frontiers | Research Topics

Adapting drug repurposing to overturn drug resistance in cancer

Edited by
Eswar Shankar, Dharmaraja Allimuthu and Vish Subramaniam

Published in
Frontiers in Pharmacology
Frontiers in Cell and Developmental Biology
Frontiers in Oncology

ISSN 1664-8714
ISBN 978-2-8325-2406-0
DOI 10.3389/978-2-8325-2406-0

About Frontiers

Frontiers is more than just an open access publisher of scholarly articles: it is a pioneering approach to the world of academia, radically improving the way scholarly research is managed. The grand vision of Frontiers is a world where all people have an equal opportunity to seek, share and generate knowledge. Frontiers provides immediate and permanent online open access to all its publications, but this alone is not enough to realize our grand goals.

Frontiers journal series

The Frontiers journal series is a multi-tier and interdisciplinary set of open-access, online journals, promising a paradigm shift from the current review, selection and dissemination processes in academic publishing. All Frontiers journals are driven by researchers for researchers; therefore, they constitute a service to the scholarly community. At the same time, the *Frontiers journal series* operates on a revolutionary invention, the tiered publishing system, initially addressing specific communities of scholars, and gradually climbing up to broader public understanding, thus serving the interests of the lay society, too.

Dedication to quality

Each Frontiers article is a landmark of the highest quality, thanks to genuinely collaborative interactions between authors and review editors, who include some of the world's best academicians. Research must be certified by peers before entering a stream of knowledge that may eventually reach the public - and shape society; therefore, Frontiers only applies the most rigorous and unbiased reviews. Frontiers revolutionizes research publishing by freely delivering the most outstanding research, evaluated with no bias from both the academic and social point of view. By applying the most advanced information technologies, Frontiers is catapulting scholarly publishing into a new generation.

What are Frontiers Research Topics?

Frontiers Research Topics are very popular trademarks of the *Frontiers journals series*: they are collections of at least ten articles, all centered on a particular subject. With their unique mix of varied contributions from Original Research to Review Articles, Frontiers Research Topics unify the most influential researchers, the latest key findings and historical advances in a hot research area.

Find out more on how to host your own Frontiers Research Topic or contribute to one as an author by contacting the Frontiers editorial office: frontiersin.org/about/contact

Adapting drug repurposing to overturn drug resistance in cancer

Topic editors

Eswar Shankar — The Ohio State University, United States

Dharmaraja Allimuthu — Indian Institute of Technology Kanpur, India

Vish Subramaniam — The Ohio State University, United States

Citation

Shankar, E., Allimuthu, D., Subramaniam, V., eds. (2023). *Adapting drug repurposing to overturn drug resistance in cancer*. Lausanne: Frontiers Media SA. doi: 10.3389/978-2-8325-2406-0

The authors declare that the research was conducted in the absence of any commercial or financial relationships that could be construed as a potential conflict of interest

Table of contents

frontiers | Frontiers in Cell and Developmental Biology

TYPE Editorial
PUBLISHED 28 April 2023
DOI 10.3389/fcell.2023.1191682

OPEN ACCESS

EDITED AND REVIEWED BY
Shyamala Maheswaran,
Massachusetts General Hospital and Harvard Medical School, United States

*CORRESPONDENCE
Dharmaraja Allimuthu,
atdharma@iitk.ac.in
Eswar Shankar,
shankar.109@osu.edu
Vish Subramaniam,
subramaniam.1@osu.edu

RECEIVED 22 March 2023
ACCEPTED 03 April 2023
PUBLISHED 28 April 2023

CITATION
Shankar E, Subramaniam V and Allimuthu D (2023), Editorial: Adopting drug repurposing to overcome drug resistance in cancer.
Front. Cell Dev. Biol. 11:1191682.
doi: 10.3389/fcell.2023.1191682

Editorial: Adopting drug repurposing to overcome drug resistance in cancer

Eswar Shankar[1]*, Vish Subramaniam[1,2]* and Dharmaraja Allimuthu[3]*

[1]Department of Internal Medicine, Division of Medical Oncology, The Ohio State University Comprehensive Cancer Center, Columbus, OH, United States, [2]Department of Mechanical and Aerospace Engineering, The Ohio State University, Columbus, OH, United States, [3]Department of Chemistry, Indian Institute of Technology Kanpur, Kanpur, Uttar Pradesh, India

KEYWORDS

cancer drug resistance, drug repurposing, FDA-approved drugs, natural product, combination therapy

Editorial on the Research Topic
Adopting drug repurposing to overturn drug resistance in cancer

Introduction

Despite significant technological advances the etiology of cancer and mechanism disease progression, and their translation into therapeutic benefits has been considerably slow. Traditional drug discovery efforts employing unbiased or target-based approaches involving natural products or small-molecule screening have created several therapeutics, but the entire process is tedious. Drug repurposing, also called drug repositioning, reprofiling, or retasking, identifies opportunities to use approved or investigational drugs that are outside the scope of the original medical indications (Ashburn and Thor, 2004). This strategy can be advantageous over developing an entirely new drug or formulation for a condition. It lowers the risk of failure as the repurposed drug's safety has already been determined and found to be safe in preclinical models and humans through completed early-stage trials; thus, from a safety point of view, the drug is less likely to fail in subsequent efficacy trials (Breckenridge and Jacob, 2019). Drug resistance is a recurrent issue in oncology (Maxmen, 2016; Dharmaraja, 2017; Nikolaou et al., 2018) and researchers are actively pursuing innovative strategies to mitigate its impact. These approaches encompass a range of interventions, including immuno-oncological treatments that elicit the immune system's response to target cancer cells (Dawe et al., 2020), combination therapies employing multiple drugs to attack cancer cells at different levels (Obenauf, 2022), and precision medicine that focuses on the molecular pathways underlying drug resistance to optimize treatment outcomes (Tsimberidou et al., 2020). These novel techniques aim to surmount the challenges of drug resistance in cancers and enhance patient outcomes. Repurposing drugs for cancer treatment has emerged as an increasingly attractive strategy as it can reduce the time to regulatory approval (Bertolini et al., 2015; Clohessy and Pandolfi, 2015; Corsello et al., 2017; Pantziarka, 2017; Pushpakom et al., 2019). In this Research Topic, we have collated research reports exploring the utility of organic small molecules, natural

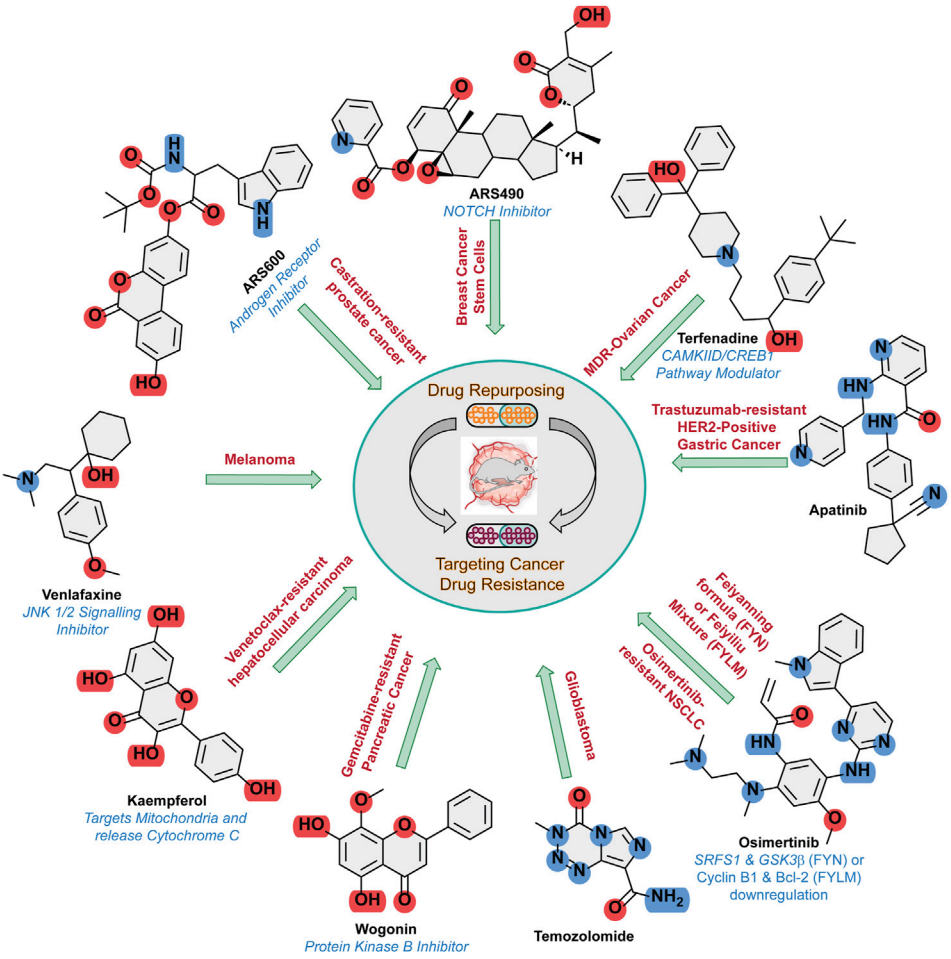

FIGURE 1
Summary of repurposed small molecules and their mechanism of actions to tackle drug resistance in the panel of cancers mentioned.

products, Chinese herbal medicines, and antibodies as combinatorial therapies to target drug resistance in cancers (Figure 1).

Small molecules in combination therapy for cancer treatment

Small molecules with promising anticancer effects have a high possibility of becoming commercialized. Therefore, there is growing enthusiasm for exploring small molecules to advance the potency of existing anticancer therapeutics. A report by Chandrasekaran et al. has identified a tyrosinated-urolithin A derivative, ARS-600, as an effective inhibitor (EC_{50}: <920 nM) of castration-resistant prostate cancer (CRPC) in xenografted castrated and non-castrated mice. The mechanism of the lead molecules was found to be the ubiquitination of the androgen receptor and its splice variant ARV7 resulting in signal inhibition in CRPC cells. Similarly, Saran et al. have identified a Withaferin A analog, ASR490, as an inhibitor of NOTCH-NICD (an active form of Notch1) in breast cancer stem cells at nanomolar concentrations. ASR490 triggers autophagy in cells to prevent cancer progression in *in vivo* xenograft models. High-throughput screening of bioactive molecules could help with the rapid identification of potential therapeutics and could provide insights into the mechanism of action. Huang et al. performed a quantitative high-throughput combinational screening of the LOPAC library (1,280 molecules, Sigma) and identified terfenadine (TFD) as a potential sensitizer of multidrug-resistant (MDR) ovarian cancer cells to doxorubicin. Here TFD molecule exerts a synergistic effect with doxorubicin against the survival of MDR ovarian cancer. They established that the mechanism of TFD function is not the manipulation of its canonical targets (Histamine receptor 1 or ether-a-go-go-related gene (hERG) channel), but direct modulation of the calcium-mediated signaling (CAMKIID/CREB1) pathway. Another small molecule-based combination therapeutic strategy with a flavonoid natural product, wogonin, was studied by Zhang et al. They show that gemcitabine-resistant pancreatic cancer cells became sensitive to gemcitabine when co-treated with wogonin. Subsequent mechanism-of-action analysis revealed suppression of the protein kinase B (Akt) signaling pathway with wogonin treatment resulting in apoptosis induction *in vivo*. Niu et al. have demonstrated that an antidepressant and antineoplastic drug, venlafaxine, could be used to control melanoma in mouse models. Venlafaxine induced

apoptosis in melanoma through its interaction with JNK1/2 signaling to promote translocation of Nur77 to mitochondria, which triggered the activation of Bcl-2, cleaved caspase-3, and poly-ADP ribose polymerase (PARP) in mouse models.

Natural products and herbal medicines that help overcome drug resistance

Natural products are a rich source of structurally diverse chemical scaffolds for the screening and identification of unique therapeutic candidates. This should not be a surprise given the successful development of taxanes as chemotherapeutic agents since the 1960s (Weaver, 2014). Chen et al. explored the therapeutic potential of kaempferol (KPL), a flavonoid natural product isolated from persimmon leaves. Here, they evaluate the efficacy of KPL on resensitizing drug-resistant hepatocellular carcinoma (HepG2) cells to venetoclax (ABT-199), a therapeutic approved to treat leukemia. The combination of KPL with ABT-199 demonstrated the induction of apoptosis through the disruption of mitochondrial membrane potential and the release of cytochrome C into mitochondria and cytoplasm, triggering apoptosis. The downstream apoptotic signature was observed in the reduction in anti-apoptotic proteins such as Bcl-2, Bcl-xL, and Mcl-1 and the upregulation of cleaved caspase. Traditional Chinese medicines have been used for the treatment of cancer for several decades. For example, Sang et al. showed that feiyanning formula (FYN), a Chinese herbal medicine cocktail prescribed for the treatment of lung cancer, could be exploited for targeting osimertinib-resistant non-small cell lung cancer (NSCLC). FYN has been shown to downregulate SRSF1 and GSK3β and thereby modulate the Wnt/β-catenin pathway in osimertinib-resistant NSCLC, HCC827OR, and PC9OR cells. Further, FYN (250 μg/mL) was found to elicit a synergistic effect with osimertinib (4 μM), an epidermal growth factor receptor (EGFR) tyrosine kinase inhibitor, on osimertinib-resistant NSCLC cells after 48 h of treatment and to prevent cell proliferation and migration; the combination suppressed tumor growth in mouse xenograft models of lung adenocarcinoma. Another Chinese herbal formula, feiyiliu mixture (FYLM), was described as sensitizing mutant EGFR-NSCLC to osimertinib by Shi et al. The major components of FYLM, characterized by mass spectrometry, included several antioxidant components such as quercetin, apigenin, formononetin, scutellarin, and oleanolic acid. EGFR-Del19/T790M/C797S mutant NSCLC is resistant to osimertinib; when combined with FYLM, the cells underwent apoptosis. It was shown that FYLM reduced EGFR phosphorylation and downregulated cyclin B1 and Bcl-2 while upregulating levels of cleaved caspase-3 to promote apoptosis *in vivo*. Peng et al. performed a metadata analysis of 31,263 patients treated with 16 Chinese herbal injections (CHIs) in combination with Western medicines. In a detailed analysis of 16 CHIs used either alone or in combination to treat cancer in China, a few were shown to be exceptionally beneficial in terms of reducing gastrointestinal adverse reactions, the incidence of thrombocytopenia, and the incidence of leukopenia when combined with Western medicines.

Antibody and nanocarrier systems targeting drug resistance

Antibodies and antibody-drug conjugates (ADCs) that have been approved by the FDA for use in cancer treatment are promising classes of cancer therapies and precision medicines. However, the inherent reduction in activity due to *de novo* resistance development in the phenotype has prompted the combination therapies evolution of ADCs with chemotherapeutics. Lv et al. describe a case report of overcoming trastuzumab resistance in human epidermal growth factor receptor 2 (HER2)-positive gastric cancer by treating it with a triple regimen of apatinib and camrelizumab with trastuzumab. This issue also includes a research article on nanoparticle-based drug delivery systems for cancer treatment. Here, Wu et al. have developed a trifunctional, covalent nanocarrier system (Pep-1@PDA-TMZ) as a chemotherapeutic and photothermal therapeutic (PTT) to treat glioblastoma. This Pep-1@PDA-TMZ is based on dopamine polymeric nanoparticles covalently linked to a glioblastoma drug, temozolomide (TMZ), and Pep-1, a cell-penetrating peptide for enabling blood-brain barrier (BBB) breach. The conjugate Pep-1@PDA-TMZ was shown to penetrate cells effectively and was delivered specifically to the therapeutic site with a 77% inhibition of U87 cells in tumor-bearing nude mice *in vivo* recorded upon irradiation. This Research Topic also includes reviews by Xia et al. and Wang et al. that comprehensively discuss combination therapeutic strategies to overcome PARP-mediated drug resistance in breast and gynecological cancers.

This Research Topic assembles research reports targeting a wide range of cancers and mechanisms centered around overcoming drug resistance by utilizing drug repurposing or therapies using combinations of drugs (Figure 1).

Author contributions

ES led the team of DA and VS as Guest Editors of this Research Topic and the team closely interacted throughout the editorial process, by defining the subjects to be treated and by acting as handling editors of the manuscripts submitted to the Research Topic and writing the Editorial. All authors contributed to the article and approved the submitted version.

Acknowledgments

We thank Angela Dahlberg, Senior Editor, Division of Medical Oncology, The Ohio State University Wexner Medical Center, for the final language editing to improve the clarity of presentation.

Conflict of interest

The authors declare that the research was conducted in the absence of any commercial or financial relationships that could be construed as a potential conflict of interest.

Publisher's note

References

Ashburn, T. T., and Thor, K. B. (2004). Drug repositioning: Identifying and developing new uses for existing drugs. *Nat. Rev. Drug Discov.* 3, 673–683. doi:10.1038/nrd1468

Bertolini, F., Sukhatme, V. P., and Bouche, G. (2015). Drug repurposing in oncology-patient and health systems opportunities. *Nat. Rev. Clin. Oncol.* 12, 732–742. doi:10.1038/nrclinonc.2015.169

Breckenridge, A., and Jacob, R. (2019). Overcoming the legal and regulatory barriers to drug repurposing. *Nat. Rev. Drug Discov.* 18, 1–2. doi:10.1038/nrd.2018.92

Clohessy, J. G., and Pandolfi, P. P. (2015). Mouse hospital and co-clinical trial project-from bench to bedside. *Nat. Rev. Clin. Oncol.* 12, 491–498. doi:10.1038/nrclinonc.2015.62

Corsello, S. M., Bittker, J. A., Liu, Z., Gould, J., Mccarren, P., Hirschman, J. E., et al. (2017). The drug repurposing hub: A next-generation drug library and information resource. *Nat. Med.* 23, 405–408. doi:10.1038/nm.4306

Dawe, D. E., Harlos, C. H., and Juergens, R. A. (2020). Immuno-oncology-the new paradigm of lung cancer treatment. *Curr. Oncol.* 27, S78–s86. doi:10.3747/co.27.5183

Dharmaraja, A. T. (2017). Role of reactive oxygen species (ROS) in therapeutics and drug resistance in cancer and bacteria. *J. Med. Chem.* 60, 3221–3240. doi:10.1021/acs.jmedchem.6b01243

Maxmen, A. (2016). Busting the billion-dollar myth: How to slash the cost of drug development. *Nature* 536, 388–390. doi:10.1038/536388a

Nikolaou, M., Pavlopoulou, A., Georgakilas, A. G., and Kyrodimos, E. (2018). The challenge of drug resistance in cancer treatment: A current overview. *Clin. Exp. Metastasis* 35, 309–318. doi:10.1007/s10585-018-9903-0

Obenauf, A. C. (2022). Mechanism-based combination therapies for metastatic cancer. *Sci. Transl. Med.* 14, eadd0887. doi:10.1126/scitranslmed.add0887

Pantziarka, P. (2017). Scientific advice - is drug repurposing missing a trick? *Nat. Rev. Clin. Oncol.* 14, 455–456. doi:10.1038/nrclinonc.2017.69

Pushpakom, S., Iorio, F., Eyers, P. A., Escott, K. J., Hopper, S., Wells, A., et al. (2019). Drug repurposing: Progress, challenges and recommendations. *Nat. Rev. Drug Discov.* 18, 41–58. doi:10.1038/nrd.2018.168

Tsimberidou, A. M., Fountzilas, E., Nikanjam, M., and Kurzrock, R. (2020). Review of precision cancer medicine: Evolution of the treatment paradigm. *Cancer Treat. Rev.* 86, 102019. doi:10.1016/j.ctrv.2020.102019

Weaver, B. A. (2014). How Taxol/paclitaxel kills cancer cells. *Mol. Biol. Cell* 25, 2677–2681. doi:10.1091/mbc.E14-04-0916

frontiers | Frontiers in Pharmacology

TYPE Review
PUBLISHED 25 August 2022
DOI 10.3389/fphar.2022.967633

OPEN ACCESS

EDITED BY
Eswar Shankar,
The Ohio State University, United States

REVIEWED BY
Tribhuwan Yadav,
Massachusetts General Hospital and Harvard Medical School, United States
Prem P. Kushwaha,
Case Western Reserve University, United States

*CORRESPONDENCE
Li Yang,
zdsfyyangli@163.com
Huaiwu Lu,
luhuaiwu@mail.sysu.edu.cn

SPECIALTY SECTION
This article was submitted to Pharmacology of Anti-Cancer Drugs, a section of the journal Frontiers in Pharmacology

RECEIVED 13 June 2022
ACCEPTED 04 August 2022
PUBLISHED 25 August 2022

CITATION
Wang N, Yang Y, Jin D, Zhang Z, Shen K, Yang J, Chen H, Zhao X, Yang L and Lu H (2022), PARP inhibitor resistance in breast and gynecological cancer: Resistance mechanisms and combination therapy strategies. *Front. Pharmacol.* 13:967633. doi: 10.3389/fphar.2022.967633

PARP inhibitor resistance in breast and gynecological cancer: Resistance mechanisms and combination therapy strategies

Nannan Wang[1], Yan Yang[2], Dongdong Jin[1,3], Zhenan Zhang[1], Ke Shen[1], Jing Yang[1], Huanhuan Chen[1], Xinyue Zhao[1], Li Yang[1,3]* and Huaiwu Lu[4]*

[1]Department of Obstetrics and Gynecology, The Third Affiliated Hospital of Zhengzhou University, Zhengzhou, China, [2]Department of Biochemistry and Molecular Biology, School of Basic Medical Sciences, Xinxiang Medical University, Xinxiang, China, [3]Zhengzhou Key Laboratory of Endometrial Disease Prevention and Treatment, Zhengzhou, China, [4]Department of Gynaecological Oncology, Sun Yat Sen Memorial Hospital, Guangzhou, China

Breast cancer and gynecological tumors seriously endanger women's physical and mental health, fertility, and quality of life. Due to standardized surgical treatment, chemotherapy, and radiotherapy, the prognosis and overall survival of cancer patients have improved compared to earlier, but the management of advanced disease still faces great challenges. Recently, poly (ADP-ribose) polymerase (PARP) inhibitors (PARPis) have been clinically approved for breast and gynecological cancer patients, significantly improving their quality of life, especially of patients with BRCA1/2 mutations. However, drug resistance faced by PARPi therapy has hindered its clinical promotion. Therefore, developing new drug strategies to resensitize cancers affecting women to PARPi therapy is the direction of our future research. Currently, the effects of PARPi in combination with other drugs to overcome drug resistance are being studied. In this article, we review the mechanisms of PARPi resistance and summarize the current combination of clinical trials that can improve its resistance, with a view to identify the best clinical treatment to save the lives of patients.

KEYWORDS

PARP inhibitor, PARP inhibitor resistance, breast cancer, gynecological cancer, combination therapy, ATR/CHK1/WEE1 pathway, targeted drugs

1 Introduction

According to statistics, in 2020, breast cancer had the highest incidence among women in the world, followed by cervical cancer (CC), endometrial cancer (EC), and ovarian cancer (OC) (Sung et al., 2021; Grossman et al., 2018). These cancers seriously endanger women's physical and mental health. Treatment methods for the cancers mentioned above generally include radical surgical resection, radiotherapy, and chemotherapy (Brown et al., 2020; Butala et al., 2021; Rütten et al., 2021). Although the treatments as mentioned earlier can significantly prolong the survival of patients, the

overall prognosis is still unsatisfactory. OC patients have about a 70% probability of recurrence within 3 years after standard treatment (Sung et al., 2021; Ledermann et al., 2018). The 5-years survival rate of early breast cancer patients can reach more than 90%, but the survival rate of advanced cancer patients is only 30%. Compared with the other molecular subtypes of breast cancer, triple-negative breast cancer has the worst prognosis because it does not respond to endocrine or targeted therapy (Sung et al., 2021; Ovcaricek et al., 2011). Advanced EC and CC patients also have a poor prognosis (Cohen et al., 2019; Crosbie et al., 2022). Progression-free survival (PFS) is progressively shorter in patients despite continued treatment at relapse (Poveda et al., 2021).

Recently, the advent of targeted drugs has given new hope to cancer patients, which can prolong the life of these patients, improve their quality of life, and cause less damage to the body. Poly (ADP-ribose) polymerase (PARP) inhibitors (PARPis) are one of these drugs, of which olaparib, lucaparib, niraparib, and talazoparib have been approved for use clinical treatment, including breast, ovarian, lung and prostate cancers (Poveda et al., 2021; Hao et al., 2021; Wang et al., 2020; Mirza et al., 2020; Molinaro et al., 2020). It is the first drug to target and induce the death of BRCA1/BRCA2-deficient cells on a synthetic lethal basis (Bryant et al., 2005). Currently, PARPi has become the first-line regimen for OC treatment (Poveda et al., 2021). A single-center real-world study of patients with platinum-resistant ovarian cancer (PROC) treated with PARPi showed that after the use of PARPi in 17 patients, the objective response rate (ORR) was 47%, and the median progression-free survival (PFS) was 8.2 months (5.3–11.3), overall survival (OS) was 14.9 months (11.2–18.5) (Agarwal et al., 2021). Despite the success of PARPi in targeting BRCA-deficient tumors, the emergence of acquired resistance to PARPi is a hurdle that we need to overcome, with more than two-thirds of patients on long-term PARPi therapy eventually developing acquired resistance (Hodgson et al., 2018; Lin et al., 2019). Therefore, understanding the mechanism of PARPi resistance and then finding alternative treatment strategies to improve the benefits of PARPi treatment is the top priority of our research. This article discusses some of the possible mechanisms of PARPi resistance and combined treatment strategies to improve the sensitivity of PARPi in cancer treatment.

2 Mechanisms of PARP inhibitors

There are many mechanisms in cells to recognize and repair DNA damage, so that damaged DNA can be repaired in time to maintain normal physiological functions, mainly including homologous recombination (HR), non-homologous end joining (NHEJ), BER (base excision repair), and mismatch repair (MMR) (Hoeijmakers, 2001). PARP1/2 is crucial in repairing DNA single-strand breaks (SSB) (Langelier et al., 2012). When the DNA single strand breaks, it rapidly recognizes and binds to the DNA damage site, and catalyzes the PARylation of various proteins including itself; i.e., PARP protein and NAD^+ (Nicotinamide adenine dinucleotide), PAR (poly ADP-ribose) chains bind and recruit other DNA repair-related proteins to initiate the DNA repair process (Fisher et al., 2007; Pascal and Ellenberger, 2015). With the PARylation of PARP1/2 proteins, the chromatin gradually becomes relaxed, and the PARP protein automatically detaches from the DNA damage site. On the one hand, PARPi can block this process, so that the PARP proteins and other DNA repair proteins cannot be detached from the DNA chain (Wang et al., 2019). This is called, "PARP trapping." This is also the reason why PARPi is more destructive towards cancer cells than knocking out the PARP gene itself (Kim et al., 2020); on the other hand, PARPi can competitively bind to the NAD^+ site, directly inhibit the activity of PARP1/2, and block the DNA repair process mediated by it, so that the SSB in DNA cannot be repaired and converted into DNA double-strand break (DSB).

There are two main repair pathways for DSB, homologous recombination (HR) repair pathway and non-homologous end joining (NHEJ) repair pathway. HR repair (HRR) is a rigorous, high-fidelity repair pathway that contributes to genetic stability. The HRR process involves the participation of various proteins, such as BRCA1, BRCA2, RAD51, and ATM. If the above genes are mutated and lose their original activity, it will lead to homologous recombination deficiency (HRD). At this time, the proportion of NHEJ in the repair process of DSB is increased. Compared with the high fidelity of HRR, the repair of NHEJ does not require the participation of homologous DNA templates; hence, its error rate is extremely high, which easily leads to DNA aberrations and cell death (Betermier et al., 2014; Le Guen et al., 2014). PARPi treatment blocks SSB repair in cancer cells, while cells with BRCA mutations are unable to rely on the HR pathway to repair DSBs and switch to a low-fidelity NHEJ pathway to repair DNA, causing genomic instability and cell death, a so-called "synthesis lethal effect" (Figure 1) (Fishman-Lobell et al., 1992; van Wietmarschen and Nussenzweig, 2018). A recently proposed new theory suggests that in BRCA-deficient cells, PARPi leads to the accumulation of ssDNA gaps through a trans-cellular cycle (Cong et al., 2021). That is, PARPi stimulates the restart of PrimPol to induce the production of ssDNA gaps in S-phase, and the accumulated ssDNA gaps are transformed into DSBs in the next S-phase. The continuous use of PARPi in BRCA-deficient cells leads to the inability of DSBs to be repaired in time and eventually kills tumor cells (Simoneau et al., 2021; Tirman et al., 2021).

3 Mechanisms of resistance to PARP inhibitors

With the approval of PARPi as a first-line clinical drug, more and more patients have increased clinical benefits, but with it

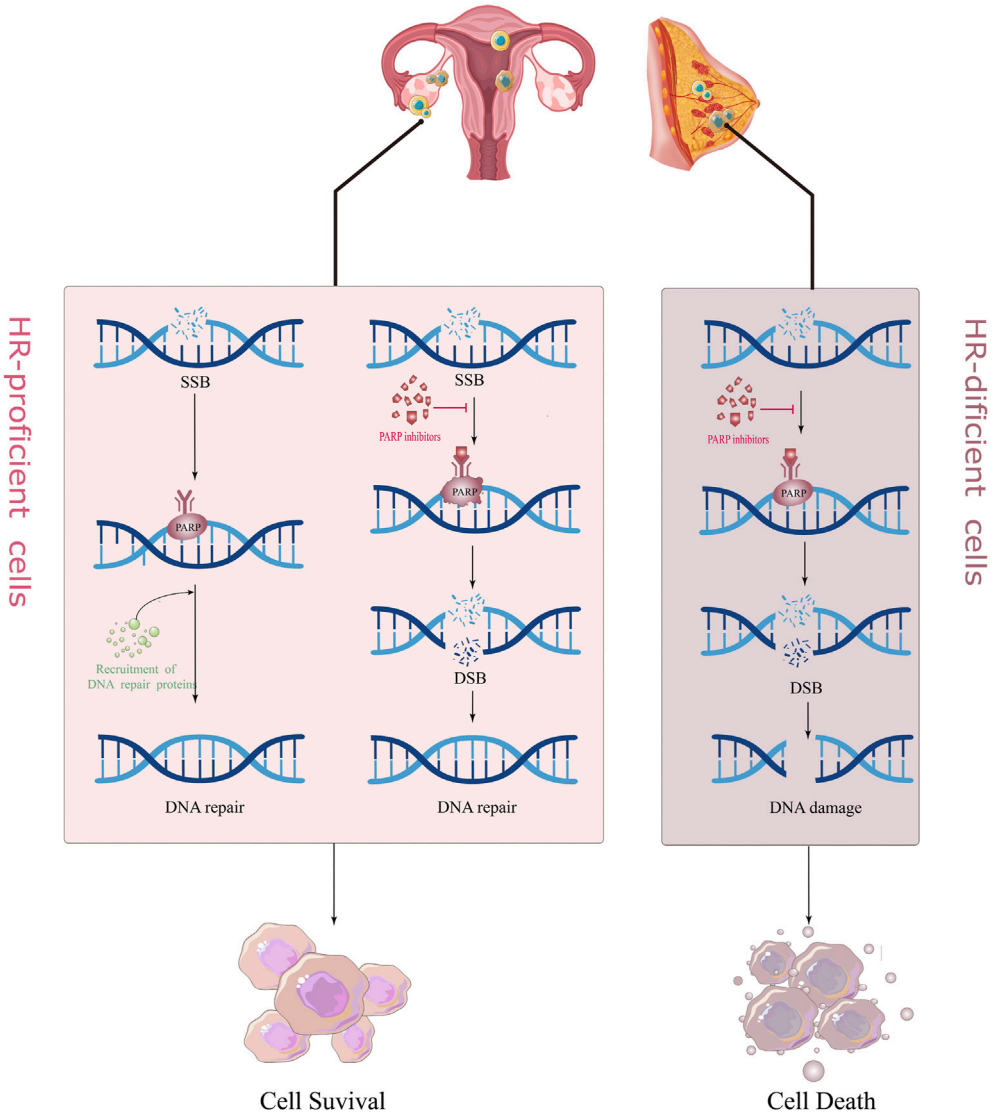

FIGURE 1
The mechanism of action of PARP inhibitors for "synthetically lethality."

comes an increase in the incidence of new or acquired resistance to PARPi. An in-depth understanding of the mechanism of PARPi resistance will help us understand and overcome the occurrence of clinical resistance. Numerous preclinical and clinical studies have explored PARPi resistance to identify combination therapy strategies and appropriate populations.

3.1 Recovery of replication fork stability

The replication fork is a significant step in DNA damage repair and checkpoint activation during replication in the cell cycle. Many abnormalities in DNA replication can lead to stalled replication forks, leading to genomic instability and cell death if stalled replication forks fail to restart (Cox et al., 2000). PARP1, BRCA1/2, and RAD51 exert essential roles in protecting replication forks from nuclease attack and regulating the accumulation of reversed forks (Chaudhuri et al., 2016; Schaaf et al., 2016; Ronson et al., 2018). However, in BRCA-mutated cells, down-regulation of the nuclease MRE11 and cross-linking endonuclease MUS81 due to a series of molecular mechanisms ultimately leads to fork protection and enhanced DNA damage repair (DDR), ultimately leading to PARPi resistance (Figure 2A) (Bryant et al., 2009; Rondinelli et al., 2017).

EZH2, a methyltransferase involved in histone methylation, rapidly locates at the replication fork after replication fork

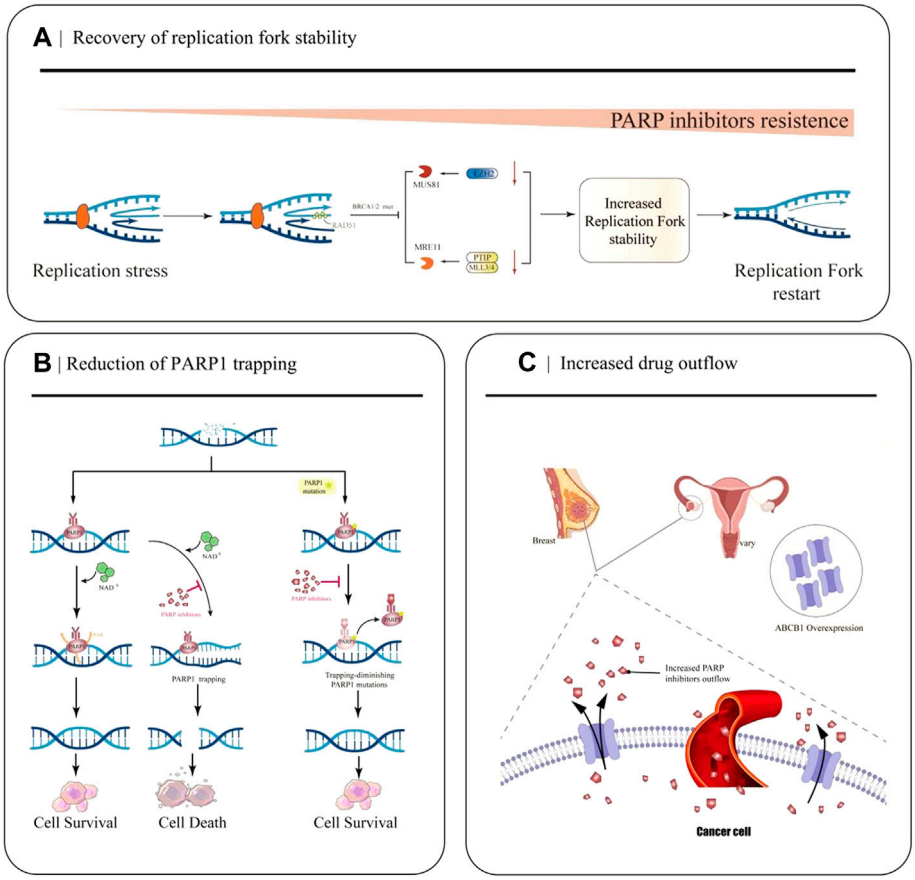

FIGURE 2
Partial mechanisms of PARP inhibitor resistance in cancer. **(A)** Restoration of replication fork stability leads to PARP inhibitor resistance. When EZH2 or MLL3/4-PTIP is deficient, MUS81 and MRE11 recruitment fails, the replication fork is less attacked, and the replication fork is stable. **(B)** Decreased PARP1 trapping contributes to the development of PARP inhibitor resistance. PARP inhibitors reduce the catalytic activity of PARP1, so that PARP remains bound to DNA and cannot undergo subsequent repair. PARP1 mutations reduce PARP capture. **(C)** Increased drug efflux mediated by ABCB1 overexpression leads to a decrease in effective concentration in cancer cells and increased resistance to PARPi.

stagnation and promotes MUS81, a crossover junction endonuclease, to attack the replication fork, causing replication fork degradation (Rondinelli et al., 2017). The MLL3/4 complex protein PTIP can recruit the nuclease MRE11 into the stalled replication fork, resulting in degradation of the stalled replication fork (Zhang et al., 2014). In BRCA1 and BRCA2 mutated cells, EZH2 and PTIP activities are downregulated at the fork, and MUS81 and MRE11 recruitment is reduced, ultimately leading to the stabilization of the replication fork and the development of PARPi resistance.

Furthermore, recent studies have found that the lysine acetyltransferase 2B, KAT2B (often called PCAF), is associated with the degradation of stalled replication forks. Kim et al. (2020) showed that in BRCA-deficient cells, PCAF first utilizes its own structure to bind to stalled replication forks, and then acetylates H4K8 to promote the recruitment of MRE11 and EXO1 nucleases to the replication fork, which further promotes fork degradation. Loss of PCAF promotes the resistance of BRCA1/2-deficient cells to PARPi treatment.

3.2 Reduction of PARP1 trapping

After identifying DNA damage, PARP1 is rapidly activated and it binds to the site of DNA breakage sites. Then it catalyzes the formation of multiple protein PAR chains, including itself with NAD^+ as the substrate, thus realizing its function (Wang et al., 2006). PARPi inhibits the catalytic activity of PARP1, which keeps PARP bound to DNA and prevents subsequent repair (Figure 2B). Recently, Stephen et al.used the CRISPR-Cas9 technology to screen PARP1 point mutation fragments that lead to PARPi resistance, and they found PARP1 p. R591C mutation (c.1771C>T) in an olaparib-resistant ovarian cancer patient.

Mutations enhance PARP1 dissociation from DNA and reduce PARP trapping, suggesting that PARP1 mutations are associated with the emergence of a drug-resistant phenotype, and experiments have confirmed that point mutations outside the ZnF domain may also lead to PARP inhibition resistance by reducing PARP1 trapping (Pettitt et al., 2018).

3.3 Increased drug outflow

Studies have demonstrated that the occurrence of PARPi resistance is associated with increased ABCB1-mediated drug efflux. ABCB1 (P-gp, p-glycoprotein, also known as MDR1), a drug efflux transporter belonging to the ATP-binding cassette (ABC) transporter superfamily, encodes the multidrug resistance protein (Figure 2C) (Li et al., 2015). It has a very wide substrate specificity, and it is highly expressed in many tumors, especially in drug-resistant breast cancer and OC (Christie et al., 2019). With the up-regulation of ABCB 1a/1b genes, the expression of P-gp efflux transporter increases, resulting in a decrease in the effective intracellular drug concentration, thus, leading to PARPi resistance (F. Martins et al., 2021). In 2020, a quantitative mass spectrometry imaging (LC-MS/MS) assay showed that in a P-gp-overexpressing ovarian cancer model, niraparib was unevenly distributed within the tumor, reducing the efficacy of drug treatment; thus, suggesting that it is resistant to PARPi(Morosi et al., 2020).

The relationship between the two was first discovered by Rottenberg et al. The group's experiments demonstrated that in a breast tumor model, the emergence of PARPi-acquired resistance is related to upregulation of P-gp expression, and that the P-gp inhibitor tariquidar can reverse its overexpression (Rottenberg et al., 2008). Similarly, *in vitro* experiments by Margarida et al. demonstrated that ABCB 1a/1b attenuated brain penetration and promoted systemic elimination of niraparib in mice, with partial reversal of resistance following treatment with the ABCB1 inhibitor Elacridar (F. Martins et al., 2021). A clinical study (NCT02681237) found that ABCB1 was upregulated in 15% of patients in the progression group after using PARPi. Clinically, PARPi resistance is significantly relevant to increased drug efflux and decreased accumulation of PARPis in tumor cells (Lheureux et al., 2020). Therefore, a more in-depth study of the relationship between the expression and role of ABCB1 and PARPi resistance is crucial for clinical medicine.

3.4 PARG depletion

PARylation is a PARP-mediated post-translational modification of proteins that controls key mechanisms such as the DNA damage response in cells (O'Sullivan et al., 2019). PARP1 is the primary target of PARylation, and the resulting PAR chains recruit downstream protein repair factors. Poly (ADPribose) glycohydrolase (PARG) can reverse PARylation and catalyze PAR strand breaks; thus, its loss reduces PARP1 capture, rescues PARP1-dependent DNA damage signaling, and ultimately leads to PARPi resistance (Figure 3A) (Francica and Rottenberg, 2018; O'Sullivan et al., 2019). A number of studies have demonstrated that the loss of PARG is related to the occurrence of acquired resistance to PARPi. Experiments in breast cancer cell models have demonstrated the correlation between the two (Gogola et al., 2018). Interestingly, many studies of PARPi-resistant cells treated with PARG inhibitors have shown that PARG inhibitors can improve the development of PARPi resistance (Gogola et al., 2018). The PARG protein was highly expressed in 34% of OC tumors, and the use of PARG inhibitors resulted in decreased cell migration compared with the use of PARG inhibitors alone. Inhibition of PARG enhances the therapeutic effect of cisplatin and PARPi on ovarian cancer cells (Chen and Yu, 2019).

3.5 Loss of SLFN11

The SLFN11 protein encoded by the Schlafen11 (SLFN11) gene can cause the degradation of specific tRNAs and then inhibit the expression of DNA damage repair-related proteins when activated. Therefore, in normal cells, SLFN11 inhibits DNA repair when DNA is broken. However, the SLFN11 gene is generally silenced in cancer cells, making these cancer cells more capable of DNA repair and conferring resistance to PARPi (Figure 3B) (Li et al., 2012). Loss of SLFN11 conferred resistance to three PARPis (olaparib, rucaparib, and veliparib) in an *in vitro* assay in small cell lung cancer and a dataset analysis in 2017 (Lok et al., 2017). The EVOLVE clinical trial (NCT02681237) exploratory study of anti-angiogenic drugs combined with PARPi in patients with PARPi-resistant ovarian cancer showed the following findings: BRCA1/2 or RAD51B reversion (19%) at the time of PARPi progression; ABCB1 upregulation (15%); and down-regulation of SLFN11 (7%) (Lheureux et al., 2020).

3.6 The alteration of the ATR/CHK1/WEE1 pathway

Besides PARPi, the ATR/CHK1/WEE1 pathway also plays a decisive role in DNA damage recognition and repair. When sensing DNA damage and replication fork pressure, replication protein A (RPA) binds to the site of damage and then recruits and activates Ataxia-telangiectasia and RAD3-related protein (ATR) at the site. When ATR is activated by RPA, it starts to activate its effector proteins, CHK1 and WEE1, which eventually leads to cell stagnation in the G2-M and S phases, preventing the cells from entering mitosis to reduce the replication pressure and trigger the

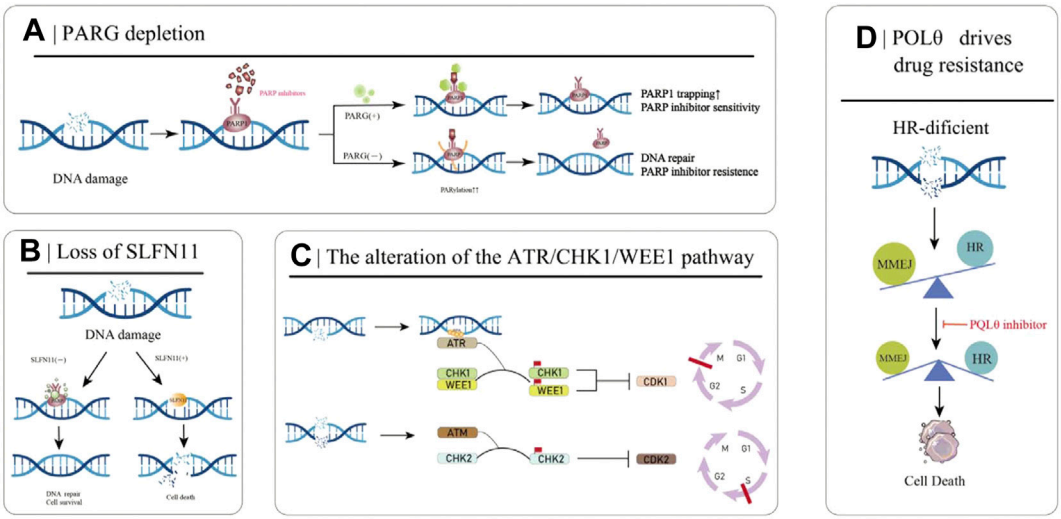

FIGURE 3
Partial mechanisms of PARP inhibitor resistance in cancer. **(A)** PARG deletion leads to PARPI resistance. **(B)** Loss of SLFN11 enhances DSB repair capacity, ultimately leading to PARPi resistance. **(C)** The ATR/CHK/WEE1 signaling pathway arrests the cell cycle to reduce replication stress and promote DSB repair. **(D)** HR-deficient cells rely on MMEJ for DSB repair, which is mediated by POLθ. Inhibition of POLθ in HR-deficient cells results in cell death.

appropriate DNA repair pathways (Figure 3C) (Petermann and Caldecott, 2006; Yekezare et al., 2013). PARPi induces strong replication stress after cancer treatment, which activates the ATR/CHK1/WEE1 pathway. Studies have shown that the ATR/CHK1/WEE1 pathway can promote DNA repair, and inhibition of this pathway can resensitize tumor cells to PARPi (Kim et al., 2017).

Cell cycle protein-dependent kinase (CDK) mainly regulates cell cycle and gene transcription process. The expression of DNA repair proteins such as ATR and BRCA1/2 is downregulated by CDK12 knockdown (Bajrami et al., 2014; Naidoo et al., 2018). Inhibition of CDK12 induces the generation of BRCAness phenotype, thus reversing PARPi drug resistance.

3.7 POLQ drives drug resistance

Microhomology-mediated end joining (MMEJ) is an uncommonly used DSB repair pathway other than HR and NHEJ, driven by low-fidelity DNA polymerase theta (Polθ, also known as POLQ). It recognizes 5-25bp homologous sequences and directly connects the broken DNA ends. Due to the frequent deletion and dislocation of homologous fragments, MMEJ is a low-fidelity DSB repair pathway compared to HR (Chang et al., 2017). In HR-deficient cancer cells, DSB repair is dependent on MMEJ repair, and inhibition of this pathway results in failure of DNA to repair properly and increases genomic instability (Figure 3D). The expression of Polθ is negatively correlated with HR activity, and Polθ binds to RAD51 and inhibits its mediated DNA recombination. Knockdown of Polθ in HR-proficient cells resulted in increased HR activity and upregulation of RAD51 activity, whereas knockdown of Polθ in HR-deficient cells resulted in cell death (Ceccaldi et al., 2015; Mateos-Gomez et al., 2015). Therefore, on the one hand, inhibiting the Polθ gene in HR-deficient tumors induces tumor cell death through a "synthetic lethal" mechanism, and on the other hand, targeting PARPi-resistant cells caused by 53BP1/Shieldin complex deficiency, is a promising strategy for the treatment of PARPi-resistant patients.

3.8 Restoration of homologous recombination repair

With the approval of PARPi as a first-line clinical drug, more and more patients have obtained increased clinical benefits, but with it comes an increase in the incidence of new or acquired resistance to PARPi. An in-depth understanding of the mechanism of PARPi resistance will help us understand and overcome the occurrence of clinical resistance (Figure 4). Numerous preclinical and clinical studies have explored PARPi resistance to identify combination therapy strategies and appropriate populations.

3.8.1 Restoration of the BRCA1/2 function

To our knowledge, BRCA1 and BRCA2 are critical genes in HR-dependent DSB repair, and the loss of their function can directly lead to defects in the HR-repair pathway (Wang and

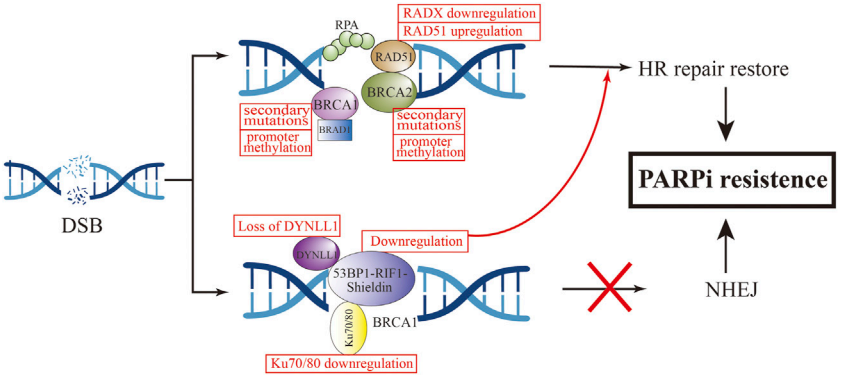

FIGURE 4
Mechanism of HR-dependent pathway leading to PARPi resistance.

Figg, 2008). The most common cause of functional restoration of the HR pathway is secondary mutations in BRCA1/2 genes (Barber et al., 2013; Waks et al., 2020). Reverse mutations of BRCA1 and BRCA2 have been demonstrated in high-grade OC cells that are resistant to platinum and PARPi drugs (Shroff et al., 2018). This is due to the reverse mutation correcting the ORF of the primary mutant BRCA1/2. For example, in Ashkenazi Jewish populations, which lack wild-type BRCA2, but carry the c.6174d frameshift mutation of BRCA2, this mutation can result in truncation of BRCA2 protein expression (Edwards et al., 2008). Subsequent further cellular experiments have found that the deletion of the c.6174d mutation and subsequent restoration of the ORF function leads to the expression of new BRCA isoforms, resulting in acquired resistance to PARPi. To investigate the relationship between BRCA reverse mutations and PARPi re sistance, an ARIEL2 trial sequenced the circulating cell-free DNA (cfDNA) of 92 patients with BRCA-mutated OC before and after rucaparib treatment. The PFS of the group with BRCA reverse mutation was 7.2 months less than that of the group without reverse mutation (1.8 vs. 9.0 months, HR, 0.12; 95%CI, 0.05–0.26; $p < 0.0001$) (Swisher et al., 2017).

In addition to reverse mutation of the gene, the reason for restoration of BRCA1/2 function is also related to promoter methylation. Experiments have demonstrated that BRCA1 promoter methylation defects have been detected in some OC ovarian cancer samples. Bianco T et al. observed that unmethylated samples had lower BRCA1 RNA expression levels compared to samples with high BRCA1 methylation. Methylation status of the BRCA1 promoter is associated with BRCA1 silencing, and hypomethylation are correlated with different degrees of BRCA1 repression and different degrees of HR recovery (Bianco et al., 2000). Hence, we can consider that BRCA1 promoter methylation is a useful predictor of the response to PARPi.

3.8.2 Increased expression of RAD51 and secondary mutations in its homologous and paralogous genes

RAD51 is a conserved universal recombinase that forms helical filaments at ssDNA and promotes double-strand repair of broken DNA. On the one hand, it binds to SWI/SNF-related matrix-associated actin-dependent regulator of chromatin subfamily A-like protein 1 (SMARCAL1) at stalled replication forks to repair replication forks and promote fork inversion (Baumann and West, 1998; Arnaudeau, 2001). On the other hand, RAD51 protects newly synthesized DNA from nuclease degradation and pro. motes subsequent DNA synthesis (Hashimoto et al., 2010).

Detecting the expression of RAD51 foci in OC patient-derived xenografts and scoring HR status according to BRCA1/2 status showed that the expression of RAD51 foci was strongly negatively correlated with olaparib responsiveness (Guffanti et al., 2022). In olaparib-treated tumor models, the percentage of RAD51-positive cells was 1.25 ± 0.25% in the four PARPi-sensitive models and 66.54 ± 2.70% in the 14 PARPi-resistant models ($p < 0.0001$). It shows that the high expression of RAD51 is related to the occurrence of PARPi resistance (Castroviejo-Bermejo et al., 2018). Clinical studies have further confirmed the relationship between RAD51 lesions and PARPi. Tumor samples from ovarian patients were stained and scored for RAD51. The results showed that the RAD51 score of PARPi-resistant tumor samples was higher than that of PARPi-sensitive samples, and was negatively correlated with the clinical efficacy of PARPi (Cruz et al., 2018). Similarly, four of eight patients with metastatic BC carrying BRCA1/2 mutations who were treated with PARPi or platinum developed BRCA reversal mutations, and a significant increase in RAD51 expression after drug resistance was found by detecting changes in protein

expression in tumor tissues before and after drug resistance (Waks et al., 2020).

It has been confirmed that in addition to BRCA1/2 mutations, RAD51 secondary mutations can also lead to the occurrence of PARPi resistance. Experiments by Olga Kondrashova et al. (2017) showed that mutations in the RAD51C/D genes confer sensitivity to PARPi treatment, but secondary mutations in these genes were detected in ovarian cancer patients who relapsed after rucaparib treatment. It may be that these secondary mutations restore the open reading frame (ORF) of RAD51, thereby restoring HR function and ultimately leading to rucaparib resistance. Further cellular experiments demonstrated that knockdown of RAD51C in the OVCAR8 cell line increased the sensitivity of cisplatin and rucaparib, and reintroduction of wild-type RAD51C cDNA could be observed to restore resistance to PARPi in cells. Conversely, introduction of RAD51C with primary mutation cDNA did not restore resistance. Not only rucaparib, but RAD51C cDNA containing secondary mutations conferred resistance to olaparib, niraparib, tarazopanib, and veliparib. Experiments by Nesic et al. (2021) found that methylation of RAD51 (meRAD51C) sensitizes ovarian cancer models to niraparib and rucaparib treatment, and that if meRAD51C deletion occurs, resistance to PARPi treatment occurs. Recently, a new protein was discovered that can antagonize the activity of RAD51, namely RADX. RADX antagonizes the recruitment of RAD51 at replication forks and inhibits its accumulation at the forks. Conversely, loss of RADX restores replication fork stability, conferring resistance to PARPi in BRCA2-deficient cells. RADX acts as a regulator of RAD51 to regulate stability at replication forks, which can serve as a biomarker for predicting PARPi response (Dungrawala et al., 2017). Additionally, a genome-wide screening found that loss of the ubiquitin ligase HUWE1 induces increased RAD51 expression and promotes partial restoration of HRR in BRCA2-deficient cells, thereby promoting olaparib resistance (Clements et al., 2020).

3.8.3 Defects of non-homologous end joining

In HRD cells, NHEJ plays a major repair role (Betermier et al., 2014; Le Guen et al., 2014). NHEJ does not rely on homologous DNA sequences and directly joins DSB ends by a DNA ligase. But NHEJ is more error-prone than HRR due to deletions or insertions of nucleotide sequences, eventually causing genome instability and ultimately cell death (Grabarz et al., 2012). When the NHEJ regulatory factor is deleted, HR is reactivated, leading to the occurrence of acquired drug resistance.

TP53-binding protein (53BP1) is a protein involved in NHEJ activation, which is normally regulated by BRCA1 to maintain the balance between HR and NHEJ (Bothmer et al., 2010). 53BP1 can protect terminal DNA from excision, thereby inhibiting HR repair (Hong et al., 2016). In BRCA1-mutated cells, loss of 53BP1 restores HR repair by promoting the excision of terminal DNA (Bunting et al., 2010; Chen et al., 2022). Animal experiments demonstrated that knockout of 53BP1 in a mouse breast cancer tumor model with BRCA1 mutations can make PARPi resistant (Jaspers et al., 2013). Decreased expression of 53BP1 was found by whole-exome sequencing and analysis of the HGSOC PDX model with BRCA1 mutations and resistance to olaparib (Parmar et al., 2019). In OC patients with HRD, low expression levels of 53BP1 were associated with suboptimal response to PARPis (Hurley et al., 2019). These *in vitro* and *in vivo* studies have demonstrated that 53BP1 deletion specifically mediates PARPi resistance in BRCA1-mutated tumors. Interestingly, 53BP1 does not appear to mediate PARPi resistance in BRCA2-mutated tumors (Bouwman et al., 2010; Yang et al., 2017).

In the mechanism of mediating HR repair, 53BP1 does not act independently, and the 53BP1-Rap interacting factor (RIF1)-Shieldin axis cooperates with each other in this process (Mirman and de Lange, 2020). 53BP1 controls DNA 5′ excision through RIF1, and REV7 inhibits RIF1 expression (Zimmermann et al., 2013). The Shieldin complex consists of the regulator of viral particle protein expression (REV7), SHLD1, SHLD2, and SHLD3. This complex interacts with 53BP1 to protect DNA ends from excision, promote NHEJ activity, increase the error rate of DNA repair, and promote tumor cell death (Xu et al., 2015; Noordermeer et al., 2018). PARPi resistance also develops when effector expression on this axis is reduced. Dev et al. (2018) found that SHLD1/2 can antagonize the effect of HR, and its reduction is associated with acquired resistance to olaparib.

In addition to the above mechanisms, a novel 53BP1 interactor, DYNLL1, was recently discovered using CRISPR knockout screening technology (He et al., 2018). In BRCA1-deficient tumor cells, DYNLL1 promotes 53BP1 oligomerization to stimulate NHEJ (Becker et al., 2018), and through its interaction with MRE11 Inhibition of DNA end excision (He et al., 2018), the combination of these two effects leads to genomic instability. Low PFS was found to be significantly associated with reduced DYNLL1 expression in patients with BRCA1-mutated OC following chemotherapy. Cellular experiments demonstrated that up-regulation of DYNLL1 expression could reverse the resistance of tumor cells to olaparib. The role of DYNLL1 in DNA repair appears to be effective only in BRCA1-deficient cells, not BRCA2.

Several other recent studies have revealed the role of Ku 70/80 and EZH2 in regulating NHEJ activity in tumor cells. In BRCA-mutated breast and ovarian cancer cell lines, overexpression of miRNA-622 renders them insensitive to olaparib and veliparib treatment. Yang et al. proposed the following mechanism by which miR622 desensitizes PARPi: it downregulats the expression of Ku 70/80, thereby reducing NHEJ activity and restoring HR activity (Choi et al., 2016). EZH2 regulates NHEJ expression in OC cells with high expression of coactivator-associated arginine methyltransferase 1 (CARM1) independent of HR. This study demonstrated that

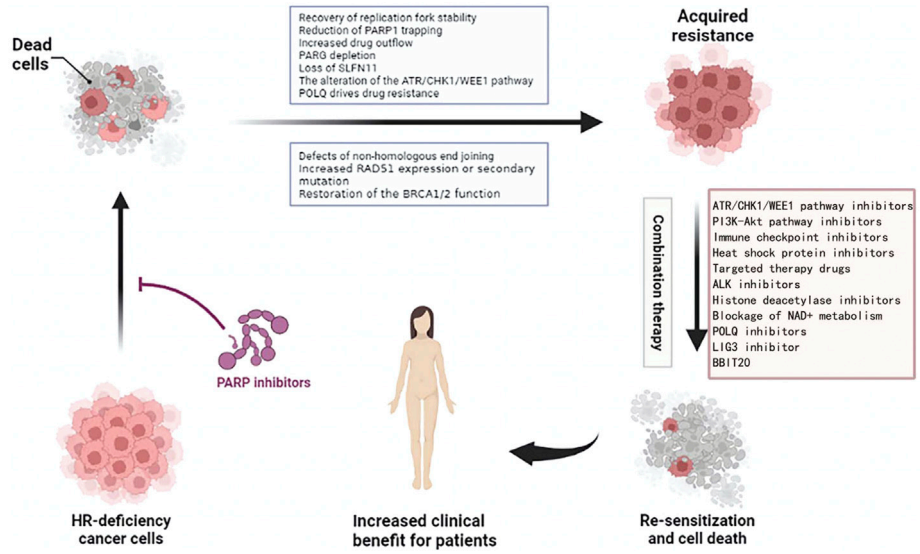

FIGURE 5
Combination treatment options for ovarian cancer resistant to PARPi. Figures have been created with BioRender.com.

tumor cells with high EZH2 expression were not sensitive to PARPi treatment, and in patient-derived xenografts, EZH2 inhibitors sensitize CARM1-high OCs to PARPi (Karakashev et al., 2020).

The 53BP1-RIF1-Shieldin axis, Ku70/80 and EZH2 can all regulate the expression of NHEJ. Among them, 53BP1 can antagonize the effect of HR through two pathways, namely BRCA1-dependent and BRCA1-independent, which further indicates that PARPi acquired drug resistance. The occurrence is not caused by a single mechanism, and clearer and deeper mechanisms are waiting for us to explore.

4 Overcoming resistance to PARPi

Whether it is congenital or acquired resistance to PARPi, we urgently need new treatments to solve this problem (Figure 5). At present, some clinical trials on the combination of PARPi are under study, and we hope to develop a clinical drug regimen for reversing PARPi resistance.

4.1 Combined use of PARPi and the ATR/CHK1/WEE1 pathway inhibitors

Studies have confirmed that drugs, such as ATR inhibitor (AZD6738) and CHK1 inhibitor (MK8776), can reverse the resistance of ovarian cancer cells to olaparib *in vitro*. Interestingly, their combined therapeutic effects with PARPis are independent of HR expression. The effects of ATRi and CHK1i were more pronounced in BRCA-deficient PARPi-resistant cells than in BRCA-proficient cells (Gralewska et al., 2020). This may be because ATR exerts an important role in RAD51 foci formation, and ATRi inhibits the loading of RAD51 onto the stalled forks and causes enhanced fork degradation and eventual cell death. The effect of the combination of these two was also verified in an *in vivo* model. In a mouse ovarian cancer orthotopic model, the use of ATRi resensitized mice to PARPi and increased the sensitivity of PARPi and platinum-based drugs (Kim et al., 2020). A Phase II clinical trial of ceralasertib (ATRi) as monotherapy or in combination with olaparib in ARID1A deletion or non-deletion gynecological cancers (including ovarian, endometrial, cervical, etc.), and treatment outcome will be measured in RECIST v1.1 (Banerjee et al., 2021). In breast cancer, concomitant administration of a CHK1 inhibitor and olaparib restored the sensitivity of BRCA1-deficient resistant triple negative breast cancer (TNBC) cells (Moustafa et al., 2021).

A phase II clinical trial (NCT03579316) compared a WEE1 inhibitor (adavotinib) with or without olaparib in patients with recurrent PARPi-resistant ovarian cancer. The ORR for monotherapy and combination therapy was 23% vs. 29%, and the median PFS was 5.5 vs. 6.8 months. However, grade 3/4 toxicities occurred in both groups, most commonly neutropenia and thrombocytopenia, and these toxicities could be controlled by interruption of treatment or dose reduction (Westin et al., 2021).

Dinaciclib is an inhibitor of CDK1, CDK2, CDK5 and CDK9, and also has some inhibitory activity against CDK12. In BRCA mutant triple negative breast cancer (TNBC) cells, the use of

TABLE 1 Ongoing or completed clinical trials of ATR/CHK1/WEE1 pathway inhibitors combination with PARPi.

	Clinicaltrials. Gov registration/Study name	Phase	Condition or disease	Patients (n)	Combination	Results
Ongoing	NCT04267939	Ib	Advanced solid tumors, including PARP inhibitor resistant OC	56	BAY1895344 (ATRi) + Niraparib	MTD and/or RP2D Incidence of TEAEs Severity of TEAEs-DLT
	CAPRI/NCT03462342	II	ROC (platinum-sensitive or platinum-resistant)	86	AZD6738 (ATRi) + Olaparib	Incidence of TEAEs RRPFS
	NCT04149145	I	PARP inhibitor resistant recurrent OC	40	M4344 (ATRi) + Niraparib	Percentage of patients with TEAEs MTD ORR PFS
	NCT04065269	II	Gynaecological Cancers with ARID1A Loss or no Loss	40	AZD6738 (ATRi) + Olaparib or AZD6738 alone	ORR (complete or partial response)
	NCT03579316	II	PARP inhibitor resistant recurrent OC	104	AZD1775(WEE1i) + Olaparib or AZD1775 alone	ORR DCR
Completed	NCT02723864	I	Refractory solid tumors	53	M6620 (ATRi) + Veliparib + Cisplatin	Incidence of adverse events PR:13.6%
	NCT03057145 Do et al. (2021) PMID: 34131002	I	Advanced solid tumors, including HGSOC with BRCA1/2 mutation	29	Prexasertib (CHKi) +Olaparib	MTD: prexasertib 70 mg/m2 iv and olaparib 100 mg, bid BRCA1mut, PARPi resistant, HGSOC (N = 18): PR 22.22%

DCR-disease control rate; DLT-dose limiting toxicities; MTD-maximum tolerated dose; ORR-overall response rate; OS- overall survival; PFS- progression free survival; RFS- relapse-free survival; RR-response rate; TEAEs- treatment emergent adverse events.

CDK12 inhibitors restored the sensitivity of tumor cells to PARPi, and this effect was also observed in a patient-derived PDX model (Johnson et al., 2016).

The ongoing or completed clinical trials (https://clinicaltrials.gov/) of ATR/CHK1/WEE1 pathway inhibitors combination with PARPi are summarized in Table 1.

4.2 Combined use of PARPi and the PI3K-Akt pathway inhibitors

The phosphoinositide 3-kinase/Akt (PI3K/Akt) signaling pathway regulates many key processes in tumorigenesis and development (Lorusso, 2016). The PI3K/Akt pathway inhibitors have been confirmed to make cancer cells sensitive to PARPi by down-regulating HRR (Mukhopadhyay et al., 2019). Preclinical studies have shown that in TNBC models, the use of PI3K inhibitors down-regulates BRCA1/2, thus, down-regulating HRR and sensitizing cancer cells to PARPi (Park et al., 2013). Combined application of these two is the focus of the current research (Table 2).

For example, PI3K inhibitors, NVP-BEZ235 and VS-5584, down-regulate HRR and make OC cells with BRCA1 mutations and recombination sensitive to PARPi (olaparib and rucaparib), and studies have shown that NVP-BEZ235 reduces the expression of RAD51. In a preclinical study in TNBC, the PI3K inhibitor BKM120 significantly reduced proliferation of TNBC cell lines by assisting olaparib to block PARP-mediated DNA SSB repair by inhibiting the expression of PARP1 and PARP2 (Li et al., 2021). In 2017, a phase I dose escalation study on the combination of BKM120 and olaparib in the treatment of high-grade serous OC and BC showed that the combination of BKM120 and olaparib was clinically beneficial (the remission rate in patients with advanced OC was 29%, BC patients with a remission rate of 28%) and can be assured of its safety (Matulonis et al., 2017). Phase 1b trial (NCT01623349) of olaparib and another PI3Kα-specific inhibitor (alpelisib) demonstrated partial responses in 36% and stable disease in 50% of 28 patients with BRCA wild-type OC(Konstantinopoulos et al., 2019). Similarly, the combination of these two drugs has also achieved promising results in TNBC. Among the 17 TNBC patients treated, the ORR was 18%, and 59% had control, and the associated adverse events were hyperglycemia (18%) and rash (12%) (Westin et al., 2021).

Currently, NCT01589861 is undergoing Phase II trials of BKM120 and Lapatinib to determine the clinical effect of the combination. Based on a series of preclinical studies, we have reason to believe that this study will achieve satisfactory results. The combination of Akt inhibitors and PARPis can also increase the sensitivity of cancer cells to PARPi. A clinical trial (NCT02208375) investigated the efficacy of olaparib in combination with an Akt inhibitor (capivasertib) in patients with PARP-resistant recurrent EC, TNBC, and OC -- 5 of the

TABLE 2 Phase II clinical trials of PARPis plus other drugs in OC/TNBC with published results.

Clinicaltrials. Gov identifier/ Study name	Condition or disease	Treatment arm	Patients	Key outcome measures
NCT02734004/MEDIOLA	BRCA1/2-mutated metastatic breast cancer	durvalumab + olaparib	30	DCR of 12 weeks: 80% (N = 24), 90% CI, 64.3–90.9
NCT03579316	Recurrent PARPi-resistant ovarian cancer	adavosertib	35	ORR: 23% (90% CI) CBR: 63% (90% CI) PFS: 5.5 months (90%CI)
		Adavosertib + olaparib	35	ORR: 29% (90% CI) CBR: 89% (90% CI) PFS: 6.8 months (90%CI)
NCT02657889	Triple-negative Breast Cancer	Pembrolizumab + niraparib	55	ORR:21%, (90% CI, 12%–33%) DCR:49%, (90% CI, 36%–62%) CR:5 patients (9%) PR: 5 patients (9%) SD: 13 patients (24%)
	Ovarian cancer		60	ORR: 18% (90% CI, 11%–29%) DCR: 65% (90% CI, 54%–75%) CR:3 patients (5%) PR: 8 patients (13%) SD: 28 patients (47%)
NCT02354131/AVANOVA2	Platinum-sensitive recurrent ovarian cancer	Niraparib plus bevacizumab	48	PFS:11·9 months (95% CI 8·5–16·7)
		Niraparib	49	PFS: 5.5 months (95% CI 8·5–16·7)

13 treated patients achieved a clinical benefit in the combination study (Yap et al., 2020). The combined application of these two drugs deserves further clinical exploration to overcome the occurrence of PARPi resistance.

4.3 Combined use of PARPi and immune checkpoint inhibitors

Immune checkpoints regulate the breadth and strength of immune responses, leading to immune escape and avoiding damage and destruction of normal tissues by the immune system, at present, more researches are on cytotoxic T lymphocyte-associated protein 4 (CTLA-4) and programmed cell death 1 (PD-1) (Pardoll, 2012). CTLA4 and PD-1 compete with CD28 for binding to B7 molecules on antigen presenting cells (APCs), transmits inhibitory signals to T cells, and inhibit their proliferation and activation (Linsley et al., 1994). Immune checkpoint therapy can block inhibitory checkpoints (eg, CTLA-4, PD-1), thereby restoring efficient T cell function and activating the immune system (Zhang et al., 2021). At present, the use of immune checkpoint inhibitors (ICI) has achieved preliminary results in clinical trials, and the most widely used ICI in clinical practice are CTLA-4 inhibitors and PD-1/PD-L1 inhibitors.

The interaction between tumor immune response-related mechanisms and DNA damage is critical in cancer therapy, and one of the most important pathways is cGAS-cGAMP-STING pathway. PARPis release broken double-stranded DNA after treating tumors and dsDNA stimulates STING upregulation, resulting in the production of type I interferon ϒ and pro-inflammatory cytokines (Ding et al., 2018; Li and Chen, 2018; Shen et al., 2019); that is, antitumor immune responses can be mediated after PARPi treatment. Experiments by Meng J et al. (2021) demonstrated that niraparib-induced DNA damage activates the STING pathway *in vitro* and *in vivo*, and increases the expression of membrane PD-L1 and total PD-L1 in OC cells. After combined use of PD-L1 inhibitor, cancer cells are resensitized to T cell killing through mechanisms such as immunomodulation, so as to enhance the antitumor effect. And there was no notable difference in body weight between mice that who were administered the combined

drug and the single drug group, indicating that it is a safe option. Therefore, we have reason to believe that the combination of PARPis and immunomodulators may have a stronger effect on inhibiting tumor growth and blocking immune escape.

There are currently more than 20 clinical trials investigating the effectiveness of ICIs in breast cancer and advanced gynecological tumors, but the results are not satisfactory. The ORR of ICIs alone is less than 10% (Maiorano et al., 2021). Niraparib in combination with pembrolizumab (a PD-1 inhibitor) was evaluated in a Phase I/II TOPACIO trial in the treatment of advanced or metastatic TNBC or recurrent OC. In TNBC, the objective response rate (ORR) was 21% and the disease control rate (DCR) was 49% in 47 curative evaluable populations, and the median duration of response (DOR) was not reached at the time of data cut-off. Among 15 patients with BRCA mutations with evaluable efficacy, the ORR and DCR were 47% and 80%, respectively, and the median PFS was 8.3 months. In the 27 cases of BRCA wild-type with evaluable efficacy and in the cohort with BRCA1/2 mutations, ORR and DCR were 45% and 73%, respectively (Vinayak et al., 2019). Among 60 patients with ovarian cancer whose efficacy could be evaluated, the ORR and DCR were 18% and 65%, respectively. ORRs were consistent in each subgroup according to the sensitivity of platinum chemotherapy, whether bevacizumab was used in the past, whether BRCA had mutation or homologous recombination deficiency (HRD). A phase I/II MEDIOLA trial investigating the effects of treatment with olaparib and durvalumab (a PD-L1 inhibitor) in patients with BRCA-mutant metastatic breast cancer, 80% of 30 eligible and treated patients had disease at 12 weeks was controlled, but this trial did not set up an olaparib-alone arm to investigate whether adding durvalumab would increase the clinical benefit of olaparib (Domchek et al., 2020).

A phase II multicohort trial (NCT02912572) investigating the clinical benefit of avelumab (a PD-L1 inhibitor) versus the PARP inhibitor talazoparib in patients with microsatellite stable (MSS) recurrent/persistent endometrial cancer showed that only 3 1 patient had a partial response (ORR = 8.6%) with a PFS of 25.8% at 6 months (Konstantinopoulos et al., 2020). There are several ongoing clinical trials (NCT03016338, NCT03694262) investigating the clinical benefit of combining ICI and PARPi with other drugs in the treatment of endometrial cancer.

Cytotoxic T lymphocyte-associated protein 4 (CTLA-4) acts as an immune checkpoint and downregulates the immune response. Compared with PD-L1 inhibitors, CTLA4 inhibitors have been less studied. A preliminary preclinical study conducted in a BRCA1-deficient mouse model of OC showed that the long-term survival of mice was improved when they were treated with CTLA-4 inhibitors in a synergistic treatment with PARPi (veliparib) (Higuchi et al., 2015). In a clinical trial (NCT02571725) on treatment of patients with recurrent OC with BRCA deficiency, using olaparib and tremelimumab (CTLA4 inhibitor), the Phase 1/2 experiment is underway (Fumet et al., 2020).

However, it seems that the combined use of ICIs and PARPis has not achieved the expected effect, and most experiments only discuss the effect of combined use without setting a PARPis alone group to compare how much additional clinical benefit can be obtained by adding ICIs. Why did the combination of the two not achieve a more significant therapeutic effect? Jennifer et al. suggested that the reason may be macrophage-mediated immunosuppression. Macrophages have an MI-like anti-tumor phenotype and an M2-like tumor-promoting phenotype (Locati et al., 2020). PARPi treatment induces macrophage differentiation to M2 phenotype under the mediation of sterol regulatory element-binding protein 1 (SREBP1) and promotes the expression of colony-stimulating factor receptor (CSF-1R) required for self-survival, while CSF-1R-positive macrophages inhibit the function of T cells and promote tumor growth and invasion. Previous experiments have demonstrated that inhibition of CSF-1R reduces the production of the M2 phenotype in macrophages, and tumor growth is suppressed in mice lacking CSF-1R (Denardo et al., 2011). In BRCA1-deficient TNBC mice treated with olaparib alone, the PFS was 63 days, the PFS increased to 82.5 days after the combination of a CSF-1R inhibitor and olaparib, and 80% of the tumors in the combination group were completely eliminated on the 34th day. In addition, it was found that the use of olaparib and CSF-1R inhibitors in the BRCA-proficient mouse tumor model had no significant therapeutic effect, indicating that tumor immunotherapy was related to BRCA status.

Further studies found that the use of SREBP1 inhibitor reversed the high expression of CSF-1R induced by PARP inhibitor. In an aggressive TNBC mouse model, treatment with PARPi + SREBP1 inhibitor + CSF-1 inhibitor significantly improved tumor growth inhibition compared to CSF-1 inhibitor + olaparib (Mehta et al., 2021).

4.4 Combined use of PARPi and heat shock protein inhibitors

Studies have shown that heat shock protein 90 (HSP90) is highly expressed in lung cancer, breast cancer, and many other cancers (Katoh et al., 2000; Workman and Powers, 2007). HSP90 stabilizes protein conformation through multi-molecular chaperone complexes, promotes the proliferation and growth of cancer cells, and affects many oncogene-related pathways. HSP90 can restore the HR function of cells and make them resistant to PARP by stabilizing the BRCA terminal domain. Studies have shown that the use of the HSP inhibitor 17-allylamino-17-demethoxygeldanamycin (17-AAG) in many cancers degrades BRCA through the ubiquitin-proteasome pathway, making it vulnerable to PARPi. Resensitization demonstrated that dual-target inhibitors of PARP and HSP90 have stronger selective cytotoxicity against tumors (Stecklein et al., 2012). A current preclinical trial on the

combination of HSP90 inhibitor onalespib (at13387) and PARPi in the treatment of ovarian cancer shows that in the mouse OC patient-derived xenograft (PDX) model, onalespib can obtain a good therapeutic effect in patients with acquired PARPi resistance without any obvious toxic and side effects. In the subsequent phase I clinical study, a total of 28 patients with advanced solid cancer were enrolled, of which two patients with BRCA-mutated HGSOC who had previously received Olaparib and onalespib therapy had stable disease after 24 weeks of treatment. Overall, 68% of patients had stable disease, 32% had progressive disease, and 32% experienced clinical benefit from the regimen (Konstantinopoulos et al., 2022). At present, the HSP90 inhibitor TAS-116 (pimitespib) has achieved great results in the treatment of gastric stromal tumors, significantly prolonged PFS compared to the original treatment (Doi et al., 2019; Saito et al., 2020). It is expected that other HSP90 inhibitors will achieve good therapeutic effects in gynecological tumors.

4.5 PARPi combined with targeted therapy drugs

The targeted drugs currently studied in combination with PARP for the treatment of cancer mainly include anti-angiogenic drugs (such as bevacizumab) and EGFR-targeted drugs (such as cetuximab).

Anti-angiogenic drugs make tumor cells achieve a hypoxic state by inhibiting tumor angiogenesis, causing DNA damage in tumor cells, and the most characteristic feature is DNA DSB; at this time, DNA replication pressure increases, and then the expression of HRR pathway-related proteins, such as RAD51 and BRCA1/2, is down-regulated through various ways, and the final result is HRR defects. Therefore, in combination with antiangiogenic drugs, it may increase tumor sensitivity to PARPi. Bevacizumab inhibits the vascular endothelial growth factor (VEGF) to inhibit tumor growth and invasion. In the phase II trial of AVANOVA2, one group of patients with recurrent ovarian cancer received niraparib alone and the other group received niraparib and bevacizumab in combination. PFS was significantly improved (11.9 vs 5.5 months, $p < 0.001$). In another clinical study of olaparib combined with cediranib in the treatment of patients with OC, the effect of the combination therapy was stronger than that of monotherapy, especially in the non-BRCA mutation group. The PAOLA phase III trial enrolled 806 patients with advanced high-grade ovarian cancer to receive olaparib or olaparib in combination with bevacizumab. Compared with bevacizumab alone, treatment with PARPi significantly improved the patients' survival rate. Progression-free survival (22.1 vs. 16.6 months; HR 0.59; 95% CI, 0.49–0.72; $p < 0.001$). Among patients with HRD-positive ovarian cancer, the combination group had the most significant benefit, with a median PFS of 37.3 months in the combination group and 17.7 months in the bevacizumab-alone group (HR, 0.33; 95% CI, 0.25–0.45), among HRD-positive patients without BRCA mutations, median PFS was 28.1 months in combination therapy versus 16.6 months in monotherapy (HR, 0.43; 95%) CI, 0.28–0.66). Adverse events occurred in 31% of patients in both groups, with a higher rate in the bevacizumab plus olaparib group than in the bevacizumab alone group. Olaparib plus bevacizumab as first-line maintenance therapy provided significant antitumor activity and safety in HRD-positive patients regardless of BRCA status (Ray-Coquard et al., 2019).

Cetuximab acts on the epidermal growth factor receptor (EGFR) and blocks the intracellular signal transduction pathway by inhibiting tyrosine kinase (TK) bound to EGFR, thereby inhibiting cancer cell proliferation and inducing apoptosis. *In vitro* experiments on head and neck tumors demonstrate that inhibition of EGFR with cetuximab (C225) sensitizes cells to PARPi (ABT-888) (Nowsheen et al., 2011). This is because C225 reduces NHEJ and HR-mediated DSB repair, resulting in DNA damage that persists after PARPi use. Through this mechanism, C225 can make the head and neck tumor cells susceptible to PARP inhibition. Therefore, the combination of C225 and ABT-888 may be an innovative therapeutic strategy, but this combination method has not been currently used in gynecological tumors, and further research is needed.

4.6 PARPi combined with ALK inhibitors

Ceritinib is an ALK kinase inhibitor for first-line ALK-positive treatment-naïve patients. It can inhibit the complex I of the mitochondrial electron transport chain, which cooperates with PARPis to generate reactive oxygen species, and then reactive oxygen species can induce DNA damage (Friboulet et al., 2014). Repair of this damage requires the participation of PARP. These mechanisms suggest that ceritinib combined with PARPis may increase its therapeutic efficacy in cancer. The combination of ceritinib and olaparib showed superior cancer inhibition in OC cell lines, and also in the HGSOC PDX model; the results showed that ceritinib monotherapy had no significant effect, but it could increase the therapeutic effect of olaparib in the PDX model (Kanakkanthara et al., 2022), and this result provides the basis for the clinical study on the combination of these two. There is currently no clinical trial to further explore the effect of the combined use of these two drugs on the clinical benefit of patients, which is also the direction of future research.

4.7 PARPi combined with histone deacetylase inhibitors

Histone deacetylase inhibitors (HDACi) can reduce the expression of HRR-related proteins (Roos and Krumm, 2016; Wilson et al., 2022). Vorinostat is the first HDACi to be

developed. *In vitro*, transcriptome sequencing results showed that the expression of HR repair-related molecules was decreased in OC cell lines treated with the HDACi panobinostat. Likewise, the combined use of PARPi and HDACi enhanced DNA damage and decreased HR repair capacity (Wilson et al., 2022). *In vivo* experiments showed that HDACi combined with PARPi significantly inhibited the growth of xenograft tumors compared with the two drugs alone--OC and TNBC increased the antitumor effect after treatment with the two drugs (Yalon et al., 2016). Olaparib in combination with Entestat, a novel HDAC inhibitor, is being studied in a phase I/II clinical trial (NCT03924245) in the treatment of relapsed, platinum-refractory or resistant HGSOC and fallopian tube cancer. Key outcome measures are MTD and ORR.

4.8 PARPi combined with drugs targeting NAD^+ metabolism

PARP1 uses oxidized NAD^+ as a substrate for PARylation, which plays a key role in DNA repair and cell signal transduction. Inhibition of NAD^+ production modulates PARPi responsiveness. Over-activation of PARP1 caused by oxidative stress and DNA damage can cause a rapid decrease in intracellular NAD^+ concentration, resulting in a rapid decline in the level of intracellular energy metabolism (Houtkooper et al., 2010). Cells maintain the level of NAD^+ through the salvage pathway, and nicotinamide phosphoribosyltransferase (NAMPT) exerts its biological function as the rate-limiting enzyme of the NAD^+ salvage synthesis pathway (Tateishi et al., 2015). Bajrami et al. observed that knockdown of NAMPT in TNBC cell lines increases olaparib sensitivity. Olaparib alone caused a 36% inhibition of cell survival in BRCA-deficient TNBC cell lines, which was increased to 72% when the NAMPT inhibitor (FK866) was added. *In vivo* experiments were carried out in the TNBC model of nude mice, and olaparib, FK866, and olaparib plus FK866 were used to treat xenograft model mice. The results showed that compared with any single drug treatment, the drugs in the combination group significantly inhibited the tumors growth, and two nude mice in the combined group ($n = 10$) had complete tumor regression at 39 days. FK866 can significantly inhibit the growth and proliferation of OC cells both *in vitro* and *in vivo*, but there is no study to explore the effect of combination therapy (Bajrami et al., 2012). In addition, $NADP^+$,a derivative of NAD^+ competes with PARP to bind to the NAD^+ site and inhibits PARylation. It can be regarded as an endogenous PARP inhibitor. When the $NADP^+$ content in cancer cells is high, it will confer PARPis sensitivity (Bian et al., 2019). In conclusion, the relationship between the regulation of NAD^+ metabolism and PARPi sensitivity is still in its infancy, and more preclinical and clinical studies are needed to explore the link between the two, in order to utilize the metabolic fragility of cancer cells to improve PARPi sensitivity.

4.9 PARPi combined with POLQ inhibitor

In addition to being an antibiotic, novobiocin (NVB) can also inhibit the activity of POLQ ATPase. Both *in vivo* and *in vitro* experiments have demonstrated that NVB can induce HR-deficient tumor cell death (Zhou et al., 2021). ART558 is a small-molecule Polθ inhibitor that has a synergistic effect with PARPi, and it has a stronger inhibitory effect on cells (including ovarian cancer and breast cancer cells) when used at the same time in BRCA1/2 mutant cells. Interestingly, tumor cells were more sensitive to POLQ inhibitors when the expression of 53BP1 in BRCA-deficient cells was reduced, suggesting that ART558 may resensitize patients with acquired resistance to PARPi by inhibiting DNA end excision protection (Zatreanu et al., 2021). ART4215 is the first Polθ inhibitor to enter clinical development and is currently undergoing clinical trials of ART4215 as monotherapy or in combination with PARPi inhibitors in advanced solid tumors, and treatment is still ongoing. POLQ inhibitors are promising drugs either as an alternative to or in combination with PARP inhibitors.

4.10 PARPi combined with LIG3 inhibitor

Single-stranded DNA gaps are created after PARPi treatment, and DNA ligase III (LIG3) is a known DNA repair factor that catalyzes DNA end joining (Taylor et al., 2000). Inhibition of LIG3 in BRCA1-deficient cells and in BRCA1/53BP1 double-deficient cells promotes PARPi-induced accumulation of single-stranded DNA gaps, ultimately leading to accumulation of chromosomal aberrations and cell death. Experiments showed that compared with parental cells, the sensitivity of tumor cells to PARPi was significantly increased after LIG3 knockout; PARPi-resistant cells regained sensitivity to PARPi after LIG3 depletion. Reversal of PARPi resistance by LIG3 is due to increased single-stranded DNA gap independent of HR (Paes Dias et al., 2021). The combined effect of the two needs further animal experiments and clinical trials to verify.

4.11 PARPi combined with BBIT20

In addition to the above chemical drugs, a natural monoterpene indole alkaloid derivative, namely dregamine 5-bromo-pyridin-2-ylhydrazone (BBIT20), has also made new progress in reversing PARPi resistance. BRCA1-associated ring domain protein (BARD1) binds to BRCA1 to form BRCA1-BARD1, which can self-localize to DSB and promote HR-mediated DSB repair. BBIT20 can inhibit the interaction

between BRCA1 and BARD1, resulting in decreased BRCA1 expression, especially in nuclear BRCA1, thereby inhibiting HRR. BBIT20 significantly enhanced olaparib in patient-derived OC cells and TNBC cells without inducing drug resistance. BBIT20 and olaparib were then used to treat OC xenograft mouse models, respectively, and the results showed that BBIT20 inhibited tumor growth more strongly than olaparib (Raimundo et al., 2021). These preclinical studies show that BBIT20 has a very promising application in the treatment of cancer, whether as a single drug or a combination drug.

5 Conclusion and future outlook

An increasing number of preclinical and clinical studies help us understand the mechanism of PARP inhibitor resistance. At present, the use of PARPis as first-line maintenance therapy for breast and ovarian cancer is satisfactory, and its clinical application range is gradually expanding (such as pancreatic cancer and prostate cancer). However, there are many troublesome problems behind the surprise of PARPis, and the occurrence of acquired drug resistance is one of the problems that cannot be ignored. The development of PARPi resistance, as described in this paper, is caused by a variety of mechanisms, most of which have been studied in cell lines and mouse models, but the actual clinical treatment is different from pure preclinical research. Many patients have developed resistance to drugs, such as platinum or paclitaxel, before using PARPi treatment, which will lead to the generation of PARPi cross-resistance. Therefore, the resistance of PARPi in clinical treatment may be different from preclinical studies. More clinical samples and studies are needed to further determine a more comprehensive mechanism of PARPi resistance.

In order to solve the problem of PARPi resistance, we studied the therapeutic effect of PARPis combined with other drugs in order to improve its therapeutic effect, PARPis plus ATR/CHK1/WEE1 pathway inhibitors, PARPis plus PI3K/Akt pathway inhibitors, PARPis plus ICIs, PARPis plus HSP90 inhibitors, PARPis plus targeted therapy drugs, PARPis plus ALK inhibitors, PARPis plus HDACis, PARPis plus drugs targeting NAD^+ metabolism, and PARPis plus POLQ inhibitor have shown certain effects in preclinical and clinical studies. But with so many types of drugs, which one will bring the greatest benefit to the patient? Will the combination drug produce more toxic and side effects while improving the efficacy and prolong the survival of patients, and will the quality of life of patients decrease? Can patients afford the financial stress of multiple medications? These are hot issues of clinical concern.

According to the existing clinical studies, PARPis combined with the ATR/CHK1/WEE1 pathway inhibitors is the current choice that takes into account the clinical benefits and safety. The patients' PFS and OS have been significantly improved, and the adverse reactions are also within the range of patients' tolerance. In recent years, ICIs, as revolutionary drugs for tumor treatment, have made great progress in clinical treatment as a single treatment plan, but unfortunately they have not achieved 1 + 1>2 effect in combination with PARPis; the therapeutic effect of combined targeted drugs is acceptable, but the incidence of adverse reactions in patients is greatly increased. Research on other drugs is currently mostly concentrated in preclinical studies, with no clinical trials or experiments in progress. According to the mechanism analysis, POLQ inhibitor induces tumor cell death from two aspects and seems to be a more promising drug. Finally, further exploration of biomarkers associated with PARPi response and clinical classification based on them to determine which combination therapy is most suitable for patients will allow for more individualized clinical treatment.

Author contributions

Conceptualization: LY and HL; writing: Original draft preparation, NW and YY; writing: Review and editing, NW and DJ; literature search: JY and KS; visualization: HC, XZ; data analysis and investigation: ZZ; supervision: LY. All authors have read and agreed to the published version of the manuscript.

Funding

This work was supported by the Natural Science Foundation of Henan (222300420266) and the Key Scientific Research Project of Higher Education of Henan Province (22A310007).

Conflict of interest

The authors declare that the research was conducted in the absence of any commercial or financial relationships that could be construed as a potential conflict of interest.

Publisher's note

References

Agarwal, A., Baghmar, S., Dodagoudar, C., Qureshi, S., Khurana, A., Vaibhav, V., et al. (2021). PARP inhibitor in platinum-resistant ovarian cancer: Single-center real-world experience. *JCO Glob. Oncol.* 7, 506–511. doi:10.1200/GO.20.00269

Arnaudeau, C., Rozier, L., Cazaux, C., Defais, M., Jenssen, D., and Helleday, T. (2001). RAD51 supports spontaneous non-homologous recombination in mammalian cells, but not the corresponding process induced by topoisomerase inhibitors. *Nucleic Acids Res.* 29 (3), 662–667. doi:10.1093/nar/29.3.662

Bajrami, I., Frankum, J. R., Konde, A., Miller, R. E., Rehman, F. L., Brough, R., et al. (2014). Genome-wide profiling of genetic synthetic lethality identifies CDK12 as a novel determinant of PARP1/2 inhibitor sensitivity. *Cancer Res.* 74 (1), 287–297. doi:10.1158/0008-5472.CAN-13-2541

Bajrami, I., Kigozi, A., Van Weverwijk, A., Brough, R., Frankum, J., Lord, C. J., et al. (2012). Synthetic lethality of PARP and NAMPT inhibition in triple-negative breast cancer cells. *EMBO Mol. Med.* 4 (10), 1087–1096. doi:10.1002/emmm.201201250

Banerjee, S., Stewart, J., Porta, N., Toms, C., Leary, A., Lheureux, S., et al. (2021). ATARI trial: ATR inhibitor in combination with olaparib in gynecological cancers with ARID1A loss or no loss (ENGOT/GYN1/NCRI). *Int. J. Gynecol. Cancer* 31 (11), 1471–1475. doi:10.1136/ijgc-2021-002973

Barber, L. J., Sandhu, S., Chen, L., Campbell, J., Kozarewa, I., Fenwick, K., et al. (2013). Secondary mutations inBRCA2 associated with clinical resistance to a PARP inhibitor. *J. Pathol.* 229 (3), 422–429. doi:10.1002/path.4140

Baumann, P., and West, S. C. (1998). Role of the human RAD51 protein in homologous recombination and double-stranded-break repair. *Trends biochem. Sci.Regular* 23 (7), 247–251. doi:10.1016/S0968-0004(98)01232-8

Becker, J. R., Cuella-Martin, R., Barazas, M., Liu, R., Oliveira, C., Oliver, A. W., et al. (2018). The ASCIZ-DYNLL1 axis promotes 53BP1-dependent non-homologous end joining and PARP inhibitor sensitivity. *Nat. Commun.* 9 (1), 5406. doi:10.1038/s41467-018-07855-x

Betermier, M., Bertrand, P., and Lopez, B. S. (2014). Is non-homologous end-joining really an inherently error-prone process? *PLoS Genet.* 10 (1), e1004086. doi:10.1371/journal.pgen.1004086

Bian, C., Zhang, C., Luo, T., Vyas, A., Chen, S., Liu, C., et al. (2019). NADP+ is an endogenous PARP inhibitor in DNA damage response and tumor suppression. *Nat. Commun.* 10 (1), 693. doi:10.1038/s41467-019-08530-5

Bianco, T., Chenevix-Trench, G., Walsh, D. C., Cooper, J. E., and Dobrovic, A. (2000). Tumour-specific distribution of BRCA1 promoter region methylation supports a pathogenetic role in breast and ovarian cancer. *Carcinogenesis* 21 (2), 147–151. doi:10.1093/carcin/21.2.147

Bothmer, A., Robbiani, D. F., Feldhahn, N., Gazumyan, A., Nussenzweig, A., and Nussenzweig, M. C. (2010). 53BP1 regulates DNA resection and the choice between classical and alternative end joining during class switch recombination. *J. Exp. Med.* 207 (4), 855–865. doi:10.1084/jem.20100244

Bouwman, P., Aly, A., Escandell, J. M., Pieterse, M., Bartkova, J., van der Gulden, H., et al. (2010). 53BP1 loss rescues BRCA1 deficiency and is associated with triple-negative and BRCA-mutated breast cancers. *Nat. Struct. Mol. Biol.* 17 (6), 688–695. doi:10.1038/nsmb.1831

Brown, K. A., Andreopoulou, E., and Andreopoulou, P. (2020). Endocrine therapy-related endocrinopathies-biology, prevalence and implications for the management of breast cancer. *Oncol. Hematol. Rev.* 16 (1), 17–22. doi:10.17925/ohr.2020.16.1.17

Bryant, H. E., Petermann, E., Schultz, N., Jemth, A. S., Loseva, O., Issaeva, N., et al. (2009). PARP is activated at stalled forks to mediate Mre11-dependent replication restart and recombination. *EMBO J.* 28 (17), 2601–2615. doi:10.1038/emboj.2009.206

Bryant, H. E., Schultz, N., Thomas, H. D., Parker, K. M., Flower, D., Lopez, E., et al. (2005). Specific killing of BRCA2-deficient tumours with inhibitors of poly(ADP-ribose) polymerase. *Nature* 434 (7035), 913–917. doi:10.1038/nature03443

Bunting, S. F., Callén, E., Wong, N., Chen, H., Polato, F., Gunn, A., et al. (2010). 53BP1 inhibits homologous recombination in brca1-deficient cells by blocking resection of DNA breaks. *Cell.* 141 (2), 243–254. doi:10.1016/j.cell.2010.03.012

Butala, A. A., Patel, R. R., Manjunath, S., Latif, N. A., Haggerty, A. F., Jones, J. A., et al. (2021). Palliative radiation therapy for metastatic, persistent, or recurrent epithelial ovarian cancer: Efficacy in the era of modern technology and targeted agents. *Adv. Radiat. Oncol.* 6 (1), 100624. doi:10.1016/j.adro.2020.11.009

Castroviejo-Bermejo, M., Cruz, C., Llop-Guevara, A., Gutierrez-Enriquez, S., Ducy, M., Ibrahim, Y. H., et al. (2018). A RAD51 assay feasible in routine tumor samples calls PARP inhibitor response beyond BRCA mutation. *EMBO Mol. Med.* 10 (12), e9172. doi:10.15252/emmm.201809172

Ceccaldi, R., Liu, J. C., Amunugama, R., Hajdu, I., Primack, B., Petalcorin, M. I. R., et al. (2015). Homologous-recombination-deficient tumours are dependent on Polθ-mediated repair. *Nature* 518 (7538), 258–262. doi:10.1038/nature14184

Chang, H. H. Y., Pannunzio, N. R., Adachi, N., and Lieber, M. R. (2017). Non-homologous DNA end joining and alternative pathways to double-strand break repair. *Nat. Rev. Mol. Cell. Biol.* 18 (8), 495–506. doi:10.1038/nrm.2017.48

Chaudhuri, A. R., Callen, E., Ding, X., Gogola, E., Duarte, A. A., Lee, J., et al. (2016). Erratum: Replication fork stability confers chemoresistance in BRCA-deficient cells. *Nature* 539 (7629), 456. doi:10.1038/nature19826

Chen, D., Gervai, J. Z., Póti, Á., Németh, E., Szeltner, Z., Szikriszt, B., et al. (2022). BRCA1 deficiency specific base substitution mutagenesis is dependent on translesion synthesis and regulated by 53BP1. *Nat. Commun.* 13 (1), 226. doi:10.1038/s41467-021-27872-7

Chen, S., and Yu, X. (2019). Targeting dePARylation selectively suppresses DNA repair-defective and PARP inhibitor-resistant malignancies. *Sci. Adv.* 5 (4), eaav4340. doi:10.1126/sciadv.aav4340

Choi, Y. E., Meghani, K., Brault, M., Leclerc, L., He, Y. J., Day, T. A., et al. (2016). Platinum and PARP inhibitor resistance due to overexpression of MicroRNA-622 in BRCA1-mutant ovarian cancer. *Cell. Rep.* 14 (3), 429–439. doi:10.1016/j.celrep.2015.12.046

Christie, E. L., Pattnaik, S., Beach, J., Copeland, A., Rashoo, N., Fereday, S., et al. (2019). Multiple ABCB1 transcriptional fusions in drug resistant high-grade serous ovarian and breast cancer. *Nat. Commun.* 10 (1), 1295. doi:10.1038/s41467-019-09312-9

Clements, K. E., Schleicher, E. M., Thakar, T., Hale, A., Dhoonmoon, A., Tolman, N. J., et al. (2020). Identification of regulators of poly-ADP-ribose polymerase inhibitor response through complementary CRISPR knockout and activation screens. *Nat. Commun.* 11 (1), 6118. doi:10.1038/s41467-020-19961-w

Cohen, P. A., Jhingran, A., Oaknin, A., and Denny, L. (2019). Cervical cancer. *Lancet* 393 (10167), 169–182. doi:10.1016/S0140-6736(18)32470-X

Cong, K., Peng, M., Kousholt, A. N., Lee, W. T. C., Lee, S., Nayak, S., et al. (2021). Replication gaps are a key determinant of PARP inhibitor synthetic lethality with BRCA deficiency. *Mol. Cell.* 81 (15), 3128–3144.e7. e7. doi:10.1016/j.molcel.2021.06.011

Cox, M. M., Goodman, M. F., Kreuzer, K. N., Sherratt, D. J., Sandler, S. J., and Marians, K. J. (2000). The importance of repairing stalled replication forks. *Nature* 404 (6773), 37–41. doi:10.1038/35003501

Crosbie, E. J., Kitson, S. J., Mcalpine, J. N., Mukhopadhyay, A., Powell, M. E., and Singh, N. (2022). Endometrial cancer. *Lancet* 399 (10333), 1412–1428. doi:10.1016/S0140-6736(22)00323-3

Cruz, C., Castroviejo-Bermejo, M., Gutiérrez-Enríquez, S., Llop-Guevara, A., Ibrahim, Y. H., Gris-Oliver, A., et al. (2018). RAD51 foci as a functional biomarker of homologous recombination repair and PARP inhibitor resistance in germline BRCA-mutated breast cancer. *Ann. Oncol.* 29 (5), 1203–1210. doi:10.1093/annonc/mdy099

Denardo, D. G., Brennan, D. J., Rexhepaj, E., Ruffell, B., Shiao, S. L., Madden, S. F., et al. (2011). Leukocyte complexity predicts breast cancer survival and functionally regulates response to chemotherapy. *Cancer Discov.* 1 (1), 54–67. doi:10.1158/2159-8274.CD-10-0028

Dev, H., Chiang, T. W., Lescale, C., de Krijger, I., Martin, A. G., Pilger, D., et al. (2018). Shieldin complex promotes DNA end-joining and counters homologous recombination in BRCA1-null cells. *Nat. Cell. Biol.* 20 (8), 954–965. doi:10.1038/s41556-018-0140-1

Ding, L., Kim, H., Wang, Q., Kearns, M., Jiang, T., Ohlson, C. E., et al. (2018). PARP inhibition elicits STING-dependent antitumor immunity in brca1-deficient ovarian cancer. *Cell. Rep.* 25 (11), 2972–2980.e5. e5. doi:10.1016/j.celrep.2018.11.054

Do, K. T., Kochupurakkal, B., Kelland, S., de Jonge, A., Hedglin, J., Powers, A., et al. (2021). Phase 1 combination study of the CHK1 inhibitor prexasertib and the PARP inhibitor olaparib in high-grade serous ovarian cancer and other solid tumors. *Clin. Cancer Res.* 27 (17), 4710–4716. doi:10.1158/1078-0432.CCR-21-1279

Doi, T., Kurokawa, Y., Sawaki, A., Komatsu, Y., Ozaka, M., Takahashi, T., et al. (2019). Efficacy and safety of TAS-116, an oral inhibitor of heat shock protein 90, in patients with metastatic or unresectable gastrointestinal stromal tumour refractory to imatinib, sunitinib and regorafenib: A phase II, single-arm trial. *Eur. J. Cancer* 121, 29–39. doi:10.1016/j.ejca.2019.08.009

Domchek, S. M., Postel-Vinay, S., Im, S., Park, Y. H., Delord, J., Italiano, A., et al. (2020). Olaparib and durvalumab in patients with germline BRCA-mutated metastatic breast cancer (MEDIOLA): An open-label, multicentre, phase 1/2,

basket study. *Lancet. Oncol.* 21 (9), 1155–1164. doi:10.1016/S1470-2045(20)30324-7

Dungrawala, H., Bhat, K. P., Le Meur, R., Chazin, W. J., Ding, X., Sharan, S. K., et al. (2017). RADX promotes genome stability and modulates chemosensitivity by regulating RAD51 at replication forks. *Mol. Cell.* 67 (3), 374–386.e5. e5. doi:10.1016/j.molcel.2017.06.023

Edwards, S. L., Brough, R., Lord, C. J., Natrajan, R., Vatcheva, R., Levine, D. A., et al. (2008). Resistance to therapy caused by intragenic deletion in BRCA2. *Nature* 451 (7182), 1111–1115. doi:10.1038/nature06548

Fisher, A. E. O., Hochegger, H., Takeda, S., and Caldecott, K. W. (2007). Poly(ADP-Ribose) polymerase 1 accelerates single-strand break repair in concert with poly(ADP-ribose) glycohydrolase. *Mol. Cell. Biol.* 27 (15), 5597–5605. doi:10.1128/MCB.02248-06

Fishman-Lobell, J., Rudin, N., and Haber, J. E. (1992). Two alternative pathways of double-strand break repair that are kinetically separable and independently modulated. *Mol. Cell. Biol.* 12 (3), 1292–1303. doi:10.1128/mcb.12.3.1292-1303.1992

Francica, P., and Rottenberg, S. (2018). Mechanisms of PARP inhibitor resistance in cancer and insights into the DNA damage response. *Genome Med.* 10 (1), 101. doi:10.1186/s13073-018-0612-8

Friboulet, L., Li, N., Katayama, R., Lee, C. C., Gainor, J. F., Crystal, A. S., et al. (2014). The ALK inhibitor ceritinib overcomes crizotinib resistance in non–small cell lung cancer. *Cancer Discov.* 4 (6), 662–673. doi:10.1158/2159-8290.CD-13-0846

Fumet, J., Limagne, E., Thibaudin, M., Truntzer, C., Bertaut, A., Rederstorff, E., et al. (2020). Precision medicine phase II study evaluating the efficacy of a double immunotherapy by durvalumab and tremelimumab combined with olaparib in patients with solid cancers and carriers of homologous recombination repair genes mutation in response or stable after olaparib treatment. *BMC Cancer* 20 (1), 748. doi:10.1186/s12885-020-07253-x

Gogola, E., Duarte, A. A., de Ruiter, J. R., Wiegant, W. W., Schmid, J. A., de Bruijn, R., et al. (2018). Selective loss of PARG restores PARylation and counteracts PARP inhibitor-mediated synthetic lethality. *Cancer Cell.* 33 (6), 1078–1093.e12. doi:10.1016/j.ccell.2018.05.008

Grabarz, A., Barascu, A., Guirouilh-Barbat, J., and Lopez, B. S. (2012). Initiation of DNA double strand break repair: Signaling and single-stranded resection dictate the choice between homologous recombination, non-homologous end-joining and alternative end-joining. *Am. J. Cancer Res.* 2 (3), 249–268.

Gralewska, P., Gajek, A., Marczak, A., Mikuła, M., Ostrowski, J., [liwińska, A., et al. (2020). PARP inhibition increases the reliance on ATR/CHK1 checkpoint signaling leading to synthetic lethality—an alternative treatment strategy for epithelial ovarian cancer cells independent from HR effectiveness. *Int. J. Mol. Sci.* 21 (24), 9715. doi:10.3390/ijms21249715

Grossman, D. C., Curry, S. J., Owens, D. K., Barry, M. J., Davidson, K. W., Doubeni, C. A., et al. (2018). Screening for ovarian cancer: US preventive services task force recommendation statement. *JAMA* 319 (6), 588–594. doi:10.1001/jama.2017.21926

Guffanti, F., Alvisi, M. F., Anastasia, A., Ricci, F., Chiappa, M., Llop-Guevara, A., et al. (2022). Basal expression of RAD51 foci predicts olaparib response in patient-derived ovarian cancer xenografts. *Br. J. Cancer* 126 (1), 120–128. doi:10.1038/s41416-021-01609-1

Hao, J., Liu, Y., Zhang, T., He, J., Zhao, H., An, R., et al. (2021). Efficacy and safety of PARP inhibitors in the treatment of advanced ovarian cancer: An updated systematic review and meta-analysis of randomized controlled trials. *Crit. Rev. Oncol. Hematol.* 157, 103145. doi:10.1016/j.critrevonc.2020.103145

Hashimoto, Y., Ray Chaudhuri, A., Lopes, M., and Costanzo, V. (2010). Rad51 protects nascent DNA from Mre11-dependent degradation and promotes continuous DNA synthesis. *Nat. Struct. Mol. Biol.* 17 (11), 1305–1311. doi:10.1038/nsmb.1927

He, Y. J., Meghani, K., Caron, M. C., Yang, C., Ronato, D. A., Bian, J., et al. (2018). DYNLL1 binds to MRE11 to limit DNA end resection in BRCA1-deficient cells. *Nature* 563 (7732), 522–526. doi:10.1038/s41586-018-0670-5

Higuchi, T., Flies, D. B., Marjon, N. A., Mantia-Smaldone, G., Ronner, L., Gimotty, P. A., et al. (2015). CTLA-4 blockade synergizes therapeutically with PARP inhibition in BRCA1-deficient ovarian cancer. *Cancer Immunol. Res.* 3 (11), 1257–1268. doi:10.1158/2326-6066.CIR-15-0044

Hodgson, D. R., Dougherty, B. A., Lai, Z., Fielding, A., Grinsted, L., Spencer, S., et al. (2018). Candidate biomarkers of PARP inhibitor sensitivity in ovarian cancer beyond the BRCA genes. *Br. J. Cancer* 119 (11), 1401–1409. doi:10.1038/s41416-018-0274-8

Hoeijmakers, J. H. (2001). Genome maintenance mechanisms for preventing cancer. *Nature* 411 (6835), 366–374. doi:10.1038/35077232

Hong, R., Ma, F., Zhang, W., Yu, X., Li, Q., Luo, Y., et al. (2016). 53BP1 depletion causes PARP inhibitor resistance in ATM-deficient breast cancer cells. *BMC Cancer* 16 (1), 725. doi:10.1186/s12885-016-2754-7

Houtkooper, R. H., Cantó, C., Wanders, R. J., and Auwerx, J. (2010). The secret life of NAD+: An old metabolite controlling new metabolic signaling pathways. *Endocr. Rev.* 31 (2), 194–223. doi:10.1210/er.2009-0026

Hurley, R. M., Wahner Hendrickson, A. E., Visscher, D. W., Ansell, P., Harrell, M. I., Wagner, J. M., et al. (2019). 53BP1 as a potential predictor of response in PARP inhibitor-treated homologous recombination-deficient ovarian cancer. *Gynecol. Oncol.* 153 (1), 127–134. doi:10.1016/j.ygyno.2019.01.015

Jaspers, J. E., Kersbergen, A., Boon, U., Sol, W., van Deemter, L., Zander, S. A., et al. (2013). Loss of 53BP1 causes PARP inhibitor resistance inBrca1 -mutated mouse mammary tumors. *Cancer Discov.* 3 (1), 68–81. doi:10.1158/2159-8290.CD-12-0049

Johnson, S. F., Cruz, C., Greifenberg, A. K., Dust, S., Stover, D. G., Chi, D., et al. (2016). CDK12 inhibition reverses de novo and acquired PARP inhibitor resistance in BRCA wild-type and mutated models of triple-negative breast cancer. *Cell. Rep.* 17 (9), 2367–2381. doi:10.1016/j.celrep.2016.10.077

Kanakkanthara, A., Hou, X., Ekstrom, T. L., Zanfagnin, V., Huehls, A. M., Kelly, R. L., et al. (2022). Repurposing ceritinib induces DNA damage and enhances PARP inhibitor responses in high-grade serous ovarian carcinoma. *Cancer Res.* 82 (2), 307–319. doi:10.1158/0008-5472.CAN-21-0732

Karakashev, S., Fukumoto, T., Zhao, B., Lin, J., Wu, S., Fatkhutdinov, N., et al. (2020). EZH2 inhibition sensitizes CARM1-high, homologous recombination proficient ovarian cancers to PARP inhibition. *Cancer Cell.* 37 (2), 157–167.e6. e6. doi:10.1016/j.ccell.2019.12.015

Katoh, M., Koninkx, J., and Schumacher, U. (2000). Heat shock protein expression in human tumours grown in severe combined immunodeficient mice. *Cancer Lett.* 161 (1), 113–120. doi:10.1016/s0304-3835(00)00601-7

Kim, C., Wang, X., and Yu, Y. (2020). PARP1 inhibitors trigger innate immunity via PARP1 trapping-induced DNA damage response. *eLife* 9, e60637. doi:10.7554/eLife.60637

Kim, H., George, E., Ragland, R. L., Rafail, S., Zhang, R., Krepler, C., et al. (2017). Targeting the ATR/CHK1 Axis with PARP inhibition results in tumor regression inBRCA -mutant ovarian cancer models. *Clin. Cancer Res.* 23 (12), 3097–3108. doi:10.1158/1078-0432.CCR-16-2273

Kim, H., Xu, H., George, E., Hallberg, D., Kumar, S., Jagannathan, V., et al. (2020). Combining PARP with ATR inhibition overcomes PARP inhibitor and platinum resistance in ovarian cancer models. *Nat. Commun.* 11 (1), 3726. doi:10.1038/s41467-020-17127-2

Kim, J. J., Lee, S. Y., Choi, J., Woo, H. G., Xhemalce, B., and Miller, K. M. (2020). PCAF-mediated histone acetylation promotes replication fork degradation by MRE11 and EXO1 in BRCA-deficient cells. *Mol. Cell.* 80 (2), 327–344.e8. e8. doi:10.1016/j.molcel.2020.08.018

Kondrashova, O., Nguyen, M., Shield-Artin, K., Tinker, A. V., Teng, N. N. H., Harrell, M. I., et al. (2017). Secondary somatic mutations RestoringRAD51C andRAD51D associated with acquired resistance to the PARP inhibitor rucaparib in high-grade ovarian carcinoma. *Cancer Discov.* 7 (9), 984–998. doi:10.1158/2159-8290.CD-17-0419

Konstantinopoulos, P. A., Barry, W. T., Birrer, M., Westin, S. N., Cadoo, K. A., Shapiro, G. I., et al. (2019). Olaparib and α-specific PI3K inhibitor alpelisib for patients with epithelial ovarian cancer: A dose-escalation and dose-expansion phase 1b trial. *Lancet. Oncol.* 20 (4), 570–580. doi:10.1016/S1470-2045(18)30905-7

Konstantinopoulos, P. A., Cheng, S. C., Supko, J. G., Polak, M., Wahner-Hendrickson, A. E., Ivy, S. P., et al. (2022). Combined PARP and HSP90 inhibition: Preclinical and phase 1 evaluation in patients with advanced solid tumours. *Br. J. Cancer* 126 (7), 1027–1036. doi:10.1038/s41416-021-01664-8

Konstantinopoulos, P. A., Gockley, A. A., Xiong, N., Tayob, N., Krasner, C. N., Buss, M., et al. (2020). LBA35 Phase II study of PARP inhibitor talazoparib and PD-L1 inhibitor avelumab in patients (pts) with microsatellite stable (MSS) recurrent/persistent endometrial cancer. *Ann. Oncol.* 31, S1165. doi:10.1016/J.ANNONC.2020.08.2265

Langelier, M., Planck, J. L., Roy, S., and Pascal, J. M. (2012). Structural basis for DNA damage–dependent poly(ADP-ribosyl)ation by human PARP-1. *Science* 336 (6082), 728–732. doi:10.1126/science.1216338

Le Guen, T., Ragu, S., Guirouilh-Barbat, J., and Lopez, B. S. (2014). Role of the double-strand break repair pathway in the maintenance of genomic stability. *Mol. Cell. Oncol.* 2 (1), e968020. doi:10.4161/23723548.2014.968020

Ledermann, J. A., Raja, F. A., Fotopoulou, C., Gonzalez-Martin, A., Colombo, N., Sessa, C., et al. (2018). Newly diagnosed and relapsed epithelial ovarian carcinoma: ESMO clinical practice guidelines for diagnosis, treatment and follow-up. *Ann. Oncol.* 29, iv259. doi:10.1093/annonc/mdy157

Lheureux, S., Oaknin, A., Garg, S., Bruce, J. P., Madariaga, A., Dhani, N. C., et al. (2020). Evolve: A multicenter open-label single-arm clinical and translational phase II trial of cediranib plus olaparib for ovarian cancer after PARP inhibition progression. *Clin. Cancer Res.* 26 (16), 4206–4215. doi:10.1158/1078-0432.CCR-19-4121

Li, M., Kao, E., Gao, X., Sandig, H., Limmer, K., Pavon-Eternod, M., et al. (2012). Codon-usage-based inhibition of HIV protein synthesis by human schlafen 11. *Nature* 491 (7422), 125–128. doi:10.1038/nature11433

Li, S., Zhang, W., Yin, X., Xing, S., Xie, H. Q., Cao, Z., et al. (2015). Mouse ATP-binding cassette (ABC) transporters conferring multi-drug resistance. *Anticancer. Agents Med. Chem.* 15 (4), 423–432. doi:10.2174/1871520615666150129212723

Li, T., and Chen, Z. J. (2018). The cGAS–cGAMP–STING pathway connects DNA damage to inflammation, senescence, and cancer. *J. Exp. Med.* 215 (5), 1287–1299. doi:10.1084/jem.20180139

Li, Y., Wang, Y., Zhang, W., Wang, X., Chen, L., and Wang, S. (2021). BKM120 sensitizes BRCA-proficient triple negative breast cancer cells to olaparib through regulating FOXM1 and Exo1 expression. *Sci. Rep.* 11 (1), 4774. doi:10.1038/s41598-021-82990-y

Lin, K. K., Harrell, M. I., Oza, A. M., Oaknin, A., Ray-Coquard, I., Tinker, A. V., et al. (2019). BRCA reversion mutations in circulating tumor DNA predict primary and acquired resistance to the PARP inhibitor rucaparib in high-grade ovarian carcinoma. *Cancer Discov.* 9 (2), 210–219. doi:10.1158/2159-8290.CD-18-0715

Linsley, P. S., Greene, J. L., Brady, W., Bajorath, J., Ledbetter, J. A., and Peach, R. (1994). Human B7-1 (CD80) and B7-2 (CD86) bind with similar avidities but distinct kinetics to CD28 and CTLA-4 receptors. *Immun. Camb. Mass.)* 1 (9), 793–801. doi:10.1016/S1074-7613(94)80021-9

Locati, M., Curtale, G., and Mantovani, A. (2020). Diversity, mechanisms, and significance of macrophage plasticity. *Annu. Rev. Pathol.* 15 (1), 123–147. doi:10.1146/annurev-pathmechdis-012418-012718

Lok, B. H., Gardner, E. E., Schneeberger, V. E., Ni, A., Desmeules, P., Rekhtman, N., et al. (2017). PARP inhibitor activity correlates withSLFN11 expression and demonstrates synergy with temozolomide in small cell lung cancer. *Clin. Cancer Res.* 23 (2), 523–535. doi:10.1158/1078-0432.CCR-16-1040

Lorusso, P. M. (2016). Inhibition of the PI3K/AKT/mTOR pathway in solid tumors. *J. Clin. Oncol.* 34 (31), 3803–3815. doi:10.1200/JCO.2014.59.0018

Maiorano, B. A., Maiorano, M. F. P., Lorusso, D., and Maiello, E. (2021). Ovarian cancer in the era of immune checkpoint inhibitors: State of the art and future perspectives. *Cancers* 13 (17), 4438. doi:10.3390/cancers13174438

Martins, M. L. F., Loos, N. H. C., Mucuk, S., de Jong, D., Lebre, M. C., et al. (2021). P-glycoprotein (ABCB1/MDR1) controls brain penetration and intestinal disposition of the PARP1/2 inhibitor niraparib. *Mol. Pharm.* 18 (12), 4371–4384. doi:10.1021/acs.molpharmaceut.1c00553

Mateos-Gomez, P. A., Gong, F., Nair, N., Miller, K. M., Lazzerini-Denchi, E., and Sfeir, A. (2015). Mammalian polymerase θ promotes alternative NHEJ and suppresses recombination. *Nature* 518 (7538), 254–257. doi:10.1038/nature14157

Matulonis, U. A., Wulf, G. M., Barry, W. T., Birrer, M., Westin, S. N., Farooq, S., et al. (2017). Phase I dose escalation study of the PI3kinase pathway inhibitor BKM120 and the oral poly (ADP ribose) polymerase (PARP) inhibitor olaparib for the treatment of high-grade serous ovarian and breast cancer[J]. *Annals Oncol.* 28 (3), 512–518. doi:10.1093/annonc/mdw672

Mehta, A. K., Cheney, E. M., Hartl, C. A., Pantelidou, C., Oliwa, M., Castrillon, J. A., et al. (2021). Targeting immunosuppressive macrophages overcomes PARP inhibitor resistance in BRCA1-associated triple-negative breast cancer. *Nat. Cancer* 2 (1), 66–82. doi:10.1038/s43018-020-00148-7

Meng, J., Peng, J., Feng, J., Maurer, J., Li, X., Li, Y., et al. (2021). Niraparib exhibits a synergistic anti-tumor effect with PD-L1 blockade by inducing an immune response in ovarian cancer. *J. Transl. Med.* 19 (1), 415. doi:10.1186/s12967-021-03073-0

Mirman, Z., and de Lange, T. (2020). 53BP1: A DSB escort. *Genes. Dev.* 34 (1-2), 7–23. doi:10.1101/gad.333237.119

Mirza, M. R., Coleman, R. L., González-Martín, A., Moore, K. N., Colombo, N., Ray-Coquard, I., et al. (2020). The forefront of ovarian cancer therapy: Update on PARP inhibitors. *Ann. Oncol.* 31 (9), 1148–1159. doi:10.1016/j.annonc.2020.06.004

Molinaro, E., Andrikou, K., Casadei-Gardini, A., and Rovesti, G. (2020). BRCA in gastrointestinal cancers: Current treatments and future perspectives. *Cancers* 12 (11), 3346. doi:10.3390/cancers12113346

Morosi, L., Matteo, C., Ceruti, T., Giordano, S., Ponzo, M., Frapolli, R., et al. (2020). Quantitative determination of niraparib and olaparib tumor distribution by mass spectrometry imaging. *Int. J. Biol. Sci.* 16 (8), 1363–1375. doi:10.7150/ijbs.41395

Moustafa, D., Elwahed, M. R. A., Elsaid, H. H., and Parvin, J. D. (2021). Modulation of Early Mitotic Inhibitor 1 (EMI1) depletion on the sensitivity of PARP inhibitors in BRCA1 mutated triple-negative breast cancer cells. *PLoS One* 16 (1), e0235025. doi:10.1371/journal.pone.0235025

Mukhopadhyay, A., Drew, Y., Matheson, E., Salehan, M., Gentles, L., Pachter, J. A., et al. (2019). Evaluating the potential of kinase inhibitors to suppress DNA repair and sensitise ovarian cancer cells to PARP inhibitors. *Biochem. Pharmacol.* 167, 125–132. doi:10.1016/j.bcp.2018.10.011

Naidoo, K., Wai, P. T., Maguire, S. L., Daley, F., Haider, S., Kriplani, D., et al. (2018). Evaluation of CDK12 protein expression as a potential novel biomarker for DNA damage response-targeted therapies in breast cancer. *Mol. Cancer Ther.* 17 (1), 306–315. doi:10.1158/1535-7163.MCT-17-0760

Nesic, K., Kondrashova, O., Hurley, R. M., Mcgehee, C. D., Vandenberg, C. J., Ho, G., et al. (2021). AcquiredRAD51C promoter methylation loss causes PARP inhibitor resistance in high-grade serous ovarian carcinoma. *Cancer Res.* 81 (18), 4709–4722. doi:10.1158/0008-5472.CAN-21-0774

Noordermeer, S. M., Adam, S., Setiaputra, D., Barazas, M., Pettitt, S. J., Ling, A. K., et al. (2018). The shieldin complex mediates 53BP1-dependent DNA repair. *Nature* 560 (7716), 117–121. doi:10.1038/s41586-018-0340-7

Nowsheen, S., Bonner, J. A., Lobuglio, A. F., Trummell, H., Whitley, A. C., Dobelbower, M. C., et al. (2011). Cetuximab augments cytotoxicity with poly (adp-ribose) polymerase inhibition in head and neck cancer. *PLoS One* 6 (8), e24148. doi:10.1371/journal.pone.0024148

O'Sullivan, J., Tedim Ferreira, M., Gagné, J., Sharma, A. K., Hendzel, M. J., Masson, J., et al. (2019). Emerging roles of eraser enzymes in the dynamic control of protein ADP-ribosylation. *Nat. Commun.* 10 (1), 1182. doi:10.1038/s41467-019-08859-x

Ovcaricek, T., Frkovic, S., Matos, E., Mozina, B., and Borstnar, S. (2011). Triple negative breast cancer - prognostic factors and survival. *Radiol. Oncol.* 45 (1), 46–52. doi:10.2478/v10019-010-0054-4

Paes Dias, M., Tripathi, V., van der Heijden, I., Cong, K., Manolika, E., Bhin, J., et al. (2021). Loss of nuclear DNA ligase III reverts PARP inhibitor resistance in BRCA1/53BP1 double-deficient cells by exposing ssDNA gaps. *Mol. Cell.* 81 (22), 4692–4708.e9. e9. doi:10.1016/j.molcel.2021.09.005

Pardoll, D. M. (2012). Immunology beats cancer: A blueprint for successful translation. *Nat. Immunol.* 13 (12), 1129–1132. doi:10.1038/ni.2392

Park, Y. H., Jung, H. H., Ahn, J. S., and Im, Y. (2013). Statin induces inhibition of triple negative breast cancer (TNBC) cells via PI3K pathway. *Biochem. Biophys. Res. Commun.* 439 (2), 275–279. doi:10.1016/j.bbrc.2013.08.043

Parmar, K., Kochupurakkal, B. S., Lazaro, J., Wang, Z. C., Palakurthi, S., Kirschmeier, P. T., et al. (2019). The CHK1 inhibitor prexasertib exhibits monotherapy activity in high-grade serous ovarian cancer models and sensitizes to PARP inhibition. *Clin. Cancer Res.* 25 (20), 6127–6140. doi:10.1158/1078-0432.CCR-19-0448

Pascal, J. M., and Ellenberger, T. (2015). The rise and fall of poly(ADP-ribose): An enzymatic perspective. *DNA Repair* 32, 10–16. doi:10.1016/j.dnarep.2015.04.008

Petermann, E., and Caldecott, K. W. (2006). Evidence that the ATR/Chk1 pathway maintains normal replication fork progression during unperturbed S phase. *Cell. Cycle* 5 (19), 2203–2209. doi:10.4161/cc.5.19.3256

Pettitt, S. J., Krastev, D. B., Brandsma, I., Drean, A., Song, F., Aleksandrov, R., et al. (2018). Genome-wide and high-density CRISPR-Cas9 screens identify point mutations in PARP1 causing PARP inhibitor resistance. *Nat. Commun.* 9 (1), 1849. doi:10.1038/s41467-018-03917-2

Poveda, A., Floquet, A., Ledermann, J. A., Asher, R., Penson, R. T., Oza, A. M., et al. (2021). Olaparib tablets as maintenance therapy in patients with platinum-sensitive relapsed ovarian cancer and a BRCA1/2 mutation (SOLO2/ENGOT-Ov21): A final analysis of a double-blind, randomised, placebo-controlled, phase 3 trial. *Lancet. Oncol.* 22 (5), 620–631. doi:10.1016/S1470-2045(21)00073-5

Raimundo, L., Paterna, A., Calheiros, J., Ribeiro, J., Cardoso, D., Piga, I., et al. (2021). BBIT20 inhibits homologous DNA repair with disruption of the BRCA1-BARD1 interaction in breast and ovarian cancer. *Br. J. Pharmacol.* 178 (18), 3627–3647. doi:10.1111/bph.15506

Ray-Coquard, I., Pautier, P., Pignata, S., Pérol, D., González-Martín, A., Berger, R., et al. (2019). Olaparib plus bevacizumab as first-line maintenance in ovarian cancer. *N. Engl. J. Med.* 381 (25), 2416–2428. doi:10.1056/NEJMoa1911361

Rondinelli, B., Gogola, E., Yucel, H., Duarte, A. A., van de Ven, M., van der Sluijs, R., et al. (2017). EZH2 promotes degradation of stalled replication forks by recruiting MUS81 through histone H3 trimethylation. *Nat. Cell. Biol.* 19 (11), 1371–1378. doi:10.1038/ncb3626

Ronson, G. E., Piberger, A. L., Higgs, M. R., Olsen, A. L., Stewart, G. S., Mchugh, P. J., et al. (2018). PARP1 and PARP2 stabilise replication forks at base excision repair intermediates through Fbh1-dependent Rad51 regulation. *Nat. Commun.* 9 (1), 746. doi:10.1038/s41467-018-03159-2

Roos, W. P., and Krumm, A. (2016). The multifaceted influence of histone deacetylases on DNA damage signalling and DNA repair. *Nucleic Acids Res.* 21 (44), 10017–10030. doi:10.1093/nar/gkw922

Rottenberg, S., Jaspers, J. E., Kersbergen, A., van der Burg, E., Nygren, A. O. H., Zander, S. A. L., et al. (2008). High sensitivity of BRCA1-deficient mammary tumors to the PARP inhibitor AZD2281 alone and in combination with platinum drugs. *Proc. Natl. Acad. Sci. U. S. A.* 105 (44), 17079–17084. doi:10.1073/pnas.0806092105

Rütten, H., Verhoef, C., van Weelden, W. J., Smits, A., Dhanis, J., Ottevanger, N., et al. (2021). Recurrent endometrial cancer: Local and systemic treatment options. *Cancers* 13 (24), 6275. doi:10.3390/cancers13246275

Saito, Y., Takahashi, T., Obata, Y., Nishida, T., Ohkubo, S., Nakagawa, F., et al. (2020). TAS-116 inhibits oncogenic KIT signalling on the Golgi in both imatinib-naive and imatinib-resistant gastrointestinal stromal tumours. *Br. J. Cancer* 122 (5), 658–667. doi:10.1038/s41416-019-0688-y

Schaaf, L., Schwab, M., Ulmer, C., Heine, S., Mürdter, T. E., Schmid, J. O., et al. (2016). Hyperthermia synergizes with chemotherapy by inhibiting PARP1-dependent DNA replication arrest. *Cancer Res.* 76 (10), 2868–2875. doi:10.1158/0008-5472.CAN-15-2908

Shen, J., Zhao, W., Ju, Z., Wang, L., Peng, Y., Labrie, M., et al. (2019). PARPi triggers the STING-dependent immune response and enhances the therapeutic efficacy of immune checkpoint blockade independent of BRCAness. *Cancer Res.* 79 (2), 311–319. doi:10.1158/0008-5472.CAN-18-1003

Shroff, R. T., Hendifar, A., Mcwilliams, R. R., Geva, R., Epelbaum, R., Rolfe, L., et al. (2018). Rucaparib monotherapy in patients with pancreatic cancer and a known deleterious BRCA mutation. *JCO Precis. Oncol.* 2018, 1–15. doi:10.1200/PO.17.00316

Simoneau, A., Xiong, R., and Zou, L. (2021). The trans cell cycle effects of PARP inhibitors underlie their selectivity toward BRCA1/2-deficient cells. *Genes. Dev.* 35 (17-18), 1271–1289. doi:10.1101/gad.348479.121

Stecklein, S. R., Kumaraswamy, E., Behbod, F., Wang, W., Chaguturu, V., Harlan-Williams, L. M., et al. (2012). BRCA1 and HSP90 cooperate in homologous and non-homologous DNA double-strand-break repair and G2/M checkpoint activation. *Proc. Natl. Acad. Sci. U. S. A.* 109 (34), 13650–13655. doi:10.1073/pnas.1203326109

Sung, H., Ferlay, J., Siegel, R. L., Laversanne, M., Soerjomataram, I., Jemal, A., et al. (2021). Global cancer statistics 2020: GLOBOCAN estimates of incidence and mortality worldwide for 36 cancers in 185 countries. *Ca. Cancer J. Clin.* 71 (3), 209–249. doi:10.3322/caac.21660

Swisher, E. M., Lin, K. K., Oza, A. M., Scott, C. L., Giordano, H., Sun, J., et al. (2017). Rucaparib in relapsed, platinum-sensitive high-grade ovarian carcinoma (ARIEL2 Part 1): An international, multicentre, open-label, phase 2 trial. *Lancet. Oncol.* 18 (1), 75–87. doi:10.1016/S1470-2045(16)30559-9

Tateishi, K., Wakimoto, H., Iafrate, A. J., Tanaka, S., Loebel, F., Lelic, N., et al. (2015). Extreme vulnerability of IDH1 mutant cancers to NAD+ depletion. *Cancer Cell.* 28 (6), 773–784. doi:10.1016/j.ccell.2015.11.006

Taylor, R. M., Whitehouse, C. J., and Caldecott, K. W. (2000). The DNA ligase III zinc finger stimulates binding to DNA secondary structure and promotes end joining. *Nucleic Acids Res.* 28 (18), 3558–3563. doi:10.1093/nar/28.18.3558

Tirman, S., Quinet, A., Wood, M., Meroni, A., Cybulla, E., Jackson, J., et al. (2021). Temporally distinct post-replicative repair mechanisms fill PRIMPOL-dependent ssDNA gaps in human cells. *Mol. Cell.* 81 (19), 4026–4040.e8. e8. doi:10.1016/j.molcel.2021.09.013

van Wietmarschen, N., and Nussenzweig, A. (2018). Mechanism for synthetic lethality in BRCA-deficient cancers: No longer lagging behind. *Mol. Cell.* 71 (6), 877–878. doi:10.1016/j.molcel.2018.08.045

Vinayak, S., Tolaney, S. M., Schwartzberg, L., Mita, M., Mccann, G., Tan, A. R., et al. (2019). Open-label clinical trial of niraparib combined with pembrolizumab for treatment of advanced or metastatic triple-negative breast cancer. *JAMA Oncol.* 5 (8), 1132–1140. doi:10.1001/jamaoncol.2019.1029

Waks, A. G., Cohen, O., Kochupurakkal, B., Kim, D., Dunn, C. E., Buendia, B. J., et al. (2020). Reversion and non-reversion mechanisms of resistance to PARP inhibitor or platinum chemotherapy in BRCA1/2-mutant metastatic breast cancer. *Ann. Oncol.* 31 (5), 590–598. doi:10.1016/j.annonc.2020.02.008

Wang, J., Zhang, Y., Yuan, L., Ren, L., Zhang, Y., and Qi, X. (2020). Comparative efficacy, safety, and acceptability of single-agent poly (ADP-ribose) polymerase (PARP) inhibitors in BRCA -mutated HER2 -negative metastatic or advanced breast cancer: A network meta-analysis. *Aging (Albany, NY.)* 13 (1), 450–459. doi:10.18632/aging.202152

Wang, M., Wu, W., Wu, W., Rosidi, B., Zhang, L., Wang, H., et al. (2006). PARP-1 and Ku compete for repair of DNA double strand breaks by distinct NHEJ pathways. *Nucleic Acids Res.* 34 (21), 6170–6182. doi:10.1093/nar/gkl840

Wang, W., and Figg, W. D. (2008). Secondary BRCA1 and BRCA2 alterations and acquired chemoresistance. *Cancer Biol. Ther.* 7 (7), 1004–1005. doi:10.4161/cbt.7.7.6409

Wang, Y., Luo, W., and Wang, Y. (2019). PARP-1 and its associated nucleases in DNA damage response. *DNA Repair* 81, 102651. doi:10.1016/j.dnarep.2019.102651

Westin, S. N., Coleman, R. L., Fellman, B. M., Yuan, Y., Sood, A. K., Soliman, P. T., et al. (2021). Effort: EFficacy of adavosertib in parp ResisTance: A randomized two-arm non-comparative phase II study of adavosertib with or without olaparib in women with PARP-resistant ovarian cancer. *J. Clin. Oncol.* 39 (15), 5505. doi:10.1200/JCO.2021.39.15_suppl.5505

Wilson, A. J., Gupta, V. G., Liu, Q., Yull, F., Crispens, M. A., and Khabele, D. (2022). Panobinostat enhances olaparib efficacy by modifying expression of homologous recombination repair and immune transcripts in ovarian cancer. *Neoplasia* 24 (2), 63–75. doi:10.1016/j.neo.2021.12.002

Workman, P., and Powers, M. V. (2007). Chaperoning cell death: A critical dual role for Hsp90 in small-cell lung cancer. *Nat. Chem. Biol.* 3 (8), 455–457. doi:10.1038/nchembio0807-455

Xu, G., Chapman, J. R., Brandsma, I., Yuan, J., Mistrik, M., Bouwman, P., et al. (2015). REV7 counteracts DNA double-strand break resection and affects PARP inhibition. *Nature* 521 (7553), 541–544. doi:10.1038/nature14328

Yalon, M., Tuval-Kochen, L., Castel, D., Moshe, I., Mazal, I., Cohen, O., et al. (2016). Overcoming resistance of cancer cells to PARP-1 inhibitors with three different drug combinations. *PLoS One* 11 (5), e0155711. doi:10.1371/journal.pone.0155711

Yang, Z. M., Liao, X. M., Chen, Y., Shen, Y. Y., Yang, X. Y., Su, Y., et al. (2017). Combining 53BP1 with BRCA1 as a biomarker to predict the sensitivity of poly(ADP-ribose) polymerase (PARP) inhibitors. *Acta Pharmacol. Sin.* 38 (7), 1038–1047. doi:10.1038/aps.2017.8

Yap, T. A., Kristeleit, R., Michalarea, V., Pettitt, S. J., Lim, J. S. J., Carreira, S., et al. (2020). Phase I trial of the PARP inhibitor olaparib and AKT inhibitor capivasertib in patients with BRCA1/2 - and non–BRCA1/2 -mutant cancers. *Cancer Discov.* 10 (10), 1528–1543. doi:10.1158/2159-8290.CD-20-0163

Yekezare, M., Gómez-González, B., and Diffley, J. F. X. (2013). Controlling DNA replication origins in response to DNA damage – inhibit globally, activate locally. *J. Cell. Sci.* 126 (6), 1297–1306. doi:10.1242/jcs.096701

Zatreanu, D., Robinson, H. M. R., Alkhatib, O., Boursier, M., Finch, H., Geo, L., et al. (2021). Polθ inhibitors elicit BRCA-gene synthetic lethality and target PARP inhibitor resistance. *Nat. Commun.* 12 (1), 3636. doi:10.1038/s41467-021-23463-8

Zhang, X., Liu, C., Nepal, S., Yang, C., Dou, W., and Chen, J. (2014). A hybrid approach for scalable sub-tree anonymization over big data using MapReduce on cloud. *J. Comput. Syst. Sci.* 80 (5), 1008–1020. doi:10.1016/j.jcss.2014.02.007

Zhang, X., Wang, Y., Gari, A., Qu, C., and Chen, J. (2021). Pan-cancer analysis of PARP1 alterations as biomarkers in the prediction of immunotherapeutic effects and the association of its expression levels and immunotherapy signatures. *Front. Immunol.* 12, 721030. doi:10.3389/fimmu.2021.721030

Zhou, J., Gelot, C., Pantelidou, C., Li, A., Yücel, H., Davis, R. E., et al. (2021). A first-in-class polymerase theta inhibitor selectively targets homologous-recombination-deficient tumors. *Nat. Cancer* 2 (6), 598–610. doi:10.1038/s43018-021-00203-x

Zimmermann, M., Lottersberger, F., Buonomo, S. B., Sfeir, A., and de Lange, T. (2013). 53BP1 regulates DSB repair using Rif1 to control 5′ end resection. *Science* 339 (6120), 700–704. doi:10.1126/science.1231573

frontiers | Frontiers in Pharmacology

TYPE Original Research
PUBLISHED 01 November 2022
DOI 10.3389/fphar.2022.1032069

OPEN ACCESS

EDITED BY
Eswar Shankar,
The Ohio State University, United States

REVIEWED BY
Ashish Tyagi,
Texas A&M University, United States
Balaji Chandrasekaran,
Texas A&M University, United States

*CORRESPONDENCE
Ming Tatt Lee,
mingtatt7286@outlook.com

SPECIALTY SECTION
This article was submitted to Pharmacology of Anti-Cancer Drugs, a section of the journal Frontiers in Pharmacology

RECEIVED 30 August 2022
ACCEPTED 17 October 2022
PUBLISHED 01 November 2022

CITATION
Chen L, Jiang X, Gao S, Liu X, Gao Y, Kow ASF, Tham CL and Lee MT (2022), Sensitization effect of kaempferol from persimmon leaves on HepG2 hepatoma cells with ABT-199 resistance and its molecular mechanisms.
Front. Pharmacol. 13:1032069.
doi: 10.3389/fphar.2022.1032069

Sensitization effect of kaempferol from persimmon leaves on HepG2 hepatoma cells with ABT-199 resistance and its molecular mechanisms

Li Chen[1,2], Xudong Jiang[2], Si Gao[2], Xueping Liu[2], Ying Gao[3], Audrey Siew Foong Kow[1], Chau Ling Tham[4] and Ming Tatt Lee[1]*

[1]Faculty of Pharmaceutical Sciences, UCSI University, Kuala Lumpur, Malaysia, [2]Department of Pharmacology, College of Medicine, Guangxi University of Science and Technology, Liuzhou, China, [3]International Ginseng Institute, School of Agriculture, Middle Tennessee State University, Murfreesboro, TN, United States, [4]Department of Biomedical Sciences, Faculty of Medicine and Health Sciences, Universiti Putra Malaysia, Serdang, Selangor, Malaysia

ABT-199 (venetoclax) is the first-in-class selective B-cell lymphoma 2 (BCL2) inhibitor, which is known to be ineffective towards liver cancer cells. Here, we investigated the efficacy and the underlying molecular processes of the sensitization effect of kaempferol isolated from persimmon leaves (KPL) on the ABT-199-resistant HepG2 cells. The effects of various doses of KPL coupled with ABT-199 on the proliferation of HepG2 cells and on the H22 liver tumor-bearing mouse model were examined, as well as the underlying mechanisms. Our findings showed that ABT-199 alone, in contrast to KPL, had no significant impact on hepatoma cell growth, both *in vitro* and *in vivo*. Interestingly, the combination therapy showed significantly higher anti-hepatoma efficacy. Mechanistic studies revealed that combining KPL and ABT-199 may promote both early and late apoptosis, as well as decrease the mitochondrial membrane potential in HepG2 cells. Western blot analysis showed that combination of KPL and ABT-199 significantly reduced the expression of the anti-apoptotic proteins Bcl-2, Bcl-xL, and Mcl-1, raised the expression of Bax and cleaved caspase 3, and enhanced cytochrome C release and Bax translocation. Therefore, KPL combined with ABT-199 has a potential application prospect in the treatment of hepatocellular carcinoma.

KEYWORDS

hepatocarcinoma, preclinical model, kaempferol, persimmons leaves, ABT-199, Bcl-2, Mcl-1, chemoresistance

1 Introduction

Hepatocellular carcinoma (HCC), the most common type of primary liver cancer, is one of the most well-known harmful tumours. The death rate is second to gastric cancer and cellular breakdown in the lungs and is the fifth driving reason for tumour-related deaths in the world (Siegel et al., 2018). Most patients with HCC rely on chemotherapy and radiotherapy for treatment, but conventional chemotherapy and radiotherapy often fail to achieve satisfactory results (Liu et al., 2015). Although surgical removal can be regarded as curative treatment therapy, recurrence remains as a major issue (Qian et al., 2021). Furthermore, liver cancer is often diagnosed at advanced stages, which surgical intervention may not be feasible. Therefore, finding new therapeutic drugs and therapeutic targets has become an urgent task for medical researchers.

ABT-199 (Venetoclax) is the first Bcl-2 inhibitor approved by FDA for the treatment of patients with chronic lymphocytic leukemia, small lymphocytic lymphoma (SLL) and acute myeloid leukemia (AML) (Cang et al., 2015; Deeks, 2016). Several reports on the therapeutic potentials of ABT-199 on chronic lymphocytic leukemia (Souers et al., 2013), breast cancer (Vaillant et al., 2013) and other malignant hematologic cancers and solid tumours (Itchaki and Brown, 2016; Shi et al., 2021; Weller et al., 2022). To the best of our knowledge, there's no reports to date demonstrating the effects of ABT-199 in HCC. Many tumour cells over-express Mcl-1 protein, resulting in the imbalance of interaction between anti-apoptotic members and pro-apoptotic members, leading to malignant proliferation of tumour cells. Studies have reported that, as an important anti-apoptotic protein, Mcl-1 is also over-expressed in hepatocellular carcinoma (Fleischer et al., 2006), which is one of the important factors of HCC drug resistance (Sieghart et al., 2006). The rational for the combination of agents based on the mechanism of antineoplastic drugs and the dynamics of proliferation is gaining attention in the field of tumour chemotherapy in recent years, and it is also one of the effective methods to overcome tumour resistance (Boshuizen and Peeper, 2020).

Persimmon leaves are the fresh or dried leaves of *Diospyros kaki* L. f., a species of the Ebenaceae family. Previous literature demonstrated that persimmon leaves have many ethnopharmacological properties, such as reducing blood pressure, hemostasis, reducing blood sugar, reducing blood lipid, antioxidant, antibacterial, liver protection, anti-tumour, etc (Kim et al., 2020a; Kim et al., 2020b). In our previous studies, we found that the ethyl acetate part of persimmon leaves and the total flavones of persimmon leaves could inhibit the tumour growth of H22 tumour-bearing mice (Chen et al., 2018). We also showed that the total flavones extracted from persimmon leaves had significant inhibitory effects on liver cancer and breast cancer, by regulating the redox state and increasing the level of ROS in cells to promote apoptosis (Chen et al., 2020). The main active components of total flavonoids in persimmon leaves are kaempferol, quercetin and its glycosides (Liu et al., 2012; Xie et al., 2015). Among these flavonoids, several studies have confirmed that kaempferol has broad-spectrum anti-tumour activities against liver cancer, breast cancer, colon cancer, prostate cancer, bladder cancer, cervical cancer, etc (Wang et al., 2019; Zhang et al., 2022). Epidemiological studies showed that dietary intake of flavonoids, including kaempferol, is correlated with low incidences of liver cancer (Zamora-Ros et al., 2013). Previous molecular studies have shown that kaempferol inhibits HepG2 cell proliferation, migration, and invasion, as well as cell viability in a dose- and time-dependent manner (Zhu et al., 2018). Furthermore, treatment with kaempferol can induce apoptosis and cause cell cycle arrest at the G2/M phase, thus preventing tumour cell migration and invasion (Huang et al., 2013; Sharma et al., 2021). Interestingly, previous research has linked kaempferol's anti-tumour effect to Bcl-2 family proteins that regulate the endogenous mitochondrial apoptosis pathway, which can downregulate Bcl-2 and Mcl-1 while increasing Bax protein expression (Imran et al., 2019; Zhu and Xue, 2019; Afroze et al., 2022). Therefore, in this study, we hypothesized that KPL can increase the sensitivity of hepatocarcinoma cells that is resistant to ABT-199, by down-regulating the expression of Mcl-1. Furthermore, we examined the sensitization effect and elucidated the underlying molecular mechanism of the selective Bcl-2 inhibitor ABT-199 combined with KPL on HepG2 cell lines *in vitro* and *in vivo*.

2 Materials and methods

2.1 Cell-line and animals

HepG2 cells were purchased from Stem Cell Bank, Chinese Academy of Sciences (SCB, Shanghai, China), and were routinely cultured according to the protocol provided by SCB.

H22 ascites tumour mice were obtained from Guangxi Institute of Traditional Chinese Medicine and Pharmaceutical Science. Six-week-old Kunming mice (male and female, SPF) were purchased from Human SJA Laboratory Animal Co., Ltd., weighing at 18–22 g (Certificate No. SYXK 2019–0017, Changsha, China). All animal experimentations reported in this study were carried out in accordance with the guidelines for the use and care of experimental animals and were approved by the Experimental Animals Committee at Guangxi University of Science and Technology. The mice were housed at room temperature between 20–26°C, the humidity was 40–70%, under a 14:10 light/dark cycle. The mice had free access to feed and drinking water for the whole experimentation period.

2.2 Chemicals and reagents

Silica gel column chromatography was purchased from Marine Chemical plant (Qingdao, China). Petroleum ether 60, ethyl acetate, chloroform, methanol and glacial acetic acid were purchased from Xilong Chemical Co., Ltd. (Guangzhou, China). Dimethyl Sulfoxide (DMSO) was purchased from Kulaibo Technology Co., Ltd. (Beijing, China). Eagle's minimum essential medium (EMEM), trypsin, and fetal bovine serum (FBS) were purchased from Shuangru Biotechnology Co., Ltd. (Shanghai, China). Persimmon (*Diospyros* kaki L.) leaves were purchased from Yaoyuan Trading Inc. (Anguo City, Hebei Province, China) (Batch No. 161011). ABT-199 and kaempferol reference standards were purchased from TargetMol (MA, United States).

Cell counting kit-8 (CCK-8), RIPA lysis buffer, PMSF solution, Quick block solution, primary antibody dilution buffer, secondary antibody dilution buffer, SDS-PAGE gel preparation kit, Tris buffered saline, SDS-PAGE electrophoresis buffer, pre-stained color protein ladder, cell mitochondria isolation kit, 4% paraformaldehyde fix solution and crystal violet staining solution were purchased from Beyotime (Shanghai, China). Hoechst 33,342, Annexin V, and propidium iodide (PI) were purchased from BD BioSciences (San Jose, CA, United States). JC-1 mitochondrial membrane potential assay kit was purchased from Cayman Chemical (MI, United States). Polyvinylidene difluoride (PVDF) membrane and ECL reagent were purchased from Millipore (MA, United States). BCA protein assay kit was purchased from Merck (novagen series, Germany). The manufactures and catalogue numbers of antibodies used in this study are listed as follows, Bcl-2 (Cell Signaling Technology, MA, United States, #4223T, 1: 1000), Bcl-xL (Cell Signaling Technology, MA, United States, # 2764T, 1:1000), Bax (Cell Signaling Technology, MA, United States, #5023T, 1:1000), Mcl-1 (Cell Signaling Technology, MA, United States, #5453T, 1:1000), Caspase 3 (Cell Signaling Technology, MA, United States, #9665T, 1:1000), α-Tubulin (Cell Signaling Technology, MA, United States, #2125S, 1:1000), Cyt C (Cell Signaling Technology, MA, United States, #4280T, 1:1000), secondary antibody (horseradish peroxidase-conjugated goat anti-rabbit) (Cell Signaling Technology, MA, United States, sub-packaged by Asbio Technology, # as006, 1:1000).

2.3 Kaempferol isolated from persimmon leaves (KPL) and the content determination

Kaempferol from persimmon leaves (KPL) was isolated from the total flavonoids of persimmon leaves by the Pharmacological Laboratory of Pharmacy, Department of Medicine, Guangxi University of Science and Technology. The extraction method was described by Chen et al. previous studies (Chen et al., 2018; Chen et al., 2020). Briefly, 20.0 g of persimmon leaves was separated by silica gel column chromatography (360.0 g, 200~300 mesh sieves). The crude powder was obtained by gradient elution of petroleum ether 60 - ethyl acetate (100:0 → 100:1 → 80:1 → 50:1 → 20:1 → 10:1 → 5: 1 → 2:1 → 0:100, V/V). The compound in powder form (12.4 mg) was obtained by repeated silica gel column chromatography with chloroform - methanol - glacial acetic acid (75:15:1, V/V) as eluent. The content of KPL was determined by HPLC, and the standard curve was prepared with different concentrations of kaempferol reference materials. Chromatographic conditions: the chromatographic column is Ultimate XB-C18 (5 μm, 4.6 mm × 250 mm); the mobile phase was acetonitrile: 0.2% phosphoric acid aqueous solution = 32: 68; the flow rate was 1.0 ml/min; the detection wavelength was 360 nm; the column temperature was room temperature; the sample volume was 20 μL.

2.4 Cell culture

HepG2 cell line used in this study was cultured in EMEM medium, supplemented with 10% FBS, 100 U/ml of penicillin and 100 U/ml of streptomycin at a 37°C incubator (Thermo, United States) supplied with 5% CO_2. The cells in the logarithmic growth phase were applied in the following assays.

2.5 Cell growth inhibition assays of ABT-199

Cells (5×10^3 cells/well) were seeded in 96-well plates, cultured overnight to allow cells attachment, and treated with ABT-199 at the concentrations of 1, 2, 5, 10 and 15 μM respectively. After 48 h treatment, 10 μL of CCK-8 dye was added into each well to a final concentration (v/v) of 10% and incubated for another 2 h. Subsequently, the absorbance (OD) was measured at 450 nm by Multiskan GO microplate reader of multi-wavelength measurement system (Thermo Scientific, MA, United States). Cell growth inhibition rate was evaluated as the ratio of the absorbance of the treated samples to that of the negative control samples and analyzed by Prism 6 software (GraphPad Software Inc. San Diego, CA, United States). All experiments were carried out in triplicate. The formula of cell growth inhibition (%) is as follows:

$$\text{growth inhibition (\%)} = \left(1 - \frac{\text{ODT}}{\text{ODC}}\right) \times 100\%$$

Where ODT is the average OD value of the treated samples and ODC is the average OD value of the negative control samples.

2.6 Cell growth inhibition assays of ABT-199 combined with KPL

According to the preliminary experimental results (Figure 1A), the growth inhibition rate (%) of ABT-199 on HepG2 cells at the above five different concentrations were all less than 2% without

significant difference, indicating that ABT-199 did not inhibit the proliferation of HepG2 cells. Thus, 2 μM of ABT-199 was selected for the subsequent experiments. Cells (5×10^3 cells/well) were seeded in 96-well plates, cultured overnight to allow cells attachment, and treated with KPL at the concentration of 10, 50, 100, 200 and 300 μM alone or combined with 2 μM of ABT-199 to the corresponding wells for 48 h. Cell growth inhibition assays were conducted as described in Section 2.5 (Cell growth inhibition assays of ABT-199).

2.7 Colony forming assay

Cells were seeded in 6-well plates at 1×10^5 cells/well and incubated overnight. The cells were next treated with KPL at the concentration of 100 and 200 μM alone or combined with ABT-199 at 2 μM to the corresponding wells. After treatment for 24 h, the culture medium was discarded and fresh complete medium was added to continue the culture. The culture medium was changed every 3–4 days until there were colonies visible to the naked eye (about 14 days). After that, the culture solution was discarded, 4% paraformaldehyde was added to the wells and the cells were fixed for 10min. After fixation, the cells were washed with distilled water and stained with crystal violet staining solution for 10 min. After staining, the staining solution was removed through repeated washing. Photos were taken and the formation of cell clones in each group was compared by using Image J (NIH, United States). The experiment was carried out in quadruplicate as described previously with minor modifications (He et al., 2020).

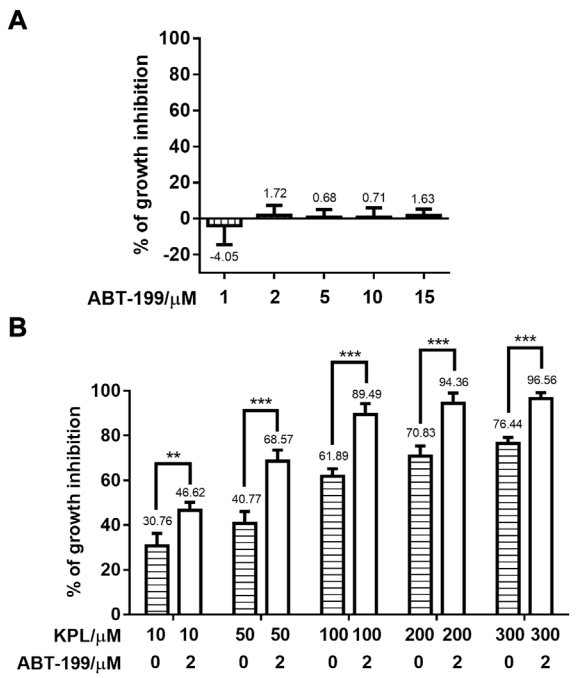

FIGURE 1
Effect of KPL combined with ABT-199 on the growth inhibition of HepG2 cells. **(A)** Growth inhibition percentage (%) of different concentrations of ABT-199 against HepG2 cell line. Cells were seeded in a 96-well plate and treated with 1–15 μM ABT-199 for 48 h, and the growth inhibition percentage of cells was detected with CCK-8 kit. **(B)** Growth inhibition percentage (%) of different concentrations of KPL combined with 2 μM ABT-199 on HepG2 cell line. Cells were seeded in a 96-well plate and treated with 10–300 μM KPL for 48 h with or without 2 μM ABT-199, and the growth inhibition percentage of cells was determined by CCK-8 kit. Values are means ± SD ($n = 4$). $^{**}p < 0.01$, $^{***}p < 0.001$ *versus* the same concentration KPL only group.

2.8 Apoptosis assay

HepG2 cells were seeded in a 96-well clear bottom black plate at a density of 5×10^3 cells/well and cultured overnight. Following attachment, cells were treated with KPL at the concentration of 100 and 200 μM alone or combined with ABT-199 at 2 μM to the corresponding wells for 24 h. The negative control group was treated with complete medium only. Each treatment group had four replicates. After treatment for 24 h, 1 μL Hoechst 33342, 5 μL PI, and 5 μL FITC-Annexin V were added to each well. Apoptosis in each group was evaluated and analyzed by ArrayScan VTI High Content Screening reader (Thermo Scientific, MA, United States). The Excitation/Emission wavelengths for Hoechst 33,342, FITC-Annexin V, and PI were 350/461 nm, 494/518 nm, and 535/617 nm, respectively (Alsaif et al., 2017).

2.9 Determination of mitochondrial membrane potential

Cells were seeded in 6-well plates at 3×10^5 cells/well and incubated overnight. The cells were next treated with KPL at the concentration of 100 and 200 μM alone or combined with ABT-199 at 2 μM to the corresponding wells. After treatment for 24 h, the culture medium was discarded, and the cells were washed with PBS. Then JC-1 Staining Solution with the final concentration of 10 μg/ml was added to the cells followed by incubation in the dark at 37°C for 30 min. The supernatant was discarded, and the cells were washed with assay buffer before observation. The images were observed in dark and captured under TS2-FL ECLIPSE inverted fluorescence microscope (Nikon Imaging Japan Inc.).

2.10 Western blot assay

The effects of KPL combined with ABT-199 on apoptosis-related proteins were detected in the total protein of HepG2 cells. Cells were seeded in 6-well plates at 5×10^5 cells/well and incubated overnight. After the cells were treated with corresponding reagents for 24 h, the culture medium was discarded and the cells were washed with PBS. Then, the cells were lysed with RIPA containing

protease inhibitor PMSF, and centrifuged at 1.2×10^4 g for 15 min at 4°C to collect the supernatant. The effects of KPL combined with ABT-199 on Cyt C release and Bax translocation in HepG2 cells were detected in mitochondria and cytoplasmic proteins. The mitochondria proteins were isolated according to the instruction of cell mitochondria isolation kit manual (Cayman Chemical, MI, United States). All the proteins concentration was quantified by the BCA method.

Equal amounts of protein (20–40 μg) were separated by 12% SDS-PAGE gel electrophoresis and transferred onto PVDF membranes. After blocking with 5% TBST milk, the membranes were hybridized with primary antibodies: Bcl-2, Bcl-xL, Bax, Mcl-1, Caspase 3, cleaved caspase 3, Cyt C and α-Tubulin. The ratio of primary antibody and primary antibody diluent is 1:1000. All the membranes were incubated with their respective primary antibodies overnight at 4°C and the corresponding horseradish-peroxidase-conjugated secondary antibodies for 1 h at room temperature. α-Tubulin was used as the housekeeping protein. The blots were developed using ECL reagent and visualized by an automatic chemiluminescence imaging system (GelView 6000 Pro, Guangzhou bolutang Instrument Co., Ltd.), and the protein levels were quantified using Image J software.

2.11 Animal models and experimental design

The solid tumour model was established using the method previously described (Chen et al., 2018). In brief, four ascites tumour mice with H22 cells passaged in the abdominal cavity for 7–9 days were taken, the mice were sacrificed, and ascites were collected under sterile conditions. The ascites was diluted to 1×10^6 cells/mL with normal saline and 0.2 ml of the ascites was inoculated subcutaneously to healthy Kunming mice in the armpit of the right forelimb. After 24 h inoculation, the mice were randomly divided into 4 groups with 10 mice in each group (half male and half female): control, ABT-199 (100 mg/kg), KPL (100 mg/kg), KPL (100 mg/kg) +ABT-199 (100 mg/kg). The mice were treated by intraperitoneal injection (*i.p.*) daily for 10 continuous days. On the 11th day, the mice were sacrificed by cervical dislocation, the tumour weights were measured, and the tumour inhibition rates were calculated using the following formula:

$$\text{tumour inhibition (\%)} = \frac{\text{tumour weight in model group (g)} - \text{tumour weight in experimental group (g)}}{\text{tumour weight in model group (g)}} \times 100\%$$

2.12 Statistical analysis

The experimental data were analysed by SPSS 25.0 statistical software (IBM, Chicago, IL, United States), and the measurement data were expressed as mean ± SD. One-way analysis of variance (ANONA) followed by Tukey's *post hoc* test was used for comparison between multiple groups. $p < 0.05$ is considered as statistically significant.

3 Results

3.1 Identification and content determination of KPL

The compound, KPL, was in the form of yellow acicular crystal with the melting point of 276–278°C. KPL was soluble in chloroform, methanol, ethyl acetate and acetone but insoluble in petroleum ether and water. The compound was presented as yellow in the 10% sulfuric acid ethanol test and showed positive in the ferric chloride reaction and magnesium hydrochloride powder reaction. The ^{13}C NMR data (Table 1) of KPL is consistent with the ^{13}C NMR data of kaempferol reported in the previous literature (Chen et al., 2018; Chen et al., 2020). Therefore, it is concluded that the compound isolated from PLF was KPL, and the content of KPL was 91.23% as determined by HPLC.

3.2 The inhibitory effect of KPL and ABT-199 co-administration on the growth of Mcl-1 overexpressing HepG2 cell line

HepG2 cell line with high expression of Mcl-1 (Yu et al., 2016) was employed in this study. First, we examined the potential growth inhibition effect of ABT-199, ranging from 1–15 μM using CCK-8 staining. As shown in Figure 1A, the growth inhibitory effect of ABT-199 at all tested concentrations were lower than 2%, which showed that ABT-199 had no inhibitory effect against HepG2 cell line, proving that hepatoma cells were insensitive to ABT-199. ABT-199 at 2 μM was chosen as the combination treatment with KPL for the subsequent experiments. As shown in Figure 1B, KPL alone (horizontal slashed bars, 10–300 μM) significantly inhibited the growth of HepG2 cells, in a concentration-dependent manner. Interestingly, when combined with 2.0 μM of ABT-199, the inhibitory effect of KPL is significantly higher at each tested concentration, as compared with KPL alone. These results indicate that KPL may have sensitization effect on HepG2 cells for ABT-199.

3.3 The inhibitory effect of KPL combined with ABT-199 on colony-forming ability of HepG2 cells

To further investigate the effect of KPL combined with ABT-199 on the proliferation of HepG2 hepatoma cells, the changes of cell clone formation of HepG2 after being treated with KPL combined with ABT-199 for 24 h were detected by crystal violet staining. As

TABLE 1 ^{13}C NMR data of KPL (100 MHz, DMSO d6).

C position	Experimental value δc	Reference value δc	C position	Experimental value δc	Reference value δc
C-2	146.9	146.1	C-9	161.3	160.5
C-3	136.6	135.5	C-10	103.8	102.9
C-4	176.5	175.7	C-1′	122.6	121.6
C-5	157.1	156.0	C-2′, 6′	130.4	129.3
C-6	98.8	98.2	C-3′, 5′	116.4	115.3
C-7	164.7	163.8	C-4′	159.8	159.0
C-8	94.2	93.4			

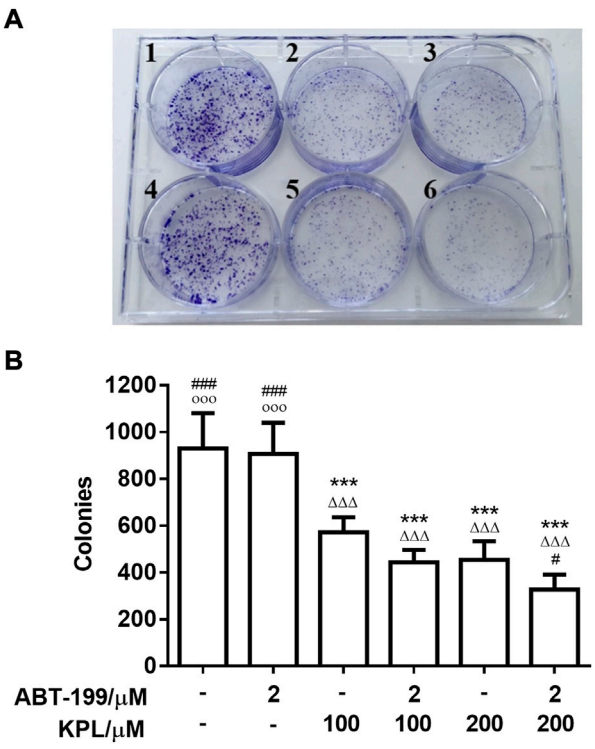

FIGURE 2
The experimental results of clone formation of HepG2 cells treated with KPL and ABT-199 for 24 h. **(A)** Colony formation assay was conducted to investigate growth *in vitro* after treatment with KPL at the concentration of 100 and 200 μM alone or combined with ABT-199 at 2 μM for 14 days. The colonies were visualized with the images. 1: Negative control, 2: KPL 100 μM, 3: KPL 200 μM, 4: ABT-199 2 μM, 5: KPL 100 μM + ABT-199 2 μM, 6: KPL 200 μM + ABT-199 2 μM. **(B)** The corresponding histogram showed the colony numbers. Values are means ± SD ($n = 4$). $^{***}p < 0.001$ *versus* negative control group; $\Delta\Delta\Delta p<0.001$ *versus* ABT-199 alone group; $^{\#}p < 0.05$, $^{\#\#\#}p < 0.001$ *versus* KPL 100 μM group; $^{ooo}p < 0.001$ *versus* KPL 200 μM group.

shown in Figure 2A, in HepG2 cells treated with ABT-199 (2 μM) alone, the number of colonies were not significantly different from the control group, in contrast with KPL alone groups (100–200 μM). However, the number of colonies at all concentration of KPL combined with ABT-199 were significantly lower than that of the negative control group and ABT-199 alone. As shown in Figures 2A,B, the number of colonies formed was smaller and less in a concentration-dependent manner, which was consistent with the results of CCK-8 (Figure 1).

3.4 The effect of KPL combined with ABT-199 on tumour growth and tumour cell necrosis in H22 tumour-bearing mice

Next, we employed the H22 solid liver cancer-bearing mice model to determine whether systemic administration of ABT-199 combined with KPL could inhibit tumour growth in mice. The *in vivo* dose of ABT-199 (100 mg/kg, *i.p.*) was selected based on previous similar studies (Pan et al., 2014; Peirs et al., 2014). In our preliminary study, we found that treatment with 100 mg/kg and 200 mg/kg (*i.p.*) of KPL displayed similar efficacy, thus 100 mg/kg KPL was selected for *in vivo* experiment. After repeated treatment with *i.p.* ABT-199 alone or combined with KPL for 10 days, the tumour weights were measured, and the tumour inhibition percentages were calculated. As showed in Figures 3A,C, compared with the control group (2.188 ± 0.256 g), the tumour weight of ABT-199 only group (2.047 ± 0.275 g) was not significantly reduced, but the tumour weight of KPL only group (1.412 ± 0.206 g) and KPL combined with ABT-199 group (0.716 ± 0.105 g) were significantly reduced ($p < 0.001$). Noticeably, the tumour inhibition by KPL-ABT-199 co-treatment group was significantly higher than ABT-199 alone and KPL alone groups (Figures 3C,D). These results also indicate that the KPL displayed a significant sensitization effect *in vivo*, which is consistent with the *in vitro* findings in Figure 1 and Figure 2.

We also conducted a hematoxylin-eosin (H&E) pathological analysis with the tumour sections to confirm the sensitization effect of KPL *in vivo*. The H&E staining in Figure 3 demonstrated that the tumour cells in the control group were irregularly arranged, with large volume, large nucleocytoplasmic ratio and obvious atypia. The morphological characteristics of tumour cells in ABT-199 only group

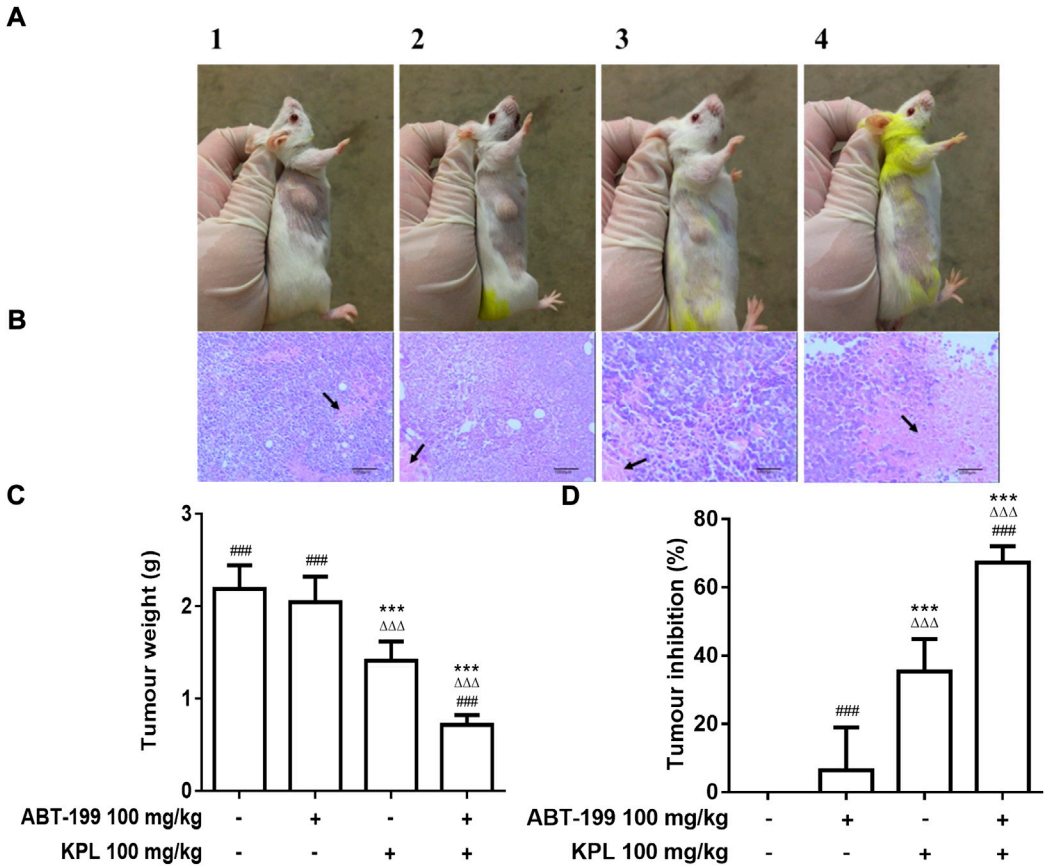

FIGURE 3
The effect of KPL combined ABT-199 on tumour growth and tumour cells necrosis in H22 tumour-bearing mice. **(A)** Representative images of the tumors in various groups. The size of tumors in each group can be seen with the naked eye: compared with the control group, the tumour size of KPL only group and KPL combined with ABT-199 group were significantly reduced, whereas the KPL combined with ABT-199 group were more significantly reduced. A1: Control group, A2: ABT-199 100 mg/kg group, A3: KPL 100 mg/kg group, A4: KPL 100 mg/kg + ABT-199 100 mg/kg group. **(B)** Histological examination of tumour tissues from H22 tumor-bearing mice. The tumorus were sectioned and stained with H&E. The necrotic tumor foci were indicated by the black arrows. B1: Control group, B2: ABT-199 100 mg/kg group, B3: KPL 100 mg/kg group, B4: KPL 100 mg/kg + ABT-199 100 mg/kg group. **(C)** Tumor weights of the mice in each group at the end of the experiment. **(D)** Tumor inhibition percentage of the various treatments. Magnification: 100 ×. Values are means ± SD (n = 10). ***$p < 0.001$ *versus* negative control group; $^{\Delta\Delta\Delta}p < 0.001$ *versus* ABT-199 alone group; $^{\#\#\#}p < 0.001$ *versus* KPL alone group.

were the same as those in the control group; In KPL only group, there were flake necrosis and less pathological mitosis in tumour tissue; In ABT-199 combined with KPL group, the tumour sections exhibited notably different histological features, obvious flake coagulation necrosis was observed in the tumour tissue, the necrosis area were significantly larger than that in other groups, the tumour nucleus were pyknosis, and the necrotic cells were mainly located between loosely arranged cells. The experimental results showed that KPL could enhance the anti-hepatoma effect of ABT-199.

3.5 The effect of KPL combined with ABT-199 on apoptosis of HepG2 cells

In this study, we investigated whether the inhibitory effect of KPL combined with ABT-199 can be related to the induction of apoptosis. We utilised the Hoechst 33342/FITC-Annexin V/PI triple staining assay to detect apoptosis in HepG2 cells. The findings in Figures 4A,B showed that after Hoechst 33342 staining, the nuclei of cells treated by ABT-199 appeared dark blue, similar to the negative control group, with no significant difference in nuclear area between the two groups. However, in the HepG2 cells that were treated with all concentrations of KPL and KPL combined with ABT-199, the nuclei area was significantly decreased ($p < 0.001$), and appeared bright blue, which is one of the classical hallmarks of apoptosis. As shown in Figures 4A,C,D, Annexin V and PI staining of cells in the negative control group and ABT-199 only group showed almost no fluorescence, indicating that there was almost no apoptosis, but cells treated with all concentrations of KPL, the fluorescence intensity of both FITC-Annexin V and PI was significantly increased, especially KPL combined with ABT-199 group ($p < 0.01$ or $p < 0.001$). The number of cells were less than that of KPL only group, due to the

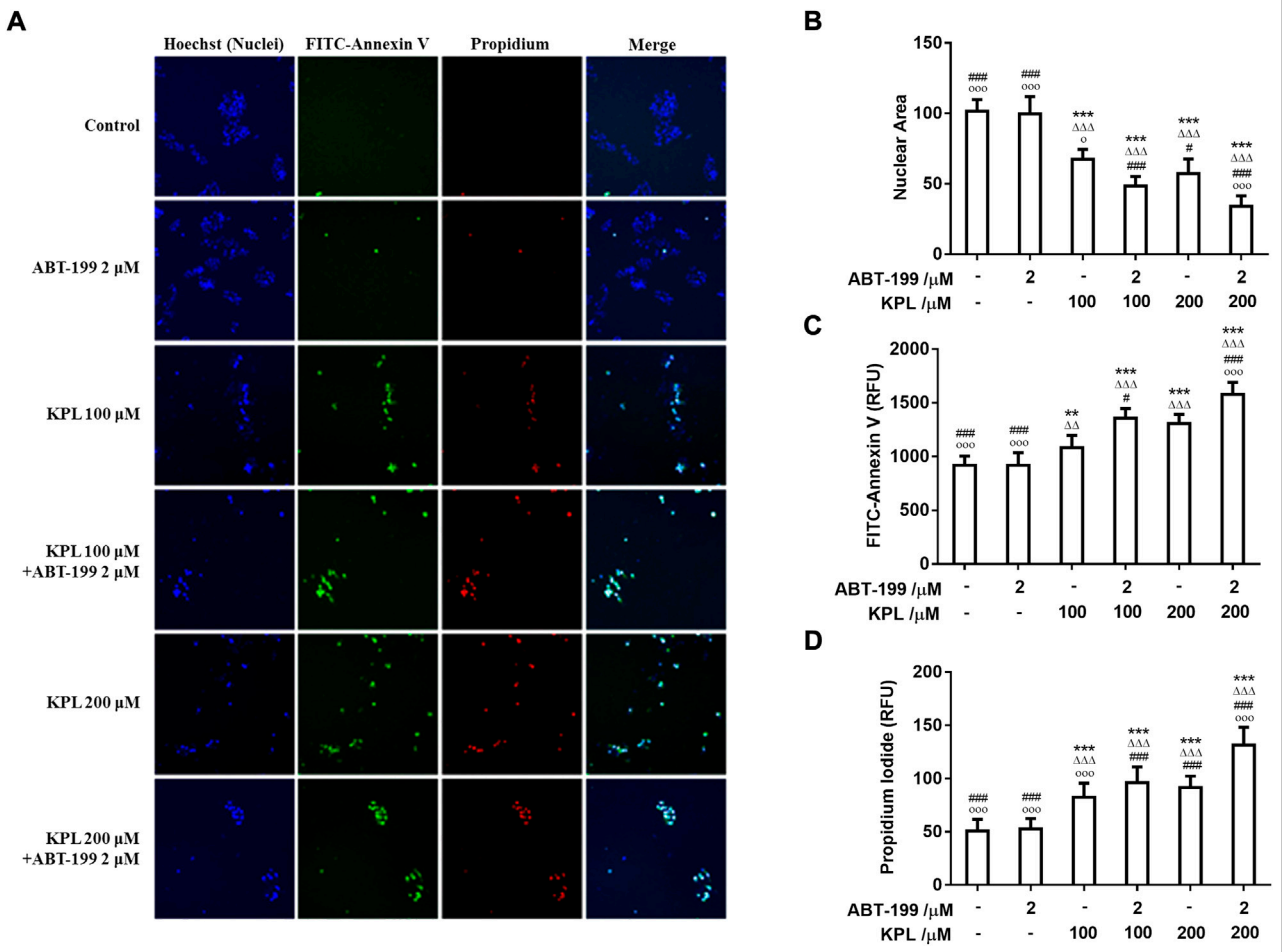

FIGURE 4
The effect of KPL combined with ABT-199 on apoptosis of HepG2 cells. **(A)** Representative images of cell apoptosis in various groups. Different concentrations of KPL with or without 2 μM ABT-199 were treated on HepG2 cells for 24 h, and then the apoptosis was detected by Hoechst 33342/FITC-Annexin V/PI triple staining. The images were collected by an Arrayscan VT1 HCS reader. Merged images were the composition of images of the same field from three different channels. **(B)** The effects of various concentrations of KPL with or without ABT-199 on the nuclear area. **(C)** Fluorescence intensity of FITC Annexin V staining in HepG2 cells treated by various concentrations of KPL with or without ABT-199. **(D)** Fluorescence intensity of PI staining in HepG2 cells treated by various concentrations of KPL with or without ABT-199. Values are means ± SD (n = 12). $^{**}p < 0.01$, $^{***}p < 0.001$ *versus* negative control group; $^{\Delta\Delta}p < 0.01$, $^{\Delta\Delta\Delta}p<0.001$ *versus* ABT-199 alone group; $^{\#}p < 0.05$, $^{\#\#\#}p < 0.001$ *versus* KPL 100 μM group; $^{\circ}p < 0.05$, $^{\circ\circ\circ}p < 0.001$ *versus* KPL 200 μM group.

combined treatment inhibited the cells' proliferation. The results implied that KPL combined with ABT-199 could promote the early and late apoptosis of HepG2 cells.

3.6 The effect of KPL combined with ABT-199 on mitochondrial membrane potential of HepG2 cells

One of the significant signs of early-stage apoptosis is the decrease of mitochondrial membrane potential (Elmore, 2007). In this study, JC-1 fluorescent probe was used to detect the changes of mitochondrial membrane potential after KPL combined with ABT-199 treatment of HepG2 cells. JC-1 staining results were shown in Figures 5A,B. The effect of cells treated with ABT-199 alone was not significantly different from the negative control group, which demonstrated bright red fluorescence. The weak green fluorescence in these cells indicated that JC-1 existed in the aggregated form in mitochondria and with high mitochondrial membrane. However, in KPL alone (100 μM and 200 μM) treatment group and KPL combined with the ABT-199 treatment group, the red fluorescence intensity in mitochondria decreased significantly and the green

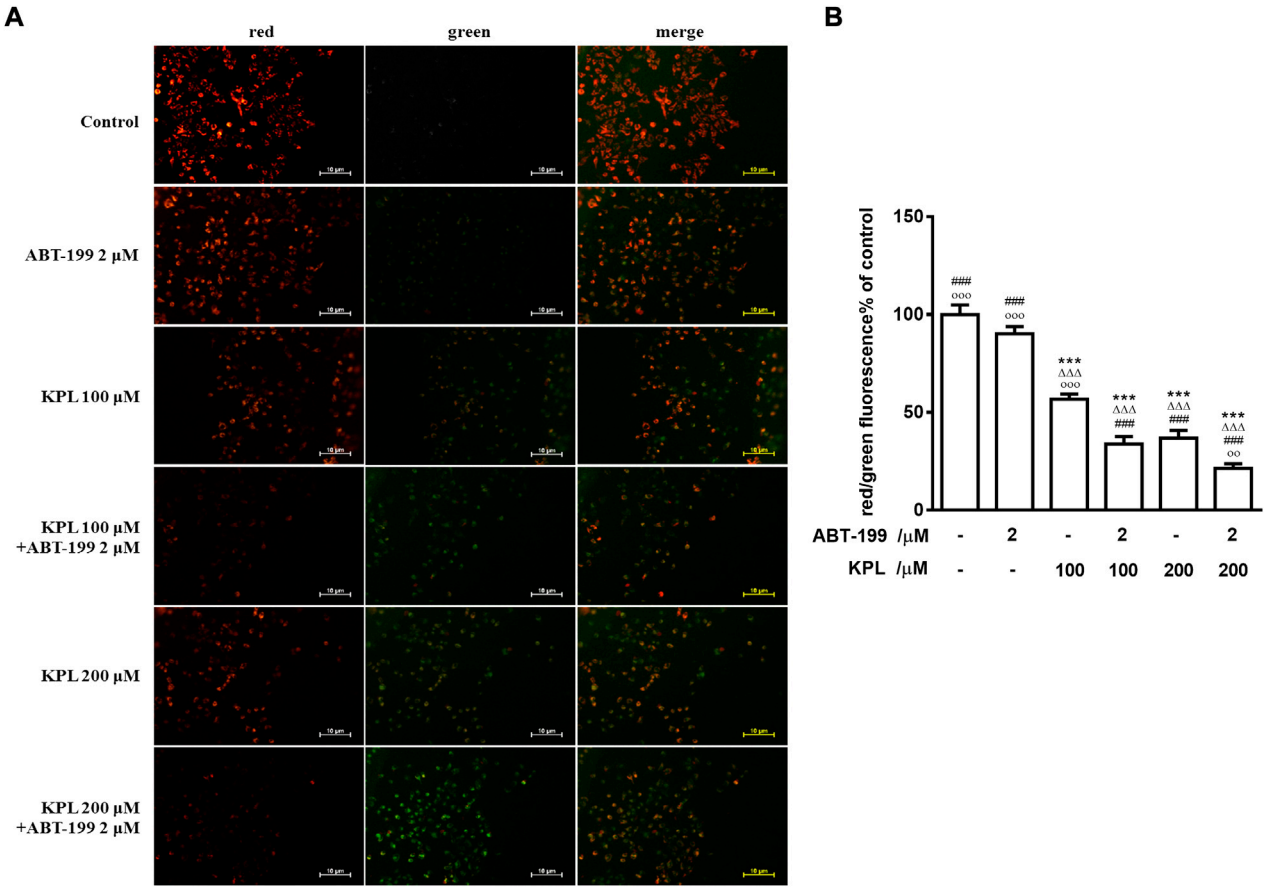

FIGURE 5
The effect of KPL combined with ABT-199 on mitochondrial membrane potential of HepG2 cells. **(A)** Representative images of double immunofluorescent staining for JC-1. Different concentrations of KPL with or without 2 μM ABT-199 were treated on HepG2 cells for 24 h, and then the changes of mitochondrial membrane potential were detected with JC-1 dye. The negative group was untreated. The images were collected by inverted fluorescence microscope. Magnification = 100 ×. **(B)** The ratio of red and green fluorescence intensity. Values are means ± SD (n = 12). ***p < 0.001 *versus* negative control group; $^{\Delta\Delta\Delta}p$<0.001 *versus* ABT-199 alone group; $^{\#\#\#}p$ < 0.001 *versus* KPL 100 μM group; $^{\circ\circ}p$ < 0.01, $^{\circ\circ\circ}p$ < 0.001 *versus* KPL 200 μM group.

fluorescence in cytoplasm increased significantly. These findings indicated that JC-1 in mitochondria existed in the form of monomer with low mitochondrial membrane potential. The results showed that ABT-199 alone could not reduce the mitochondrial membrane potential of HepG2 cells, but the mitochondrial membrane potential decreased significantly after being combined with KPL.

3.7 The effects of KPL combined with ABT-199 on endogenous mitochondrial apoptosis pathway-related proteins in HepG2 cells

To further explore the molecular mechanism of KPL combined with ABT-199 against HCC, we have proceeded with the Western Blot technique. In this experiment, Mcl-1 inhibitor UMI-77 was used as the positive control. As shown in Figures 6A,B, when the HepG2 cells were treated with ABT-199 alone, there was no significant difference in the expression level of anti-apoptotic protein Mcl-1 compared with the negative control group; ABT-199 combined with UMI-77, an Mcl-1 inhibitor, also showed no significant difference in the expression of Mcl-1 compared with UMI-77 alone. The above results showed that ABT-199 could not directly inhibit the expression of Mcl-1. KPL alone and combined with ABT-199 could significantly inhibit the expression level of anti-apoptotic protein Mcl-1 (p < 0.001), and the inhibition intensity was similar to that of UMI-77 alone and UMI-77 combined with ABT-199. The findings from the present study also indicated that ABT-199 alone was insensitive to Mcl-1 and Bcl-xL in HepG2 cells. Interestingly, ABT-199 combined with KPL, compared with the negative control group, the expression of Bcl-2, including Mcl-1 and

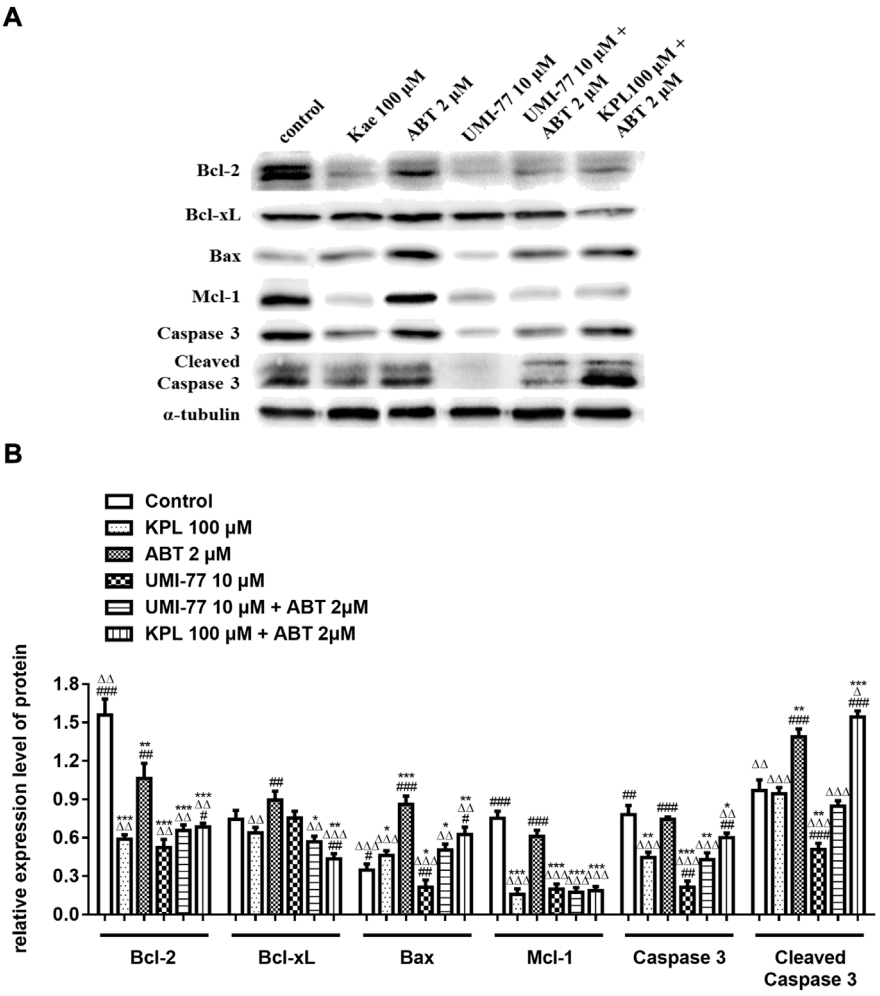

FIGURE 6
The effects of KPL combined with ABT-199 on caspase-3, cleaved caspase-3, Bcl-2, Bcl-xL, Bax and Mcl-1 proteins in HepG2 cells. **(A)** The expression levels of Bcl-2, Bcl-xL, Bax, Mcl-1, caspase 3 and cleaved caspase 3 were examined by western blotting analysis. α-tubulin was used as internal control. **(B)** The relative expression level of Bcl-2, Bcl-xL, Bax, Mcl-1, caspase-3 and cleaved caspase-3. α-tubulin was used as internal control. Relative expression of target protein = expression of target protein/expression of internal control protein. Values are means ± SD (n = 3). *$p < 0.05$, **$p < 0.01$, ***$p < 0.001$ *versus* negative control group; $^{\Delta\Delta\Delta}p<0.001$ *versus* ABT-199 alone group; $^{\#\#\#}p < 0.001$ *versus* KPL 100 μM group.

Bcl-xL, had decreased significantly ($p < 0.001$), indicating that KPL can enhance the inhibitory effect of ABT-199 on Bcl-2, Mcl-1 and Bcl-xL expression. It can also be observed from Figure 6 that compared with the negative control group, ABT-199 alone can significantly enhance the expression of Bax ($p < 0.001$), and even significantly greater than in ABT-199 combined with KPL. As reported in Figure 6, compared with the negative control group, there was no significant difference in the expression of caspase-3 when ABT-199 was applied alone ($p > 0.05$), but the expression of caspase-3 in other groups decreased significantly. Furthermore, as compared with the negative control group, KPL alone and UMI-77 combined with ABT-199 had no significant effect on the expression of cleaved caspase-3 after activation ($p > 0.05$), but ABT-199 alone and ABT-199 combined with KPL significantly increased the expression of cleaved caspase-3 ($p < 0.01$ or $p < 0.001$). ABT-199, as a selective Bcl-2 inhibitor, can cause apoptosis by interfering with the interaction among Bcl-2 proteins, subsequently promote Bax from cytoplasm to mitochondria, and mediate the release of cytochrome C from the mitochondria to cytoplasm. As shown in Figures 7A,B, in KPL alone (100 μM and 200 μM) treatment groups and KPL combined with ABT-199 treatment group, cytochrome C was released into the cytoplasm, therefore the expression of cytochrome C in mitochondria was reduced. It is interesting to note that the expression of cytochrome C in mitochondria of the combined treatment was less than that of KPL alone treatment, indicating that combined treatment can promote the release of cytochrome C into the cytoplasm. In addition, after treatment, the pro-apoptotic protein Bax was translocated to mitochondria, and its

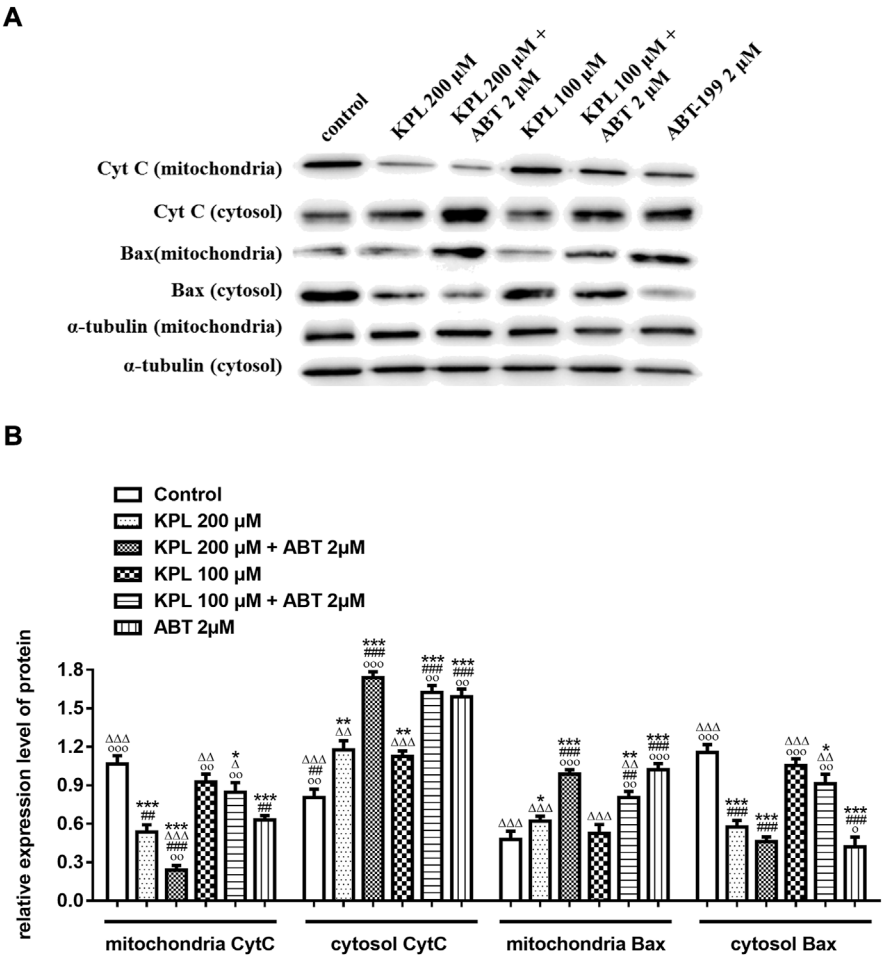

FIGURE 7
The effects of KPL combined with ABT-199 on cytochrome C release and Bax translocation in HepG2 cells were detected in mitochondria and cytoplasmic proteins by Western blot assay. **(A)** The expression levels of cytochrome C release and Bax in mitochondria and cytoplasmic were examined by western blotting analysis. α-tubulin was used as the internal control. **(B)** The relative expression levels of cytochrome C release and Bax in the mitochondria and the cytoplasm. α-tubulin was used as the internal control for relative expression of target.

expression in mitochondria increased, and the expression of Bax of combined treatment was more than that of KPL only treatment. Western blot results showed that the inhibitory effect of KPL combined with ABT-199 on the proliferation of hepatoma HepG2 cells may be related to KPL downregulating Mcl-1, thereby regulating the Bcl-2 protein family in the endogenous mitochondrial pathway of ABT-199 regulating apoptosis.

4 Discussion

In this study, we first evaluated the sensitization effects of KPL on HepG2 hepatoma cells for ABT-199. The results of CCK-8 method and colony formation assay indicated that treatment with ABT-199 alone did not affect the hepatoma cells, but in combination with KPL, it could significantly inhibit the proliferation and the colony forming ability of HepG2 cells. To further verify the sensitization effect of KPL on ABT-199 *in vivo*, the H22 liver cancer bearing mouse model was employed, evaluated *via* the weight and pathological sections of tumour tissue.

Apoptosis is an important biological phenomenon of eukaryotic cells. In tumour suppression therapy, inducing tumour cell apoptosis is an important therapeutic strategy. To study the mechanism of KPL on ABT-199-sensitized hepatocellular carcinoma, Hoechst 33342 staining and JC-1 staining were used to observe the effect of KPL combined with ABT-199 on apoptosis of HepG2 cells. The results of apoptosis showed that KPL combined with ABT-199 could promote the early and late apoptosis of HepG2 cells, suggesting that the inhibitory effect of KPL combined with ABT-199 on cell proliferation was related to the induction of

apoptosis. It was found that the apoptosis of different cell lines *via* varied factors was accompanied by the decline of mitochondrial membrane potential. The mitochondrial membrane potential began to decline before the pathological changes in the early stage of apoptosis, even earlier than DNA fragmentation (Salvioli et al., 2000). In this study, the JC-1 staining results showed that in the groups of combined medication, the red fluorescence intensity in mitochondria decreased significantly and the green fluorescence in cytoplasm increased significantly, indicating that JC-1 in mitochondria existed in the form of monomer, and the mitochondrial membrane potential was low (Zhao et al., 2018), demonstrating that the role of KPL in enhancing ABT-199 on inhibiting HepG2 cell proliferation and promoting apoptosis was related to the endogenous mitochondrial pathway.

When the cells were injured, the mitochondrial membrane potential decreased, and the membrane permeability increased. A series of apoptotic factors will be released, resulting in apoptosis. Bcl-2 family proteins are important proteins in the regulation of the apoptosis signaling pathway (REF), including the mitochondrial-mediated endogenous apoptosis pathway. The functions of the anti-apoptotic protein Bcl-2 and the pro-apoptotic protein Bax are diametrically opposed: Bcl-2 is a mitochondrial outer membrane protein, which can inhibit the release of cytochrome C with a pro-apoptotic effect from mitochondria to cytoplasm and then inhibit apoptosis (Naseri et al., 2015); anti-apoptotic protein Mcl-1 blocks the release of cytochrome C from mitochondria by interacting with pro-apoptotic factors of Bcl-2 protein family, such as Bim and Bak, so as to prevent cells from entering the process of apoptosis (Chen and Fletcher, 2017). Bax is a nuclear coding protein existing in advanced eukaryotes, which can be translocated to the outer membrane of mitochondria to mediate cell apoptosis. Bax itself can form a homodimer or heterodimer with Bcl-2. When Bcl-2 was highly expressed in cells, the heterodimer of Bcl-2 and Bax increased and the trend of apoptosis decreased; when Bax is highly expressed in cells, the homodimer formed by Bax itself is dominant, and it antagonizes the effect of Bcl-2, it will be prone to apoptosis (Oltvai et al., 1993; Naseri et al., 2015; Guo et al., 2018). Caspase is a cysteine aspartate specific protease that exists in the cytoplasm and plays an extremely key role in the process of apoptosis. Caspase-3 is located downstream of the cascade reaction. As a protein that cuts the cell structure, caspase-3 can directly cause cell apoptosis (Kirsch et al., 1999; Pisani et al., 2020). Caspase-3 activation is an important indicator for determining the state of cell apoptosis (Tyas et al., 2000; Brentnall et al., 2013; Nichani et al., 2020). When cells are stimulated by apoptosis signals or other harmful substances, caspase-3 will be activated into an active cleaved caspase-3. Cleaved caspase-3 participates in the process of cell apoptosis by cutting specific substrates, DNA dependent protein kinases, actin, lamin, *etc*. Therefore, the high expression of cleaved caspase-3 can induce tumour cell apoptosis, and it is one of the key proteins that promote cell apoptosis (Hou et al., 2015; Manning and Toker, 2017).

Studies have shown that Mcl-1, an important anti-apoptotic protein in the mitochondrial apoptotic pathway, is overexpressed in liver cancer cells and liver cancer stem cells (Zhang et al., 2019). The increased expression of Mcl-1 is also one of the potential mechanisms of ABT-199 resistance (Niu et al., 2016). Because of the binding of ABT-199 with Bcl-2, although it prevents the interaction between Bim and Bcl-2, free Bim will be bound by the anti-apoptotic protein Mcl-1, which then blocks the signal of apoptosis transmitted by Bim, thus hindering apoptosis (Niu et al., 2016; Conage-Pough and Boise, 2018). In the signal transduction of apoptosis, anti-apoptotic proteins Bcl-xL and Bcl-2 can be combined by apoptosis promoter protein Bid and factors with similar functions to cause cytochrome C outflow (Shamas-Din et al., 2013), which further activates caspase-3 and caspase-7 to execute apoptosis (Galluzzi et al., 2012). Bcl-xL is a protein encoded by Bcl-2-like 1 gene and a major member of the Bcl-2 family. In terms of anti-apoptosis, Bcl-xL is more potent than Bcl-2 and Mcl-1 (Fiebig et al., 2006; Chen et al., 2015), and overexpression of Bcl-xL can reduce apoptosis in cells (Fuchsluger et al., 2011). Therefore, the high expression of Bcl-xL in tumour cells suggests that it is related to tumour chemoresistance (Liu et al., 1999). ABT-199 has a strong inhibitory effect on Bcl-2 and can promote the apoptosis of tumour cells with high Bcl-2 expression. However, ABT-199 as a BH3-mimetic has a weak inhibitory effect on Mcl-1, Bcl-xL and Bcl-w (Cang et al., 2015; Luedtke et al., 2017), our experiment results also proved it. The western blot results indicated that KPL could downregulate the expression of Bcl-2, Mcl-1 and caspase 3, and upregulate the expression of Bax. On the other hand, ABT-199 could downregulate the expression of Bcl-2 and upregulate the expression of Bax and cleaved caspase-3. When the HepG2 cells were co-treated with KPL and ABT-199, the expression of Bcl-2, Mcl-1 and Bcl-xL were significantly downregulated, and the expression of Bax, caspase-3 and cleaved caspase-3 were upregulated. But from Figure 6 we can see that compared with the negative control group, ABT-199 alone can significantly enhance the expression of Bax, and even significantly greater than in ABT-199 combined with KPL. This may be related to ABT-199's ability to prevent the anti-apoptotic Bcl-2 from binding to pro-apoptotic Bax and Bak-1 proteins (Bordeleau et al., 2018). This also shows that, although ABT-199 can up-regulate the expression of Bax protein, the inhibition of ABT-199 on Mcl-1, Bcl-xL and Bcl-w is very weak, so from our experimental results, we can see that ABT-199 alone has little effect on the apoptosis of HepG2 cells with high expression of Mcl-1. KPL combined with ABT-199 could inhibit the expression of

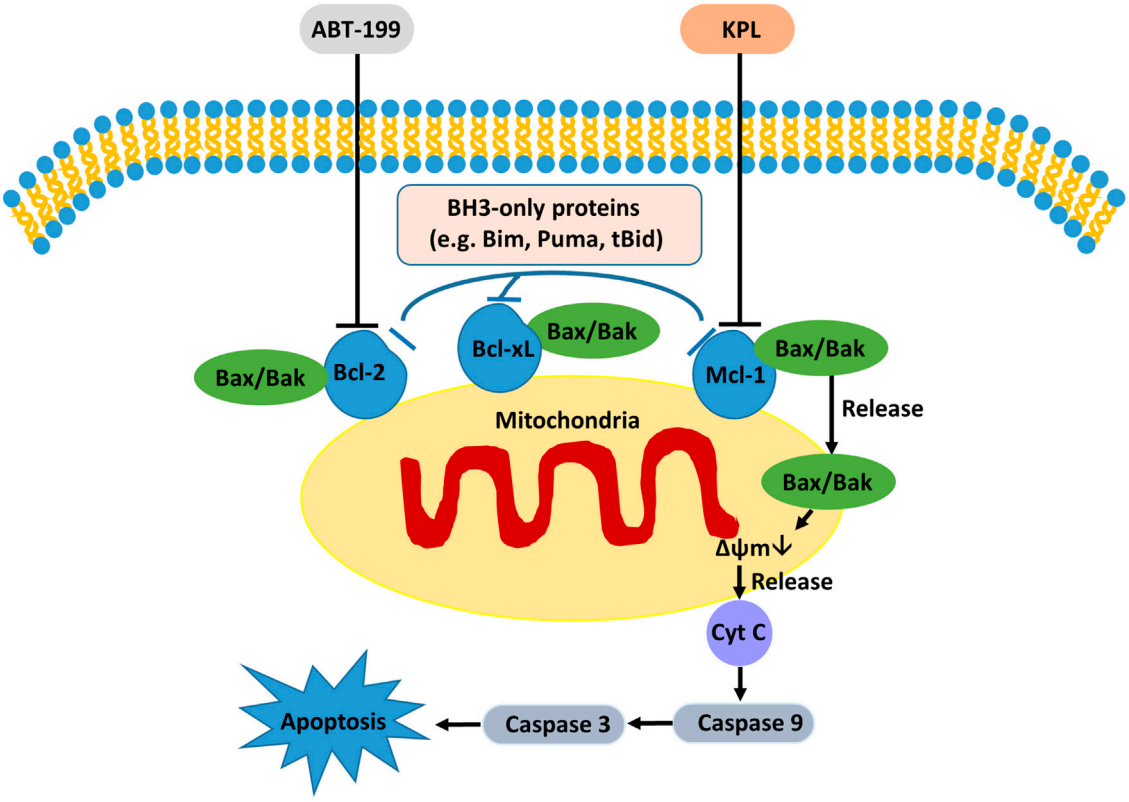

FIGURE 8
The possible molecular mechanism of KPL sensitizing ABT-199 against the proliferation of HepG2 cells.

Bcl-2, Bcl-xL and Mcl-1, change the conformation of Bax and move to the surface of mitochondria, form pores on the mitochondrial membrane, and then reduce the mitochondrial membrane potential, release the apoptotic factor cytochrome C to the cytoplasm, trigger the cascade reaction of the caspase family, activate the effector caspase 3, and lead to apoptosis. Therefore, KPL combined with ABT-199 had a mutual sensitization effect on the Bcl-2 proteins family in the endogenous mitochondrial pathway of apoptosis, thus inducing HepG2 hepatoma cells apoptosis. The molecular mechanism of KPL sensitising ABT-199 against HepG2 cells is shown in Figure 8.

5 Conclusion

In conclusion, KPL can enhance the sensitivity of ABT-199 to hepatoma cells, inhibit the proliferation of HepG2 cells and induce apoptosis. The anti-proliferation effect of KPL combined with ABT-199 may be related to the down-regulation of Mcl-1 by KPL, which enhances ABT-199 regulates the Bcl-2 protein family in the endogenous mitochondrial pathway of apoptosis. Therefore, KPL combined with ABT -199 has a potential application prospect in the treatment of hepatocellular carcinoma, and can be used as a new strategy for the treatment of hepatocellular carcinoma patients. At present, Mcl-1 expression is mainly through the activation of Janus kinase/signal transducer and activator of transcription (JAK/STAT) signal pathway, phosphatidylinositol 3-kinase (PI-3K) signal pathway, mitogen activated protein kinase (MAPK) signaling pathway plays a role (Booy et al., 2011; Chou et al., 2013). The present study has yet to examine the signaling pathway of KPL sensitized ABT-199 in down-regulating Mcl-1, which may be an interesting research topic in the future. Furthermore, similar pharmacological studies on ABT-199 and KPL combination therapy in other HCC cell lines should be conducted in the future to augment the findings in the current study, in order to provide a stronger basis for the translational potential in clinical setting.

Data availability statement

The raw data supporting the conclusion of this article will be made available by the authors, without undue reservation.

Ethics statement

The animal study was reviewed and approved by the Experimental Animals Committee at Guangxi University of Science and Technology.

Author contributions

Conceptualization, LC and ML; Methodology, LC, SG, YG, XJ, and XL; Formal Analysis, LC, SG, YG, XJ, and XL; Investigation, LC, SG, YG, and XL; Writing—Original Draft Preparation, LC.; Writing—Review and Editing, CT, AK, and ML; Supervision, CT and ML; Funding Acquisition, LC, CT, AK, and ML.

Funding

The study was supported by grants from the Natural Science Foundation of Guangxi, China (2016GXNSFBA380080), Fundamental Research Grant Scheme, Ministry of Higher Education, Malaysia (FRGS/1/2021/WAB13/UCSI/02/1 and FRGS/1/2018/SKK10/UPM/02/2) and UCSI University Research Excellence and Innovation Grant, Malaysia (REIG-FPS-2020/065 and REIG-FPS-2022/006).

Conflict of interest

The authors declare that the research was conducted in the absence of any commercial or financial relationships that could be construed as a potential conflict of interest.

Publisher's note

All claims expressed in this article are solely those of the authors and do not necessarily represent those of their affiliated organizations, or those of the publisher, the editors and the reviewers. Any product that may be evaluated in this article, or claim that may be made by its manufacturer, is not guaranteed or endorsed by the publisher.

References

Afroze, N., Pramodh, S., Almutary, A. G., Rizvi, T. A., Rais, N., Raina, R., et al. (2022). Kaempferol regresses carcinogenesis through a molecular cross talk involved in proliferation, apoptosis and inflammation on human cervical cancer cells, HeLa. *Appl. Sci.* 12, 3155. doi:10.3390/app12063155

Alsaif, G., Almosnid, N., Hawkins, I., Taylor, Z., Knott, D. L. T., Handy, S., et al. (2017). Evaluation of fourteen aurone derivatives as potential anti-cancer agents. *Curr. Pharm. Biotechnol.* 18, 384–390. doi:10.2174/1389201018666170502112303

Booy, E. P., Henson, E. S., and Gibson, S. B. (2011). Epidermal growth factor regulates Mcl-1 expression through the MAPK-Elk-1 signalling pathway contributing to cell survival in breast cancer. *Oncogene* 30, 2367–2378. doi:10.1038/onc.2010.616

Bordeleau, M. E., Bisaillon, R., Thiollier, C., Krosl, J., Lehnertz, B., Lavallee, V. P., et al. (2018). Genetic characterization of ABT-199 sensitivity in human AML. *Blood* 132 (1), 283. doi:10.1182/blood-2018-99-113062

Boshuizen, J., and Peeper, D. S. (2020). Rational cancer treatment combinations: An urgent clinical need. *Mol. Cell.* 78, 1002–1018. doi:10.1016/j.molcel.2020.05.031

Brentnall, M., Rodriguez-Menocal, L., De Guevara, R. L., Cepero, E., and Boise, L. H. (2013). Caspase-9, caspase-3 and caspase-7 have distinct roles during intrinsic apoptosis. *BMC Cell. Biol.* 14, 32. doi:10.1186/1471-2121-14-32

Cang, S., Iragavarapu, C., Savooji, J., Song, Y., and Liu, D. (2015). ABT-199 (venetoclax) and BCL-2 inhibitors in clinical development. *J. Hematol. Oncol.* 8, 129. doi:10.1186/s13045-015-0224-3

Chen, H. C., Kanai, M., Inoue-Yamauchi, A., Tu, H. C., Huang, Y., Ren, D., et al. (2015). An interconnected hierarchical model of cell death regulation by the BCL-2 family. *Nat. Cell. Biol.* 17, 1270–1281. doi:10.1038/ncb3236

Chen, L., and Fletcher, S. (2017). Mcl-1 inhibitors: A patent review. *Expert Opin. Ther. Pat.* 27, 163–178. doi:10.1080/13543776.2017.1249848

Chen, L., Guo, Y., Alsaif, G., and Gao, Y. (2020). Total flavonoids isolated from Diospyros kaki L. F. Leaves induced apoptosis and oxidative stress in human cancer cells. *Anticancer Res.* 40, 5201–5210. doi:10.21873/anticanres.14523

Chen, L., Wei, Y., Zhao, S., Zhang, M., Yan, X., Gao, X., et al. (2018). Antitumor and immunomodulatory activities of total flavonoids extract from persimmon leaves in H22 liver tumor-bearing mice. *Sci. Rep.* 8, 10523. doi:10.1038/s41598-018-28440-8

Chou, C. H., Lai, S. L., Chen, C. N., Lee, P. H., Peng, F. C., Kuo, M. L., et al. (2013). IL-6 regulates mcl-1L expression through the JAK/PI3K/akt/CREB signaling pathway in hepatocytes: Implication of an anti-apoptotic role during liver regeneration. *PLoS One* 8, e66268. doi:10.1371/journal.pone.0066268

Conage-Pough, J. E., and Boise, L. H. (2018). Phosphorylation alters Bim-mediated Mcl-1 stabilization and priming. *FEBS J.* 285, 2626–2640. doi:10.1111/febs.14505

Deeks, E. D. (2016). Venetoclax: First global approval. *Drugs* 76, 979–987. doi:10.1007/s40265-016-0596-x

Elmore, S. (2007). Apoptosis: A review of programmed cell death. *Toxicol. Pathol.* 35, 495–516. doi:10.1080/01926230701320337

Fiebig, A. A., Zhu, W., Hollerbach, C., Leber, B., and Andrews, D. W. (2006). Bcl-XL is qualitatively different from and ten times more effective than Bcl-2 when expressed in a breast cancer cell line. *BMC Cancer* 6, 213. doi:10.1186/1471-2407-6-213

Fleischer, B., Schulze-Bergkamen, H., Schuchmann, M., Weber, A., Biesterfeld, S., Muller, M., et al. (2006). Mcl-1 is an anti-apoptotic factor for human hepatocellular carcinoma. *Int. J. Oncol.* 28, 25–32. doi:10.3892/ijo.28.1.25

Fuchsluger, T. A., Jurkunas, U., Kazlauskas, A., and Dana, R. (2011). Anti-apoptotic gene therapy prolongs survival of corneal endothelial cells during storage. *Gene Ther.* 18, 778–787. doi:10.1038/gt.2011.20

Galluzzi, L., Kepp, O., Trojel-Hansen, C., and Kroemer, G. (2012). Mitochondrial control of cellular life, stress, and death. *Circ. Res.* 111, 1198–1207. doi:10.1161/CIRCRESAHA.112.268946

Guo, X. X., Li, X. P., Zhou, P., Li, D. Y., Lyu, X. T., Chen, Y., et al. (2018). Evodiamine induces apoptosis in SMMC-7721 and HepG2 cells by suppressing NOD1 signal pathway. *Int. J. Mol. Sci.* 19, E3419. doi:10.3390/ijms19113419

He, L. J., Yang, D. L., Chen, H. Y., Huang, J. H., Zhang, Y. J., Qin, H. X., et al. (2020). A novel imidazopyridine derivative exhibits anticancer activity in breast cancer by inhibiting wnt/β-catenin signaling. *Onco. Targets. Ther.* 13, 10111–10121. doi:10.2147/OTT.S266752

Hou, X., Tong, Q., Wang, W., Xiong, W., Shi, C., and Fang, J. (2015). Dihydromyricetin protects endothelial cells from hydrogen peroxide-induced oxidative stress damage by regulating mitochondrial pathways. *Life Sci.* 130, 38–46. doi:10.1016/j.lfs.2015.03.007

Huang, W., Tsai, S., Peng, S., Lin, M., Chiang, J., Chiu, Y., et al. (2013). Kaempferol induces autophagy through AMPK and AKT signaling molecules

and causes G2/M arrest via downregulation of CDK1/cyclin B in SK-HEP-1 human hepatic cancer cells. *Int. J. Oncol.* 42, 2069–2077. doi:10.3892/ijo.2013.1909

Imran, M., Salehi, B., Sharifi-Rad, J., Aslam Gondal, T., Saeed, F., Imran, A., et al. (2019). Kaempferol: A key emphasis to its anticancer potential. *Molecules* 24, E2277. doi:10.3390/molecules24122277

Itchaki, G., and Brown, J. R. (2016). The potential of venetoclax (ABT-199) in chronic lymphocytic leukemia. *Ther. Adv. Hematol.* 7, 270–287. doi:10.1177/2040620716655350

Kim, H. S., Suh, J. S., Jang, Y. K., Ahn, S. H., Raja, G., Kim, J. C., et al. (2020). Anti-cancer potential of persimmon (Diospyros kaki) leaves via the PDGFR-Rac-JNK pathway. *Sci. Rep.* 10, 18119. doi:10.1038/s41598-020-75140-3

Kim, K.-A., Lee, C. H., Kang, T. K., Yang, S. J., Lee, C. Y., Lee, W.-B., et al. (2020). Effect of persimmon leaves (Diospyros kaki) on goblet cell density and inflammation in experimental dry eye model. *Appl. Biol. Chem.* 63, 45. doi:10.1186/s13765-020-00529-7

Kirsch, D. G., Doseff, A., Chau, B. N., Lim, D. S., de Souza-Pinto, N. C., Hansford, R., et al. (1999). Caspase-3-dependent cleavage of Bcl-2 promotes release of cytochrome c. *J. Biol. Chem.* 274, 21155–21161. doi:10.1074/jbc.274.30.21155

Liu, C. Y., Chen, K. F., and Chen, P. J. (2015). Treatment of liver cancer. *Cold Spring Harb. Perspect. Med.* 5, a021535. doi:10.1101/cshperspect.a021535

Liu, L., Liu, R. L., Zhang, J., and Zhang, Z. Q. (2012). Study on the PEG-based microwave-assisted extraction of flavonoid compounds from persimmon leaves. *J. Sep. Sci.* 35, 3412–3420. doi:10.1002/jssc.201200495

Liu, R., Page, C., Beidler, D. R., Wicha, M. S., and Nunez, G. (1999). Overexpression of Bcl-x(L) promotes chemotherapy resistance of mammary tumors in a syngeneic mouse model. *Am. J. Pathol.* 155, 1861–1867. doi:10.1016/S0002-9440(10)65505-8

Luedtke, D. A., Niu, X., Pan, Y., Zhao, J., Liu, S., Edwards, H., et al. (2017). Inhibition of Mcl-1 enhances cell death induced by the Bcl-2-selective inhibitor ABT-199 in acute myeloid leukemia cells. *Signal Transduct. Target. Ther.* 2, 17012. doi:10.1038/sigtrans.2017.12

Manning, B. D., and Toker, A. (2017). AKT/PKB signaling: Navigating the network. *Cell.* 169, 381–405. doi:10.1016/j.cell.2017.04.001

Naseri, M. H., Mahdavi, M., Davoodi, J., Tackallou, S. H., Goudarzvand, M., and Neishabouri, S. H. (2015). Up regulation of Bax and down regulation of Bcl2 during 3-NC mediated apoptosis in human cancer cells. *Cancer Cell. Int.* 15, 55. doi:10.1186/s12935-015-0204-2

Nichani, K., Li, J., Suzuki, M., and Houston, J. P. (2020). Evaluation of caspase-3 activity during apoptosis with fluorescence lifetime-based cytometry measurements and phasor analyses. *Cytom. A* 97, 1265–1275. doi:10.1002/cyto.a.24207

Niu, X., Zhao, J., Ma, J., Xie, C., Edwards, H., Wang, G., et al. (2016). Binding of released Bim to mcl-1 is a mechanism of intrinsic resistance to ABT-199 which can be overcome by combination with daunorubicin or cytarabine in AML cells. *Clin. Cancer Res.* 22, 4440–4451. doi:10.1158/1078-0432.CCR-15-3057

Oltvai, Z. N., Milliman, C. L., and Korsmeyer, S. J. (1993). Bcl-2 heterodimerizes *in vivo* with a conserved homolog, Bax, that accelerates programmed cell death. *Cell.* 74, 609–619. doi:10.1016/0092-8674(93)90509-o

Pan, R., Hogdal, L. J., Benito, J. M., Bucci, D., Han, L., Borthakur, G., et al. (2014). Selective BCL-2 inhibition by ABT-199 causes on-target cell death in acute myeloid leukemia. *Cancer Discov.* 4, 362–375. doi:10.1158/2159-8290.CD-13-0609

Peirs, S., Matthijssens, F., Goossens, S., Van de Walle, I., Ruggero, K., de Bock, C. E., et al. (2014). ABT-199 mediated inhibition of BCL-2 as a novel therapeutic strategy in T-cell acute lymphoblastic leukemia. *Blood* 124, 3738–3747. doi:10.1182/blood-2014-05-574566

Pisani, C., Ramella, M., Boldorini, R., Loi, G., Billia, M., Boccafoschi, F., et al. (2020). Apoptotic and predictive factors by Bax, Caspases 3/9, Bcl-2, p53 and Ki-67 in prostate cancer after 12 Gy single-dose. *Sci. Rep.* 10, 7050. doi:10.1038/s41598-020-64062-9

Qian, X., Zheng, H., Xue, K., Chen, Z., Hu, Z., Zhang, L., et al. (2021). Recurrence risk of liver cancer post-hepatectomy using machine learning and study of correlation with immune infiltration. *Front. Genet.* 12, 733654. doi:10.3389/fgene.2021.733654

Salvioli, S., Dobrucki, J., Moretti, L., Troiano, L., Fernandez, M. G., Pinti, M., et al. (2000). Mitochondrial heterogeneity during staurosporine-induced apoptosis in HL60 cells: Analysis at the single cell and single organelle level. *Cytometry* 40, 189–197. doi:10.1002/1097-0320(20000701)40:3<189::aid-cyto3>3.0.co;2-6

Shamas-Din, A., Kale, J., Leber, B., and Andrews, D. W. (2013). Mechanisms of action of Bcl-2 family proteins. *Cold Spring Harb. Perspect. Biol.* 5, a008714. doi:10.1101/cshperspect.a008714

Sharma, N., Biswas, S., Al-Dayan, N., Alhegaili, A. S., and Sarwat, M. (2021). Antioxidant role of kaempferol in prevention of hepatocellular carcinoma. *Antioxidants (Basel)* 10, 1419. doi:10.3390/antiox10091419

Shi, Y., Ye, J., Yang, Y., Zhao, Y., Shen, H., Ye, X., et al. (2021). The basic research of the combinatorial therapy of ABT-199 and homoharringtonine on acute myeloid leukemia. *Front. Oncol.* 11, 692497. doi:10.3389/fonc.2021.692497

Siegel, R. L., Miller, K. D., and Jemal, A. (2018). Cancer statistics, 2018. *Ca. Cancer J. Clin.* 68, 7–30. doi:10.3322/caac.21442

Sieghart, W., Losert, D., Strommer, S., Cejka, D., Schmid, K., Rasoul-Rockenschaub, S., et al. (2006). Mcl-1 overexpression in hepatocellular carcinoma: A potential target for antisense therapy. *J. Hepatol.* 44, 151–157. doi:10.1016/j.jhep.2005.09.010

Souers, A. J., Leverson, J. D., Boghaert, E. R., Ackler, S. L., Catron, N. D., Chen, J., et al. (2013). ABT-199, a potent and selective BCL-2 inhibitor, achieves antitumor activity while sparing platelets. *Nat. Med.* 19, 202–208. doi:10.1038/nm.3048

Tyas, L., Brophy, V. A., Pope, A., Rivett, A. J., and Tavare, J. M. (2000). Rapid caspase-3 activation during apoptosis revealed using fluorescence-resonance energy transfer. *EMBO Rep.* 1, 266–270. doi:10.1093/embo-reports/kvd050

Vaillant, F., Merino, D., Lee, L., Breslin, K., Pal, B., Ritchie, M. E., et al. (2013). Targeting BCL-2 with the BH3 mimetic ABT-199 in estrogen receptor-positive breast cancer. *Cancer Cell.* 24, 120–129. doi:10.1016/j.ccr.2013.06.002

Wang, X. N., Yang, Y. T., An, Y. T., and Fang, G. (2019). The mechanism of anticancer action and potential clinical use of kaempferol in the treatment of breast cancer. *Biome Pharmacother.* 117, 109086. doi:10.1016/j.biopha.2019.109086

Weller, S., Toenniessen, A., Schaefer, B., Beigl, T., Muenchow, A., Bopple, K., et al. (2022). The BCL-2 inhibitor ABT-199/venetoclax synergizes with proteasome inhibition via transactivation of the MCL-1 antagonist NOXA. *Cell. Death Discov.* 8, 215. doi:10.1038/s41420-022-01009-1

Xie, C., Xie, Z., Xu, X., and Yang, D. (2015). Persimmon (Diospyros kaki L.) leaves: A review on traditional uses, phytochemistry and pharmacological properties. *J. Ethnopharmacol.* 163, 229–240. doi:10.1016/j.jep.2015.01.007

Yu, Q., Liu, Z. Y., Chen, Q., and Lin, J. S. (2016). Mcl-1 as a potential therapeutic target for human hepatocelluar carcinoma. *J. Huazhong Univ. Sci. Technol. Med. Sci.* 36, 494–500. doi:10.1007/s11596-016-1614-7

Zamora-Ros, R., Fedirko, V., Trichopoulou, A., González, C. A., Bamia, C., Trepo, E., et al. (2013). Dietary flavonoid, lignan and antioxidant capacity and risk of hepatocellular carcinoma in the European prospective investigation into cancer and nutrition study. *Int. J. Cancer* 133, 2429–2443. doi:10.1002/ijc.28257

Zhang, H., Li, G., Chen, G., Zhang, Y., Pan, J., Tang, H., et al. (2019). Targeting Mcl-1 inhibits survival and self-renewal of hepatocellular cancer stem-like cells. *Clin. Res. Hepatol. Gastroenterol.* 43, 292–300. doi:10.1016/j.clinre.2018.11.004

Zhang, Y. M., Chen, J. Q., Fang, W. X., Liang, K. Y., Li, X. N., Zhang, F., et al. (2022). Kaempferol suppresses androgen-dependent and androgen-independent prostate cancer by regulating Ki67 expression. *Mol. Biol. Rep.* 49, 4607–4617. doi:10.1007/s11033-022-07307-2

Zhao, M. X., Cai, Z. C., Zhu, B. J., and Zhang, Z. Q. (2018). The apoptosis effect on liver cancer cells of gold nanoparticles modified with lithocholic acid. *Nanoscale Res. Lett.* 13, 304. doi:10.1186/s11671-018-2653-8

Zhu, G., Liu, X., Li, H., Yan, Y., Hong, X., and Lin, Z. (2018). Kaempferol inhibits proliferation, migration, and invasion of liver cancer HepG2 cells by down-regulation of microRNA-21. *Int. J. Immunopathol. Pharmacol.* 32, 2058738418814341–12. doi:10.1177/2058738418814341

Zhu, L., and Xue, L. (2019). Kaempferol suppresses proliferation and induces cell cycle arrest, apoptosis, and DNA damage in breast cancer cells. *Oncol. Res.* 27, 629–634. doi:10.3727/096504018X15228018559434

frontiers | Frontiers in Oncology

TYPE Original Research
PUBLISHED 10 November 2022
DOI 10.3389/fonc.2022.1068443

OPEN ACCESS

EDITED BY
Eswar Shankar,
The Ohio State University,
United States

REVIEWED BY
Prem P. Kushwaha,
Case Western Reserve University,
United States
Kate Ormiston,
The Ohio State University,
United States

*CORRESPONDENCE
Wei Zheng
wzheng@mail.nih.gov

SPECIALTY SECTION
This article was submitted to Pharmacology of Anti-Cancer Drugs, a section of the journal Frontiers in Oncology

RECEIVED 12 October 2022
ACCEPTED 25 October 2022
PUBLISHED 10 November 2022

CITATION
Huang W, Yang S, Cheng Y-S, Sima N, Sun W, Shen M, Braisted JC, Lu W and Zheng W (2022) Terfenadine resensitizes doxorubicin activity in drug-resistant ovarian cancer cells *via* an inhibition of CaMKII/CREB1 mediated ABCB1 expression. *Front. Oncol.* 12:1068443. doi: 10.3389/fonc.2022.1068443

Terfenadine resensitizes doxorubicin activity in drug-resistant ovarian cancer cells *via* an inhibition of CaMKII/CREB1 mediated ABCB1 expression

Wei Huang[1,2], Shu Yang[2], Yu-Shan Cheng[2], Ni Sima[1], Wei Sun[2], Min Shen[2], John C. Braisted[2], Weiguo Lu[1,3] and Wei Zheng[2]*

[1]Women's Hospital, School of Medicine, Zhejiang University, Hangzhou, China, [2]National Center for Advancing Translational Sciences (NCATS), National Institutes of Health (NIH), Bethesda, MD, United States, [3]Women's Reproductive Health Research Laboratory of Zhejiang Province, Women's Hospital, School of Medicine, Zhejiang University, Hangzhou, China

Ovarian cancer is one of the most lethal gynecological malignancies. Recurrence or acquired chemoresistance is the leading cause of ovarian cancer therapy failure. Overexpression of ATP-binding cassette subfamily B member 1 (ABCB1), commonly known as P-glycoprotein, correlates closely with multidrug resistance (MDR). However, the mechanism underlying aberrant ABCB1 expression remains unknown. Using a quantitative high-throughput combinational screen, we identified that terfenadine restored doxorubicin sensitivity in an MDR ovarian cancer cell line. In addition, RNA-seq data revealed that the Ca2+-mediated signaling pathway in the MDR cells was abnormally regulated. Moreover, our research demonstrated that terfenadine directly bound to CAMKIID to prevent its autophosphorylation and inhibit the activation of the cAMP-responsive element-binding protein 1 (CREB1)-mediated pathway. Direct inhibition of CAMKII or CREB1 had the same phenotypic effects as terfenadine in the combined treatment, including lower expression of ABCB1 and baculoviral IAP repeat-containing 5 (BIRC5, also known as survivin) and increased doxorubicin-induced apoptosis. In this study, we demonstrate that aberrant regulation of the Ca2+-mediated CAMKIID/CREB1 pathway contributes to ABCB1 over-expression and MDR creation and that CAMKIID and CREB1 are attractive targets for restoring doxorubicin efficacy in ABCB1-mediated MDR ovarian cancer.

KEYWORDS

drug-resistant, ovarian cancer, terfenadine, CaMKII, doxorubicin

Introduction

Ovarian cancer is one of the worst cancers and the major cause of mortality among gynecologic tumors (1). Due to the absence of clear early-stage symptoms, more than 75% of ovarian cancer patients are diagnosed at an advanced stage, with a 5-year survival rate of 20% (2–4). Currently, debulking surgery followed by chemotherapy is the usual treatment for ovarian cancer in an advanced stage (5). However, the development of tumor resistance during treatment is common and poses challenges in ovarian cancer therapy (6, 7). Indeed, over 80% of cases respond to first-line treatment, yet 70% of patients experience cancer recurrence within the first three years (8).

Overexpression of ATP binding cassette subfamily B member 1 (ABCB1) is a well-known molecular mechanism responsible for multidrug resistance (MDR) in malignancies such as ovarian cancer (6, 9, 10). ABCB1, also known as P-glycoprotein 1 (P-gp), is an ATP-driven efflux transporter that pumps substrates from cells. To protect organs from toxins, it is abundantly distributed in the blood-brain barrier, placenta, kidneys, and intestines (11). Numerous anticancer medicines, including doxorubicin, vincristine, paclitaxel, anthracyclines, and taxanes, are ABCB1 substrates (10, 11). Hence, overexpression of ABCB1 in cancer cells decreases intracellular concentrations of these drugs and produces MDR (12). Since co-administration of an effective ABCB1 modulator with anticancer drugs was deemed to be a viable strategy for overcoming ABCB1-mediated MDR malignancies, efforts have been made to generate ABCB1 inhibitors in the past few decades. Despite the fact that numerous ABCB1 inhibitors have been developed, their clinical translation has been limited due to their low binding affinities, excessive toxicity, or non-specificity (13, 14), indicating the need for new ABCB1 transporter inhibitors or strategies to overcome the MDR caused by ABCB1 overexpression.

Terfenadine is a histamine receptor H1 (HRH1) antagonist that was once employed to treat allergy disorders. Recent studies have demonstrated that terfenadine inhibits cell growth and induces apoptosis in neoplastic mast cells, melanoma cells, and breast cells *via* altering intracellular calcium homeostasis, caspase activation, and the mitochondrial pathway (15–19). Moreover, a synergistic effect of terfenadine and anticancer drugs has been demonstrated in the treatment of breast cancer and lung cancer (20, 21). However, it is unknown how terfenadine functions in this combinational therapy. Intriguingly, terfenadine has been related to a decrease in calcium influx caused by L-type calcium channels (LTCC) activation in rat and human cells (22, 23), showing terfenadine can regulate intracellular calcium homeostasis. Calcium works as a second messenger in cells to activate the downstream RNA polymerase to trigger gene transcription, which is involved in various cellular processes, such as cell division, proliferation, *etc.* (24, 25). Ca^{2+} signaling alterations are linked to carcinogenesis, tumor development, and metastasis (26). Moreover, it has been found that calcium signaling is connected with drug resistance. Activation of transient receptor potential channels, for instance, is associated with chemoresistance in a number of malignancies (27).

In this work, using quantitative high-throughput combinational screening (qHTCS), we found that terfenadine reverses doxorubicin resistance in MDR ovarian cancer cells. In addition, we demonstrate that terfenadine interacts directly with calcium/calmodulin dependent protein kinase II delta (CAMK2D) and inhibits the subsequent ectopic activation of the CAMK2/cAMP responsive element binding protein 1 (CREB1) pathway in an ABCB1-mediated MDR ovarian cancer line, A2780-ADR. In fact, either the CAMK2 or CREB1 inhibitor resensitizes doxorubicin-resistant ovarian cancer cells, showing that the CAMK2/CREB1 pathway is a suitable target pathway for future therapeutic development.

Materials and methods

Compounds and antibodies

Terfenadine was purchased from Sigma-Aldrich (catalog number: T9625). Topotecan, paclitaxel, KN62, and KN93 were obtained from Selleck Chemicals (catalog number: S1231, S1150, S7422, and S7423). Rhodamine 123 was purchased from MedChemExpress (catalog number: HY-D0186) Antibodies used in experiments are listed in Table S1.

Cell culture

All the human ovarian cancer cell lines were purchased from Sigma-Aldrich. Cells were cultured in RPMI 1640 medium with 10% fetal bovine serum (FBS) and 100 U/mL penicillin-streptomycin at 37°C with 5% CO_2.

Quantitative high-throughput combinational screening

ATP content assay (Promega) was conducted according to the manufacture's protocols. Briefly, A2780-ADR cells were plated at 500 cells/well in 5 μL of RPMI 1640 medium with 10% FBS and 100 U/mL penicillin-streptomycin in white, solid-bottom 1,536-well plates and incubated 4 h at 37°C. Four concentrations of compounds from the library of pharmacologically active compounds (LOPAC, Sigma-Aldrich) consists of 1,280 small molecules, the NIH Chemical Genomics Center Pharmaceutical (NPC) collection with 4,265 compounds (28), as well as the Mechanism Interrogation Plate (MIPE) with 1,920 compounds were added to assay plates at 23 nL/well using a pintool station (WAKO Scientific Solutions, San Diego, CA).

After a 72-h incubation at 37°C with 5% CO_2, the mixture of ATP LITE assay reagents was added to the assay plates at 5 μL/well. After incubation for the indicated time, the luminescence signal in the plates were detected using a ViewLux plate reader (PerkinElmer).

Rhodamine123 accumulation assay

A2780-ADR cells were seeded onto 96-well plates at a density of 5,000 cells/well. The cells were pretreated with 2.5 to 10 μM terfenadine for different time. After pretreatment, the cells were incubated with 5 μM Rhodamine123 (Rh123) in culture medium and kept in the dark at 37°C with 5% CO_2 for 60 min. Plates were then washed twice with pre-warmed PBS, filled with 100 μl/well PBS, and measured using a Tecan reader at 485 nm excitation and 535 nm emission.

Caspase activity assay and ATP content cell viability assay

Caspase-3/7 activity assay (Caspase-Glo, Promega) and ATP content cell viability assay (CellTiter-Glo, Promega) were conducted according to the manufactures' protocols. Ovarian cancer cells were plated at 3,000 to 5,000 cells/well in 100 μL of complete culture medium in white, solid-bottom 96-well plates and incubated overnight at 37°C with 5% CO_2. Compounds were added to the assay plates at indicated concentrations at 100 μL/well diluted in medium. After a 24 h (caspase 3/7 assay and ATP content cell viability assay) incubation at 37°C with 5% CO_2, the mixtures of assay reagents at 100 μL/well were added to the assay plates. After incubation for the indicated times from the protocols, the luminescence signal in assays plates were detected in a ViewLux plate reader.

RNA-sequencing analysis

RNA-sequencing analysis of A2780 and A2780-ADR was performed by Q2 Solutions as previously described (29, 30). RNA was isolated by Qiagen miRNeasy Mini Kit. cDNA libraries were generated using Illumina TruSeq Stranded mRNA sample preparation kit (Illumina # RS-122-2103). Read counts of each sample were normalized with DESeq and ran a negative binomial two sample test to find significant genes in higher transcript abundance in either sample. RNA sequencing data have been deposited in Gene Expression Omnibus (GEO) under accession number GSE177038.

Western blotting

Cells were lysed in RIPA buffer (Cell Signaling Technology) supplemented with protease inhibitors (cOmplete ULTRA Tablets, EDTA-free, Roche) and phosphatase inhibitor cocktail (PhosSTOP, Roche). The cell lysates were centrifuged at 16,000 rpm for 30 min. Supernatant was collected for protein quantitation with a BCA assay kit (Pierce BCA Protein Assay Kit, Thermo Fisher Scientific). The supernatant with similar protein concentrations were subsequently applied to Bis-Tris or Tris-Acetate gels for protein separation. Proteins were transferred to polyvinylidene difluoride (PVDF) membrane by dry transfer (iBlot 2 Gel Transfer Device, both from Thermo Fisher Scientific) or tank wet transfer. Immunoblot analysis was performed with indicated antibodies and the chemiluminescence signal was visualized with Luminata Forte Western HRP substrate (EMD Millipore) in a BioSpectrum system (UVP, LLC). The chemiluminescence intensity of the band was calculated in the VisionWorks LS software (UVP, LLC).

Cellular thermal shift assay

CETSA was performed as previously described (31). A2780-ADR cells were harvested, rinsed with PBS, and re-suspended in detergent-free buffer (25 mM HEPES pH 7.0, 20 mM $MgCl_2$, 2 mM DTT) supplemented with protease inhibitors and phosphatase inhibitor cocktail. The cell suspensions were lysed *via* three freeze-thaw cycles with liquid nitrogen. The cell lysates were centrifuged at 16,000 rpm for 20 min at 4 °C to pellet the cell debris from the soluble fraction. The soluble portion were diluted in detergent-free buffer and divided into two aliquots, with or without 600 μM terfenadine treatment. After 60 min incubation at room temperature, each sample was divided into 12 small aliquots in 50 μL/tube and individually heated at different temperatures (37 to 70 °C with 3 °C interval) for 3 min in a thermal cycler (Eppendorf), followed by immediate 3 min cooling cycle on ice. The heated samples were centrifuged at 20,000 × g for 20 min at 4 °C to remove the precipitates from the soluble fractions. The supernatant was examined by western blotting with CAMKII antibody. The relative chemiluminescence intensity of each sample at different temperatures was used to plot the temperature dependent melting curve. The apparent aggregation temperature (T_{agg}) was calculated by nonlinear regression. The statistically significance between two curves were analyzed by extra sum-of-squares F test. All data represent mean ± SEM of at least 3 replicates.

Data analysis

The primary screen data were analyzed using customized software developed internally (32). All data from the cell-based assays were presented as the mean ± standard error of the mean (SEM) with at least three independent experiments unless otherwise stated. Half maximal inhibitory concentrations (IC_{50}) of doxorubicin or compounds were calculated using Prism software (version 7, GraphPad Software, San Diego, CA). All imaging data are presented as the mean ± SEM and represent data from cells in at least 10 fields from three or more independent experiments. The two-tailed unpaired Student's test of the mean was used for single comparisons of statistical significance between experimental groups. One-way analysis of variance (ANOVA) with Bonferroni test was used for multiple comparisons. Bliss independence with Prism or SynergyFinder (33) was used to define synergistic or additive effects.

Results

Terfenadine restores doxorubicin activity to MDR ovarian cancer cells

To explore potential novel therapies for ABCB1-mediated MDR ovarian cancer cases in the clinic, we conducted a qHTCS against an ABCB1-overexpressing MDR ovarian cancer cell line, A2780-ADR. Compared to the parental A2780 cells, the A2780-ADR cells exhibited a higher expression and overall activity of ABCB1, as demonstrated by a considerable rise in protein level in Western blot detection and a significantly reduced cellular accumulation of Rho123, an ABCB1 substrate (Figures 1A, B and Figure S1A). The IC_{50} values of three ABCB1 substrates (doxorubicin, topotecan, and paclitaxel) for the A2780-ADR cells were 7.08 uM, 0.0081 uM, and 0.88 uM, which were

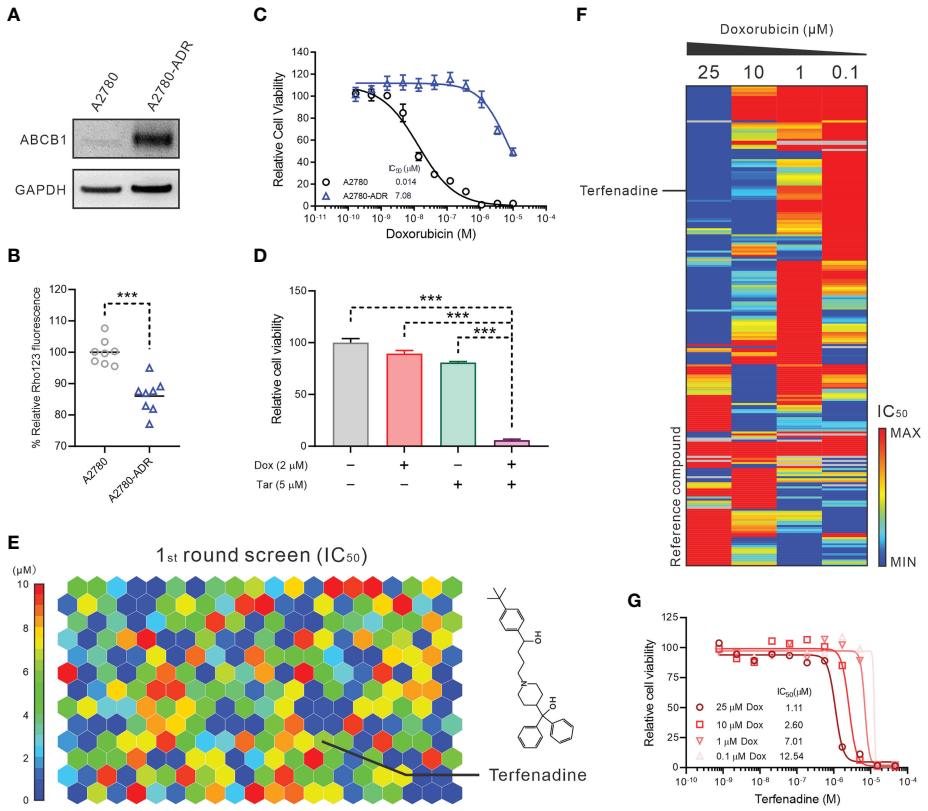

FIGURE 1
Terfenadine restores the activity of doxorubicin in MDR ovarian cancer cells. **(A)** Western blot analysis of ABCB1 in multidrug resistance (MDR) ovarian cancer cells A2780-ADR and its parental cell A2780. A representative image was shown here. **(B)** Rho123 accumulation in A2780-ADR and its parental cell A2780. **(C)** Dose-response curves of doxorubicin in MDR ovarian cancer cells A2780-ADR and its parental cell A2780. **(D)** Cell viability of MDR ovarian cancer cells A2780-ADR treated with 2 μM doxorubicin (Dox), 5 μM tariquidar (Tar), or both for 48 hours. DMSO was used as a non-treated control. **(E)** The heatmap shows 246 compounds were identified that efficiently inhibited the proliferation of A2780-ADR cells as monotherapy in the first round of screening. The color represents the IC_{50} of each compound, as the scale bar showed. **(F)** The heatmap shows enrichment of A2780-ADR for a strong response to specific drug categories (columns) combined with doxorubicin (rows). Drug-category-response scores are based on IC_{50} (μM). **(G)** A2780-ADR dose-response curves to terfenadine in the presence of 0.1, 1, 10, and 25 μM doxorubicin (Dox). Statistical analysis was performed using a two-tailed t-test. ***p<0.001.

significantly higher than 14 nM, 0.95 nM, and 0.0016 nM, respectively, for the A2780 cells (Figure 1C and Figures S1B, C). In the presence of tariquidar, a specific ABCB1 inhibitor, their anticancer effectiveness against A2780-ADR cells also increased (34) (Figure 1D and Figures S1D–F).

The qHTCS was performed in two stages. In the first stage, we examined 6,016 pharmacologically active compounds as single drugs at five doses in a luminescent cell viability assay to narrow down the compound pairs. 246 compounds were found that effectively inhibit the proliferation of A2780-ADR cells with an IC_{50} < 10 μM (Figure 1E). To further identify compounds that showed combination effects with doxorubicin, these 246 compounds were evaluated at 11 concentrations in combination with four doxorubicin concentrations at 0.1, 1, 10, and 25 μM, separately. Consequently, 24 compounds were identified as doxorubicin synergistic compounds in A2780-ASR cells, as indicated by the decreasing IC_{50} of each drug as the doxorubicin dose rose (Figure 1F and Table S2). Terfenadine was selected for further investigation (Figure 1G) since the mechanism of terfenadine and doxorubicin combination is unknown and terfenadine's anticancer activity has been described (15, 16).

Terfenadine resensitizes doxorubicin-induced apoptosis in MDR ovarian cancer cells

With an IC_{50} of 4.8 μM, the inhibitory activity of terfenadine as a single agent was confirmed in MDR A2780-ADR cells (Figure 2A). As evidenced by the shifted toxicity curve in MDR cells, the combined treatment significantly decreased the IC_{50} of doxorubicin in a dose-dependent manner, indicating the potential synergistic effect of these two drugs (Figure 2B).

To quantify these enhanced anticancer effects, we computed the combinational index (CI) (CI<1, synergism; CI=1, additive; CI>1, antagonism) (35). The mean CI value was 0.35, showing that the interaction in A2780-ADR cells is synergistic (Figure 2C). To further evaluate the synergism and determine the best synergistic concentration, effects were investigated using a dose-response matrix and analyzed using the zero interaction potency (ZIP) model (33, 36). As a result, terfenadine exhibited a synergistic effect with doxorubicin. The average ZIP synergy scores for A2780 cells and A2780-ADR cells were 2.874 and 4.403, respectively (Figures 2D, E). Notably, in resistant cells, the synergy score reached 49.80 when resistant cells were treated with 3.33 μM terfenadine and 1.11 μM doxorubicin, which was higher than the highest score of 22.39 in sensitive cells, showing a greater synergistic effect in MDR cells than in their parental cells, indicating that terfenadine will target the abnormally activated pathway associated with ABCB1 overexpression in MDR cells. In addition, the combination therapy lowered cell counts in a nuclear staining-based counting assay (Figure 2F), enhanced caspase-3/7 activity (Figure 2G), and promoted PARP cleavage (Figure 2H and Figure S2A), suggesting that the A2780-ADR cells were induced to undergo apoptosis. During the expanded testing, terfenadine had a comparable effect on the toxicity of paclitaxel and topotecan for A2780-ADR cells (Figures S2B, C).

Neither hERG nor H1R were the functional targets of terfenadine in the combination

To investigate the mechanism underlying this synergistic effect, we first examined two conventional terfenadine targets: the histamine H1 receptor (H1R) (37) and the human ether-a-go-go-related gene (hERG) channel (38). Terfenadine was reported as an antagonist of the H1R and is a prodrug that is converted to fexofenadine in the liver (37). Nevertheless, it was withdrawn from the market due to its ability to inhibit the hERG channel (38). The dose-response curve for doxorubicin as monotherapy was nearly comparable to the dose-response curve for doxorubicin in conjunction with the H1R-specific inhibitor fexofenadine (39) (Figure 3A). The CI for doxorubicin and fexofenadine was 0.9819, showing that their effect was additive, not synergistic (Figures 3A, B). In a second attempt, tannic acid (TA), a blocker of the hERG channel, was recruited (40). Even while TA decreased cell viability at higher concentrations, the dose-response curve for the combined therapy was similar to that of the doxorubicin treatment alone (Figure 3C). The CI value for the combination of doxorubicin and TA was 1.1867, showing that there was no synergy between the two drugs (Figures 3C, D). In addition, western blot revealed no difference in H1R and KCNH2 protein expression between A2780 and A2780-ADR cells, indicating that these proteins are not essential for MDR development (Figure 3E and Figure S3). These findings indicated that the synergistic effect of terfenadine and doxorubicin was not the result of terfenadine inhibiting the H1R or the hERG channel.

Terfenadine increased the intracellular accumulation of doxorubicin in MDR ovarian cancer cells by repressing ABCB1

We questioned whether terfenadine impacts the expression or function of ABCB1 in these MDR ovarian cancer cells, as ABCB1 overexpression was essential for the chemoresistance of A2780-ADR. Indeed, terfenadine decreased the expression of the ABCB1 protein in a dose-dependent manner (Figure 3F and Figure S4A). The reduction of ABCB1 was also found following doxorubicin and terfenadine treatment (Figure 3G and Figure S4B). In addition, in the ABCB1 activity experiment, terfenadine boosted Rho123 accumulation dose-dependently, indicating the decreased cellular ABCB1 activity. The Rho123 signal achieved a plateau when the concentration exceeded 5 μM (Figure 3H). In a time-

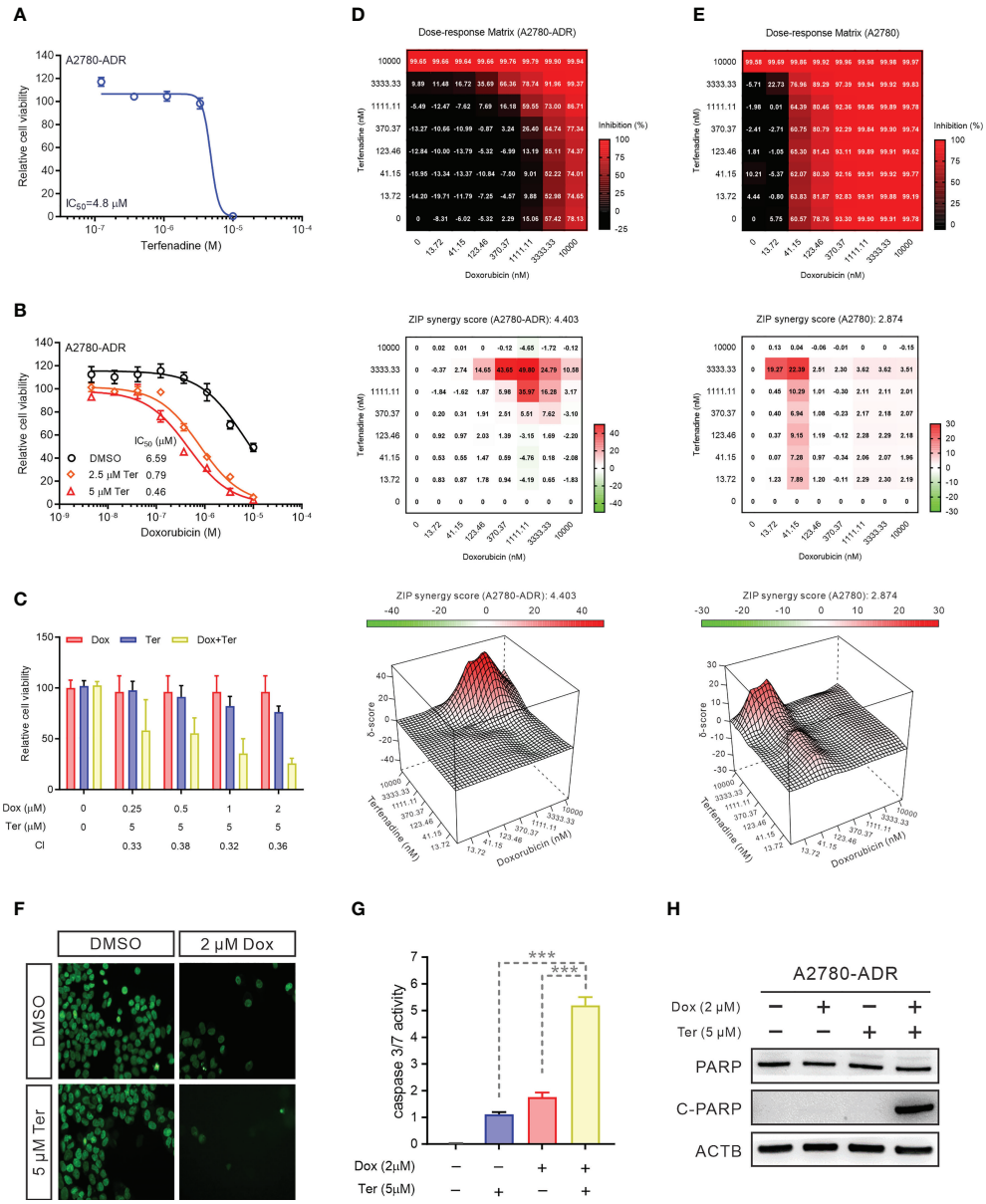

FIGURE 2
Terfenadine restores doxorubicin-induced apoptosis in MDR ovarian cancer cells **(A)** Terfenadine dose-response curves of MDR ovarian cancer cells. **(B)** Dose-response curves for doxorubicin in MDR ovarian cancer cells in the absence or presence of terfenadine (Ter). **(C)** A Bar graph showing the synergistic effects of terfenadine (Ter) and doxorubicin (Dox) on MDR ovarian cancer cells. Calculated CI values are presented below the plots. **(D, E)** Synergy matrixes (bottom) and surface plots (top) show the synergy between doxorubicin and terfenadine on A2780 **(D)** and A2780-ADR **(E)** cells (n = 3). **(F)** Nuclear staining of MDR ovarian cancer cells treated with the indicated concentration of doxorubicin (Dox), terfenadine (Ter) or both. DMSO was used as a non-treated control. **(G)** Caspase3/7 activity in MDR ovarian cancer cells treated with the indicated concentration of doxorubicin (Dox), terfenadine (Ter) or both. DMSO was used as a non-treated control. **(H)** Western blot analysis of PARP in MDR ovarian cancer cells after treated with 2 μM doxorubicin (Dox), 5 μM terfenadine (Ter), or both for 24 h. ACTB was used as the loading control. All values represent the mean ± SEM (n = 3 replicates). Western blot images were shown as one of three repeated experiments. Statistical analysis was performed using two tailed t-test (*** $p < 0.001$).

course study, the intracellular level of Rho123 continued to increase until terfenadine-induced apoptosis occurred (Figure 3I). Moreover, combination treatment significantly enhanced doxorubicin levels in A2780-ADR cells (Figures 3J, K). These findings imply that terfenadine decreased the expression and activity of the multidrug efflux pump ABCB1 in A2780-ADR cells, which resulted in the accumulation of doxorubicin and apoptosis.

10.3389/fonc.2022.1068443

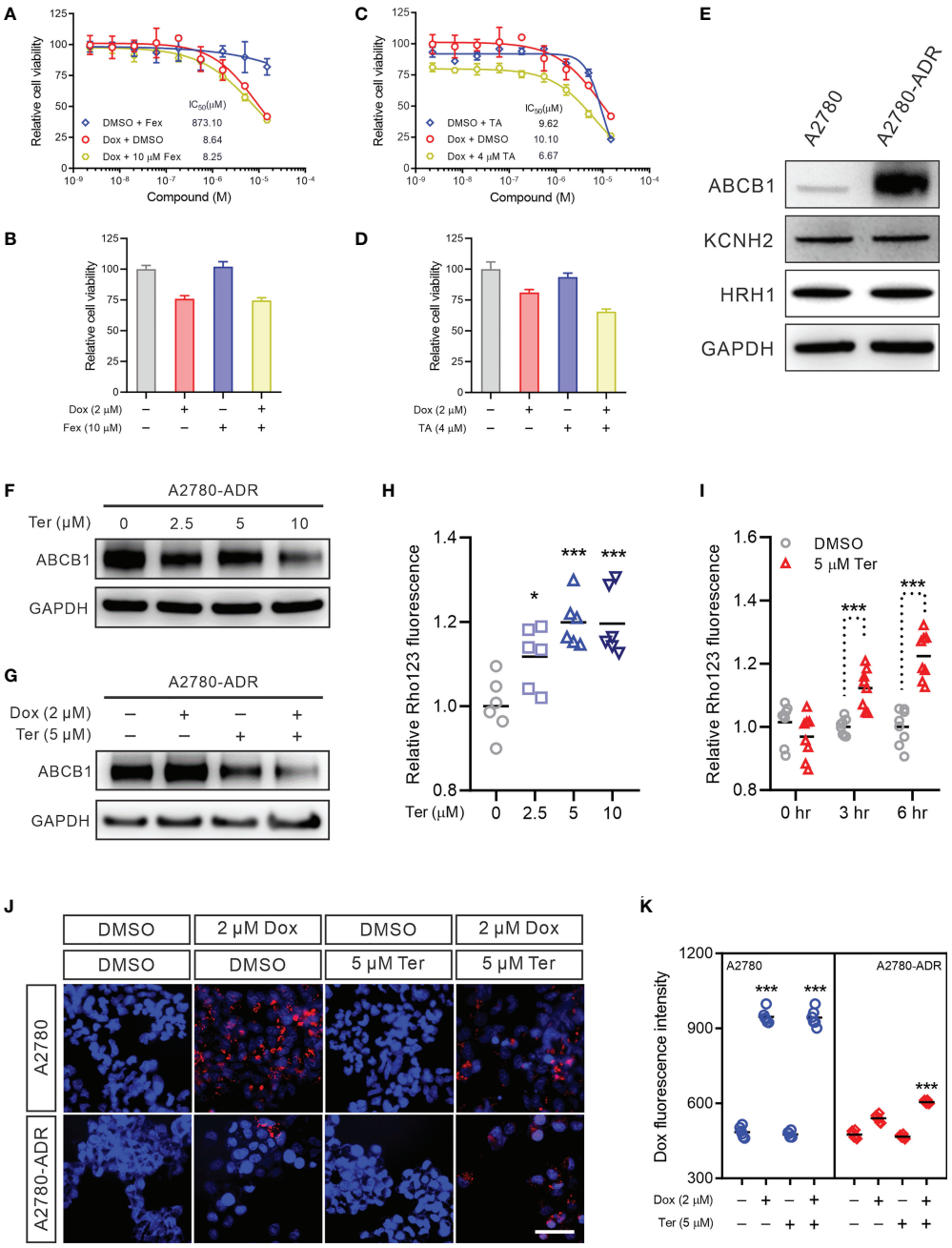

FIGURE 3
Terfenadine reverses MDR in ovarian cancer cells by repressing ABCB1 expression **(A)** Dose-response curves for doxorubicin (Dox) in the presence or absence of 10 μM fexofenadine (Fex) in MDR ovarian cancer cells. **(B)** Cell viability of MDR ovarian cancer cells treated with 2 μM doxorubicin (Dox), 10 μM fexofenadine (Fex), or both for 48 hours. DMSO was used as a non-treated control. **(C)** Dose-response curves of the MDR ovarian cancer cells to doxorubicin (Dox) in the presence or absence of 4 μM tannic acid (TA). **(D)** Cell viability of MDR ovarian cancer cells treated with 2 μM doxorubicin (Dox), 5 μM tannic acid (TA), or both for 48 hours. DMSO was used as a non-treated control. **(E)** Western blot analysis of hERG channel (KCNH2) and HRH1 in MDR ovarian cancer cell and its sensitive parental A2780 cell. **(F)** ABCB1 Western blot analysis in MDR cells treated with the indicated terfenadine (Ter) concentration. DMSO was used as a non-treated control. GAPDH was used as a loading control. **(G)** ABCB1 Western blot in MDR cells treated with 2 μM doxorubicin (Dox), 5 μM terfenadine (Ter), or both. DMSO was used as a non-treated control. GAPDH was used as a loading control. **(H)** Rho123 accumulation in MDR ovarian cancer cells treated with the indicated concentration of terfenadine (Ter) for 6 h. **(I)** Rho123 accumulation in MDR ovarian cancer cells treated for indicated time with 5 μM terfenadine (Ter). **(J, K)** Doxorubicin intracellular accumulation in MDR ovarian cancer cells or its parental sensitive A2780 cells treated for 6 hours with 2 μM doxorubicin (Dox), 5 μM terfenadine (Ter), or both. All values represent the mean ± SEM (n = 3 replicates). All values represent the mean ± SEM (n = 3 replicates). Western blot images were shown as one of three repeated experiments. Statistical analysis was carried out using a two-tailed t-test (* $p < 0.05$, *** $p < 0.001$).

Calcium pathway was altered in MDR cells

To further investigate the potential targets and mechanisms of drug resistance, we used RNA-seq to assess the transcriptional differences between A2780 and A2780-ADR. A total of 5,694 genes with a fold change of > 2 and a p-value < 0.05 were identified as differentially expressed genes (DEGs) (Figure 4A), including 2,755 genes that were over-expressed and 2,939 genes that were under-expressed in the A2780-ADR cells. The gene ontology (GO) enrichment study revealed 13 calcium-related biological processes which caught our attention (Figure 4B). The

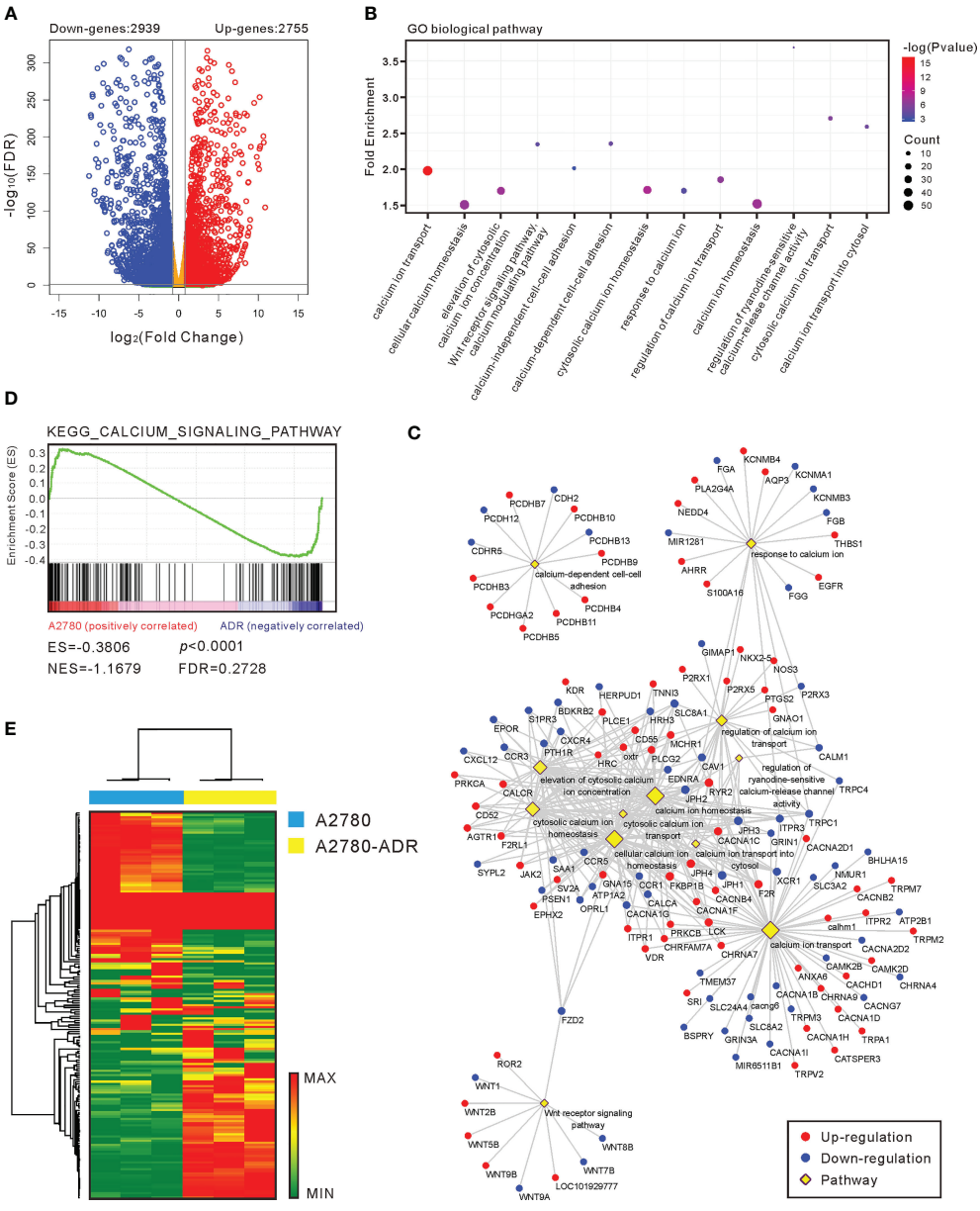

FIGURE 4
Calcium pathway is important in MDR generation. **(A)** A volcano plot of the genes that were up- and down-regulated in A2780-ADR cells versus A2780 cells. The genes are considered significant changes when the p-value is < 0.05 and the fold change is > 2-fold. **(B)** Gene ontology (GO) enrichment analysis revealed that 13 calcium-related biological pathways were activated in the A2780-ADR cell when compared to its parental A2780 cell. **(C)** Gene-Pathway network showed most of the DEGs were clustered in the processes of cytosolic calcium ion transport, homeostasis, and response. **(D)** The KEGG calcium signaling pathway (p < 0.0001) was also exhibited the significance in gene set enrichment analysis (GSEA). **(E)** Heatmap: the unsupervised hierarchical clustering showed 177 genes regarding calcium pathway showed the perfect separation in the GSEA.

Gene-Pathway network showed that the majority of DEGs were clustered in the cytosolic calcium ion transport, homeostasis, and response processes (Figure 4C), indicating this MDR cell line possessed abnormal calcium signaling.

In addition to the preliminary analysis, a gene set enrichment analysis (GSEA) was conducted to identify probable biological pathway enrichment from the Kyoto Encyclopedia of Genes and Genomes (KEGG) pathway database. This study uncovered the difference in the KEGG calcium signaling pathway ($p<0.0001$) as well (Figure 4D). Using all 177 genes involved in the calcium pathway, unsupervised hierarchical clustering revealed a clear separation of these two cell types (Figure 4E), demonstrating a major modification in the calcium homeostasis of MDR cells. Collectively, these findings suggest that the calcium signaling pathway is associated with the MDR phenotype in the A2780-ADR cells.

Terfenadine overcomes MDR by inhibiting the CAMK2/CREB1 pathway

Among the proteins implicated in the calcium signaling pathway, RNA-seq data revealed dysregulation of calcium/calmodulin-dependent protein kinase II (CaMK2) members. Specifically, *CAMK2D* is highly up-regulated, and *CAMK2B* is down-regulated (Figure 5A). The rise of CAMK2D and its active form, phosphorylated-CAMK2D (T286), in A2780-ADR cells was confirmed by Western blotting (Figure 5B and Figure S5A). In addition, we detected an increase in the phosphorylation of CREB1 at S133, although RNA and protein levels remained unchanged (Figures 5B, C and Figure S5A). As revealed by these results, they indicated the CAMK2/CREB1 pathway was overactive in the A2780-ADR cells.

To determine if terfenadine blocked the CAMK2/CREB1 pathway, the expression of related proteins was measured following terfenadine administration. After 24 hours of treatment, dose-dependent reductions in CAMK2D and phosphorylated CAMK2D were observed. Meanwhile, CREB1, ABCB1, and baculoviral inhibitor of apoptosis repeat-containing 5 (BIRC5) were also reduced (Figure 5D and Figure S5B). The protein BIRC5, also known as survivin, suppresses apoptosis by inhibiting caspase activation. As CREB1 is a transcription factor located in the nuclei and is activated by direct binding of CAMK2, we also examined their levels in the nuclei and found that terfenadine dose-dependently decreased the CAMK2D and the phosphorylated CREB1 in the nuclei (Figures 5D, E and Figures S6A, B), indicating a decrease in the activating and nuclear entry of CAMK2D in the presence of terfenadine.

A cellular thermal shift assay (CETSA) was conducted to assess if terfenadine directly binds to CAMK2D to prevent its activation. CAMK2D's apparent aggregation temperature (T_{agg}) was evaluated in the absence or presence of terfenadine in A2780-ADR cell lysates (Figure 5F and Figure S6C). The best-fit curve for the terfenadine-treated group shifted significantly from that of the DMSO control ($p< 0.001$). Figure 5G shows that terfenadine reduced the T_{agg} of CaMK2D protein from 57.4 to 54.2°C, indicating that it thermally destabilized CAMK2D. Together with the other studies demonstrating that CREB1 regulates ABCB1 expression (41, 42), our findings suggest that terfenadine may prevent cells from apoptosis by regulating the Ca^{2+}-mediated CAMK2/CREB1 pathway through binding directly to CAMK2D, thereby causing its destabilization in cells and reducing the activation of CREB1 and subsequent ABCB1 expression.

CAMK2/CREB1 pathway is the promising therapeutics target for the ABCB1 mediated MDR of ovarian cancer

To confirm further that CAMK2D was a target for MDR combination therapy, we recruited KN62, a CaMK2 specific inhibitor, for our investigation (43). KN62 reduced the expression and activity of ABCB1 in A2780-ADR cells, consistent with the terfenadine therapy (Figures 6A, B and Figure S7A). Moreover, KN62 inhibited the expression of BIRC5 and the phosphorylation of both CAMK2D and CREB1 in A2780-ADR cells (Figure 6A). The IC_{50} of doxorubicin dropped from 2.4 μM (doxorubicin alone) to 0.17 μM (doxorubicin paired with 5 μM KN62) in A2780-ADR cells when KN62 was administered in combination with doxorubicin (Figure 6C). This was a synergistic combination ($CI < 1$) (Figure 6D). Notably, KN62 had the same effect as terfenadine in the combination with doxorubicin, decreasing ABCB1 and BIRC5 expression and increasing cleaved PARP (Figures 6E, F). Although the phosphorylated CAMK2D was lowered in either terfenadine or KN62 treatment alone, there was no difference in CAMK2D phosphorylation in combination treatments with either of them with doxorubicin. In contrast, CREB1 phosphorylation remained lower in the combined treatment, indicating that CAMK2 inhibitors repressed the CAMK2/CREB1 pathway (Figures 6E. F and Figures S8A, B). Furthermore, KN93, another CAMK2-specific inhibitor, reduced ABCB1 activity and increased doxorubicin-induced cell death in A2780-ADR cells (Figures S9A, B). These findings suggest that inhibiting CAMK2 could resensitize MDR cells to doxorubicin.

To determine if blocking CREB1 would similarly resensitize MDR cells to doxorubicin, A2780-ADR cells were treated with the selective CREB1 inhibitor 3i (also known as 666-15 (44). Consistent with the CAMK2 inhibitors, ABCB1 and BIRC5, along with CREB1 phosphorylation, decreased after treatment with 666-15 (Figure 6G and Figure S7B). Under the 666-15 treatment, the total ABCB1 activity similarly dropped in a dose-dependent manner (Figure 6H). In addition, the combination of doxorubicin and 666-15 killed MDR cells A2781-ADR

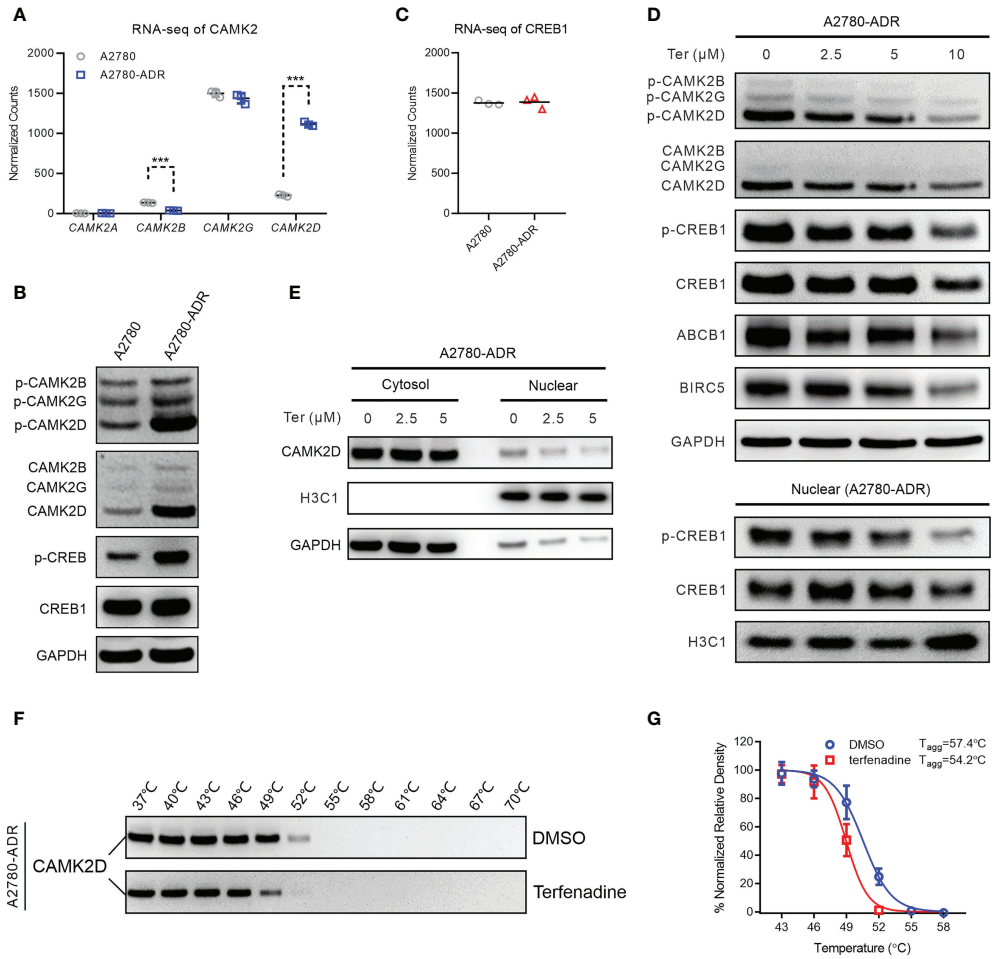

FIGURE 5
Terfenadine overcomes MDR in ovarian cancer cells by inhibiting the CAMK2/CREB-mediated pathway. **(A)** Normalized read counts of the CAMK2 family in MDR ovarian cancer cells and its parental sensitive ovarian cells (A2780) obtained in the RNA-seq analysis. **(B)** Western blot analysis of p-CAMK2 (T286), CAMK2 (pan), p-CREB1 (s133), and CREB1 in MDR sensitive ovarian cells (A2780). GAPDH was used as the loading control. **(C)** RNA-seq normalized read counts of CREB1 in MDR ovarian cancer cells and its parental sensitive ovarian cancer cells A2780. **(D)** Upper panel: Western blot analysis of p-CAMKII (T286), CAMKII (pan), p-CREB1 (s133), CREB1, ABCB1, and BIRC5 in MDR ovarian cancer cells treated for 24 hours with terfenadine (Ter). GAPDH was used as the loading control. Lower panel: Western blot analysis of CREB1 and p-CREB1 (s133) in the nucleus of MDR ovarian cancer cells treated with terfenadine (Ter) for 6 h. Histone H3 (H3C1) was used as the loading control. **(E)** Western blot analysis of CAMK2D in the cytosol or nucleus of terfenadine (Ter)-treated MDR ovarian cancer cells for 6 hours. GAPDH and H3C1 were used as the loading controls for cytosol protein and nucleus protein, respectively. **(F, G)** Cellular thermal shift assay (CETSA) for the binding of terfenadine to CAMKIID in MDR ovarian cancer cell lysate. **(F)** Representative western blot images for the CESTA. **(G)** T_{agg} curves of CaMKIID in MDR ovarian cancer cells in the presence of DMSO or 600 μM of terfenadine. All statistical analysis was performed using a two-tailed t-test (*** $p < 0.001$).

synergistically (CI < 1) (Figure 6I). Together, inhibition of the Ca^{2+} mediated CAMK2D/CREB1 pathway appears to be a promising therapeutic target for doxorubicin resensitization in ABCB1-mediated MDR ovarian cancer.

Discussion

Resistance to chemotherapy, whether inherited or acquired, is a significant obstacle in cancer treatment. Several mechanisms of drug resistance have been postulated, with the multiplication and expression of phosphorylated ABCB1 protein, an energy-dependent drug efflux pump, being one of the most extensively investigated (45). Studies *in vitro* have demonstrated that high levels of ABCB1 expression are associated with MDR in multiple cell lines and that the degree of overexpression correlates with the amount of resistance (46). Research on patients with ovarian cancer has found that high levels of ABCB1 expression are inversely related to chemotherapy response and progression-free survival (47). Consequently, ovarian cancer patients continue to

10.3389/fonc.2022.1068443

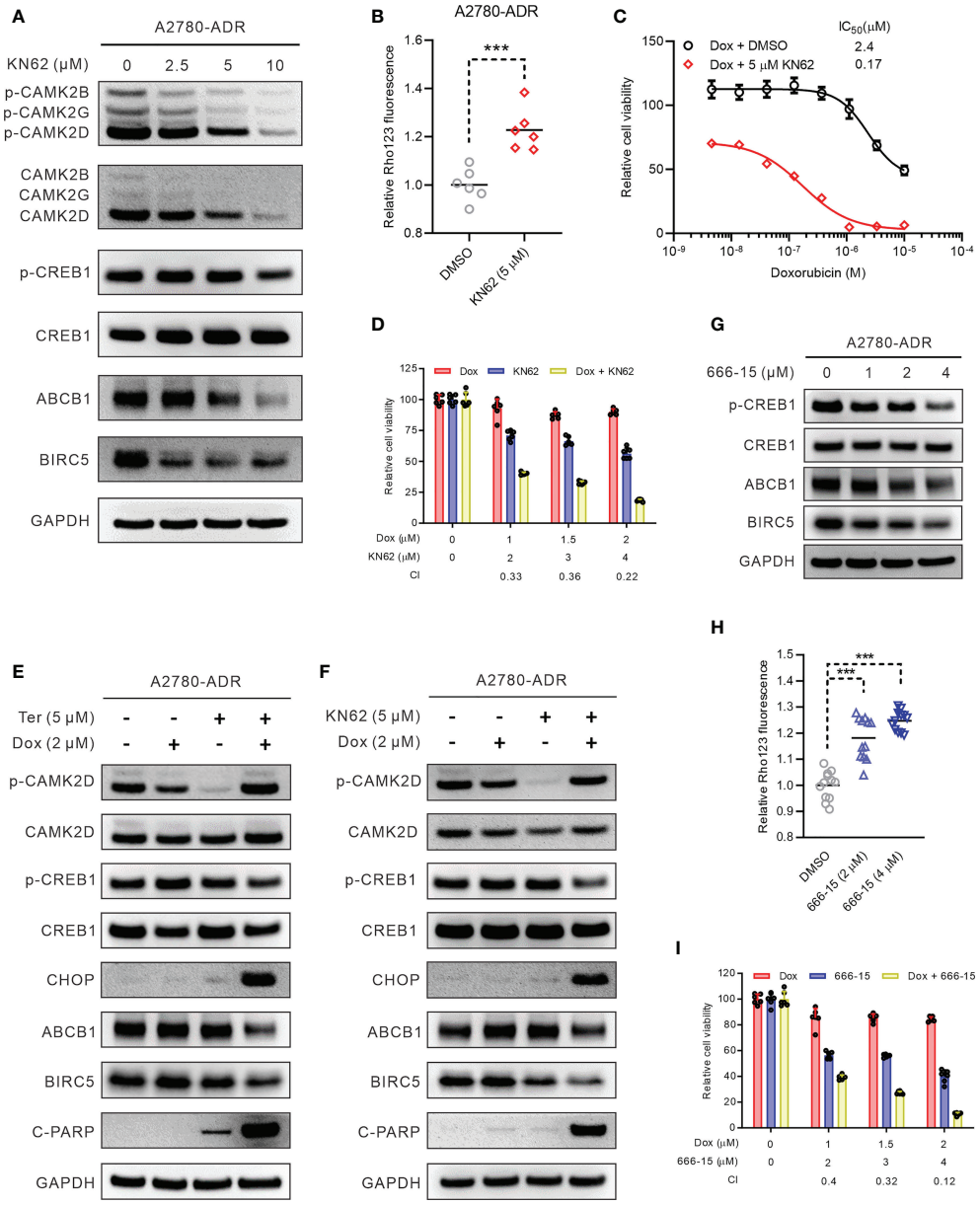

FIGURE 6
Inhibiting the CAMK2/CREB pathway reversed MDR in ovarian cancer cells. **(A)** Western blot of p-CAMK2 (T286), CAMK2 (pan), ABCB1, p-CREB1 (s133), CREB1, and BIRC5 in KN62-treated MDR ovarian cancer cells for 24 h. **(B)** Rho123 accumulation in MDR ovarian cancer cells treated for 6 h with 5 μM KN62. DMSO was used as non-treated control. Statistical analysis was performed using a two-tailed t-test (*** $p < 0.001$). **(C)** Dose-response curves of MDR ovarian cancer cells to doxorubicin (Dox) in the presence or absence of 5 μM KN62. **(D)** Synergistic effects of KN62 and doxorubicin (Dox) on MDR ovarian cancer cell killing. The bar graph shows the cell viability of MDR ovarian cancer cells treated for 48 h with doxorubicin, KN62, or both. Calculated CI values are presented below the plots. **(E)** Western blot of p-CAMK2 (T286), CAMK2 (pan), ABCB1, p-CREB1, CREB1, c-PARP, CHOP, and BIRC5 in MDR ovarian cancer cells treated for 24 h with 2 μM doxorubicin (Dox), 5 μM terfenadine (Ter), or both. **(F)** Western blot of p-CAMK2 (T286), CAMK2 (pan), ABCB1, p-CREB1, CREB1, c-PARP, CHOP, and BIRC5 in MDR ovarian cancer cells treated for 24 h with 2 μM doxorubicin (Dox), 5 μM KN62, or both. **(G)** Western blot of ABCB1, p-CREB1 (s133), CREB1, and BIRC5 in MDR ovarian cancer cells treated for 24 h with 666-15. **(H)** Rho123 accumulation in MDR ovarian cancer cells treated for 6 h with 666-15. DMSO was used as non-treated control. Statistical analysis was performed using a one-way ANOVA with Tukey's HSD correction (*** $p < 0.001$). **(I)** Synergistic effects of 666-15 and doxorubicin (Dox) on MDR ovarian cancer cell killing. The bar graph shows the cell viability of MDR ovarian cancer cells treated for 48 h with doxorubicin, 666-15, or both. Calculated CI values are presented below the plots.

be in need of a therapeutic for effectively overcoming MDR. Using qHTCS, this work found a group of doxorubicin potentiators in an ABCB1-mediated MDR ovarian cancer cell line. Among these, we demonstrated that terfenadine restored the activity of doxorubicin by inhibiting the CAMK2/CREB1 pathway, resulting in decreased expression of ABCB1 and BIRC5. In addition, inhibiting the CAMK2/CREB1 pathway resensitized MDR ovarian cancer cells to not only doxorubicin but also paclitaxel and topotecan, which are clinically employed to treat ovarian cancer (48).

Terfenadine has been shown to restore the activity of doxorubicin in the MCF-7/ADR human breast cancer cells and the L1210/VMDRC.06 murine leukemia cells (49), and the activity of epirubicin in killing drug-resistant non-small cell lung cancer (20). In spite of this, the target and mechanism by which terfenadine restores chemotherapeutic activity in MDR cancer cells remain unknown. Notably, neither H1R nor hERG inhibitors were able to duplicate the synergistic effects of terfenadine on the MDR cancer cells, indicating that other biological mechanisms may be involved in the reversal of chemosensitivity. To investigate the unique target of terfenadine in combinational chemotherapy for MDR cancer, the global gene expression of doxorubicin-sensitive and -resistant cell lines was profiled using RNA sequence. Importantly, calcium signaling-related pathways were shown to be aberrantly regulated in MDR cells, indicating that calcium homeostasis was disrupted. Indeed, our work demonstrated the abnormal expression of CAMK2 family members, particularly CAMK2D, which is dramatically overexpressed in MDR cells, and terfenadine treatment inhibits the CAMK2D phosphorylation in a manner comparable to that of the CAMK2 inhibitor KN62.

Intriguingly, terfenadine has been related to a decrease in calcium influx caused by L-type calcium channels (LTCC) activation in rat cerebellar neurons and human atrial myocytes (22, 23), showing terfenadine can regulate intracellular calcium homeostasis. However, the target of terfenadine for this function remains unclear. Moreover, activation of CAMK2 can further activate LTCC by binding to and phosphorylating the COOH terminus of LTCC (50, 51). Using the CETSA assay, we demonstrated the direct binding of terfenadine to CAMK2D in our study, as indicated by a protein melting curve shift after the addition of terfenadine to the cell lysate. Interestingly, the melting curve of the CAMK2D protein was shifted to the right in the presence of terfenadine, indicating instability of the CAMK2D protein upon heating when bound to terfenadine. As equilibrium binding ligands typically increase protein thermal stability by a factor proportionate to the concentration and affinity of the ligand, the CETSA assay will typically demonstrate a leftward change in the melting curve of the protein (52). However, multiple situations have been reported experimentally in which equilibrium-binding ligands destabilize proteins, i.e., decrease the melting temperature of the protein by an amount proportionate to the ligand's concentration and affinity (53, 54). This type of protein instability may cause aggregation and degradation of target proteins in cells, resulting in further protein reduction. In our study, we demonstrated that terfenadine administration lowered CAMK2 protein in a dose-dependent manner. Based on our findings, it is possible to speculate that terfenadine's inhibition of CAMK2 protein leads to the deactivation of LTCC, thereby reducing calcium influx in neurons and myocytes.

Unfortunately, terfenadine has been linked to cardiac death in at least 125 and 14 cases in the United States and United Kingdom, respectively (55), and the Food and Drug Administration (FDA) recommended its removal from the market in 1997 due to its pro-arrhythmic risk for long QT-related Torsades de Pointes (TdPs) (56, 57). Although numerous structural derivatives with a relatively low toxicity profile, such as fexofenadine (58), have been developed, their activity and target for MDR cancer treatment have yet to be investigated. Therefore, it is preferable to identify pharmacologically accessible downstream targets in this calcium cascade for MDR treatment. In recent years, CAMK2 has garnered a great deal of attention for its pivotal role in the arrhythmias of chronic illness (59). The isoform-specific inhibitor of CAMK2D (the main cardiac isoform of CAMK2) could be used to target the cardiac-specific pathology of autonomously activated CAMK2 in diabetes (60), while avoiding off-target effects in other tissues, such as α and β isoforms of CAMK2, and disruption of memory formation in the hippocampus (61). A recent clinical trial revealed that the CAMK2 inhibitor appears to be well accepted and safe among patients (62), suggesting that it should pave the way for future development of CAMK2 inhibitors in other conditions, such as the treatment of MDR cancer patients.

Considering that CAMK2 activation can phosphorylate and activate CREB1 (63) and that phosphorylated CREB1 binds to the CRE binding site in the ABCB1 promoter and promotes ABCB1 expression (64), CAMK2 activation will induce ABCB1 expression in cancer cells, resulting in MDR. Therefore, reducing CREB1 activity is an additional promising MDR cancer therapeutic target. In fact, CREB has already been identified as a candidate for oncogenic signaling in a variety of tumor types (65), particularly in leukemia and glioma (66, 67). In the current work, an aberrant increase in CREB1 phosphorylation was observed in MDR cells, and inhibition of CREB1 decreased ABCB1 expression and activity, indicating that CREB1 is a viable target for MDR reversal in cancer therapy. Despite the recent developments, CREB inhibitors are exclusively used in preclinical research. The lack of pharmacokinetic and pharmacodynamic responses, as well as

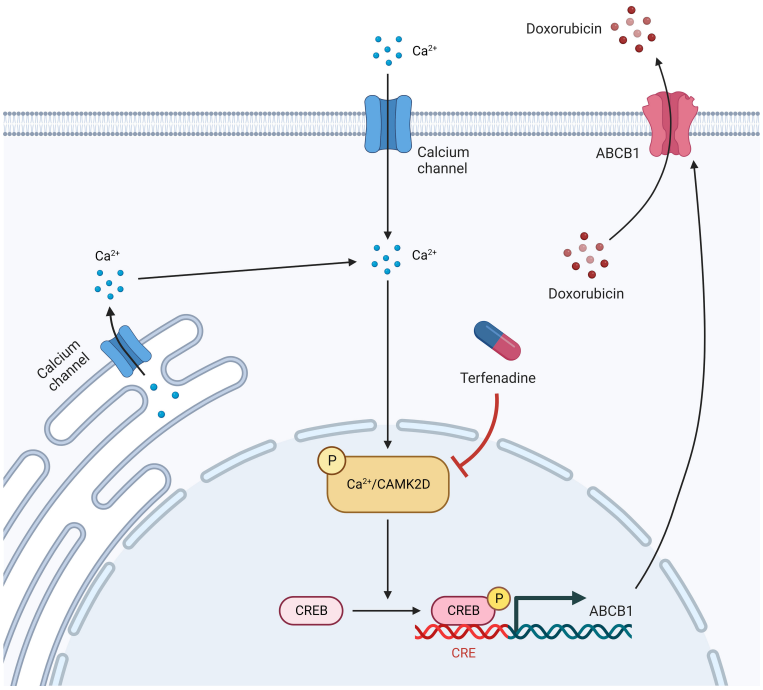

FIGURE 7
An illustration of terfenadine function in combinational treatment with doxorubicin.

toxicity reports, makes it unlikely that any of them will be used in clinical practice currently, despite the fact that some of them look to be highly promising. In addition, the use of CREB inhibitors has been hampered by numerous limitations, such as lower bioactivity in living systems and off-target binding. This necessitates a more comprehensive characterization and development prior to clinical application.

In this study, we reported that the CAMK2/CREB pathway, particularly CAMK2D, is a promising target for reversing ABCB1-mediated drug resistance in ovarian cancer (Figure 7). However, the *in vivo* activity of their inhibitors requires further investigation. Additionally, we demonstrated once more that integrating qHTCS and gene expression data is an effective approach for identifying novel agents with combinational effects and their underlying mechanisms.

Data availability statement

The datasets presented in this study can be found in online repositories. The names of the repository/repositories and accession number(s) can be found on: https://www.ncbi.nlm.nih.gov/, GSE177038.

Author contributions

WL and WZ conceived the research and designed the study. WH, SY, NS, and WS performed the experiments. WH, SY, Y-SC, MS and JB analyzed the data. SY, Y-SC and WZ wrote, reviewed, and edited the manuscript. All authors contributed to the article and approved the submitted version.

Funding

This work was partially supported by the intramural research programs of the National Center for Advancing Translational Sciences, National Institutes of Health, and the Natural Science foundation of Zhejiang Province (LY19H160046 to WH). This work was also supported by grants from National Natural Science Foundation of China (81974403 to NS).

Acknowledgments

The authors thank the compound management group at NCATS, NIH for their professional support and Dr. DeeAnn Visk, a medical writer and editor, for editing the manuscript.

Conflict of interest

The authors declare that the research was conducted in the absence of any commercial or financial relationships that could be construed as a potential conflict of interest.

Publisher's note

All claims expressed in this article are solely those of the authors and do not necessarily represent those of their affiliated organizations, or those of the publisher, the editors and the reviewers. Any product that may be evaluated in this article, or claim that may be made by its manufacturer, is not guaranteed or endorsed by the publisher.

Supplementary material

The Supplementary Material for this article can be found online at: https://www.frontiersin.org/articles/10.3389/fonc.2022.1068443/full#supplementary-material

References

1. Siegel RL, Miller KD, Jemal A. Cancer statistics, 2019. *CA Cancer J Clin* (2019) 69(1):7–34. doi: 10.3322/caac.21551

2. Glajzer J, Grabowski JP, Sehouli J, Pfisterer J. Recurrent treatment in ovarian cancer patients: What are the best regimens and the order they should be given? *Curr Treat Options Oncol* (2020) 21(6):49. doi: 10.1007/s11864-020-00747-7

3. Hacker NF, Rao A. Surgery for advanced epithelial ovarian cancer. *Best Pract Res Clin Obstet Gynaecol* (2017) 41:71–87. doi: 10.1016/j.bpobgyn.2016.10.007

4. Torre LA, Trabert B, DeSantis CE, Miller KD, Samimi G, Runowicz CD, et al. Ovarian cancer statistics, 2018. *CA Cancer J Clin* (2018) 68(4):284–96. doi: 10.3322/caac.21456

5. Della Pepa C, Tonini G, Pisano C, Di Napoli M, Cecere SC, Tambaro R, et al. Ovarian cancer standard of care: Are there real alternatives? *Chin J Cancer* (2015) 34(1):17–27. doi: 10.5732/cjc.014.10274

6. Pokhriyal R, Hariprasad R, Kumar L, Hariprasad G. Chemotherapy resistance in advanced ovarian cancer patients. *biomark Cancer* (2019) 11:1179299X19860815. doi: 10.1177/1179299X19860815

7. Ozols RF. Challenges for chemotherapy in ovarian cancer. *Ann Oncol* (2006) 17 Suppl 5:v181–7. doi: 10.1093/annonc/mdj978

8. Ledermann JA, Raja FA, Fotopoulou C, Gonzalez-Martin A, Colombo N, Sessa C, et al. Newly diagnosed and relapsed epithelial ovarian carcinoma: Esmo clinical practice guidelines for diagnosis, treatment and follow-up. *Ann Oncol* (2013) 24 Suppl 6:vi24–32. doi: 10.1093/annonc/mdt333

9. Adamska A, Falasca M. Atp-binding cassette transporters in progression and clinical outcome of pancreatic cancer: What is the way forward? *World J Gastroenterol* (2018) 24(29):3222–38. doi: 10.3748/wjg.v24.i29.3222

10. Ween MP, Armstrong MA, Oehler MK, Ricciardelli C. The role of abc transporters in ovarian cancer progression and chemoresistance. *Crit Rev Oncol Hematol* (2015) 96(2):220–56. doi: 10.1016/j.critrevonc.2015.05.012

11. Hodges LM, Markova SM, Chinn LW, Gow JM, Kroetz DL, Klein TE, et al. Very important pharmacogene summary: Abcb1 (Mdr1, p-glycoprotein). *Pharmacogenet Genomics* (2011) 21(3):152–61. doi: 10.1097/FPC.0b013e3283385a1c

12. Li L, Xu QH, Dong YH, Li GX, Yang L, Wang LW, et al. Mir-181a upregulation is associated with epithelial-to-Mesenchymal transition (Emt) and multidrug resistance (Mdr) of ovarian cancer cells. *Eur Rev Med Pharmacol Sci* (2016) 20(10):2004–10.

13. Yang X, Li X, Duan Z, Wang X. An update on circumventing multidrug resistance in cancer by targeting p-glycoprotein. *Curr Cancer Drug Targets* (2018) 18(7):677–96. doi: 10.2174/1568009617666170623114524

14. Coley HM. Overcoming multidrug resistance in cancer: Clinical studies of p-glycoprotein inhibitors. *Methods Mol Biol* (2010) 596:341–58. doi: 10.1007/978-1-60761-416-6_15

15. Blaya B, Nicolau-Galmes F, Jangi SM, Ortega-Martinez I, Alonso-Tejerina E, Burgos-Bretones J, et al. Histamine and histamine receptor antagonists in cancer biology. *Inflamm Allergy Drug Targets* (2010) 9(3):146–57. doi: 10.2174/187152810792231869

16. Fernandez-Nogueira P, Noguera-Castells A, Fuster G, Recalde-Percaz L, Moragas N, Lopez-Plana A, et al. Histamine receptor 1 inhibition enhances antitumor therapeutic responses through extracellular signal-regulated kinase (Erk) activation in breast cancer. *Cancer Lett* (2018) 424:70–83. doi: 10.1016/j.canlet.2018.03.014

17. Hadzijusufovic E, Peter B, Gleixner KV, Schuch K, Pickl WF, Thaiwong T, et al. H1-receptor antagonists terfenadine and loratadine inhibit spontaneous growth of neoplastic mast cells. *Exp Hematol* (2010) 38(10):896–907. doi: 10.1016/j.exphem.2010.05.008

18. Jangi SM, Diaz-Perez JL, Ochoa-Lizarralde B, Martin-Ruiz I, Asumendi A, Perez-Yarza G, et al. H1 histamine receptor antagonists induce genotoxic and caspase-2-Dependent apoptosis in human melanoma cells. *Carcinogenesis* (2006) 27(9):1787–96. doi: 10.1093/carcin/bgl021

19. Jangi SM, Ruiz-Larrea MB, Nicolau-Galmes F, Andollo N, Arroyo-Berdugo Y, Ortega-Martinez I, et al. Terfenadine-induced apoptosis in human melanoma cells is mediated through Ca2+ homeostasis modulation and tyrosine kinase activity, independently of H1 histamine receptors. *Carcinogenesis* (2008) 29 (3):500–9. doi: 10.1093/carcin/bgm292

20. An L, Li DD, Chu HX, Zhang Q, Wang CL, Fan YH, et al. Terfenadine combined with epirubicin impedes the chemo-resistant human non-small cell lung cancer both in vitro and in vivo through emt and notch reversal. *Pharmacol Res* (2017) 124:105–15. doi: 10.1016/j.phrs.2017.07.021

21. Jangi SM, Asumendi A, Arlucea J, Nieto N, Perez-Yarza G, Morales MC, et al. Apoptosis of human T-cell acute lymphoblastic leukemia cells by diphenhydramine, an H1 histamine receptor antagonist. *Oncol Res* (2004) 14(7-8):363–72. doi: 10.3727/0965040041292369

22. Diaz-Trelles R, Fernandez-Sanchez MT, Marini AM, Novelli A. Antihistamine terfenadine inhibits calcium influx, cgmp formation, and nmda receptor-dependent neurotoxicity following activation of l-type voltage sensitive calcium channels. *Neurotox Res* (2002) 4(1):15–24. doi: 10.1080/10298420290007583

23. Hove-Madsen L, Llach A, Molina CE, Prat-Vidal C, Farre J, Roura S, et al. The proarrhythmic antihistaminic drug terfenadine increases spontaneous calcium release in human atrial myocytes. *Eur J Pharmacol* (2006) 553(1-3):215–21. doi: 10.1016/j.ejphar.2006.09.023

24. Wang S, Liu X, Chen S, Liu Z, Zhang X, Liang XJ, et al. Regulation of Ca(2+) signaling for drug-resistant breast cancer therapy with mesoporous silica nanocapsule encapsulated Doxorubicin/Sirna cocktail. *ACS Nano* (2019) 13 (1):274–83. doi: 10.1021/acsnano.8b05639

25. Williams JB, Buchanan CM, Pitt WG. Codelivery of doxorubicin and verapamil for treating multidrug resistant cancer cells. *Pharm Nanotechnol* (2018) 6(2):116–23. doi: 10.2174/2211738506666180316122620

26. Prevarskaya N, Skryma R, Shuba Y. Calcium in tumour metastasis: New roles for known actors. *Nat Rev Cancer* (2011) 11(8):609–18. doi: 10.1038/nrc3105

27. Santoni G, Morelli MB, Marinelli O, Nabissi M, Santoni M, Amantini C. Calcium signaling and the regulation of chemosensitivity in cancer cells: Role of the transient receptor potential channels. *Adv Exp Med Biol* (2020) 1131:505–17. doi: 10.1007/978-3-030-12457-1_20

28. Huang R, Southall N, Wang Y, Yasgar A, Shinn P, Jadhav A, et al. The ncgc pharmaceutical collection: A comprehensive resource of clinically approved drugs enabling repurposing and chemical genomics. *Sci Transl Med* (2011) 3(80):80ps16. doi: 10.1126/scitranslmed.3001862

29. Cai X, Li Z, Hao Q, Cheung ANY, Ngan HYS, Liu SS, et al. Autocrine activation of Jak2 by il-11 promotes platinum drug resistance. *Oncogene* (2018) 37 (29):3981–97. doi: 10.1038/s41388-018-0238-8

30. Meng Y, Chen CW, Yung MMH, Sun W, Sun J, Li J, et al. Duoxa1-mediated ros production promotes cisplatin resistance by activating atr-Chk1 pathway in ovarian cancer. *Cancer Lett* (2018) 428:104–16. doi: 10.1016/j.canlet.2018.04.029

31. Rojo M, Legros F, Chateau D, Lombès A. Membrane topology and mitochondrial targeting of mitofusins, ubiquitous mammalian homologs of the transmembrane gtpase fzo. *J Cell Sci* (2002) 115(Pt 8):1663–74. doi: 10.1242/jcs.115.8.1663

32. Wang Y, Jadhav A, Southal N, Huang R, Nguyen DT. A grid algorithm for high throughput fitting of dose-response curve data. . *Curr Chem Genomics* (2010) 4:57–66. doi: 10.2174/1875397301004010057

33. Ianevski A, He L, Aittokallio T, Tang J. Synergyfinder: A web application for analyzing drug combination dose-response matrix data. *Bioinformatics* (2017) 33 (15):2413–5. doi: 10.1093/bioinformatics/btx162

34. Martin C, Berridge G, Mistry P, Higgins C, Charlton P, Callaghan R. The molecular interaction of the high affinity reversal agent Xr9576 with p-glycoprotein. *Br J Pharmacol* (1999) 128(2):403–11. doi: 10.1038/sj.bjp.0702807

35. Chou TC, Talalay P. Quantitative analysis of dose-effect relationships: The combined effects of multiple drugs or enzyme inhibitors. *Adv Enzyme Regul* (1984) 22:27–55. doi: 10.1016/0065-2571(84)90007-4

36. Yadav B, Wennerberg K, Aittokallio T, Tang J. Searching for drug synergy in complex dose-response landscapes using an interaction potency model. *Comput Struct Biotechnol J* (2015) 13:504–13. doi: 10.1016/j.csbj.2015.09.001

37. Naclerio RM, Kagey-Sobotka A, Lichtenstein LM, Freidhoff L, Proud D. Terfenadine, an H1 antihistamine, inhibits histamine release in vivo in the human. *Am Rev Respir Dis* (1990) 142(1):167–71. doi: 10.1164/ajrccm/142.1.167

38. Roy M, Dumaine R, Brown AM. Herg, a primary human ventricular target of the nonsedating antihistamine terfenadine. *Circulation* (1996) 94(4):817–23. doi: 10.1161/01.cir.94.4.817

39. Watanabe N, Matsuda E, Masuda A, Nariai K, Shibasaki T. The effects of fexofenadine on eosinophilia and systemic anaphylaxis in mice infected with trichinella spiralis. *Int Immunopharmacol* (2004) 4(3):367–75. doi: 10.1016/j.intimp.2003.10.009

40. Chu X, Guo Y, Xu B, Li W, Lin Y, Sun X, et al. Effects of tannic acid, green tea and red wine on herg channels expressed in Hek293 cells. *PLoS One* (2015) 10 (12):e0143797. doi: 10.1371/journal.pone.0143797

41. Xia Z, Guo M, Liu H, Jiang L, Li Q, Peng J, et al. Cbp-dependent Wnt/Beta-catenin signaling is crucial in regulation of Mdr1 transcription. *Curr Cancer Drug Targets* (2015) 15(6):519–32. doi: 10.2174/1568009615666150506093643

42. Kim HG, Hien TT, Han EH, Hwang YP, Choi JH, Kang KW, et al. Metformin inhibits p-glycoprotein expression *Via* the nf-kappab pathway and cre transcriptional activity through ampk activation. *Br J Pharmacol* (2011) 162 (5):1096–108. doi: 10.1111/j.1476-5381.2010.01101.x

43. Tokumitso H, Chijiwa T, Hagiwara M, Mizutani A, Terasawa M, Hidaka H. Kn-62, 1-[N,O-Bis(5-Isoquinolinesulfonyl)-N-Methyl-L-Tyrosyl]-4-Phenylpiperazi Ne, a specific inhibitor of Ca2+/Calmodulin-dependent protein kinase ii. *J Biol Chem* (1990) 265(8):4315–20. doi: 10.1016/S0021-9258(19)39565-1

44. Xie F, Li BX, Kassenbrock A, Xue C, Wang X, Qian DZ, et al. Identification of a potent inhibitor of creb-mediated gene transcription with efficacious in vivo anticancer activity. *J medicinal Chem* (2015) 58(12):5075–87. doi: 10.1021/acs.jmedchem.5b00468

45. Gottesman MM. Mechanisms of cancer drug resistance. *Annu Rev Med* (2002) 53:615–27. doi: 10.1146/annurev.med.53.082901.103929

46. Kartner N, Shales M, Riordan JR, Ling V. Daunorubicin-resistant Chinese hamster ovary cells expressing multidrug resistance and a cell-surface p-glycoprotein. *Cancer Res* (1983) 43(9):4413–9.

47. Baekelandt MM, Holm R, Nesland JM, Trope CG, Kristensen GB. P-glycoprotein expression is a marker for chemotherapy resistance and prognosis in advanced ovarian cancer. *Anticancer Res* (2000) 20(2B):1061–7.

48. team TACSmaec. *Chemotherapy for ovarian cancer: cancer.org* (2018). Available at: https://www.cancer.org/cancer/ovarian-cancer/treating/chemotherapy.html.

49. Hait N, Gesmonde JF, Murren JR, Yang JM, Chen HX, Reiss M. Terfenadine (Seldane): A new drug for restoring sensitivity to multidrug resistant cancer cells. *Biochem Pharmacol* (1993) 45(2):401–6. doi: 10.1016/0006-2952(93)90076-9

50. Hudmon A, Schulman H, Kim J, Maltez JM, Tsien RW, Pitt GS. Camkii tethers to l-type Ca2+ channels, establishing a local and dedicated integrator of Ca2+ signals for facilitation. *J Cell Biol* (2005) 171(3):537–47. doi: 10.1083/jcb.200505155

51. Dzhura I, Wu Y, Colbran RJ, Balser JR, Anderson ME. Calmodulin kinase determines calcium-dependent facilitation of l-type calcium channels. *Nat Cell Biol* (2000) 2(3):173–7. doi: 10.1038/35004052

52. Jafari R, Almqvist H, Axelsson H, Ignatushchenko M, Lundback T, Nordlund P, et al. The cellular thermal shift assay for evaluating drug target interactions in cells. *Nat Protoc* (2014) 9(9):2100–22. doi: 10.1038/nprot.2014.138

53. Cimmperman P, Baranauskiene L, Jachimoviciute S, Jachno J, Torresan J, Michailoviene V, et al. A quantitative model of thermal stabilization and destabilization of proteins by ligands. *Biophys J* (2008) 95(7):3222–31. doi: 10.1529/biophysj.108.134973

54. Sridharan S, Kurzawa N, Werner T, Gunthner I, Helm D, Huber W, et al. Proteome-wide solubility and thermal stability profiling reveals distinct regulatory roles for atp. *Nat Commun* (2019) 10(1):1155. doi: 10.1038/s41467-019-09107-y

55. Rangno R. Terfenadine therapy: Can we justify the risks? *CMAJ* (1997) 157 (1):37–8.

56. Pawankar R, Holgate S, Rosenwasser L (eds). *Allergy frontiers: Therapy and prevention*. Tokyo: Springer (2010). Available at: https://link.springer.com/book/10.1007/978-4-431-99362-9.

57. Cruzan SM. FDA proposes to withdraw seldane approval. *FDA talk paper T97-3*. Rockville, MD: United States Food & Drug Administration.

58. Terrien MH, Rahm F, Fellrath JM, Spertini F. Comparison of the effects of terfenadine with fexofenadine on nasal provocation tests with allergen. *J Allergy Clin Immunol* (1999) 103(6):1025–30. doi: 10.1016/s0091-6749(99)70174-0

59. Nassal D, Gratz D, Hund TJ. Challenges and opportunities for therapeutic targeting of calmodulin kinase ii in heart. *Front Pharmacol* (2020) 11:35. doi: 10.3389/fphar.2020.00035

60. Veitch CR, Power AS, Erickson JR. Camkii inhibition is a novel therapeutic strategy to prevent diabetic cardiomyopathy. *Front Pharmacol* (2021) 12:695401. doi: 10.3389/fphar.2021.695401

61. Buard I, Coultrap SJ, Freund RK, Lee YS, Dell'Acqua ML, Silva AJ, et al. Camkii "Autonomy" is required for initiating but not for maintaining neuronal long-term information storage. *J Neurosci* (2010) 30(24):8214–20. doi: 10.1523/JNEUROSCI.1469-10.2010

62. Boyle AJ, Schultz C, Selvanayagam JB, Moir S, Kovacs R, Dib N, et al. Calcium/Calmodulin-dependent protein kinase ii delta inhibition and ventricular remodeling after myocardial infarction: A randomized clinical trial. *JAMA Cardiol* (2021) 6(7):762–8. doi: 10.1001/jamacardio.2021.0676

63. Yan X, Liu J, Ye Z, Huang J, He F, Xiao W, et al. Camkii-mediated creb phosphorylation is involved in Ca2+-induced bdnf mrna transcription and neurite outgrowth promoted by electrical stimulation. *PLoS One* (2016) 11(9):e0162784. doi: 10.1371/journal.pone.0162784

64. Yamagishi N, Nakao R, Kondo R, Nishitsuji M, Saito Y, Kuga T, et al. Increased expression of sorcin is associated with multidrug resistance in leukemia cells *Via* up-regulation of Mdr1 expression through camp response element-binding protein. *Biochem Biophys Res Commun* (2014) 448(4):430–6. doi: 10.1016/j.bbrc.2014.04.125

65. Sapio L, Salzillo A, Ragone A, Illiano M, Spina A, Naviglio S. Targeting creb in cancer therapy: A key candidate or one of many? an update. *Cancers (Basel)* (2020) 12(11):3166. doi: 10.3390/cancers12113166

66. Pigazzi M, Ricotti E, Germano G, Faggian D, Arico M, Basso G. Camp response element binding protein (Creb) overexpression creb has been described as critical for leukemia progression. *Haematologica* (2007) 92(10):1435–7. doi: 10.3324/haematol.11122

67. Mantamadiotis T, Papalexis N, Dworkin S. Creb signalling in neural Stem/Progenitor cells: Recent developments and the implications for brain tumour biology. *Bioessays* (2012) 34(4):293–300. doi: 10.1002/bies.201100133

frontiers | Frontiers in Pharmacology

TYPE Original Research
PUBLISHED 10 November 2022
DOI 10.3389/fphar.2022.1037620

OPEN ACCESS

EDITED BY
Eswar Shankar,
The Ohio State University, United States

REVIEWED BY
Prem P. Kushwaha,
Case Western Reserve University, United States
Deena Snoke,
University of Vermont, United States
Kate Ormiston ,
The Ohio State University, United States

*CORRESPONDENCE
Liubao Peng,
pengliubao@csu.edu.cn

SPECIALTY SECTION
This article was submitted to Pharmacology of Anti-Cancer Drugs, a section of the journal Frontiers in Pharmacology

RECEIVED 06 September 2022
ACCEPTED 20 October 2022
PUBLISHED 10 November 2022

CITATION
Peng C, Chen J, Cui W, Li S, Li J and Peng L (2022), Comparative efficacy of various CHIs combined with western medicine for non-small cell lung cancer: A bayesian network meta-analysis of randomized controlled trials. *Front. Pharmacol.* 13:1037620. doi: 10.3389/fphar.2022.1037620

Comparative efficacy of various CHIs combined with western medicine for non-small cell lung cancer: A bayesian network meta-analysis of randomized controlled trials

Ciyan Peng[1], Jing Chen[2], Wei Cui[1], Sini Li[1], Jianhe Li[1] and Liubao Peng[1]*

[1]Department of Pharmacy, The Second Xiangya Hospital of Central South University, Changsha, China, [2]Department of Pharmacy, The First Affiliated Hospital of Hunan University of Chinese Medicine, Changsha, China

Background: Given the limitations of Western medicine (WM) for the treatment of non-small cell lung cancer (NSCLC) and the wide exploration of Chinese herbal injections (CHIs), systematically evaluate the efficacy of Various CHIs Combined with WM for Non-small Cell Lung Cancer. In this study, we performed a network meta-analysis to evaluate the comparative efficacy of 16 CHIs combined with WM regimens for the treatment of NSCLC.

Methods: Literature databases were searched from their inception to November 2021, and all randomized control trials (RCTs) involving NSCLC patients treated with a combination of Chinese and WM were retrieved. Outcomes, including disease control rate, survival quality score, incidence of gastrointestinal adverse reactions, incidence of leukopenia, and incidence of thrombocytopenia, were analyzed using RevMan (5.3), Stata17, and R software. Surface under the cumulative ranking curve (SUCRA) probability values were calculated to rank the treatments examined, and clustering analysis was used to compare the effects of CHIs on different outcomes.

Results: A total of 389 studies involving 31,263 patients and 16 CHIs were included. The 16 CHIs were: Aidi injection (ADI), Huachansu injection (HCSI), oil

Abbreviations: 95% CI, 95% confidence interval; ADI, Aidi injection; CHIs, Chinese herbal injections; CM, Chinese medicine; CSI, Chansu injection; DCI, disodium cantharidinate and vitamin B6 injection; DCR, disease control rate; DLSI, Delisheng injection; FFKSI, Fufang Kushen injection; GI, gastrointestinal; HCSI, Huachansu injection; HQI, Huangqi injection; INPLASY, International platform of registered systematic review and meta-analysis protocols; KAI, Kangai injection; KLTI, Kanglaite injection; KPS, Karnofsky performance scale; NSCLC, non-small cell lung cancer; NMA, network meta-analysis; OOMI, oil of Ophiopogon injection; OR, odds ratio; RCT, randomized controlled trial; SFI, Shenfu injection; SI, Shengmai injection; SMI, Shenmai injection; SQFZI, Shenqi Fuzheng injection; SUCRA, surface under the cumulative ranking curve area; WM, western medicine; XAPI, Xiaoaiping injection; XGDTI, Xianggu Duotang injection.

of Ophiopogon injection (OOMI), disodium cantharidinate and vitamin B6 injection (DCI), Shenfu injection (SFI), Shenmai injection (SMI), Shenqi Fuzheng injection (SQFZI), Chansu injection (CSI), Delisheng injection (DLSI), Fufang Kushen injection (FFKSI), Huangqi injection (HQI), Kangai injection (KAI), Kanglaite injection (KLTI), Shengmai injection (SI), Xiangguduotang injection (XGDTI), and Xiaoaiping injection (XAPI). The results of the network meta-analysis showed that, with WM treatment as a co-intervention, CSI was most likely to improve the disease control rate (SUCRA = 80.90%), HQI had the highest probability of being the best option for improving the survival quality score (SUCRA = 82.60%), DCI had the highest probability of reducing the incidence of gastrointestinal adverse reactions (SUCRA = 85.50%), HCSI + WM had the highest probability of reducing the incidence of thrombocytopenia (SUCRA = 91.30%), while SMI had the highest probability of reducing the incidence of leukopenia (SUCRA = 79.10%).

Conclusion: CHIs combined with WM is proved to be more effective than WM alone, which may be beneficial to NSCLC patients. SMI + WM and DCI + WM are most likely the optimal CHI to improve disease control rates, survival quality score, and reduce adverse effects. This study has limitations; therefore, higher quality RCTs and real-world evidence are required to support our conclusions.

KEYWORDS

network meta-analysis, bayesian model, Chinese herbal injections, non-small cell lung cancer, combined therapy, Chinese medicine

1 Introduction

Lung cancer is the malignancy with the highest mortality and incidence rates, both worldwide and in China (Bray et al., 2018; Sung et al., 2021; Siegel et al., 2021; Alexander et al., 2020). Lung cancer brings a tremendous economic and social burden on both developing and developed countries (Minguet et al., 2016; Sung et al., 2021; Bray et al., 2018; Molina et al., 2008). Based on histology, Lung cancer can be classified as non-small cell lung cancer (NSCLC) and small cell lung cancer. Non-small cell lung cancer (NSCLC) accounts for approximately 80%–85% of all lung cancers (Miller et al., 2020; Miller et al., 2016; Miller et al., 2022).

Currently, platinum based chemotherapy is still the first-line treatment for lung cancer (Ettinger et al., 2017; Ettinger et al., 2022). However, some patients are unable to complete the recommended cycles of chemotherapy due to serious adverse events, greatly limiting its clinical application (Quoix et al., 2011; Shojaee and Nana-sinkam, 2017; Ettinger et al., 2022). With the development of modern treatment methods and biotechnology, lung cancer has entered the era of precision therapy (Soo et al., 2017; Hirsch et al., 2017; Yoneda et al., 2018). Molecular targeted drugs and immunotherapy have substantially improved the clinical efficacy of mid-to late-stage lung cancer treatment (Lemjabbar-Alaoui et al., 2015; Cho, 2017; Zhang et al., 2018; Jiang et al., 2019; Li et al., 2021). Although Immunotherapy increasing the 5-year survival rate of patients with advanced NSCLC from 5% to approximately 23% (Reck et al., 2022; Ren et al., 2021; Yoneda et al., 2018; Garon et al., 2019; Breimer et al., 2020), it is often accompanied by low antigenicity, side effects, and drug resistance for lung cancer has limitations in clinical practice (Khunger et al., 2018; Zhang et al., 2018; Xia et al., 2019; Wang et al., 2021; Stock-Martineau et al., 2021; Zhou and Zhou., 2021). Therefore, how to actively identify effective drug treatment options to reduce postoperative recurrence and metastasis, prolong the survival time of patients with advanced disease, reduce adverse effects, and improve patient quality of life remains a key challenge in the treatment of advanced lung cancer.

Chinese medicine injections (CHIs) are widely used by clinicians in China as an important component of complementary and alternative medicine for the adjuvant treatment of NSCLC (Jiao et al., 2017; Jiang et al., 2019; Xu et al., 2021; Han et al., 2016; Wu et al., 2016; He et al., 2016; Cao et al., 2017; Cao et al., 2021; Wang B et al., 2018). Many studies have documented the efficacy of Various CHIsCombined with Western Medicine for Non-small Cell Lung Cancer (Li et al., 2021; Zhang et al., 2018; Yao et al., 2020; Jiang et al., 2016; Jiang et al., 2019; Tan and Wang., 2016; Liu et al., 2017; Ma and Xu., 2017; Zheng et al., 2017; Wang G et al., 2018; Li et al., 2020; Liu et al., 2021; Xie et al., 2021). However, there are various types of CHIs, and the optimal strategy for combining CHIs with WM for treating

NSCLC remains inconclusive, which may cause difficulty for clinicians in clinical treatment. Bayesian network meta-analysis (NMA) has the advantage of combining direct and indirect evidence to compare multiple interventions (Schwingshackl et al., 2019; Watt et al., 2019; Ahn and Kang., 2021; González-Xuriguera et al., 2021; Watt and Del Giovne, 2022). Therefore, in this study, we used Bayesian network meta-analysis (NMA) method to systematically evaluate the efficacy of Various CHIs Combined with WM for Non-small Cell Lung Cancer. The objective of this NMA was to supplement the optimal strategy of NSCLC treatment and to strengthen additional insights for clinical practice in the future.

2 Methods

This study is reported in strict accordance with the standard format specifications detailed in the Preferred Reporting Items for Systematic Reviews and Meta-Analysis: PRISMA Extension Statement (Cornell, 2015; Hutton et al., 2015; Rethlefsen et al., 2021). A completed PRISMA checklist is included as an additional file (Supplementary File). The study protocol was registered and approved on the International Platform of Registered Systematic Review and Meta-Analysis Protocols (INPLASY) on 17 November 2021 (registration number: INPLASY2021110068), and the study was conducted strictly in accordance with the registered study protocol. This NMA did not require ethical approval, because the study only collected clinical data from each randomized controlled trial (RCT) and did not disclose patient information.

2.1 Search strategy

In this NMA, a comprehensive data search of the following electronic databases for RCTs of CHIs combined with WM for NSCLC was conducted from their inception to November 2021: Chinese Biological Medicine Literature, China National Knowledge Infrastructure, Wanfang, PubMed, Cochrane Library, and Embase. In addition, pharmaceutical companies that manufacture proprietary CMI were contacted to provide unpublished information regarding premarket and postmarket studies. Further, study authors were contacted to supplement incomplete reports of original papers or to provide data from unpublished studies. The search strategy was divided into three parts: CHIs, NSCLC, and RCTs. A search strategy was developed, as illustrated in Table 1 using PubMed as an example. A total of 16 CHIs that met the national standards of the Chinese Food and Drug Administration were included (https://db.yaozh.com and https://www.nmpa.gov.cn/). Detailed drug information is provided in (Table 1 and Supplementary Table S1).

2.2 Inclusion criteria

2.2.1 Study types

RCTs that reported the efficacy of the 16 CHIs combined with WM for treating NSCLC were eligible. There were no language restrictions. When outcome information was available for multiple time points, the data for the longest follow-up time point were selected.

2.2.2 Participants

All patients were pathologically and histologically diagnosed with NSCLC. There were no limitations on sex, age, race, region or nationality.

2.2.3 Interventions

Patients in control groups received only WM regimens, including DP, TP, GP, NP, and GE, where D indicates docetaxel, P cisplatin, T paclitaxel, G gemcitabine, N vinorelbine, and E gefitinib. Patients in the treatment group received CHIs together with WM therapy. To facilitate our analyses, we collapsed all agents regardless of dose. If patients had complications during the treatment, then some appropriate mitigation measures could be taken.

2.3 Outcome measures

The primary outcome indicator was DCR, where DCR was defined as complete remission + partial remission + stable. Survival quality was assessed using the Karnofsky performance scale (KPS), with improvement defined as an increase of ≥10 points in the KPS score after treatment, stability as an increase or decrease of <10 points, and a decline as a decrease of ≥10 points in the KPS score. Secondary outcome indicators were the incidence of adverse reactions, including gastrointestinal (GI) adverse reactions, leukopenia, and thrombocytopenia. Data were extracted according to the predefined definitions described in the protocol, with priority given to the earliest published report when data appeared in more than one report. RCTs were eligible if they reported one of the aforementioned outcomes.

2.4 Exclusion criteria

The exclusion criteria were as follows: 1) Other western medical treatment options (Radiotherapy, Surgical and Local interventional therapy); 2) Other traditional Chinese Medicine treatment options (Decoction for oral and external use, emotional therapy, static breathing control, acupuncture); 3) repeat publications; and 4) Studies with incomplete or incorrect data.

TABLE 1 Specific terms used to search PubMed.

#1 Non-small cell lung cancer (MeSH terms), #2 carcinoma, Non-small cell lung (title/Abstract), #3 carcinomas, Non-small-cell lung (title/Abstract), #4 lung carcinoma, Non-small-cell (title/Abstract), #5 lung carcinomas, Non-small-cell (title/Abstract), #6 Non-small-cell lung carcinoma (title/Abstract), #7 Non-small-cell lung carcinomas (title/Abstract)
#8, #1 OR #2 OR #3 OR #4 OR #5 OR #6 OR #7
#9 Aidi Injection (Title/Abstract), #10 Huachansu Injection (Title/Abstract), #11 Oil of Ophiopogon Injection (Title/Abstract), #12 Disodium Cantharidinate and Vitamin B6 Injection (Title/Abstract), #13 Shenfu Injection (Title/Abstract), #14 Shenmai Injection (Title/Abstract)
#15 Shenqifuzheng Injection (Title/Abstract), #16 Chansu Injection (Title/Abstract), #17 Delisheng Injection (Title/Abstract), #18 Fufangkushen Injection (Title/Abstract), #19 Huangqi Injection (Title/Abstract)
#20 Kangai Injection (Title/Abstract), #21 Kanglete Injection (Title/Abstract), #22 Shengmai (Title/Abstract), #23 Xiangguduotang Injection (Title/Abstract), #24 Xiaoaiping Injection (Title/Abstract)
#25 #9 OR #10 OR #11 OR #12 OR #13 OR #14 OR #15 OR #16 OR #17 OR #18 OR #19 OR #20 OR #21 OR #22 OR #23, OR #24
#26 randomized controlled trial (Publication type)
#27 controlled clinical trial (Publication type)
#28 #26 OR # 27
#28 #8 AND #25 AND #28

2.5 Data extraction and quality assessment

All retrieved studies were managed using EndNote software. After excluding duplicate studies, two researchers (Jing Chen and Sini Li) independently screened the retrieved studies according to the inclusion and exclusion criteria, and after excluding unrelated literature, such as reviews, evaluations, animal studies, and uncontrolled studies, the full text of each report was read to finalize the texts for inclusion in the study and to extract the data. Subsequently, a review team consisting of two researchers (Jianhe Li and Wei Cui) checked the accuracy of the data and assessed the quality of the included studies. Information extracted from included studies comprised: study name, study date, number of patients, sex ratio, treatment strategy, treatment procedure, and outcomes.

Two researchers (Jianhe Li and Wei Cui) independently assessed the risk of bias in included RCTs according to the risk of bias tool provided in the Cochrane Handbook for Systematic Reviews of Interventions. The following were assessed: 1) selection bias associated with random sequence generation; 2) selection bias associated with allocation concealment; 3) performance bias: blinding of participants and personnel; 4) detection bias: blinding of outcome assessments; 5) attrition bias: completeness of outcome data; 6) reporting bias: selective reporting; and 7) other sources of bias. Each factor was categorized as "low risk", "high risk", or "unclear". All discrepancies that emerged from this study were discussed by a review panel.

2.6 Data analysis

All meta-analyses were performed within a Bayesian framework using R4.11 software for statistical analysis of data and research, and a Markov chain Monte Carlo method for Bayesian inference. The parameters set in R4.11 software were as follows: number of chains, 4; tuning iterations, 50,000; simulation iterations, 100,000; thinning interval, 1; settings of tuning iterations and simulation iterations were adjusted according to the actual situation. Potential scale reduction factors were used to evaluate the convergence of Markov chains. Models were compared using the deviance information criterion, which is equal to the sum of the posterior mean of the residual deviations and the number of valid parameters. Results for comparisons of dichotomous variables were calculated as odds ratios (OR). Differences between groups were considered statistically significant when the 95% confidence interval (CI) of OR values did not contain 1. Network diagrams showing indirect comparative relationships among different interventions were generated, where the nodal areas for each intervention represent the number of patients, and the thickness of lines between different interventions represented the number of RCTs. R4.11 and Stata17 software were used to plot cumulative probability ranking, and to generate mesh and funnel plots for each intervention. A surface under the cumulative ranking area (SUCRA) curve is used to estimate the probability of ranking each intervention; the larger the area under the curve, the higher the ranking and the higher the probability that the CHIs are the best interventions (Salanti et al., 2011). Clustering analysis was used to synthesize and compare interventions with two different outcome indicators, to obtain the best choice of injection for both outcome indicators: the farther away from the origin in the clustering plot, the better the outcome indicator. Acomparison-adjusted funnel plot was used to assess potential publication bias. If points on both sides of the midline in the funnel diagram were symmetric, which meant the correction guideline was at right angles to the midline, it was considered indicative of no significant publication bias.

3 Results

3.1 Search results

A total of 2004 studies were retrieved, and 389 RCTs (Supplementary Table S2) were finally included for NMA

TABLE 2 Detailed information on Chinese herbal injections.

Chinese herbal injection (Name of the formulation)	Name of the herbal drug	Functional indications	Number of articles	Number of patients	
				Number of men	Number of women
ADI	Cantharis, ginseng, astragalus, acanthopanax senticosus	anti-tumor and immunomodulatory effects Cichello et al. (2015); Meng et al. (2018); Ge et al., 2017; Wang et al. (2018)	66	3,681	2,339
XAPI	Tongguanteng extract, polysorbate	target apoptosis and autophagy leading to the death of NSCLC cells death Jiao et al. (2018)	22	956	618
XGDTI	Lentinan	Enhance the immunity of the body and enhance thesusceptibility Xu et al. (2020); Lv et al. (2021)	18	898	497
CSI	Toad	Induce apoptosis, promote cell differentiation, increase immunity, inhibit vascular proliferation and endothelial cell proliferation Su and Niu (2001); Efferth et al. (2002)	4	114	153
DCI	Sodium cantharidate, vitamin B6	Inhibit the synthesis of protein and nucleic acid in tumor cells and reduce the level of cancer toxin Wang et al. (2019)	14	591	390
DLSI	Red Ginseng, *Astragalus*, Toad, Cantharis	Enhance the inhibition of chemotherapy on tumor metastasis Dong et al. (2014)	8	378	184
FFKSI	*Sophora* flavescens, Smilax glabra	Enhance the resistance of body cancer cells, promote the apoptosis of cancer cells, reduce the stimulation to the body, Anti inflammation, endocrine regulation and immune function improvement Zhang et al. (2013); Agrawal et al. (2014)	55	2,933	1715
HCSI	Dry Toad Skin Extract	inhibit tumor cells, reduced the ADRs in patients with advanced NSCLC Tan et al. (2021)	10	577	412
HQI	*Astragalus* membranaceus	Inhibiting tumor cell proliferation, affecting tumor tissue metabolism and Functions such as regulating immunity Sang et al. (2008)	8	331	156
KAI	*Astragalus* membranaceus, ginseng, matrine	matrine inhibits the proliferation and metastasis of tumor cells by inducing apoptosis, halting the cell cycle, and inhibiting the formation of blood vessels; *Astragalus* membranaceus induction of interferon or exert interferon-like effects, and to enhance anti-tumor effects by strengthening the activity of NK cells Zhao et al. (2012); Li, T et al. (2019); Hu et al. (2022)	37	1835	1,063
KLTI	Coix seed oil, soybean phospholipid	induction of cancer cell apoptosis, inhibition of cancer cell mitosis, execution of cancer cells, and improvement of the immune function Gui and Dai, (2020)	39	2,101	1,417
OOMI	Refined Brucea javanica oil, refined soybean phospholipid, glycerin	Alleviate adverse reactions caused by chemotherapy drugs.It should prevent leukopenia caused by chemotherapy bone marrow suppression and improve the patient's, And improve the quality of life Mo, (2010); Luo et al., (2019)	23	1,113	702
SFI	Red Ginseng, Epibolus	increase the clinical efficacy through inducing the cancer cell apoptosis, inhibiting cell proliferation metastasis, and upregulating tumor immunity Cao et al., (2017)	14	566	359
SI	Red Ginseng, Ophiopogon japonicus, Schisandra chinensis	improving quality of life in patients, immunomodulating action Lu, (2011)	11	511	220
SMI	Red Ginseng, Ophiopogon japonicus	activating the body's immune system, improving the hematopoietic function of bone marrow, regulating angiogenesis and inhibiting the growth of tumor cells Cheng et al., (2021); Zhong et al., (2020)	21	1,013	537
SQFZI	Dangshen, Huangqi	inhibiting cancer growth, promoting apoptosis, increasing chemotherapy sensitivity, and improving immune functions Li et al., (2015); Xiong et al., (2018)	39	990	1913

Note: ADI, Aidi injection; CSI, Chansu injection; DCI, disodium cantharidinate and vitamin B6 injection; DLSI, Delisheng injection; FFKSI, Fufang Kushen injection; HCSI, Huachansu injection; HQI, Huangqi injection; KAI, Kangai injection; KLTI, Kanglaite injection; OOMI, oil of Ophiopogon injection; SFI, Shenfu injection; SI, Shengmai injection; SMI, Shenmai injection; SQFZI, Shenqi Fuzheng injection; XAPI, Xiaoaiping injection; XGDTI, Xianggu Duotang injection.

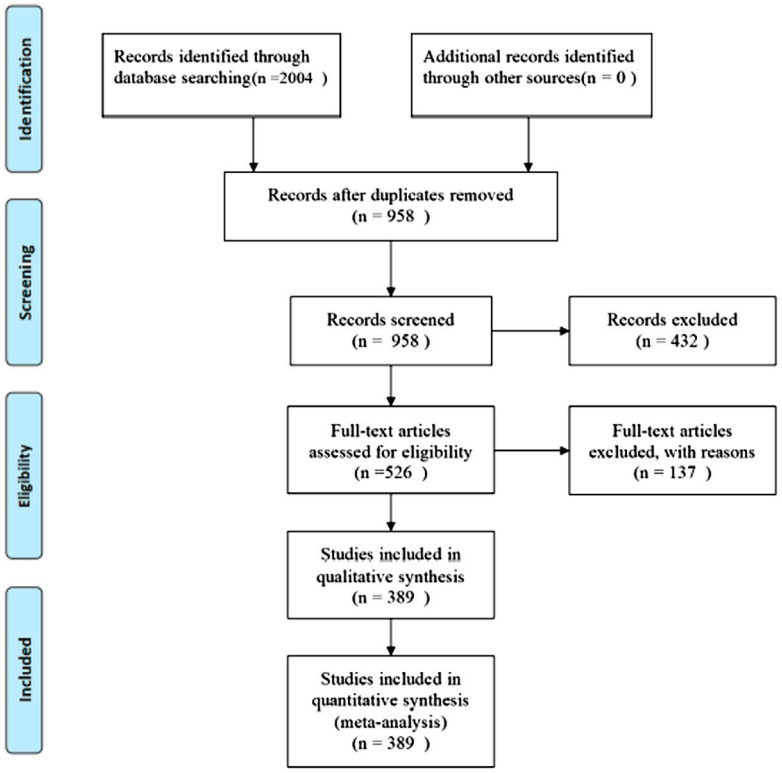

FIGURE 1
PRISMA flow diagram.

according to the pre-defined inclusion and exclusion criteria. Further details of the literature screening process are shown in Figure 1. The 389 RCTs reported 16 herbal injections used as interventions in combination with conventional WM, as follows: Aidi injection (ADI, 66 RCTs), Huachansu injection (HCSI, 10 RCTs), oil of *Ophiopogon* injection (OOMI, 23 RCTs), disodium cantharidinate and vitamin B6 injection (DCI, 14 RCTs), Shenfu injection (SFI, 14 RCTs), Shenmai injection (SMI, 21 RCTs), Shenqi Fuzheng injection (SQFZI, 39 RCTs), Chansu injection (CSI, 4 RCTs), Delisheng injection (DLSI, 8 RCTs), Fufang Kushen injection (FFKSI, 55 RCTs), Huangqi injection (HQI, 8 RCTs), Kangai injection (KAI, 37 RCTs), Kanglaite injection (KLTI, 39 RCTs), Shengmai injection (SI, 11 RCTs), Xiangguduotang injection (XGDTI, 18 RCTs), and Xiaoaiping injection (XAPI, 22 RCTs) (Table 2). Of the 389 RCTs reported, 306 reported DCR, 198 reported Survival Quality Score, 222 reported Incidence of GI Adverse Reactions, 198 reported Incidence of Leukopenia, and 113 reported Incidence of Thrombocytopenia. All included studies were published in Chinese, and the publication years were from 2003 to 2021.

3.2 Characteristics and quality of included studies

A total of 31,263 patients (15,854 in intervention groups and 15,409 in control groups) were enrolled in the 389 included studies, all of whom were diagnosed with NSCLC in hospital, based on clear diagnostic criteria. The number of people is (males:18,588, females:12,675), and patients had a mean age of 58 years. A total of 3,094 patients received ADI, 499 HCSI, 929 OOMI, 498 DCI, 462 SFI, 788 SMI, 1461 SQFZI, 142 CSI, 284 DLSI, 2373 FFKSI, 244 HQI, 1450 KAI, 1722 KLTI, 370 SI, 702 XGDTI, and 786 XAPI combined with WM therapies. Basic data about the studies analyzed in this paper are listed in (Table 2 and Supplementary Table S2). We assessed the quality of included studies according to the Cochrane Risk of Bias tool. Each evaluation principle was classified as “high risk”, “low risk”, or “unclear”. Of the 389 studies included, 59 RCTs used random number tables for group assignment, 2 used random sampling methods, and 1 applied random assignment by lottery; selection bias associated with random sequence generation in the studies was rated as “low risk”. All included studies reported complete outcome indicators, and their attrition bias was assessed as “low

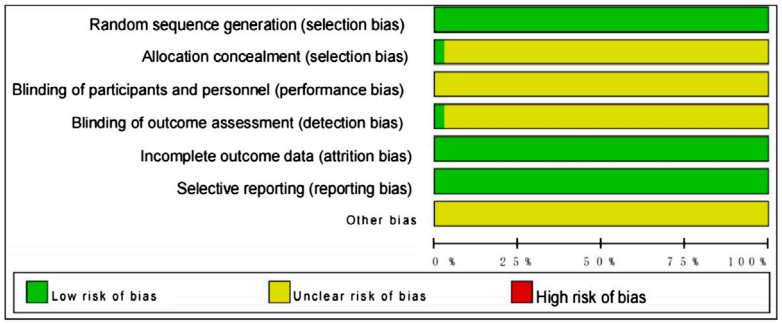

FIGURE 2
Assessment of risk of bias.

risk". Detailed results of the risk of bias assessment are shown in Figure 2.

3.3 Primary outcomes

3.3.1 DCR

DCR directly reflects the curative effect of treatments on patients and served as the main outcome index in this study. A total of 16 CHIs assessed in 306 RCTs including 25,783 patients, were included in the DCR analysis. Studies of ADI (n = 58), CSI (n = 3), DCI (n = 11), DLSI (n = 6), FFKSI (n = 42), HCSI (n = 6), HQI (n = 3), KAI (n = 32), KLTI (n = 35), OOMI (n = 18), SFI (n = 12), SI (n = 4), SMI (n = 16), SQFZI (n = 30), XAPI (n = 11), and XGDTI (n = 19), each combined with WM, were included. A network diagram is shown in Figure 3A. OR values generated by NMA are shown in Supplementary Table S1. DCR values were significantly higher in patients with NSCLC treated with ADI, CSI, DCI, DLSI, FFKSI, HCSI, KAI, KLTI, OOMI, SFI, SMI, SQFZI, XAPI, or XGDTI combined with WM than in those treated with WM alone. There was no significant difference between DCR in patients treated with HQI or SI combined with WM and those receiving WM treatment alone.

The results of the SUCRA rankings and probability values (Table 3 and Figure 4A), after ranking the effects of the interventions, indicated that CSI was most likely to improve DCR in patients with NSCLC relative to WM treatment alone (probability, 80.90%).

3.3.2 Survival quality score

Improvement in quality of survival was assessed for a total of 16 CHIs, 198 RCTs, and 14,700 patients, including studies of ADI (n = 40), CSI (n = 3), DCI (n = 11), DLSI (n = 5), FFKSI (n = 25), HCSI (n = 2), HQI (n = 1), KAI (n = 16), KLTI (n = 18), OOMI (n = 9), SFI (n = 7), SI (n = 6), SMI (n = 8), SQFZI (n = 21), XAPI (n = 12), and XGDTI (n = 14), each combined with WM. A network diagram is shown in Figure 3B. OR values generated by NMA are shown in Supplementary Table S2. Compared with the control group treated with WM alone, survival quality scores of patients with NSCLC treated with WM combined with all CHIs were significantly improved.

After ranking the effects of each intervention, the results of the SUCRA ranking and probability values (Table 3 and Figure 4B) indicated that HQI was most likely to improve survival quality score in patients with NSCLC, compared with controls treated with WM alone (probability, 82.60%).

3.4 Secondary outcomes

3.4.1 Incidence of GI adverse reactions

A total of 16 CHIs, 222 RCTs, and 18,720 patients were included in analysis of GI adverse reactions, comprising studies of ADI (n = 45), CSI (n = 1), DCI (n = 8), DLSI (n = 5), FFKSI (n = 30), HCSI (n = 4), HQI (n = 1), KAI (n = 22), KLTI (n = 22), OOMI (n = 16), SFI (n = 9), SI (n = 6), SMI (n = 10), SQFZI (n = 21), XAPI (n = 8), and XGDTI (n = 14), each combined with WM. A network diagram is shown in Figure 3C. The OR values generated by NMA are presented in Supplementary Table S3. The rate of GI adverse reactions in patients with NSCLC treated with WM combined with ADI, DCI, CSI, DLSI, FFKSI, HCSI, KAI, KLTI, HQI, SFI, SMI, SQFZI, XAPI, or XGDTI was significantly lower than that in patients treated with WM alone. There was no significant difference in GI adverse events between patients receiving OOMI or SI combined with WM and those treated with WM alone.

After ranking the effects of each intervention, the results of the SUCRA rankings and probability values (Table 3 and Figure 4C) indicated that DCI was most likely to reduce the incidence of leukopenia in patients with NSCLC relative to WM treatment alone (probability, 85.50%).

3.4.2 Incidence of leukopenia

Incidence of leukopenia was analyzed for a total of 16 CHIs, in 198 RCTs, and 16,187 patients, comprising studies on ADI (n = 37) CSI (n = 1), DCI (n = 10), DLSI (n = 2), FFKSI (n = 27),

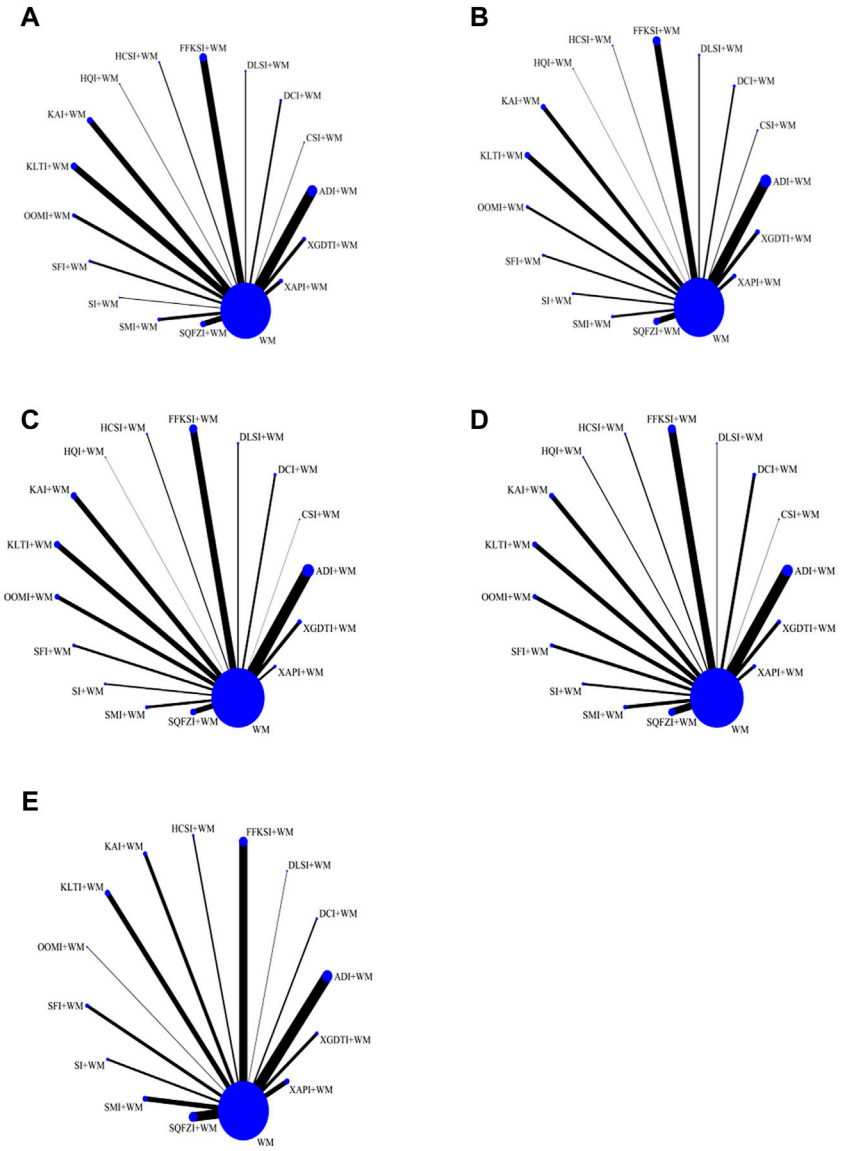

FIGURE 3
Network graphs for different outcomes. **(A)** Disease control rate. **(B)** Survival quality score. **(C)** Incidence of gastrointestinal adverse reactions. **(D)** Incidence of leukopenia. **(E)** Incidence of thrombocytopenia.

HCSI (n = 4), HQI (n = 3), KAI (n = 16), KLTI (n = 16), OOMI (n = 13), SFI (n = 10), SI (n = 7), SMI (n = 11), SQFZI (n = 23), XAPI (n = 6), and XGDTI (n = 12), each combined with WM. A network diagram is shown in Figure 3D. The OR values generated by NMA are presented in Supplementary Table S4. The incidence of leukopenia in patients with NSCLC treated with a combination of WM and ADI, DCI, OOMI, DLSI, FFKSI, HCSI, KAI, KLTI, SFI, SI, SMI, SQFZI, XAPI, or XGDTI was significantly lower than that in patients treated with WM alone. HQI or CSI combined with WM did not significantly alter the incidence of leukopenia relative to WM treatment alone.

After ranking the effects of each intervention, the results of the SUCRA rankings and probability values (Table 3 and Figure 4D) indicated that SMI was most likely to reduce leukopenia incidence in patients with NSCLC compared with WM alone, with a probability of 79.10%.

3.5 Incidence of thrombocytopenia

Analysis of the incidence of thrombocytopenia included a total of 14 CHIs, 113 RCTs, and 12,648 patients in studies of ADI (n =

TABLE 3 Surface under the cumulative ranking probabilities analysis (SUCRA) results for five outcome measures.

Interventions	Disease control rate (%)	Survival quality score (%)	Incidence of gastrointestinal adverse reactions (%)	Incidence of leukopenia (%)	Incidence of thrombocytopenia
ADI + WM	58.20	46.70	36.20	58.60	44.60%
CSI + WM	80.90	28.30	79.20	41.90	—
DCI + WM	67.80	82.20	85.50	63.20	87.40%
DLSI + WM	46.30	52.50	64.20	61.50	77.80%
FFKSI + WM	34.80	39.70	71.70	70.90	48.50%
HCSI + WM	69.10	44.20	75.80	26.00	91.30%
HQI + WM	51.50	82.60	16.10	13.10	—
KAI + WM	73.00	67.10	57.40	70.70	70.10%
KLTI + WM	40.20	31.30	44.20	58.40	53.70%
OOMI + WM	60.00	36.10	8.00	58.50	19.70%
SFI + WM	36.90	33.40	46.30	27.70	56.50%
SI + WM	9.40	70.60	27.70	41.50	8.70%
SMI + WM	80.60	60.30	67.70	79.10	67.00%
SQFZI + WM	56.30	49.30	76.20	67.40	26.90%
XAPI + WM	37.90	64.60	29.50	65.50	28.30%
XGDTI + WM	43.80	60.80	58.80	43.10	63.30%
WM	3.30	0.10	5.60	2.90	6.10%

The greater the SUCRA, the greater the likelihood that it will be the best intervention.

21), DCI (n = 3), DLSI (n = 1), FFKSI (n = 17), HCSI (n = 3), KAI (n = 7), KLTI (n = 10), OOMI (n = 1), SFI (n = 6), SI (n = 4), SMI (n = 9), SQFZI (n = 17), XAPI (n = 5), and XGDTI (n = 6), each combined with WM. A network diagram is shown in Figure 3E. OR values generated by NMA are presented in Supplementary Table S5. The incidence of leukocytopenia in patients with NSCLC treated with a combination of WM and ADI, DCI, HQI, DLSI, CSI, FFKSI, HCSI, KAI, KLTI, SFI, SMI, SQFZI, XAPI, or XGDTI was significantly lower than that in patients treated with WM alone; there was no significant difference between patients treated with OOMI or SI combined with WM and those receiving WM alone.

After ranking the effects of each intervention, the results of the SUCRA rankings and probability values (Table 3 and Figure 4E) indicated that HCSI was most likely to reduce the incidence of thrombocytopenia in patients with NSCLC compared with WM alone (probability, 91.30%).

3.6 Cluster analysis

Cluster analysis based on SUCRA is illustrated in Figure 5. First, cluster analysis was conducted on DCR and survival quality score. Among eligible treatments, SMI + WM and CSI + WM achieved superior effects over the others in improving DCR and survival quality score, while WM alone ranked toward the bottom. Next, cluster analyses were performed on DCR, survival quality score, and other outcomes. The results revealed that SMI + WM, DCI + WM, and HQI + WM were the highest ranked among the eligible interventions.

3.7 Publication bias

To assess whether the primary results of this study were affected by reporting bias, we generated Acomparison-adjusted funnel plot. The points on both sides of the center line of the funnel plot were basically symmetrical from left to right; therefore, we assumed that there was no small sample effect. There was an angle between the correction guideline and the centerline, suggesting that our findings may have been influenced by publication bias to some extent (Figure 6).

4 Discussion

The severity of NSCLC has been widely recognized due to its high mortality rates and heavy economic burden (Bray et al., 2018; Miller et al., 2022). Currently, a combination of CHIs and WM is widely adopted in China and has achieved the desired efficacy (Cao et al., 2017; Chen, 2018; Duan et al., 2018; Wang J et al., 2018; Cao et al., 2019; Wang et al., 2019; Feng et al., 2020; Zhu et al., 2022). As aim of this study was to supplement the optimal strategy of NSCLC treatment and to strengthen additional insights for clinical practice in the future, this NMA incorporated 389 RCTs, which included 31,263 patients, comparing the efficacy of Sixteen CHIs combined

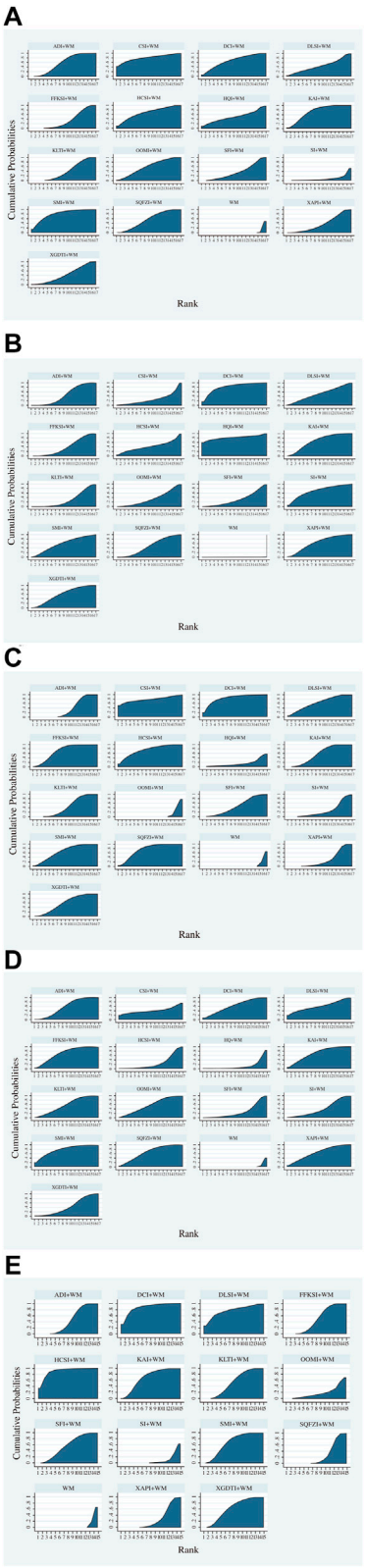

FIGURE 4
Surface under the cumulative ranking curve area plots for each outcome analyzed (The larger the area under the curve, the higher the ranking and the higher the probability that the CHIs are the best interventions). **(A)** Disease control rate. **(B)** Survival quality score. **(C)** Incidence of gastrointestinal adverse reactions. **(D)** Incidence of leukopenia. **(E)** Incidence of thrombocytopenia.

(*Continued*)

FIGURE 4 (Continued)
higher the ranking and the higher the probability that the CHIs are the best interventions). **(A)** Disease control rate. **(B)** Survival quality score. **(C)** Incidence of gastrointestinal adverse reactions. **(D)** Incidence of leukopenia. **(E)** Incidence of thrombocytopenia.

with WM *versus* WM alone. According to the results of the cluster analysis and the SUCRA, all eligible CHIs combined with WM were associated with a more beneficial effect than WM alone. Moreover, SMI + WM and DCI + WM are most likely the optimal CHIs to improve disease control rates, survival quality score, and reduce adverse effects. Hence, the efficacy of SMI + WM and DCI + WM should be considered for patients with NSCLC. However, according to the results of the ORs, there was no significant difference between DCR in patients treated with HQI or SI combined with WM and those receiving WM treatment alone. It is worth noting that there are major differences in the numbers of males and females analyzed in this current NMA. Therefore, clinical treatment decisions should be cautious guided by the specific situation and the clinicians experience. The OR and SUCRA values for some treatment strategies generated in this study were very close; therefore, despite clear advantages over other treatment strategies, they do not represent definitive treatment strategy choices in clinical care.

Shenmai injection (SMI), is derived from a well-known traditional Chinese formula, Shendong Yin, in which the primary pharmacological activity constituents are ginsenosides and Ophiopogon (Liu et al., 2018; Xu et al., 2019; Nag et al., 2012; Chen et al., 2021). Several pharmacological studies reported that SMI has antitumor efficacy and is effective in regulating immune function, enhancing body immunity, and reducing the side effects of chemotherapy (Sun et al., 2020; Li S. Y., 2019; Fang et al., 2018). Ginsenoside Rg3 (the preparation named SMI), a principal pharmacological component of Ginseng, has the potential to reverse drug resistance, inhibit the proliferation of NSCLC cells, and protect DNA integrity (Jiang et al., 2017; Liu L et al., 2019). The undelying mechanism may be that they can attenuate the resistance of cisplatin in lung cancer by inhibiting Akt and NF-KB, resuming immunity, and regulating DNA damage in NSCLC cells by activating the VRK1/P53BP1 pathway (Jiang et al., 2017; Liu T et al., 2019). These findings reveal the impact of ginsenoside Rg3 on DNA damage and downregulating PD-L1, and it opens a new window for developing new drugs based on ginsenoside Rg3 and presents a foundation for developing new therapeutic strategies for cancers. Sodium cantharidinate (SCA), a semi-synthetic derivative of cantharidin, is chemically synthesized from cantharidin and sodium hydroxide (molecular formula, $C_{10}H_{12}Na_2O_5$). SCA (the preparation named DCI) has the potential to enhance immune function and inhibit the adhesion, invasion, and metastasis of tumor cells (Wang G et al., 2018; Tao et al., 2017; Wen et al., 2013; Wu et al., 2021). Their an mechanisim may be that they can promote the proliferation of T lymphocytes, secrete the cytokine interleukin-2, inhibits the secretion

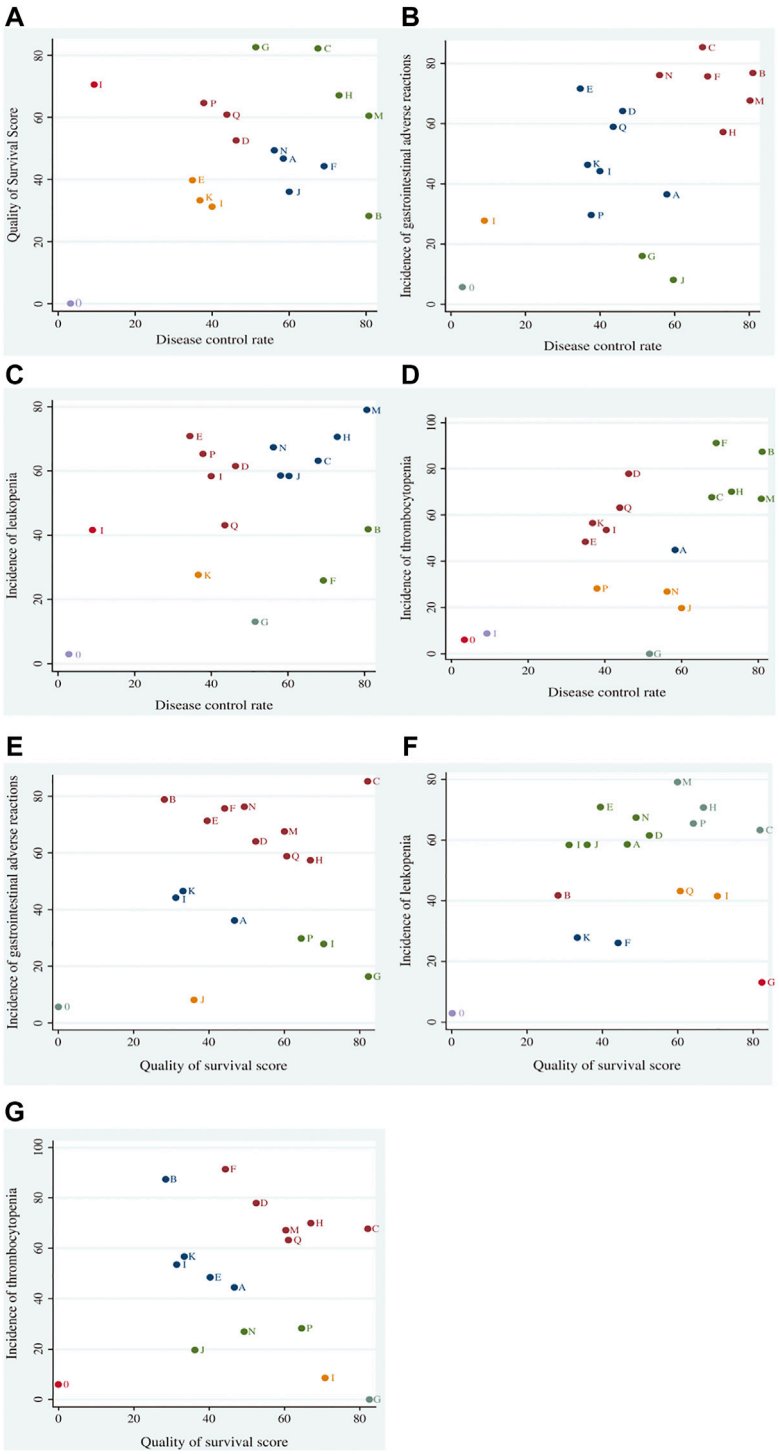

FIGURE 5
Cluster analysis plots for outcomes. Cluster analysis plot of: **(A)** disease control rate (DCR) and survival quality score, **(B)** DCR and incidence of gastrointestinal adverse reactions, **(C)** DCR and incidence of leukopenia, **(D)** DCR and incidence of thrombocytopenia, **(E)** survival quality score and incidence of gastrointestinal adverse reactions, **(F)** survival quality score and incidence of leukopenia, and **(G)** survival quality score and incidence of thrombocytopenia. Interventions located in the upper right corner indicate optimal therapies for two different outcomes, as follows: A, adi + wm; B, csi + wm; C, dci + wm; D, dlsi + wm; E, flksi + wm; F, hcsi + wm; G, hqi + wm; H, kai + wm; I, klti + wm; J, oomi + wm; K, sfi4-wm; L, si + wtn; M, smi + win; N, sqfzi + wm; 0, wm; P, xapi + wm; Q, xgdti + wm.

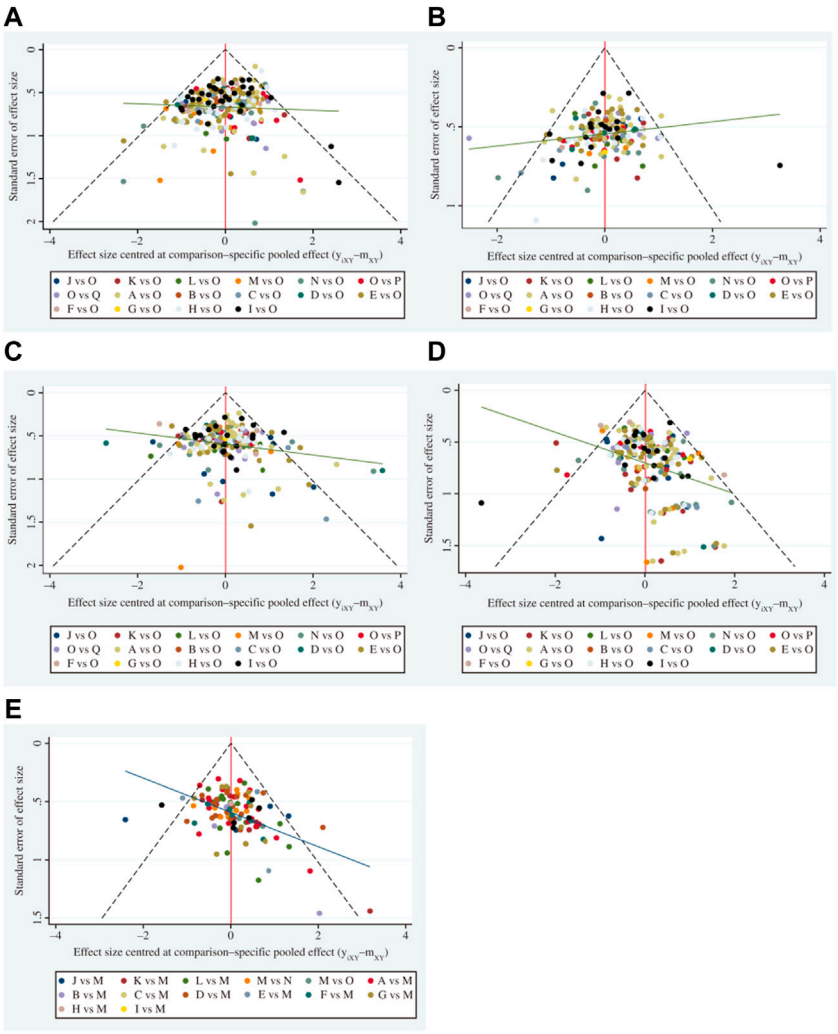

FIGURE 6
Funnel plots (A comparison-adjusted funnel plot was used to assess potential publication bias. If points on both sides of the midline in the funnel diagram were symmetric, which meant the comection guideline was at right angles to the midline, it was considered indicative of no significant publication bias). **(A)** Disease control rate. **(B)** Survival quality score. **(C)** Incidence of gastrointestinal adverse reactions. **(D)** Incidence of leukopenia. **(E)** Incidence of thrombocytopenia. A, adi + wm; B, csi + wm; C, dci + wm; D, dlsi + wm; E, fflcsi + wm; F, hcsi + wm; G, hqi + wm; H, kai + wm; I, klti + wm; J, oomi + wm; K, sfi + wm; L, si + wm; M, smi + wm; N, sqfzi + wm; 0, win; P, xapi + wm; Q, xgdti + wm.

of interleukin-8, downregulates the protein expression of VEGF and MMP-9, restrain the formation of new blood vessels, and control tumor cell adhesion (Tao et al., 2017; Wen et al., 2013; Wu et al., 2021). In addition, SCA could reduce the hematopoietic system toxicity of chemoradiotherapy by shortening the bone marrow maturation, releasing leukocytes' time, and promoting the differentiation of hematopoietic stem cells into granulocyte/monocyte progenitor cells, as well as increasing white blood cell counts (Wu et al., 2021). Chansu injection (CSI) combined with WM is considered as the best intervention for improving the Disease Control Rate (DCR). Pharmacological studies have revealed that it has good anti-tumor and anti-inflammatory effects, possibly due to its main active ingredient-Toad (Su et al., 2001). The antitumor mechanism of this combination strategy may be that they can induce apoptosis of A549 cells, suppress the survivin mRNA and protein, and increase caspase-3 activity (Morishita et al., 1992; Wang et al., 2009; Wang et al., 2012).

The safety of CHIs should also be evaluated alongside their effectiveness. Although the incidences of ADRs/ADEs were low in this NMA, approximately two-thirds of eligible RCTs did not report ADRs/ADEs, implying that these analyses did not take the safety issue seriously. While describing ADRs/ADEs, this NMA observed that an appropriate course of treatment is essential in treatment. Moreover, appropriate dosage, solution, and syndrome differentiation should also be emphasized.

The present study has some limitations that should be considered when interpreting the findings: 1) The methodological quality of the included studies was not very high. Only 62 of the 389 RCTs described the correct generation of random sequences and no studies mentioned allocation concealment or blinding. 2) The included studies spanned a relatively long period of time and were published in Chinese journals, and their findings may not be fully generalizable to other locations. 3) Most included RCTs compared CHIs combined with WM for treatment of NSCLC, and there was a lack of direct comparisons of two or more CHIs. 4) The sample sizes included in the RCTs varied in size and significant differences may not be detected by studies with small sample sizes. If the sample size is increased, to balance the number of RCTs targeting different types of CHI could improve the statistical power of the data and the credibility of the NMA. 5) Most relevant RCTs did not report the CHIs dosage and ADRs/ADEs, In terms of the above limitations, more rigorous RCTs with high quality are needed to verify the value of CHIs combined with WM for patients with NSCLC.

Although this study has some limitations, it is the first to comprehensively assess the efficacy and safety of CHIs in combination with WM for treatment of NSCLC, using a NMA to rank DCR, survival quality scores, incidence of GI adverse events, incidence of leukopenia, and incidence of thrombocytopenia. This NMA provides clinicians with a detailed comparison of common treatment strategies and may provide a reference for clinical application.

5 Conclusion

Overall, this NMA provides a comprehensive and integrated evaluation and summary of the findings using CHIs for treatment of NSCLC. The current evidence indicates that CHIs combined with WM might have a more beneficial effect on NSCLC patients than WM alone, particularly SMI + WM and DCI + WM. It is imperative for clinicians to consider the efficacy of CHIs when diagnosing and treating patients. Future studies should include high quality RCTs, and real-world data are needed to confirm and support the findings of this NMA.

Data availability statement

The original contributions presented in the study are included in the article/Supplementary Material, further inquiries can be directed to the corresponding author.

Author contributions

CP and SL conceived and designed the network meta-analysis. CP, JC, WC, SL, JL, and LP performed the network meta-analysis. JL and WC assessed the quality of the network meta-analysis. CP, JC, WC, SL, JL, and LP analyzed study data, CP and JC wrote the paper. All authors read and approved the final version of the manuscript.

Funding

This study was supported by the Scientific Foundation of Hunan Provincial Health and Health Commission (No. 202213052746).

Acknowledgments

We thank the Hunan Province Evidence-Based Medicine Center for their support.

Conflict of interest

The authors declare that the research was conducted in the absence of any commercial or financial relationships that could be construed as a potential conflict of interest.

Publisher's note

Supplementary material

The Supplementary Material for this article can be found online at: https://www.frontiersin.org/articles/10.3389/fphar.2022.1037620/full#supplementary-material

References

Agrawal, A., Purandare, N., Shah, S., Puranik, A., Banavali, S., and Rangarajan, V. (2014). Response assessment in metronomic chemotherapy: RECIST or PERCIST? *Indian J. Nucl. Med.* 29 (2), 74–80. doi:10.4103/0972-3919.130285

Ahn, E., and Kang, H. (2021). Concepts and emerging issues of network meta-analysis. *Korean J. Anesthesiol.* 74 (5), 371–382. doi:10.4097/kja.21358

Alexander, M., Kim, S. Y., and Cheng, H. (2020). Update 2020: Management of non-small cell lung cancer. *Lung* 198 (6), 897–907. doi:10.1007/s00408-020-00407-5

Bray, F., Ferlay, J., Soerjomataram, I., Siegel, R. L., Torre, L. A., and Jemal, A. (2018). Global cancer statistics 2018: GLOBOCAN estimates of incidence and mortality worldwide for 36 cancers in 185 countries. *Ca. Cancer J. Clin.* 68 (6), 394–424. doi:10.3322/caac.21492

Breimer, L. H., Nousios, P., Olsson, L., and Brunnstrom, H. (2020). Immune checkpoint inhibitors of the PD-1/PD-L1-axis in non-small cell lung cancer: Promise, controversies and ambiguities in the novel treatment paradigm. *Scand. J. Clin. Lab. Invest.* 80 (5), 360–369. doi:10.1080/00365513.2020.1742369

Cao, A., He, H., Jing, M., Yu, B., and Zhou, X. (2017). Shenfu injection adjunct with platinum-based chemotherapy for the treatment of advanced non-small-cell lung cancer: A meta-analysis and systematic review. *Evidence-based complementary Altern. Med.* 2017, 1068751. doi:10.1155/2017/1068751

Cao, A., He, H., Wang, Q., Li, L., An, Y., and Zhou, X. (2019). Evidence of Astragalus injection combined platinum-based chemotherapy in advanced nonsmall cell lung cancer patients: A systematic review and meta-analysis. *Medicine* 98 (11), e14798. doi:10.1097/MD.0000000000014798

Cao, W., Chen, H. D., Yu, Y. W., and Li, N. (2021). Changing profiles of cancer burden worldwide and in China: A secondary analysis of the global cancer statistics 2020. *Chin. Med. J.* 134 (7), 783–791. doi:10.1097/CM9.0000000000001474

Chen, G. (2018). Effects of Shenfu injection on chemotherapy-induced adverse effects and quality of life in patients with advanced nonsmall cell lung cancer: A systematic review and meta-analysis. *J. Cancer Res. Ther.* 14, S549–S555. doi:10.4103/0973-1482.187299

Chen, Y., Sun, Y., Zhao, Q., Liu, C., and Wang, C. (2021). Shenmai injection enhances cisplatin-induced apoptosis through regulation of Mfn2-dependent mitochondrial dynamics in lung adenocarcinoma A549/DDP cells. *Cancer Drug resist.* 4 (4), 1047–1060. doi:10.20517/cdr.2021.94

Cheng, L., Liu, W., Zhong, C., Ni, P., Ni, S., Wang, Q., et al. (2021). Remodeling the homeostasis of pro-and anti-angiogenic factors by Shenmai injection to normalize tumor vasculature for enhanced cancer chemotherapy. *J. Ethnopharmacol.* 270, 113770. doi:10.1016/j.jep.2020.113770

Cho, J. H. (2017). Immunotherapy for non-small-cell lung cancer: Current status and future obstacles. *Immune Netw.* 17 (6), 378–391. doi:10.4110/in.2017.17.6.378

Cichello, S. A., Yao, Q., Dowell, A., Leury, B., and He, X. Q. (2015). Proliferative and inhibitory activity of siberian ginseng (eleutherococcus senticosus) extract on cancer cell lines; A-549, XWLC-05, HCT-116, CNE and beas-2b. *Asian pac. J. Cancer Prev.* 16 (11), 4781–4786. doi:10.7314/apjcp.2015.16.11.4781

Cornell, J. E. (2015). The PRISMA extension for network meta-analysis: Bringing clarity and guidance to the reporting of systematic reviews incorporating network meta-analyses. *Ann. Intern. Med.* 162 (11), 797–798. doi:10.7326/M15-0930

Dong, X. L., Gong, Y., Chen, Z. Z., and Wang, Y. j. (2014). Delisheng Injection , a Chinese medicinal compound, enhanced the effect of cis-platinum on lung carcinoma cell line PGCL3. *Chin. J. Integr. Med.* 20 (4), 286–291. doi:10.1007/s11655-013-1335-0

Duan, B., Xie, J., Rui, Q., Zhang, W., and Xi, Z. (2018). Effects of Shengmai injection add-on therapy to chemotherapy in patients with non-small cell lung cancer: A meta-analysis. *Support. Care Cancer* 26 (7), 2103–2111. doi:10.1007/s00520-018-4167-4

Efferth, T., Davey, M., Olbrich, A., Rucker, G., Gebhart, E., and Davey, R. (2002). Activity of drugs from traditional Chinese medicine toward sensitive and MDR1- or MRP1-overexpressing multidrug-resistant human CCRF-CEM leukemia cells. *Blood Cells Mol. Dis.* 28 (2), 160–168. doi:10.1006/bcmd.2002.0492

Ettinger, D. S., Wood, D. E., Aisner, D. L., Akerley, W., Bauman, J., Chirieac, L. R., et al. (2017). Non-small cell lung cancer, version 5.2017, NCCN clinical practice guidelines in oncology. *J. Natl. Compr. Canc. Netw.* 15 (4), 504–535. doi:10.6004/jnccn.2017.0050

Ettinger, D. S., Wood, D. E., Aisner, D. L., Akerley, W., Bauman, J. R., Bharat, A., et al. (2022). Non-small cell lung cancer, version 3.2022, NCCN clinical practice guidelines in oncology. *J. Natl. Compr. Canc. Netw.* 20 (5), 497–530. doi:10.6004/jnccn.2022.0025

Fang, T., Li, J., and Wu, X. (2018). Shenmai injection improves the postoperative immune function of papillary thyroid carcinoma patients by inhibiting differentiation into Treg cells via miR-103/GPER1 axis. *Drug Dev. Res.* 79 (7), 324–331. doi:10.1002/ddr.21459

Feng, F., Huang, J., Wang, Z., Zhang, J., Han, D., Wu, Q., et al. (2020). Xiao-ai-ping injection adjunct with platinum-based chemotherapy for advanced non-small-cell lung cancer: A systematic review and meta-analysis. *BMC Complement. Med. Ther.* 20 (1), 3. doi:10.1186/s12906-019-2795-y

Garon, E. B., Hellmann, M. D., Rizvi, N. A., Carcereny, E., Leighl, N. B., Ahn, M. J., et al. (2019). Five-year overall survival for patients with advanced non–small-cell lung cancer treated with pembrolizumab: Results from the phase I KEYNOTE-001 study. *J. Clin. Oncol.* 37 (28), 2518–2527. doi:10.1200/JCO.19.00934

González-Xuriguera, C. G., Vergara-Merino, L., Garegnani, L., Ortiz-Munoz, L., and Meza, N. (2021). Introduction to network meta-analysis for evidence synthesis. *Medwave* 21 (6), e8315. doi:10.5867/medwave.2021.06.8315

Gui, X. M., Dai, L., Yuan, Q. W., and Fan, X. M. (2020). Effect of Kanglaite injection in the treatment of advanced non-small cell lung cancer with chemotherapy drugs and its effect on CD~+_ 3、CD~+_ 4、NK、CD~+_ 4/CD~+_ 8. Effect of level. *Chin. J. Traditional Chin. Med.* 38 (5), 147–150. doi:10.13193/j.issn.1673-7717.2020.05.034

Han, Y., Wang, H., Xu, W., Cao, B., Han, L., Jia, L., et al. (2016). Chinese herbal medicine as maintenance therapy for improving the quality of life for advanced non-small cell lung cancer patients. *Complement. Ther. Med.* 24, 81–89. doi:10.1016/j.ctim.2015.12.008

He, X. R., Han, S. Y., and Li, P. P. (2016). Injectable Chinese herbal formula Kang'ai for nonsmall cell lung cancer: Trial sequential analysis of 2, 259 participants from 31 randomized controlled trials. *J. Cancer Res. Ther.* 12 (2), 735–743. doi:10.4103/0973-1482.150411

Hu, J. D., and Wang, Y. (2022). Research progress on the anti-tumor mechanism of matrine Chinese. *J. Traditional Chin. Med.* 40 (5), 171–175. doi:10.13193/j.issn.1673-7717.2022.05.040

Hutton, B., Salanti, G., Caldwell, D. M., Chaimani, A., Schmid, C. H., Cameron, C., et al. (2015). The PRISMA extension statement for reporting of systematic reviews incorporating network meta-analyses of health care interventions: Checklist and explanations. *Ann. Intern. Med.* 162 (11), 777–784. doi:10.7326/M14-2385

Jiang, Y., Liu, L. S., Shen, L. P., Han, Z. F., Jian, H., Liu, J. X., et al. (2016). Traditional Chinese medicine treatment as maintenance therapy in advanced non-small-cell lung cancer: A randomized controlled trial. *Complement. Ther. Med.* 24, 55–62. doi:10.1016/j.ctim.2015.12.006

Jiang, Y., Liu, L. S., Shen, L. P., Liu, J. X., Jiang, G. N., Gu, A. Q., et al. (2019). Traditional Chinese medicine treatment as adjuvant therapy in completely resected stage IB-iiia non-small-cell lung cancer: Study protocol for a multicenter, double-blind, randomized, placebo-controlled trial. *Clin. Lung Cancer* 20 (5), e541–e547. doi:10.1016/j.cllc.2019.05.011

Jiang, Z., Yang, Y., Yang, Y., Zhang, Y., Yue, Z., Pan, Z., et al. (2017). Ginsenoside Rg3 attenuates cisplatin resistance in lung cancer by downregulating PD-L1 and resuming immune. *Biomed. Pharmacother. = Biomedecine Pharmacother.* 96, 378–383. doi:10.1016/j.biopha.2017.09.129

Jiao, L., Dong, C., Liu, J., Chen, Z., Zhang, L., Xu, J., et al. (2017). Effects of Chinese medicine as adjunct medication for adjuvant chemotherapy treatments of non-small cell lung cancer patients. *Sci. Rep.* 7, 46524. doi:10.1038/srep46524

Jiao, Y. N., Wu, L. N., Xue, D., Liu, X. J., Tian, Z. H., Jiang, S. T., et al. (2018). Marsdenia tenacissima extract induces apoptosis and suppresses autophagy through ERK activation in lung cancer cells. *Cancer Cell Int.* 18, 149. doi:10.1186/s12935-018-0646-4

Khunger, M., Jain, P., Rakshit, S., Pasupuleti, V., Hernandez, A. V., Stevenson, J., et al. (2018). Safety and efficacy of PD-1/PD-L1 inhibitors in treatment-naive and chemotherapy-refractory patients with non-small-cell lung cancer: A systematic review and meta-analysis. *Clin. Lung Cancer* 19 (3), e335–e348. doi:10.1016/j.cllc.2018.01.002

Lemjabbar-Alaoui, H., Hassan, O. U., Yang, Y. W., and Buchanan, P. (2015). Lung cancer: Biology and treatment options. *Biochim. Biophys. Acta* 1856 (2), 189–210. doi:10.1016/j.bbcan.2015.08.002

Li, L., Sha, Z., Wang, Y., Yang, D., Li, J., Duan, Z., et al. (2019). Pre-treatment with a combination of Shenmai and Danshen injection protects cardiomyocytes against hypoxia/reoxygenation- and H2O2-induced injury by inhibiting mitochondrial permeability transition pore opening. *Exp. Ther. Med.* 17 (6), 4643–4652. doi:10.3892/etm.2019.7462

Li, S. Y., Q, X. M., and Li, Ke. (2019). Research progress on immunoregulatory effect and mechanism of astragalus polysaccharides. *J. China Med. Univ.* (05), 685–689. doi:10.13753/j.issn.1007-6611.2019.05.030

Li, T., Song, S. L., and Huang, G. (2020). Research progress of immune mechanism and treatment status of Chinese medicine for lung cancer. *J. Tradit. Chin. Med.* 48, 62–66. doi:10.19664/j.cnki.1002-2392.200016

Li, W., Xu, Q., He, Y. F., Liu, Y., Yang, S. B., Wang, Z., et al. (2015). Anti-tumor effect of steamed codonopsis lanceolata in H22 tumor-bearing mice and its possible mechanism. *Nutrients* 7 (10), 8294–8307. doi:10.3390/nu7105395

Li, Z., Feiyue, Z., and Gaofeng, L. (2021). Traditional Chinese medicine and lung cancer--From theory to practice. *Biomed. pharmacotherapy=Biomedecine Pharmacother.* 137, 111381. doi:10.1016/j.biopha.2021.111381

Liu, L., Liu, Q., and Fang, Z. (2017). Research progress of Chinese medicine treatment for non-small cell lung cancer. *J. Shandong Univ. Tradit. Chin. Med.* 41, 386–388. doi:10.16294/j.cnki.1007-659x.2017.04.027

Liu, Q., Wu, H., Wang, J., and Li, X. M. (2018). Effects of Shenmai injection on the values of CO, SV, and ef in patients undergoing off-pump coronary artery bypass graft: A randomized, clinical trial. *Medicine* 97 (10), e0085. doi:10.1097/MD.0000000000010085

Liu, S. X., He, H. H., Jia, R., Du, J., Lin, S., and Li, Y. (2021). Research progress on mechanism of traditional Chinese medicine in treating lung cancer. *Clin. Res. Tradit. Chin. Med.* (5), 132–134.

Liu, T., Zuo, L., Guo, D., Chai, X., Xu, J., Cui, Z., et al. (2019). Ginsenoside Rg3 regulates DNA damage in non-small cell lung cancer cells by activating VRK1/P53BP1 pathway. *Biomed. Pharmacother. = Biomedecine Pharmacother.* 120, 109483. doi:10.1016/j.biopha.2019.109483

Lu, X. (2011). Effect of Shengmai injection combined with chemotherapy on quality of life and immune function of advanced non-small cell lung cancer. *Shaanxi Tradit. Chin. Med.* 32 (04), 389–391.

Luo, L. H., Song, Z. H., Yang, J. J., Li, H. J., Kang, G. Q., and Shi, X. (2019). Effect of Brucea javanica oil emulsion combined with TP chemotherapy on immune function of patients with advanced non-small cell lung cancer. *World Tradit. Chin. Med.* 14 (8), 2087–2091.

Lv, L., Deng, M. H., and Guo, L. Y. (2021). Effect of lentinan as adjuvant therapy on immune function of patients with non-small cell lung cancer. *China Health Stand. Manag.* 12 (14), 101–104.

Ma, C., and Xu, L. (2017). Research progress of Chinese medicine in the treatment of lung cancer. *Chin. J. Tradit. Chin. Med.* 35, 1100–1103. doi:10.13193/j.issn.1673-7717.2017.05.013

Meng, Q., Pan, J., Liu, Y., Chen, L., and Ren, Y. (2018). Anti-tumour effects of polysaccharide extracted from Acanthopanax senticosus and cell-mediated immunity. *Exp. Ther. Med.* 15 (2), 1694–1701. doi:10.3892/etm.2017.5568

Miller, K. D., Fidler-Benaoudia, M., Keegan, T. H., Hipp, H. S., Jemal, A., and Siegel, R. L. (2020). Cancer statistics for adolescents and young adults, 2020. *Ca. Cancer J. Clin.* 70 (6), 443–459. doi:10.3322/caac.21637

Miller, K. D., Nogueira, L., Devasia, T., Mariotto, A. B., Yabroff, K. R., Jemal, A., et al. (2022). Cancer treatment and survivorship statistics, 2022. *Ca. Cancer J. Clin.* 72 (5), 409–436. doi:10.3322/caac.21731

Miller, K. D., Siegel, R. L., Lin, C. C., Mariotto, A. B., Kramer, J. L., Rowland, J. H., et al. (2016). Cancer treatment and survivorship statistics, 2016. *Ca. Cancer J. Clin.* 66 (4), 271–289. doi:10.3322/caac.21349

Minguet, J., Smith, K. H., and Bramlage, P. (2016). Targeted therapies for treatment of non-small cell lung cancer--Recent advances and future perspectives. *Int. J. Cancer* 138 (11), 2549–2561. doi:10.1002/ijc.29915

Mo, S. X. (2010). Effect of Brucea javanica oil emulsion combined with chemotherapy on immune function of patients with non-small cell lung cancer after surgery. *J. Mod. Integr. Chin. West. Med.* 19 (9), 1098–1099.

Molina, J. R., Yang, P., Cassivi, S. D., Schild, S. E., and Adjei, A. A. (2008). Non-small cell lung cancer: Epidemiology, risk factors, treatment, and survivorship. *Mayo Clin. Proc.* 83 (5), 584–594. doi:10.4065/83.5.584

Morishita, S., Shoji, M., Oguni, Y., Ito, C., HiguchiM.and SakanashiM. (1992). Pharmacological actions of "kyushin, " a drug containing toad venom: Cardiotonic and arrhythmogenic effects, and excitatory effect on respiration. *Am. J. Chin. Med.* 20, 245–256. doi:10.1142/S0192415X92000254

Nag, S. A., Qin, J. J., Wang, W., Wang, M. H., Wang, H., and Zhang, R. (2012). Ginsenosides as anticancer agents: *In vitro* and *in vivo* activities, structure-activity relationships, and molecular mechanisms of action. *Front. Pharmacol.* 3, 25. doi:10.3389/fphar.2012.00025

Quoix, E., Zalcman, G., Oster, J. P., Westeel, V., Pichon, E., Lavole, A., et al. (2011). Carboplatin and weekly paclitaxel doublet chemotherapy compared with monotherapy in elderly patients with advanced non-small-cell lung cancer: IFCT-0501 randomised, phase 3 trial. *Lancet (London, Engl.* 378 (9796), 1079–1088. doi:10.1016/S0140-6736(11)60780-0

Reck, M., Remon, J., and Hellmann, M. D. (2022). First-line immunotherapy for non-small-cell lung cancer. *J. Clin. Oncol.* 40 (6), 586–597. doi:10.1200/JCO.21.01497

Ren, S., Xiong, X., You, H., Shen, J., and Zhou, P. (2021). The combination of immune checkpoint blockade and angiogenesis inhibitors in the treatment of advanced non-small cell lung cancer. *Front. Immunol.* 12, 689132. doi:10.3389/fimmu.2021.689132

Rethlefsen, M. L., Kirtley, S., Waffenschmidt, S., Ayala, A. P., Moher, D., Page, M. J., et al. (2021). PRISMA-S: An extension to the PRISMA statement for reporting literature searches in systematic reviews. *Syst. Rev.* 10 (1), 39. doi:10.1186/s13643-020-01542-z

Salanti, G., Ades, A. E., and Ioannidis, J. P. (2011). Graphical methods and numerical summaries for presenting results from multiple-treatment meta-analysis: An overview and tutorial. *J. Clin. Epidemiol.* 64 (2), 163–171. doi:10.1016/j.jclinepi.2010.03.016

Sang, G. Y., Wei, S., and Liu, C. (2008). Research progress on anti-tumor mechanism and clinical application of Astragalus membranaceus. *Shizhen Tradit. Chin. Med.* 19 (12), 3032–3034.

Schwingshackl, L., Schwarzer, G., Rücker, G., and Meerpohl, J. J. (2019). Perspective: Network meta-analysis reaches nutrition research: Current status, scientific concepts, and future directions. *Adv. Nutr.* 10 (5), 739–754. doi:10.1093/advances/nmz036

Shojaee, S., and Nana-Sinkam, P. (2017). Recent advances in the management of non-small cell lung cancer. *F1000Res.* 6, 2110. doi:10.12688/f1000research.11471.1

Siegel, R. L., Miller, K. D., Fuchs, H. E., and Jemal, A. (2021). Cancer statistics, 2021. *Ca. Cancer J. Clin.* 71 (1), 7–33. doi:10.3322/caac.21654

Stock-Martineau, S., Magner, K., Jao, K., and Wheatley-Price, P. (2021). Challenges of immunotherapy in stage IV non-small-cell lung cancer. *JCO Oncol. Pract.* 17 (8), 465–471. doi:10.1200/OP.20.00949

Su, Y. H., and Niu, X. (2001). Review on the pharmacodynamic effect of bufonis preparation. *J. Beijing Univ. Traditional Chin. Med.* 2001 (2), 51–54.

Sun, Y., Chen, Y., Xu, M., Liu, C., Shang, H., and Wang, C. (2020). Shenmai injection supresses glycolysis and enhances cisplatin cytotoxicity in cisplatin-resistant A549/DDP cells via the AKT-mTOR-c-myc signaling pathway. *Biomed. Res. Int.* 2020, 9243681. doi:10.1155/2020/9243681

Sung, H., Ferlay, J., Siegel, R. L., Laversanne, M., Soerjomataram, I., Jemal, A., et al. (2021). Global cancer statistics 2020: GLOBOCAN estimates of incidence and mortality worldwide for 36 cancers in 185 countries. *Ca. Cancer J. Clin.* 71 (3), 209–249. doi:10.3322/caac.21660

Tan, X., Liang, X., Xi, J., Guo, S., Meng, M., Chen, X., et al. (2021). Clinical efficacy and safety of Huachansu injection combination with platinum-based chemotherapy for advanced non-small cell lung cancer: A systematic review and meta-analysis of randomized controlled trials. *Medicine* 100 (36), e27161. doi:10.1097/MD.0000000000027161

Tan, Y., and Wang, Y. (2016). Research progress in Chinese medicine for non-small cell lung cancer. J. Liaoning Univ. *Tradit. ChinMed.* 18, 128–130. doi:10.13194/j.issn.1673-842x

Tao, R., Sun, W. Y., Yu, D. H., Qiu, W., Yan, W. Q., Ding, Y. H., et al. (2017). Sodium cantharidinate induces HepG2 cell apoptosis through LC3 autophagy pathway. *Oncol. Rep.* 38 (2), 1233–1239. doi:10.3892/or.2017.5779

Wang, B., Wang, X., and Li, Z. (2018). Research progress of Chinese medicine in the treatment of lung cancer. *J. Tradit. Chin. Med.* 33, 371–374. doi:10.16368/j.issn.1674-8999.2018.03.090

Wang, G., Dong, J., and Deng, L. (2018). Overview of cantharidin and its analogues. *Curr. Med. Chem.* 25 (17), 2034–2044. doi:10.2174/0929867324666170414165253

Wang, J., Jin, Y., Xu, Z., Zheng, Z., and Wan, S. (2009). Involvement of caspase-3 activity and survivin downregulation in cinobufocini-induced apoptosis in A 549 cells. *Exp. Biol. Med.* 234 (5), 566–572. doi:10.3181/0811-RM-326

Wang, J., Li, G., Yu, L., Mo, T., Wu, Q., and Zhou, Z. (2018). Aidi injection plus platinum-based chemotherapy for stage IIIB/IV non-small cell lung cancer: A meta-analysis of 42 RCTs following the PRISMA guidelines. *J. Ethnopharmacol.* 221, 137–150. doi:10.1016/j.jep.2018.04.013

Wang, J. Y., Chen, L., Zheng, Z., Wang, Q., Guo, J., and Xu, L. (2012). Cinobufocini inhibits NF-κB and COX-2 activation induced by TNF-α in lung adenocarcinoma cells. *Oncol. Rep.* 27 (5), 1619–1624. doi:10.3892/or.2012.1647

Wang, M., Herbst, R. S., and Boshoff, C. (2021). Toward personalized treatment approaches for non-small-cell lung cancer. *Nat. Med.* 27 (8), 1345–1356. doi:10.1038/s41591-021-01450-2

Wang, Z., Feng, F., Wu, Q., Jin, Y., Gu, J., Xu, Y., et al. (2019). Disodium cantharidinate and vitamin B6 injection adjunct with platinum-based chemotherapy for the treatment of advanced non-small-cell lung cancer: A meta-analysis. *Evidence-based complementary Altern. Med.* 2019, 9386273. doi:10.1155/2019/9386273

Watt, J., and Del Giovane, C. (2022). Network meta-analysis. *Methods Mol. Biol.* 2345, 187–201. doi:10.1007/978-1-0716-1566-9_12

Watt, J., Tricco, A. C., Straus, S., Veroniki, A. A., Naglie, G., and Drucker, A. M. (2019). Research techniques made simple: Network meta-analysis. *J. Invest. Dermatol.* 139 (1), 4–12. e1. doi:10.1016/j.jid.2018.10.028

Wen, S. Q., Chen, Q., and Hu, M. (2013). Experimental study on the inhibitory effect of sodium cantharidinate on human hepatoma HepG2 cells. *Afr. J. Tradit. Complement. Altern. Med.* 11 (1), 131–134. doi:10.4314/ajtcam.v11i1.20

Wu, L., Deng, C., Zhang, H., Weng, J., Wu, Y., Zeng, S., et al. (2021). Efficacy and safety of docetaxel and sodium cantharidinate combination vs. Either agent alone as second-line treatment for advanced/metastatic NSCLC with wild-type or unknown EGFR status: An open-label, randomized controlled, prospective, multi-center phase III trial (Cando-L1). *Front. Oncol.* 11, 769037. doi:10.3389/fonc.2021.769037

Wu, X., Chung, V., Lu, P., Poon, S. K., Hui, E. P., Lau, A. Y. L., et al. (2016). Chinese herbal medicine for improving quality of life among nonsmall cell lung cancer patients: Overview of systematic reviews and network meta-analysis. *Medicine* 95 (1), e2410. doi:10.1097/MD.0000000000002410

Xia, L., Liu, Y., and Wang, Y. (2019). PD-1/PD-L1 blockade therapy in advanced non-small-cell lung cancer: Current status and future directions. *Oncologist* 24, S31–S41. doi:10.1634/theoncologist.2019-IO-S1-s05

Xie, Y. A. G., Shen, K. P., and Lu, Y. L. (2021). Research progress in Chinese medicine for non-small cell lung cancer. *Chin. J. Traditional Chin. Med.* 36, 2846–2851.

Xiong, Y., Zhao, Q., Gu, L., Liu, C., and Wang, C. (2018). Shenqi Fuzheng injection reverses cisplatin resistance through mitofusin-2-mediated cell cycle arrest and apoptosis in A549/DDP cells. *Evidence-based complementary Altern. Med.* 2018, 8258246. doi:10.1155/2018/8258246

Xu, H., Liu, Y., Wang, D., and Zhang, Z. (2019). Shenmai injection maintains blood-brain barrier integrity following focal cerebral ischemia via modulating the expression and trafficking of occludin in lipid rafts. *J. Ethnopharmacol.* 237, 55–63. doi:10.1016/j.jep.2019.03.034

Xu, L. L., Zhang, S. F., Wang, Y. L., Luo, Y. B., Fang, Z. H., Fang, Y., et al. (2021). The efficacy of long-term Chinese herbal medicine use on lung cancer survival time: A retrospective two-center cohort study with propensity score matching. *Evid. Based. Complement. Altern. Med.* 2021, 5522934. doi:10.1155/2021/5522934

Xu, S., Zhao, S. K., Ren, F., Ren, D., Wang, Y. Y., and Song, Z. Q. (2020). Progress and prospect of new adjuvant targeting and immunotherapy for non-small cell lung cancer. *Chin. Clin. Oncol.* 47 (6), 299–303.

Yao, C., Su, L., Zhang, F., Zhu, X., Zhu, Y., Wei, L., et al. (2020). Thevebioside, the active ingredient of traditional Chinese medicine, promotes ubiquitin-mediated SRC-3 degradation to induce NSCLC cells apoptosis. *Cancer Lett.* 493, 167–177. doi:10.1016/j.canlet.2020.08.011

Yoneda, K., Imanishi, N., Ichiki, Y., and Tanaka, F. (2018). Immune checkpoint inhibitors (ICIs) in non-small cell lung cancer (NSCLC). *J. UOEH* 40 (2), 173–189. doi:10.7888/juoeh.40.173

Zhang, B. B., Song, Z. H., He, C. X., Yu, X. M., Lou, G. Y., Hong, D., et al. (2013). Clinical efficacy of different doses of gemcitabine combined with carboplatin in first-line treatment of advanced non-small cell lung cancer. *J. Oncol.* (12), 977–980.

Zhang, X. W., Liu, W., Jiang, H. L., and Mao, B. (2018). Chinese herbal medicine for advanced non-small-cell lung cancer: A systematic review and meta-analysis. *Am. J. Chin. Med.* 46 (5), 923–952. doi:10.1142/S0192415X18500490

Zhao, R., and Gao, Y. X. (2012). Research progress on immune regulation of astragalus polysaccharides. *Clin. Res. Traditional Chin. Med.* 4 (5), 4–6.

Zheng, J. B., Li, B. X., Cheng, Q. W., Li, D., and Lin, H. S. (2017). Research progress in post-operative treatment of non-small cell lung cancer patients with traditional Chinese medicine China. *Cancer Clin. Rehabil.* (1), 125–128. doi:10.13455/j.cnki.cjcor.2017.01.36

Zhong, C., Jiang, C., Ni, S., Wang, Q., Cheng, L., Wang, H., et al. (2020). Identification of bioactive anti-angiogenic components targeting tumor endothelial cells in Shenmai injection using multidimensional pharmacokinetics. *Acta Pharm. Sin. B* 10 (9), 1694–1708. doi:10.1016/j.apsb.2019.12.011

Zhou, F., and Zhou, C. C. (2021). Immunotherapy in non-small cell lung cancer: Advancements and challenges. *Chin. Med. J.* 134 (10), 1135–1137. doi:10.1097/CM9.0000000000001338

Zhu, D., Xu, Y., Feng, F., Wang, Z., Han, D., and Zhou, X. (2022). Effect of kangai injection combined with platinum-based chemotherapy on the immune function of patients with advanced non-small-cell lung cancer: A meta-analysis. *Phytomedicine.* 100, 154088. doi:10.1016/j.phymed.2022.154088

frontiers | Frontiers in Pharmacology

TYPE Original Research
PUBLISHED 29 November 2022
DOI 10.3389/fphar.2022.1019451

OPEN ACCESS

EDITED BY
Eswar Shankar,
The Ohio State University, United States

REVIEWED BY
Balaji Chandrasekaran,
Texas A&M University, United States
Prem P. Kushwaha,
Case Western Reserve University, United States

*CORRESPONDENCE
Ling Bi,
biling@shyueyanghospital.com
Yabin Gong,
gongyabin@hotmail.com

†These authors have contributed equally to this work and share first authorship

SPECIALTY SECTION
This article was submitted to Pharmacology of Anti-Cancer Drugs, a section of the journal Frontiers in Pharmacology

RECEIVED 15 August 2022
ACCEPTED 15 November 2022
PUBLISHED 29 November 2022

CITATION
Sang S, Sun C, Ding R, Jiang J, Han Y, Gan S, Bi L and Gong Y (2022), Feiyanning formula modulates the molecular mechanism of osimertinib resistance in lung cancer by regulating the Wnt/β-catenin pathway. *Front. Pharmacol.* 13:1019451. doi: 10.3389/fphar.2022.1019451

Feiyanning formula modulates the molecular mechanism of osimertinib resistance in lung cancer by regulating the Wnt/β-catenin pathway

Shuliu Sang[1†], Chenbing Sun[1†], Rongzhen Ding[1,2], Jingjie Jiang[1], Yang Han[1], Shanshan Gan[1], Ling Bi[1*] and Yabin Gong[1*]

[1]Department of Oncology, Yueyang Hospital of Integrated Traditional Chinese and Western Medicine, Shanghai University of Traditional Chinese Medicine, Shanghai, China, [2]Institutional Key Laboratory of Vascular Biology and Translational Medicine in Hunan Province, Hunan University of Chinese Medicine, Changsha, China

Feiyanning Formula (FYN), a Chinese herbal formula derived from summarized clinical experience, is proven to have anti-tumor effects in lung cancer patients. Osimertinib, a third-generation epidermal growth factor receptor-tyrosine kinase inhibitor (EGFR-TKI), can improve progression-free survival and overall survival of patients but drug resistance is inevitable. The current study evaluated the effects of FYN in osimertinib-resistant HCC827OR and PC9OR cells. FYN preferentially inhibited the proliferation and migration of HCC827OR and PC9OR cells. Moreover, FYN and osimertinib exhibited synergistic inhibitory effects on proliferation and migration. Real-time qPCR (RT-qPCR) and western blotting results indicated that FYN downregulated gene and protein levels of GSK3β and SRFS1, which are enriched in the Wnt/β-catenin pathway. Besides, FYN inhibited tumor growth and exhibited synergistic effects with osimertinib *in vivo*. Collectively, the results suggested that FYN exerted an anti-osimertinib resistance effect *via* the Wnt/β-catenin pathway.

KEYWORDS

Feiyanning formula, osimertinib, drug resistance, lung cancer, Wnt/β-catenin pathway

Introduction

Lung cancer is the most prevalent tumor globally and ranks first in cancer mortality (Siegel et al., 2022). The most common treatment for early stage lung cancer is surgery, whereas chemotherapy, radiotherapy, targeted therapy, and immunotherapy are commonly used in progressive cases (Lemjabbar-Alaoui et al., 2015). Unfortunately, most patients experience recurrence and metastasis after surgery, which foreshadows a poor prognosis (Schegoleva et al., 2021). To improve outcomes, the National Comprehensive Cancer Network recommended that histological subtypes and biomarkers be detected before treating lung cancer patients with recurrence and metastasis (Ettinger et al., 2022). As a third-generation epidermal growth factor receptor-tyrosine kinase inhibitor (EGFR-TKI), osimertinib is

recommended as the first-line treatment in patients with epidermal growth factor receptor (EGFR) mutation-positive non-small cell lung cancer (NSCLC) (Maione et al., 2015). Osimertinib promotes longer progression-free survival (18.9 months vs 10.2 months) and better overall survival (38.6 vs. 31.8 months) than former generation EGFR-TKIs (Passaro et al., 2021), but the development of resistance is inevitable. In past decades, the mechanisms involved in osimertinib resistance have not been entirely expounded there has been no practical way to improve the situation. However, herbal compounds have exhibited outstanding potential therapeutic value recently.

Several recent studies have investigated the effects of Chinese herbal compounds on EGFR-TKI resistance (Hu et al., 2020; Tan et al., 2020). Feiyanning Formula (FYN) is an anti-cancer formula consisting of *Astragalus membranaceus, Ganoderma lucidum, Paris polyphylla,* and other Chinese herbs. In our previous clinical study, FYN combined with chemotherapy prolonged the survival of advanced NSCLC patients (Gong et al., 2018). Recent studies have shown that FYN can induce apoptosis in lung adenocarcinoma cells by activating the mitochondrial pathway (Zhu et al., 2021). However, the mechanism by which FYN delays drug resistance has not been reported yet.

In this study, the effects of FYN combined with osimertinib on PC9OR and HCC827OR cell proliferation and migration were investigated. FYN combined with osimertinib had synergistic inhibitory effects against the development of osimertinib resistance *in vivo*. These findings revealed the mechanisms involved in the application of FYN the treatment of NSCLC, and provide an experimental basis for clinical application.

Materials and methods

Herbs and chemicals preparation

FYN consists of 11 Chinese herbs (Table 1). All FYN herbs were provided by the pharmacy of Shanghai Chest Hospital, Shanghai Jiao Tong University (Shanghai, China). FYN was dried into a lyophilized powder and stored at -20 ˚C. In accordance with the experimental requirements, the lyophilized FYN powder was dissolved in RPMI-1640 medium (Hyclone, United States, SH30809.01), diluted to various concentrations, then passed through a 0.22-μm filter. Osimertinib (Selleck Company, United States, S7297) was dissolved in DMSO (Absin Bioscience Inc., China, abs9187), diluted to 200 mM, then aliquoted and stored at −20˚C in the dark.

Cells and cell culture

HCC827 and PC9 cells originally obtained from the Cell Bank of Chinese Academy of Sciences (Shanghai, China) were cultured in RPMI 1640 medium supplemented with 10% fetal bovine serum (Gibco, United States, 10091148) and 1% penicillin–streptomycin (HyClone, United States, SV30010) in a humidified incubator (Thermo Fisher, United States) with 5% CO_2 at 37˚C. All cell types were verified by short tandem repeat profiling and were examined every 6 months for *Mycoplasma*.

Establishment and identification of osimertinib-resistant cell line lines

PC9 and HCC827 cells were cultured in T25 flasks at logarithmic growth stages, then osimertinib was added to establish osimertinib-resistant cell lines. PC9OR and HCC827OR cells were established in our laboratory by exposing them to stepwise and incremental concentrations of osimertinib in the range of 5–3000 nM (Table 2).

Cell viability assay

Cell proliferation was assessed *via* the CCK-8 assay. PC9OR, HCC827OR, PC9, and HCC827 cells in logarithmic growth phase were seeded into 96-well plates at a density of 5×10^3 per well, and treatments (FYN, osimertinib and FYN combined with osimertinib) were applied the next day. Five replicate wells were prepared for each group. After treatment, OD values at 450 nm were measured in each well after the addition of 10 μl CCK-8 reagent for 1–4 h without refreshing the media. The inhibition ratio was calculated *via* the following formula:

$$\text{Inhibition ratio}\ (\%) = (1 - \text{OD}_{\text{treatment}} / \text{OD}_{\text{control}}) \times 100\%$$

The IC_{50} values of osimertinib were calculated using GraphPad Prism 8.0 software.

Synergistic effect analysis

Combination treatments can result in synergistic, additive, antagonistic, or potentiative effects. These effects were evaluated by calculation of the combination index (CI) in accordance with the Chou-Talalay method. Data were analyzed using CompuSyn software (CompuSyn Inc.), and CI 0.85 to 0.90 = slight synergism, CI 0.70 to 0.85 = moderate synergism, CI 0.30 to 0.70 = synergism, CI 0.10 to 0.30 = strong synergism, and CI < 0.10 = very strong synergism.

Colony formation assay

PC9OR and HCC827OR cells were seeded into 6-well plates at a density of 1000 cells per well for 24 h before treatment. After 14 days, all wells were fixed with 4% paraformaldehyde (Biosharp Co., Ltd., China, BL539A) and stained with crystal violet (Beyotime Inc., China, C0121). After drying, the stained cells were imaged, and stained colonies containing >10 cells were counted.

TABLE 1 FYN components.

Species	Active chemicals	Herbal name	Number of components (g)
Dried root of *Astragalus membranaceus (Fisch.)*	Isoflavanone, 3,9-di-O-methylnissolin, Isorhamnetin, Jaranol, Kaempferol, Quercetin, 7-O-methylisomucronulatol, Hederagenin, Formononetin, Calycosin, Mairin, (3S,8S,9S,10R,13R,14S,17R)-10,13-dimethyl-17-[(2R,5S)-5-propan-2-yloctan-2-yl]-2,3,4,7,8,9,11,12,14,15,16,17-dodecahydro-1H-cyclopenta [a] phenanthren-3-ol, Bifendate	Huang Qi	30
Dried rhizome of *Polygonatum kingianum Coll. et Hemsl.*	4′,5-Dihydroxyflavone, Apigenin, Baicalein, 3′-Methoxydaidzein, β-sitosterol, Diosgenin, Oroxin A, Daucosterol, Dioscin, Methylprotodioscin, (+)-Syringaresinol-O-β-D-glucoside, Liriodendrin_qt	Huang Jing	30
Dried fruit of *Cornus officinalis Sieb. Et Zucc.*	Hydroxygenkwanin, Tetrahydroalstonine, Mandenol, Cornudentanone, Ethyl linolenate, Ethyl oleate (NF), β-sitosterol, Poriferast-5-en-3beta-ol, Stigmasterol, Diop, Leucanthoside, 2,6,10,14,18-pentamethylicosa-2,6,10,14,18-Pentaene, Gemin D	Shan Zhu Yu	15
Dried rhizome of *Paris polyphylla Smith var. yunnanensis (Franch.) Hand.-Mazz.*	Isorhamnetin, Kaempferol, Luteolin, Quercetin, Remerin,	Chong Lou	15

(Continued on following page)

TABLE 1 (*Continued*) FYN components.

Species	Active chemicals	Herbal name	Number of components (g)
	Stigmasterol, Daucosterol, Dioscin, Polyphyllin VII, Polyphyllin I, Polyphyllin II		
Dried rhizome of *Atractylodes macrocephala Koidz.*	Apigenin, Luteolin, Ethyl caffeate, α-Amyrin, AtractylenolideII, (3S,8S,9S,10R,13R,14S,17R)-10,13-dimethyl-17-[(2R,5S)-5-propan-2-yloctan-2-yl]-2,3,4,7,8,9,11,12,14,15,16,17-dodecahydro-1H-cyclopenta [a]phenanthren-3-ol, Atractylenolide Ⅲ, Atractylenolide I	Bai Zhu	9
Dried nest of *Polistes olivaceous (DeGeer)*	Kaempferol, Ferulic acid, β-sitosterol, 3,4,5-trihydroxy benzoic acid, Supraene, α-Carotene	Feng Fang	9
Dried plant of *Salvia chinensis Benth.*	Quercetin, Resveratrol, Oleanolic acid, Ursolic acid, β-sitosterol, Salvianolic acid C, Vanillin	Shi Jian Chuan	30
Dried skin of *Bufo gargarizans Cantor*	Cinobufagin, Cinobufotalin, β-sitosterol, Arenobufagin, Bufalin, Resibufogenin, Deacetylcinobufotalin, Bufotaline	Gan Chan Pi	6
Dried fruit body of *Ganoderma lucidum (Leyss.exFr.) Karst*	Cerevisterol, Ganosporelactone B, Methyl Ganoderic acid DM, Epoxyganoderiol B, Ganoderiol F,	Ling Zhi	15

(Continued on following page)

TABLE 1 (*Continued*) FYN components.

Species	Active chemicals	Herbal name	Number of components (g)
	Ganodermanondiol, Methyl (4R)-4-[(5R,7S,10S,13R,14R,15S,17R)-7,15-dihydroxy-4,4,10,13,14-pentamethyl-3,11-dioxo-2,5,6,7,12,15,16,17-octahydro-1H-cyclopenta [a] phenanthren-17-yl]pentanoate, Lucidumol A, Ganoderal B, Lucialdehyde B, Methyl (4R)-4-[(5R,10S,13R,14R,17R)-4,4,10,13,14-pentamethyl-3,7,11,15-tetraoxo-2,5,6,12,16,17-hexahydro-1H-cyclopenta [a]phenanthren-17-yl] pentanoate, (+)-Methyl ganolucidate A, Ganoderic acid V, Ganoderic acid X, Ganoderic aldehyde A, Lucialdehyde C, Ganolucidic acid E, Ganodermic acid T-Q, Ganoderic acid Mi, Ganoderic acid TR		
Dried pseudobulb of *Cremastra appendiculata (D.Don) Makino*	Quercetin, 2-methoxy-9,10-dihydrophenanthrene-4,5-diol, β-sitosterol, Stigmasterol, 3,4,5-trihydroxy benzoic acid, Daucosterol, Colchicine	Shan Ci Gu	15
Dried leaf of *Epimedium brevicomu Maxim.*	Chryseriol, Kaempferol, Luteolin, Quercetin, 8-Isopentenyl-kaempferol, Linoleyl acetate, Magnograndiolide, Poriferast-5-en-3beta-ol, Yinyanghuo A, Icariin, 25-epicampesterol, Anhydroicaritin, Yinyanghuo C, Yinyanghuo E	Yin Yang Huo	15

Wound healing assay

PC9OR and HCC827OR cells were inoculated in 6-well plates at 5×10^5 per well. When cells reached 90% confluence a horizontal scratch was made with a 200-μl pipette tip. After washing away floating cells with PBS, cells were treated for 24 h. Images were obtained using an inverted microscope (Leica DMI3000B, Leica Microsystems, Inc.) at different timepoints to measure scratch width.

TABLE 2 Time of cultivation with each dose.

Concentration (nM)	Time (days)
5	7
10	7
20	15
30	15
100	15
500	15
1000	20
2000	20
3000	20

Transwell assay

PC9OR and HCC827OR cells were diluted to 2×10^4 per well in serum-free 1640 medium. The cells were then seeded into the upper chambers of transwell plates and different treatments were applied for 24 h. Medium containing 15% fetal bovine serum was added to the lower chamber to enhance cell migration. After 24 h, the cells were fixed with 4% paraformaldehyde and stained with crystal violet. An inverted microscope was used for image acquisition.

Real-time qPCR (RT-qPCR) array

The Trizol reagent (Invitrogen, Thermo Fisher Scientific Inc., United States, 15596018) was used to extract total RNA from cells. The RNA was then reverse transcribed into cDNA using a cDNA synthesis kit (Bio-Rad, United States, 1708891), and gene expression profiles were analyzed by RT-qPCR array in accordance with the manufacturer's instructions. mRNA expression levels were calculated using the $2^{-\Delta\Delta Cq}$ method, and GAPDH was used as an internal reference. All primers were purchased from Sangon Biotech, and were summarized in Supplementary Table S1.

Western blotting

HCC827OR and PC9OR cells were treated with FYN at IC_{50} for 48 h to determine protein expression levels. The cells were then lysed in ice-cold RIPA buffer (Beyotime Inc., China, P0013B), and a BCA Protein Assay Kit (Beyotime Inc., China, P0010) was used to quantify protein concentrations. Total proteins in different groups were subjected to SDS-PAGE gel separation, then transferred to polyvinylidene difluoride membranes (Merck Millipore). After blocking with 5% skim milk powder at room temperature for 2 h, the membranes were incubated with primary antibodies at 4 °C overnight. Secondary antibodies were then added, and the preparations were incubated for 2 h. The probed membranes were developed with ECL solution (Sangon, Shanghai, China, C510043-0100). Primary antibodies against SRSF1 (Cat# 14908), GSK3B (Cat# 5558), β-catenin (Cat# 8480), and GAPDH (Cat# 5174) were acquired from Cell Signaling Technology. The primary antibody against PCNA (Cat# sc-56) was acquired from Santa Cruz Biotechnology.

Tumor xenograft

Female nude mice aged 4 weeks were purchased from the Shanghai SLAC Animal Laboratory (China). After acclimatization for 1 week, 1×10^7 HCC827OR cells were resuspended in 200 µl of PBS then injected subcutaneously under the left armpit of each mouse. When the mean tumor volume of all mice was approximately 100 mm^3, the mice were divided into control group, FYN group, osimertinib group, and FYN with osimertinib combination group. The preparations applied to all four groups were administered *via* oral gavage once each day. The control group was administered water. The FYN group was administered 131.86 mg FYN powder per mouse. The osimertinib group was administered 0.1 mg osimertinib per mouse. The combination group was administered 131.86 mg FYN powder and 0.1 mg osimertinib per mouse. Body weights and tumor volumes were recorded daily. Tumor volumes were measured with a digital caliper and calculated as 0.5 × length × $width^2$, and the results were presented in Supplementary Table S2. At the endpoint of the experiment, the tumors were weighted and the organs were fixed with 4% paraformaldehyde, embedded in paraffin, and stained with hematoxylin and eosin.

Statistical analysis

Data were analyzed by GraphPad Prism 8.0, and represented as means ± standard deviation. Differences between groups were assessed *via* Student's *t*-test or analysis of variance. Differences were considered statistically significant when $p < 0.05$.

Results

FYN preferentially inhibited cell proliferation and migration in osimertinib-resistant lung cancer cell lines

The rates of PC9OR and HCC827OR cell inhibition were significantly reduced compared to parental cells after 48 h of osimertinib intervention, in a dose-dependent manner (Supplementary Figure S1A). Protein levels of PCNA in HCC827OR and PC9OR cell lines were higher than in the parental counterpart (Supplementary Figure S1B), indicating enhanced cellular proliferation and invasion. FYN

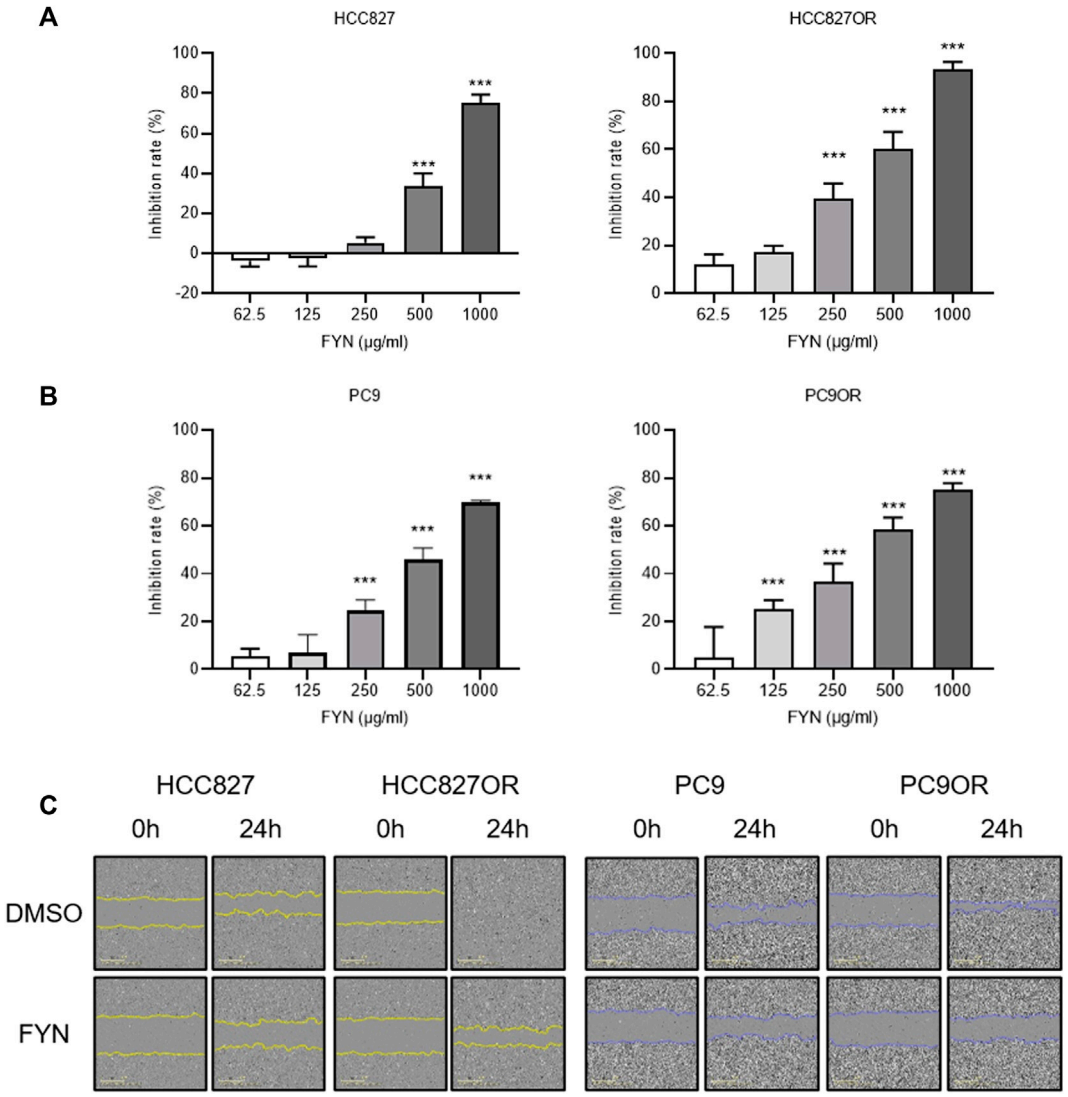

FIGURE 1
Effects of FYN on lung cancer cell proliferation and migration. **(A,B)** CCK8 results. HCC827 or HCC827OR cells **(A)** and PC9 or PC9OR cells **(B)** were treated with different concentrations of FYN for 48 h. **(C)** Cell migration was detected *via* wound healing assays. HCC827 or HCC827OR cells were treated for 24 h with 250 μg/ml FYN, and PC9 or PC9OR cells were treated for 24 h with 125 μg/ml FYN. *$p < 0.05$, **$p < 0.01$, ***$p < 0.001$.

preferentially suppressed cellular proliferation and migration in osimertinib-resistant HCC827OR and PC9OR cells, and it had higher potency and efficacy than in the parental HCC827 and PC9 cells (Figures 1A–C).

Synergistic effect of FYN with osimertinib on resistant lung cancer cell lines

To investigate the synergistic effect of FYN with EGFR-TKI, CCK-8 assays and colony formation assays were performed. The effects of the combination of FYN and osimertinib on the viability of HCC827OR and PC9OR cells were assessed. The combination exhibited more significant inhibition compared with osimertinib alone (Figure 2A, Supplementary Figure S1C). The CI was less than 1.0 (Figure 2B), suggesting a synergistic effect of FYN and osimertinib in resistant cell lines. Colony formation assays indicated that the combination substantially inhibited the long-term proliferation of HCC827OR and PC9OR cells (Figure 3A). Thus, the combination exhibited significant inhibition of the viability of drug-resistant cells.

Transwell assays and wound-healing assays were performed to investigate the effects of the combination of

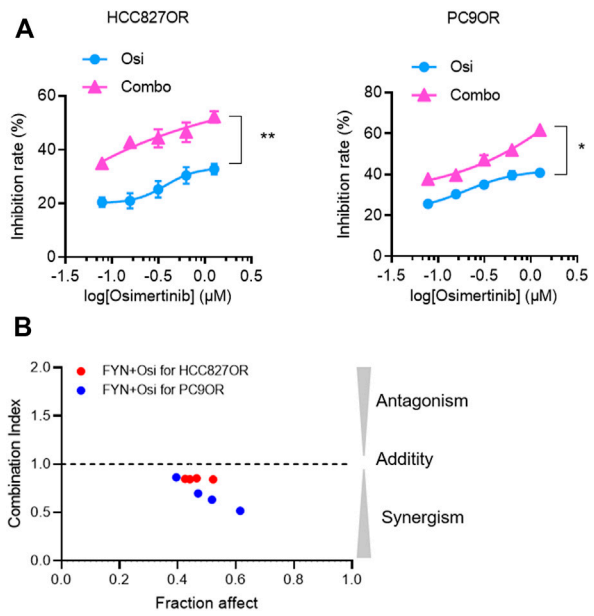

FIGURE 2
Synergistic effects of FYN with osimertinib on osimertinib-resistant NSCLC cells lines. **(A)** HCC827OR cells were treated for 48 h with 4 μM osimertinib alone, or in combination with 250 μg/ml FYN. PC9OR cells were treated for 48 h with 6 μM osimertinib alone, or in combination with 500 μg/ml FYN. **(B)** Synergistic effects of 250 μg/ml FYN on HCC827OR cells (red circles), or 500 μg/ml FYN on PC9OR cells (blue circles), combined with various dose of osimertinib. CI (combination index) value was calculated as described in Materials and Methods. Osi, osimertinib; FYN, Feiyanning Formula; Combo, combination of Feiyanning Formula and osimertinib. *$p < 0.05$, **$p < 0.01$.

FYN and osimertinib on migration and invasion. Cell migration was enhanced in HCC827OR and PC9OR cell lines compared to the parental lines (Figure 1C). Cell migration was inhibited after 24 h of treatment with the combination of FYN and osimertinib in HCC827OR and PC9OR cell lines, compared to control and osimertinib alone ($p < 0.05$) (Figure 3B). Consistent results were obtained in wound-healing assays (Figure 3C).

FYN downregulated mRNA expression in the Wnt/β-catenin pathway

RT-qPCR array analysis was performed after 48 h of treatment with an IC_{50} dose of FYN in HCC827OR cell lines. mRNA levels of c-MYC, GSK3B, PIK3CA, Slug, and SRSF1 were downregulated (Figures 4A,C). c-MYC, GSK3B, Slug, and SRSF1 were downregulated after 48 h of exposure to FYN in PC9OR cell lines (Figure 4D). KEGG analysis of the genes above indicated they were primarily enriched differentially expressed genes in the Wnt/β-catenin pathway (Figure 4B).

FYN reduced the expression of SRSF1, GSK3B, and β-catenin

The differentially expressed genes were screened *via* the GEPIA website (http://gepia.cancer-pku.cn/). SRSF1 and GSK3B were filtered through "overall survival", and high expression was associated with a poorer prognosis than low expression in a subset of lung adenocarcinoma patients (Figure 5A). Western blotting results indicated that FYN could significantly downregulate SRSF1 and GSK3B protein expression in HCC827OR and PC9OR cells. Since the Wnt/β-catenin pathway mainly regulates downstream signaling pathways with β-catenin as the core node, we investigated the expression of β-catenin in HCC827OR and PC9OR cells after FYN intervention. FYN could downregulate β-catenin, suggesting that the Wnt/β-catenin pathway may be involved in FYN's effects on osimertinib resistance (Figure 5B).

FYN suppressed tumor growth *in vivo*

To validate the synergistic effects of FYN with osimertinib *in vivo*, murine subcutaneous xenograft experiments were performed. In HCC827OR xenografts (Figures 6A,B, Supplementary Table S2), compared with the control group tumor growth was inhibited in the other three groups, particularly in the combination group ($p < 0.05$). No lesions were observed in heart, kidney, liver, spleen, or lung tissues in the combination group (Figure 6C). Considering that the tumor volume of the control group met the ethical requirements, 7 mice in the control group, 7 mice in the FYN group, 4 mice in the osimertinib group, and 4 mice in the combination group were terminated after 30 days of treatment. Due to the small volumes of tumors, 3 mice in the osimertinib group and 3 mice in the combination group were retained for further observation under prolonged intervention. Tumor volume increased significantly after 20 days in the osimertinib group, which may indicate the development of resistance. Compared with the osimertinib group, tumor growth was significantly inhibited in the combination group, suggesting that FYN could partly against the adapt resistance of osimertinib (Figure 6D).

Discussion

Most drug resistance development occurred after treatment with former generations of EGFR-TKIs, with a progression-free survival of 10–14 months (Zhang et al., 2019; Wu et al., 2020). T790M mutation was believed to be the culprit. Osimertinib has been used as a first-line treatment in NSCLC patients with EGFR Mutations due to significant therapeutic effects on both common EGFR mutations (Del19 and L858R) and T790M resistance mutations (Popat, 2018). However, the development of resistance remains inevitable

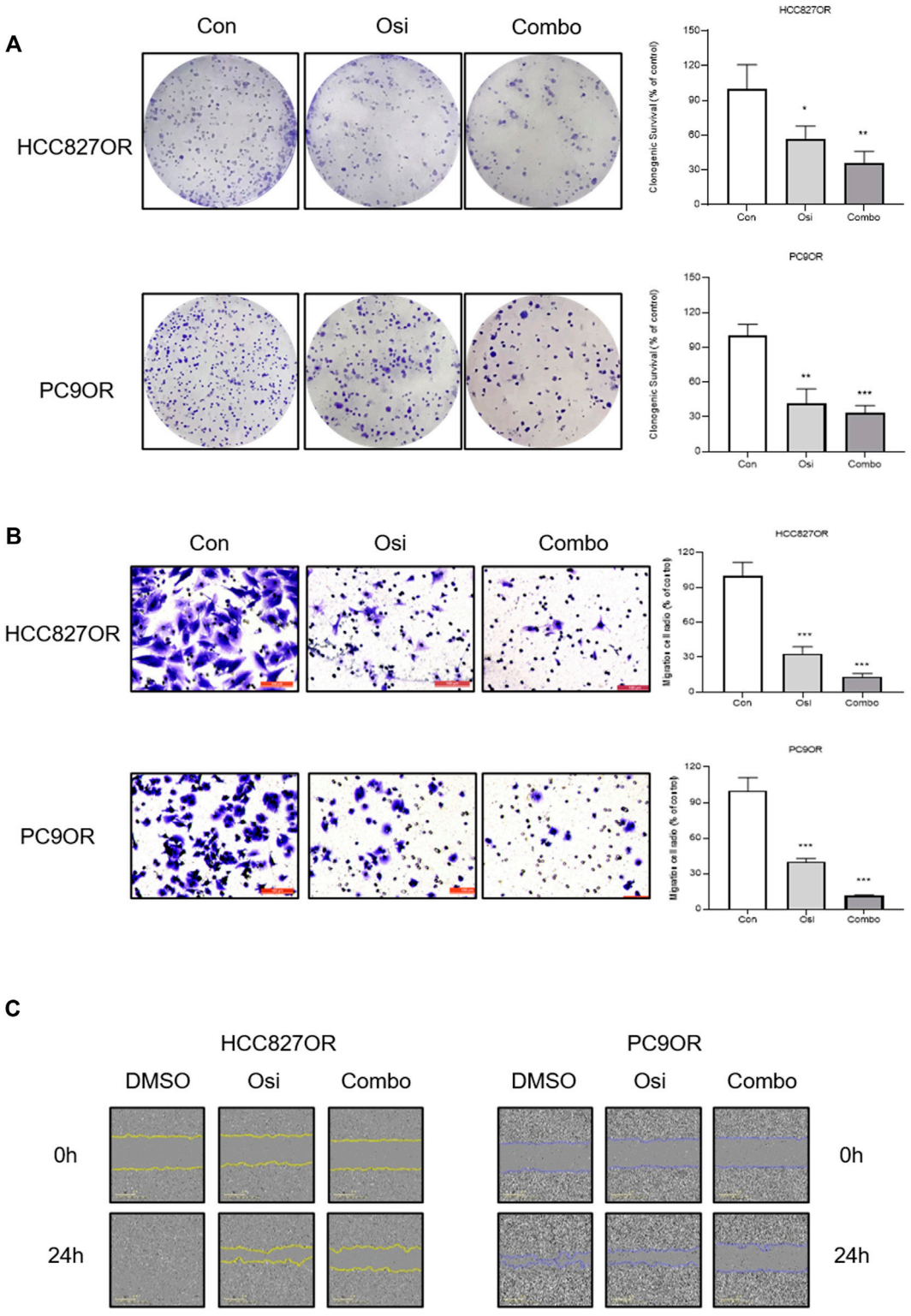

FIGURE 3
The synergistic effect of FYN with osimertinib on cell proliferation and migration. Resistant HCC827 cells were treated with 1 μM osimertinib alone or in combination with 250 μg/ml FYN. Resistant PC9 cells were treated with 1 μM osimertinib alone or in combination with 125 μg/ml FYN. **(A)** Clonogenic assays results of HCC827OR and PC9OR and the cells were treated for 14 days. **(B)** Cell migration was detected by transwell assays or **(C)** wound healing assays for 24 h. Con, control; Osi, osimertinib; Combo, combination of Feiyanning Formula with osimertinib. *$p < 0.05$, **$p < 0.01$, ***$p < 0.001$.

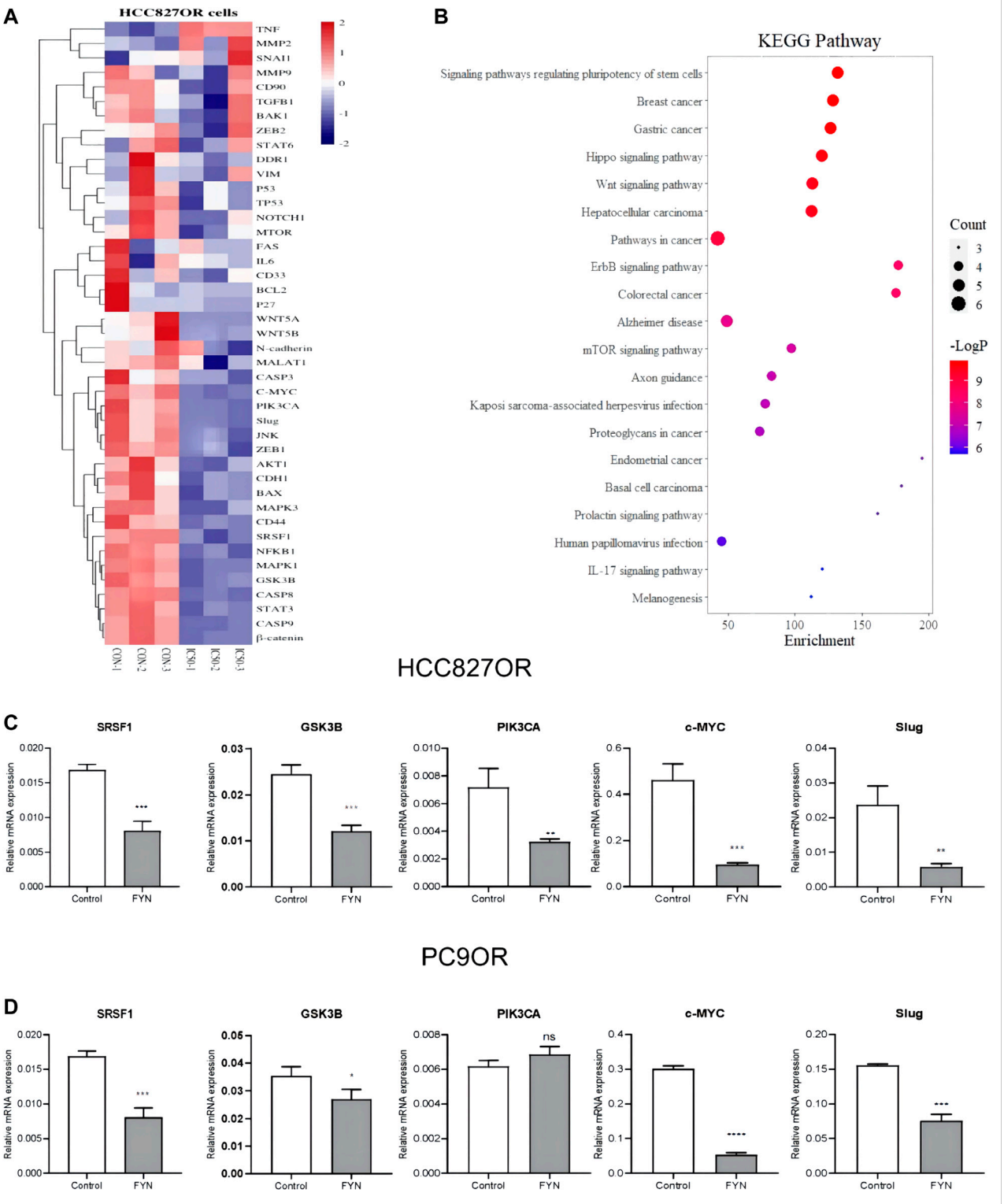

FIGURE 4
FYN downregulated the mRNA levels of genes enriched in the Wnt/β-catenin pathway. HCC827OR cells treated with FYN at IC_{50} for 48 h were harvested for analysis **(A)** Heatmap of target mRNA expression in control HCC827OR cells and FYN-treated HCC827OR cells. **(B)** KEGG analysis mostly enriched differentially expressed genes in the Wnt/β-catenin pathway. **(C and D)** mRNA levels in HCC827OR cells **(C)** and PC9OR cells **(D)** were measured by qPCR. FYN, Feiyanning Formula. *$p < 0.05$, **$p < 0.01$, ***$p < 0.001$.

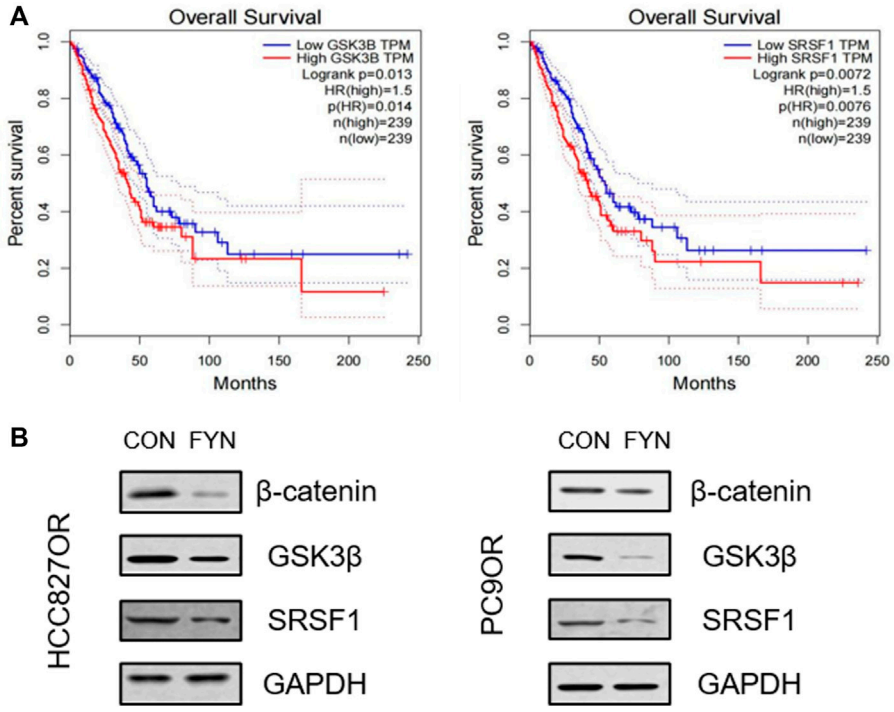

FIGURE 5
FYN reduced SRSF1, GSK3β, and β-catenin protein levels. **(A)** Correlations between overall survival in LUAD patients and GSK3β and SRSF1 expression, analyzed using the GEPIA website. **(B)** HCC827OR cells were treated with FYN at IC_{50} or isovolumetric 1640 medium for 48 h for analysis. Protein levels of SRSF1, GSK3B, and β-catenin were determined by western blotting. Con, control; FYN, Feiyanning Formula.

(Du et al., 2021). Resistance mechanisms such as C797S site mutations, MET and HER2 amplification, bypass activation, and conversion to NSCLC are reportedly involved (He et al., 2021). Traditional Chinese Medicine combined with targeted therapy can reportedly prolong survival and delay drug resistance (Zhang et al., 2018; Jiao et al., 2019; Lu et al., 2021). Abundant herbal monomers combined with osimertinib had the effect of delaying drug resistance. The mechanisms involved included tumor stem cell inhibition, regulation of reactive oxygen species, and alteration of downstream pathways (Hu et al., 2020; Lai et al., 2021). In contrast, research on herbal formulas remains at blurred stages. Therefore, it is necessary to determine the mechanisms of FYN in drug resistance regulation.

FYN contains 11 herbs and exhibits anti-cancer effects (Xu et al., 2011). Although FYN can inhibit the protective autophagy induced by cisplatin in NSCLC cells (Zheng et al., 2021), whether it can modulate osimertinib resistance in NSCLC remains unclear. In the current study, FYN inhibited the viability of HCC827OR and PC9OR cells in a dose-dependent manner. FYN combined with osimertinib could enhance the inhibition of cell viability, inhibit colony formation, and suppress invasion and migration. These observations indicated that FYN had synergistic effects.

Numerous studies have shown that the Wnt/β-catenin pathway is a major contributor to the development of drug resistance to EGFR-TKIs (Wang et al., 2020; Yan et al., 2022). The Wnt signaling pathway is involved in a variety of physiological processes including cell proliferation, developmental metabolism, and cell migration. Moreover its abnormal activation is associated with tumor growth (Koni et al., 2020; Yu et al., 2021; Liu et al., 2022). In the current study, the differential genes were screened using PCR array. According to KEGG analysis, these genes are primarily enriched in the Wnt/β-catenin pathway. FYN downregulated the expression of SRSF1 and GSK3B. SRSF1 is a multifunctional protein involved in RNA metabolism. It induces a cancer cell cycle, proliferation, apoptosis, tumorigenic angiogenesis, and metastasis (Sokół et al., 2017). Upregulation of SRSF1 activates the Wnt pathway, promoting tumor growth (Malakar et al., 2017; Zhang et al., 2021), which may be related to the accumulation of β-catenin proteins (Fu et al., 2013). Glycogen synthase kinase-3β is a serine/threonine kinase that participates in various signaling pathways including Wnt/β-catenin. It also has anti-tumor effects (Domoto et al., 2016; Lin et al., 2020). This is consistent with results in the current study, implying that the Wnt/β-catenin pathway is the core pathway involved in FYN against osimertinib resistance.

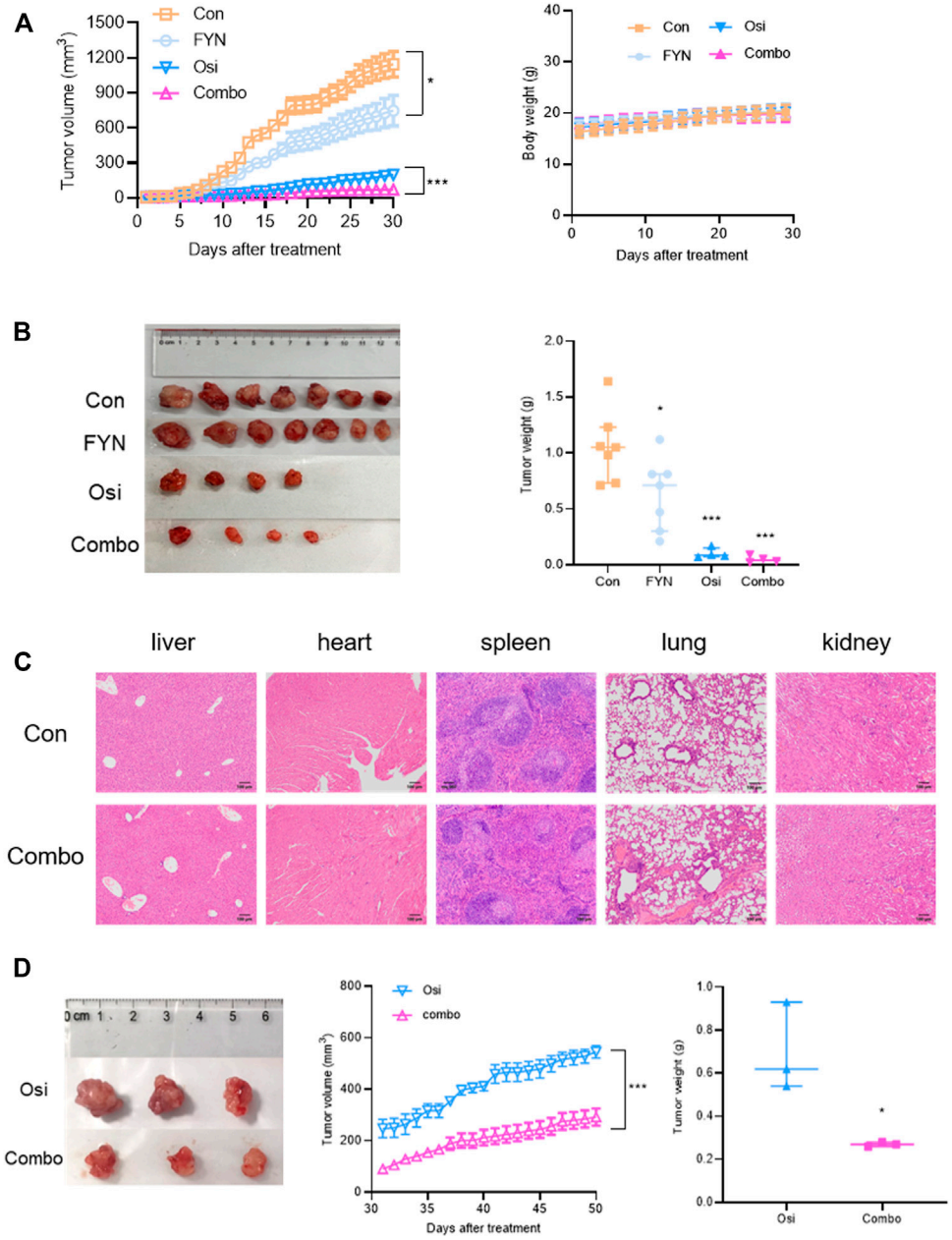

FIGURE 6
FYN combined with osimertinib suppressed tumor growth in mouse xenograft models of lung adenocarcinoma. **(A)** Tumor growth curve and body weight of subcutaneous HCC827OR xenografts (n = 7). **(B)** Mice in the control group (n = 7), FYN group (n = 7), osimertinib group (n = 4) and combination group (n = 4) were anaesthetized to determine tumor volumes and weights 30 days after treatment. **(C)** Organs of mice in the control group and the combination group were harvested 30 days after treatment and stained with hematoxylin and eosin. **(D)** Tumor growth curves and tumor weights of 3 mice in the osimertinib group and 3 mice in the combination group. Con, control; FYN, Feiyanning Formula. Osi, osimertinib; Combo, combination of Feiyanning Formula and osimertinib. *p < 0.05, **p < 0.01, ***p < 0.001.

Conclusion

The combination of FYN and osimertinib may inhibit the cellular activities of osimertinib-resistant cells *in vitro* and *in vivo*, leading to anti-tumor effects. In this study, FYN downregulated the mRNA expression of SRSF1, β-catenin, and GSK3B. FYN delayed osimertinib resistance by regulating the Wnt/β-catenin pathway. The current study provided scientific evidence for the application of Chinese herbal medicine on NSCLC treatment, particularly in combination with EGFR-TKI.

Data availability statement

The raw data supporting the conclusion of this article will be made available by the authors, without undue reservation.

Ethics statement

The animal study was reviewed and approved by the Ethics Committee of Yueyang Hospital of Integrated Traditional Chinese and Western Medicine.

Author contributions

SS and SC contributed equally. SS, SC, and DR performed experimental work. SS and SC prepared the original draft of the report. JJ, HH, and GS performed data curation. BL and GY designed the study, and reviewed and edited the manuscript. All authors have read and approved the final manuscript.

Funding

This work was supported by grants from the National Natural Science Foundation of China (grant number No.82074339, No.82274143, the Natural Science Foundation of Shanghai, China (No.20ZR1459400) and the Shanghai Sailing Program (No.21YF1448200).

Conflict of Interest

The authors declare that the research was conducted in the absence of any commercial or financial relationships that could be construed as a potential conflict of interest.

Publisher's note

All claims expressed in this article are solely those of the authors and do not necessarily represent those of their affiliated organizations, or those of the publisher, the editors and the reviewers. Any product that may be evaluated in this article, or claim that may be made by its manufacturer, is not guaranteed or endorsed by the publisher.

Supplementary material

The Supplementary Material for this article can be found online at: https://www.frontiersin.org/articles/10.3389/fphar.2022.1019451/full#supplementary-material

SUPPLEMENTARY FIGURE S1

Effects of osimertinib on the proliferation of different lung cancer cell lines. **(A)** Effects of osimertinib on HCC827 and PC9 osimertinib sensitivity in parental (white) and osimertinib-resistant (gray) cells. Cells were treated with various concentrations of osimertinib for 48 h and tested *via* the CCK8 assay. **(B)** Protein levels of PCNA were measured *via* western blotting. **(C)** CCK8 results. HCC827OR cells were treated with 4 μM Osimertinib with FYN and PC9OR cells were treated for 48 h with 6 μM osimertinib with FYN for 48 h. ~P, parental cell lines; ~OR, osimertinib-resistant cell lines. $*p < 0.05$, $**p < 0.01$, $***p < 0.001$.

References

Domoto, T., Pyko, I. V., Furuta, T., Miyashita, K., Uehara, M., Shimasaki, T., et al. (2016). Glycogen synthase kinase-3β is a pivotal mediator of cancer invasion and resistance to therapy. *Cancer Sci.* 10710, 1363–1372. doi:10.1111/cas.13028

Du, X., Yang, B., An, Q., Assaraf, Y. G., Cao, X., and Xia, J. (2021). Acquired resistance to third-generation EGFR-TKIs and emerging next-generation EGFR inhibitors. *Innovation.* 22, 100103. doi:10.1016/j.xinn.2021.100103

Duchartre, Y., Kim, Y. M., and Kahn, M. (2016). The Wnt signaling pathway in cancer. *Crit. Rev. Oncol. Hematol.* 99, 141–149. doi:10.1016/j.critrevonc.2015.12.005

Ettinger, D. S., Wood, D. E., Aisner, D. L., Akerley, W., Bauman, J. R., Bharat, A., et al. (2022). Non-small cell lung cancer, version 3.2022, NCCN clinical practice guidelines in oncology. *J. Natl. Compr. Canc. Netw.* 205, 497–530. doi:10.6004/jnccn.2022.0025

Fu, Y., Huang, B., Shi, Z., Han, J., Wang, Y., Huangfu, J., et al. (2013). SRSF1 and SRSF9 RNA binding proteins promote Wnt signalling-mediated tumorigenesis by enhancing β-catenin biosynthesis. *EMBO Mol. Med.* 55, 737–750. doi:10.1002/emmm.201202218

Gong, Y., Xu, Z., Jin, C., Deng, H., Wang, Z., Zhou, W., et al. (2018). Treatment of advanced non-small-cell lung cancer with Qi-nourishing essence-replenishing Chinese herbal medicine combined with chemotherapy. *Biol. Proced. Online* 20, 9. doi:10.1186/s12575-018-0074-9

He, J., Huang, Z., Han, L., Gong, Y., and Xie, C. (2021). Mechanisms and management of 3rd-generation EGFR-TKI resistance in advanced non-small cell lung cancer (Review). *Int. J. Oncol.* 595, 90. doi:10.3892/ijo.2021.5270

Hu, X., Zhang, Z. Y., Wu, L. W., Zeng, L. H., Chen, H., Zhu, H. J., et al. (2020). A natural anthraquinone derivative shikonin synergizes with AZD9291 against wtEGFR NSCLC cells through reactive oxygen species-mediated endoplasmic reticulum stress. *Phytomedicine* 68, 153189. doi:10.1016/j.phymed.2020.153189

Jiao, L., Xu, J., Sun, J., Chen, Z., Gong, Y., Bi, L., et al. (2019). Chinese herbal medicine combined with EGFR-TKI in EGFR mutation-positive advanced pulmonary adenocarcinoma (catla): A multicenter, randomized, double-blind, placebo-controlled trial. *Front. Pharmacol.* 10, 732. doi:10.3389/fphar.2019.00732

Koni, M., Pinnarò, V., and Brizzi, M. F. (2020). The Wnt signalling pathway: A tailored target in cancer. *Int. J. Mol. Sci.* 2120, E7697. doi:10.3390/ijms21207697

Lai, L., Shen, Q., Wang, Y., Chen, L., Lai, J., Wu, Z., et al. (2021). Polyphyllin I reverses the resistance of osimertinib in non-small cell lung cancer cell through regulation of PI3K/Akt signaling. *Toxicol. Appl. Pharmacol.* 419, 115518. doi:10.1016/j.taap.2021.115518

Lemjabbar-Alaoui, H., Hassan, O. U., Yang, Y. W., and Buchanan, P. (2015). Lung cancer: Biology and treatment options. *Biochim. Biophys. Acta* 18562, 189–210. doi:10.1016/j.bbcan.2015.08.002

Lin, J., Song, T., Li, C., and Mao, W. (2020). GSK-3β in DNA repair, apoptosis, and resistance of chemotherapy, radiotherapy of cancer. *Biochim. Biophys. Acta. Mol. Cell Res.* 18675, 118659. doi:10.1016/j.bbamcr.2020.118659

Liu, J., Xiao, Q., Xiao, J., Niu, C., Li, Y., Zhang, X., et al. (2022). Wnt/β-catenin signalling: Function, biological mechanisms, and therapeutic opportunities. *Signal Transduct. Target. Ther.* 71, 3. doi:10.1038/s41392-021-00762-6

Lu, Y., Sun, C., Jiao, L., Liu, Y., Gong, Y., and Xu, L. (2021). Chinese herbal medicine combined with first-generation EGFR-TKIs in treatment of advanced non-small cell lung cancer with EGFR sensitizing mutation: A systematic review and meta-analysis. *Front. Pharmacol.* 12, 698371. doi:10.3389/fphar.2021.698371

Maione, P., Sacco, P. C., Sgambato, A., Casaluce, F., Rossi, A., and Gridelli, C. (2015). Overcoming resistance to targeted therapies in NSCLC: Current approaches and clinical application. *Ther. Adv. Med. Oncol.* 75, 263–273. doi:10.1177/1758834015595048

Malakar, P., Shilo, A., Mogilevsky, A., Stein, I., Pikarsky, E., Nevo, Y., et al. (2017). Long noncoding RNA MALAT1 promotes hepatocellular carcinoma development by SRSF1 upregulation and mTOR activation. *Cancer Res.* 775, 1155–1167. doi:10.1158/0008-5472.CAN-16-1508

Passaro, A., Jänne, P. A., Mok, T., and Peters, S. (2021). Overcoming therapy resistance in EGFR-mutant lung cancer. *Nat. Cancer* 24, 377–391. doi:10.1038/s43018-021-00195-8

Popat, S. (2018). Osimertinib as first-line treatment in EGFR-mutated non-small-cell lung cancer. *N. Engl. J. Med.* 3782, 192–193. doi:10.1056/NEJMe1714580

Schegoleva, A. A., Khozyainova, A. A., Fedorov, A. A., Gerashchenko, T. S., Rodionov, E. O., Topolnitsky, E. B., et al. (2021). Prognosis of different types of non-small cell lung cancer progression: Current state and perspectives. *Cell. Physiol. biochem.* 55S2, 29–48. doi:10.33594/000000340

Siegel, R. L., Miller, K. D., Fuchs, H. E., and Jemal, A. (2022). Cancer statistics, 2022. *Ca. Cancer J. Clin.* 721, 7–33. doi:10.3322/caac.21708

Sokół, E., Bogusławska, J., and Piekiełko-Witkowska, A. (2017). The role of SRSF1 in cancer. *Postepy Hig. Med. Dosw.* 710, 422–430. doi:10.5604/01.3001.0010.3825

Tan, Q., Lin, S., Zeng, Y., Yao, M., Liu, K., Yuan, H., et al. (2020). Ginsenoside Rg3 attenuates the osimertinib resistance by reducing the stemness of non-small cell lung cancer cells. *Environ. Toxicol.* 356, 643–651. doi:10.1002/tox.22899

Wang, Q., Liao, J., He, Z., Su, Y., Lin, D., Xu, L., et al. (2020). LHX6 affects erlotinib resistance and migration of EGFR-mutant non-small-cell lung cancer HCC827 cells through suppressing Wnt/β-catenin signaling. *Onco. Targets. Ther.* 13, 10983–10994. doi:10.2147/OTT.S258896

Wu, L., Ke, L., Zhang, Z., Yu, J., and Meng, X. (2020). Development of EGFR TKIs and options to manage resistance of third-generation EGFR TKI osimertinib: Conventional ways and immune checkpoint inhibitors. *Front. Oncol.* 10. 602762. doi:10.3389/fonc.2020.602762

Xu, Z. Y., Jin, C. J., Zhou, C. C., Wang, Z. Q., Zhou, W. D., Deng, H. B., et al. (2011). Treatment of advanced non-small-cell lung cancer with Chinese herbal medicine by stages combined with chemotherapy. *J. Cancer Res. Clin. Oncol.* 1377, 1117–1122. doi:10.1007/s00432-011-0975-3

Yan, R., Fan, X., Xiao, Z., Liu, H., Huang, X., Liu, J., et al. (2022). Inhibition of DCLK1 sensitizes resistant lung adenocarcinomas to EGFR-TKI through suppression of Wnt/β-Catenin activity and cancer stemness. *Cancer Lett.* 531, 83–97. doi:10.1016/j.canlet.2022.01.030

Yu, F., Yu, C., Li, F., Zuo, Y., Wang, Y., Yao, L., et al. (2021). Wnt/β-catenin signaling in cancers and targeted therapies. *Signal Transduct. Target. Ther.* 61, 307. doi:10.1038/s41392-021-00701-5

Zhang, C., Yang, Y., Yi, L., Paizula, X., Xu, W., and Wu, X. (2021). HOXD antisense growth-associated long noncoding RNA promotes triple-negative breast cancer progression by activating Wnt signaling pathway. *J. Breast Cancer* 243, 315–329. doi:10.4048/jbc.2021.24.e24

Zhang, X. W., Liu, W., Jiang, H. L., and Mao, B. (2018). Chinese herbal medicine for advanced non-small-cell lung cancer: A systematic review and meta-analysis. *Am. J. Chin. Med.* 465, 923–952. doi:10.1142/S0192415X18500490

Zhang, Y. C., Zhou, Q., and Wu, Y. L. (2019). Clinical management of third-generation EGFR inhibitor-resistant patients with advanced non-small cell lung cancer: Current status and future perspectives. *Cancer Lett.* 459, 240–247. doi:10.1016/j.canlet.2019.05.044

Zheng, Z., Ma, Y., Wang, L., Deng, H., Wang, Z., Li, J., et al. (2021). Chinese herbal medicine Feiyanning cooperates with cisplatin to enhance cytotoxicity to non-small-cell lung cancer by inhibiting protective autophagy. *J. Ethnopharmacol.* 276, 114196. doi:10.1016/j.jep.2021.114196

Zhu, L. M., Shi, H. X., Sugimoto, M., Bandow, K., Sakagami, H., Amano, S., et al. (2021). Feiyanning Formula induces apoptosis of lung adenocarcinoma cells by activating the mitochondrial pathway. *Front. Oncol.* 11, 690878. doi:10.3389/fonc.2021.690878

frontiers | Frontiers in Pharmacology

TYPE Original Research
PUBLISHED 23 December 2022
DOI 10.3389/fphar.2022.1068855

OPEN ACCESS

EDITED BY
Eswar Shankar,
The Ohio State University, United States

REVIEWED BY
Balaji Chandrasekaran,
Texas A&M University, United States
Mohit Vashishta,
Texas A&M University, United States
Prem P. Kushwaha,
Case Western Reserve University, United States

*CORRESPONDENCE
Gary Guishan Xiao,
gxiao@dlut.edu.cn

SPECIALTY SECTION
This article was submitted to Pharmacology of Anti-Cancer Drugs, a section of the journal Frontiers in Pharmacology

RECEIVED 13 October 2022
ACCEPTED 14 December 2022
PUBLISHED 23 December 2022

CITATION
Zhang T, Liu M, Liu Q and Xiao GG (2022), Wogonin increases gemcitabine sensitivity in pancreatic cancer by inhibiting Akt pathway.
Front. Pharmacol. 13:1068855.
doi: 10.3389/fphar.2022.1068855

Wogonin increases gemcitabine sensitivity in pancreatic cancer by inhibiting Akt pathway

Tianli Zhang, Mengmeng Liu, Qing Liu and Gary Guishan Xiao*

State Key Laboratory of Fine Chemicals, Department of Pharmaceutical Sciences, School of Chemical Engineering, Dalian University of Technology, Dalian, China

Pancreatic cancer has a high degree of malignancy and a low 5-year survival rate, and drug resistance is one of the main factors leading to poor prognosis of pancreatic cancer. Wogonin is a flavonoid drug isolated from Scutellaria baicalensis, which has certain antitumor activity. Hence the purpose of this study was to investigate whether wogonin can be used to enhance the sensitivity of pancreatic cancer to gemcitabine chemotherapy, and investigate its possible sensitization mechanism. *In vitro,* MTT assay showed that wogonin increased gemcitabine cytotoxicity in gemcitabine-resistant pancreatic cancer cells. *In vivo,* Wogonin combined with gemcitabine was found to inhibit tumor growth in orthotopic pancreatic cancer mouse model. In order to explore the sensitization mechanism, the differentially expressed genes (DEGs) of the gemcitabine-resistant cell line Panc-1 and the gemcitabine-sensitive cell line Bxpc-3 were screened through the GEO database, and 15 differentially expressed genes were obtained by intersecting with the potential targets of wogonin. Gene Ontology and KEGG enrichment analysis was performed. Bioinformatics results predicted that wogonin promoted pancreatic cancer cell apoptosis by inhibiting protein kinase B (Akt) signaling, thereby enhancing the sensitivity of gemcitabine to Pancreatic cancer. The above results were also verified by flow cytometry and Western blotting experiments. In conclusion, wogonin may enhance the sensitivity of gemcitabine by inhibiting Akt pathway.

KEYWORDS

wogonin, pancreatic cancer, gemcitabine, sensitization, drug resistance, mechanism

1 Introduction

The rate of pancreatic cancer incidence in 2020 was 4.9 per 100000 for both sexes together, while mortality rate was 4.5 per 100000 from a global perspective (Ilic and Ilic, 2022). Pancreatic cancer is a malignant tumor with high degree of malignancy, difficult clinical detection and poor prognosis (Bray et al., 2018; Mcguigan et al., 2018; Park et al., 2021). The main risk factors associated with pancreatic cancer include factors such as alcoholism, smoking, obesity, diabetes, family history, and genetics (Ren and Wang, 2020; Hu et al., 2021). The early treatment of pancreatic cancer is mainly adjuvant gemcitabine chemotherapy after surgical resection, and the use of

gemcitabine/nab-paclitaxel in the advanced treatment of pancreatic cancer can improve the poor prognosis to a certain extent (Neoptolemos et al., 2018). Although gemcitabine is used as a first-line drug for pancreatic cancer chemotherapy, it often leads to poor clinical outcomes due to the inherent drug resistance of pancreatic cancer cells (Yang et al., 2021). Therefore, for gemcitabine resistance, quercetin (Lee et al., 2015), Ginsenoside Rg3 (Zou et al., 2020) and Ursolic (Lin et al., 2020) has been reported to promote apoptosis of pancreatic cancer cells and enhance gemcitabine sensitivity. These findings prompted us to investigate whether other phytochemicals could sensitize pancreatic cancer cells to gemcitabine.

We selected one of the active ingredients wogonin according to the optimal toxicokinetic ADME rules (OB = 30.68% > 30% and DL = 0.23 > 0.18) (Liu et al., 2013) in the TCMSP database. Wogonin is a flavonoid compound extracted from the root of Scutellaria baicalensis (Banik et al., 2022). It has antioxidant activity, and anti-inflammatory, anti-tumor, immunomodulatory, neuroprotective effects (Huynh et al., 2020). Wogonin also acts as a chemosensitizer, reducing drug resistance in cancer therapy. When wogonin is used in combination with anticancer drugs such as etoposide, doxorubicin, 5-FU, and cisplatin (Huynh et al., 2017), it can induce tumor cell apoptosis (Wu et al., 2021) and protect normal cells from side effects.

Xing et al, (2019). Reported that wogonin enhanced the sensitivity of ovarian cancer cells to gemcitabine by inhibiting the PI3K/Akt signaling pathway. However, whether wogonin can enhance gemcitabine sensitivity and its sensitizing mechanism remain to be explored. Therefore, this study intends to preliminarily investigate whether wogonin has a sensitizing effect on the Pancreatic cancer by inhibiting the Akt signaling pathway.

2 Materials and methods

2.1 Materials and reagents

Wogonin (Cat. MB6663-20 mg) was purchased from Meilunbio (Dalian, China); Gemcitabine (Cat. PHR2582-50 mg) was purchased from Sigma Aldrich (St Louis, MO, United States); EDTA-free trypsin (C0207) was purchased from Beyotime Biotechnology (Shanghai, China); the anti-β-actin antibody (Cat. 66009-1-lg) was purchased from Proteintech (Rosemont, IL, United States) and antibodies against pAKT (Thr) antibody (Cat.ab131474), Akt (Cat.ab8805), BAD (Cat.ab32455) and Bcl-2 (Cat.ab32124) were purchased from Abcam (Massachusetts, United States). The anti-rabbit Ki67 (Cat. ab15580) was also purchased from Abcam.

2.2 Cell culture and MTT assays

Pancreatic cancer cell lines (PANC-1, BXPC-3, PANC-02) were purchased from the Peking Union Medical College Cell Bank (Beijing, China). All these cells were cultured in DMEM medium supplemented with 10% FBS. Panc-1 and Bxpc-3 cells were plated in 96-well plates, and treated with Gemcitabine or Wogonin for 72 h MTT assays. MTT was then performed as previously described (Zhang et al., 2022)

2.3 Annexin-V assay

The Annexin V-FITC Apoptosis Detection Kit (Cat. C1062S) was were purchased from the Beyotime Biotechnology (Shanghai, China). The Panc-1 cells were cultivated to the logarithmic growth phase, and treated with 10 μM, 20 μM, 40 μM, and 100 μM wogonin for 72 h, digested with EDTA-free trypsin, and then terminated with serum. Cells were washed with PBS twice and then esponded with 195 μl Annexin V-FITC binding solution, subsequently added 5 μl Annexin V-FITC and 10 μl PI for 10–20 min in the dark. Finally, flow cytometry was used to detect cell apoptosis. (PI and Annexin concentrations in the kit are inconvenient for the reagent supplier to provide)

2.4 Western blotting

Panc-1 cells were treated with 10, 20, 40, 100 μM Wogonin for 72 h. Total protein was extracted from the Panc-1 cells and from pancreatic tissue of Control group, Gem group and Gem + Wog group. Western blotting was then performed as previously described (Domenichini et al., 2019)

2.5 Animals

C57BL/6 mice were purchased from Liaoning Changsheng Biotechnology Co., Ltd. (Benxi, China). 2×10^6 Mouse derived PANC-02 cells were injected into the pancreas tissue of male C57BL/6 mice to generate orthotopic pancreatic cancer mouse model. Eighteen mice were divided into three groups: Control group, Gemcitabine group (Gem group), and Gemcitabine Wogonin combined group (Gem + Wog group). Mice in the Gem group were intraperitoneally injected with gemcitabine (25 $mgkg^{-1}$ i. g.) on the seventh and 14th days; Gem + Wog group were intraperitoneally injected with gemcitabine (25 $mgkg^{-1}$ i. g.) on the seventh and 14th days, along with intragastric administration of Wogonin (50 $mgkg^{-1}$ i. p.) in 7–21 days per day. Body weight were measured every 2 days. After 21 days, The mice were sacrificed and pancreas tumors were collected for mechanism research.

2.6 Histochemical staining

The collected pancreatic tumors were immersed in 4% paraformaldehyde, embedded in paraffin, and cut into small pieces. Pancreatic sections were then stained with Ki67 antibody according to the manufacturer's instructions and simple images were obtained by using a light microscope at ×100 magnification (Zheng et al., 2020). IHC images were quantified by ImageJ.

2.7 Statistical analysis

The experimental data were analyzed using GraphPad Prism 8.0.1 statistical analysis software (GraphPad, San Diego, CA, United States). A two-tailed Student's t-test or one-way analysis of variance (ANOVA) was used for statistical analyses. The following terminology was used to show statistical significance: $^{*}p < 0.05$, $^{**}p < 0.01$, $^{***}p < 0.001$.

2.8 Potential targets of wogonin

The active components of the drug can exert related biological functions through related targets. The active ingredients were screened in TCMSP (https://tcmsp-e.com/) according to the optimal toxicokinetic ADME rules. Wogonin (OB = 30.68, DL = 0.23) was obtained as possible core active components of pancreatic cancer. Genecards (https://www.genecards.org/),SwissTargetPrediction (https://new.swisstargetprediction.ch/),BATMAN-TCM(http://bionet.ncpsb.org.cn/batman-tcm/),PharmMapper (Wang et al., 2016; Wang et al., 2017) (http://www.lilab-ecust.cn/pharmmapper/) were used to predict the potential targets of wogonin.

2.9 Identification of differentially expressed genes

GEO2R was used to identify DEGs between gemcitabine-resistant cell line Panc-1 and the gemcitabine-sensitive cell line Bxpc-3. A criteria of $p < 0.05$ and $|\log FC| \geq 2$ were considered to be statistically significant. Then, the online software Venny 2.1.0 (http://bioinfogp.cnb.csic.es/tools/venny/index.html) was used to screen out overlapping DEGs. The Venn diagram was also drawn by Venny 2.1.0. (Song et al., 2020).

2.10 Construction of a "drug—targets—disease" network

The candidate targets of wogonin and protein markers of pancreatic cancer gemcitabine resistance-related genes were uploaded to IPA (Ingenuity Pathway Analysis, version 2019) for network and pathway analysis. IPA was used to construct pathways and networks based on interactions between genes and proteins. Through the "Compare" module in IPA, the pathways and networks involved in gemcitabine resistance-related genes and wogonin candidate targets in pancreatic cancer were identified.

2.11 Go and KEGG enrichment analysis

Metascape (https://metascape.org/gp/index.html#/main/step1) was used for GO and KEGG enrichment analysis. GO (Gene Ontology) terms are divided into CC (Cellular Component), biological process BP (Biological Process) and molecular function MF (Molecular Function). Set the filter condition MinOverlap = 3, $p < 0.01$.

3 Results

3.1 Wogonin increased gemcitabine cytotoxicity in gemcitabine-resistant pancreatic cancer cells

MTT assay was performed to assess the antiproliferative effects of pancreatic cancer cells by gemcitabine and wogonin treatment for 72 h. Panc-1 and Bxpc-3 pancreatic cancer cell lines were treated with gemcitabine at different concentrations (0, 0.08, 0.15, 0.3, 0.6, 1.3, 2.5, 5 and 10 μM) for 72 h. Panc-1 cell vitality decreased by 21.0%–37.7%, and Bxpc-3 cell viability decreased by 53.8%–66.9%, which displayed significant antiproliferative effects. (Figure 1A). As described in the literature (Cao et al., 2015), Panc-1 pancreatic cancer cell line is naturally resistant to gemcitabine, while Bxpc-3 pancreatic cancer cell line is sensitive to gemcitabine.

Gemcitabine-resistant pancreatic cancer cells Panc-1 was incubated with wogonin at different concentrations (0, 1.3, 2.5, 5, 10, 20, 40, 80, and 160 μM). Wogonin inhibited the growth of Panc-1 cells in dose-and time-dependent manners. MTT test showed that IC50 value of wogonin was 73.3 μM and the dose-effect curve exhibited that 10 μM wogonin displayed no significant antiproliferative effects on Panc-1 cells (survival rate was 94.1%); 20 μM wogonin displayed weak antiproliferative effects (survival rate was 78.7%) (Figure 1B)

10 and 20 μM wogonin were combined with different concentrations (0, 0.04, 0.08, 0.15, 0.3, 0.6, 1.3, 2.5, 5 and 10 μM) of gemcitabine for 72 h. As shown in Figure 1C, at gemcitabine concentrations of 0.04, 0.08 and 0.16 μM, 10 μM wogonin significantly enhanced sensitive of Panc-1 cells to gemcitabine ($p < 0.001$). At gemcitabine concentrations of 0.31 and 0.63 μM, Wogonin could slightly enhance the sensitivity of Panc-1 cells to gemcitabine ($p < 0.05$). When the

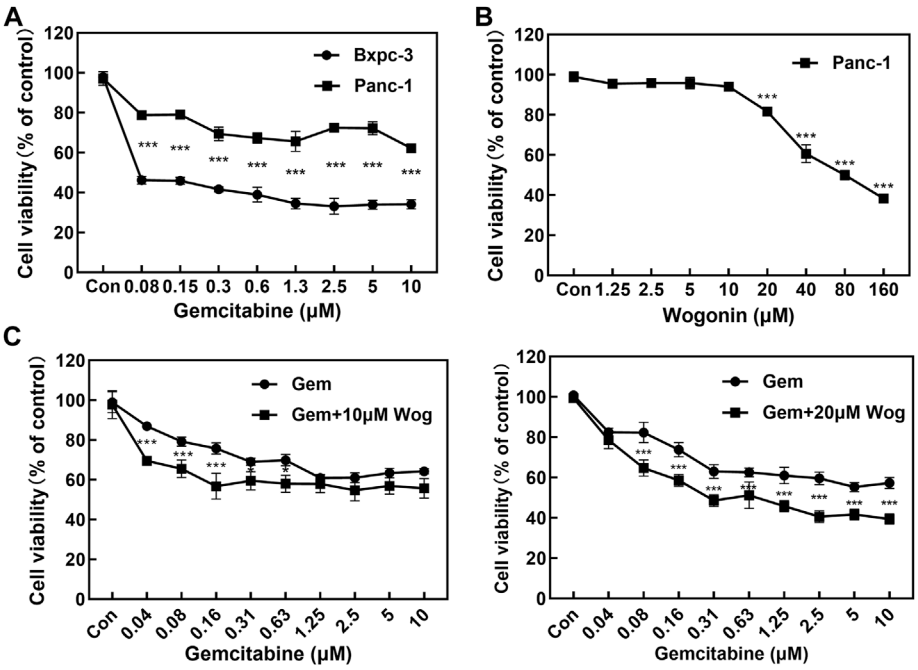

FIGURE 1
Wogonin combined with gemcitabine inhibits the proliferation of pancreatic cancer cells. **(A)** The cell viability of Panc-1 and Bxpc-3 cells treated with gemcitabine was assessed using MTT assay at 72 h. Compared with Bxpc-3, Gemcitabine displayed no significant antiproliferative effects to Panc-1 cell. **(B)** The cell viability of Panc-1 treated with wogonin was assessed using MTT assay at 72 h. The cell viability decreased with the elevated concentration of wogonin. **(C)** Sensitizing effect of wogonin in Panc-1 cells to gemcitabine. Cells were treated with gemcitabine (0, 0.04, 0.08, 0.15, 0.3, 0.6, 1.3, 2.5, 5 and 10 μM), Gem + Wog (10 μM) and Gem + Wog (20 μM) for 72 h and cell viability was determined by MTT assay. *$p < 0.05$, **$p < 0.01$, ***$p < 0.001$ vs. controls.

concentration of wogonin was increased to 20 μM, combined with 0.08, 0.16, 0.31, 0.63, 1.25, 2.5, 5, 10 μM of gemcitabine could further significantly inhibit the proliferation of Panc-1 cells. These results showed that the wogonin could significantly increase gemcitabine cytotoxicity in gemcitabine-resistant pancreatic cancer cells.

3.2 Prediction of targets for wogonin sensitization

In order to explore the possible mechanism of wogonin sensitization, two gene chips (GSE15550, GSE97594) were found in the GEO database. By comparing the gemcitabine-resistant cell line Panc-1 and the gemcitabine-sensitive cell line Bxpc-3, differentially expressed genes (DEGs) related to gemcitabine resistance in pancreatic cancer were obtained. Based on the criteria of $p < 0.05$ and $|\log FC| \geq 2$, a total of 1865 DEGs were obtained in GSE15550, including 917 up-regulated genes and 948 down-regulated genes. In gene chip GSE97594, 1980 DEGs were identified, including 1064 up-regulated genes and 916 down-regulated genes. The DEGs were used to build a volcano map (Figure 2A) Venn 2.1.0 was used to screen for common DEGs between GSE15550 and GSE97594. The obtained 851 genes were differentially expressed genes (DEGs) related to gemcitabine resistance (Figure 2B). Through GeneCards, TCMSP, SwissTargetPrediction, BATMAN-TCM, PharmMapper and IPA databases, 251 potential targets related to wogonin were obtained (Figure 2C). Potential targets of wogonin were intersected with 851 DEGs, and 15 DEGs were obtained (Figure 2D). These fifteen DEGs, including AKT2, CCL2, HSP90AA1, PDE5A, PTGS1, BCHE, SERPINB5, CA2, SRC, DGKA, HIF1A, PTGS2, ABCA1, DPYD, and AKR1C3 were potential target of wogonin to enhance gemcitabine sensitivity in pancreatic cancer.

3.3 Prediction of the sensitization mechanism of wogonin

Through IPA (Ingenuity Pathway Analysis) software, a "wogonin-target-gemcitabine resistance" network map was constructed. Wogonin may enhance the sensitivity of gemcitabine in pancreatic cancer by inhibiting AKT2, CCL2, HSP90AA1, PDE5A, or activating PTGS1, BCHE, SERPINB5, CA2, SRC, DGKA, HIF1A, PTGS2, ABCA1, DPYD and AKR1C3 (Figure 3A).

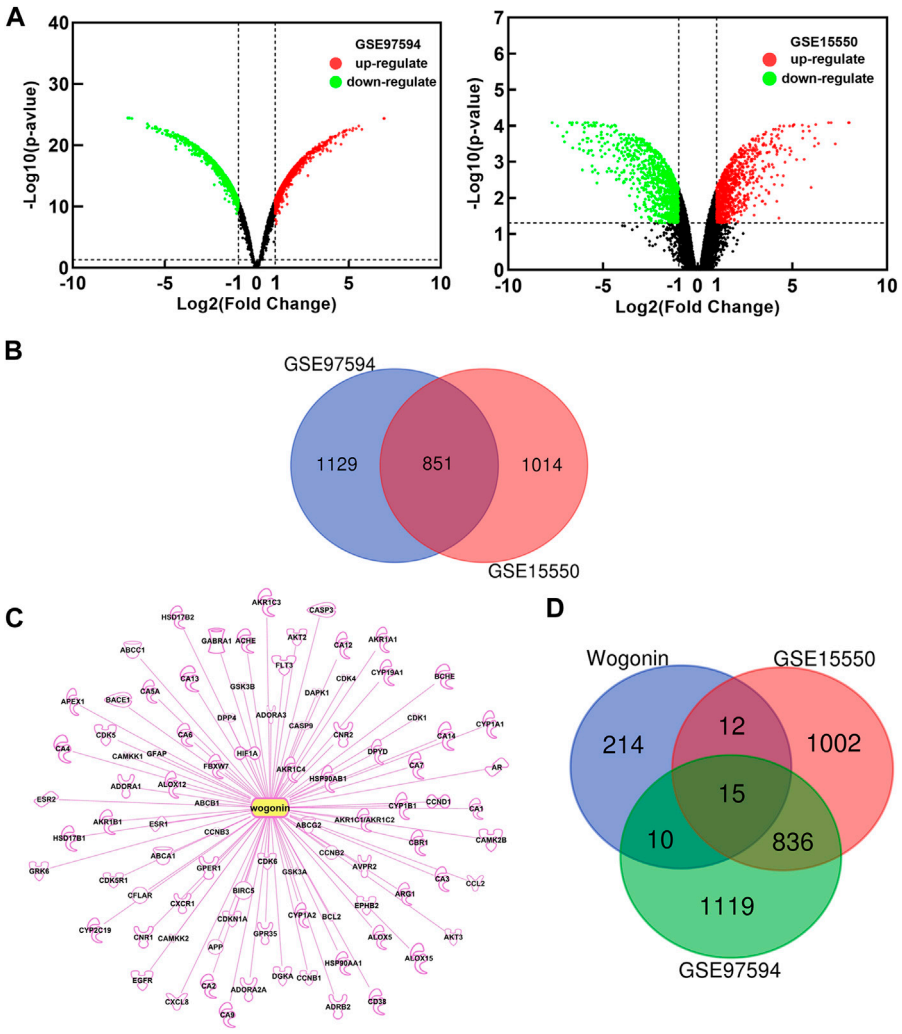

FIGURE 2
Potential target of wogonin to enhance gemcitabine sensitivity. **(A)**Diferential genes volcano map analyzed by GEO chips. Global gene expression of gemcitabine-resistant cell line Panc-1 vs gemcitabine-sensitive cell line Bxpc-3 **(B)** Venn diagram of 851 DEGs related to gemcitabine resistance **(C)** Potential targets of wogonin **(D)** Venn diagram of 15 DEGs related to wogonin sensitization in gemcitabine-resistant pancreatic cancer.

GO and KEGG enrichment analysis for the 15 DEGs were performed using the Metascape. The enriched GO terms were divided into CC, BP, and MF ontologies. The results of GO analysis indicated that DEGs were mainly enriched in BPs, including response to fluid shear stress, cyclooxygenase pathway, response to steroid hormone, protein kinase B signaling, learning, positive regulation of transmembrane transport, peptide transport, and ribonucleotide metabolic process (Figure 3B). MF analysis showed that the DEGs were significantly enriched in heme binding, phosphotransferase activity, ubiquitin protein ligase binding, protein homodimerization activity, and hydrolase activity. For the cell component, the DEGs were enriched in membrane raft and axon. In addition, the results of KEGG pathway analysis showed that DEGs were mainly enriched in pathways in Fluid shear stress and atherosclerosis, Regulation of lipolysis in adipocytes, IL-17 signaling pathway, and Choline metabolism in cancer.

As shown in Figure 2A, wogonin can down-regulate the expression of AKT2 and enhance the sensitivity of gemcitabine to pancreatic cancer cell; As shown in Figure 3B, the differentially expressed genes for wogonin sensitization were enriched in protein kinase B (Akt) signaling. In summary, we selected protein kinase B (Akt) signaling pathway (GO:0043491). Through the KEGG website (https://www.kegg.jp/), we can hypothesize that wogonin can promote the apoptosis of gemcitabine-resistant cell lines by inhibiting Akt and its downstream apoptosis-related proteins BAD and Bcl-2 (Figure 3C), and was verified by follow-up experiments.

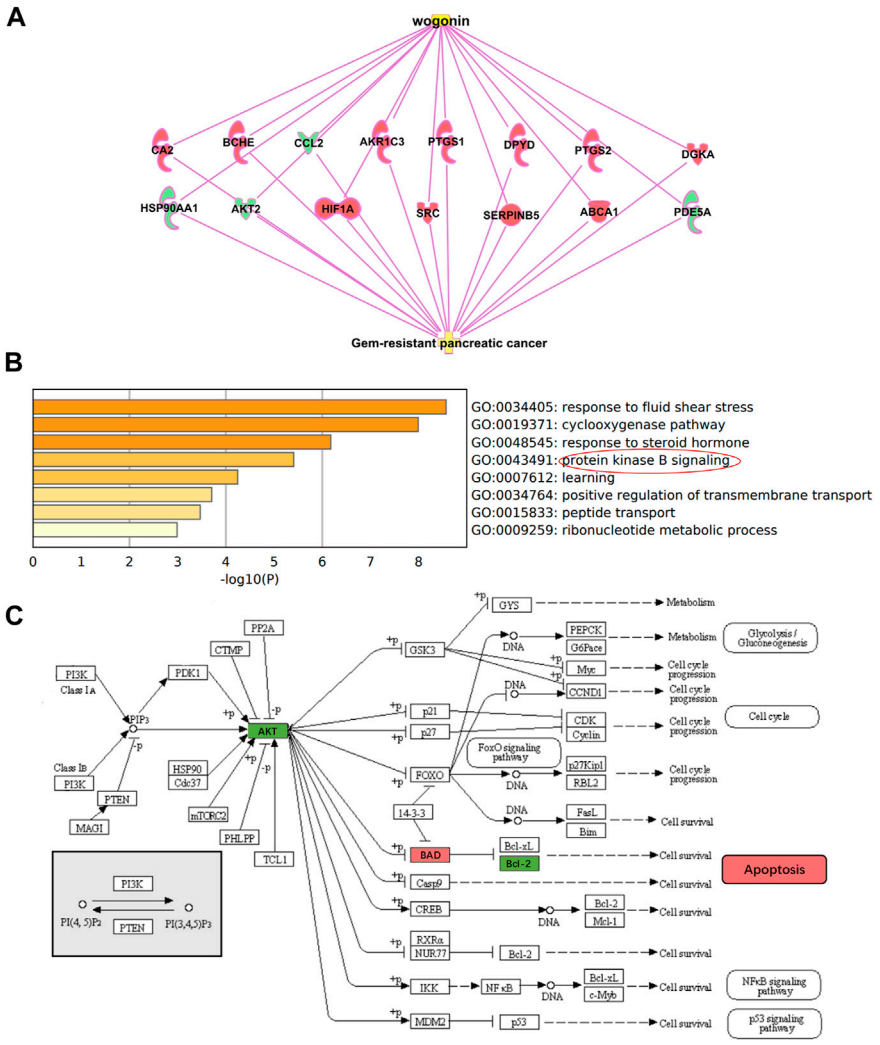

FIGURE 3
Potential mechanism of wogonin sensitization **(A)** "wogonin-target-gemcitabine resistance" network map. Wogonin can enhance gemcitabine sensitivity by downregulating AKT2. **(B)** Go enrichment analysis of 15 DEGs, which were enriched in protein kinase B (Akt) signaling. **(C)** Hypothesis on the sensitization mechanism of wogonin to gemcitabine in pancreatic cancer.

3.4 Wogonin promoted apoptosis of Panc-1 cells by inhibiting Akt pathway

The expression of Akt pathway was verified by WB experiment. The gemcitabine-resistant pancreatic cell line Panc-1 was selected, and wogonin at final concentrations of 10, 20, 40, and 100 μM was added. After 72 h of incubation, the cell protein was extracted and the expression of Akt, p-Akt, BAD, Bcl-2 was detected. As shown in Figure 4A, with the increase of wogonin concentration, the protein expression of Akt remained unchanged, while the protein expression of p-Akt decreased significantly, and the protein expression of the pro-apoptotic gene Bad increased. The protein expression of the anti-apoptotic gene Bcl-2 decreased, which was consistent with the bioinformatics conclusions.

Cell apoptosis was detected by flow cytometry. In Panc-1 cells, 10, 20, 40, 100 μM wogonin was added, and the apoptosis of Panc-1 was detected after 72 h of incubation. Annexin V-FITC and PI double staining positive means late apoptotic cells. Under the action of 10 μM wogonin, it had a certain promotion effect on the apoptosis of Panc-1 ($p < 0.05$), and under the action of 20, 40 and 100 μM wogonin, it significantly promoted the late apoptosis of cells ($p < 0.001$), which was consistent with Western blot results (Figure 4B). We can conclude that wogonin can promote the apoptosis of Gemcitabine-resistant pancreatic cell line Panc-1 by inhibiting Akt signaling.

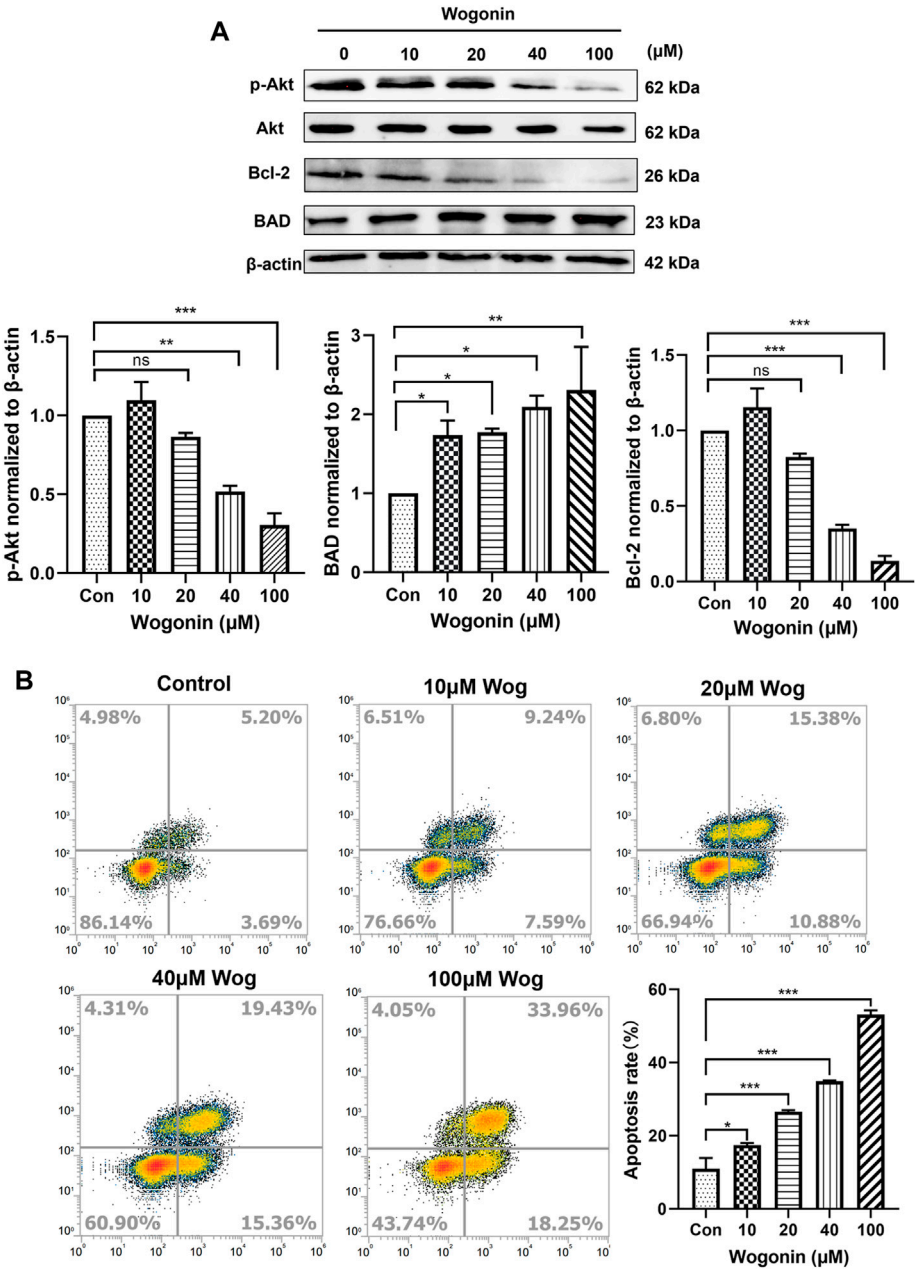

FIGURE 4
Wogonin promoted apoptosis of Panc-1 cells by inhibiting Akt pathway **(A)**gemcitabine-resistant cell line Panc-1 was treated with 10, 20, 40 and 100 μM wogonin for 72 h, then the protein levels of Akt, p-Akt, BAD and Bcl-2 were detected by western blot. **(B)**Flow cytometry was used to detect the apoptosis of Panc-1 cells treated with different concentrations of wogonin for 72 h $^{*}p < 0.05$, $^{**}p < 0.01$, $^{***}p < 0.001$ vs. controls.

3.5 Wogonin inhibitd pancreatic cancer *in vivo* by inhibiting Akt pathway

In order to explore the sensitization effect of wogonin on gemcitabine in pancreatic cancer, we generated orthotopic pancreatic cancer mouse model in C57BL/6 mice and administered the drugs on time. The experimental design is shown in the timeline (Figure 5A) and in the method of animals. As shown in Figure 5B, compared with the Control group, the body weight of the mice in the Gem group (25 mg/kg) and the Gem + Wog group (25 mg/kg Gem +50 mg/kg Wog) had no downward trend. Compared with the Control group, the tumor size of Gem + Wog group was significantly reduced ($p < 0.05$) (Figure 5D). The tumor inhibition rates in Gem group and

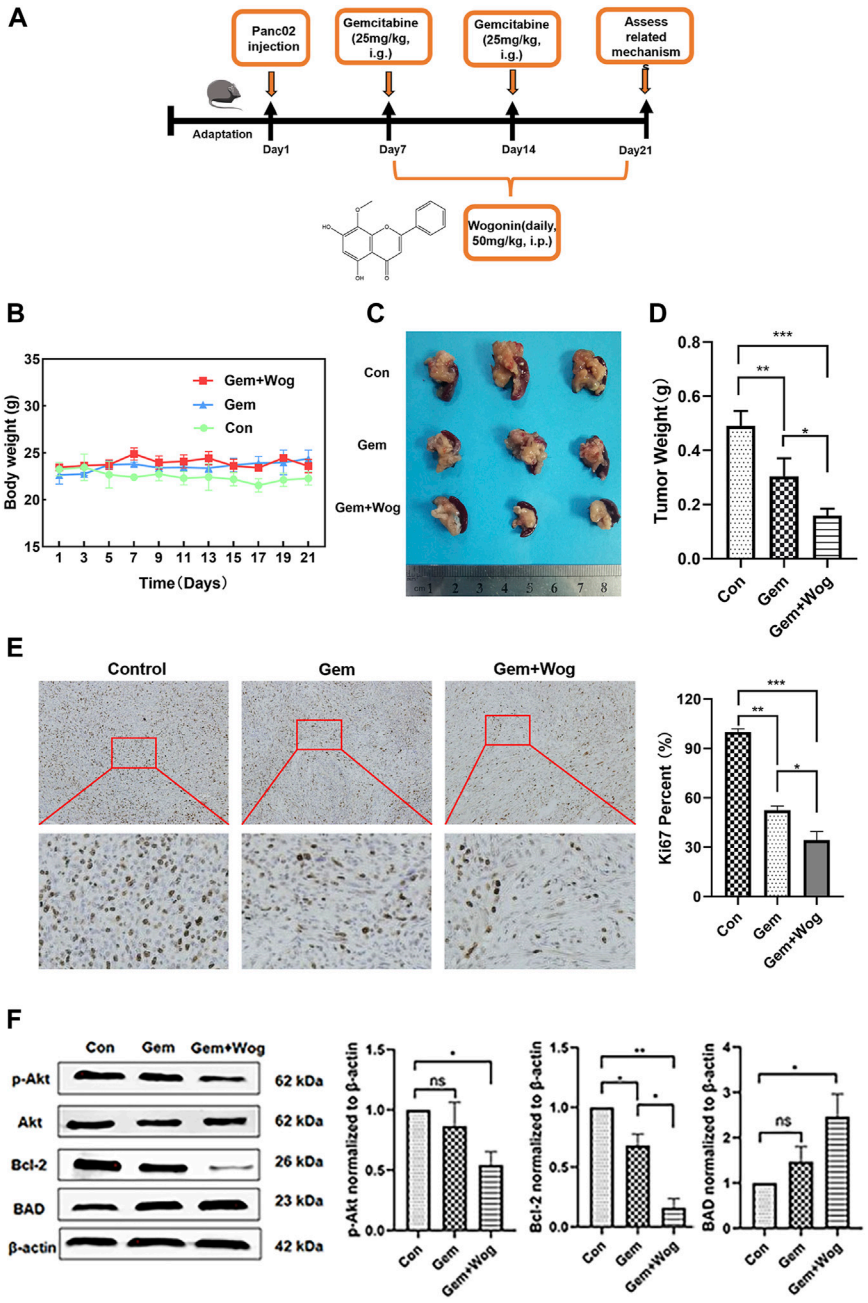

FIGURE 5
Wogonin inhibitd pancreatic cancer *in vivo* by inhibiting Akt pathway **(A)**Orthotopic pancreatic cancer mouse model experimental design **(B)** Body weight changes of mice in Con group, Gem group and Gem + Wog group within 21 days **(C)** Tumor size **(D)** Tumor weight **(E)** The fixed sections of mouse pancreas and pancreatic cancer were stained with Ki67 to detect tumor proliferation **(F)** After cryopreservation of mouse pancreatic tumors, Western Blot was detected to compare the expression of p-AKT, AKT, BAD and bcl-2 proteins in Con group, Gem group and Gem + Wog group. *$p < 0.05$, **$p < 0.01$, * **$p < 0.001$ vs. controls.

Gem + Wog group were 26.2% and 59.6%, respectively, and the tumor inhibition rate in the Gem + Wog group was significantly higher than that in the Gem group. The combination of wogonin and gemcitabine can inhibit the growth of pancreatic in tumor, and the effect is better than that of gemcitabine alone. Ki67 staining indicated tissue proliferation (Kreipe, 2018). Gem + Wog group significantly reduced the degree of tissue malignancy (Figure 5E). As shown in Figure 5F, the expression of p-Akt protein decreased, the expression of its downstream pro-apoptotic gene BAD increased, and the expression of anti-

apoptotic gene Bcl-2 decreased, which was consistent with the *in vitro* experiments. The results showed that wogonin combined with gemcitabine inhibited the Akt signaling pathway *in vivo*, and inhibited the growth of orthotopic pancreatic cancer.

4 Discussion

Wogonin can induce senescence of breast cancer cells (Yang et al., 2020) and promote apoptosis of cervical cancer (Kim et al., 2013) and gastric cancer cells (Hong et al., 2018). Research shows that wogonin can cooperate with chemotherapy drugs such as docetaxel (Wang et al., 2018) and cisplatin (Xu et al., 2021) to achieve better anti-tumor effect. In this study, through bioinformatics analysis and experimental verification, it is showed that wogonin may enhance gemcitabine sensitivity in pancreatic cancer.

Wogonin can inhibit tumor proliferation and invasion (Liu et al., 2016). Through the MTT assay, it was demonstrated that wogonin inhibited the proliferation of pancreatic cancer cells. At the concentration of 10 μM, wogonin could also sensitize Panc-1 cell to gemcitabine (Figure 1).

In order to explore the sensitization mechanism of wogonin to gemcitabine, the bioinformatics method was used to predict potential target. Bioinformatics prediction showed that the sensitizing target of wogonin is associated with AKT2, and GO analysis indicated that DEGs are inriched in protein kinase B (Akt) signaling (Figure 2, Figure 3). According to Yu et al, (2010)expression of the apoptosis-related genes Bcl-2 and BAD are associated with chemosensitivity. BAD and Bcl-2 are also potential target of wogonin in glioma (Wang et al., 2021). The results of flow cytometry and Western blot showed that wogonin may enhance the sensitivity of pancreatic cancer cells to gemcitabine by inhibiting p-Akt, anti-apoptotic gene Bcl-2, activating pro-apoptotic gene BAD, and promoting apoptosis of Panc-1 (Figure 4, Figure 5).

Meanwhile, bioinformatics predicted that wogonin could enhance gemcitabine sensitivity of pancreatic cancer by inhibiting AKT2, CCL2, HSP90AA1, PDE5A, and activating PTGS1, BCHE, SERPINB5, CA2, SRC, DGKA, HIF1A, PTGS2, ABCA1, DPYD, AKR1C3. According to the literature, AKT2 (Chen et al., 2012), CCL2 (Monti et al., 2004), HSP90 (Ghadban et al., 2017), CA2 (Zhao et al., 2021), SRC (Lin et al., 2019), HIF1A (Xu et al., 2021), ABCA1 (Shen and Yan, 2021), DPYD (Delhorme et al., 2022) and AKR1C3 (Phoo et al., 2021) are associated with drug resistance. The biological process of wogonin sensitization to gemcitabine includes: response to fluid shear stress, cyclooxygenase pathway, response to steroid hormones, positive regulation of transmembrane transport, peptide transport, and ribonucleoside acid metabolism process (Figure 3). And the results would be more reliable if gemcitabine resistant cells of the Pancreatic cancer were constructed and the Orthotopic pancreatic cancer mouse model was constructed. This study has not been experimentally verified, and further research is needed.

5 Conclusion

Our study demonstrates that wogonin inhibits the proliferation of Pancreatic cancer cells both *in vivo* and *invitro*. Through bioinformatics analysis and experimental verification, the mechanism of wogonin sensitizing gemcitabine in pancreatic cancer may be through inhibition of Akt pathway. Therefore, wogonin may be a novel drug with sensitizing effect in pancreatic cancer.

Data availability statement

The raw data supporting the conclusion of this article will be made available by the authors, without undue reservation.

Ethics statement

The animal study was reviewed and approved by Dalian Univercity of Technology.

Author contributions

Study conception and design: GX, TZ; data collection: ML; analysis and interpretation of results: QL; draft manuscript preparation: TZ and GX. All authors reviewed the results and approved the final version of the manuscript.

Funding

This work was supported by the National Natural Science Foundation of China (No. 81770846 and No. 81803024), Hirshberg Foundation for Pancreatic Cancer Research (GX20171003858 and GX20191005878), and Fundamental Research Funds from the Dalian Universities of Technology under Grant No. DUT17ZD308.

Conflict of interest

The authors declare that the research was conducted in the absence of any commercial or financial relationships that could be construed as a potential conflict of interest.

Publisher's note

All claims expressed in this article are solely those of the authors and do not necessarily represent those of their

affiliated organizations, or those of the publisher, the editors and the reviewers. Any product that may be evaluated in this article, or claim that may be made by its manufacturer, is not guaranteed or endorsed by the publisher.

Supplementary material

The Supplementary Material for this article can be found online at: https://www.frontiersin.org/articles/10.3389/fphar.2022.1068855/full#supplementary-material

References

Banik, K., Khatoon, E., Harsha, C., Rana, V., Parama, D., Thakur, K. K., et al. (2022). Wogonin and its analogs for the prevention and treatment of cancer: A systematic review. *Phytother. Res.* 36, 1854–1883. doi:10.1002/ptr.7386

Bray, F., Ferlay, J., Soerjomataram, I., Siegel, R. L., Torre, L. A., and Jemal, A. (2018). Global cancer statistics 2018: GLOBOCAN estimates of incidence and mortality worldwide for 36 cancers in 185 countries. *CA Cancer J. Clin.* 68 (6), 394–424. doi:10.3322/caac.21492

Cao, J., Yang, J., Ramachandran, V., Arumugam, T., Deng, D., Li, Z., et al. (2015). TM4SF1 promotes gemcitabine resistance of pancreatic cancer *in vitro* and *in vivo*. *PLoS One* 10 (12), e0144969doi:10.1371/journal.pone.0144969

Chen, D., Niu, M., Jiao, X., Zhang, K., Liang, J., and Zhang, D. (2012). Inhibition of AKT2 enhances sensitivity to gemcitabine via regulating PUMA and NF-κB signaling pathway in human pancreatic ductal adenocarcinoma. *Int. J. Mol. Sci.* 13 (1), 1186–1208. doi:10.3390/ijms13011186

Delhorme, J. B., Bersuder, E., Terciolo, C., Vlami, O., Chenard, M. P., Martin, E., et al. (2022). CDX2 controls genes involved in the metabolism of 5-fluorouracil and is associated with reduced efficacy of chemotherapy in colorectal cancer. *Biomed. Pharmacother.* 147, 112630doi:10.1016/j.biopha.2022.112630

Domenichini, A., Edmands, J. S., Adamska, A., Begicevic, R. R., Paternoster, S., and Falasca, M. (2019). Pancreatic cancer tumorspheres are cancer stem-like cells with increased chemoresistance and reduced metabolic potential. *Adv. Biol. Regul.* 72, 63–77. doi:10.1016/j.jbior.2019.02.001

Ghadban, T., Dibbern, J. L., Reeh, M., Miro, J. T., Tsui, T. Y., Wellner, U., et al. (2017). HSP90 is a promising target in gemcitabine and 5-fluorouracil resistant pancreatic cancer. *Apoptosis* 22 (3), 369–380. doi:10.1007/s10495-016-1332-4

Hu, J. X., Zhao, C. F., Chen, W. B., Liu, Q. C., Li, Q. W., Lin, Y. Y., et al. (2021). Pancreatic cancer: A review of epidemiology, trend, and risk factors. *World J. Gastroenterol.* 27 (27), 4298–4321. doi:10.3748/wjg.v27.i27.4298

Huynh, D. L., Ngau, T. H., Nguyen, N. H., Tran, G. B., and Nguyen, C. T. (2020). Potential therapeutic and pharmacological effects of wogonin: An updated review. *Mol. Biol. Rep.* 47 (12), 9779–9789. doi:10.1007/s11033-020-05972-9

Huynh, D. L., Sharma, N., Kumar, S. A., Singh, S. S., Zhang, J. J., Mongre, R. K., et al. (2017). Anti-tumor activity of wogonin, an extract from Scutellaria baicalensis, through regulating different signaling pathways. *Chin. J. Nat. Med.* 15 (1), 15–40. doi:10.1016/S1875-5364(17)30005-5

Ilic, I., and Ilic, M. (2022). International patterns in incidence and mortality trends of pancreatic cancer in the last three decades: A joinpoint regression analysis. *World J. Gastroenterol.* 28 (32), 4698–4715. doi:10.3748/wjg.v28.i32.4698

Kim, M. S., Bak, Y., Park, Y. S., Lee, D. H., Kim, J. H., Kang, J. W., et al. (2013). Wogonin induces apoptosis by suppressing E6 and E7 expressions and activating intrinsic signaling pathways in HPV-16 cervical cancer cells. *Cell Biol. Toxicol.* 29 (4), 259–272. doi:10.1007/s10565-013-9251-4

Kreipe, H. (2018). Ki67: Biological intertumor variance versus variance of assay. *Pathologe* 39 (2), 272–277. doi:10.1007/s00292-018-0502-2

Lee, S. H., Lee, E. J., Min, K. H., Hur, G. Y., Lee, S. H., Lee, S. Y., et al. (2015). Quercetin enhances chemosensitivity to gemcitabine in lung cancer cells by inhibiting heat shock protein 70 expression. *Clin. Lung Cancer* 16 (6), e235–e243. doi:10.1016/j.cllc.2015.05.006

Lin, J. H., Chen, S. Y., Lu, C. C., Lin, J. A., and Yen, G. C. (2020). Ursolic acid promotes apoptosis, autophagy, and chemosensitivity in gemcitabine-resistant human pancreatic cancer cells. *Phytother. Res.* 34 (8), 2053–2066. doi:10.1002/ptr.6669

Lin, Y. P., Wu, J. I., Tseng, C. W., Chen, H. J., and Wang, L. H. (2019). Gjb4 serves as a novel biomarker for lung cancer and promotes metastasis and chemoresistance via Src activation. *Oncogene* 38 (6), 822–837. doi:10.1038/s41388-018-0471-1

Liu, H., Wang, J., Zhou, W., Wang, Y., and Yang, L. (2013). Systems approaches and polypharmacology for drug discovery from herbal medicines: An example using licorice. *J. Ethnopharmacol.* 146 (3), 773–793. doi:10.1016/j.jep.2013.02.004

Liu, X., Tian, S., Liu, M., Jian, L., and Zhao, L. (2016). Wogonin inhibits the proliferation and invasion, and induces the apoptosis of HepG2 and Bel7402 HCC cells through NFκB/Bcl-2, EGFR and EGFR downstream ERK/AKT signaling. *Int. J. Mol. Med.* 38 (4), 1250–1256. doi:10.3892/ijmm.2016.2700

Mcguigan, A., Kelly, P., Turkington, R. C., Jones, C., Coleman, H. G., and Mccain, R. S. (2018). Pancreatic cancer: A review of clinical diagnosis, epidemiology, treatment and outcomes. *World J. Gastroenterol.* 24 (43), 4846–4861. doi:10.3748/wjg.v24.i43.4846

Monti, P., Marchesi, F., Reni, M., Mercalli, A., Sordi, V., Zerbi, A., et al. (2004). A comprehensive *in vitro* characterization of pancreatic ductal carcinoma cell line biological behavior and its correlation with the structural and genetic profile. *Virchows Arch.* 445 (3), 236–247. doi:10.1007/s00428-004-1053-x

Neoptolemos, J. P., Kleeff, J., Michl, P., Costello, E., Greenhalf, W., and Palmer, D. H. (2018). Therapeutic developments in pancreatic cancer: Current and future perspectives. *Nat. Rev. Gastroenterol. Hepatol.* 15 (6), 333–348. doi:10.1038/s41575-018-0005-x

Park, W., Chawla, A., and O'Reilly, E. M. (2021). Pancreatic cancer: A review. *JAMA* 326 (9), 851–862. doi:10.1001/jama.2021.13027

Phoo, N., Dejkriengkraikul, P., Khaw-On, P., and Yodkeeree, S. (2021). Transcriptomic profiling reveals AKR1C1 and AKR1C3 mediate cisplatin resistance in signet ring cell gastric carcinoma via autophagic cell death. *Int. J. Mol. Sci.* 22 (22), 12512. doi:10.3390/ijms222212512

Ren, H., and Wang, C. F. (2020). Diagnosis, treatment and prognosis evaluation of pancreatic cancer by microRNA. *Zhonghua Zhong Liu Za Zhi* 42 (11), 903–906. doi:10.3760/cma.j.cn112152-20190313-00152

Shen, Y., and Yan, Z. (2021). Systematic prediction of drug resistance caused by transporter genes in cancer cells. *Sci. Rep.* 11 (1), 7400. doi:10.1038/s41598-021-86921-9

Song, D., Tian, J., Hu, Y., Wei, Y., Lu, H., Wang, Y., et al. (2020). Identification of biomarkers associated with diagnosis and prognosis of gastroesophageal junction adenocarcinoma-a study based on integrated bioinformatics analysis in GEO and TCGA database. *Med. Baltim.* 99 (51), e23605doi:10.1097/MD.0000000000023605

Wang, T., Long, F., Jiang, G., Cai, H., Jiang, Q., Cheng, K., et al. (2018). Pharmacokinetic properties of wogonin and its herb-drug interactions with docetaxel in rats with mammary tumors. *Biomed. Chromatogr.* 32, e4264doi:10.1002/bmc.4264

Wang, X., Pan, C., Gong, J., Liu, X., and Li, H. (2016). Enhancing the enrichment of pharmacophore-based target prediction for the polypharmacological profiles of drugs. *J. Chem. Inf. Model.* 56 (6), 1175–1183. doi:10.1021/acs.jcim.5b00690

Wang, X., Shen, Y., Wang, S., Li, S., Zhang, W., Liu, X., et al. (2017). PharmMapper 2017 update: A web server for potential drug target identification with a comprehensive target pharmacophore database. *Nucleic Acids Res.* 45 (W1), W356-W360–W360. doi:10.1093/nar/gkx374

Wang, Z., Cheng, L., Shang, Z., Li, Z., Zhao, Y., Jin, W., et al. (2021). Network pharmacology for analyzing the key targets and potential mechanism of wogonin in gliomas. *Front. Pharmacol.* 12, 646187doi:10.3389/fphar.2021.646187

Wu, K., Teng, M., Zhou, W., Lu, F., Zhou, Y., Zeng, J., et al. (2021). Wogonin induces cell cycle arrest and apoptosis of hepatocellular carcinoma cells by activating hippo signaling. *Anticancer Agents Med. Chem.* 22, 1551–1560. doi:10.2174/1871520621666210824105915

Xing, F., Sun, C., Luo, N., He, Y., Chen, M., Ding, S., et al. (2019). Wogonin increases cisplatin sensitivity in ovarian cancer cells through inhibition of the phosphatidylinositol 3-kinase (PI3K)/Akt pathway. *Med. Sci. Monit.* 25, 6007–6014. doi:10.12659/MSM.913829

Xu, F., Huang, M., Chen, Q., Niu, Y., Hu, Y., Hu, P., et al. (2021). LncRNA HIF1A-AS1 promotes gemcitabine resistance of pancreatic cancer by enhancing glycolysis through modulating the AKT/YB1/HIF1 pathway. *Cancer Res.* 81 (22), 5678–5691. doi:10.1158/0008-5472.CAN-21-0281

Xu, J., Zhang, B., Chu, Z., Jiang, F., and Han, J. (2021). Wogonin alleviates cisplatin-induced cardiotoxicity in mice via inhibiting gasdermin D-mediated pyroptosis. *J. Cardiovasc Pharmacol.* 78 (4), 597–603. doi:10.1097/FJC.0000000000001085

Yang, D., Guo, Q., Liang, Y., Zhao, Y., Tian, X., Ye, Y., et al. (2020). Wogonin induces cellular senescence in breast cancer via suppressing TXNRD2 expression. *Arch. Toxicol.* 94 (10), 3433–3447. doi:10.1007/s00204-020-02842-y

Yang, J., Xu, J., Zhang, B., Tan, Z., Meng, Q., Hua, J., et al. (2021). Ferroptosis: At the crossroad of gemcitabine resistance and tumorigenesis in pancreatic cancer. *Int. J. Mol. Sci.* 22 (20), 10944. doi:10.3390/ijms222010944

Yu, B., Sun, X., Shen, H. Y., Gao, F., Fan, Y. M., and Sun, Z. J. (2010). Expression of the apoptosis-related genes BCL-2 and BAD in human breast carcinoma and their associated relationship with chemosensitivity. *J. Exp. Clin. Cancer Res.* 29 (1), 107. doi:10.1186/1756-9966-29-107

Zhang, W. T., Zhang, J. J., Shao, Q., Wang, Y. K., Jia, J. P., Qian, B., et al. (2022). FGD5-AS1 is an oncogenic lncRNA in pancreatic cancer and regulates the Wnt/β-catenin signaling pathway via miR-577. *Oncol. Rep.* 47 (1), 21. doi:10.3892/or.2021.8232

Zhao, K., Zhang, Z., Culmsee, C., Zhong, L., Pagenstecher, A., Nimsky, C., et al. (2021). Inhibition of carbonic anhydrase 2 overcomes temozolomide resistance in glioblastoma cells. *Int. J. Mol. Sci.* 23 (1), 157. doi:10.3390/ijms23010157

Zheng, N. N., Zhou, M., Sun, F., Huai, M. X., Zhang, Y., Qu, C. Y., et al. (2020). Combining protein arginine methyltransferase inhibitor and anti-programmed death-ligand-1 inhibits pancreatic cancer progression. *World J. Gastroenterol.* 26 (26), 3737–3749. doi:10.3748/wjg.v26.i26.3737

Zou, J., Su, H., Zou, C., Liang, X., and Fei, Z. (2020). Ginsenoside Rg3 suppresses the growth of gemcitabine-resistant pancreatic cancer cells by upregulating lncRNA-CASC2 and activating PTEN signaling. *J. Biochem. Mol. Toxicol.* 34 (6), e22480doi:10.1002/jbt.22480

frontiers | Frontiers in Pharmacology

TYPE Original Research
PUBLISHED 04 January 2023
DOI 10.3389/fphar.2022.1080412

OPEN ACCESS

EDITED BY
Eswar Shankar,
The Ohio State University, United States

REVIEWED BY
Annapurna Gupta,
Comprehensive Cancer Center,
United States
Kate Ormiston,
The Ohio State University, United States

*CORRESPONDENCE
Ruihe Zheng,
ruihezheng@hainmc.edu.cn,
ruihezheng@126.com

†These authors have contributed equally to this work

SPECIALTY SECTION
This article was submitted to Pharmacology of Anti-Cancer Drugs, a section of the journal Frontiers in Pharmacology

RECEIVED 26 October 2022
ACCEPTED 21 December 2022
PUBLISHED 04 January 2023

CITATION
Niu T, Wei Z, Fu J, Chen S, Wang R, Wang Y and Zheng R (2023), Venlafaxine, an anti-depressant drug, induces apoptosis in MV3 human melanoma cells through JNK1/2-Nur77 signaling pathway. *Front. Pharmacol.* 13:1080412. doi: 10.3389/fphar.2022.1080412

Venlafaxine, an anti-depressant drug, induces apoptosis in MV3 human melanoma cells through JNK1/2-Nur77 signaling pathway

Ting Niu[1†], Zhiying Wei[2†], Jiao Fu[1], Shu Chen[1], Ru Wang[1], Yuya Wang[2] and Ruihe Zheng[2*]

[1]Central Laboratory, Hainan General Hospital, Hainan Affiliated Hospital of Hainan Medical University, Haikou, China, [2]Department of Pharmacy, Hainan General Hospital, Hainan Affiliated Hospital of Hainan Medical University, Haikou, China

Introduction: Venlafaxine is one of the most commonly used anti-depressant and antineoplastic drug. Previous studies have predicted venlafaxine as an anti-cancer compound, but the therapeutic effects of venlafaxine in melanoma have not yet been demonstrated. Nur77 is an orphan nuclear receptor that highly expressed in melanoma cells and can interact with Bcl-2 to convert Bcl-2 from an antiapoptotic to a pro-apoptotic protein.

Method: We examined the effects of venlafaxine in MV3 cells *in vitro* and MV3 xenograft tumor in nude mice. Western-blot, PCR, TUNEL assay and immunofluorescence were used to reveal the growth of melanoma cells.

Results: Here, our data revealed that venlafaxine could reduce the growth, and induce apoptosis of melanoma cells through a Nur77-dependent way. Our results also showed that treatment with venlafaxine (20 mg/kg, i.p.) potently inhibited the growth of melanoma cells in nude mice. Mechanistically, venlafaxine activated JNK1/2 signaling, induced Nur77 expressions and mitochondrial localization, thereby promoting apoptosis of melanoma cells. Knockdown of Nur77 and JNK1/2, or inhibition of JNK1/2 signaling with its inhibitor SP600125 attenuated the anti-cancer effects of venlafaxine.

Conclusion: In summary, our results suggested venlafaxine as a potential therapy for melanoma.

KEYWORDS

melanoma, Nur77, venlafaxine, drug repurposing, JNK1/2 kinase

1 Introduction

Melanoma is the leading cause of skin cancer death worldwide (Cullen et al., 2020). Currently, BRAF inhibitor vemurafenib and MEK inhibitor trametinib are the most common drugs used for the treatment of melanoma (Guo et al., 2021; Chiavarini et al., 2022; Porcelli et al., 2022). However, BRAF-mutated melanomas treated with these compounds almost invariably develop resistance (Siegel et al., 2020). Further research on the molecular mechanism of melanoma and the development of novel therapeutics with high efficiency and low toxicity is highly desired. Nur77 is an orphan nuclear receptor that widely expressed in different types of tumors, including melanoma (Hsu et al., 2004; To et al., 2012). Nur77 plays diverse roles in the regulation of cell proliferation, survival, and apoptosis (Hu et al., 2017; Wu and Chen, 2018;

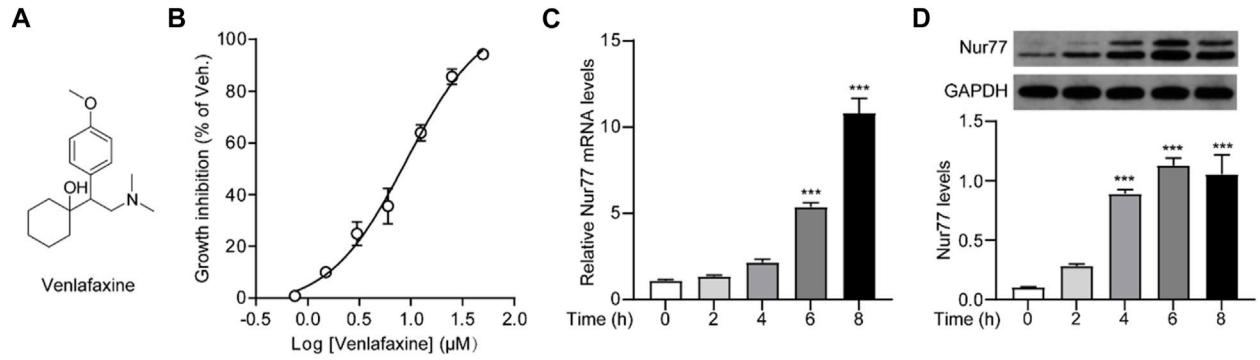

FIGURE 1
Cellular viability was correlated to Nur77 expression induced by venlafaxine. **(A)** Chemical structure of venlafaxine. **(B)** Dose-dependent inhibition of venlafaxine on the growth inhibition of MV3 cells at 72 h. **(C)** Relative mRNA expressions of Nur77 in MV3 cells were quantified after treatment with venlafaxine (10 μM) for 0–8 h. **(D)** The protein expression of Nur77 in MV3 cells was detected by Western blot after treatment with venlafaxine (10 μM) for 0–8 h. Intensity of the protein bands was quantified and normalized to loading control GAPDH. N = 3, ***, $p < .001$ vs. control (0 h).

Safe and Karki, 2021). The mitogenic and survival effect of Nur77 may be associated with its transcriptional activity in the nucleus (Zhang, 2007). On the other hand, the pro-apoptotic effect of Nur77 involves its translocation from the nucleus to mitochondria, where it interacts with Bcl-2 and converts Bcl-2 from a survival to a killer of cancer cells (Lin et al., 2004; Kolluri et al., 2008; Zhou et al., 2014; Liu et al., 2017). These complex effects of Nur77 appear to be dependent on its posttranslational modifications (Zhou et al., 2014; Liu et al., 2017). For example, phosphorylation of Nur77 by protein kinase B (AKT) promotes its nuclear shuttling, resulting in the promotion of cancer cell proliferation and invasion, while its phosphorylation by c-Jun N-terminal kinase (JNK) involves the apoptosis in certain cancer cells (Han et al., 2006; Bourhis et al., 2008; Bliss et al., 2012). Thus, targeting Nur77 may offer new strategies to develop effective melanoma therapeutics.

To date, many potent Nur77 modulators have been developed (Crean and Murphy, 2021). However, it is extremely challenging to push these compounds towards clinical application. One way to expedite drug development is to discover new uses for approved or investigational drugs. Recently, a study conducted by Bennett et al. revealed that predicted venlafaxine as an anti-cancer compound (Bennett et al., 2022). Venlafaxine is a serotonin and norepinephrine reuptake inhibitor (Figure 1A) and has been used in therapy as an anti-depressant drug since 1993 (Roseboom and Kalin, 2000). Venlafaxine also can attenuate neuropathic pain and vasomotor symptoms in women after cancer (Pinkerton and Santen, 2019; van den Beuken-van Everdingen et al., 2017). Many serotonin reuptake inhibitors, e.g., fluoxetine and desipramine could inhibit melanoma solid tumor growth *in vitro* (Kubera et al., 2009; Grygier et al., 2013). Thus, it is possible that venlafaxine can reduce melanoma cell proliferation. In addition, venlafaxine contains a two-ring group, which is commonly seen in many potent Nur77 modulators, i.g., BI1071 and Triclosan (Ha et al., 2018; Chen et al., 2019). Venlafaxine is likely to act as a Nur77 modulator, exhibiting anti-cancer activities by regulation of Nur77 signaling. So far, venlafaxine has not been explored as a therapeutic approach for melanoma and whether venlafaxine can inhibit the growth of tumor cells in animals is still unknown.

As a proof of concept, we examined the capability of venlafaxine to inhibit the growth of MV3 melanoma cells, and its effects in theNur77 expression. We also studied the molecular mechanisms involved in venlafaxine-induced MV3 cell death. Our results showed that venlafaxine could reduce the growth and induce apoptosis of MV3 cells through the JNK1/2-Nur77 signaling pathway. Our results suggested venlafaxine as a potential therapy for melanoma.

2 Materials and methods

2.1 Chemicals

All reagents were purchased from Sinopharm (Shanghai, China) unless otherwise indicated. Venlafaxine hydrochloride (Cat. #V129637), SP600125 (Cat. #S125267) and PD98059 (Cat. #P126620) were purchased from Aladdin (Shanghai, China).

2.2 Cell culture and treatment

Human melanoma (MV3) cells were purchased from the China center for type culture collection (Cat. #GDC0615). MV3 cells were cultured in DMEM medium supplemented with 10% FBS, 100 units/ml penicillin, and 100 μg/ml streptomycin in humidified 5% CO_2 atmosphere at 37°C until 80% confluence. MV3 cells were then treated with venlafaxine (0–100 μM), SP600125 (.5 μM) and PD98059 (15 μM) (a MEK/ERK inhibitor that can inhibit MEK activation and subsequent ERK phosphorylation) for 30 min, or human Nur77 siRNA (50 nM), JNK1/2 siRNA (Cell signaling, Cat. #6232S, 50 nM), ERK1/2 siRNA (Cell signaling, Cat. #6560S, 50 nM) and HiPerfect transfection reagent (Qiagen, 301704, United States) for 12 h, followed by incubation at 37°C for 0–72 h (Li et al., 2018). The siRNA sequences were described below:

Control siRNA: 5′-GCGCGCUUUGTAGGAUUCGdTdT-3′
Nur77 siRNA: 5′-CAGUCCAGCCAUGCUCCUCdTdT-3′

2.3 Cell viability

Cell viability was measured at 72 h, using the cell counting kit-8 (CCK8) according to the manufacturer's instructions (Liu J et al., 2022; Qin et al., 2022). MV3 cells were collected and incubated with a CCK-8

reagent (Dojindo, Cat. #CK04, 5 mg/ml, 10 μl) at 37°C for 60 min. The OD values of the reaction mixture were measured at the wavelength of 450 nm. The cell viability was calculated using the following formula: Cell viability (%) = OD (control) − OD (test)/OD (control) − OD (blank).

2.4 Apoptosis assay

Apoptosis assay was conducted at 0, 4 and 8 h, using a dead cell apoptosis kit with Annexin V-FITC and propidium iodide (PI) (Thermo, Cat. #V13241) according to the manufacturer's instructions (Chen et al., 2019; Li et al., 2022). MV3 cells were washed with PBS, resuspended in binding buffer, incubated with Annexin V-FITC and PI for 15 min according to the kit protocol, and analyzed immediately by cytoFLEX Flow Cytometry System (Beckman-Coulter) using FITC and PerCP.

2.5 Animals and treatments

The animal experiments were approved by the Animal Care and Use Committee of Hainan Medical University [Approval No. Med-Eth-Re (2022) 736]. Female BALB/c nude mice (20–25 g) were purchased from Shanghai SLAC Laboratory Animal Co., Ltd. Mice were maintained under specific pathogen-free conditions, group-housed in ventilated cages with controlled temperature (25°C ± 1°C) and relative humidity (55% ± 10%). Standard mouse chow and tap water were provided *ad libitum*. The nude mice were anesthetized by intravenous injection of pentobarbital sodium (25 mg/kg), followed by subcutaneous transplantation of MV3 or Nur77 knockout (Nur77 KO) MV3 melanoma cells in the right posterior axillary line (Liu Y. X et al., 2022). The dose of venlafaxine for the mice was based on the preliminary experiments and the references (Zhang et al., 2019; Madrigal-Bujaidar et al., 2021). Mice were treated with venlafaxine (20 mg/kg, i.p.) or its .1% DMSO-containing saline vehicle once daily after tumor size grew up to 50–100 mm^3. Body weight and tumor volume were measured every 3 days. Mice were sacrificed by CO_2 inhalation after 15-day drug treatment and the tumors were stripped for various assessments (Chen et al., 2019). Nur77 knockout (KO) MV3 cells were generated by CRISPR/Cas9 system using a previously reported method (Chen et al., 2019). The gRNA targeting sequence of Nur77 is 5′-ACCTTCATGGACGGCTACAC-3′. Protein lysates were prepared from tumors with previously reported method (Chen et al., 2015). Tumors were homogenized in cold 1× RIPA lysis buffer and centrifuged at 15,000 × g for 15 min at 4°C. The supernatants were collected and the protein concentration of sample was measured by Pierce BCA protein assay kit (Thermo, Cat. #23225). Ultimately, all samples were normalized to the same total protein concentration of 2 mg/ml. Frozen tumor tissues were thawed and then homogenated in Trizol reagent. Total RNA was extracted with chloroform, isopropanol, and 75% ethanol. The RNA concentration was measured with a spectrophotometer (Beckman Coulter, United States).

2.6 Western blot

Western blots were performed using the standard sodium dodecyl sulfate (SDS)-PAGE polyacrylamide gel electrophoresis method (Li et al., 2021a). The protein of cell or tumor lysates was prepared and measured by Pierce BCA protein assay kit (Thermo, Cat. #23225) (Xie et al., 2022a). The total protein (50 μg) was separated by 10% SDS-PAGE gels and transferred to a nitrocellulose membrane (Amersham Biosciences, Shanghai, China). Membranes were blocked in 5% (w/v) nonfat milk for 1 h at room temperature, washed with saline buffer (containing .05% tween-20) and then incubated at 4°C overnight with the primary antibody: Nur77 (Cell signaling, Cat. #3960S, dilution 1:500), cleaved caspase-3 (Cell signaling, Cat. #9661S, dilution 1:300), PARP (Santa Cruz, Cat. #sc-8001, dilution 1:500), p38 (Novus, Cat. #AF8691, dilution 1:500), p-p38 (Santa Cruz, Cat. #sc-166182, dilution 1:300), JNK1/2 (Santa Cruz, Cat. #sc-137019, dilution 1:800), p-JNK1/2 (R&D, Cat. #AF1205, dilution 1:400), c-Jun (Novus, Cat. #MAB8930, dilution 1:500), p-c-Jun (Cell signaling, Cat. #3270S, dilution 1:300), ERK1/2 (Cell signaling, Cat. #68303SF, dilution 1:600), p-ERK1/2 (Cell signaling, Cat. #9101S, dilution 1:300), GAPDH (Santa Cruz, Cat. #sc-47724, dilution 1:1000). The membranes were then incubated for 1 h at room temperature with horseradish peroxidase (HRP)-linked anti-rabbit IgG antibody (Santa Cruz, Cat. #sc-2004, dilution 1:5000) and detected with an electrochemiluminescence plus kit (Amersham Biosciences).

2.7 Real-time polymerase chain reaction (RT-PCR)

Total RNAs were extracted by Trizol (Invitrogen) and complemental DNA was synthesized using RevertAid First-Strand cDNA Synthesis Kits (Fermentas). RT-PCR was performed using SYBR Green dye and the Roche LightCycler® 480 II system following the manufacturer's instructions on a 7300 real-time PCR system (Applied Biosystems) using respective primers (Hu et al., 2021):

Nur77: 5′-ACCCACTTCTCCACACCTTG-3′ (forward), 5′-ACTTGGCGTTTTTCT GCACT-3′ (reverse).

β-Actin: 5′-AGAGCTACGAGCTGCCTGAC-3’ (forward), 5′-AGCACTGTGTTG GCGTACAG-3′ (reverse).

Expression data were normalized to β-Actin mRNA expression.

2.8 Histological analysis

Tumor tissues were excised, sectioned and fixed in 10% (w/v) formalin for 24 h, followed by embedding in paraffin. The specimen was embedded in paraffin and cut into 5 μm sections for further assessments (Xie et al., 2022b).

2.9 Immunofluorescence

In vitro–cultured MV3 cells were fixed with 4% paraformaldehyde, permeabilized with .1% Triton X-100 in PBS for 20 min, and then blocked with goat serum in .3 M glycine in PBS at 25°C for 1 h. Sections were then incubated at 4°C overnight with the primary antibody: Nur77 (Cell signaling, Cat. #3960S, dilution 1:500) and Bcl2 (Abcam, Cat. #ab692, dilution 1:500). Sections were rinsed with .1 M PBS and exposed to donkey secondary antibodies conjugated with Alexa Fluor 488 or 647 (Abcam, dilution 1:1,000) at room temperature for 2 h. After an additional rinse, cells were then counterstained with 4′, 6-diamidino-2-phenylindole (DAPI) for nuclear labelling (Wang et al., 2022). Fluorescence images were captured with a confocal microscope.

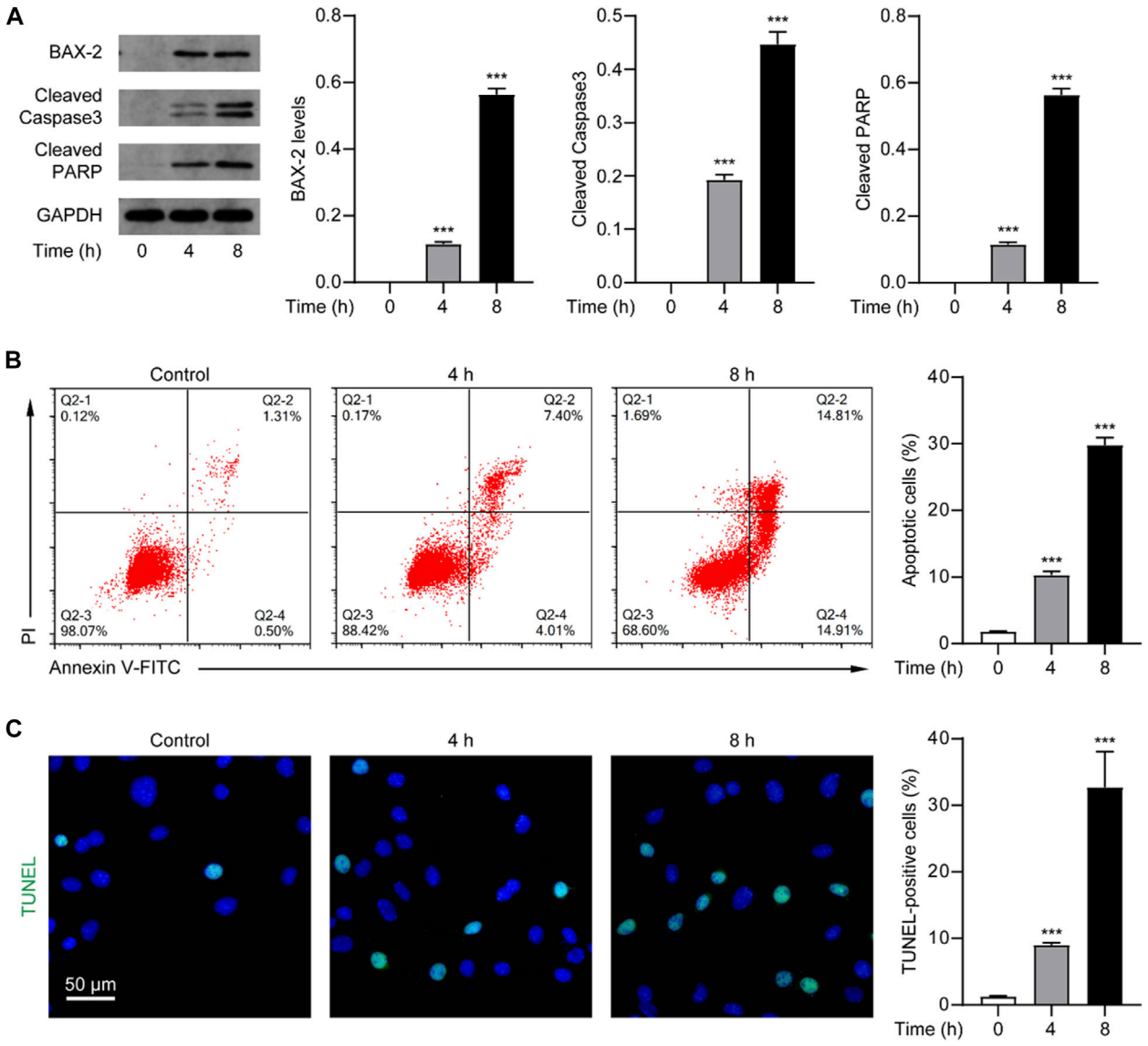

FIGURE 2
Venlafaxine induced apoptosis in MV3 cells. **(A)** The protein expression of BAX-2, cleaved caspase 3 and cleaved PARP in MV3 cells was detected by Western blot after treatment with venlafaxine (10 μM) for 0–8 h. Intensity of the protein bands was quantified and normalized to loading control GAPDH. **(B)** Apoptosis assays in MV3 cells treated with venlafaxine (10 μM) for 0–8 h were conducted by flow cytometry. **(C)** The apoptotic cells were detected by TUNEL assay in MV3 cells treated with venlafaxine (10 μM) for 0–8 h. N = 3, ***, $p < .001$ vs. control (0 h).

The paraffin-embedded tumor sections were incubated with the following primary antibodies at 4°C overnight: Nur77 (Cell signaling, Cat. #3960S, dilution 1:500), cleaved caspase-3 (Cell signaling, Cat. #9661S, dilution 1:300), Ki-67 (Abcam, Cat. #ab15580, dilution 1:800). After incubation, sections were rinsed with .1 M PBS and exposed to goat secondary antibodies conjugated with Alexa Fluor 488 or 647 (Abcam, dilution 1:1,000) at room temperature for 1 h (Li et al., 2021b). After an additional rinse, sections were then counterstained with DAPI for nuclear labelling. Fluorescence images were captured with a confocal microscope.

Reactive oxygen species (ROS) were stained with cellular ROS assay kit (deep red) (Abcam, Cat. #ab186029) according to the manufacturer's instructions. Terminal deoxynucleotidyl transferase-mediated dUTP nick end labeling (TUNEL) assays were carried out according to the manufacturer's instructions (Promega, Cat. #G7131). The number of apoptotic cells was counted by Image J.

2.10 Statistical analysis

Data are presented as means ± SEM. Analyses were performed with GraphPad Prism 9.0.5. Three or more different groups were analyzed by one-way ANOVA with Dunnett's *post hoc* multiple comparison tests. $p < .05$ was considered statistically significant.

3 Results

3.1 Cellular viability was correlated to Nur77 expression induced by venlafaxine

We first investigated whether venlafaxine could regulate the cellular viability of MV3 cells. As shown in Figure 1B, venlafaxine

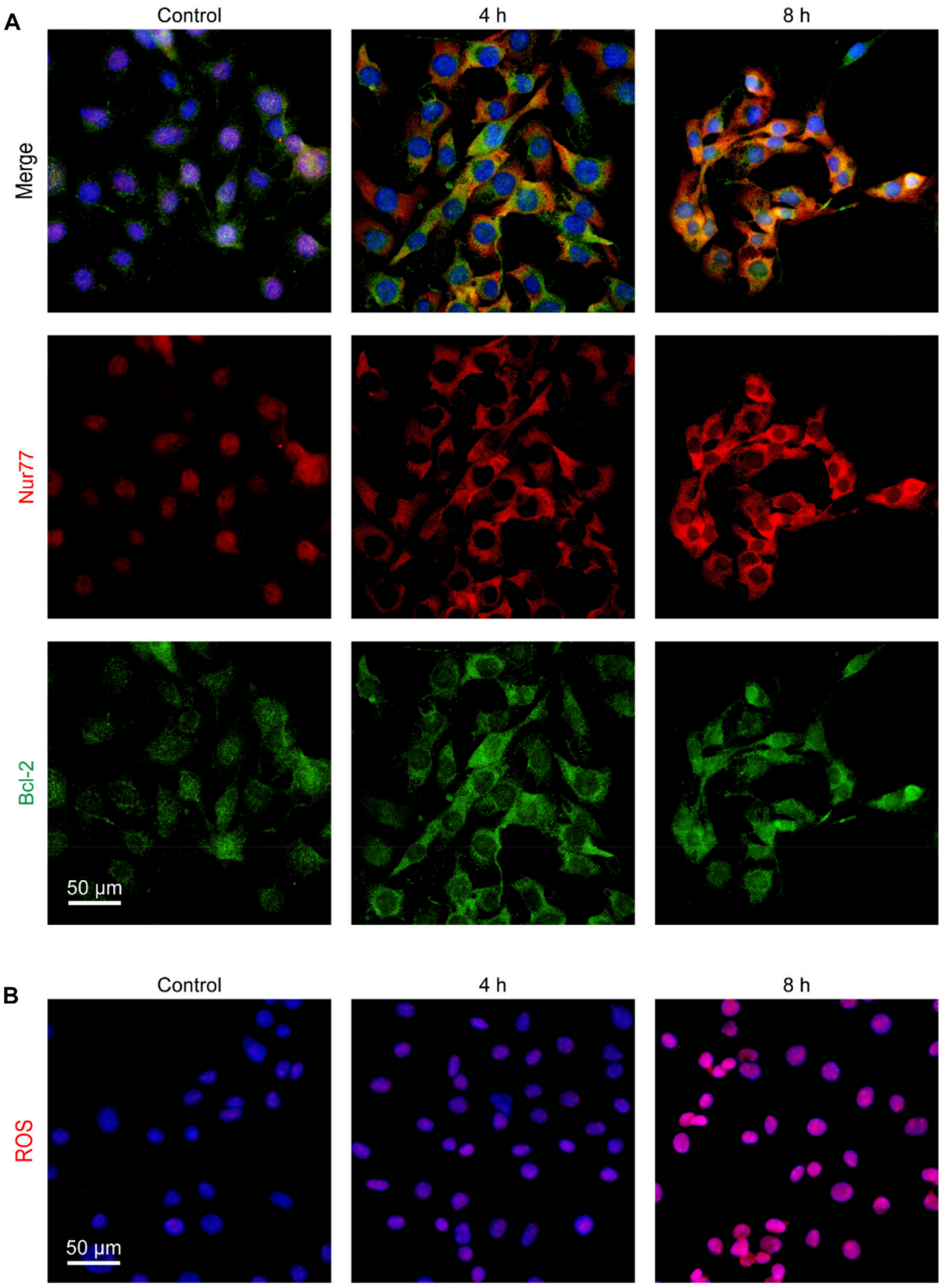

FIGURE 3
Venlafaxine induced Nur77 mitochondrial targeting and ROS production in MV3 cells. **(A)** MV3 cells treated with venlafaxine (10 μM) for 0–8 h were immunostained with Bcl-2 and Nur77 antibodies and visualized by confocal microscopy. **(B)** MV3 cells treated with the cellular ROS assay kit and visualized by confocal microscopy.

showed a great inhibition on the growth of MV3 cells with an LD_{50} = 9.01 ± .97 μM. To investigate whether the cytotoxicity effect of venlafaxine was associated with its induction of Nur77 expression, we then examined the effect of venlafaxine on Nur77 expression in MV3 cells. Based on the LD_{50} data of venlafaxine, MV3 cells were treated with venlafaxine at a

10.3389/fphar.2022.1080412

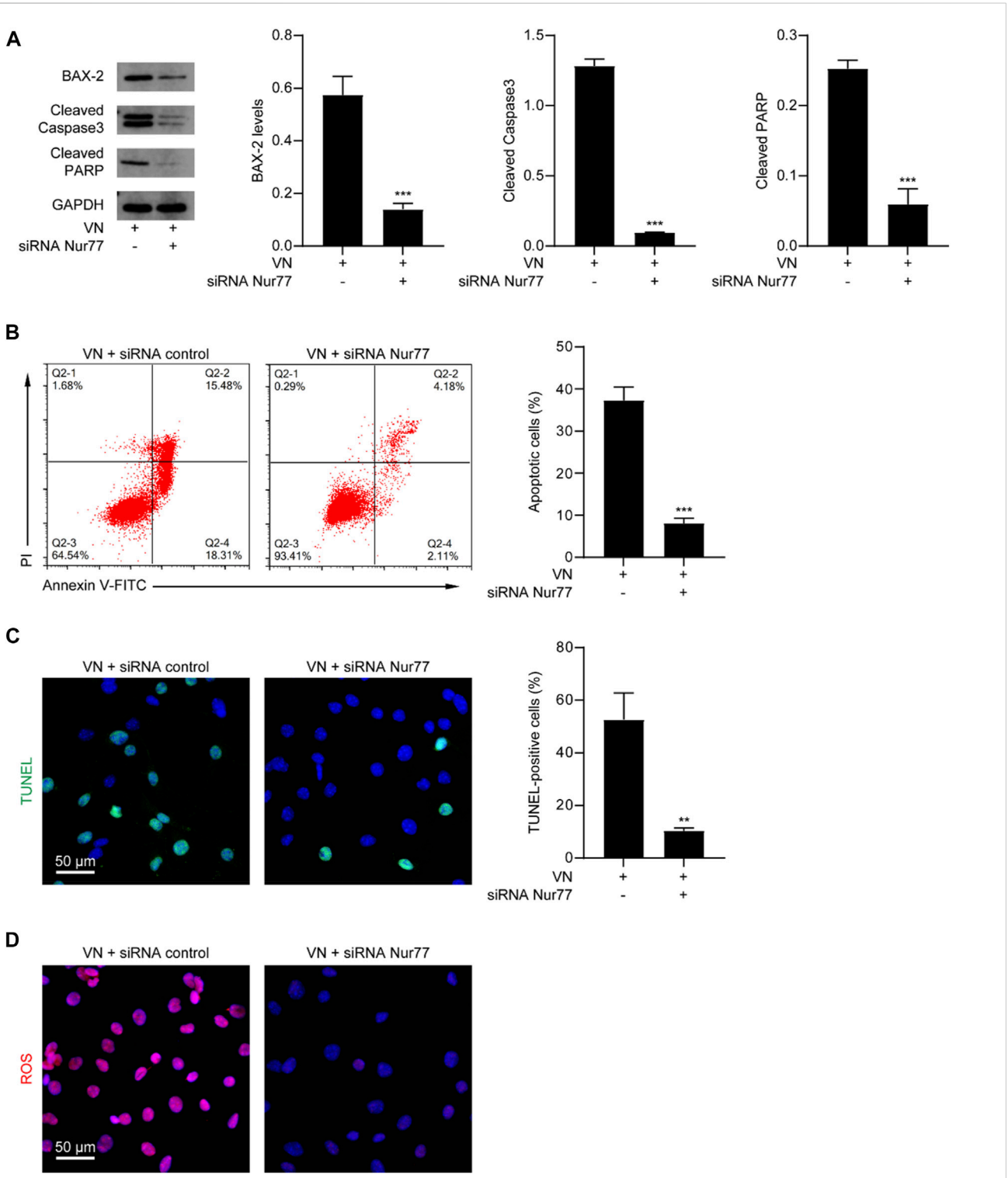

FIGURE 4
Nur77 expression was necessary for venlafaxine-induced apoptosis. MV3 cells were transfected with siRNA control or Nur77 siRNA, following by treatment with venlafaxine (10 μM) for 0–8 h. **(A)** The protein expression of BAX-2, caspase 3 and cleaved PARP in MV3 cells was detected by western blot. Inte cleaved nsity of the protein bands was quantified and normalized to loading control GAPDH. **(B)** Apoptosis assays in MV3 cells were conducted by flow cytometry. **(C)** The apoptotic cells were detected by TUNEL assay. **(D)** MV3 cells treated with the cellular ROS assay kit and visualized by confocal microscopy. N = 3, **, $p < .01$, ***, $p < .001$ vs. control.

concentration of 10 μM. qRT-PCR (Figure 1C) and western blot (Figure 1D) analyses showed that the mRNA and protein levels of Nur77 were low in MV3 cells, but were persistently elevated after venlafaxine treatment. Together, these results suggested that venlafaxine reduced the cell proliferation and introduced Nur77 expression in MV3 cells.

10.3389/fphar.2022.1080412

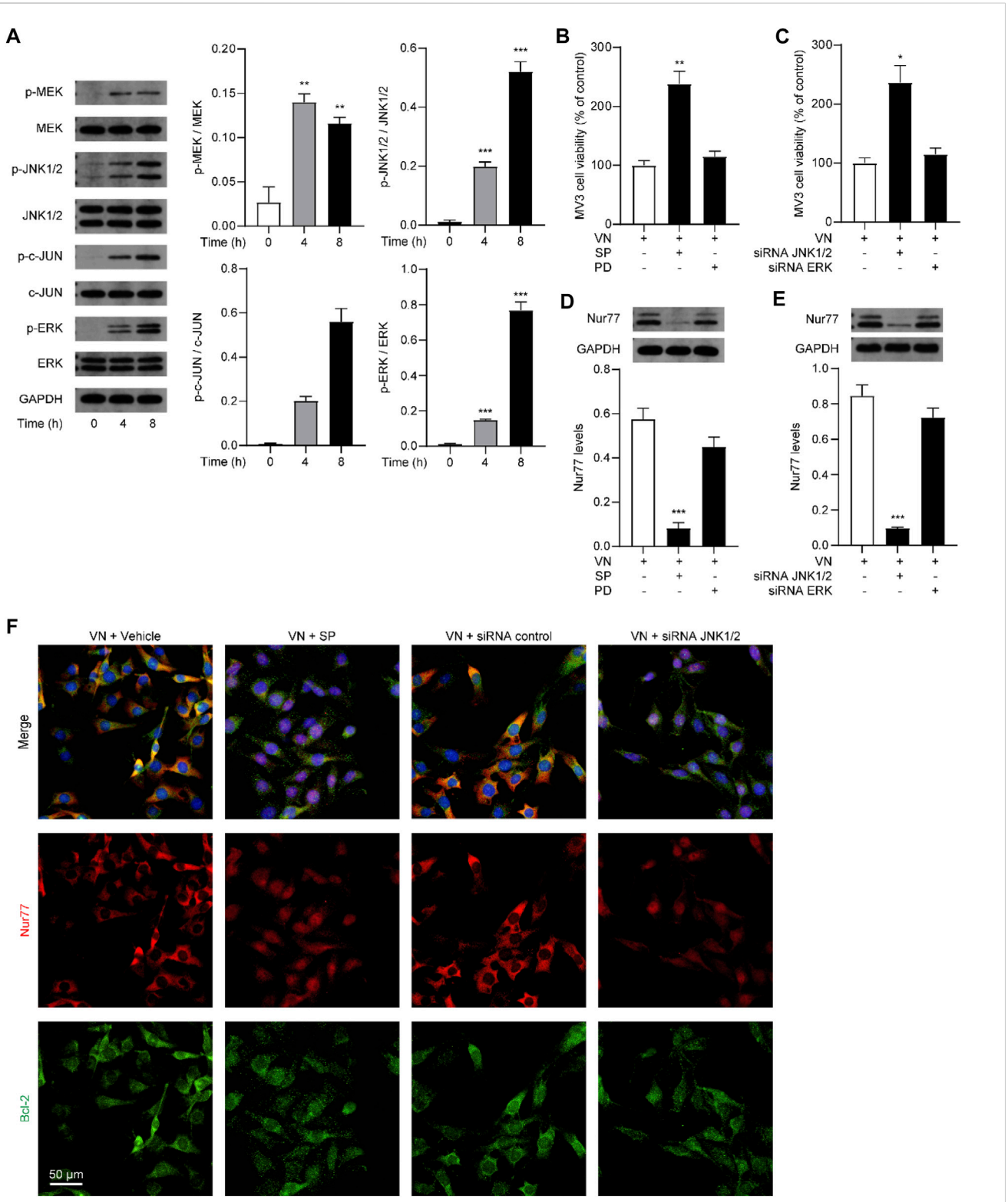

FIGURE 5
Activation of ERK1/2 signaling was necessary for venlafaxine-induced apoptosis. **(A)** Representative western-blot bands and quantification of the MAPK signal molecules abundances in MV3 cells treated with venlafaxine (10 μM) for 0–8 h **(B)** MV3 cells were treated with vehicle, JNK1/2 inhibitor SP600125 and MERK/ERK inhibitor PD98059 for 72 h. Cell viability were measured by CCK-8 kits at 72 h **(C)** MV3 cells were transfected with siRNA control, JNK1/2 siRNA, and ERK siRNA for 72 h. Cell viability were measured by CCK-8 kits at 72 h **(D,E)** Representative western-blot bands and quantification of Nur77 abundances in MV3 cells treated with venlafaxine (10 μM) for 8 h, or transfected with siRNA control, JNK1/2 siRNA, and ERK siRNA for 20 h **(F)** MV3 cells were immunostained with Bcl-2 and Nur77 antibodies and visualized by confocal microscopy. N = 3, *, $p < .05$, **, < .01, ***, $p < .001$ vs. control.

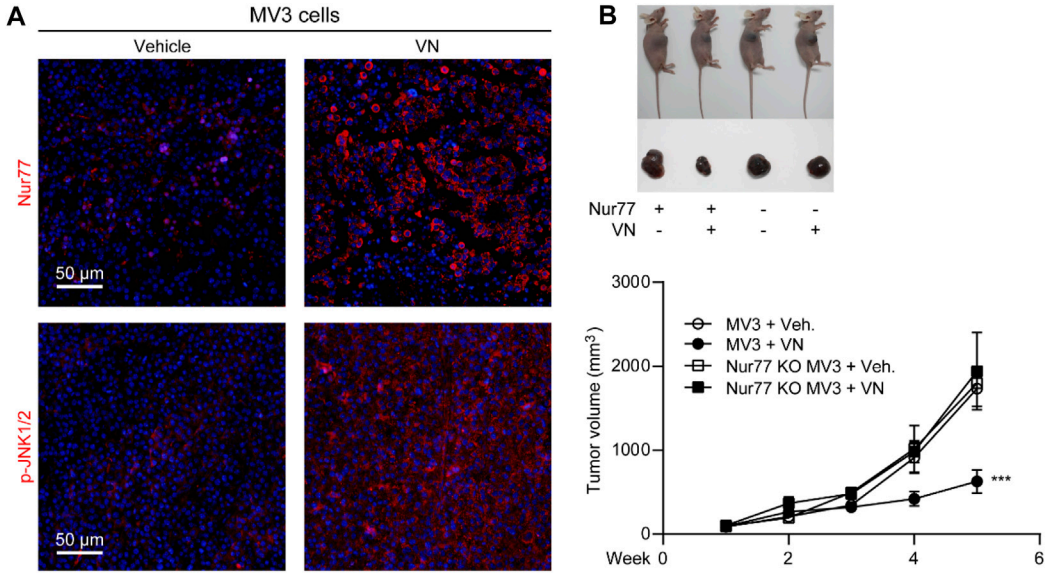

FIGURE 6
Anti-cancer efficacy of venlafaxine in mice. BALB/c nude mice bearing MV3 or Nur77 KO MV3 xenograft tumors were treated with venlafaxine (20 mg/kg, i.p.) or its vehicle once daily from week 1 to week 5 after implantation of MV3 or Nur77 KO MV3 cells. **(A)** Tumor tissues were immunostained with Nur77 and JNK1/2 antibodies and visualized by confocal microscopy. **(B)** Venlafaxine reduced cancer cell growth in nude mice through Nur77. One of five similar experiments is shown.

3.2 Venlafaxine-induced apoptosis in MV3 cells

Given that the death effect of Nur77 is associated with its induction of apoptosis, which has been observed in other studies (Zhang, 2007), we speculate that venlafaxine may exert an anti-proliferative effect through activating the Nur77-dependent apoptotic pathway. As a proof of concept, we examined the expression of BAX-2, cleaved caspase 3 and cleaved PARP, the indicators of apoptosis, in MV3 cells treated with venlafaxine (10 μM). Western-blot analysis showed that venlafaxine treatment persistently induced caspase 3 and PARP cleavage and BAX-2 expression in MV3 cells (Figure 2A). We further assessed the effect of venlafaxine on cell death using flow cytometry-based Annexin V/Propidium iodide (PI) apoptosis assay. As shown in Figure 2B, approximately 30% of MV3 cells were apoptotic when treated with venlafaxine for 8 h, whereas only about 2% of cells were apoptotic in vehicle control group. Moreover, TUNEL assay revealed extensive apoptosis in venlafaxine-treated MV3 cells (Figure 2C). Together, these results revealed that venlafaxine induces apoptosis in MV3 cells.

3.3 Venlafaxine induced Nur77 mitochondrial targeting and ROS production in MV3 cells

Nur77 can induce apoptosis by translocating to mitochondria where it binds to Bcl-2 to trigger cytochrome c release and ROS production (Lin et al., 2004; Chen et al., 2019). Thus, we further examined whether venlafaxine could induce Nur77 translocation from the nucleus to mitochondria. Immunofluorescence assay showed that Nur77 was mainly localized in the nucleus of MV3 cells, while treatment of venlafaxine promoted the mitochondrial translocation of this protein (Figure 3A). Furthermore, following Nur77 mitochondrial translocation, the production of ROS in MV3 cells was also enhanced by venlafaxine (Figure 3B). Together, these results revealed that venlafaxine induced Nur77 mitochondrial targeting and ROS production in MV3 cells.

3.4 Nur77 expression was necessary for venlafaxine-induced apoptosis

We next determined whether venlafaxine-induced apoptosis was Nur77-dependent. MV3 cells were transfected with Nur77 siRNA and subjected to venlafaxine treatment for 8 h. We found that Nur77 knockdown decreased venlafaxine-induced expressions of BAX-2, cleaved caspase 3 and cleaved PARP were in MV3 cells (Figure 4A). Furthermore, venlafaxine-induced apoptosis was rescued by transfecting with Nur77 siRNA, but not control siRNA (Figures 4B, C). Additionally, venlafaxine induced lower levels of ROS in Nur77-knockdown cells than control MV3 cells (Figure 4D). Together, these data indicated that Nur77 expression was necessary for venlafaxine-induced apoptosis.

3.5 Activation of JNK1/2 signaling was necessary for venlafaxine-induced cell death effects

Given that MAPKs play an important role in the regulation of melanoma cell survival and Nur77 post-translational modifications (Liu et al., 2017; Huo et al., 2020; Hu et al., 2021), we further studied whether venlafaxine affects Nur77 expression through MAPKs signaling. MV3 cells expressed relatively low levels of phosphorylated MEK (p-MEK), p-JNK1/2, p-c-Jun, and p-ERK. After treatment with venlafaxine, the levels of p-MEK, p-JNK1/2, p-c-Jun, and p-ERK

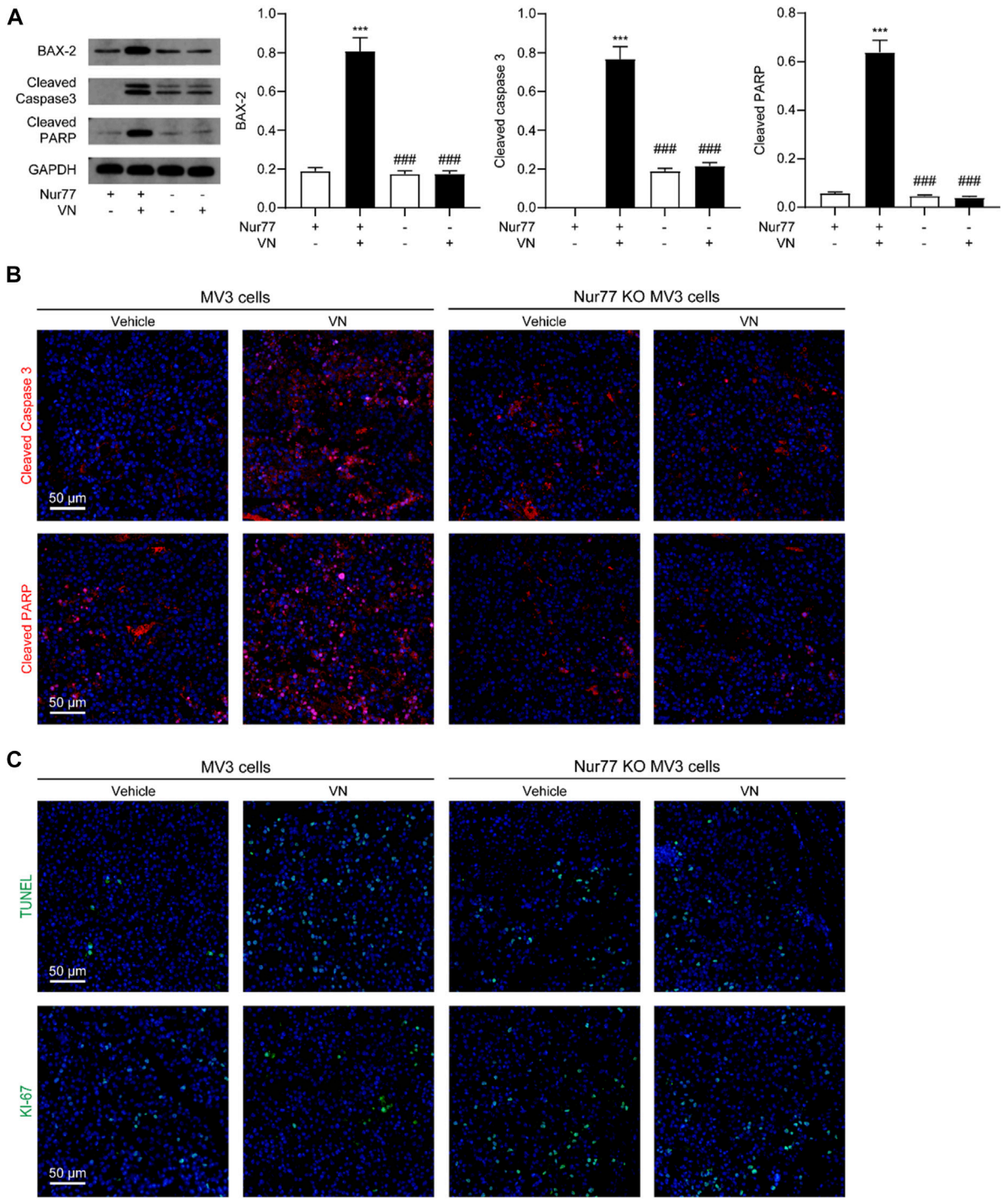

FIGURE 7
Venlafaxine-induced apoptosis *in vivo*. BALB/c nude mice bearing WT MV3 or Nur77 KO MV3 xenograft tumors were treated with venlafaxine (20 mg/kg, i.p.) or its vehicle once daily from week 1 to week 5 after implantation of MV3 or Nur77 KO MV3 cells. **(A)** Representative western-blot bands and quantification of BAX-2, cleaved caspase 3 and cleaved PARP abundances in tumor tissues. N = 5, *, $p < .05$, **, $< .01$, ***, $p < .001$ vs. MV3 vehicle control. $^{###}$, $p < .001$ vs. MV3 venlafaxine control. **(B)** Tumor tissues were immunostained with cleaved caspase 3 and cleaved PARP antibodies and visualized by confocal microscopy. **(C)** Tumor tissues were immunostained with TUNEL assay kits and antibodies and Ki-67 visualized by confocal microscopy. One of five similar experiments is shown.

were increased in MV3 cells (Figure 5A). To further study the roles of MAPK signaling in venlafaxine-induced apoptosis, MV3 cells were co-treated with venlafaxine and different inhibitors of MAPK kinases, including MEK/ERK signaling inhibitor PD98059 and JNK1/2 inhibitor SP600125. CCK8 assay showed that inhibition of JNK1/2 activity by SP600125 impaired venlafaxine-induced cell death effects, while PD98059 had no such effects (Figure 5B). Moreover, knockdown of JNK1/2 but not ERK increased cell viability in venlafaxine-treated

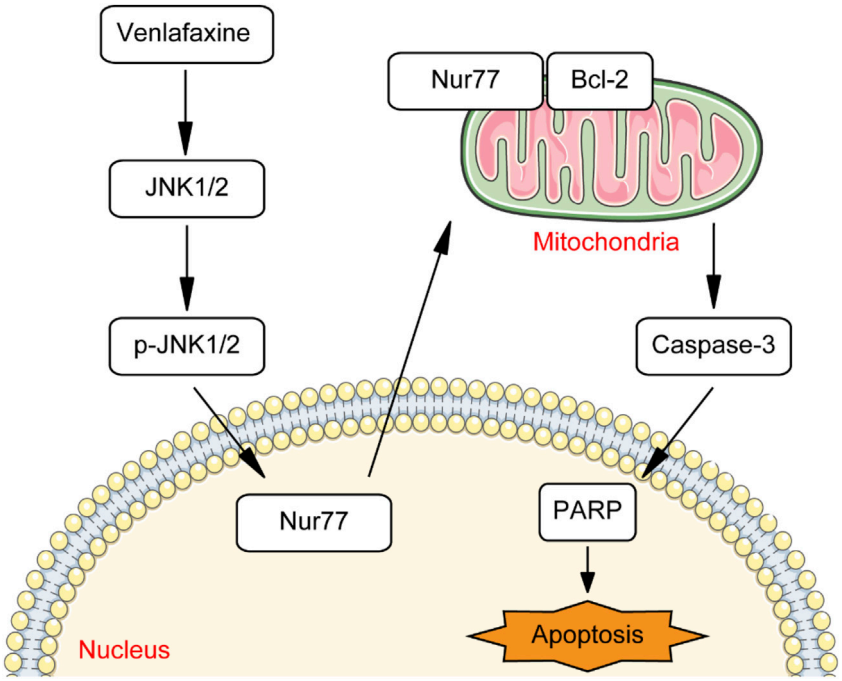

FIGURE 8
Schematic summary of venlafaxine mediated signaling pathway.

MV3 cells (Figure 5C). These data demonstrated that JNK1/2 signaling is involved in venlafaxine-induced cell death effects. Next, we examined whether venlafaxine affects Nur77 expression in MV3 cells through JNK1/2 signaling. As shown in Figures 5D, E, both genetic inactivation and pharmacological administration of JNK1/2 inhibitor SP600125 significantly suppressed venlafaxine-induced Nur77 expression, indicating that venlafaxine increases Nur77 expression in MV3 cells through activation of JNK1/2 signaling. Furthermore, blockade of JNK1/2 signaling also suppressed mitochondrial translocation of Nur77 (Figure 5F). Taken together, these data suggested that venlafaxine induced MV3 cells death through activation of JNK1/2 signaling and induction of Nur77 expression.

3.6 Anti-cancer efficacy of venlafaxine in mice

Encouraged by the *in vitro* activity of venlafaxine, we further investigated whether the induction of Nur77 by venlafaxine contribute to its growth inhibitory effect *in vivo*. BALB/c nude mice were inoculated subcutaneously with MV3 cells, and were treated with venlafaxine (20 mg/kg, i.p., once daily for 15 days) when the average tumor size grew up to 50–100 mm^3. Consistent with the *in vitro* results, treatment with venlafaxine for 15 days promoted expressions of Nur77 and activation of JNK1/2 in tumor tissues (Figure 6A). Furthermore, at the 15 days after implantation, the average tumor volume of the vehicle control group was 1,732 mm^3; and that of venlafaxine treatment group was 630 mm^3, with the inhibition ratio of tumor growth was 64% (Figure 6B). These results demonstrated that venlafaxine induced Nur77 expression and inhibit the growth of MV3 xenograft tumor *in vivo*.

To study whether venlafaxine inhibit the growth of MV3 xenograft tumor associated with its induction of apoptosis. We examined the expression of BAX-2, cleaved caspase 3 and cleaved PARP in tumor tissues. Western-blot assay and immunostaining showed that venlafaxine treatment significantly increased the level of these protein (Figures 7A, B). Additionally, immunostaining assay demonstrated that venlafaxine enhanced apoptotic cell death, as assessed by TUNEL staining, and suppressed cell proliferation, as assessed by Ki-67 immunostaining, in tumor tissues (Figure 7C). When combined, these results suggested that venlafaxine potently inhibited the growth of melanoma cells in animals through its apoptotic cell death effects.

Furthermore, we also studied the role of Nur77 in the anti-cancer effects of venlafaxine *in vivo*. We used the CRISPR/Cas9 technology to generate Nur77 knockout (KO) MV3 cells, and subcutaneously injected Nur77 KO MV3 melanoma cells into the BALB/c nude mice. At the 15 days after implantation, we found that the average tumor volume of the Nur77 KO MV3 group was similar to that of MV3 group, indicating Nur77 is not required for the growth of MV3 xenograft tumor. Furthermore, treatment with venlafaxine could not inhibit the growth of Nur77 KO MV3 xenograft tumor (Figures 6B, C), as well as the expression of BAX-2, cleaved caspase 3 and cleaved PARP in tumor tissues (Figures 7A, B). Moreover, treatment with venlafaxine had no effects on the numbers of TUNEL-positive and Ki-67-positive cells (Figure 7C). Taken together, these results suggested that venlafaxine suppresses the growth of melanoma cells through Nur77-dependent apoptotic pathway.

4 Discussion

Melanoma is one of the most aggressive and dangerous form of skin cancer (Ahmed et al., 2020). Although immunotherapies and targeted therapies are highly effective in ameliorating melanoma, their clinical use is hindered by the drug resistance (Ahmed et al., 2020). Therefore, novel approaches to melanoma treatment are still highly desired to

reduce the mortality rate of patient with melanoma. One way to rapidly develop therapeutic agents for melanoma is drug repurposing, defined as the re-application of known drugs to target new indication. Some of the classic examples of successful repurposing are minoxidil and gabapentin. Minoxidil, originally an anti-hypertensive agent, is now commonly used to promote hair re-growth (Goren and Naccarato, 2018). Gabapentin, originally used as anti-epileptics, is now used to treat neuropathic pain (Moore and Gaines, 2019). Therefore, we switch our attention from newly synthesized anti-cancer compound to approved drugs to rapidly develop therapeutic agents for melanoma. As a proof of concept, we demonstrated that anti-depressant drug venlafaxine could inhibit the growth of MV3 melanoma cells through introduction of Nur77 expression. Mechanistically, venlafaxine activates JNK1/2 signaling pathway, thus trigger expression and mitochondrial localization of Nur77. Follow mitochondrial translocation, Nur77 binds to Bcl-2 and converts Bcl-2 from a survival to a killer of cancer cells, thereby inhibiting the growth and induce apoptosis of MV3 melanoma cells (Figure 8).

A significant finding presented here is that venlafaxine can induce apoptosis of MV3 human melanoma cells through a Nur77-dependent pathway. Nur77 is an orphan nuclear receptor. It often translocate to mitochondria and binds to Bcl-2 in response to different death signals, leading to a conformation change in Bcl-2 and conversion of Bcl-2 from performing an anti-apoptotic role to a pro-apoptotic role (Lin et al., 2004; Kolluri et al., 2008). Many anti-cancer drugs, including vinblastine, vincristine, taxol, and cisplatin also induce expression of Nur77 (Deacon et al., 2003; Achkar et al., 2018). Herein, we found that venlafaxine treatment could increase Nurr77 expression and interaction with Bcl-2 (Figures 1D, 3A), resulting in ROS production (Figure 3B), and apoptosis (Figure 2A). Interestingly, the mRNA expression of Nur77 after 4 h incubation is non-significant, although there is significant protein expression at the same time point (Figures 1C, D). The reason for the discrepancies between mRNA expressions and protein expression is not clear. There may be serval reasons attributed to these results. It has been reported that Nur77 can bind to Bcl-2 after phosphorylation by JNK1/2. It is possible that the certain posttranslational modifications of Nur77 may increase the binding affinity of Bur77 to its antibody, thus a significant band of Nur77 was also observed at 4 h. Furthermore, we cannot exclude the possibility that the degradation of Nur77 was reduced in MV3 cells after 4 h incubation with venlafaxine. Future studies need to be carried out to confirm the precise reason for this result. Furthermore, the Nur77 subgroup of nuclear hormone receptors subfamily has been implicated in the pathophysiology of the central nervous system, including manic depression, Parkinson's disease, schizophrenia, and Alzheimer's disease (Liu et al., 2021). Venlafaxine also exhibits pharmacological actions in these diseases (Mazeh et al., 2004; Mokhber et al., 2014; El-Saiy et al., 2022; Zhuo et al., 2022). It is possible that venlafaxine produces therapeutic effects in these diseases through introduction of Nur77 expression.

A number of studies suggested that MAPKs, including JNK1/2 and ERK and their related upstream or downstream signal molecules such as MEK can regulate Nur77 expression (Anjum et al., 2022). Our results showed that venlafaxine could activated the JNK/c-Jun and the MERK/ERK pathway. Both pathways are documented in the literature. For example, c-Jun is a transcription factor that positively modulated Nur77 mitochondrial localization and activation by directly binding to the Nur77 DNA promoter regions (Han et al., 2006; Ming et al., 2018). The transcriptional activity of c-Jun is associated with its abundance and posttranslational modification (Han et al., 2006; Ming et al., 2018). Ha et. al. (2018) have reported that inhibition of c-Jun phosphorylation by miR-6321/Map3k1 reduced Nur77 protein expression, while activation of the JNK/c-Jun pathway by anisomycin increased Nur77 levels (Han et al., 2006). In addition, the MERK/ERK pathway plays a critical role in inducing Nur77 expression. GnRH promoted Nur77 expression in alpha T3-1 cells through ERK signaling (Bliss et al., 2012; Oliveira et al., 2021; Liu Y. X et al., 2022). Scalarane sesterterpenoid 12-deacetyl-12-epi-scalaradial induces HeLa cells apoptosis through ERK-mediated expression and phosphorylation of Nur77 (Zhou et al., 2020). Furthermore, malayoside, a cardenolide glycoside extracted from Antiaris toxicaria Lesch, also induced Nur77 expression, phosphorylation, and human non-small lung cancer cells apoptosis through ERK signaling (Hu et al., 2021). Our results showed that venlafaxine-induced Nur77 expression and cell apoptosis can be blocked by treatment with JNK1/2 inhibitor SP600125, but not MERK/ERK inhibitor PD98059, suggesting that venlafaxine may induced MV3 cell apoptosis through the JNK/c-Jun signaling.

5 Conclusion

In conclusion, our results demonstrate that venlafaxine could reduce the growth and induce apoptosis of MV3 cells through the JNK1/2-Nur77 signaling pathway. Our results also identified venlafaxine as a promising therapy for melanoma.

Data availability statement

The raw data supporting the conclusion of this article will be made available by the authors, without undue reservation.

Ethics statement

The animal study was reviewed and approved by the Animal Care and Use Committee of Hainan Medical University.

Author contributions

TN conducted most of the experiments and helped with manuscript preparation. ZW, JF, and YW conduced cell culture, western blot and analyzed data. SC and RW conduced Flow analysis. RZ and TN designed the experiments, and wrote the manuscript.

Funding

This work was supported by National Natural Science Fund Cultivating 530 Project of Hainan General Hospital (No. 2021QNXM05 to TN).

Conflict of interest

The authors declare that the research was conducted in the absence of any commercial or financial relationships that could be construed as a potential conflict of interest.

Publisher's note

References

Achkar, I. W., Abdulrahman, N., Al-Sulaiti, H., Joseph, J. M., Uddin, S., and Mraiche, F. (2018). Cisplatin based therapy: The role of the mitogen activated protein kinase signaling pathway. *J. Transl. Med.* 16, 96. doi:10.1186/s12967-018-1471-1

Ahmed, B., Qadir, M. I., and Ghafoor, S. (2020). Malignant melanoma: Skin cancer-diagnosis, prevention, and treatment. *Crit. Rev. Eukaryot. Gene Expr.* 30, 291–297. doi:10.1615/CritRevEukaryotGeneExpr.2020028454

Anjum, J., Mitra, S., Das, R., Alam, R., Mojumder, A., Bin Emran, T., et al. (2022). A renewed concept on the MAPK signaling pathway in cancers: Polyphenols as a choice of therapeutics. *Pharmacol. Res.* 184, 106398. doi:10.1016/j.phrs.2022.106398

Bennett, A. N., Huang, R. X., He, Q., Lee, N. P., Sung, W. K., and Chan, K. H. K. (2022). Drug repositioning for esophageal squamous cell carcinoma. *Front. Genet.* 13, 991842. doi:10.3389/fgene.2022.991842

Bliss, S. P., Navratil, A. M., Xie, J., Miller, A., Baccarini, M., and Roberson, M. S. (2012). ERK signaling, but not c-Raf, is required for gonadotropin-releasing hormone (GnRH)-induced regulation of Nur77 in pituitary gonadotropes. *Endocrinology* 153, 700–711. doi:10.1210/en.2011-0247

Bourhis, E., Maheux, J., Rouillard, C., and Levesque, D. (2008). Extracellular signal-regulated kinases (ERK) and protein kinase C (PKC) activities are involved in the modulation of Nur77 and Nor-1 expression by dopaminergic drugs. *J. Neurochem.* 106, 875–888. doi:10.1111/j.1471-4159.2008.05455.x

Chen, L., Chen, H., Li, Y., Li, L., Qiu, Y., and Ren, J. (2015). Endocannabinoid and ceramide levels are altered in patients with colorectal cancer. *Oncol. Rep.* 34, 447–454. doi:10.3892/or.2015.3973

Chen, X., Cao, X., Tu, X., Alitongbieke, G., Xia, Z., Li, X., et al. (2019). BI1071, a novel Nur77 modulator, induces apoptosis of cancer cells by activating the nur77-bcl-2 apoptotic pathway. *Mol. cancer Ther.* 18, 886–899. doi:10.1158/1535-7163.MCT-18-0918

Chiavarini, M., Naldini, G., Giacchetta, I., and Fabiani, R. (2022). Postmenopausal exogenous hormone therapy and melanoma risk in women: A systematic review and time-response meta-analysis. *Pharmacol. Res.* 176, 106054. the official journal of the Italian Pharmacological Society. doi:10.1016/j.phrs.2021.106054

Crean, D., and Murphy, E. P. (2021). Targeting NR4A nuclear receptors to control stromal cell inflammation, metabolism, angiogenesis, and tumorigenesis. *Front. Cell Dev. Biol.* 9, 589770. doi:10.3389/fcell.2021.589770

Cullen, J. K., Simmons, J. L., Parsons, P. G., and Boyle, G. M. (2020). Topical treatments for skin cancer. *Adv. Drug Deliv. Rev.* 153, 54–64. doi:10.1016/j.addr.2019.11.002

Deacon, K., Mistry, P., Chernoff, J., Blank, J. L., and Patel, R. (2003). p38 Mitogen-activated protein kinase mediates cell death and p21-activated kinase mediates cell survival during chemotherapeutic drug-induced mitotic arrest. *Mol. Biol. Cell* 14, 2071–2087. doi:10.1091/mbc.e02-10-0653

El-Saiy, K. A., Sayed, R. H., El-Sahar, A. E., and Kandil, E. A. (2022). Modulation of histone deacetylase, the ubiquitin proteasome system, and autophagy underlies the neuroprotective effects of venlafaxine in a rotenone-induced Parkinson's disease model in rats. *Chem. Biol. Interact.* 354, 109841. doi:10.1016/j.cbi.2022.109841

Goren, A., and Naccarato, T. (2018). Minoxidil in the treatment of androgenetic alopecia. *Dermatol Ther.* 31, e12686. doi:10.1111/dth.12686

Grygier, B., Arteta, B., Kubera, M., Basta-Kaim, A., Budziszewska, B., Leskiewicz, M., et al. (2013). Inhibitory effect of antidepressants on B16F10 melanoma tumor growth. *Pharmacol. Rep.* 65, 672–681. doi:10.1016/s1734-1140(13)71045-4

Guo, W., Wang, H., and Li, C. (2021). Signal pathways of melanoma and targeted therapy. *Signal Transduct. Target Ther.* 6, 424. doi:10.1038/s41392-021-00827-6

Ha, M., Zhang, P., Li, L., and Liu, C. (2018). Triclosan suppresses testicular steroidogenesis via the miR-6321/JNK/Nur77 cascade. *Cell Physiol. Biochem.* 50, 2029–2045. doi:10.1159/000495049

Han, Y. H., Cao, X., Lin, B., Lin, F., Kolluri, S. K., Stebbins, J., et al. (2006). Regulation of Nur77 nuclear export by c-Jun N-terminal kinase and Akt. *Oncogene* 25, 2974–2986. doi:10.1038/sj.onc.1209358

Hsu, H. C., Zhou, T., and Mountz, J. D. (2004). Nur77 family of nuclear hormone receptors. *Curr. Drug Targets Inflamm. Allergy* 3, 413–423. doi:10.2174/1568010042634523

Hu, M., Luo, Q., Alitongbieke, G., Chong, S., Xu, C., Xie, L., et al. (2017). Celastrol-induced Nur77 interaction with TRAF2 alleviates inflammation by promoting mitochondrial ubiquitination and autophagy. *Mol. Cell* 66, 141–153. doi:10.1016/j.molcel.2017.03.008

Hu, Q. Y., Zhang, X. K., Wang, J. N., Chen, H. X., He, L. P., Tang, J. S., et al. (2021). Malayoside, a cardenolide glycoside extracted from Antiaris toxicaria Lesch, induces apoptosis in human non-small lung cancer cells via MAPK-Nur77 signaling pathway. *Biochem. Pharmacol.* 190, 114622. doi:10.1016/j.bcp.2021.114622

Huo, J., Xu, S., and Lam, K. P. (2020). ASK1 mediates Nur77 expression in T-cell receptor mediated thymocyte apoptosis. *Cells* 9, 585. doi:10.3390/cells9030585

Kolluri, S. K., Zhu, X., Zhou, X., Lin, B., Chen, Y., Sun, K., et al. (2008). A short Nur77-derived peptide converts Bcl-2 from a protector to a killer. *Cancer Cell* 14, 285–298. doi:10.1016/j.ccr.2008.09.002

Kubera, M., Grygier, B., Arteta, B., Urbanska, K., Basta-Kaim, A., Budziszewska, B., et al. (2009). Age-dependent stimulatory effect of desipramine and fluoxetine pretreatment on metastasis formation by B16F10 melanoma in male C57BL/6 mice. *Pharmacol. Rep.* 61, 1113–1126. doi:10.1016/s1734-1140(09)70174-4

Li, H., Li, X., Yang, B., Su, J., Cai, S., Huang, J., et al. (2021). The retinoid X receptor alpha modulator K-80003 suppresses inflammatory and catabolic responses in a rat model of osteoarthritis. *Sci. Rep.* 11, 16956. doi:10.1038/s41598-021-96517-y

Li, X. X., Wang, Z. J., Zheng, Y., Guan, Y. F., Yang, P. B., Chen, X., et al. (2018). Nuclear receptor Nur77 facilitates melanoma cell survival under metabolic stress by protecting fatty acid oxidation. *Mol. Cell* 69, 480–492. doi:10.1016/j.molcel.2018.01.001

Li, Y., Li, Y., Xu, S., Chen, Y., Zhou, P., Hu, T., et al. (2022). Corrigendum to "N-acylethanolamine acid amidase (NAAA) exacerbates psoriasis inflammation by enhancing dendritic cell (DCs) maturation" [Pharm. Res. 185 (2022) 1-16/YPHRS_106491]. *Pharmacol. Res.* 185, 106527. doi:10.1016/j.phrs.2022.106527

Li, Y., Zhou, P., Hu, T., Ren, J., Xu, Y., Qiu, Y., et al. (2021). NAAA inhibitor F96 attenuates BBB disruption and secondary injury after traumatic brain injury (TBI). *Eur. J. Pharmacol.* 912, 174561. doi:10.1016/j.ejphar.2021.174561

Lin, B., Kolluri, S. K., Lin, F., Liu, W., Han, Y. H., Cao, X., et al. (2004). Conversion of Bcl-2 from protector to killer by interaction with nuclear orphan receptor Nur77/TR3. *Cell* 116, 527–540. doi:10.1016/s0092-8674(04)00162-x

Liu, J., Wang, G. H., Duan, Y. H., Dai, Y., Bao, Y., Hu, M., et al. (2017). Modulation of the Nur77-Bcl-2 apoptotic pathway by p38α MAPK. *Oncotarget* 8, 69731–69745. doi:10.18632/oncotarget.19227

Liu, J., Zheng, X., Li, W., Ren, L., Li, S., Yang, Y., et al. (2022). Anti-tumor effects of Skp2 inhibitor AAA-237 on NSCLC by arresting cell cycle at G0/G1 phase and inducing senescence. *Pharmacol. Res.* 181, 106259. the official journal of the Italian Pharmacological Society. doi:10.1016/j.phrs.2022.106259

Liu, L., Ma, D., Zhuo, L., Pang, X., You, J., and Feng, J. (2021). Progress and promise of nur77-based therapeutics for central nervous system disorders. *Curr. Neuropharmacol.* 19, 486–497. doi:10.2174/1570159X18666200606231723

Liu, Y. X., Xu, B. W., Niu, X. D., Chen, Y. J., Fu, X. Q., Wang, X. Q., et al. (2022). Inhibition of Src/STAT3 signaling-mediated angiogenesis is involved in the anti-melanoma effects of dioscin. *Pharmacol. Res.* 175, 105983. doi:10.1016/j.phrs.2021.105983

Madrigal-Bujaidar, E., Gomez-Gonzalez, P., Camacho-Cantera, S., Morales-Gonzalez, J. A., Madrigal-Santillan, E., and Alvarez-Gonzalez, I. (2021). Genotoxic and cytotoxic evaluation of venlafaxine in an acute and a subchronic assay in mouse. *Braz J. Biol.* 84, e251289. doi:10.1590/1519-6984.251289

Mazeh, D., Shahal, B., Saraf, R., and Melamed, Y. (2004). Venlafaxine for the treatment of depressive episode during the course of schizophrenia. *J. Clin. Psychopharmacol.* 24, 653–655. doi:10.1097/01.jcp.0000144894.37611.0a

Ming, S., Shui-Yun, W., Wei, Q., Jian-Hui, L., Ru-Tai, H., Lei, S., et al. (2018). miR-139-5p inhibits isoproterenol-induced cardiac hypertrophy by targetting c-Jun. *Biosci. Rep.* 38, BSR20171430. doi:10.1042/BSR20171430

Mokhber, N., Abdollahian, E., Soltanifar, A., Samadi, R., Saghebi, A., Haghighi, M. B., et al. (2014). Comparison of sertraline, venlafaxine and desipramine effects on depression, cognition and the daily living activities in Alzheimer patients. *Pharmacopsychiatry* 47, 131–140. doi:10.1055/s-0034-1377041

Moore, J., and Gaines, C. (2019). Gabapentin for chronic neuropathic pain in adults. *Br. J. Community Nurs.* 24, 608–609. doi:10.12968/bjcn.2019.24.12.608

Oliveira, E. A., Chauhan, J., Silva, J. R. D., Carvalho, L., Dias, D., Carvalho, D. G., et al. (2021). TOP1 modulation during melanoma progression and in adaptative resistance to BRAF and MEK inhibitors. *Pharmacol. Res. official J. Italian Pharmacol. Soc.* 173, 105911. doi:10.1016/j.phrs.2021.105911

Pinkerton, J. V., and Santen, R. J. (2019). Managing vasomotor symptoms in women after cancer. *Climacteric* 22, 544–552. doi:10.1080/13697137.2019.1600501

Porcelli, L., Di Fonte, R., Pierri, C. L., Fucci, L., Saponaro, C., Armenio, A., et al. (2022). BRAF(V600E;K601Q) metastatic melanoma patient-derived organoids and docking analysis to predict the response to targeted therapy. *Pharmacol. Res.* 182, 106323. the official journal of the Italian Pharmacological Society. doi:10.1016/j.phrs.2022.106323

Qin, Y., Xie, J., Zheng, R., Li, Y., and Wang, H. (2022). Oleoylethanolamide as a new therapeutic strategy to alleviate doxorubicin-induced cardiotoxicity. *Front. Pharmacol.* 13, 863322. doi:10.3389/fphar.2022.863322

Roseboom, P. H., and Kalin, N. H. (2000). Neuropharmacology of venlafaxine. *Depress Anxiety* 12 (1), 20–29. doi:10.1002/1520-6394(2000)12:1+<20::AID-DA3>3.0.CO;2-M

Safe, S., and Karki, K. (2021). The paradoxical roles of orphan nuclear receptor 4A (NR4A) in cancer. *Mol. Cancer Res.* 19, 180–191. doi:10.1158/1541-7786.MCR-20-0707

Siegel, R. L., Miller, K. D., Goding Sauer, A., Fedewa, S. A., Butterly, L. F., Anderson, J. C., et al. (2020). Colorectal cancer statistics, 2020. *CA Cancer J. Clin.* 70, 145–164. doi:10.3322/caac.21601

To, S. K., Zeng, J. Z., and Wong, A. S. (2012). Nur77: A potential therapeutic target in cancer. *Expert Opin. Ther. Targets* 16, 573–585. doi:10.1517/14728222.2012.680958

van den Beuken-van Everdingen, M. H., de Graeff, A., Jongen, J. L., Dijkstra, D., Mostovaya, I., Vissers, K. C., et al. (2017). Pharmacological treatment of pain in cancer patients: The role of adjuvant analgesics, a systematic review. *Pain Pract. official J. World Inst. Pain* 17, 409–419. doi:10.1111/papr.12459

Wang, T., Zheng, R., and Sun, S. (2022). Drug Repurposing: Escitalopram attenuates acute lung injury by inhibiting the SIK2/HDAC4/NF-κB signaling cascade. *Biochem. Biophys. Res. Commun.* 599, 1–8. doi:10.1016/j.bbrc.2022.02.015

Wu, L., and Chen, L. (2018). Characteristics of Nur77 and its ligands as potential anticancer compounds (Review). *Mol. Med. Rep.* 18, 4793–4801. doi:10.3892/mmr.2018.9515

Xie, X., Li, Y., Xu, S., Zhou, P., Yang, L., Xu, Y., et al. (2022). Genetic blockade of NAAA cell-specifically regulates fatty acid ethanolamides (FAEs) metabolism and inflammatory responses. *Front. Pharmacol.* 12, 817603. doi:10.3389/fphar.2021.817603

Xie, X., Wu, X., Zhao, D., Liu, Y., Du, Q., Li, Y., et al. (2022). Fluvoxamine alleviates bleomycin-induced lung fibrosis via regulating the cGAS-STING pathway. *Pharmacol. Res.* 187, 106577. the official journal of the Italian Pharmacological Society. doi:10.1016/j.phrs.2022.106577

Zhang, X. K. (2007). Targeting Nur77 translocation. *Expert Opin. Ther. Targets* 11, 69–79. doi:10.1517/14728222.11.1.69

Zhang, Y., Bi, X., Adebiyi, O., Wang, J., Mooshekhian, A., Cohen, J., et al. (2019). Venlafaxine improves the cognitive impairment and depression-like behaviors in a cuprizone mouse model by alleviating demyelination and neuroinflammation in the brain. *Front. Pharmacol.* 10, 332. doi:10.3389/fphar.2019.00332

Zhou, M., Peng, B. R., Tian, W., Su, J. H., Wang, G., Lin, T., et al. (2020). 12-Deacetyl-12-epi-Scalaradial, a scalarane sesterterpenoid from a marine sponge hippospongia sp., induces HeLa cells apoptosis via MAPK/ERK pathway and modulates nuclear receptor Nur77. *Mar. Drugs* 18, 375. doi:10.3390/md18070375

Zhou, Y., Zhao, W., Xie, G., Huang, M., Hu, M., Jiang, X., et al. (2014). Induction of Nur77-dependent apoptotic pathway by a coumarin derivative through activation of JNK and p38 MAPK. *Carcinogenesis* 35, 2660–2669. doi:10.1093/carcin/bgu186

Zhuo, C., Zhou, C., Cai, Z., Chen, J., Yang, L., Li, Q., et al. (2022). Electrical stimulus combined with venlafaxine and mirtazapine improves brain Ca(2+) activity, pre-pulse inhibition, and immobility time in a model of major depressive disorder in schizophrenia. *J. Affect Disord.* 319, 610–617. doi:10.1016/j.jad.2022.09.037

frontiers | Frontiers in Pharmacology

TYPE Review
PUBLISHED 04 January 2023
DOI 10.3389/fphar.2022.1048484

OPEN ACCESS

EDITED BY
Eswar Shankar,
The Ohio State University, United States

REVIEWED BY
Prem P. Kushwaha,
Case Western Reserve University, United States
Balaji Chandrasekaran,
Texas A&M University, United States
Annapurna Gupta,
Comprehensive Cancer Center, United States

*CORRESPONDENCE
Hairong Zhang,
sdzhhr7211@163.com
Huirong Li,
tiger.student@163.com

†These authors have contributed equally to this work and share first authorship

SPECIALTY SECTION
This article was submitted to Pharmacology of Anti-Cancer Drugs, a section of the journal Frontiers in Pharmacology

RECEIVED 19 September 2022
ACCEPTED 14 December 2022
PUBLISHED 04 January 2023

CITATION
Xia L, Ding S, Wang X, Zhang X, Zhu L, Zhang H and Li H (2023), Advances in ovarian cancer treatment using a combination of statins with other drugs. *Front. Pharmacol.* 13:1048484. doi: 10.3389/fphar.2022.1048484

Advances in ovarian cancer treatment using a combination of statins with other drugs

Lei Xia[1†], Shichao Ding[2†], Xuezhen Wang[3], Xiaoyu Zhang[3], Lin Zhu[3], Hairong Zhang[4*] and Huirong Li[4*]

[1]Department of Pathology, Shandong University of Traditional Chinese Medicine, Jinan, China, [2]Department of Internal Medicine, The Third Affiliated Hospital of Shandong First Medical University, Jinan, China, [3]School of Chinese Medicine, Shandong University of Traditional Chinese Medicine, Jinan, China, [4]Department of Obstetrics and Gynecology, Shandong Provincial Third Hospital, Jinan, China

New anti-cancer drugs are constantly being developed, especially targeted drugs. Although these drugs have achieved significant clinical efficacy, they do not play a significant role in ovarian cancer. Moreover, the research cycle and costs of such drugs are often huge. The repositioning of conventional drugs has gradually become a concern. Statins, as traditional lipid-lowering drugs, play a role mainly by inhibiting HMGCR. In recent years, epidemiological studies and *in vitro* experiments have confirmed its anti-cancer effect, especially the effect of anti-ovarian cancer. The mutation rate of TP53 in ovarian cancer is as high as 95%, while HMGCR is often highly expressed in TP53 mutant tumors. However, the effect of prospective clinical trials is not ideal. This result seems understandable considering that it seems unrealistic for a lipid-lowering drug to completely inhibit tumor growth. Therefore, statins play more synergistic roles in the treatment of ovarian cancer. Because ovarian cancer is a highly heterogeneous tumor, it may be a good choice to deeply understand the mechanism of statins in the treatment of ovarian cancer and achieve precise treatment by combining it with other drugs.

KEYWORDS

statins, ovarian cancer, synergistic effect, HMGCoA reductase, progress

1 Introduction

Ovarian cancer is a common malignant tumor reported in women and is also one of the gynecological tumors with the highest mortality rate. There are 239,000 new cases of ovarian cancer and 152,000 deaths of ovarian cancer every year in the world (GBD 2019 Stroke Collaborators, 2021). The incidence rate of Ovarian cancer in 2035 is

Abbreviations: HMG-CoA, 3-hydroxy-3-methyglutaryl-coenzyme A; HMGCR, HMG-CoA reductase; MVA, mevalonic acid; PARP, poly ADP-ribose polymerase; FPP, farnesyl pyrophosphate; GGPP, geranylgeranyl pyrophosphate; GGT, geranylgeranyltransferase; ABCB1, ATP-binding cassette subfamily B member 1; MVD, mevalonate (diphospho) decarboxylase; VDCA1, voltage-dependent anion-selective channel protein 1; FDPS, Farnesyl diphosphate synthase; IDI, isopentenyl-diphosphate delta Isomerase; SREBPs, sterol regulatory element-binding proteins.

estimated to be 371,000 (an increase of 55%), and the number of deaths is estimated to be 254,000 (an increase of 67%). Most ovarian cancers are diagnosed at stage III and IV (Torre et al., 2018), when 5-year survival is less than 30% (Torre et al., 2018; Peres et al., 2019). Although routine treatment has demonstrated therapeutic outcomes, 70% of patients with ovarian cancer relapse and develop chemoresistance, and have a shorter survival time. New targeted drugs have been widely used in the treatment of tumors, but the effect is not ideal in the treatment of ovarian cancer, especially relapsed and drug-resistant ovarian cancer. It is therefore critical to identify novel drugs for patients who are dissatisfied with the clinical treatment effects. Due to the long development cycle and the high cost of new drugs, the repositioning of traditional drugs has gradually attracted people's attention. Drug repositioning refers to the method of determining new target molecules and disease indications for approved drugs (National Academy of Sciences, 1975). When compared with traditional new drug research and development, it has a lower cost and shorter cycle.

Statins—hyperlipidemia drugs (Schachter, 2005)—have recently been discovered to have anti-cancer properties manifested through the inhibition of the cell cycle, anti-tumor proliferation (Kobayashi et al., 2015), induction of apoptosis and autophagy (Kobayashi et al., 2015; Hutchinson and Marignol, 2017), and increasing the chemotherapy sensitivity of tumors (Hutchinson and Marignol, 2017). Particularly, it plays an important role in anti-ovarian cancer. Some people believe that this is closely related to the characteristics of ovarian cancer and the target of statins. The main target of statins is HMGCR. The expression of HMGCR in TP53 mutant cells is generally increased, while the proportion of TP53 mutations in ovarian cancer cells is as high as 95%.

Several epidemiological studies and *in vitro* testing have also demonstrated that statins have anti-ovarian cancer effects (Liu et al., 2009; Xie et al., 2017; Li and ZHOU, 2018). For example, some studies (Xie et al., 2017; Urpilainen et al., 2018) have reported that the overall survival rate of patients taking statins is significantly higher than that of patients not taking statins. Even after the diagnosis of ovarian cancer, the overall survival rate of patients taking statins was significantly higher (Li and Zhou, 2018; Harding et al., 2019; Kim et al., 2022). However, some data showed the opposite results. For instance, some studies reported that statins can reduce the recurrence rate of ovarian cancer, but have no impact on the overall survival rate (Lavie et al., 2013; Bar et al., 2016; Chen et al., 2016). On the other hand, some studies believe that the use of statins can prevent the occurrence of ovarian cancer (Lavie et al., 2013; Zhang et al., 2019), while others believe that the use of statins cannot prevent the occurrence of ovarian cancer (Baandrup, 2015). Moreover, some studies found that the use of statins did not have a different effect on different ovarian cancer subtypes (Couttenier et al., 2017), but other studies showed that statins have a more obvious therapeutic effect on non-serous papillary epithelial cell ovarian cancer subtypes. It has been suggested that it may be related to the type of statin, lipophile and hydrophilic statins may have different effects on ovarian cancer (Jiao et al., 2020), and lipophile statins are more effective in reducing tumor progression because they have less liver selectivity than hydrophilic statins (Kato et al., 2010; Majidi et al., 2021).

In addition, the prospective clinical trials using statins to treat ovarian cancer have mostly been unsatisfactory (Altwairgi, 2015). The reason may be related to the type of ovarian cancer and the dosage of statins. On one hand, ovarian cancer exhibits high heterogeneity, the histological classification of ovarian cancer is complex with over 100 types having been identified (Granström et al., 2008). Ovarian cancer treatment pathways are targeted at the type and depend on histopathological diagnosis. Ovarian cancer can be divided into epithelial, sex cord-stromal, and germ-cell tumor types. Among these, epithelial ovarian cancer is the most common one and can be further categorized into serous, mucinous, endometrioid, and clear cell cancers according to their cell types. In addition, ovarian cancer can be low-grade or high-grade, based on the degree of malignancy. The biological characteristics of the two types of tumors are extremely different as are their genetic backgrounds. The common mutations in HGSOC were TP53 (96%), BRCA1/2 (23%) and HRD (homologous recombination defect) mutation (50%); The common mutations in clear cell carcinoma are PIK3CA, ARD1A, PTEN and microsatellite instability (MSI); Common mutations in endometrioid carcinoma are CTNNB1, ARID1A, PTEN, MSI; The common mutations in mucinous carcinoma are KRAS, HER2 and CDKN2A mutations; In LGSOC, mutations such as BRAF, KRAS, NRAS, ERBB2 and PIK3CA are more common (Schachter, 2005).

The anti-tumor effect of statins is not limited to HMGCR inhibition, but it has different anti-tumor effects against different tumors. On the other hand, in several studies, the drug dosage is often utilized for hypercholesterolemia treatment, which may have resulted in the plasma concentration of the drug being lower than that necessary for inducing cell apoptosis *in vitro* tests (Robinson et al., 2013). However, large-dose statins may cause myalgia and other adverse effects.

It is undeniable that, although some studies have shown that there is no difference in the survival time between the simple use of statins and the simple use of chemotherapy drugs, epidemiological investigations often combine statins on the basis of conventional treatment. Therefore, the anti-tumor effect of statins is mainly reflected by the combination with other therapies, or it mainly plays an auxiliary role. Therefore, it is important to better understand its anti-ovarian cancer mechanism and the synergistic role with other drugs, which has a significant role in improving the overall clinical efficacy and reducing adverse drug reactions.

This study examined research on the mechanism of statin treatment of ovarian cancer and how the therapeutic effects can

TABLE 1 Synergistic effect of statins with other drugs in the treatment of ovarian cancer.

	Drugs	Cell models	Potential	References
			The mechanism	
1	Zoledronic acid + fluvastatin	22 pre-treated ovarian carcinomas	Activates the tricarboxylic acid cycle, autophagy	Robinson et al. (2013)
2	Fluvastatin + cisplatin	CAOV3 SKOV3	Induction of apoptosis	Mctaggart (2006)
			Inhibition of GGT	
			Inhibition of Ras, Rho, Rab	
3	Lovastatin + doxorubicin	A2780ADR	Inhibiting P-glycoprotein.	De Wolf et al. (2017)
4	Oxysterols + statins	SKOV-3	Inhibition of SREBPs	Lipper et al. (2019)
		OVCAR-8		
5	Carboplatin + simvastatin	A2780, Ovcar-5, Ovcar-8 Igrov-1	Unclear	Liu et al. (2009)
6	Paclitaxel + simvastatin	A2780, Ovcar-5, Ovcar-8 Igrov-1	Unclear	Liu et al. (2009)
7	Paclitaxel + simvastatin	ES2	Inhibition of VDCA1 binding to tubulin	Abdullah et al. (2019), Kobayashi et al. (2022)
8	Panobinostat + simvastatin	ES2	Inhibition of HDAC	Kobayashi et al. (2022)
9	Prednisolone + pitavastatin	Ovsaho, Cov-318, Cov-362, Ovcar-3, Ovcar-4	Inhibition of MVA pathway;	Svensmark and Brakebusch (2019)
			HMGCR and FDPS were reduced	
10	ABT-737 + pitavastatin	Igrov-1	PARP cleavage	Jeon and Osborne (2012)
			Bcl-xL was reduced	
11	Pictilisib + pitavastatin	OVCAR3	Inhibiting NF-κB	Jeon and Osborne (2012)
			PTEN modulation	
12	Atorvastatin + JQ1	Hey, SKOV3	Inhibiting c-Myc	Jones et al. (2017)

be improved through drug combinations. This study aimed to obtain ideas for application in future fundamental research and clinical treatment (Table 1).

2 Treatment by inhibiting the mevalonic acid (MVA) pathway

Statins' anti-tumor effect mainly blocks the MVA pathway by inhibiting HMGCR. HMGCR is considered a metabolic oncogene that promotes tumor growth and development (Clendening et al., 2010). HMGCR is commonly seen in TP53-mutated tumor cells, and the TP53 mutation rate in ovarian cancer cells is as high as 95% (Freed-Pastor and Prives, 2016). De Wolf et al. investigated 12 ovarian tumor cell lines and found that HMGCR was upregulated in ovarian tumor cells when compared to that in normal ovarian surface epithelial cells (De Wolf et al., 2017). Combining HMGCR with other MVA pathway antagonists may achieve a sound synergistic anti-ovarian cancer effect (Figure 1).

2.1 Synergistic blocking of protein isoprenylation by statins and MVA pathway inhibitor

FPP, GGPP, and cholesterol are intermediate and end-products of the MVA pathway. FPP and GGPP, for example, can provide isopentenyl groups, thereby allowing isoprenylation of multiple small GTPase binding proteins and anchoring them to the cell membrane (e.g., Ras and Rho). Membrane localization is, therefore, necessary for these proteins to function, and several oncogenes interfering with the isoprenylation of these proteins can have an anti-tumor effect (Mctaggart, 2006; Svensmark and Brakebusch, 2019).

Ibandronate and zoledronic acid are FPP synthase inhibitors, which limit the production of FPP and GGPP and thus inhibit the isoprenylation of the relevant proteins (Kobayashi et al., 2015; Pletcher et al., 2017). These drugs can inhibit various tumors (Green, 2004), and the combination of statins with zoledronic acid has synergistic inhibitory effects on the growth of ovarian cancer cells (Abdullah et al., 2017).

TABLE 2 Summary of the evidence regarding impact of statin therapy on risk and survival of ovarian cancer.

Type of study	Size of population	Primary outcome variable	Conclusion	References
Retrospective cohort	8,629	Risk of ovarian cancer	Improved survival among use statin after diagnosis, especially in endometrioid cancer and those who use statin for long.	Feng et al. (2021)
Case control study	Cases, 4,103; matched controls, 58,706	Risk of epithelial ovarian cancer	Decreased risk seen in mucinous ovarian cancer. No association with epithelial subtype	Baandrup et al. (2015)
Retrospective cohort	442	Progression-free survival and disease-specific survival	Improved survival among statin users was not seen except in non-serous papillary epithelial ovarian cancer	Habis et al. (2014)
Case control study	Cases, 12; matched controls, 126	Risk of ovarian cancer and survival	Decreased risk along with improved survival was reported	Lavie et al. (2013)
Retrospective cohort	73,336	Risk of ovarian cancer	Non-significant decrease in ovarian cancer risk was found	Yu et al. (2009)
Retrospective cohort	126	Progression-free survival and overall survival	Improved survival was seen in statin users	Elmore et al. (2008)
Retrospective cohort	361,859	Risk of ovarian cancer	No association was found	Friedman et al. (2008)
Case control study	Cases, 91; controls, 7,393	Risk of ovarian cancer	Statins have no substantial effect on ovarian cancer risk	Abdullah et al. (2019)
Retrospective cohort	997	Risk of ovarian cancer	No difference in frequency of cancer between statin users/non-users was reported	Clearfield et al. (2001)
Retrospective cohort	421	Mortality rate of ovarian cancer	Pre-diagnostic use of statins was observed to be associated with decreased mortality	Urpilainen et al. (2018)

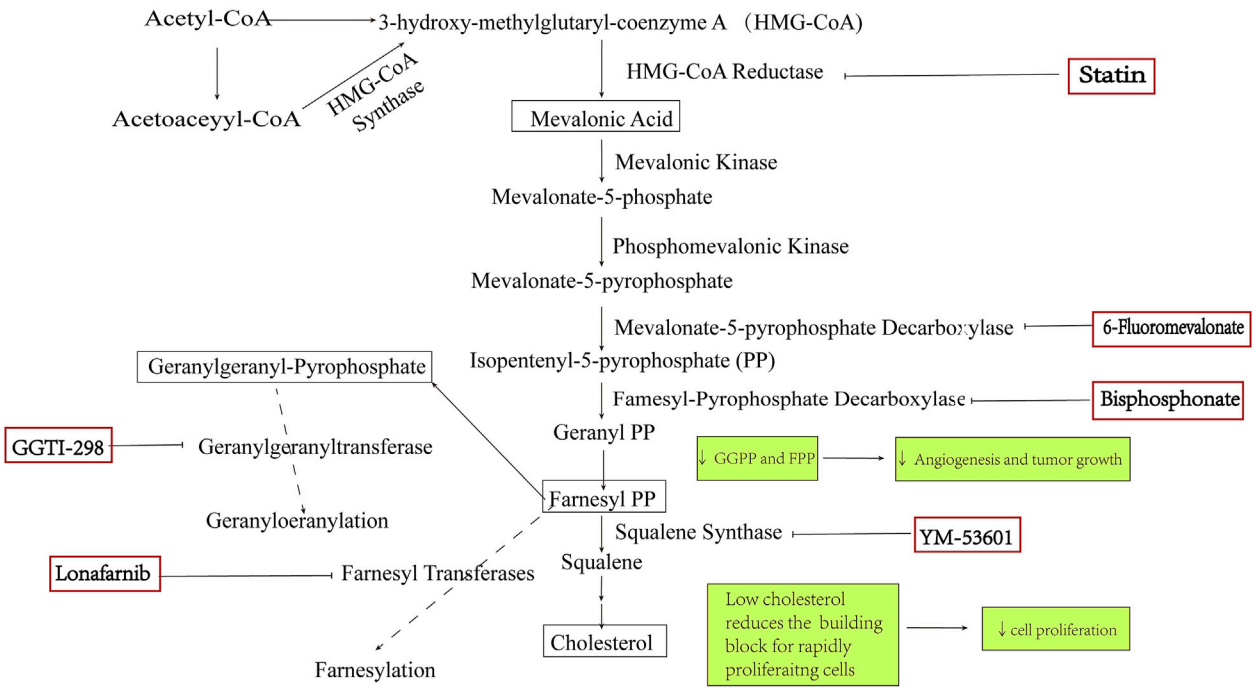

FIGURE 1
MVA pathway and the related inhibitors.

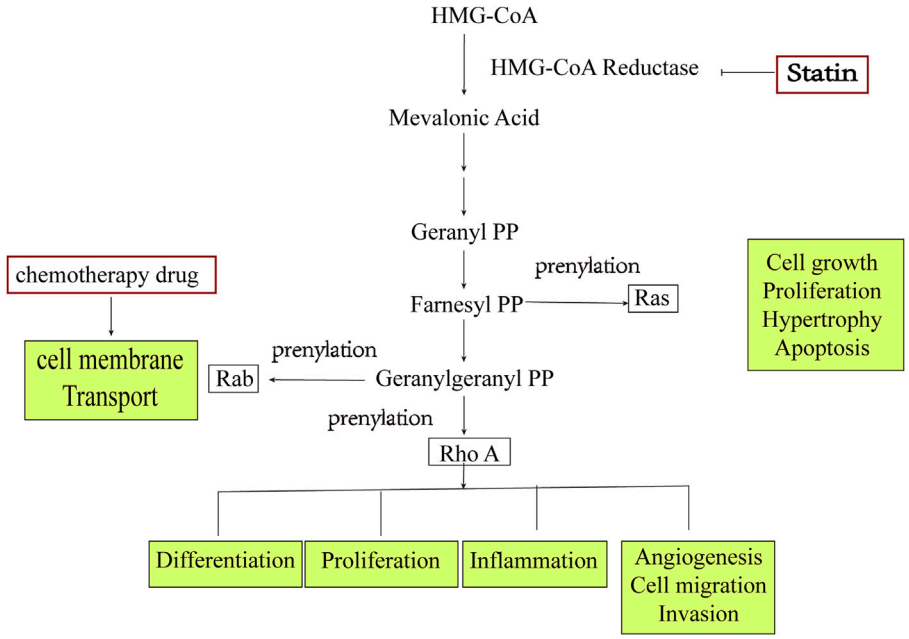

FIGURE 2
Effect of statins on small GTPase and its potential antitumor effects.

Other targets in the isoprenylation pathway have also been investigated to identify their effects on ovarian cancer. The cumulative results demonstrated that lonafarnib (farnesyl transferase inhibitor) and GGTI-298 (geranylgeranyl transferase inhibitor) can inhibit the proliferation of SKOV3 and OVCAR5 cells by inhibiting isoprenylation. By inhibiting the MVA pathway, 6-fluoromevalonate (mevalonate pyrophosphate decarboxylasyrophose inhibitor) and YM-53601 (squalene synthase inhibitor) could inhibit tumor cells. However, a higher dosage of 6-fluoromevalonate and YM-53601 is warranted (Kobayashi et al., 2017). By inhibiting the MVA pathway, drugs can induce cell autophagy. Nevertheless, whether these drugs and statins have a synergistic anti-ovarian cancer effect needs further verification (Figure 1).

2.2 Combination of statins and cisplatin blocks the small GTPase signaling pathway

Among the diverse isoprenylated proteins, the small GTPase superfamily, which comprises Ras, Rho, and Rab, has attracted significant attention. In addition, it has been demonstrated that lovastatin and simvastatin can inhibit the proliferation of ovarian cancer cells, induce apoptosis, and cause cell-cycle arrest (Kato et al., 2010; Martirosyan et al., 2010), which is closely related to the inhibition of Ras, Rho, and Rab (Taylor-Harding et al., 2010). Meanwhile, it was found that fluvastatin and cisplatin possess synergistic cytotoxicity (Taylor-Harding et al., 2010). Accordingly, a hypothesis was proposed that Rab1 protein regulated the cell membrane transport and cell growth and that the detection of unmodified Rab1 protein might lead to the synergistic effect of fluvastatin and cisplatin combination therapy. Robinson et al. (2013) reported that statins alone could reduce cell activity and proliferation and increase cell apoptosis and autophagy. A superposition effect was discovered when the experimental cells were exposed to statins and carboplatin or paclitaxel, although the specific mechanism was not explored in depth. Nevertheless, some scholars (Martirosyan et al., 2010) claim that the combination of lovastatin and cisplatin has synergistic effects only at high concentrations (Figure 2).

2.3 Combination of statins and prednisone promotes apoptosis of ovarian cancer cells

Previous studies (Abdullah et al., 2019) have demonstrated that prednisolone has minimal influence on the caspase 3/7 activity in ovarian cancer cells. However, pivastatin combined with prednisolone significantly increased the caspase activation when compared to that by pivastatin alone. Scholars have also investigated the expression of MVA pathway-related genes as prednisolone regulates gene expression by binding to glucocorticoid receptors. They found that neither pitavastatin nor prednisolone alone had any effect on HMGCR, GGTI-β, IDI1, MVD, and FDPS levels, but they could reduce the GGTII-β expression. Pitavastatin with prednisolone reduced the levels of GGTII-β and resulted in

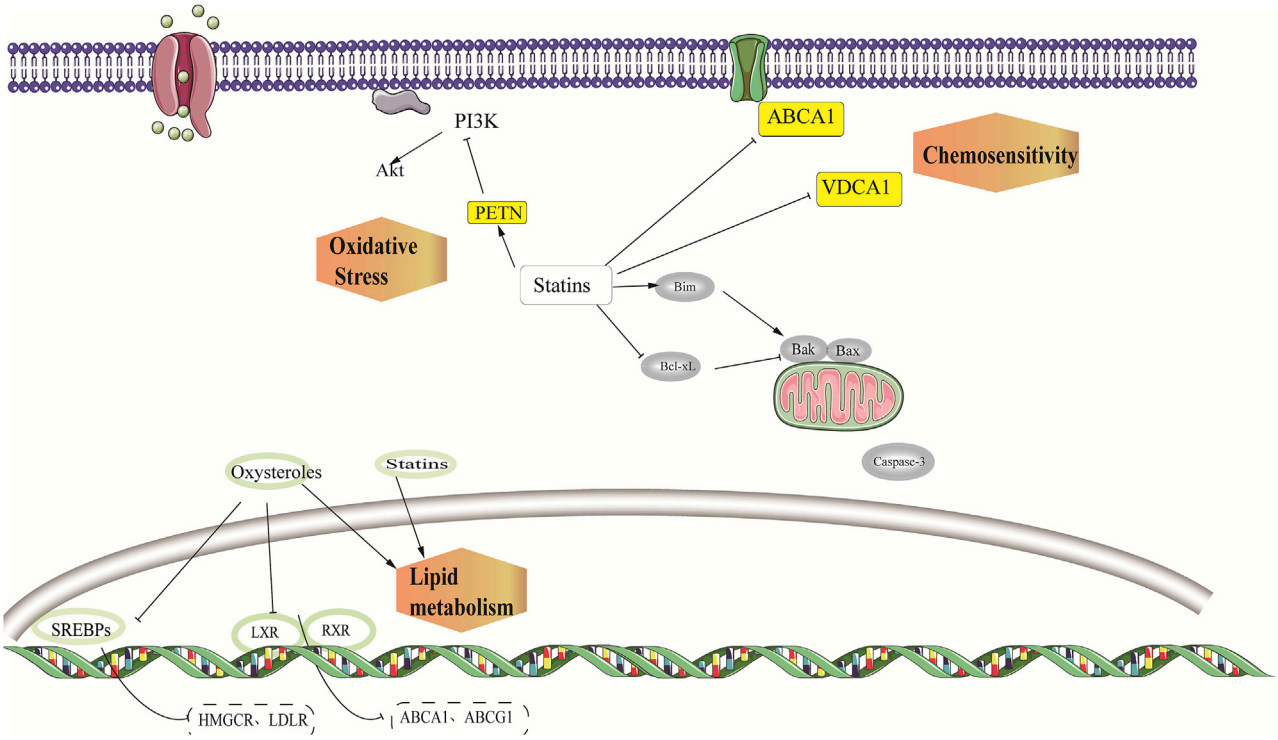

FIGURE 3
Other potential antitumor effects of statins.

significantly lower levels of HMGCR and FDPS. In addition, the combination of prednisolone and pivastatin led to a significant PARP accumulation relative to that of either drug individually (Abdullah et al., 2019).

3 Inhibition of tumor growth by metabolic reprogramming

Aerobic glycolysis is common in tumor cells. Aerobic glycolysis can lead to increased acidic substances, inhibiting immune cell function, and promoting tumor metastasis. Acetyl CoA increased, whereas lactate decreased significantly in statins-treated cells. It was also found through the analysis of other metabolites that metabolites related to the tricarboxylic acid cycle increased significantly and that their metabolic characteristics were similar to those of normal cells (Figure 3).

3.1 Inhibition of tumor growth by VDAC1

VDAC1 was demonstrated to be a positively correlated gene with statin response in ovarian cancer cells (Kobayashi et al., 2022). VDAC1 encodes a 30-kDa channel protein found in the outer mitochondrial membrane (Mannella and Bonner, 1975). VDAC may transport substrates for energy metabolism from the cytoplasm to the intermembrane zone and metabolites from the intermembrane zone to the cytoplasm as it can non-selectively penetrate substances with a molecular weight of about 6,000 Da. Therefore, it is an essential protein for effective energy metabolism in the mitochondria (Rostovtseva et al., 2006). By binding to hexokinase, VDAC regulates glycolysis and interacts with mitochondrial respiration (the rate-limiting enzyme of glycolysis) (Pastorino et al., 2002; Mazure, 2017). VDAC1 expression is upregulated in several human cancer cell lines when compared to normal cell lines. VDAC1 is thus a potential therapeutic target for cancer. In addition, statins have a regulating effect on VDAC1 (Baandrup, 2015; Lipper et al., 2019).

Paclitaxel and panopistat have synergistic anti-ovarian cancer effects (Kobayashi et al., 2022). Paclitaxel is an effective anti-tumor drug that can stoichiometrically and specifically bind to the β-tubulin subunit in tubulin. The VDAC 1 expression may be involved in the synergistic effect of statins and paclitaxel. Tubulin can regulate VDAC *via* a functional interaction between dimer tubulin and VDAC1 (Rostovtseva et al., 2008). Tubulin and VDAC interact at the C-terminal tail of tubulin, which then penetrates the lumen of the VDAC barrel and functions as a plug. Because of the length of the C-terminal tail, which is about the length of the VDAC pore, the C-terminal tail is negatively charged and the VDAC-related domain is positively charged,

which contributes to tubulin and VDAC binding (Mazure, 2017). Statins are one of the promising drugs for targeting VDAC; hence, the synergistic antitumor effect of paclitaxel and statins may be related to microtubules and VDAC binding (Reina And De Pinto, 2017; Fang And Maldonado, 2018).

3.2 Cholesterol metabolism affected the proliferation of ovarian cancer cells

Elevated cholesterol levels could decrease progression-free survival in ovarian cancer patients (Li et al., 2010). Statins reduce cholesterol synthesis by inhibiting the MVA pathway. Statins can induce HMGCR increase through the sterol reaction in some statin-resistant tumor cells, rather than in statin-sensitive cells. This type of feedback depends on SREBPs (Jeon and Osborne, 2012). Oxysterol inhibits SREBP activation by preventing protein processing and nuclear transport. Indeed, statins-oxysterol combination treatment could significantly enhance statin cytotoxicity in ovarian cancer cells (Casella et al., 2014). This drug combination is effective against statins-sensitive cells and has a synergistic effect on statin-resistant cells. The mechanism may be related to the inhibition of SREBPs activity, and, thus, a decrease in the intracellular cholesterol content. LXRs bind to oxysterol and active LXRs can inhibit the growth of ovarian cancer cells. Notably, 25HC was used in this study, and the results showed that 25HC had no significant effect on promoting apoptosis or proliferation in ovarian cancer cells (Casella et al., 2014), despite past research suggesting that HC might promote tumor growth. 27HC was tested in another study (He et al., 2019), which could be metabolized by cholesterol through CYP27A1. Moreover, 27HC has been shown to inhibit the growth of ovarian cancer cells. Whether 27HC can cooperate with the anti-tumor effect of statins warrants further verification. Moreover, 27HC may promote the metastasis of ovarian cancer cells, which needs further consideration.

4 Other mechanisms

4.1 Induction of cell apoptosis by the PI3K/AKT signal pathway

The PI3K/AKT signaling pathway promotes tumor cell proliferation and anti-apoptosis and is overexpressed in 45% of high-grade ovarian cancer (Cancer Genome Atlas Research Network, 2011). Statins can inhibit PI3K activation by inhibiting NF-κB, which promotes the expression of PTEN and reduces AKT activation (Ghosh-Choudhury et al., 2010; Miraglia et al., 2012). The investigation of OVCAR3, OVCAR8, A2780, and Igrov-1 constitutively activated by the PI3K/AKT signaling pathway revealed that the combination of pictilisib and pivastatin had a synergistic inhibitory effect on OVCAR3 but an antagonistic effect on A2780 and Igrov (De Wolf et al., 2018). This observation may be attributed to the low expression of PTEN in A2780 and Igrov cells, which results in an inability to reduce AKT activation.

Simvastatin inhibited the PI3K/AKT pathway in SKOV3 and HEY cells, increased the active oxygen level to cause DNA damage, induced ER stress, and reduced the VEGF expression, thus playing an anti-proliferation and metastasis role in ovarian cancer (Stine et al., 2016). Moreover, after lovastatin intervention, total glutathione, reduced glutathione, and oxidized glutathione levels in the ovarian cancer cells were significantly decreased (Kobayashi et al., 2017) (Figure 3).

4.2 Induction of cell apoptosis by the Bcl-2 superfamily

The Bcl-2 family includes pro-apoptotic proteins, anti-apoptotic proteins, and pro-apoptotic proteins of BH-3-only. Herein, the anti-apoptotic protein acted by binding with the pro-apoptotic proteins or BH-3-only proteins. Past studies (De Wolf et al., 2018) have demonstrated that pivastatin had no significant effect on Bcl-2 alone, although it could promote the expression of the pro-apoptotic protein Bim and decrease the expression of the anti-apoptotic protein Bcl-XL. Moreover, Bcl-XL was highly expressed in ovarian cancer (Lee et al., 2019).

ABT-737 is a BH3 mimetic inhibitor, and the combination of pivastatin and ABT-737 significantly promoted ovarian cancer cell death (De Wolf et al., 2018). Pivastatin may increase Bim and decrease Bcl-xL, accelerating ABT-737, antagonizing Bcl-xL, and inducing Bim release, which finally activated the cell-specific apoptosis process. A relatively significant synergistic effect can be found in Igrov cells, but none in A2780 cells, which may be due to the low expression of Bcl-xL but a high expression of Mcl-1 in A2780 cells. Furthermore, ABT-737 could inhibit Bcl-xL, Bcl-2, and Bcl-w, but not Mcl-1, Bcl-B, or Bfl-1 (Witham et al., 2007) (Figure 3). However, some studies have determined that simvastatin could inhibit TNF-α-induced NF-κB activation, leading to the downregulation of cyclin D1, Bcl-2, MMP9, and VEGF (Ahn et al., 2007).

4.3 Anti-tumor chemoresistance mediated by p-gp

ABCB1 encodes p-gp, and increasing its expression can accelerate drug excretion, which is one of the critical mechanisms of tumor chemoresistance (Waghray and Zhang, 2018). Past studies (Martirosyan et al., 2010) noted no significant synergistic effect between statins and cisplatin or doxorubicin and statins for chemotherapy-sensitive A2780 cells; however, there was a significant synergistic effect between lovastatin and adriamycin in chemo-resistant A2780ADR cells. Moreover, adriamycin treatment increased the expression of p-gp in A2780 cells, while statins could affect the inhibitory effect of

the p-gp overexpression. Meanwhile, the adriamycin level of the chemo-resistant cell strain rose. However, because the p-gp expression was not considered in the cells, the combination of statins and adriamycin demonstrated no significant synergistic effect in treating A2780 cells. Therefore, the authors proposed that statins had therapeutic effects on ovarian cancer *via* the MVA pathway, could antagonize drug chemoresistance by inhibiting p-glycoprotein and had synergistic effects with the use of chemotherapeutic drugs (Figure 3).

4.4 Anti-tumor effect mediated by Myc

C-Myc is associated with both cell proliferation and the cell cycle. Statins may induce cell growth arrest by inhibiting c-Myc. In some studies, three statins were used to intervene in ovarian cancer cells OVCAR8 and its multidrug chemo-resistant cell strain NCI-ADR/RES. The results demonstrated that all three statins could inhibit cell proliferation without causing cell apoptosis while also arresting the G1 and S phases. Meanwhile, statins accelerated c-Myc degradation and inhibited c-Myc protein synthesis, indicating that statins interfere with c-Myc biosynthesis, which exists not only in chemotherapy-sensitive ovarian cancer cells but also in multi-chemo-resistant cells. JQ1 is a c-Myc inhibitor, and Jones et al. found that JQ1 combined with Atorvastatin had a synergistic inhibitory effect on c-Myc and a synergistic anti-ovarian cancer effect (Jones et al., 2017).

Hence, we believe that statins can be clinically applied in chemo-resistant tumor cells. However, after ceasing the administration, the cell proliferation gradually recovered, indicating the significance of statin action time in cancer treatment (Rao and Rao, 2021) (Figure 3).

5 Discussion

Although several studies have demonstrated that statins play an important role in the prevention and treatment of ovarian cancer, most of these studies are retrospective in nature and often combined with the use of statins on the basis of conventional treatment (Table 2). The results of ovarian cancer treated with statins alone are full of contradictions (Robinson et al., 2013; Chen et al., 2016; Wang et al., 2019), and some studies even believe that statins can promote the occurrence of ovarian cancer (Desai et al., 2018). On the one hand, this contradiction is related to the positioning of statins. It is difficult to imagine that an anti-lipid drug can completely kill tumor cells. Therefore, statins may need to be applied together with other drugs to better play an anti-tumor role. On the other hand, it may also be related to the high heterogeneity of ovarian cancer.

Some studies (Baandrup et al., 2015; Verdoodt et al., 2017; Feng et al., 2021) believe that statins have obvious effects in the treatment of endometrioid and mucinous carcinoma, but not in serous or mucinous carcinoma. In serous ovarian cancer, statins have a protective effect only after diagnosis (Hanley et al., 2021). Therefore, the protective effect of statins may be limited to certain specific subtypes, but, even for a certain subtype, the biological characteristics of cancer cells are different.

At present, the sample size of the ongoing or completed clinical trials is small. Although the sample size of the retrospective trials can be relatively large, the data collected is not precise enough. Therefore, the data collection of relevant retrospective studies should be more detailed and targeted. For example, not only the type of statin, the type of ovarian cancer, but also the conventional treatment method should be considered, and relevant clinical studies should look for appropriate molecular markers on the basis of existing studies, rather than simply relying on tissue type.

6 Conclusion and prospect

The anti-tumor effect of statins not only affects the MVA pathway by inhibiting HMGCR, but also may affect cell proliferation, apoptosis and drug resistance through metabolic reprogramming, Bcl-2 family and other pathways. Moreover, statins can exert synergistic anti-ovarian cancer effect by combining with a variety of drugs. However, the current clinical studies mainly focus on the combined use of statins and chemotherapy drugs. Combination with other drugs is less common. A thorough understanding of the working mechanism of statins is expected to facilitate the achievement of "precision treatment" by using them either alone or in combination, thereby improving the overall clinical efficacy. Furthermore, suitable tumor markers are essential and should be investigated in the future.

Author contributions

LX and HZ designed the study; SD, XW, XZ, and ZL researched the literature and wrote the manuscript; and HZ and HL reviewed the manuscript.

Acknowledgments

The authors would like to thank all reviewers who participated in the review, as well as MJEditor (www.mjeditor.com), for providing English editing services during the preparation of this manuscript.

Conflict of interest

The authors declare that the research was conducted in the absence of any commercial or financial relationships that could be construed as a potential conflict of interest.

Publisher's note

References

Abdullah, M. I., Abed, M. N., Khanim, F., and Richardson, A. (2019). Screening a library of approved drugs reveals that prednisolone synergizes with pitavastatin to induce ovarian cancer cell death. *Sci. Rep.* 9 (1), 9632. doi:10.1038/s41598-019-46102-1

Abdullah, M. I., Abed, M. N., and Richardson, A. (2017). Inhibition of the mevalonate pathway augments the activity of pitavastatin against ovarian cancer cells. *Sci. Rep.* 7 (1), 8090. doi:10.1038/s41598-017-08649-9

Ahn, K. S., Sethi, G., and Aggarwal, B. B. (2007). Simvastatin potentiates TNF-alpha-induced apoptosis through the down-regulation of NF-kappaB-dependent antiapoptotic gene products: Role of IkappaBalpha kinase and TGF-beta-activated kinase-1. *J. Immunol. Baltim. Md* 178 (4), 2507–2516. doi:10.4049/jimmunol.178.4.2507

Altwairgi, A. K. (2015). Statins are potential anticancerous agents (review) [J]. *Oncol. Rep.* 33 (3), 1019–1039. doi:10.3892/or.2015.3741

Baandrup, L., Dehlendorff, C., Friis, S., Olsen, J. H., and Kjær, S. K. (2015). Statin use and risk for ovarian cancer: A Danish nationwide case-control study. *Br. J. cancer* 112 (1), 157–161. doi:10.1038/bjc.2014.574

Baandrup, L. (2015). Drugs with potential chemopreventive properties in relation to epithelial ovarian cancer-a nationwide case-control study. *Dan. Med. J.* 62, B5117.

Bar, D., Lavie, O., Stein, N., Feferkorn, I., and Shai, A. (2016). The effect of metabolic comorbidities and commonly used drugs on the prognosis of patients with ovarian cancer. *Eur. J. obstetrics, Gynecol. reproductive Biol.* 207, 227–231. doi:10.1016/j.ejogrb.2016.09.005

Cancer Genome Atlas Research Network (2011). Integrated genomic analyses of ovarian carcinoma. *Nature* 474 (7353), 609–615. doi:10.1038/nature10166

Casella, C., Miller, D. H., Lynch, K., and Brodsky, A. S. (2014). Oxysterols synergize with statins by inhibiting SREBP-2 in ovarian cancer cells. *Gynecol. Oncol.* 135 (2), 333–341. doi:10.1016/j.ygyno.2014.08.015

Chen, H. Y., Wang, Q., Xu, Q. H., Yan, L., Gao, X. F., Lu, Y. H., et al. (2016). Statin as a combined therapy for advanced-stage ovarian cancer: A propensity score matched analysis. *BioMed Res. Int.* 2016, 9125238. doi:10.1155/2016/9125238

Clearfield, M., Downs, J. R., Weis, S., Whitney, E. J., Kruyer, W., Shapiro, D. R., et al. (2001). Air force/Texas coronary atherosclerosis prevention study (AFCAPS/TexCAPS): Efficacy and tolerability of long-term treatment with lovastatin in women. *J. women's health & gender-based Med.* 10 (10), 971–981. doi:10.1089/152460901317193549

Clendening, J. W., Pandyra, A., Boutros, P. C., El Ghamrasni, S., Khosravi, F., Trentin, G. A., et al. (2010). Dysregulation of the mevalonate pathway promotes transformation. *Proc. Natl. Acad. Sci. U. S. A.* 107 (34), 15051–15056. doi:10.1073/pnas.0910258107

Couttenier, A., Lacroix, O., Vaes, E., Cardwell, C. R., De Schutter, H., and Robert, A. (2017). Statin use is associated with improved survival in ovarian cancer: A retrospective population-based study. *PloS one* 12 (12), e0189233. doi:10.1371/journal.pone.0189233

De Wolf, E., Abdullah, M. I., Jones, S. M., Menezes, K., Moss, D. M., Drijfhout, F. P., et al. (2017). Dietary geranylgeraniol can limit the activity of pitavastatin as a potential treatment for drug-resistant ovarian cancer. *Sci. Rep.* 7 (1), 5410. doi:10.1038/s41598-017-05595-4

De Wolf, E., De Wolf, C., and Richardson, A. (2018). ABT-737 and pictilisib synergistically enhance pitavastatin-induced apoptosis in ovarian cancer cells. *Oncol. Lett.* 15 (2), 1979–1984. doi:10.3892/ol.2017.7516

Desai, P., Wallace, R., Anderson, M. L., Howard, B. V., Ray, R. M., Wu, C., et al. (2018). An analysis of the association between statin use and risk of endometrial and ovarian cancers in the Women's Health Initiative. *Gynecol. Oncol.* 148 (3), 540–546. doi:10.1016/j.ygyno.2018.01.006

Elmore, R. G., Ioffe, Y., Scoles, D. R., and Karlan, B. Y. (2008). Impact of statin therapy on survival in epithelial ovarian cancer. *Gynecol. Oncol.* 111 (1), 102–105. doi:10.1016/j.ygyno.2008.06.007

Fang, D., and Maldonado, E. N. (2018). VDAC regulation: A mitochondrial target to stop cell proliferation. *Adv. cancer Res.* 138, 41–69. doi:10.1016/bs.acr.2018.02.002

Feng, J. L., Dixon-Suen, S. C., Jordan, S. J., and Webb, P. M. (2021). Statin use and survival among women with ovarian cancer: An Australian national data-linkage study. *Br. J. cancer* 125 (5), 766–771. doi:10.1038/s41416-021-01460-4

Freed-Pastor, W., and Prives, C. (2016). Targeting mutant p53 through the mevalonate pathway. *Nat. Cell Biol.* 18 (11), 1122–1124. doi:10.1038/ncb3435

Friedman, G. D., Flick, E. D., Udaltsova, N., Chan, J., Quesenberry, C. P., Jr, and Habel, L. A. (2008). Screening statins for possible carcinogenic risk: Up to 9 years of follow-up of 361, 859 recipients. *Pharmacoepidemiol. drug Saf.* 17 (1), 27–36. doi:10.1002/pds.1507

GBD 2019 Stroke Collaborators (2021). Global, regional, and national burden of stroke and its risk factors, 1990-2019: A systematic analysis for the global burden of disease study 2019 [J]. *Lancet Neurology* 20 (10), 795–820. doi:10.1016/S1474-4422(21)00252-0

Ghosh-Choudhury, N., Mandal, C. C., Ghosh-Choudhury, N., and Ghosh Choudhury, G. (2010). Simvastatin induces derepression of PTEN expression via NFkappaB to inhibit breast cancer cell growth. *Cell. Signal.* 22 (5), 749–758. doi:10.1016/j.cellsig.2009.12.010

Granström, C., Sundquist, J., and Hemminki, K. (2008). Population attributable fractions for ovarian cancer in Swedish women by morphological type. *Br. J. cancer* 98 (1), 199–205. doi:10.1038/sj.bjc.6604135

Green, J. R. (2004). Bisphosphonates: Preclinical review. *Oncol.* 9, 3–13. doi:10.1634/theoncologist.9-90004-3

Habis, M., Wroblewski, K., Bradaric, M., Ismail, N., Yamada, S. D., Litchfield, L., et al. (2014). Statin therapy is associated with improved survival in patients with non-serous-papillary epithelial ovarian cancer: A retrospective cohort analysis. *PloS one* 9 (8), e104521. doi:10.1371/journal.pone.0104521

Hanley, G. E., Kaur, P., Berchuck, A., Chase, A., Grout, B., Deurloo, C. M., et al. (2021). Cardiovascular medications and survival in people with ovarian cancer: A population-based cohort study from British columbia, Canada. *Gynecol. Oncol.* 162 (2), 461–468. doi:10.1016/j.ygyno.2021.05.021

Harding, B. N., Delaney, J. A., Urban, R. R., and Weiss, N. S. (2019). Use of statin medications following diagnosis in relation to survival among women with ovarian cancer [J]. Cancer epidemiology, biomarkers & prevention : A publication of the American association for cancer research. *cosponsored by Am. Soc. Prev. Oncol.* 28 (7), 1127–1133. doi:10.1158/1055-9965.EPI-18-1194

He, S., Ma, L., Baek, A. E., Vardanyan, A., Vembar, V., Chen, J. J., et al. (2019). Host CYP27A1 expression is essential for ovarian cancer progression. *Endocrine-related cancer* 26 (7), 659–675. doi:10.1530/ERC-18-0572

Hutchinson, J., and Marignol, L. (2017). Clinical potential of statins in prostate cancer radiation therapy. *Anticancer Res.* 37 (10), 5363–5372. doi:10.21873/anticanres.11962

Jeon, T. I., and Osborne, T. F. (2012). SREBPs: Metabolic integrators in physiology and metabolism. *Trends Endocrinol. metabolism TEM* 23 (2), 65–72. doi:10.1016/j.tem.2011.10.004

Jiao, X. F., Li, H. L., Jiao, X. Y., Guo, Y. C., Zhang, C., Yang, C. S., et al. (2020). Ovary and uterus related adverse events associated with statin use: An analysis of the FDA adverse event reporting system. *Sci. Rep.* 10 (1), 11955. doi:10.1038/s41598-020-68906-2

Jones, H. M., Fang, Z., Sun, W., Clark, L. H., Stine, J. E., Tran, A. Q., et al. (2017). Atorvastatin exhibits anti-tumorigenic and anti-metastatic effects in ovarian cancer *in vitro*. *Am. J. cancer Res.* 7 (12), 2478–2490.

Kato, S., Smalley, S., Sadarangani, A., Chen-Lin, K., Oliva, B., Branes, J., et al. (2010). Lipophilic but not hydrophilic statins selectively induce cell death in gynaecological cancers expressing high levels of HMGCoA reductase. *J. Cell. Mol. Med.* 14 (5), 1180–1193. doi:10.1111/j.1582-4934.2009.00771.x

Kim, D. S., Ahn, H. S., and Kim, H. J. (2022). Statin use and incidence and mortality of breast and gynecology cancer: A cohort study using the national health insurance claims database. *Int. J. cancer* 150 (7), 1156–1165. doi:10.1002/ijc.33869

Kobayashi, Y., Kashima, H., Rahmanto, Y. S., Banno, K., Yu, Y., Matoba, Y., et al. (2017). Drug repositioning of mevalonate pathway inhibitors as antitumor agents for ovarian cancer. *Oncotarget* 8 (42), 72147–72156. doi:10.18632/oncotarget.20046

Kobayashi, Y., Kashima, H., Wu, R. C., Jung, J. G., Kuan, J. C., Gu, J., et al. (2015). Mevalonate pathway antagonist suppresses formation of serous tubal intraepithelial carcinoma and ovarian carcinoma in mouse models. *Clin. cancer Res. official J. Am. Assoc. Cancer Res.* 21 (20), 4652–4662. doi:10.1158/1078-0432.CCR-14-3368

Kobayashi, Y., Takeda, T., Kunitomi, H., Chiwaki, F., Komatsu, M., Nagai, S., et al. (2022). Response predictive markers and synergistic agents for drug repositioning of statins in ovarian cancer. *Pharm. (Basel, Switz.* 15 (2), 124. doi:10.3390/ph15020124

Lavie, O., Pinchev, M., Rennert, H. S., Segev, Y., and Rennert, G. (2013). The effect of statins on risk and survival of gynecological malignancies. *Gynecol. Oncol.* 130 (3), 615–619. doi:10.1016/j.ygyno.2013.05.025

Lee, J. M., Minasian, L., and Kohn, E. C. (2019). New strategies in ovarian cancer treatment. *Cancer* 125, 4623–4629. doi:10.1002/cncr.32544

Li, A. J., Elmore, R. G., Chen, I. Y., and Karlan, B. Y. (2010). Serum low-density lipoprotein levels correlate with survival in advanced stage epithelial ovarian cancers. *Gynecol. Oncol.* 116 (1), 78–81. doi:10.1016/j.ygyno.2009.09.027

Li, X., and Zhou, J. (2018). Impact of postdiagnostic statin use on ovarian cancer mortality: A systematic review and meta-analysis of observational studies. *Br. J. Clin. Pharmacol.* 84 (6), 1109–1120. doi:10.1111/bcp.13559

Lipper, C. H., Stofleth, J. T., Bai, F., Sohn, Y. S., Roy, S., Mittler, R., et al. (2019). Redox-dependent gating of VDAC by mitoNEET. *Proc. Natl. Acad. Sci. U. S. A.* 116 (40), 19924–19929. doi:10.1073/pnas.1908271116

Liu, H., Liang, S. L., Kumar, S., Weyman, C. M., Liu, W., and Zhou, A. (2009). Statins induce apoptosis in ovarian cancer cells through activation of JNK and enhancement of Bim expression. *Cancer Chemother. Pharmacol.* 63 (6), 997–1005. doi:10.1007/s00280-008-0830-7

Majidi, A., Na, R., Jordan, S. J., De Fazio, A., and Webb, P. M.OPAL Study Group (2021). Statin use and survival following a diagnosis of ovarian cancer: A prospective observational study. *Int. J. cancer* 148 (7), 1608–1615. doi:10.1002/ijc.33333

Mannella, C. A., and Bonner, W. D. J. R. (1975). Biochemical characteristics of the outer membranes of plant mitochondria. *Biochimica biophysica acta* 413 (2), 213–225. doi:10.1016/0005-2736(75)90105-4

Martirosyan, A., Clendening, J. W., Goard, C. A., and Penn, L. Z. (2010). Lovastatin induces apoptosis of ovarian cancer cells and synergizes with doxorubicin: Potential therapeutic relevance. *BMC cancer* 10, 103. doi:10.1186/1471-2407-10-103

Mazure, N. M. (2017). VDAC in cancer. *Biochimica biophysica acta Bioenergetics* 1858 (8), 665–673. doi:10.1016/j.bbabio.2017.03.002

Mctaggart, S. J. (2006). Isoprenylated proteins, Isoprenylated proteins [J]. *Cell. Mol. life Sci. CMLS* 63 (3), 255–267. doi:10.1007/s00018-005-5298-6

Miraglia, E., HöGBERG, J., and Stenius, U. (2012). Statins exhibit anticancer effects through modifications of the pAkt signaling pathway. *Int. J. Oncol.* 40 (3), 867–875. doi:10.3892/ijo.2011.1223

National Academy of Sciences (1975). "The national academies collection: Reports funded by national institutes of health [M]," in *Drug repurposing and repositioning: Workshop summary* Washington (DC): National Academies Press. 2014, Copyright by the National Academy of Sciences. All rights reserved. 2014.

Pastorino, J. G., Shulga, N., and Hoek, J. B. (2002). Mitochondrial binding of hexokinase II inhibits Bax-induced cytochrome c release and apoptosis. *J. Biol. Chem.* 277 (9), 7610–7618. doi:10.1074/jbc.M109950200

Peres, L. C., Cushing-Haugen, K. L., KöBEL, M., Harris, H. R., Berchuck, A., Rossing, M. A., et al. (2019). Invasive epithelial ovarian cancer survival by histotype and disease stage. *J. Natl. Cancer Inst.* 111 (1), 60–68. doi:10.1093/jnci/djy071

Pletcher, M. J., Pignone, M., Jarmul, J. A., Moran, A. E., Vittinghoff, E., and Newman, T. (2017). Population impact & efficiency of benefit-targeted versus risk-targeted statin prescribing for primary prevention of cardiovascular disease. *J. Am. Heart Assoc.* 6 (2), e004316. doi:10.1161/JAHA.116.004316

Rao, P. S., and Rao, U. S. (2021). Statins decrease the expression of c-Myc protein in cancer cell lines. *Mol. Cell. Biochem.* 476 (2), 743–755. doi:10.1007/s11010-020-03940-2

Reina, S., and De Pinto, V. (2017). Anti-cancer compounds targeted to VDAC: Potential and perspectives. *Curr. Med. Chem.* 24 (40), 4447–4469. doi:10.2174/0929867324666170530074039

Robinson, E., Nandi, M., Wilkinson, L. L., Arrowsmith, D. M., Curtis, A. D. M., and Richardson, A. (2013). Preclinical evaluation of statins as a treatment for ovarian cancer. *Gynecol. Oncol.* 129 (2), 417–424. doi:10.1016/j.ygyno.2013.02.003

Rostovtseva, T. K., Kazemi, N., Weinrich, M., and Bezrukov, S. M. (2006). Voltage gating of VDAC is regulated by nonlamellar lipids of mitochondrial membranes. *J. Biol. Chem.* 281 (49), 37496–37506. doi:10.1074/jbc.M602548200

Rostovtseva, T. K., Sheldon, K. L., Hassanzadeh, E., Monge, C., Saks, V., Bezrukov, S. M., et al. (2008). Tubulin binding blocks mitochondrial voltage-dependent anion channel and regulates respiration. *Proc. Natl. Acad. Sci. U. S. A.* 105 (48), 18746–18751. doi:10.1073/pnas.0806303105

Schachter, M. (2005). Chemical, pharmacokinetic and pharmacodynamic properties of statins: An update. *Fundam. Clin. Pharmacol.* 19 (1), 117–125. doi:10.1111/j.1472-8206.2004.00299.x

Stine, J. E., Guo, H., Sheng, X., Han, X., Schointuch, M. N., Gilliam, T. P., et al. (2016). The HMG-CoA reductase inhibitor, simvastatin, exhibits anti-metastatic and anti-tumorigenic effects in ovarian cancer. *Oncotarget* 7 (1), 946–960. doi:10.18632/oncotarget.5834

Svensmark, J. H., and Brakebusch, C. (2019). Rho GTPases in cancer: Friend or foe? [J]. *Oncogene* 38 (50), 7447–7456. doi:10.1038/s41388-019-0963-7

Taylor-Harding, B., Orsulic, S., Karlan, B. Y., and Li, A. J. (2010). Fluvastatin and cisplatin demonstrate synergistic cytotoxicity in epithelial ovarian cancer cells. *Gynecol. Oncol.* 119 (3), 549–556. doi:10.1016/j.ygyno.2010.08.017

Torre, L. A., Trabert, B., Desantis, C. E., Miller, K. D., Samimi, G., Runowicz, C. D., et al. (2018). Ovarian cancer statistics, 2018 [J]. *CA a cancer J. Clin.* 68 (4), 284–296. doi:10.3322/caac.21456

Urpilainen, E., Marttila, M., Hautakoski, A., Arffman, M., Sund, R., Ilanne-Parikka, P., et al. (2018). Prognosis of ovarian cancer in women with type 2 diabetes using metformin and other forms of antidiabetic medication or statins: A retrospective cohort study. *BMC cancer* 18 (1), 767. doi:10.1186/s12885-018-4676-z

Verdoodt, F., Kjaer Hansen, M., Kjaer, S. K., Pottegard, A., Friis, S., and Dehlendorff, C. (2017). Statin use and mortality among ovarian cancer patients: A population-based cohort study. *Int. J. cancer* 141 (2), 279–286. doi:10.1002/ijc.30738

Waghray, D., and Zhang, Q. (2018). Inhibit or evade multidrug resistance P-glycoprotein in cancer treatment. *J. Med. Chem.* 61 (12), 5108–5121. doi:10.1021/acs.jmedchem.7b01457

Wang, Y., Ren, F., Song, Z., Chen, P., Liu, S., and Ouyang, L. (2019). Statin use and the risk of ovarian and endometrial cancers: A meta-analysis. *BMC cancer* 19 (1), 730. doi:10.1186/s12885-019-5954-0

Witham, J., Valenti, M. R., De-Haven-Brandon, A. K., Vidot, S., Eccles, S. A., Kaye, S. B., et al. (2007). The Bcl-2/Bcl-XL family inhibitor ABT-737 sensitizes ovarian cancer cells to carboplatin. *Clin. cancer Res. official J. Am. Assoc. Cancer Res.* 13 (23), 7191–7198. doi:10.1158/1078-0432.CCR-07-0362

Xie, W., Ning, L., Huang, Y., Liu, Y., Zhang, W., Hu, Y., et al. (2017). Statin use and survival outcomes in endocrine-related gynecologic cancers: A systematic review and meta-analysis. *Oncotarget* 8 (25), 41508–41517. doi:10.18632/oncotarget.17242

Yu, O., Boudreau, D. M., Buist, D. S., and Miglioretti, D. L. (2009). Statin use and female reproductive organ cancer risk in a large population-based setting. *Cancer causes control CCC* 20 (5), 609–616. doi:10.1007/s10552-008-9271-1

Zhang, Q. S., Deater, M., Phan, N., Marcogliese, A., Major, A., Guinan, E. C., et al. (2019). Combination therapy with atorvastatin and celecoxib delays tumor formation in a Fanconi anemia mouse model. *Pediatr. blood cancer* 66 (1), e27460. doi:10.1002/pbc.27460

frontiers | Frontiers in Pharmacology

TYPE Case Report
PUBLISHED 09 January 2023
DOI 10.3389/fphar.2022.1067557

OPEN ACCESS

EDITED BY
Eswar Shankar,
The Ohio State University, United States

REVIEWED BY
Ashish Tyagi,
Texas A&M University, United States
Daniele Mengato,
University Hospital of Padua, Italy

*CORRESPONDENCE
Xiaobing Chen,
zlyychenxb0807@zzu.edu.cn

SPECIALTY SECTION
This article was submitted to Pharmacology of Anti-Cancer Drugs, a section of the journal Frontiers in Pharmacology

RECEIVED 12 October 2022
ACCEPTED 13 December 2022
PUBLISHED 09 January 2023

CITATION
Lv H, He Y, Nie C, Du F and Chen X (2023), Adding of apatinib and camrelizumab to overcome *de novo* trastuzumab resistance of HER2-positive gastric cancer: A case report and literature review.
Front. Pharmacol. 13:1067557.
doi: 10.3389/fphar.2022.1067557

Adding of apatinib and camrelizumab to overcome *de novo* trastuzumab resistance of HER2-positive gastric cancer: A case report and literature review

Huifang Lv, Yunduan He, Caiyun Nie, Feng Du and Xiaobing Chen*

The Affiliated Cancer Hospital of Zhengzhou University, Henan cancer hospital, Zhengzhou, China

Background: Studies confirmed that trastuzumab plus fluorouracil-based chemotherapy improves the survival to more than 1 year in human with human epidermal growth factor receptor-2 (HER2)-positive advanced gastric cancer. However, there are still a small proportion of patients who do not benefit from trastuzumab treatment.

Case summary: Here, we described a case report of *de novo* trastuzumab resistance in HER2-positive gastric cancer. Concomitant cyclin-E1 (CCNE1) and HER2 amplification are associated with *de novo* trastuzumab resistance. Genomic analysis demonstrated CCNE1 amplification and TP53 mutation in a HER2-positive gastric cancer patient. This patient achieved significant survival benefit and good safety when the patient received triple regimens consisting of trastuzumab, apatinib, and camrelizumab.

Conclusion: Trastuzumab plus camrelizumab plus apatinib has the potential efficacy in HER2-positive gastric cancer patients who were previously treated with trastuzumab plus chemotherapy. This may lead to a new solution to trastuzumab resistance.

KEYWORDS

trastuzumab, resistance, camrelizumab, apatinib, gastric cancer, case report, literature review

Introduction

In the past decade, treatment based on precision medicine or individualized treatment has changed the outlook of many types of cancers (Nelson et al., 2021). Gastric cancer (GC) patients have evolved from treatment based on its molecular characteristics or its tumor microenvironment. Human epidermal growth factor receptor-2 (HER2) is closely related to the prognosis of gastric cancer (Lv et al., 2020). Since the advent of trastuzumab, survival has been significantly prolonged in advanced HER2-positive GC, and the treatment of GC has entered the era of targeted therapy (Bang et al., 2010).

Unfortunately, a small proportion of patients could not benefit from trastuzumab treatment (*de novo* resistance). Even if someone benefits from the treatment, drug resistance to trastuzumab often appears after 1 year (acquired resistance). Once trastuzumab treatment fails, chemotherapy, including paclitaxel, docetaxel, or irinotecan, with or without ramucirumab is suggested to be the second-line treatment regimen (Hironaka et al., 2013; Wilke et al., 2014). New drugs have been explored in the second-line or aforementioned treatment of gastric cancer. Unfortunately, most of the clinical studies showed negative results (Ohtsu et al., 2013; Dutton et al., 2014; Bang et al., 2017). Antibody–drug conjugate (ADC) drugs have been successfully used in HER2-positive breast cancer (Modi et al., 2020; Montemurro et al., 2020). In addition to trastuzumab emtansine (T-DM1) failure in gastric cancer, the trials that involved trastuzumab deruxtecan (DS-8201a) and disitamab vedotin (RC48) have achieved positive results in gastric cancer (Thuss-Patience et al., 2017; Shitara et al., 2020; Xu et al., 2021). DS-8201a has been approved for the second-line treatment of gastric cancer by the US Food and Drug Administration (FDA), and ADC-RC48 is also used for the third-line treatment by the China National Medical Products Administration (NMPA).

Immune checkpoint inhibitors (ICIs) have changed the outcome of advanced tumors (Ribas and Wolchok, 2018). However, only 15 percent can benefit from programmed cell death 1 (PD-1) inhibitors alone. Therefore, the current research mainly focuses on the exploration of different immunotherapy combination treatment modalities (Hegde et al., 2016). Nivolumab combined with chemotherapy significantly improved the progression-free survival (PFS) and overall survival (OS) in the first-line treatment of HER2-negative gastric cancer patients (Janjigian et al., 2021), while in HER2-positive gastric cancer, pembrolizumab plus trastuzumab and chemotherapy recently showed a superior efficacy (Janjigian et al., 2020). In addition, a recent study showed that ICIs and anti-angiogenic drugs have synergistic effects on anti-tumor treatment (Galluzzi et al., 2016). The combination of immunotherapy and anti-angiogenic drugs has also been explored in gastric cancer. Regorafenib combined with nivolumab was approved to show survival benefits in patients with advanced gastric cancer in the REGONIVO study (Fukuoka et al., 2020). Lenvatinib plus pembrolizumab showed active anti-tumor activity in the EPOC1706 study (Kawazoe et al., 2020). However, most patients cannot afford them due to their high prices in China.

Apatinib, an anti-angiogenic drug, has been approved for the third-line treatment of GC and granted marketing approval by the NMPA (Li et al., 2016). Camrelizumab, the PD-1 blockades, has been approved effective in the treatment of lymphoma, esophageal squamous cancer, non-small cell lung cancer, and liver cancer by the NMPA (Nie et al., 2019; Qin et al., 2020; Luo et al., 2021; Zhou et al., 2021). In addition, camrelizumab has been approved as an orphan drug in hepatocellular carcinoma by

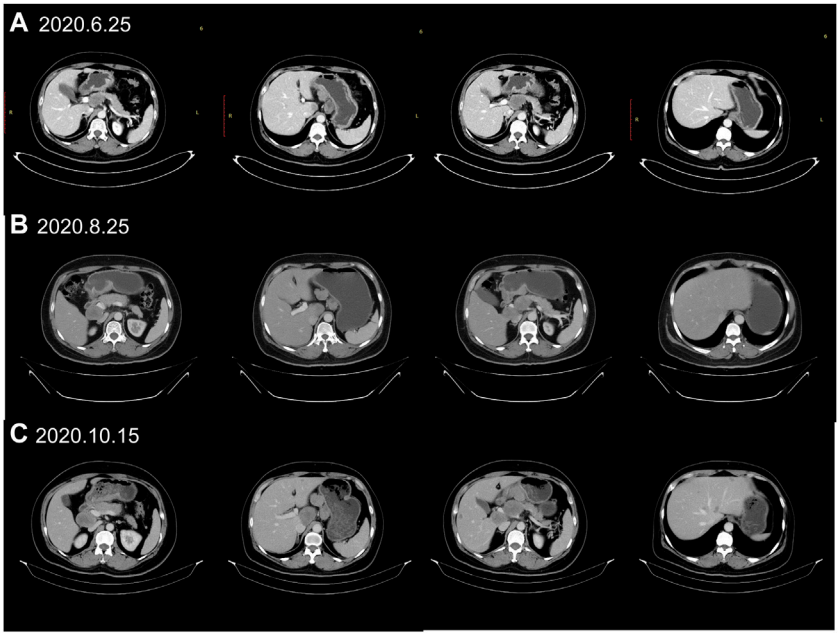

FIGURE 1
Treatment protocol before trastuzumab therapy. **(A)** CT scans (2020.6.25) showed the patient's baseline disease; **(B)** CT scans (2020.8.25) demonstrated progressive disease (PD) in multiple lymph nodes metastases when first-line chemotherapy failed. **(C)** CT scans (2020.10.15) revealed new liver metastases when the second-line chemotherapy failed.

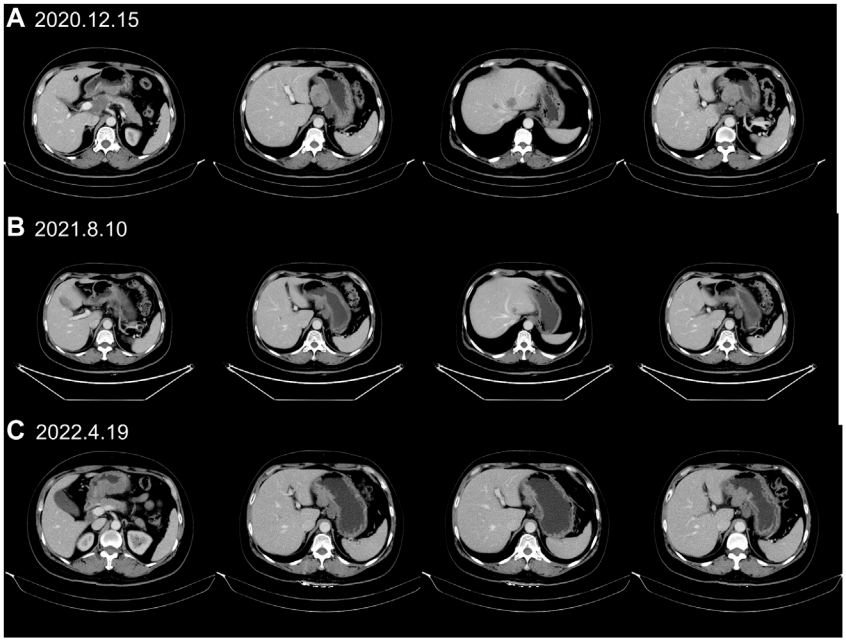

FIGURE 2
CT scans identified liver lesions during trastuzumab treatment. **(A)** CT scans (2020.12.15) demonstrated progressive disease (PD) in liver metastases after trastuzumab plus chemotherapy treatment. **(B)** CT (2021.8.10) showed that liver lesions had markedly shrunken 8 months after trastuzumab, apatinib and camrelizumab treatment. **(C)** The PR status (2022.4.19) continued with trastuzumab, apatinib and camrelizumab treatment until upper gastrointestinal bleeding happened.

the US FDA. Camrelizumab combined with chemotherapy followed by camrelizumab plus apatinib demonstrated an encouraging anti-tumor activity as the first-line therapy for patients with advanced adenocarcinoma in a phase II trial (Peng et al., 2021). Here, we described a specific case which apatinib and camrelizumab combined with trastuzumab could overcome trastuzumab resistance and primary chemotherapy resistance. This made a preliminary exploration of the treatment of triplet regimens (trastuzumab, camrelizumab, and apatinib) to overcome trastuzumab resistance in HER2-positive gastric cancer patients.

TABLE 1 Gene alterations in live metastasis.

Type	Result
NGS	
TMB	8.64 Muts/Mb
MSI	MSS
HER2 amplification	CN = 49.2
CCNE1 amplification	CN = 16.0
TP53 mutation	45.70%
IHC	
HER2	3+

Case presentation

A 55-year-old female suffered from abdominal pain. The information was as follows: KPS 90, H: 168 cm, W: 62 kg, and BSA: 1.7 kg/m^2. She has no family history and genetic history. Gastroscopy showed a huge lump on the antrum of the stomach. The gastric biopsy revealed adenocarcinoma. CT (2020.6.25) scans demonstrated gastric antrum lesions with multiple metastases of hepatogastric and retroperitoneal lymph nodes (Figure 1A). The patient received two cycles of oxaliplatin plus capecitabine (oxaliplatin 200 mg d1; capecitabine 1.5 bid, d1–14, q21d). CT scans (2020.8.25) revealed disease progression in multiple lymph nodes (Figure 1B). Then, the patient was administered oxaliplatin plus capecitabine, along with docetaxel for one cycle (oxaliplatin 200 mg d1; capecitabine 1.5 bid, d1–14; and docetaxel 100 mg d1, q21d). New liver lesions appeared, and the primary tumor and lymph nodes increased (2020.10.15, Figure 1C). Then, the patient visited our hospital. Immunohistochemistry (IHC) revealed that tumor cells were HER2 3+ and negative for PD-L1 in gastric lesions (Figures 3A–C). The patient received trastuzumab plus docetaxel for two cycles. Trastuzumab was administered by intravenous infusion at

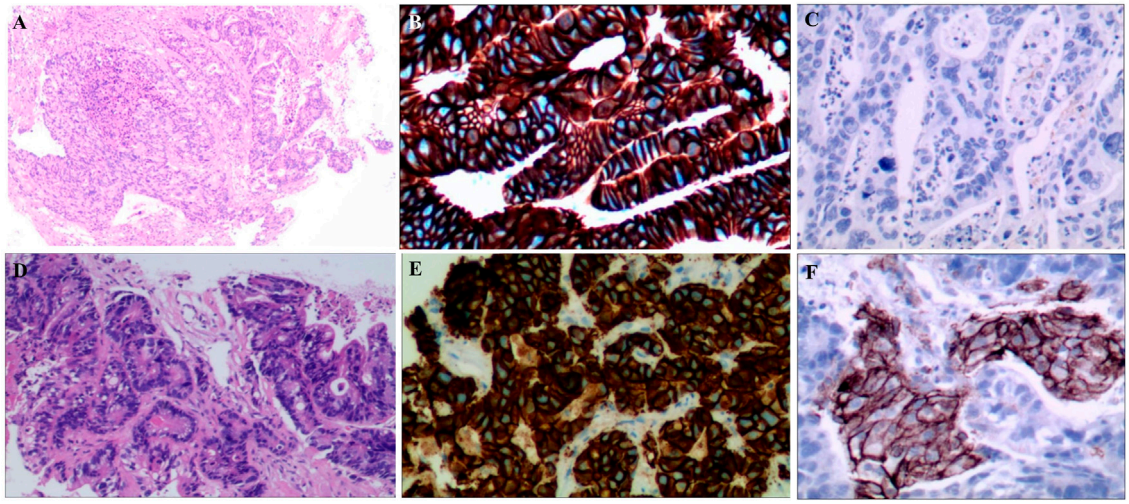

FIGURE 3
(A). HE staining of gastric lesions (×400); **(B)**. HER2 positive on gastric cancer cells; **(C)**: PD-L1 negative on gastric cancer cells; **(D)**: HE staining of liver lesions (×400); **(E)**: HER2 positive on liver lesions; **(F)**: PD-L1 positive on liver lesions.

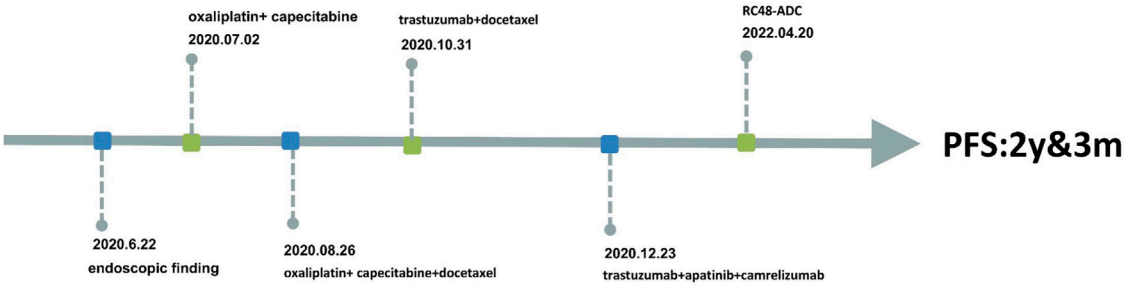

FIGURE 4
Information of this case report has been organized into a timeline.

a dose of 8 mg/kg on day 1 of the first cycle, followed by 6 mg/kg every 3 weeks. Docetaxel was administered at a dose of 120 mg on day 1 at 21 days intervals. CT scans (2020.12.15) showed increased liver lesions (Figure 2A). A multi-gene next-generation sequencing (NGS) testing was performed on liver lesions. Genomic profiling showed HER2 amplification (fold change, 49.2), cyclin-E1 (CCNE1) amplification (fold change, 16.0), and TP53 mutation (Table 1). IHC confirmed HER2 3+ and PD-L1 positive in liver lesions (Figures 3D–F). It is believed that CCNE1 amplification may be related to the resistance of HER2 monoclonal antibody and is associated with poor prognosis in HER2-positive gastric cancer. Then, the patient received trastuzumab, apatinib, and camrelizumab for eight cycles. Camrelizumab was intravenously administered with a dose of 200 mg at 21 days intervals. Apatinib was orally administered with a dose of 250 mg each day. The clinical efficacy was evaluated by imaging examination every 6 weeks. The optimal efficacy was partial response (PR) (2021.8.10, Figure 2B). During the treatment, the patient had moderate anemia and underwent two blood transfusions. The triple regimens continued until upper gastrointestinal bleeding took place, and the patient had to discontinue apatinib (2022.4.19, Figure 3C). Subsequently, she switched to ADC-RC48. A summary of her treatment history is illustrated in Figure 4. During the whole treatment, the patient provided written informed consent each time.

Discussion

Trastuzumab plus chemotherapy significantly improved the survival of gastric cancer (Bang et al., 2010), whereas most

patients develop resistance about 1 year later. Overcoming trastuzumab resistance is still a difficult problem in the clinic until now. Different approaches have been explored recently in the second-line or aforementioned treatment of HER2-positive GC. Lapatinib, a small molecule tyrosine kinase inhibitor, blocks the downstream signaling of HER2. Adding lapatinib to paclitaxel cannot prolong PFS (3.7 m vs. 3.2 m, $p = .33$) and OS (10.2 m vs. 10.0 m, $p = .20$) in patients who progressed after trastuzumab plus chemotherapy in the TyTAN trial (Satoh et al., 2014). ADC drugs have dual antibody-dependent cell-mediated cytotoxicity (ADCC) and cytotoxicity effect. Due to bystander killing effect, DS-8201a had a better OS in patients who failed to respond to trastuzumab (12.5 m vs. 8.4 m, $p = .0097$) (Shitara et al., 2020). RC48-ADC had a similar result (OS = 7.6 m) (Xu et al., 2021). Margetuximab, an Fc-modified anti-HER2 agent, has more powerful ADCC. It demonstrated that margetuximab plus pembrolizumab has a synergistic anti-tumor activity, and better survival was achieved in patients who were previously treated with trastuzumab (OS = 12.9 months) (Catenacci et al., 2020). In addition, trastuzumab beyond progression was explored in HER2-positive gastric cancer. However, continuous use of trastuzumab plus switched chemotherapeutic agents after first-line treatment progression failed to improve PFS (3.2 and 3.7 months, $p = .33$) (Makiyama et al., 2020). However, an Ib/II trial illustrated that continuous use of trastuzumab plus ramucirumab and paclitaxel have a promising activity in patients who failed the first-line trastuzumab plus standard chemotherapy trial (OS: 13.6 months; PFS: 7.2 months) (Sun et al., 2021).

The mechanism of trastuzumab-acquired resistance has been explored in gastric cancer in recent years, but it is still unclear. It is considered that trastuzumab resistance is mainly related to HER2 receptor mutations, activation of MET, HER3, or FGFR receptors, or activation of downstream signaling such as PI3K/AKT and MAPK (Augustin et al., 2022). In contrast, substantially less effort has been devoted to investigating *de novo* trastuzumab resistance in gastric cancer. Gastric cancer was divided into four subtypes in The Cancer Genome Atlas (TCGA) project: tumors positive for Epstein–Barr virus (EBV); microsatellite unstable tumors (MSI); genomically stable tumors (GS), and tumors with chromosomal instability (CIN). A CIN subtype often harbors HER2 amplification, focal amplification of receptor tyrosine kinases (RTKs), and cell cycle regulatory gene amplification (Cancer Genome Atlas Research Network, 2014). It is believed that preexisting specific gene copy-number alterations that often co-occur with HER2 amplification might be co-drivers of tumorigenesis or may reflect intratumor heterogeneity, which would reveal the possible mechanism of *de novo* resistance to HER2-directed therapy (Kim et al., 2014).

CCNE1, one of the cell cycle regulatory genes, is overexpressed in multiple tumors. CCNE1 can lead to chromosomal instability which may contribute to tumorigenesis. In HER2-positive gastric cancer, patients with CCNE1 amplification have a poorer benefit than the patients without CCNE1 amplification. However, in the MSK cohort, there was no difference between patients with or without CCNE1 amplification (Janjigian et al., 2018). The result is controversial. Genomic analysis is often performed to identify the genetic alterations and is helpful for better selection of treatment regimens now. Previous studies showed that CCNE1 amplification is related to *de novo* trastuzumab resistance (Kim et al., 2014). In this case study, NGS testing demonstrated HER2 amplification, CCNE1 amplification, and TP53 mutation. Unfortunately, there is no specific drug for patients with CCNE1 amplification so far. In this case report, this patient achieved survival benefits when she received triple regimens consisting of trastuzumab, apatinib, and camrelizumab. She has a good quality of life and is very satisfied with her treatment regimen until now. This may lead to a new solution for trastuzumab resistance.

We have to admit that the mechanism of trastuzumab resistance is complicated, and the strategy in trastuzumab resistance is still an urgent problem to be solved in HER2-positive gastric cancer. The addition of apatinib and camrelizumab to trastuzumab has good efficacy and high safety in patients with *de novo* trastuzumab resistance. It needs to be further verified in clinical practices.

Data availability statement

The original contributions presented in the study are included in the article/Supplementary Material; further inquiries can be directed to the corresponding author.

Ethics statement

The studies involving human participants were reviewed and approved by the Medical Ethics Committee of Henan Provincial Cancer Hospital. The patients/participants provided their written informed consent to participate in this study. Written informed consent was obtained from the individual(s) for the publication of any potentially identifiable images or data included in this article.

Author contributions

HL and YH wrote the first draft of the manuscript. HL, YH, and FD treated the patient and acquired the data. CN and XC revised the manuscript. All authors contributed to the article and approved the submitted version.

Conflict of interest

The authors declare that the research was conducted in the absence of any commercial or financial relationships that could be construed as a potential conflict of interest.

Publisher's note

References

Augustin, J. E., Soussan, P., and Bass, A. J. (2022). Targeting the complexity of ERBB2 biology in gastroesophageal carcinoma. *Ann. Oncol.* 33, 1134–1148. doi:10.1016/j.annonc.2022.08.001

Bang, Y. J., Van Cutsem, E., Feyereislova, A., Chung, H. C., Shen, L., Sawaki, A., et al. (2010). Trastuzumab in combination with chemotherapy versus chemotherapy alone for treatment of HER2-positive advanced gastric or gastro-oesophageal junction cancer (ToGA): A phase 3, open-label, randomised controlled trial. *Lancet* 376, 687–697. doi:10.1016/S0140-6736(10)61121-X

Bang, Y. J., Xu, R. H., Chin, K., Lee, K. W., Park, S. H., Rha, S. Y., et al. (2017). Olaparib in combination with paclitaxel in patients with advanced gastric cancer who have progressed following first-line therapy (GOLD): A double-blind, randomised, placebo-controlled, phase 3 trial. *Lancet Oncol.* 18, 1637–1651. doi:10.1016/S1470-2045(17)30682-4

Cancer Genome Atlas Research Network (2014). Comprehensive molecular characterization of gastric adenocarcinoma. *Nature* 513, 202–209. doi:10.1038/nature13480

Catenacci, D. V. T., Kang, Y. K., Park, H., Uronis, H. E., Lee, K. W., Ng, M. C. H., et al. (2020). Margetuximab plus pembrolizumab in patients with previously treated, HER2-positive gastro-oesophageal adenocarcinoma (CP-MGAH22-05): A single-arm, phase 1b-2 trial. *Lancet Oncol.* 21, 1066–1076. doi:10.1016/S1470-2045(20)30326-0

Dutton, S. J., Ferry, D. R., Blazeby, J. M., Abbas, H., Dahle-Smith, A., Mansoor, W., et al. (2014). Gefitinib for oesophageal cancer progressing after chemotherapy (COG): A phase 3, multicentre, double-blind, placebo-controlled randomised trial. *Lancet Oncol.* 15, 894–904. doi:10.1016/S1470-2045(14)70024-5

Fukuoka, S., Hara, H., Takahashi, N., Kojima, T., Kawazoe, A., Asayama, M., et al. (2020). Regorafenib plus nivolumab in patients with advanced gastric or colorectal cancer: An open-label, dose-escalation, and dose-expansion phase Ib trial (REGONIVO, EPOC1603). *J. Clin. Oncol.* 38, 2053–2061. doi:10.1200/JCO.19.03296

Galluzzi, L., Zitvogel, L., and Kroemer, G. (2016). Immunological mechanisms underneath the efficacy of cancer therapy. *Cancer Immunol. Res.* 4, 895–902. doi:10.1158/2326-6066.CIR-16-0197

Hegde, P. S., Karanikas, V., and Evers, S. (2016). The where, the when, and the how of immune monitoring for cancer immunotherapies in the era of checkpoint inhibition. *Clin. Cancer Res.* 22, 1865–1874. doi:10.1158/1078-0432.CCR-15-1507

Hironaka, S., Ueda, S., Yasui, H., Nishina, T., Tsuda, M., Tsumura, T., et al. (2013). Randomized, open-label, phase III study comparing irinotecan with paclitaxel in patients with advanced gastric cancer without severe peritoneal metastasis after failure of prior combination chemotherapy using fluoropyrimidine plus platinum: WJOG 4007 trial. *J. Clin. Oncol.* 31, 4438–4444. doi:10.1200/JCO.2012.48.5805

Janjigian, Y. Y., Maron, S. B., Chatila, W. K., Millang, B., Chavan, S. S., Alterman, C., et al. (2020). First-line pembrolizumab and trastuzumab in HER2-positive oesophageal, gastric, or gastro-oesophageal junction cancer: An open-label, single-arm, phase 2 trial. *Lancet Oncol.* 21, 821–831. doi:10.1016/S1470-2045(20)30169-8

Janjigian, Y. Y., Sanchez-Vega, F., Jonsson, P., Chatila, W. K., Hechtman, J. F., Ku, G. Y., et al. (2018). Genetic predictors of response to systemic therapy in esophagogastric cancer. *Cancer Discov.* 8, 49–58. doi:10.1158/2159-8290.CD-17-0787

Janjigian, Y. Y., Shitara, K., Moehler, M., Garrido, M., Salman, P., Shen, L., et al. (2021). First-line nivolumab plus chemotherapy versus chemotherapy alone for advanced gastric, gastro-oesophageal junction, and oesophageal adenocarcinoma (CheckMate 649): A randomised, open-label, phase 3 trial. *Lancet* 398, 27–40. doi:10.1016/S0140-6736(21)00797-2

Kawazoe, A., Fukuoka, S., Nakamura, Y., Kuboki, Y., Wakabayashi, M., Nomura, S., et al. (2020). Lenvatinib plus pembrolizumab in patients with advanced gastric cancer in the first-line or second-line setting (EPOC1706): An open-label, single-arm, phase 2 trial. *Lancet Oncol.* 21, 1057–1065. doi:10.1016/S1470-2045(20)30271-0

Kim, J., Fox, C., Peng, S., Pusung, M., Pectasides, E., Matthee, E., et al. (2014). Preexisting oncogenic events impact trastuzumab sensitivity in ERBB2-amplified gastroesophageal adenocarcinoma. *J. Clin. Invest.* 124, 5145–5158. doi:10.1172/JCI75200

Li, J., Qin, S., Xu, J., Xiong, J., Wu, C., Bai, Y., et al. (2016). Randomized, double-blind, placebo-controlled phase III trial of apatinib in patients with chemotherapy-refractory advanced or metastatic adenocarcinoma of the stomach or gastroesophageal junction. *J. Clin. Oncol.* 34, 1448–1454. doi:10.1200/JCO.2015.63.5995

Luo, H., Lu, J., Bai, Y., Mao, T., Wang, J., Fan, Q., et al. (2021). Effect of camrelizumab vs placebo added to chemotherapy on survival and progression-free survival in patients with advanced or metastatic esophageal squamous cell carcinoma: The ESCORT-1st randomized clinical trial. *JAMA* 326, 916–925. doi:10.1001/jama.2021.12836

Lv, H., Zhang, J., Sun, K., Nie, C., Chen, B., Wang, J., et al. (2020). Corrigendum: Expression of human epidermal Growth factor receptor-2 status and programmed cell death protein-1 ligand is associated with prognosis in gastric cancer. *Front. Oncol.* 10, 672599. doi:10.3389/fonc.2021.672599

Makiyama, A., Sukawa, Y., Kashiwada, T., Kawada, J., Hosokawa, A., Horie, Y., et al. (2020). Randomized, phase II study of trastuzumab beyond progression in patients with HER2-positive advanced gastric or gastroesophageal junction cancer: WJOG7112G (T-ACT study). *J. Clin. Oncol.* 38, 1919–1927. doi:10.1200/JCO.19.03077

Modi, S., Saura, C., Yamashita, T., Park, Y. H., Kim, S. B., Tamura, K., et al. (2020). Trastuzumab deruxtecan in previously treated HER2-positive breast cancer. *N. Engl. J. Med.* 382, 610–621. doi:10.1056/NEJMoa1914510

Montemurro, F., Delaloge, S., Barrios, C. H., WueRstlein, R., Anton, A., Brain, E., et al. (2020). Trastuzumab emtansine (T-DM1) in patients with HER2-positive metastatic breast cancer and brain metastases: Exploratory final analysis of cohort 1 from KAMILLA, a single-arm phase IIIb clinical trial. *Ann. Oncol.* 31, 1350–1358. doi:10.1016/j.annonc.2020.06.020

Nelson, R. S., Seligson, N. D., Bottiglieri, S., Carballido, E., Cueto, A. D., Imanirad, I., et al. (2021). UGT1A1 guided cancer therapy: Review of the evidence and considerations for clinical implementation. *Cancers (Basel)* 13, 1566. doi:10.3390/cancers13071566

Nie, J., Wang, C., Liu, Y., Yang, Q., Mei, Q., Dong, L., et al. (2019). Addition of low-dose decitabine to anti-PD-1 antibody camrelizumab in relapsed/refractory classical hodgkin lymphoma. *J. Clin. Oncol.* 37, 1479–1489. doi:10.1200/JCO.18.02151

Ohtsu, A., Ajani, J. A., Bai, Y. X., Bang, Y. J., Chung, H. C., Pan, H. M., et al. (2013). Everolimus for previously treated advanced gastric cancer: Results of the randomized, double-blind, phase III GRANITE-1 study. *J. Clin. Oncol.* 31, 3935–3943. doi:10.1200/JCO.2012.48.3552

Peng, Z., Wei, J., Wang, F., Ying, J., Deng, Y., Gu, K., et al. (2021). Camrelizumab combined with chemotherapy followed by camrelizumab plus apatinib as first-line therapy for advanced gastric or gastroesophageal junction adenocarcinoma. *Clin. Cancer Res.* 27, 3069–3078. doi:10.1158/1078-0432.CCR-20-4691

Qin, S., Ren, Z., Meng, Z., Chen, Z., Chai, X., Xiong, J., et al. (2020). Camrelizumab in patients with previously treated advanced hepatocellular carcinoma: A multicentre, open-label, parallel-group, randomised, phase 2 trial. *Lancet Oncol.* 21, 571–580. doi:10.1016/S1470-2045(20)30011-5

Ribas, A., and Wolchok, J. D. (2018). Cancer immunotherapy using checkpoint blockade. *Science* 359, 1350–1355. doi:10.1126/science.aar4060

Satoh, T., Xu, R. H., Chung, H. C., Sun, G. P., Doi, T., Xu, J. M., et al. (2014). Lapatinib plus paclitaxel versus paclitaxel alone in the second-line treatment of HER2-amplified advanced gastric cancer in asian populations: TyTAN--a randomized, phase III study. *J. Clin. Oncol.* 32, 2039–2049. doi:10.1200/JCO.2013.53.6136

Shitara, K., Bang, Y. J., Iwasa, S., Sugimoto, N., Ryu, M. H., Sakai, D., et al. (2020). Trastuzumab deruxtecan in previously treated HER2-positive gastric cancer. *N. Engl. J. Med.* 382, 2419–2430. doi:10.1056/NEJMoa2004413

Sun, Y. R., Chang, G. K., Minkyu, J., Hyo, S. K., Choon-Kun, L., Hei-Cheul, J., et al. (2021). *Multicenter phase Ib/II study of second-line trastuzumab, ramucirumab, and paclitaxel in patients with HER2-positive advanced gastric or*

gastroesophageal junction cancer (HER-RAM study). Alexandria, Virginia, United States: American Society of Clinical Oncology.

Thuss-Patience, P. C., Shah, M. A., Ohtsu, A., Van Cutsem, E., Ajani, J. A., Castro, H., et al. (2017). Trastuzumab emtansine versus taxane use for previously treated HER2-positive locally advanced or metastatic gastric or gastro-oesophageal junction adenocarcinoma (GATSBY): An international randomised, open-label, adaptive, phase 2/3 study. *Lancet Oncol.* 18, 640–653. doi:10.1016/S1470-2045(17)30111-0

Wilke, H., Muro, K., Van Cutsem, E., Oh, S. C., Bodoky, G., Shimada, Y., et al. (2014). Ramucirumab plus paclitaxel versus placebo plus paclitaxel in patients with previously treated advanced gastric or gastro-oesophageal junction adenocarcinoma (RAINBOW): A double-blind, randomised phase 3 trial. *Lancet Oncol.* 15, 1224–1235. doi:10.1016/S1470-2045(14)70420-6

Xu, Y., Wang, Y., Gong, J., Zhang, X., Peng, Z., Sheng, X., et al. (2021). Phase I study of the recombinant humanized anti-HER2 monoclonal antibody-MMAE conjugate RC48-ADC in patients with HER2-positive advanced solid tumors. *Gastric Cancer* 24, 913–925. doi:10.1007/s10120-021-01168-7

Zhou, C., Chen, G., Huang, Y., Zhou, J., Lin, L., Feng, J., et al. (2021). Camrelizumab plus carboplatin and pemetrexed versus chemotherapy alone in chemotherapy-naive patients with advanced non-squamous non-small-cell lung cancer (CameL): A randomised, open-label, multicentre, phase 3 trial. *Lancet Respir. Med.* 9, 305–314. doi:10.1016/S2213-2600(20)30365-9

frontiers | Frontiers in Pharmacology

TYPE Original Research
PUBLISHED 18 January 2023
DOI 10.3389/fphar.2023.1081612

OPEN ACCESS

EDITED BY
Eswar Shankar,
The Ohio State University, United States

REVIEWED BY
Wei Shao,
Westlake University, China
Vaibhav Singh,
Case Western Reserve University,
United States

*CORRESPONDENCE
Lianhui Wang,
iamlhwang@njupt.edu.cn
Yufu Zhu,
fugle99@126.com
Hengzhu Zhang,
zhanghengzhu@sina.com

SPECIALTY SECTION
This article was submitted to Pharmacology of Anti-Cancer Drugs, a section of the journal Frontiers in Pharmacology

RECEIVED 27 October 2022
ACCEPTED 03 January 2023
PUBLISHED 18 January 2023

CITATION
Wu H, Zhang T, Liu Q, Wei M, Li Y, Ma Q, Wang L, Zhu Y and Zhang H (2023), Polydopamine-based loaded temozolomide nanoparticles conjugated by peptide-1 for glioblastoma chemotherapy and photothermal therapy. *Front. Pharmacol.* 14:1081612. doi: 10.3389/fphar.2023.1081612

Polydopamine-based loaded temozolomide nanoparticles conjugated by peptide-1 for glioblastoma chemotherapy and photothermal therapy

Hao Wu[1,2], Tianyi Zhang[3], Qi Liu[4], Min Wei[1,2], Yuping Li[2], Qiang Ma[2], Lianhui Wang[5]*, Yufu Zhu[6]* and Hengzhu Zhang[2]*

[1]Graduate School of Dalian Medical University, Dalian, China, [2]Department of Neurosurgery, Clinical Medical College, Yangzhou University, Yangzhou, China, [3]Nanjing University, Nanjing, China, [4]Department of Neurosurgery, The First Hospital of Yu Lin, Yulin, China, [5]Institute of Advanced Materials, Nanjing University of Posts and Telecommunications, Nanjing, China, [6]Department of Neurosurgery, The Affiliated Hospital of Xuzhou Medical University, Xuzhou, China

Purpose: Nanoparticles (NPs) of the polydopamine (PDA)-based,loaded with temozolomide (TMZ) and conjugated with Pep-1 (Peptide-1) as a feasible nano-drug delivery system were constructed and utilized for chemotherapy (CT) and photothermal therapy (PTT) of glioblastoma (GBM).

Method: PDA NPs were synthesized from dopamine (DA) hydrochloride and reacted with TMZ to obtain the PDA-TMZ NPs and then the PDA NPs and the PDA-TMZ NPs were conjugated and modified by Pep-1 to obtain the Pep-1@PDA NPs and Pep-1@PDA-TMZ NPs *via* the Schiff base reaction (SBR), respectively.Their dimensions, charge, and shape were characterized by dynamic light scattering (DLS) and scanning electron microscope (SEM). The assembly of TMZ was verified by Fourier-transform infrared spectroscopy (FT-IR) and ultraviolet and visible spectroscopy (UV-Vis). The biostability of both the nanocarrier and the synthetic NPs were validated using water and fetal bovine serum (FBS). The antitumor activities of the PDA-TMZ NPs and Pep-1@PDA-TMZ NPs were verified in U87 cells and tumor-bearing nude mice.

Results: The prepared PDA NPs, PDA-TMZ NPs, Pep-1@PDA NPs, and Pep-1@PDA-TMZ NPs were regular and spherical, with dimension of approximately 122, 131, 136, and 140 nm, respectively. The synthetic nanoparticles possessed good dispersity, stability,solubility, and biocompatibility. No obvious toxic side effects were observed, and the loading rate of TMZ was approximately 50%.*In vitro* research indicated that the inhibition ratio of the Pep-1@PDA-TMZ NPs combined with 808 nm laser was approximately 94% for U87 cells and *in vivo* research was approximately 77.13%, which was higher than the ratio of the other groups ($p < 0.05$).

Abbreviations: CBTRUS, central Brain Tumour Registry of the United States; CT, chemotherapy; DA, dopamine; DCC, N,N′dicyclohexylcarbodiimide; DLS, dynamic Light Scattering; DMAP, 4-dimethylaminopyridine; DMF, N,N-dimethylformamide; EE, encapsulation efficiency; EPR, enhanced permeability and retention; FBS, fetal bovine serum; GBM, glioblastoma multiforme; GSCs, glioma stem cells; H&E, hematoxylin andeosin; IL-13Rα2, interleukin-13 receptor α2; LR, loading rate; MGMT, O6-methylguanine-DNA methyltransferase; NIR, near-infrared; NPs, nanoparticles; PDA, polydopamine; PEG, polyethylene glycol; Pep-1, peptide-1; PTT, photothermal; SEM, scanning Electron Microscope; TEM, transmission Electron Microscope; TMZ, temozolomide; UV-Vis, ultraviolet-visible.

Conclusion: Pep-1 was conjugated and modified to PDA-TMZ NPs, which can serve as a new targeted drug nano-delivery system and can offer a CT and PTT integration therapy against GBM. Thus, Pep-1@PDA-TMZ NPs could be a feasible approach for efficient GBM therapy, and further provide some evidence and data for clinical transformation so that gradually conquer GBM.

KEYWORDS

temozolomide, polydopamine, PEP-1, glioblastoma, nanoparticles, chemo/photothermal therapy

1 Introduction

In clinical practice, GBM is the most common malignancy in the brain. GBM originates from glioma cells (Ostrom et al., 2020). Unfortunately, it is the survival rate of 5-years is only 23.5% (Ostrom et al., 2020). Currently, postoperative radiotherapy (RT) and CT are the conventional GBM treatment programs (Batash et al., 2017; Glaser et al., 2017). However, identifying which radiotherapy-based approach combined with chemotherapy are effective is a challenge due to GBM specificity, including diverse sites, histological types, and heterogeneity (Pearson and Regad, 2017). Postoperative CT, which can inhibit GBM recurrence, is often used to manage glioma, and these approaches directly affect the survival prognoses of the patients; TMZ, a clinical first-line chemotherapy drug for GBM treatment, has significant antitumor activity by inducing apoptosis to destroy glioma cells (Wang Y. et al., 2021). However, the dissolvability and stability of TMZ is relatively poorer in water and its half-life is only approximately 1.8 h. Moreover, TMZ can be instantly eliminated from *in vivo* circulation (Saenz del Burgo et al., 2014). TMZ also has some deficiencies, including inferior tumor targeting, considerable toxicities or adverse effects, drug resistance *via* DNA repair, and the regulation of several signaling pathways. The therapeutic effect of GBM remains unsatisfactory, even though timely operation and postoperative CT (Yu et al., 2022). GBM remains a challenging and valuable research topic. Basic researches and clinical trials exploring the RT and CT of postoperative GBM have paid closer and higher attention to the types of diverse nano-delivery system in recent years, because nano-delivery system can enhance the targeting ability of TMZ, even trigger and control the release of TMZ, and augment its biological half-life period to inhibit its degradation in the acidic environment of the tumor (Nie et al., 2019; Wang L. et al., 2021). The super-strong adhesion, better photothermal conversion and good biocompatibility of PDA, and its capacity to promote the molecular biology characteristics and upgrade bioavailability, supports the use of PDA with TMZ to improve delivery (Bi et al., 2018). Meanwhile, the PTT of PDA is beneficial for enhanced tumor therapy due to the synergistic effect, especially some multi-mode therapeutics such as the photodynamic therapy (PDT) combined with the PTT can convert molecular oxygen (O_2) into cytotoxic reactive oxygen species (ROS) to destroy tumor cells. (Shao et al., 2020). More, Pep-1, a specific IL-13Ra2 ligand, was proved to improve the ability of traversing the blood brain barrier (BBB) and cytomembrane and targeted to GBM. Pep-1 can carry efficiently nanoparticles to traverse the BBB and enter into the nucleus (Wang et al., 2019).

In this study, we designed a covalent self-assembly strategy by introducing dynamic Schiff base bonds (Sbb C=N) into the PDA NPs The formation of Sbb C=N occurred between the PDA amine group and the carbonyl groups of Pep-1 and TMZ *via* cross-linking during the SBR. Sbb C=N endowed the PDA-based NPs with pH-dependent degradation properties. After encapsulating TMZ, the versatile drug nano-delivery system Pep-1@PDA-TMZ NPs displayed that Pep-1 can be utilized as the promising accelerator entering tumor cells and the PDA NPs were the transport carrier; the system also demonstrated that pH-smart, responsive drug release is possible in the acidic tumor microenvironment (TEM) (Figure 1). The combination of carrier and drug can achieve the effects of synergistic antitumor by delivering CT and PTT. Pep-1@PDA-TMZ NPs with good biodegradability, pH-responsive drug release, and synergistic therapy are promising approach for optimizing the therapeutic efficacy of GBM (Zhang et al., 2015) (Figure 2).

2 Material and methods

2.1 Materials

Dopamine hydrochloride, Temozolomide,Temozolomide acid, Coumarin-6 and 2.5% Isoflurane were purchased from Sigma-Aldrich (St.Louis, United States). NH_2-PEG-NH_2 Amine, Tris-HCl,*N,N*-dimethylformamide (DMF), *N,N′*-dicyclohexylcar-bodiimide, 4-dimethylaminopyridine and Pep-1 were purchased from Nanjing Peptide Biotech Co., Ltd. All chemicals in cell experiments were purchased from Keygen Biotech Co., Ltd. (Nanjing, China).

2.2 Instruments and characterization

Ultraviolet and Visible Spectroscopy (UV-Vis) was conducted using a UV-3600 spectrophotometer (Shimadzu, Japan). Fourier-transform infrared spectroscopy (FT-IR) was performed and recorded on a Shimadzu IR Prestige-21 spectrometer by dispersing the sample in a KBr press. An EVO18 Scanning electron microscope (SEM) was utilized to obtain images, and the size of NPs was tested by using a Zeta PALS. The confocal laser scanning microscope (CLSM) images were attained using an FV1000 (Olympus, Japan). A Fotric 225 photothermal camera was utilized to record the temperature and capture images.

2.3 Cell lines and animals information

2.3.1 Cell lines information

U87 cells were purchased from Nanjing Key gen Co., Ltd. The complete medium was 90% DMEM with 10% FBS; they were grown in an incubator at 37°C and 5% CO_2 with saturated humidity. U87 cells were incubated for 24 h, followed by replacing the old culture with a medium containing different concentrations of the PDA NPs, PDA-TMZ NPs, Pep-1@PDA NPs, and Pep-1@PDA-TMZ NPs (200 μg/mL each) for a further 6 h incubation.

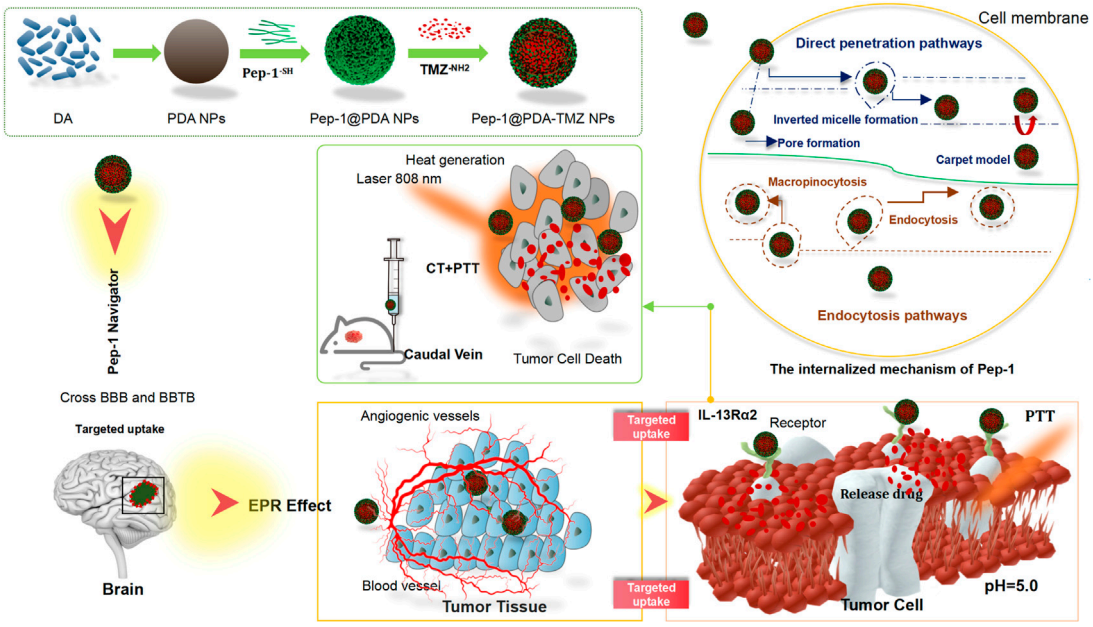

FIGURE 1
Graphical demonstration to display the synthesis of the Pep-1@PDA-TMZ NPs and the chemotherapy and photothermal therapy of Pep-1@PDA-TMZ NPs for glioblastoma.

2.3.2 Animal information

BALB/c nude mice were purchased from Shanghai Experimental Animal Co., Ltd. The Laboratory Animal Use License was SYXK (Su) 2017-0040. Mice were 4 weeks old and male, and five animals were assigned to each group. Eight groups were formed, requiring a total of 40 animals.

2.3.3 Ethics statement

Studies involving animal participants were reviewed and approved by the Experimental Animal Welfare Ethics Committee of Nanjing Ramda Pharmaceutical Co., Ltd. (No. IACUC-20220502).

2.4 Methods

2.4.1 Synthesis of PDA NPs

DA (2 mg) was mixed in Tris-HCl (10 ml, 10 mM, pH 8.5) and stirred at room temperature using a magnetic stirring apparatus (500 rpm) for 8 h. Subsequently, the mixture was centrifuged at 12,000 rpm for 20 min using a centrifugal machine, washed several times with deionized water, then centrifuged at 12,000 rpm for 20 min, finally removed from the supernatant liquid, and the PDA NPs were collected.

2.4.2 PDA-TMZ NPs synthesis

Because the metabolite of TMZ is Temozolomide acid *in vivo,* they have the identical cytotoxicity and antitumor effects. We selected Temozolomide acid to replace TMZ. Temozolomide acid (3 mg),NH_2-PEG-NH_2 Amine, (10 mg), and *N,N′*-dicyclohexylcar-bodiimide (2 mg) were mixed in anhydrous *N,N*-dimethylformamide (DMF, 1 mL).4-dimethylaminopyridine (2 mg) was then added, the mixture was reacted in an N_2 atmosphere, and was stirred for 24 h at room temperature, and TMZ-PEG-NH_2 was obtained. Next, TMZ-PEG-NH_2 (3 mg) and PDA NPs (10 mg) were dissolved into the aqueous solution with vigorous stirring at room temperature. The mixture was then emulsified by ultrasonication for 10 min. Subsequently, the mixture was centrifuged at 14,000 rpm for 20 min and was washed thrice with water then continued to centrifuged at 14,000 rpm for 20 min to remove supernatant liquid and collect the PDA-TMZ NPs.

2.4.3 Pep-1@PDA NPs synthesis

By adopting the above mentioned methods,Pep-1 (3 mg) was reacted with PDA NPs (10 mg) at 26°C to collect the Pep-1@PDA NPs.

2.4.4 Pep-1@PDA-TMZ NPs synthesis

By adopting the above mentioned methods,Pep-1 (3 mg) and the PDA-TMZ NPs (10 mg) were mixed with an aqueous solution with vigorous stirring at 26°C to collect the Pep-1@PDA-TMZ NPs. Thereafter, FT-IR and UV-Vis were used for analyzing and characterizing.

2.4.5 LR and EE of Pep-1@PDA-TMZ NPs

The loading rates (LR) and encapsulation efficiency (EE) of Pep-1@PDA-TMZ NPs were calculated by using UV-Vis. The different concentrations of TMZ (4,6,8,10, and 16 μg/mL) were prepared, and the standard curve of TMZ was drawn with DMF as the control to obtain the linear regression equation. The LR and EE were calculated using the following formula (Liu et al., 2013).

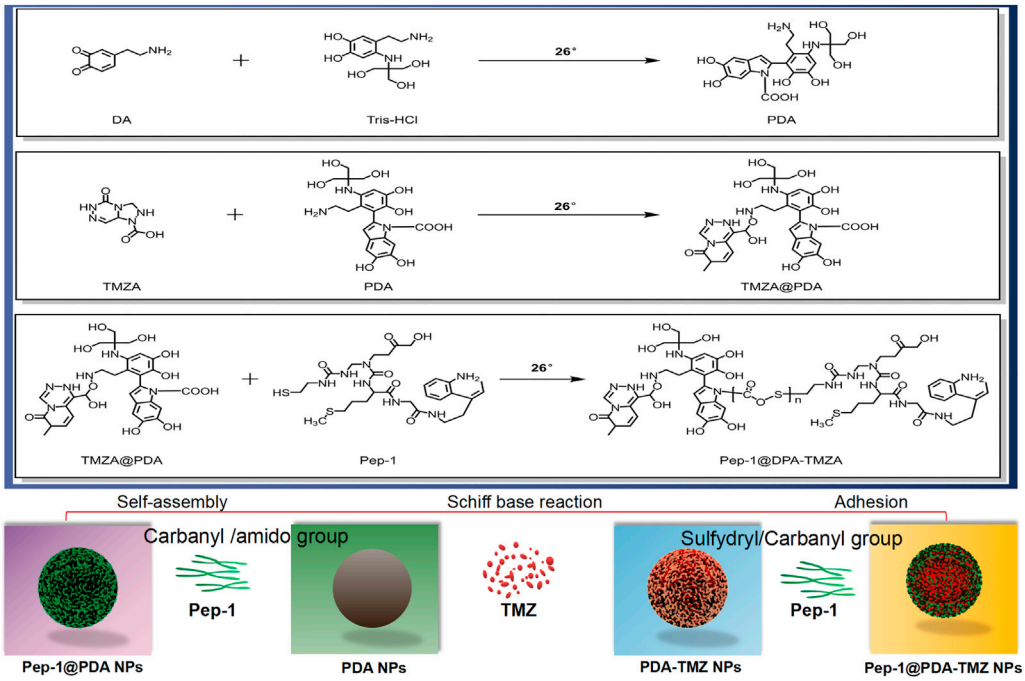

FIGURE 2
The features of the different NPs.

$$LR(\%) = \frac{W0 - Wf}{W0} \times 100\%$$

$$EE(\%) = \frac{W0 - Wf}{Ws} \times 100\%$$

where W_0 represents the weight of the original TMZ,W_f represents the free TMZ, and Ws represents the weight of the complex after lyophilization.

2.4.6 Biostability of NPs

To evaluate the stability of PDA NPs,PDA-TMZ NPs,Pep-1@PDA NPs, and Pep-1@PDA-TMZ NPs, we measured the potential of PDA NPs and Pep-1@PDA NPs by DLS. Meanwhile, water and 100% FBS were used to dissolve PDA NPs and Pep-1@PDA NPs. After 7 days, the transparency and clarification of PDA NPs and Pep-1@PDA NPs were verified respectively.

2.4.7 pH-dependent release of TMZ

We added PDA-TMZ NPs and Pep-1@PDA-TMZ NPs in pH 5.0,4.0, and 7.4 PBS and then in succession shook at 25 °C respectively. The old PBS solution was replaced with a fresh one every 2 h, and the bulk volume of the solution remained unchanged. The supernatant liquid was tested by using UV-Vis. The typical absorption values of TMZ were utilized to draw the cumulative release graph of TMZ. The following formula was utilized to calculate the cumulative release rate (CRR) (Mei et al., 2020):

$$CRR(\%) = \frac{\text{Total release mass of TMZ}}{\text{Total mass TMZ loaded in Pep} - 1@PDA - TMZ\ NPs\ (PDA - TMZ\ NPs)} \times 100\%$$

2.4.8 Analysis of PTT conversion rate

To study the photothermal conversion efficiency of PDA NPs, PDA-TMZ NPs, Pep-1@PDA NPs, and Pep-1@PDA-TMZ NPs, the temperature variations of PDA NPs, PDA-TMZ NPs, Pep-1@PDA NPs, and Pep-1@PDA-TMZ NPs at different concentrations (set as 50, 100, 150, 200, and 250 μg/mL) were recorded under with 808 nm laser irritation. Furthermore, the temperature was recorded at different time points (set as 0, 1, 2, 3, 4, 5, 6, 7, 8, 9, and 10 min) *via* infrared thermography, for which water was set as the control group. The photothermal conversion efficiency (η) of the nanoparticles were calculated, according to reported method (Zhang et al., 2017).

2.4.9 Endocytosis analysis of NPs

Human malignant glioma U87 cell lines were used to observe the cellular uptake of PDA-TMZ NPs and Pep-1@PDA-TMZ NPs using CLSM. The U87 cells were seeded into a 96-well plate at a density of 5×10^4 cells per well, after 24 h incubation, U87 cells were incubated with PDA NPs, PDA-TMZ NPs, Pep-1@PDA NPs, and Pep-1@PDA-TMZ NPs at identical concentrations at 37°C for 1 h. To investigate the influences of incubation at different time points on U87 cellar uptake, U87 cells were incubated with the PDA-TMZ NPs and Pep-1@PDA-TMZ NPs (200 μg/mL) for 0.5, 1, 2, 4, 6, 8, 10, and 12 h at 37°C, respectively. The 96-well plates were stained with CCK-8 for 6 h. Finally, the cellular uptake dynamic behavior and outcome of PDA NPs, PDA-TMZ NPs, Pep-1@PDA NPs, and Pep-1@PDA-TMZ NPs were surveyed *via* CLSM.

2.4.10 Cytotoxicity evaluation of NPs

U87 cells plated in a 96-well plates with a density of 1×10^4 cells per well were incubated with the different concentrations (50, 100, 150, 200, and 250 μg/mL) of PDA NPs, PDA-TMZ NPs, Pep-1@PDA NPs, and Pep-1@PDA-TMZ NPs for 24 h. Subsequently, the experimental group was irradiated with the 808 nm laser (1 W/cm^2) for 10 min, and the control group without irradiation. Then

use CCK-8 to incubate for 6 h and then test cell viability. Optical density values were measured using a microplate reader to obtain cell viability data. For cytotoxicity experiments by CLSM U87 cells were seeded in confocal dishes and incubated for 24 h, and the control group without irradiation, followed by replacing the old culture with a medium containing different concentrations of PDA NPs, PDA-TMZ NPs, Pep-1@PDA NPs, and Pep-1@PDA-TMZ NPs (250 μg/mL each) for a further 6 h incubation. After 808 nm (1 W/cm^2) laser irradiation for 10 min, staining was performed using 10 μL PI (1 mg/mL) and 10 μL of Calcein-AM (20 μg/mL) for 20 min. The CLSM images were obtained *via* Hoechst 33342.

2.4.11 *In vivo* evaluation of live anticancer performance in mice

2.4.11.1 Construction of the tumor nude mouse model

U87 cell were collected at 5 × 10^7/mL density. By subcutaneous inoculation, 0.1 ml was implanted in the right axilla of each mouse, and the experiments were performed when the tumor volume of all mice were grown for 3 weeks.

2.4.11.2 Anesthesia time and method

When the tumor volume of all mice grew to approximately 80 mm^3, the anesthesia method was inhalation, and the narcotic drug was 2.5% isoflurane.

2.4.11.3 Therapeutic schedule

When the tumor volume in each of the 40 mice grew to approximately 80 mm^3, the tumor-bearing nude mice were freely divided into eight groups, and each had five tumor-bearing nude mice, then respectively injected *via* the caudal vein with 150 μl of saline, Pep-1@PDA NPs, PDA-TMZ NPs, and Pep-1@PDA-TMZ NPs 12 h later, the tumor site of corresponding groups were exposed to 808 nm laser for 10 min (1 W/cm^2). The concentration of coumarin-6, TMZ, PDA, and Pep-1 were 200 200, 200, and 100 μg/mL, respectively.When all trials were completed, the nude mice were killed by euthanasia with carbon dioxide. The tumor slices of mice treated with saline, Pep-1@PDA NPs, PDA-TMZ NPs, and Pep-1@PDA-TMZ NPs at 24 h after irradiation were stained with hematoxylin and eosin (H&E), moreover, the H&E images of major organs were obtained after 14 days of treatment.

2.4.11.4 Observational indicators

To collect the experimental data, the day of drug injection was recorded as day 0. The body weight and tumor volume (TV) of each mouse were measured every second day. TV was calculated using the following equation.

$$\mathbf{TV} = \times \mathbf{a} \times \mathbf{b}^2$$

where **a** and **b** represent the long and short diameters (in mm),respectively.

The relative tumor volume (RTV) were calculated using the following formula:

$$\mathbf{RTV} = \mathbf{V_t}/\mathbf{V_0}$$

where V_0 is the TV, as calculated by separate-cage administration, and V_t is the TV, as calculated at each measurement.

The tumor growth inhibition rate was calculated as follows:

$$\text{Inhibition rate}(\%) = \frac{\text{Mean tumor weight of the control group} - \text{Mean tumor weight of the treatment group}}{\text{Meant tumor weight of the control group}} \times 100\%$$

Pathological sections of tumor tissue, H&E staining, and routine blood examination were utilized to verify the safety of NPs.

2.4.11.5 Statistical analysis

All experimental results were expressed as mean ± standard deviation and one-way ANOVA was conducted using GraphPad Prism software (version 6.0; GraphPad, San Diego, CA, United States), and statistical significance was considered at a p-value <0.05.

3 Results

3.1 Morphological characterization of NPs

The shape of PDA NPs, PDA-TMZ NPs, Pep-1@PDA NPs, and Pep-1@PDA-TMZ NPs were regular and spherical, and the characterization analysis of DLS and SEM indicated that the dimensions of the above NPs were approximately 120, 125, 135, and 140 nm, respectively, with well-proportioned dimensions and smooth surfaces that could be lightly traverse and could attach to the tumor location *via* the enhanced permeability and retention (EPR) effect (Zheng et al., 2020). The Pep-1@PDA-TMZ NPs dimensions gradually increased, indicating that TMZ and Pep-1 were successfully loaded (Figure 3).

3.2 Assembly analysis of Pep-1@PDA-TMZ NPs

The chemical composition of the Pep-1@PDA-TMZ NPs was analyzed by UV-Vis and FT-IR. The FT-IR of Pep-1@PDA-TMZ NPs possessed new peak value at 1626, 3421, and 2,912 cm^{-1}, which conformed to Pep-1 and TMZ. Above relatively typical peaks value indicated that Pep-1 and TMZ had been successfully conjugated to the PDA NPs (Supplementary Figure S1A). Moreover, the peak value of TMZ (1,699 cm^{-1}) and that of Pep-1 (1,683 cm^{-1}) merged into a single peak at 1,626 cm^{-1}, signifying the formation of the Sbb (C = N). Furthermore, the UV-Vis spectrum verified the typical peak value of TMZ at 329 nm, Pep-1 at 229 nm, and PDA at 285 nm. Meanwhile, Pep-1@PDA-TMZ NPs demonstrated relatively broader absorption at 329 nm (Supplementary Figure S1B). Therefore, the assembly of the carbonyl group of Pep-1and TMZ with the PDA amino group formed Sbb (C=N). Therefore, we speculated that the SBR have formed.

3.3 Stability of the Pep-1@PDA NPs

The stability of NPs are of significance for antitumor treatment. The zeta potential of PDA NPs,PDA-TMZ NPs, Pep-1@PDA NPs and Pep-1@PDA-TMZ NPs was approximately −22.4, −34.6, −32.7, and −25 mV, respectively (Figure 4), which can ensure these PDA NPs, PDA-TMZ NPs, Pep-1@PDA NPs, and Pep-1@PDA-TMZ NPs should not be eliminated easily in the body circulation. Afterwards, PDA NPs and Pep-1@PDA NPs were dissolved in water and FBS to carefully observe their dissolution. After 7 days, the solutions maintained a homogeneous brightness. Thereby, the

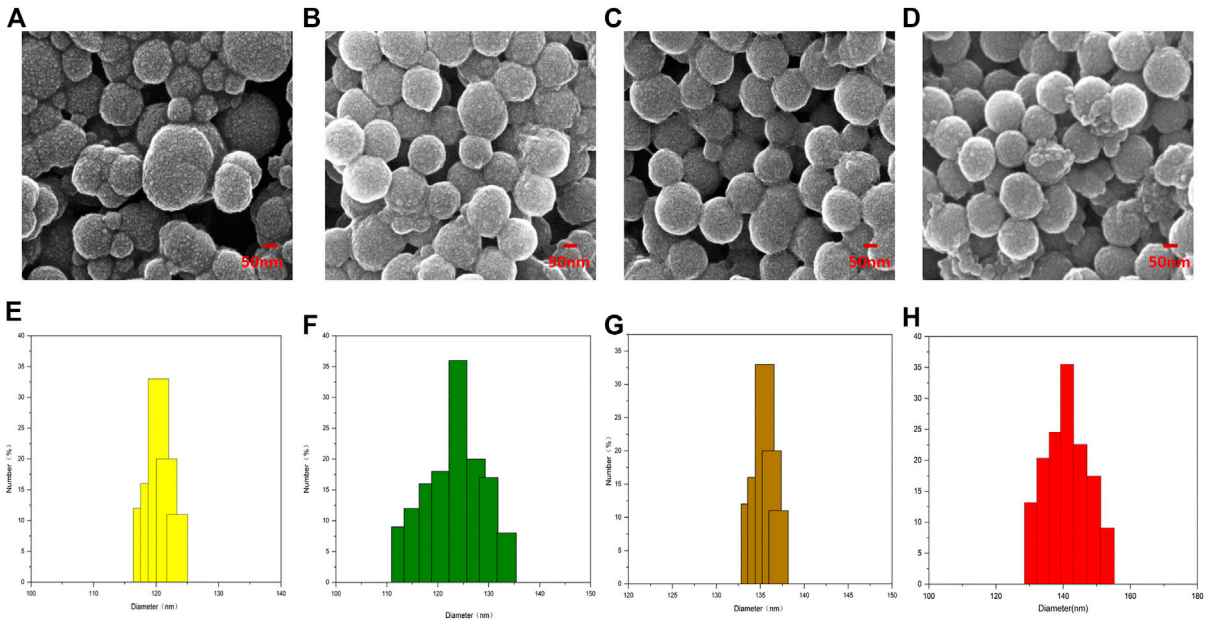

FIGURE 3
The Characterization of different NPs: **(A–D)** SEM **(E–H)**; The size and distribution of different NPs.

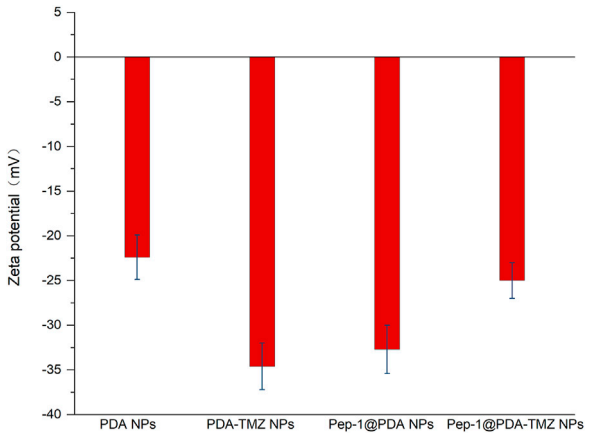

FIGURE 4
The zeta potential of the different NPs.

results proved that the solubility and stability of PDA NPs and Pep-1@PDA NPs were relatively good (Supplementary Figure S2).

3.4 Encapsulation and release of TMZ

To calculate the LR and EE of PDA-TMZ NPs and Pep-1@PDA-TMZ NPs, TMZ (10 μg/mL) was dissolved to DMF and analyzed by UV-Vis spectroscopy, which denoted that the standard absorption peak value of TMZ occurred at approximately 329 nm (Supplementary Figure S3A), and this peak value can be utilized to calculate the content of TMZ. Supplementary Figure S3B presented the absorbance of different concentrations of TMZ. The EE and LR of PDA-TMZ NPs and Pep-1@PDA-TMZ NPs were approximately 48.5% and 10.3%, 50%, and 10.40%, respectively.

The trials verified that the Sbb C = N of PDA-TMZ NPs and Pep-1@PDA-TMZ NPs can be break, to cause the release of TMZ in certain acidic environments. To prove pH-dependent respond release of PDA-TMZ NPs and Pep-1@PDA-TMZ NPs loaded with TMZ, pH = 7.4, 5.0, and 4.0 were utilized to simulate the normal physiological condition and acidic TME. When pH = 7.4, the total cumulative release rate (CRR) of TMZ of PDA-TMZ NPs and Pep-1@PDA-TMZ NPs over 24 h was approximately 25.5% and 32%, and when pH = 5.0, CRR was approximately 52.4% and 56.1%. However, interestingly, when pH = 4.0, CRR reached approximately 57% and 57.3% (Figure 5A). Therefore, PDA-TMZ NPs and Pep-1@PDA-TMZ NPs can cause more Sbb C=N breakage under the acidic TME. PDA-TMZ NPs and Pep-1@PDA-TMZ NPs have lower adverse effects on normal cells and are safe, trustworthy, and efficient in antitumor activity.

To investigate whether PTT therapy in the acidic environment has a good impact on TMZ release from PDA-TMZ NPs and Pep-1@PDA-TMZ NPs.The results proved that the release rate of TMZ can be enhanced considerably to about 65.9% and 66.1% *via* 808 nm laser irradiation (Figure 5B). Hence, the, PTT effect of PDA-TMZ NPs and Pep-1@PDA-TMZ NPs could cause the dissociation of more Sbb C=N and accelerate the release of TMZ The PDA-TMZ NPs and Pep-1@PDA-TMZ NPs can serve as nano-drug delivery systems against GBM and should be good pH-responsive drug-release nanocarriers.

3.5 PTT conversion rate of NPs

After 10 min of 808 nm laser irradiation, the PTT was assessed, and the temperature variation at different the PDA-TMZ NPs and Pep-1@PDA-TMZ NPs concentrations were tested using thermography. The temperature of the PDA-TMZ NPs and Pep-1@PDA-TMZ NPs solution rose from 33.7°C to 73.8°C, and 33°C–72.6°C (Figure 6). But, regrettably, the temperature of the PDA-TMZ NPs and Pep-1@PDA-TMZ

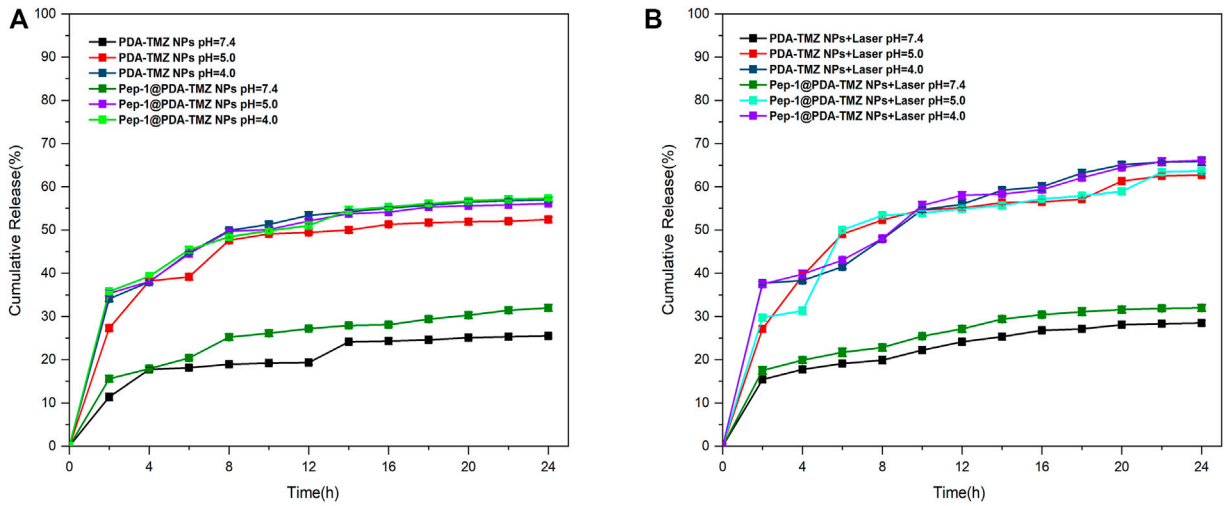

FIGURE 5
(A) TMZ release curve of the PDA-TMZ NPs in different pH values of PBS. **(B)** TMZ release curve of the Pep-1@PDA-TMZ NPs with 808 nm laser irradiation in different pH values of PBS.

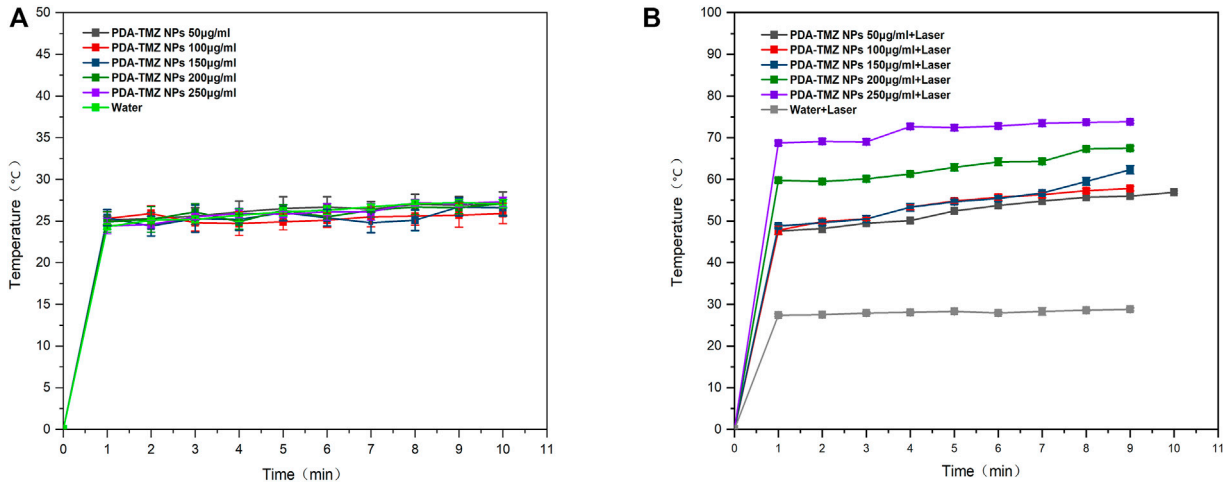

FIGURE 6
(A) The temperature variation of the PDA-TMZ NPs (different concentrations). **(B)** The temperature variation of PDA-TMZ NPs (different concentrations with laser).

NPs almost did not change without laser irradiation, and almost close to room temperature (Figure 7). Therefore, the PDA-TMZ NPs and Pep-1@PDA-TMZ NPs exhibited relatively better PTT effects. The photothermal conversion efficiency of the Pep-1@PDA NPs was further calculated to be 49.2%, according to previous reported method (Supplementary Figure S4) (Zhang et al., 2017).

3.6 Endocytosis analysis

The endocytosis of PDA-TMZ NPs and Pep-1@PDA-TMZ NPs was explored. PDA-TMZ NPs and Pep-1@PDA-TMZ NPs in U87 cells were evaluated by using CLSM (Figure 8). The cells were stained and showed blue fluorescence. The drug-loaded NPs displayed green fluorescence after entering U87 cells. After co-incubation for 6 h with U87 cells, Pep-1@PDA-TMZ NPs were successfully endocytosed into the nucleus of U87 cells. However, the PDA-TMZ NPs failed to endocytose into nucleus of U87 cells, but they only stayed around the cytoplasm. Thus, the PDA-based NPs modified with Pep-1 had a strong affinity and penetrating power in U87 cells and could enhance the effectiveness of antitumor therapy by carrying chemotherapy drugs. Therefore, the Pep-1@PDA-TMZ NPs have wide potential for tumor-targeted therapy.

3.7 Cytotoxicity evaluation

After incubation for 6 h, CCK-8 was used for analyzying NPs activity in cells. The associated cytotoxicity of PDA NPs, PDA-TMZ NPs, Pep-1@PDA NPs, and Pep-1@PDA-TMZ NPs to U87 cells were

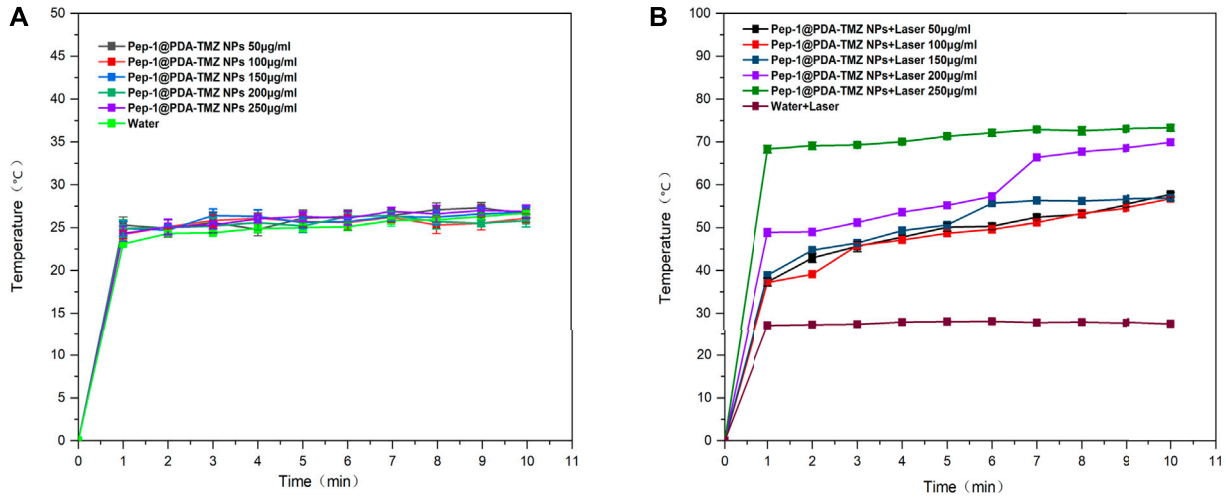

FIGURE 7
(A) The temperature of the Pep-1@PDA-TMZ NPs (different concentrations). **(B)** The temperature of the Pep-1@PDA-TMZ NPs (different concentrations with laser).

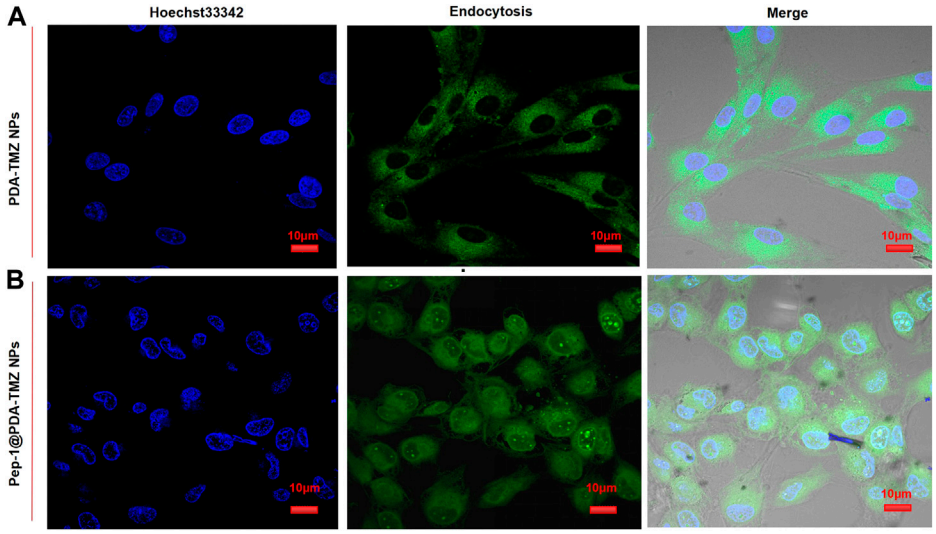

FIGURE 8
(A) The PDA-TMZ NPs gathered in the cytoplasm of U87 cells. **(B)** The Pep-1@PDA-TMZ NPs were endocytosed by the nucleus of U87 cells (green fluorescence).

tested. As revealed in Supplementary Figure S5, the PDA NPs and Pep-1@PDA NPs had slight impact on the activity of U87 cells. Above results further indicated that the particles possessed good biocompatibility and had no obvious toxicities or adverse effects. U87 cells with at different concentrations of PDA-TMZ NPs and Pep-1@PDA-TMZ NPs were incubated for 6 h. The experimental group was irradiated with an 808 nm laser for 10 min, while the control group was not irradiated. Post treatment, the result proved that the inhibition rate of the experimental groups were more prominent than the control groups, hence proving the associated antitumor effect of CT and PTT. Furthermore, cytotoxicity to cancer cells was obviously augmented with increasing the dosage of TMZ, which demonstrated dosage positive correlation. When the dosage of the PDA-TMZ NPs and Pep-1@PDA-TMZ NPs were increased to 300 μg/mL and were associated with PTT therapy, the inhibition rates in U87 cells were approximately 80% and 94%, respectively (Figures 9A, B). The therapeutic effects of the Pep-1@PDA-TMZ NPs were relatively better than those of the PDA-TMZ NPs after co-incubation with U87 cells for 6 h. Thus, the PDA-TMZ NPs conjugated by Pep-1 were more prominent against malignant GBM cells and could further promote the effect and activity of antitumor.

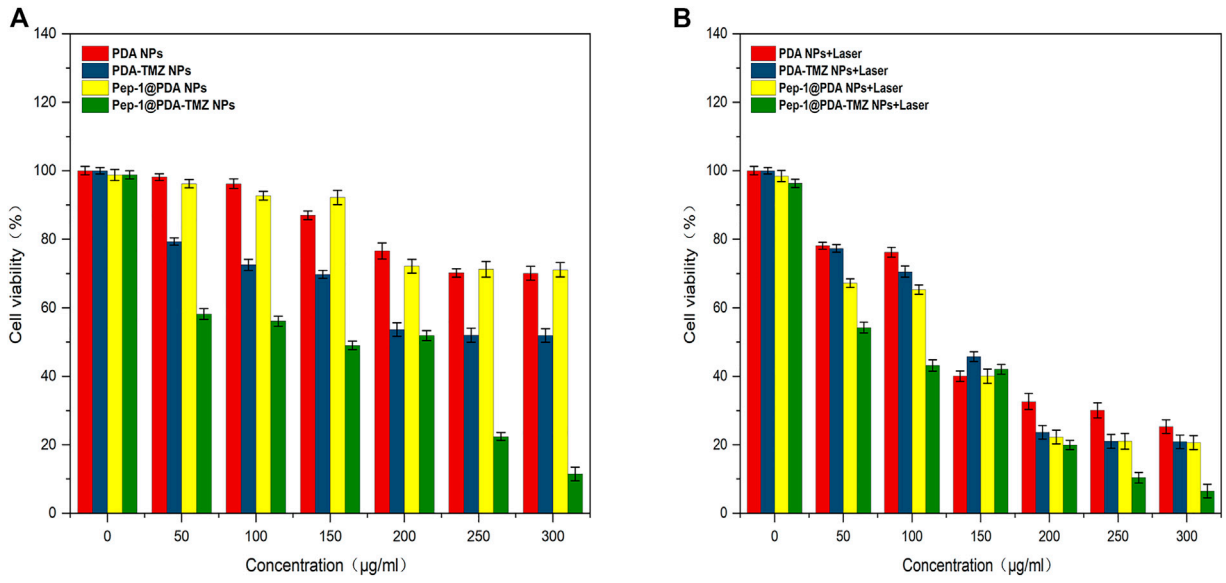

FIGURE 9
(A) The inhibition rate of the different NPs (without Laser). **(B)** The inhibition rate of the different NPs (with laser).

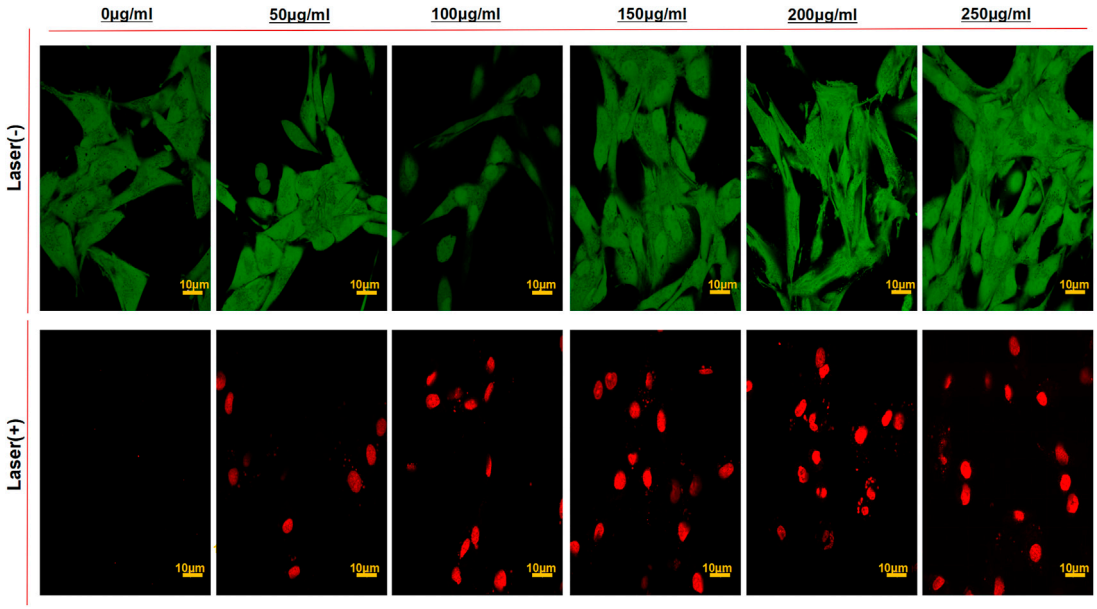

FIGURE 10
The CLSM images of U87 cells stained with Calcein-AM/PI to visualize cell viabilities treated by the PDA-TMZ NPs and Pep-1@PDA-TMZ NPs with or without 808 nm laser (Green:live; Red:death).

To further inspect the antitumor activity of Pep-1@PDA-TMZ NPs *in vitro*, the viability of U87 cells (staining of live dead cells) was assessed using CLSM (Figure 10). After U87 cells incubated with the different dosage of the Pep-1@PDA-TMZ NPs combined with 808 nm laser irradiation indicated the survival rates of U87 cells markedly reduced than without irradiation. Thus, the Pep-1@PDA-TMZ NPs presented stronger CT and PTT, which offer more confidences and evidences to us in the subsequent *in vivo* trials.

3.8 *In vivo* anticancer effect of Pep-1@PDA-TMZ NPs

In consideration of the antitumor therapeutic effect of Pep-1@PDA-TMZ NPs was relatively satisfying *in vitro*, the antitumor effect of an integration therapy of CT and PTT of the Pep-1@PDA-TMZ NPs was verified utilizing U87 cells in tumor-bearing nude mice *in vivo*. When the mice TV increased to approximately 80 mm^3, Pep-1@PDA-TMZ NPs

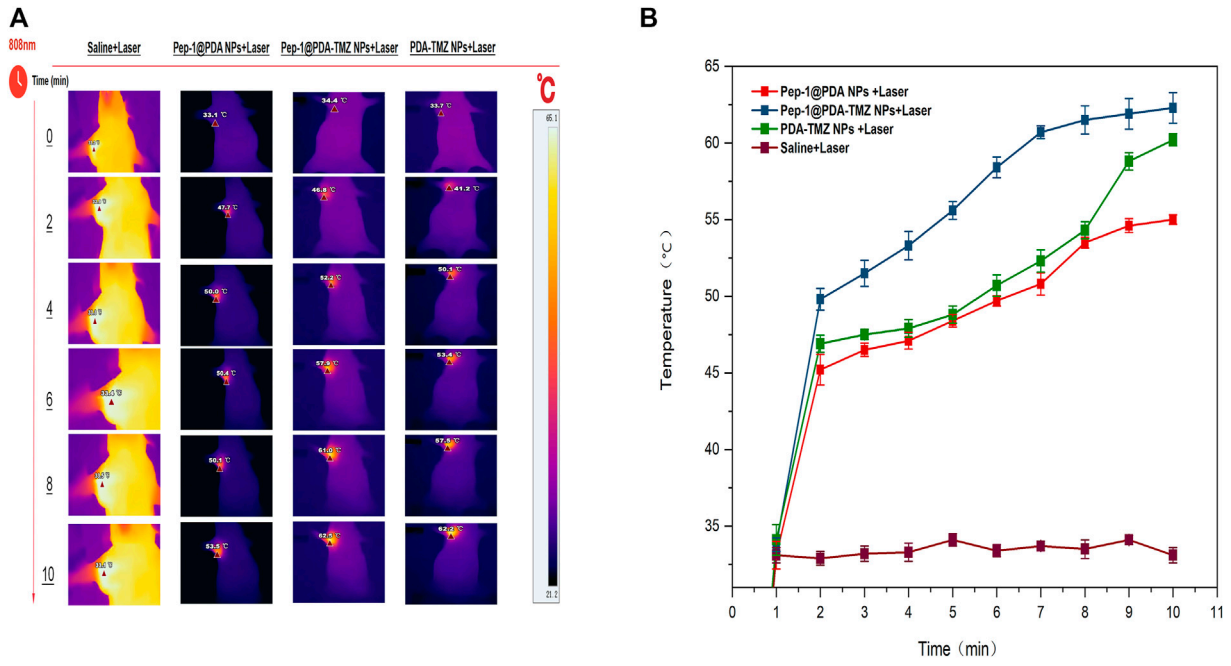

FIGURE 11
(A) The thermal images and **(B)** temperature rise curves of tumor sites in tumor-bearing nude mice within 10 min post laser irradiation.

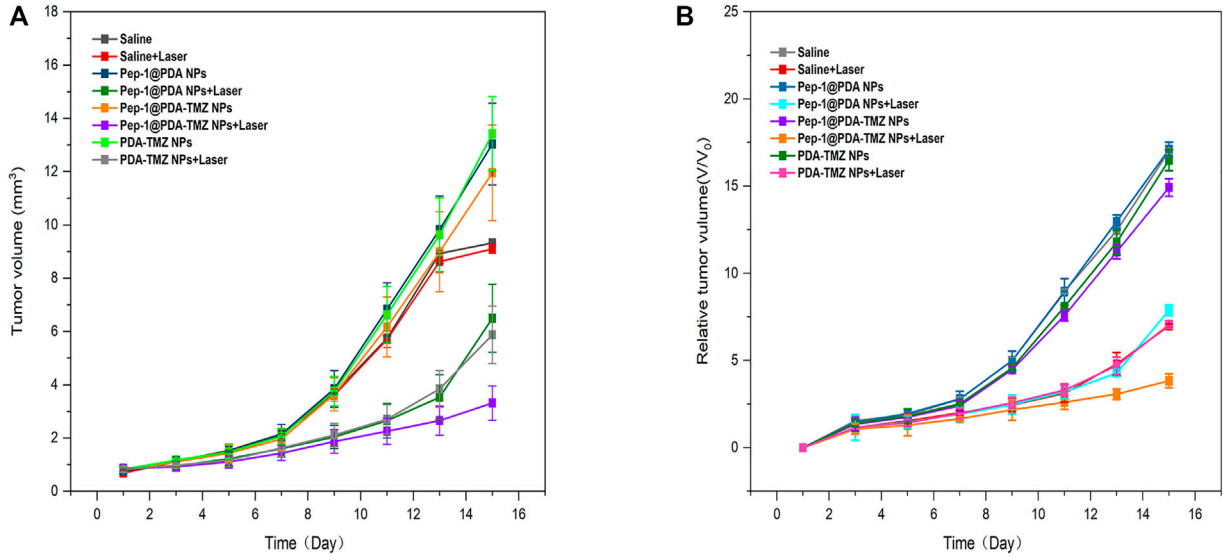

FIGURE 12
(A) The tumor volume change of tumor-bearing mice after different treatments denoted. **(B)** Relative tumor volume of tumor-bearing mice after different treatments denoted.

(200 μg/mL, 150 μL) were injected into the nude mice *via* the caudal vein. The PDA-TMZ NPs and Pep-1@PDA NPs were set as the control groups. The temperatures at the tumor site of nude mice injected with the Pep-1@PDA-TMZ NPs were promptly increased to approximately 60°C within 7 min (Figure 11). The antitumor therapeutic effect of nude mice denoted that the growth of tumors treated with Pep-1@PDA NPs was slightly inhibited without laser irradiation. In comparison, the growth of tumors treated with PDA-TMZ NPs and Pep-1@PDA-TMZ NPs with laser irradiation was considerably inhibited due to the association of CT and PTT, but Pep-1@PDA-TMZ NPs was relatively superior. In addition, the safety of Pep-1@PDA-TMZ NPs was evaluated *via* with an *in vivo* antitumor activity analysis. Finally, the volume of tumors and RTV of

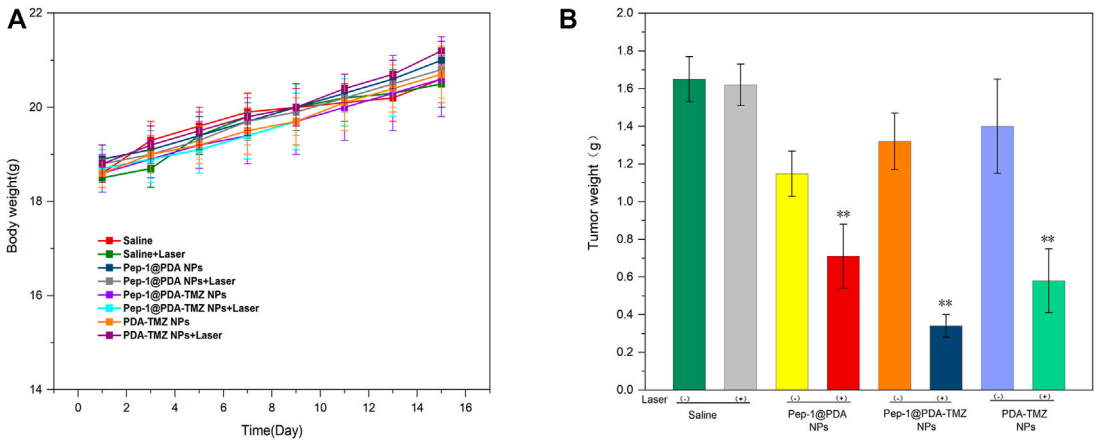

FIGURE 13
(A) The body weight of the tumor-bearing mice after different treatments. **(B)** Tumor weight of the tumor-bearing mice after different treatments.

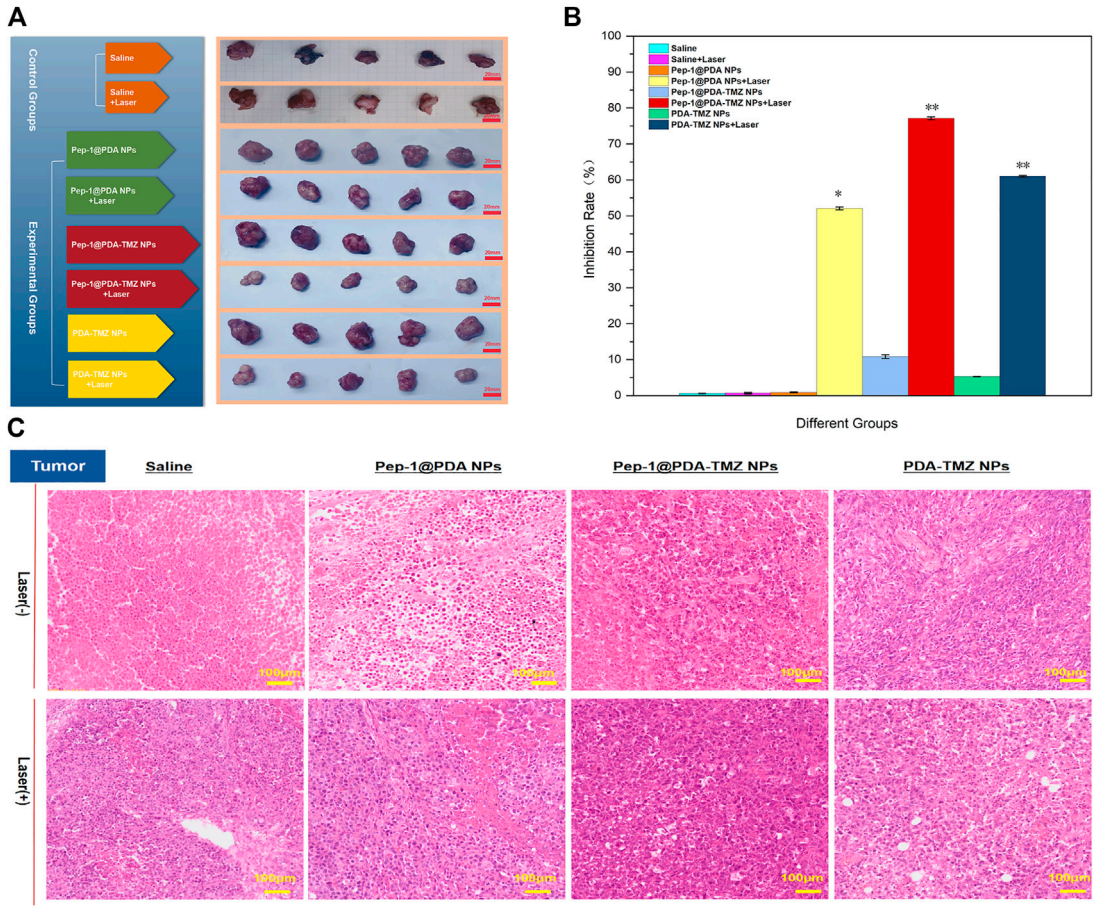

FIGURE 14
(A) *In vivo* PTT combined with CT efficacy of the NPs. **(B)** The tumor inhibition by different groups of drugs. *$p < 0.05$,**$p < 0.01$; **(C)** The H&E images of tumor treated with the Saline, Pep-1@PDA NPs, Pep-1@PDA-TMZ NPs, and PDA-TMZ NPs at 24 h post irradiation (808 nm, 1 W/cm^2, and 10 min).

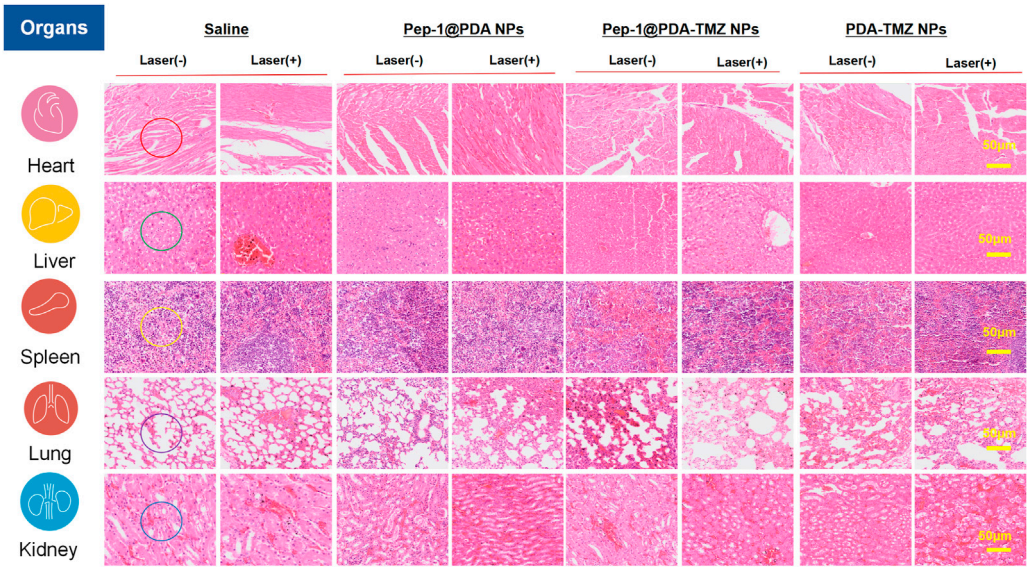

FIGURE 15
H&E staining of the major organs in nude mice. After treatment of Saline, Pep-1@PDA NPs, Pep-1@PDA-TMZ NPs, and PDA-TMZ NPs Heart: The myocardial fibers are aligned (red circle); liver: No significant vacuolization (green circle), spleen: No obvious irregular shape of white pulp (yellow circle); lung: No obvious lymphocyte infifiltration (purple circle) and kidney: No obvious nephrotoxicity (bule circle).

nude mice in each group was monitored (Figures 12A, B). During the experiment, the body and tumor weight of mice in all groups increased (Figures 13A, B), thereby validating the good biocompatibility of the Pep-1@PDA-TMZ NPs.

In conclusion, compared with the other groups,Pep-1@PDA-TMZ NPs with Laser had the best antitumor performance (Figures 14A, B).Figure 14C presented the H&E staining of tumor site. The images depicted that no obvious apoptosis occurred in the Pep-1@PDA NPs and Pep-1@PDA NPs + Laser groups or in the PDA-TMZ NPs groups, whereas PDA-TMZ NPs + Laser and Pep-1@PDA-TMZ NPs groups indicated partial apoptosis. The Pep-1@PDA-TMZ NPs + Laser denoted evident apoptosis and rupture.

To systematically investigate the toxicity of Pep-1@PDA-TMZ NPs toward major organs in nude mice, the H&E stained assay of each organ was conducted. There was no visible damage to the heart (no cardiac muscle fibers disorder), liver (no significant vacuolization), spleen (no obvious irregular shape of white pulp), lung (no obvious lymphocyte infifiltration), or kidney tissues (no obvious nephrotoxicity) in nude mice of Pep-1@PDA-TMZ NPs (Figure 15) and no significantly alter white blood cells, lymphocytes, neutrophils, platelet count, or hemoglobin level. Supplementary Figure S6 displayed blood routine examination of post-treatment nude mice. These results indicated the safety and biocompatibility of Pep-1@PDA-TMZ NPs for GBM treatment. Nevertheless, further investigation should be conducted to ensure the *in vivo* safety and biocompatibility of Pep-1@PDA-TMZ NPs.

4 Discussion

In clinical practice, the traits of GBM include high mortality and low postoperative survival. The standard of the treatment is surgery combined with RT and CT. But the overall therapeutic effects are extremely frustrating, meanwhile, side-effects associated with therapies were severe (Thaci et al., 2014).

Photothermal therapy (PTT) is an emerging physicochemical treatment method with high selectivity and minimal invasiveness, in which light energy is converted to thermal energy *via* near-infrared light irradiation from an external auxiliary light source. The rapidly increasing temperature is used to conquer targeted tumor cells through photothermal effects. PDA can be used as a photothermal therapeutic agent, the research shown that PDA had no significant damage to the surrounding normal tissues and with reduced side effects. This study demonstrated the superior photothermal effects of PDA. We found the prepared stable and well-dispersed PDA-based NPs with an advanced photothermal conversion rate of 49.2%. The dispersion temperature of these PDA-based NPs was rapidly increased by 73.8°C *via* 808 nm laser irradiation (1 W/cm^2) for 10 min at a concentration of 200 μg/mL in U87 cells. PDA-based NPs are an appropriate drug delivery system for high-efficiency loading of antitumor drugs with improved side effect (Milletti, 2012; Guidotti et al., 2017; Farokhi et al., 2019; Dai et al., 2021). PDA contains amino groups and catechol that can encapsulate other materials, including TMZ, Doxorubicin (DOX), and paclitaxel (PTX) (Guidotti et al., 2017). Additionally, its advantages include excellent adhesion capabilities, PTT effects, PDT effects, good the photothermal conversion efficiency (compare with some reported PDA nanoparticles, such as PSBTBT@PDA NPs,PDA-PEG/DOX (Wang et al., 2016))) and pH-responsive drug-release properties (Liu et al., 2014; Shao et al., 2020). The photothermal therapy of PDA can be combined with photodynamic therapy to treat tumors. In photodynamic therapy, photosensitizers can convert molecular oxygen (O_2) into cytotoxic reactive oxygen species (ROS), especially singlet oxygen ($^1O_2$), which can kill tumor cells. However, up to now, only a few studies have reported the combination of photothermal therapy of polydopamine-based and photodynamic therapy for tumor treatment. Hence, PDA can

become a potential nanocarrier for antitumor therapy (Liu et al., 2014), but the PDA-based NPs are inefficient for active tumor targeting.

The current study has confirmed that almost all GBM highly express the IL-13 receptor. IL-13Rα2, a monomer of IL-13, is a highly affinity receptor encoded by the X chromosome and consists of 380 amino acids, 17 amino acid domains and 26 amino acid signal sequences. However, IL-13Rα2 was rarely expressed in normal brain cells but highly expressed in GBM. This specificity makes it an ideal target for therapeutic in GBM. Some studies also confirmed that Pep-1 is a peptide ligand capable of highly specific binding to IL-13Rα2 and has the highest affinity. Furthermore, the expression of the IL-13Rα2 receptor has also been shown to harbor in tumor-infiltrating cells, tumor-initiating cells, or GSCs and neovascularization (Knudson et al., 2022). Research of Wang indicated that Pep-1 can invade glioma tumor cell nuclei *via* IL-13Rα2-mediated endocytosis (Wang et al., 2019). Lin also demonstrated that IL-13Rα2 was over-expressed in GBM and that a nano-delivery system constructed utilizing Pep-1 was efficient at impeding tumor proliferation *via* the regulation of the JNK signaling pathway (Lin et al., 2021). In our work,Pep-1carried NPs could permeate U87 cells and enter the cell nucleus *via* transmembrane mechanisms (Pandya et al., 2012; Wang et al., 2015; Jiang et al., 2016; Lv et al., 2016; Jiang et al., 2017; Jiao et al., 2017; Wang et al., 2017; Guo et al., 2019; Wang et al., 2020; Choi et al., 2021) According to cell experiments, we tracked the endocytosis of PDA-TMZ NPs and Pep-1@PDA-TMZ NPs by coumarin-6 labeling. The results showed that Pep-1@PDA-TMZ NPs were successfully endocytosed into the nucleus of U87 cells. However, the PDA-TMZ NPs failed to endocytose into nucleus of U87 cells, but they only stayed around the cytoplasm. We speculate that the Pep-1@PDA-TMZ NPs could be targeted to GBM *via* IL-13Rα2-mediated endocytosis, However, the specific transmembrane mechanisms of Pep-1 carried NPs need to be further explored in the future research, including the involvement of other signaling pathways.

In conclusion, Pep-1 was conjugated and modified to the PDA@TMZ NPs, which can not only afford an integration treatment of CT and PTT therapy against GBM, but can also enhance the velocity and accuracy of targeted entry into tumor location, indicating that the Pep-1@PDA-TMZ NPs combined with PTT therapy are more effective than single CT or PTT treatment at gradually wiping out tumor tissues, suggesting that Pep-1@PDA-TMZ NPs could be a promising approach as novel, targeted,nano-delivery systems for GBM therapy and further offer some evidence and data for clinical transformation and so that gradually conquer GBM.

Data availability statement

The raw data supporting the conclusion of this article will be made available by the authors, without undue reservation.

Author contributions

HW and TZ are co-first authors. HW and TZ contributed equally to this work. HW and TZ design of the work; QL and MW the acquisition analysis, QM interpretation of data; LY the creation of new software used in the work; HZ, LW, and YZ have drafted and guided the work or substantively revised it. All authors read and approved the final manuscript.

Funding

This study was supported by grants from the National Natural Science Foundation of China (No. 82172603) and the Natural Science Foundation of Jiangsu Province (No. BK20190241).

Acknowledgments

The authors give their thanks to all those who have helped with this issue.

Conflict of interest

The authors declare that the research was conducted in the absence of any commercial or financial relationships that could be construed as a potential conflict of interest.

Publisher's note

Supplementary material

The Supplementary Material for this article can be found online at: https://www.frontiersin.org/articles/10.3389/fphar.2023.1081612/full#supplementary-material

References

Batash, R., Asna, N., Schaffer, P., Francis, N., and Schaffer, M. (2017). Glioblastoma multiforme, diagnosis and Treatment;Recent literature review. *Curr. Med. Chem.* 24 (27), 3002–3009. doi:10.2174/0929867324666170516123206

Bi, D., Zhao, L., Yu, R., Li, H., Guo, Y., Wang, X., et al. (2018). Surface modification of doxorubicin-loaded nanoparticles based on polydopamine with pH-sensitive property for tumor targeting therapy. *Drug Deliv.* 25 (1), 564–575. doi:10.1080/10717544.2018.1440447

Choi, Y. J., Kim, D. W., Shin, M. J., Yeo, H. J., Yeo, E. J., Lee, L. R., et al. (2021). PEP-1-GLRX1 reduces dopaminergic neuronal cell loss by modulating MAPK and apoptosis signaling in Parkinson's disease. *Mol. (Basel, Switz.* 26 (11), 3329. doi:10.3390/molecules26113329

Dai, G., Choi, C., Choi, C., Fong, W. P., and Ng, D. (2021). Glutathione-degradable polydopamine nanoparticles as a versatile platform for fabrication of advanced photosensitisers for anticancer therapy. *Biomaterials Sci.* 10 (1), 189–201. doi:10.1039/d1bm01482j

Farokhi, M., Mottaghitalab, F., Saeb, M. R., and Thomas, S. (2019). Functionalized theranostic nanocarriers with bio-inspired polydopamine for tumor imaging and chemo-photothermal therapy. *J. Control. release official J. Control. Release Soc.* 309, 203–219. doi:10.1016/j.jconrel.2019.07.036

Glaser, T., Han, I., Wu, L., and Zeng, X. (2017). Targeted nanotechnology in glioblastoma multiforme. *Front. Pharmacol.* 8, 166. doi:10.3389/fphar.2017.00166

Guidotti, G., Brambilla, L., and Rossi, D. (2017). Cell-penetrating peptides: From basic research to clinics. *Trends Pharmacol. Sci.* 38 (4), 406–424. doi:10.1016/j.tips.2017.01.003

Guo, X., Wu, G., Wang, H., and Chen, L. (2019). Pep-1&borneol-Bifunctionalized carmustine-loaded micelles enhance anti-glioma efficacy through tumor-targeting and BBB-penetrating. *J. Pharm. Sci.* 108 (5), 1726–1735. doi:10.1016/j.xphs.2018.11.046

Jiang, Y., Lv, L., Shi, H., Hua, Y., Lv, W., Wang, X., et al. (2016). PEGylated Polyamidoamine dendrimer conjugated with tumor homing peptide as a potential targeted delivery system for glioma. *Colloids surfaces. B, Biointerfaces* 147, 242–249. doi:10.1016/j.colsurfb.2016.08.002

Jiang, Y., Wang, X., Liu, X., Lv, W., Zhang, H., ZhangLi, M. X., et al. (2017). Enhanced antiglioma efficacy of ultrahigh loading capacity paclitaxel prodrug conjugate self-assembled targeted nanoparticles. *ACS Appl. Mater. interfaces* 9 (1), 211–217. doi:10.1021/acsami.6b13805

Jiao, Z., Li, Y., Pang, H., Zheng, Y., and Zhao, Y. (2017). Pep-1 peptide-functionalized liposome to enhance the anticancer efficacy of cilengitide in glioma treatment. *Colloids surfaces.B, Biointerfaces* 158, 68–75. doi:10.1016/j.colsurfb.2017.03.058

Knudson, K. M., Hwang, S., McCann, M. S., Joshi, B. H., Husain, S. R., and Puri, R. K. (2022). Recent advances in IL-13rα2-directed cancer immunotherapy. *Front. Immunol.* 13, 878365. doi:10.3389/fimmu.2022.878365

Lin, X. M., Shi, X. X., Xiong, L., Nie, J. H., Ye, H. S., Du, J. Z., et al. (2021). Construction of IL-13 receptor α2-targeting resveratrol nanoparticles against glioblastoma cells:therapeutic efficacy and molecular effects. *Int. J. Mol. Sci.* 22 (19), 10622. doi:10.3390/ijms221910622

Liu, Y., Ai, K., Liu, J., Deng, M., He, Y., and Lu, L. (2013). Dopamine-melanin colloidal nanospheres: An efficient near-infrared photothermal therapeutic agent for *in vivo* cancer therapy. *Adv. Mater. Deerf. Beach, Fla.)* 25 (9), 1353–1359. doi:10.1002/adma.201204683

Liu, Y., Ai, K., and Lu, L. (2014). Polydopamine and its derivative materials:synthesis and promising applications in energy, environmental, and biomedical fields. *Chem. Rev.* 114 (9), 5057–5115. doi:10.1021/cr400407a

Lv, L., Jiang, Y., Liu, X., Wang, B., Lv, W., Zhao, Y., et al. (2016). Enhanced antiglioblastoma efficacy of neovasculature and glioma cells dual targeted nanoparticles. *Mol. Pharm.* 13 (10), 3506–3517. doi:10.1021/acs.molpharmaceut.6b00523

Mei, S., Xu, X., Priestley, R. D., and Lu, Y. (2020). Polydopamine-based nanoreactors: Synthesis and applications in bioscience and energy materials. *Chem. Sci.* 11 (45), 12269–12281. doi:10.1039/d0sc04486e

Milletti, F. (2012). Cell-penetrating peptides: Classes, origin, and current landscape. *Drug Discov. today* 17 (15-16), 850–860. doi:10.1016/j.drudis.2012.03.002

Nie, E., Miao, F., Jin, X., Wu, W., Zhou, X., Zeng, A., et al. (2019). Fstl1/DIP2A/MGMT signaling pathway plays important roles in temozolomide resistance in glioblastoma. *Oncogene* 38 (15), 2706–2721. doi:10.1038/s41388-018-0596-2

Ostrom, Q. T., Patil, N., Cioffi, G., Waite, K., Kruchko, C., and Barnholtz-Sloan, J. S. (2020). CBTRUS statistical report: Primary brain and other central nervous system tumors diagnosed in the United States in 2013-2017. *Neuro-oncology* 22, iv1–iv96. doi:10.1093/neuonc/noaa200

Pandya, H., Gibo, D. M., Garg, S., Kridel, S., and Debinski, W. (2012). An interleukin 13 receptor α 2-specific peptide homes to human Glioblastoma multiforme xenografts. *Neuro-oncology* 14 (1), 6–18. doi:10.1093/neuonc/nor141

Pearson, J., and Regad, T. (2017). Targeting cellular pathways in glioblastoma multiforme. *Signal Transduct. Target. Ther.* 2, 17040. doi:10.1038/sigtrans.2017.40

Saenz del Burgo, L., Hernández, R. M. O., and Pedraz, J. L. (2014). Nanotherapeutic approaches for brain cancer management. *Nanomedicine:nanotechnology, Biol. Med.* 10 (5), 905–919. doi:10.1016/j.nano.2013.10.001

Shao, W., Yang, C., Li, F., Wu, J., Wang, N., Ding, Q., et al. (2020). Molecular design of conjugated small molecule nanoparticles for synergistically enhanced PTT/PDT. *Nano-micro Lett.* 12 (1), 147. doi:10.1007/s40820-020-00474-6

Thaci, B. C. E., Binello, E., WerbanethSampath, K. P., and Sengupta, S. (2014). Significance of interleukin-13 receptor alpha 2-targeted glioblastoma therapy. *Neuro-oncology* 16 (10), 1304–1312. doi:10.1093/neuonc/nou045

Wang, B., LvWang, L. Z., Jiang, Y., Lv, W., Liu, X., Wang, Z., et al. (2015). Improved anti-glioblastoma efficacy by IL-13Rα2 mediated copolymer nanoparticles loaded with paclitaxel. *Sci. Rep.* 5, 16589. doi:10.1038/srep16589

Wang, X., Zhang, J., Wang, Y., Wang, C., Xiao, J., Zhang, Q., et al. (2016). Multi-responsive photothermal-chemotherapy with drug-loaded melanin-like nanoparticles for synergetic tumor ablation. *Biomaterials* 81, 114–124. doi:10.1016/j.biomaterials.2015.11.037

Wang, X., Zhang, Q., Lv, L. u, J., Jiang, Y., Xin, H., Yao, Q., et al. (2017). Glioma and microenvironment dual targeted nanocarrier for improved antiglioblastoma efficacy. *Drug Deliv.* 24 (1), 1401–1409. doi:10.1080/10717544.2017.1378940

Wang, B., Wu, W., Lu, H., Wang, Z., and Xin, H. (2019). Enhanced anti-tumor of pep-1 modified superparamagnetic iron oxide/PTX loaded polymer nanoparticles. *Front. Pharmacol.* 9, 1556. doi:10.3389/fphar.2018.01556

Wang, T., Wang, C., Zheng, S., Qu, G., Feng, Z., Shang, J., et al. (2020). Insight into the mechanism of internalization of the cell-penetrating carrier peptide Pep-1 by conformational analysis. *J. Biomed. Nanotechnol.* 16 (7), 1135–1143. doi:10.1166/jbn.2020.2950

Wang, L., Tang, S., Yu, Y., Lv, Y., Wang, A., Yan, X., et al. (2021). Intranasal delivery of temozolomide-conjugated gold nanoparticles functionalized with anti-EphA3 for glioblastoma targeting. *Mol. Pharm.* 18 (3), 915–927. doi:10.1021/acs.molpharmaceut.0c00911

Wang, Y., Jiang, Y., Wei, D., Singh, P., Yu, Y., Lee, T., et al. (2021). Nanoparticle-mediated convection-enhanced delivery of a DNA intercalator to gliomas circumvents temozolomide resistance. *Nat. Biomed. Eng.* 5 (9), 1048–1058. doi:10.1038/s41551-021-00728-7

Yu, Y., Wang, A., Wang, S., Sun, Y., Chu, L., Zhou, L., et al. (2022). Efficacy of temozolomide-conjugated gold nanoparticle photothermal therapy of drug-resistant glioblastoma and its mechanism study. *Mol. Pharm.* 19 (4), 1219–1229. doi:10.1021/acs.molpharmaceut.2c00083

Zhang, D., Wu, M., Zeng, Y., Wu, L., Wang, Q., Han, X., et al. (2015). Chlorin e6 Conjugated Poly(dopamine) Nanospheres as PDT/PTT Dual-Modal Therapeutic Agents for Enhanced Cancer Therapy. *ACS Appl. Mater. interfaces* 7 (15), 8176–8187. doi:10.1021/acsami.5b01027

Zhang, J., Yang, C., Zhang, R., Chen, R., Zhang, Z., Zhang, W., et al. (2017). Biocompatible D-A semiconducting polymer nanoparticle with light-harvesting unit for highly effective photoacoustic imaging guided photothermal therapy. *Adv. Funct. Mater.* 27 (13), 1605094. doi:10.1002/adfm.201605094

Zheng, P., Ding, B., and Li, G. (2020). Polydopamine-incorporated nanoformulations for biomedical applications. *Macromol. Biosci.* 20 (12), e2000228. doi:10.1002/mabi.202000228

frontiers | Frontiers in Pharmacology

TYPE Original Research
PUBLISHED 19 January 2023
DOI 10.3389/fphar.2023.1093017

OPEN ACCESS

EDITED BY
Eswar Shankar,
The Ohio State University, United States

REVIEWED BY
Prem P. Kushwaha,
Case Western Reserve University, United States
Vaibhav Singh,
Case Western Reserve University, United States

*CORRESPONDENCE
Xin Zheng,
zhengxin66999@163.com

†These authors have contributed equally to this work and share first authorship

SPECIALTY SECTION
This article was submitted to Pharmacology of Anti-Cancer Drugs, a section of the journal Frontiers in Pharmacology

RECEIVED 08 November 2022
ACCEPTED 10 January 2023
PUBLISHED 19 January 2023

CITATION
Shi J, Hao S, Liu X, Li Y and Zheng X (2023), Feiyiliu Mixture sensitizes EGFR$^{Del19/T790M/C797S}$ mutant non-small cell lung cancer to osimertinib by attenuating the PRC1/Wnt/EGFR pathway.
Front. Pharmacol. 14:1093017.
doi: 10.3389/fphar.2023.1093017

Feiyiliu Mixture sensitizes EGFR$^{Del19/T790M/C797S}$ mutant non-small cell lung cancer to osimertinib by attenuating the PRC1/Wnt/EGFR pathway

Jingjing Shi[1,2†], Shaoyu Hao[3†], Xiantao Liu[4†], Yingying Li[1] and Xin Zheng[2*]

[1]College of First Clinical Medical, Shandong University of Traditional Chinese Medicine, Jinan, China, [2]Qingdao Hospital of Traditional Chinese Medicine (Qingdao Hiser Hospital), Qingdao, China, [3]Department of Thoracic Surgery, Shandong Cancer Hospital and Institute, Shandong First Medical University and Shandong Academy of Medical Sciences, Jinan, China, [4]Department of Respiratory Medicine, Affiliated Hospital of Shandong University of Traditional Chinese Medicine, Jinan, China

Introduction: Osimertinib is a potent epidermal growth factor receptor tyrosine kinase inhibitor (EGFR-TKI) for the treatment of patients with EGFR-mutant non-small cell lung cancer (NSCLC). However, the emergence of acquired resistance due to the EGFR-Del19/T790M/C797S mutation limits the clinical application of osimertinib. Feiyiliu Mixture (FYLM), a clinical experience formula of Chinese medicine, was used to treat lung cancer with good clinical efficacy. In this study, we aimed to investigate the mechanism by which Feiyiliu Mixture delays osimertinib resistance in EGFR-mutant cell lines and EGFR-mutant cell tumor-bearing mice.

Methods: The osimertinib-resistant cell models were established in mouse Lewis lung carcinoma (LLC) cells transfected with EGFR-Del19/T790M/C797S mutant lentivirus. In cell experiments, after 48 h of treatment with Feiyiliu Mixture-containing serum, MTT assay was used to detect the relative cell viability, and western blotting was used to detect EGFR protein phosphorylation expression. In animal experiments, C57BL/6J mice were subcutaneously injected with Lewis lung carcinoma cells stably expressing EGFR-Del19/T790M/C797S mutations to construct a xenograft model. After 2 weeks of Feiyiliu Mixture and/or osimertinib treatment, the expression of proliferation-related, apoptosis-related and PRC1/Wnt/EGFR pathway markers was detected by real-time qPCR, western blotting and immunohistochemistry.

Results: The results showed that when combined with osimertinib, Feiyiliu Mixture synergistically reduces proliferation and increases apoptosis to improve drug resistance. *In vitro*, Feiyiliu Mixture-containing serum reduced the EGFR phosphorylation. *In vivo*, Feiyiliu Mixture downregulated the expression of cyclin B1 and Bcl-2 while upregulating the level of cleaved Caspase-3 protein, indicating that Feiyiliu Mixture promotes apoptosis. Furthermore, Feiyiliu Mixture reduced the expression

Abbreviations: NSCLC, non-small cell lung cancer; EGFR, epidermal growth factor receptor; Del19, exon 19 base deletions; L858R, point mutation in exon 21; NCCN, National Comprehensive Cancer Network, TKIs, tyrosine kinase inhibitors; EMT, epithelial-mesenchymal transition; PRC1, protein regulator of cytokinesis 1; TCM, Traditional Chinese Medicine; FYLM, Feiyiliu Mixture; LLC, Lewis lung carcinoma; MOI, multiplicity of infection; ALT, alanine aminotransferase; AST, aspartate aminotransferase; ALP, alkaline phosphatase; CRE, creatinine; BUN, blood urea nitrogen.

of p-EGFR, p-Akt, PRC1 and Wnt pathway-related proteins such as β-catenin, c-Myc and c-Jun.

Conclusion: The present study identified that Feiyiliu Mixture inhibited PRC1/Wnt/EGFR pathway activation, reduced proliferation, and promoted apoptosis, thereby increasing the sensitivity of EGFR-mutant non-small cell lung cancer to osimertinib. Our study provided a new idea for Chinese medicine to play a role in enhancing efficacy and reducing toxicity in the treatment of non-small cell lung cancer.

KEYWORDS

Feiyiliu Mixture, osimertinib, acquired resistance, PRC1/Wnt/EGFR pathway, non-small cell lung cancer

1 Introduction

Lung cancer is the most common malignancy and the leading cause of cancer-related deaths, causing a huge social burden in the world (Sung et al., 2021; Siegel et al., 2022). In 2020, there are about 2.2 million new cancer cases (11.4%) and 1.8 million cancer deaths (18%) of lung cancer worldwide (Sung et al., 2021). Non-small cell lung cancer (NSCLC) made up about 85 percent of all lung cancer cases (Molina et al., 2008; Testa et al., 2018). Among them, lung adenocarcinoma is the main histological phenotype of NSCLC, accounting for approximately 55%. Patients with lung cancer are not easily detected at an early stage, and the majority of them are at an advanced stage by the time of clinical diagnosis, losing the opportunity for surgical resection. Current treatments for advanced NSCLC include cytotoxic chemotherapy, radiotherapy, targeted therapy, immunotherapy, and various combination therapies (Miller and Hanna, 2021; Gesthalter et al., 2022; Higgins et al., 2022). With the development of molecular biology research, targeted therapy guided by oncogenic drivers is considered to be an effective means to improve the overall survival and prolong progression-free survival of patients with lung adenocarcinoma (Ramalingam et al., 2020; Ettinger et al., 2022). Epidermal growth factor receptor (EGFR) is considered to be one of the most common driver oncogenes in NSCLC (Harrison et al., 2020; Russo et al., 2020; Cooper et al., 2022). Approximately 50% of Asian patients with lung adenocarcinoma have EGFR-activating mutations, mainly including exon 19 base deletions (Del19) and point mutation in exon 21 (L858R) (Sharma et al., 2007). Moreover, EGFR gene mutation is a biomarker for predicting the effectiveness of targeted therapy. Therefore, genetically mutated EGFR is an important target for targeted therapy in lung adenocarcinoma.

According to the National Comprehensive Cancer Network (NCCN) guidelines for NSCLC (Ettinger et al., 2022), tyrosine kinase inhibitors (TKIs) are recommended as first-line therapy for patients with EGFR-mutant advanced NSCLC. The first and second-generation EGFR-TKIs (gefitinib, erlotinib and afatinib) targeting EGFR tyrosine kinase domain achieved marked clinical efficacy, but unfortunately, acquired resistance occurs 9–14 months later (Park et al., 2016; Hsu et al., 2018). The mechanisms of acquired resistance to EGFR-TKIs involve the second-site mutations of EGFR (such as T790M gatekeeper mutation), activation of the bypass signaling pathways, epithelial-mesenchymal transition (EMT), the transformation of NSCLC to small cell lung cancer tissue, etc. (Westover et al., 2018; Wu and Shih, 2018). Among them, T790M mutation occurs in at least 50% of the patients (Remon et al., 2018). Osimertinib, a third-generation irreversible EGFR-TKI, selectivity targeted against both activating mutations and T790M resistance mutations. However, after 9–13 months of treatment, there was only a transient benefit followed by osimertinib resistance due to the C797S mutation (Thress et al., 2015; Du et al., 2021). Currently, there is no effective therapeutic strategy to overcome the triple mutation (Del19/T790M/C797S)-mediated drug resistance problem. Clearly, exploring the resistance mechanism and searching for new therapeutic targets to delay and reverse EGFR-TKIs resistance in lung adenocarcinoma is an urgent problem to be solved in tumor-targeted therapy and it is also essential for the treatment of NSCLC.

Research has shown that the protein regulator of cytokinesis 1 (PRC1) is associated with the mitotic process of tumor cells and is highly expressed in various carcinomas (Li et al., 2018). As well as, PRC1 promotes lung adenocarcinoma cells proliferation, metastasis and tumorigenesis by activating the Wnt/β-catenin signaling pathway (Zhan et al., 2017). Besides, the activation of EGFR and its downstream signaling pathways by the Wnt/β-catenin pathway is an important molecular mechanism for the development of EGFR-TKI resistance (Arasada et al., 2018). Hence, inhibition of the PRC1/β-catenin/EGFR pathway may be an important molecular pathway for overcoming EGFR-TKI resistance.

Traditional Chinese Medicine (TCM) has certain advantages in the treatment of chronic diseases and diseases with complex factors, especially in anti-tumor (Shao et al., 2021). In addition, TCM and molecular targeted drugs have synergistic anti-cancer effects on lung cancer patients with EGFR-TKI resistance (Li et al., 2019; Wang et al., 2021b). Feiyiliu Mixture (FYLM), a clinical experience formula of Chinese medicine, is composed of Huangqi, Banzhilian, Baizhu, Baihuasheshecao, Renshen, Fuling, Zhebeimu, Shancigu, Yiyiren and Gancao. Our previous studies have demonstrated that compared with erlotinib alone, FYLM combined with erlotinib not only inhibits tumor growth and improves symptoms but also effectively alleviates side effects in patients with advanced lung adenocarcinoma (Li, 2010). In addition, FYLM can reduce the mRNA expression of EGFR and regulate the PI3K/Akt pathway downstream of EGFR (Cao et al., 2016; Peng et al., 2019). Therefore, we speculated that FYLM may be involved in the process of EGFR-TKI resistance and may complement targeted drugs. However, the underlying molecular mechanism remains unknown.

In the present study, we aimed to investigate whether FYLM could delay osimertinib resistance by regulating the PRC1/Wnt/EGFR pathway in EGFR triple-mutant LLC cells *in vitro* and an EGFR triple-mutant xenograft mouse model *in vivo*.

2 Materials and methods

2.1 Preparation of FYLM decoction

FYLM consists of ten Chinese herbal medicines, including 18 g of Huangqi [*Astragalus membranaceus* (Fisch.) Bge.], 24 g of Banzhilian (*Scutellaria barbata* D. Don), 12 g of Baizhu (*Atractylodes macrocephala* Koidz.), 20 g of Baihuasheshecao [*Oldenlandia diffusa* (Willd.) Roxb.], 9 g of Renshen (*Panax ginseng* C. A. Mey.), 15 g of Fuling [*Poria cocos* (Schw.) Wolf], 15 g of Zhebeimu (*Fritillaria thunbergii* Miq.), 20 g of Shancigu [*Cremastra appendiculata* (D. Don) Makino], 20 g of Yiyiren [*Coix lacryma—jobi L. var. ma—yuen* (Roman.) Stapf] and 6 g of Gancao (*Glycyrrhiza uralensis* Fisch.). All the Chinese medicine pieces were provided by Bozhou Huqiao Pharmaceutical Co., Ltd (Bozhou, China) and authenticated by Prof. Feng Li of Shandong University of Traditional Chinese Medicine. For *in vivo* animal studies, all herbs (159 g in total) were soaked in ten times cold distilled water for 1 h and then decocted for 40 min. After filtering the solution, the dregs of decoction were decocted again in eight times distilled water for 30 min. After combining two filtrates, the FYLM decoction was concentrated to 66 ml under a rotary evaporator (N-1300, Shanghai Ailang Instrument Co., Ltd, Shanghai, China). At last, 2.4 g (crude drug)/ml FYLM decoction was prepared and stored at −20°C.

2.2 UPLC-Q-Orbitrap-MS analysis

The composition analysis of FYLM decoction was detected using a chromatograph (instrument model: UltiMate 3000 RS) and a Q Exactive high-resolution mass spectrometer [Thermo Fisher Scientific (China) Co. Ltd.]. 1 ml of 80% methanol was mixed with 200 µl of FYLM solution and vortexed for 10 min. After centrifugation at 20,000 g for 10 min at 4°C, the supernatant was filtered for subsequent studies. Chromatographic analysis was performed on an AQ-C18 column (150 mm × 2.1 mm, 1.8 µm, Welch) at 35°C with an injection volume of 5 µl. The chromatographic gradient elution procedure: 98% aqueous phase, 2% organic phase at 1 min; 80% aqueous phase, 20% organic phase at 5 min; 50% aqueous phase, 50% organic phase at 10 min; 20% aqueous phase, 80% organic phase at 15 min; 5% aqueous phase, 95% organic phase at 20 min; 5% aqueous phase, 95% organic phase at 27 min; 98% aqueous phase, 2% organic phase at 28 min; 98% aqueous phase, 2% organic phase at 30 min. The mass spectrometry analysis was performed using a full mass/dd-MS2 detection method with a positive and negative ion switching scan. Data collected from the high-resolution liquid mass were initially analyzed by CD2.1 (Thermo Fisher) and then compared to a database (mzCloud).

2.3 Preparation of FYLM-containing serum

Twenty male Sprague-Dawley rats (weighting 180 ± 10 g) were purchased from Vital River Laboratory Animal Technology Co., Ltd. (Beijing, China) [animal License number: SCXK (Jing) 2016-0006]. Animals were housed in a 12/12 h light/dark cycle at 23°C ± 2°C with 50%–60% relative humidity and free of the specific pathogens [Laboratory use of animal license number: SYXK(Lu)2017-0022], with free access to food and water (Geng et al., 2021).

After 1 week of adaptive feeding, the animals were randomly divided into two groups, the control group and the FYLM administration group. The clinical dose of FYLM in adults is 159 g/60 kg and the gavage dose for rats is 6.3 times the clinical dose based on body surface area. The rats of FYLM administration group were given FYLM at the dose of 16.7 g/kg by gavage. While rats in the control group were given saline gavage (1.5 ml/100 g body weight). After 6 days of continuous gavage, rats were anesthetized with 3% pentobarbital sodium (45 mg/kg, intraperitoneal injection) (Sun et al., 2004), and blood was collected from the abdominal aorta. After resting for 1 h at room temperature, the serum was obtained by centrifugation at 3,000 rpm for 15 min at 4°C. Subsequently, it was inactivated in a water bath at 57°C for 30 min. After that, the bacteria were removed by filtration through a 0.22 µm microporous membrane and stored in a refrigerator at −80°C for *in vitro* experiments.

2.4 Cell culture

Mouse Lewis lung carcinoma (LLC) cell line and human NSCLC cell line (H1975) were purchased from the Cell bank, Type Culture Collection of Chinese Academy of Sciences (Shanghai, China). LLC cells were maintained in Dulbecco's Modified Eagle Medium (DMEM, Gibco, Beijing, China) containing 10% fetal bovine serum (FBS, ExCell Bio, Shanghai, China) and 1% Penicillin Streptomycin solution (Yu et al., 2020a). H1975 cells were cultured in RPMI 1640 Medium (Invitrogen, 11875-093) with 10% FBS, 1% Glutamax (Invitrogen, 35050061), and 1% Sodium Pyruvate 100 mM Solution (Invitrogen, 11360070) (Jiang et al., 2021). All cells were cultured in a humidified incubator at 37°C and 5% CO_2.

2.5 Lentivirus transfection of LLC cells

EGFR triple-mutant cells were generated by transfection with lentiviruses harboring the gene sequence encoding $EGFR^{Del19/T790M/C797S}$ mutations in LLC cells. Construction of the overexpression lentiviral vector and concentration of viruses was performed by Shanghai Genechem Co., Ltd. (Shanghai, China). Based on the results of the pre-experiment, the optimal multiplicity of infection (MOI) for $EGFR^{Del19/T790M/C797S}$ overexpression and empty vector lentivirus infection of LLC cells was 100. Before infection, LLC cells were plated in 6-well plates at 3×10^5 cells per well overnight, and then the supernatant was replaced with 1 ml complete medium supplemented with lentivirus. After 14 h of infection, the lentivirus-containing medium was discarded and replaced with 2 ml fresh complete medium. After 72 h of infection, the stably transfected cell lines were selected by 2 µg/ml puromycin. The transfection efficiency was assessed by observing fluorescence intensity, and the $EGFR^{Del19/T790M/C797S}$ overexpression levels were identified by real-time qPCR and western blotting.

2.6 Cell viability assays

LLC triple-mutant cells and H1975 cells were seeded at 1×10^4 cells per well in 96-well plates for 24 h. Then, cells were treated with different concentrations of FYLM-containing serum. After 48 h of intervention, 100 μl medium containing 20% MTT (5 mg/ml, Solarbio, Beijing, China) was added to each well. After incubation at 37°C for 4 h, 150 μl dimethylsulfoxide (DMSO) was added to each well and shaken on a shaker at low speed for 10 min to dissolve the formazan crystals. In the end, the absorbance values of each well were measured at 490 nm (Lin et al., 2015) using a full-wavelength microplate reader (BioTek, United States).

2.7 Real-time quantitative PCR

Total RNA was extracted from cells or tumor tissues by Trizol reagent (Invitrogen, Thermo Fisher Scientific, United States). A reverse transcription reaction was performed using a 5x All-In-One RT MasterMix kit (Abm, Canada) to synthesize cDNA from total RNA. qPCR assays were detected by the SYBR Green PCR Master Mix kit (DBI Bioscience, Germany) in accordance with the manufacturer's instructions on a real-time fluorescence quantitative PCR instrument (Roche LightCycler 480II, Mannheim, Germany). The relative expression of genes was measured using the $2^{-\triangle\triangle CT}$ method (Michaelidou et al., 2013), and GAPDH was used as a normalization control. Each sample was tested three times in duplicate. The primer sequences are shown in Table 1.

2.8 Western bolting

After treatments, cells or tumor tissues were lysed for 20 min on ice in RIPA lysis buffer (Solarbio, Beijing, China) supplemented with protease inhibitor (PMSF) and phosphatase inhibitor (APExBIO, MA, United States). And then the supernatant-containing proteins were collected by centrifugation at 12,000 rpm for 20 min at 4°C. Protein concentration measurements were performed using a BCA protein assay kit (Beyotime, Shanghai, China). Protein samples of 40 μg were isolated on 8% or 12% SDS-polyacrylamide gels and transferred onto the polyvinylidene fluoride (PVDF) membranes (0.45 μm, Millipore, Billerica, MA, United States). After blocking with 5% skim milk in TBST at room temperature for 2 h, membranes were incubated separately with the specific primary antibodies at 4°C overnight. The primary antibodies were as follows: EGFR (#4267, Cell Signaling Technology, 1:1000), p-EGFR (#3777s, Cell Signaling Technology, 1:1000), Cyclin B1 (#4138, Cell Signaling Technology, 1:1000), Bcl-2 (#3498, Cell Signaling Technology, 1:1000), Cleaved Caspase-3 (#9661, Cell Signaling Technology, 1:1000), PRC1 (BM3910, BOSTER, Wuhan, China, 1:1000), β-catenin (BA0426, BOSTER, Wuhan, China, 1:1000), c-Myc (PB9092, BOSTER, Wuhan, China, 1:1000), c-Jun (#9165, Cell Signaling Technology, 1:1000), Akt (ab179463, Abcam, 1:10000), p-Akt (ab192623, Abcam, 1:1000), β-actin (BA2305, BOSTER, Wuhan, China, 1:5000), GAPDH (A00227-1, BOSTER, Wuhan, China, 1:1000). After washing 3 times with TBST for 5 min each time, the membranes were incubated with secondary antibodies conjugated to horseradish peroxidase (BOSTER, Wuhan, China, 1:5000) for 1 h at room temperature. Finally, the bands were detected by an automated chemiluminescence gel imaging system (GE Amersham Imager600, United States), and the grayscale value was measured by ImageJ software (NIH, Bethesda, MD).

2.9 Triple-mutant EGFR xenograft-bearing mouse model

6-week-old male C57BL/6J mice, weighing 18–20 g, were purchased from Jinan Pengyue experimental Animal Breeding Co., Ltd. (Jinan, China) [animal License number: SCXK(Lu)2019-0003]. LLC cells stably transfected with $EGFR^{Del19/T790M/C797S}$-mutant or empty vector lentivirus were harvested and washed 2 times with PBS. Then, 1×10^6 cells were suspended in 100 μl PBS and injected subcutaneously into the right side of the flank region of C57BL/6J mice. The equivalent dose was converted from human and mouse body surface area (9.1 times), and the dose administered to mice was 24 g/kg. Body weight and tumor volume of mice were recorded every 3 days, and tumor volume was represented by $0.5 \times \text{length} \times \text{width}^2$ (mm^3) (Chen et al., 2021). When the tumor volume reached about 200 mm^3 (7 days after tumor inoculation) (Uchibori et al., 2017), the mice were randomly divided into seven groups ($n = 5$), empty vector control group (0.5% CMC-Na, Selleckchem, Houston, TX, United States, catalog number: S6703), overexpression control group (0.5% CMC-Na, Selleckchem, Houston, TX, United States, catalog number: S6703), 24 g/kg FYLM group, 48 g/kg FYLM group, osimertinib group (50 mg/kg, AZD9291, Selleckchem, Houston, TX, United States, catalog number: S7279), osimertinib +24 g/kg FYLM group (50 mg/kg osimertinib plus 24 g/kg FYLM) and osimertinib +48 g/kg FYLM group (50 mg/kg osimertinib plus 48 g/kg FYLM). After 2 weeks of continuous gavage, the tumor tissue was obtained and stored at −80°C or fixed with paraformaldehyde for further experiments.

2.10 H&E staining

The tumor tissues were dehydrated and embedded in paraffin, and then cut into 5 μm sections. Sections were stained with hematoxylin and eosin and then observed using an optical microscope.

2.11 Serum analysis

Blood samples were collected from the mouse retro-orbital venous plexus. After resting at room temperature, the blood samples were

TABLE 1 The primer sequences used for real-time quantitative PCR.

Gene	Sequence (5′ to 3′)	
EGFR	Forward primer	GCGATTCAGCAACAACC
	Reverse primer	CATTGGGACAGCTTGGA
Akt	Forward primer	TAACGGACTTCGGGCTGT
	Reverse primer	TTCTCGTGGTCCTGGTTGT
GAPDH	Forward primer	TGTTTCCTCGTCCCGTAGA
	Reverse primer	ATCTCCACTTTGCCACTGC

TABLE 2 Chemical composition information in FYLM.

NO.	Name	Formula	Reference ion	RT [min]	Calc. MW	mzCloud best match	Corresponding herbs
1	L-Histidine	C6 H9 N3 O2	[M-H]-1	1.293	155.0683	97.8	Baizhu
2	DL-Arginine	C6 H14 N4 O2	[M+H]+1	1.388	174.1114	85.8	Baizhu
3	Choline	C5 H13 N O	[M+H]+1	1.392	103.1001	93.5	Huangqi
4	L-Glutamic acid	C5 H9 N O4	[M+H]+1	1.408	147.0529	95.3	Baizhu
5	Betaine	C5 H11 N O2	[M+H]+1	1.44	117.0791	93.2	Huangqi
6	Isocitric acid	C6 H8 O7	[M-H]-1	1.617	192.026	70.8	Renshen
7	Nicotinic acid	C6 H5 N O2	[M+H]+1	2.131	123.0322	99.8	Huangqi
8	L-Isoleucine	C6 H13 N O2	[M+H]+1	2.602	131.0946	99.8	Baizhu
9	Succinic acid	C4 H6 O4	[M-H]-1	3.116	118.0252	36.1	Shancigu
10	Uridine	C9 H12 N2 O6	[M-H]-1	3.626	244.0693	81.8	Baizhu
11	Geniposidic acid	C16 H22 O10	[M-H]-1	7.838	374.1209	86.5	Baihuasheshecao
12	Dimethyl phthalate	C10 H10 O4	[M+H]+1	8.249	194.0579	60.4	Gancao
13	Coumarin	C9 H6 O2	[M+H]+1	8.675	146.0367	60.1	Huangqi
14	Chlorogenic acid	C16 H18 O9	[M+H]+1	9.804	354.0947	99.7	Huangqi
15	4-Hydroxybenzaldehyde	C7 H6 O2	[M+H]+1	9.817	122.037	97.2	Banzhilian
16	Caffeic acid	C9 H8 O4	[M-H]-1	10.256	180.0416	99.1	Huangqi
17	Vanillin	C8 H8 O3	[M+H]+1	10.656	152.0473	94.4	Yiyiren
18	L-Tyrosine	C9 H11 N O3	[M+H]+1	11.388	181.0739	69.9	Baizhu
19	4-Methoxycinnamic acid	C10 H10 O3	[M+H]+1	11.439	178.0626	66.4	Baihuasheshecao
20	Phenylacetaldehyde	C8 H8 O	[M-H]-1	11.561	120.0561	99.6	Banzhilian
21	Quercetin	C15 H10 O7	[M+H]+1	11.706	302.0422	95.7	Banzhilian
22	Isoliquiritigenin	C15 H12 O4	[M+H]+1	11.96	256.0729	99.3	Gancao
23	Rutin	C27 H30 O16	[M-H]-1	12.965	610.1525	99.7	Baihuasheshecao
24	Apigenin	C15 H10 O5	[M+H]+1	13.291	270.0521	99.3	Banzhilian
25	Scutellarin	C21 H18 O12	[M+H]+1	13.371	462.079	98.2	Banzhilian
26	Ononin	C22 H22 O9	[M+H]+1	13.502	430.1256	98.5	Huangqi
27	Eriodictyol	C15 H12 O6	[M-H]-1	13.699	288.0634	69.9	Banzhilian
28	Baicalin	C21 H18 O11	[M+H]+1	14.594	446.0842	97.1	Banzhilian
29	Formononetin	C16 H12 O4	[M-H]-1	14.732	268.0734	99.5	Gancao
30	Daidzein	C15 H10 O4	[M-H]-1	17.534	254.0576	98.3	Huangqi
31	Soyasaponin I	C48 H78 O18	[M+H]+1	19.215	942.5178	75.5	Huangqi
32	Hispidulin	C16 H12 O6	[M-H]-1	19.444	300.0631	88.9	Banzhilian
33	Oleanolic acid	C30 H48 O3	[M-H]-1	22.062	456.3603	99.2	Gancao
34	Linoleic acid	C18 H32 O2	[M-H]-1	22.291	280.2401	100	Huangqi
35	Palmitic acid	C16 H32 O2	[M-H]-1	22.808	256.2399	100	Fuling
36	Stearic acid	C18 H36 O2	[M-H]-1	24.168	284.2715	99.5	Yiyiren

centrifuged at 1,500 g for 30 min to obtain the supernatant. According to the manufacturer's instructions, alanine aminotransferase (ALT), aspartate aminotransferase (AST), alkaline phosphatase (ALP), creatinine (CRE), blood urea nitrogen (BUN) levels in serum samples were determined using the kit from Nanjing Jiancheng (Nanjing, China).

2.12 Immunohistochemistry staining

The tumor sections were dewaxed, antigen repaired in a microwave oven, and incubated with 3% H_2O_2 for 20 min at room temperature. The sections were incubated overnight at 4°C with an anti-Ki67 antibody (GB111499, Servicebio, 1:500) and an anti-β-catenin antibody (GB11015, Servicebio, 1:1000). Finally, the protein expression of Ki67 and β-catenin was observed under the optical microscope.

2.13 TUNEL staining

TUNEL staining of tumor sections was performed to detect apoptosis using the TUNEL assay kit (G1507, Servicebio, Wuhan, China) according to the manufacturer's instructions. The paraffin sections were dewaxed, rehydrated, and incubated with proteinase K working solution for 20 min at 37°C. After incubation with 3% H_2O_2 at room temperature for 20 min, the sections were blocked with TUNEL reaction at 37°C for 1 h in a flat wet box. Positive expression was observed under an optical microscope.

2.14 Statistical analysis

The data were analyzed using SPSS 23.0 software (SPSS, Inc., Chicago, IL, United States). Mean ± standard deviation (SD) was used to reveal data. One-way ANOVA analysis followed by Fisher's least-significant difference (LSD) was used to compare multiple-group statistical differences. A value of $p < 0.05$ was considered statistically significant.

3 Results

3.1 Identification of the chemical composition of FYLM decoction

To analyze the main components of FYLM, we used combination of Ultra-Performance Liquid Chromatography and Quadrupole-Orbitrap mass spectrometry (UPLC-Q-Orbitrap-MS) method. Chinese medicine samples matched 710 compounds in mzCloud. As shown in Table 2, 36 kinds of compounds were identified by screening with the Traditional Chinese Medicine Systems Pharmacology Database and Analysis Platform (TCMSP, https://old.tcmsp-e.com/tcmsp.php). We found that the main components of huangqi include Choline, Betaine, Nicotinic acid, Coumarin, Chlorogenic acid, Caffeic acid, Ononin, Daidzein, Soyasaponin I, Linoleic acid. The main components of banzhilian include 4-Hydroxybenzaldehyde, Phenylacetaldehyde, Quercetin, Apigenin, Scutellarin, Eriodictyol, Baicalin, Hispidulin. The main components of baizhu include L-Histidine, DL-Arginine, L-Glutamic acid, L-Isoleucine, Uridine, L-Tyrosine. And the main components of baihuasheshecao include Geniposidic acid, 4-Methoxycinnamic acid, Rutin. The total ion chromatograms of FYLM were shown in Figure 1A (negative ion mode) and Figure 1B (positive ion mode). Figure 1C manifested the chemical structure formula corresponding to the typical peaks.

3.2 FYLM-containing serum inhibits the proliferation of EGFR mutant cells and reduces EGFR phosphorylation

To determine whether $EGFR^{Del19/T790M/C797S}$ is stably expressed in LLC cells, we analyzed fluorescence intensity, mRNA and protein levels of EGFR. By fluorescence microscopy, both overexpression and empty vector lentiviruses-transfected LLC cells exhibited enhanced fluorescence signals, indicating normal expression of fluorescent marker genes and successful transfection (Figure 2A). Based on the real-time qPCR results (Figure 2C), the EGFR gene expression in the overexpression group was 37-fold higher than that in the empty vector group. Similarly, the protein levels of EGFR were significantly higher in the overexpression group (Figures 2B, D). The above results suggested that LLC cells were successfully transfected with $EGFR^{Del19/T790M/C797S}$ expressing lentivirus. Next, cell viability was measured by treating with various concentrations of FYLM-containing serum for 48 h in $EGFR^{Del19/T790M/C797S}$-mutated and $EGFR^{L858R/T790M}$-mutated cells. As shown in Figure 2E, FYLM-containing serum dose-dependently inhibited the proliferation of LLC-triple mutant cells (IC_{50} = 14.27%). In addition, FYLM-containing serum can inhibit the proliferation of H1975-L858R/T790M cells (Figure 2F, IC_{50} = 17.72%). In order to further verify the effect of FYLM-containing serum on LLC-triple mutant cells, we detected the protein expression of p-EGFR by western blotting. The results suggested that low and high doses of FYLM-containing serum can reduce EGFR phosphorylation compared with the control group. In addition, the combination of FYLM-containing serum and osimertinib had a more significant inhibitory effect compared with the osimertinib alone group. However, there was no significant differences between high and low doses (Figures 2G–I).

3.3 The combination of FYLM and osimertinib inhibits tumor growth in triple-mutant EGFR xenograft mouse model

To explore the inhibitory effect of FYLM on tumor progression *in vivo*, we first constructed a xenograft mouse model harboring EGFR-Del19/T790M/C797S-mutant *via* subcutaneously inoculating LLC-triple mutant cells into C57BL/6J mice. Tumor-bearing mice were continuously orally gavage for 2 weeks with 0.5% CMC-Na, FYLM (24 g/kg/d), FYLM (48 g/kg/d), osimertinib (50 g/kg/d), a combination treatment of osimertinib (50 g/kg/d) and FYLM (24 g/kg/d), or a combination treatment of osimertinib (50 g/kg/d) and FYLM (48 g/kg/d). As a result, the body weight of mice in each group steadily increased without significant differences, and no obvious toxicity was observed compared to the control treatment group (Figures 3B, G). The tumor weight and tumor volume of the empty vector group were slightly smaller than those of the overexpression group, but the differences were not statistically significant (Figures 3C–E). FYLM or osimertinib inhibited tumor progression compared with the control group. Among them, the combination of FYLM (48 g/kg/d) and osimertinib had the most significant inhibitory effect (Figures 3H–J). Furthermore, to evaluate the safety of combination treatment with FYLM and

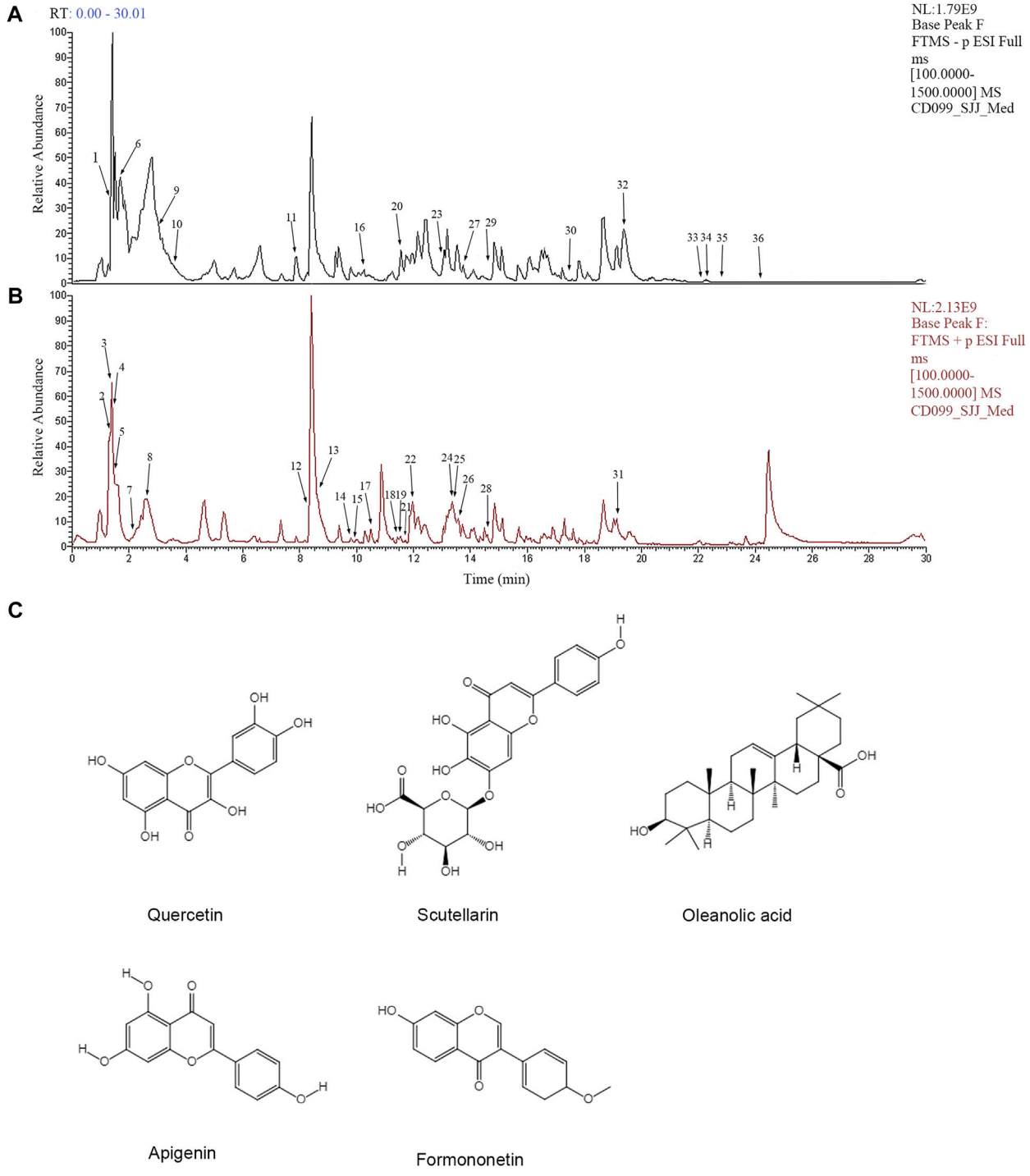

FIGURE 1
Analysis of the main chemical components of Feiyiliu Mixture (FYLM) by UPLC-Q-Orbitrap-MS in **(A)** negative ion mode and **(B)** positive ion mode. **(C)** Typical chemical structure formulas of components.

osimertinib, we measured spleen weight and biochemical analysis of liver function [alanine aminotransferase (ALT), aspartate aminotransferase (AST), alkaline phosphatase (ALP)] and kidney function [creatinine, blood urea nitrogen (BUN)]. The results showed no significant differences among the groups. Therefore, the combination of FYLM and osimertinib has no significant toxicity (Figures 4A–F).

3.4 The combination of FYLM and osimertinib inhibits cell proliferation, regulates cell cycle and promotes apoptosis in triple-mutant EGFR xenograft mouse model

HE staining revealed a decrease in nuclear density, lighter staining and lower nucleoplasm ratio in the combined treatment

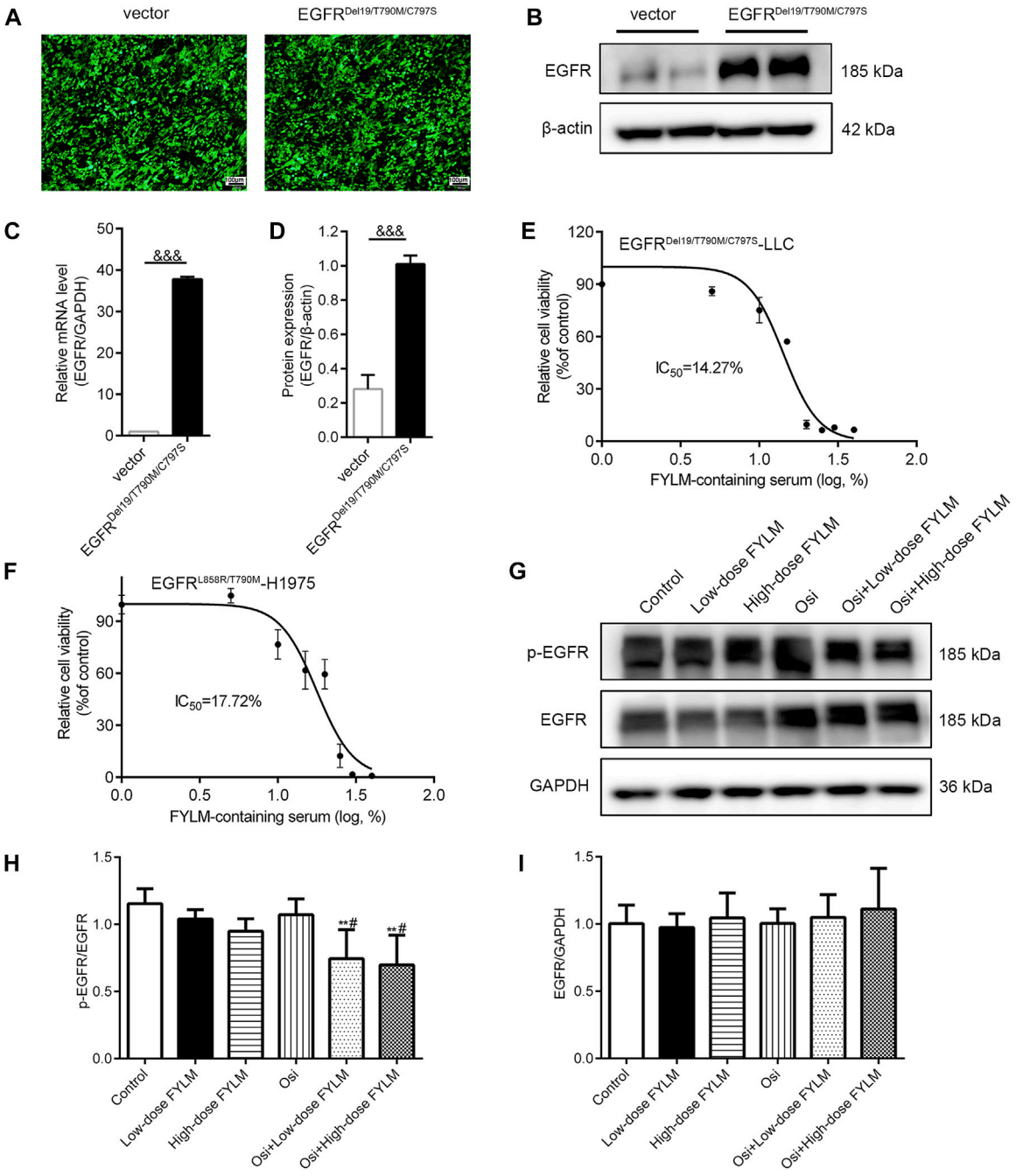

FIGURE 2
FYLM-containing serum inhibited cell proliferation and reduced EGFR phosphorylation *in vitro*. The **(A)** fluorescence intensity, **(B)** western blot and **(C)** real-time qPCR results were used to identify the transfection effect of the empty vector and EGFR$^{Del19/T790M/C797S}$ mutant lentivirus in LLC cells. **(D)** Quantitative analysis of EGFR protein levels. **(E,F)** MTT assays determined relative cell viability in LLC-EGFR-Del19/T790M/C797S cells and H1975-EGFR-L858R/T790M cells treated with FYLM-containing serum for 48 h **(G)** LLC-EGFR-Del19/T790M/C797S cells were treated with low and high doses of FYLM-containing serum and Osi alone or in combination. p-EGFR and EGFR protein were detected by western blotting. **(H,I)** Quantitative analysis of p-EGFR and EGFR protein levels. $^{\&\&\&}p < 0.001$ vs. vector; $^{**}p < 0.01$ vs. Control; $^{\#}p < 0.05$ vs. Osi. Osi, osimertinib. All data are shown as mean ± SD.

group (Figure 5A). To investigate the effect of FYLM on tumor growth, we detected the levels of cell proliferation, cell cycle, and apoptosis-related protein Ki-67, cyclin B1, Bcl-2 and cleaved Caspase-3 in xenograft mouse tumor tissues by western blot and immunohistochemistry. Consistent with the results of phenotypic experiments, the combination of FYLM and osimertinib reduced the positive expression of Ki-67 protein in a dose-dependent manner in the immunohistochemistry assay (Figure 5B). The western blot results showed that the combination of FYLM and osimertinib downregulated the protein expression level of cyclin B1 (Figures 5C, D). Furthermore, TUNEL staining results illustrated that

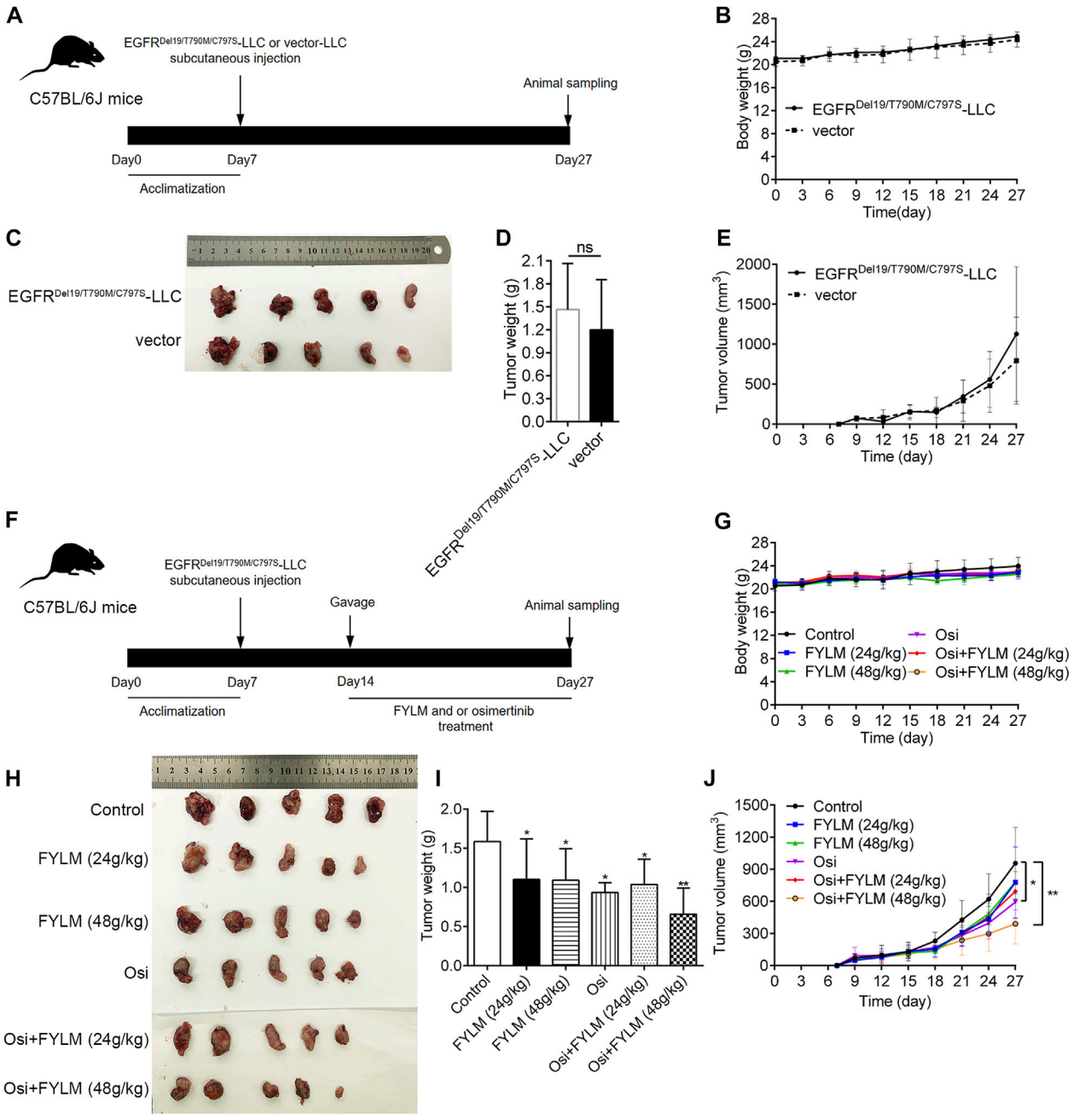

FIGURE 3
FYLM combined with osimertinib inhibited tumor progression in EGFR-Del19/T790M/C797S LLC tumor-bearing mice *in vivo*. **(A,F)** Flowchart of animal experiments. **(B,G)** Body weights of mice in each group were measured every 3 days. **(C,H)** Photograph of tumor tissues from xenograft mouse. **(D,I)** Tumor weight and **(E,J)** tumor volumes of mice were treated by FYLM and/or osimertinib for 2 weeks. *$p < 0.05$ and **$p < 0.01$ vs. Control. Osi, osimertinib. All data are shown as mean ± SD.

combination of osimertinib and FYLM (24 and 48 g/kg) increased apoptosis (Figure 6A). Moreover, western blot assays revealed that combination treatment of osimertinib and FYLM (24 and 48 g/kg) inhibited Bcl-2 expression compared with osimertinib or FYLM alone. However, cleaved Caspase-3 protein expression were upregulated in combination treatment of osimertinib and FYLM (24 g/kg) group and the combination treatment of osimertinib and FYLM (48 g/kg) group compared with the osimertinib alone group (Figures 6B–D).

3.5 The combination of FYLM and osimertinib inhibits PRC1/Wnt/EGFR pathway in triple-mutant EGFR xenograft mouse model

To clarify the mechanism synergistic anti-cancer effect of FYLM, we investigated the protein expression of PRC1, Wnt pathway-related protein (β-catenin, c-Myc, c-Jun) and EGFR pathway-related protein (p-EGFR, EGFR, p-Akt and Akt) in xenograft tumor tissues by western blot and immunohistochemistry. Immunohistochemistry

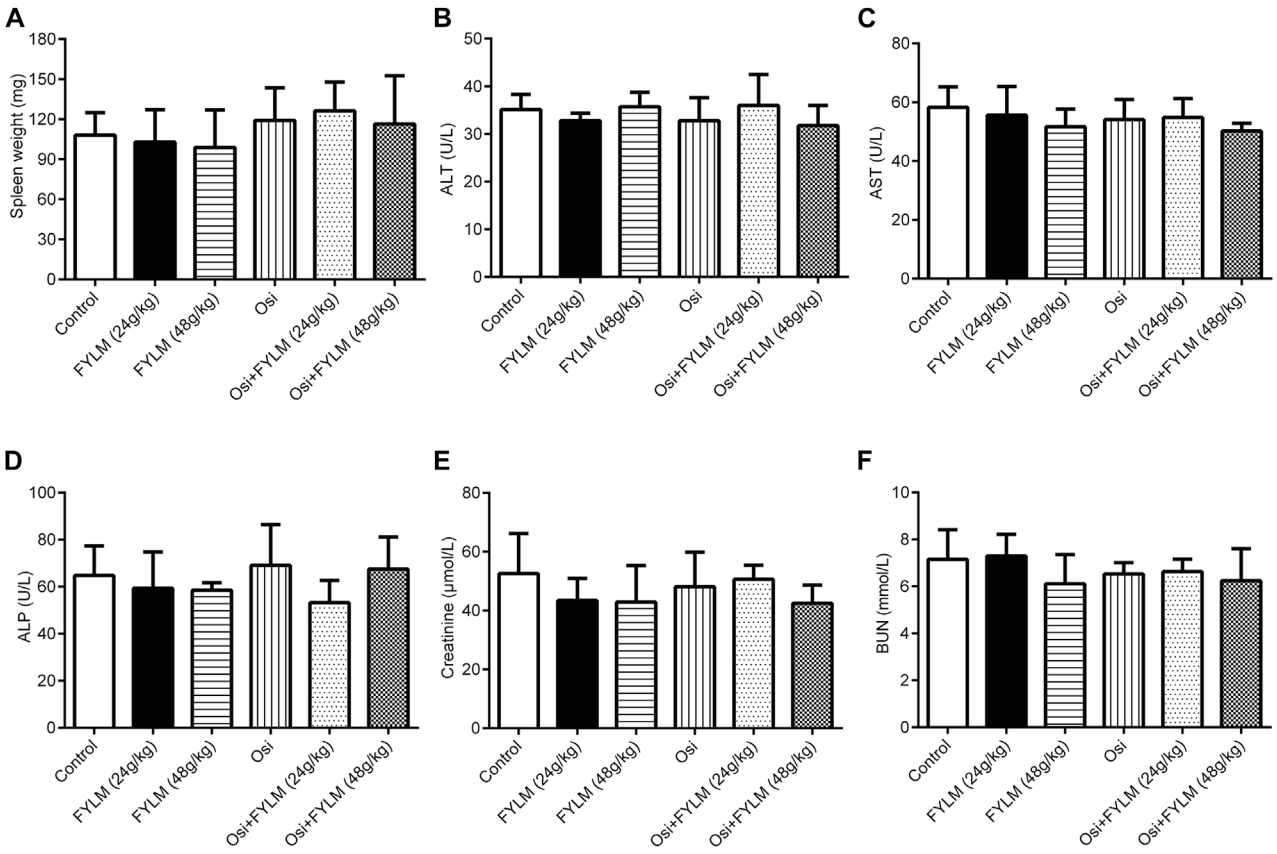

FIGURE 4
FYLM combined with osimertinib has no obvious toxicity to EGFR-Del19/T790M/C797S LLC tumor-bearing mice. **(A)** Spleen weight. **(B)** Alanine aminotransferase (ALT), **(C)** aspartate aminotransferase (AST), **(D)** alkaline phosphatase (ALP), **(E)** creatinine and **(F)** blood urea nitrogen (BUN) levels were measured after 2 weeks of drugs treatment. Osi, osimertinib. All data are shown as mean ± SD.

assays showed a decrease of β-catenin protein in both the combination treatment of osimertinib and FYLM (24 g/kg) group and the combination treatment of osimertinib and FYLM (48 g/kg) group (Figure 7A). Western blot assays revealed that combination treatment of osimertinib and FYLM (24 and 48 g/kg) suppress PRC1, β-catenin, c-Myc and c-Jun expression relative to the treatment with osimertinib or FYLM alone (Figures 7B–G). The Wnt pathway and the EGFR pathway are key pathways related to drug resistance, and they crosstalk each other. Inhibition of Wnt pathway and EGFR pathway can delay drug resistance. No significant changes in EGFR and Akt expression in the combination treatment group compared to other individual treatment groups in terms of real-time qPCR and immunoblotting of mouse tumor tissues (Figures 8A, B, E, G). However, the combination of osimertinib and FYLM (24 and 48 g/kg) reduced the expression of p-EGFR/EGFR and p-Akt/Akt ratios (Figures 8C, D, F). These results suggest that the combination of FYLM and osimertinib inhibits the PRC1/Wnt/EGFR pathway, which may be the mechanism of FYLM alleviating TKI resistance.

4 Discussion

Based on the basic treatment method of strengthening healthy qi to eliminate pathogens, FYLM consists of two types of herbs: Huangqi, Baizhu, Renshen and Gancao to replenish healthy qi; and Banzhilian, Baihuasheshecao, Fuling, Zhebeimu, Shancigu, Yiyiren to eliminate unhealthy trends. Studies have shown that during the treatment of lung cancer, whether it is surgery, radiotherapy, chemotherapy or targeted therapy, the healthy qi is obviously damaged, manifested as fatigue, gastrointestinal reactions, rashes and other side effects (Krzyzanowska et al., 2021; Mössner, 2022). In addition, Chinese medicine compounds have shown a multitude of advantages in the treatment of lung cancer, such as synergistic inhibition of tumor growth, sensitivity to targeted therapy, and reduction of toxicity (Li et al., 2016; Shao et al., 2021). Hence, the Chinese medicine compound combined with targeted drugs is a promising treatment option for the treatment of TKI-resistant NSCLC. Clinically, FYLM has a good effect on the treatment of lung cancer and can reduce the adverse reactions of patients. In this study, we analyzed the major components of FYLM using UPLC-Q-Orbitrap-MS and identified 36 chemical constituents. Among them, it has been reported that quercetin, scutellarin, oleanolic acid, apigenin and formononetin can overcome acquired resistance to EGFR-TKIs by inhibiting proliferation, promoting apoptosis and inducing autophagy *in vitro* and *in vivo* (Chen et al., 2019a; Chen et al., 2019b; Yu et al., 2020b; Huang et al., 2021; Sun et al., 2021). For example, quercetin reduced the growth of EGFR-C797S mutated NSCLC cells *via* inhibiting ALX and promoting apoptosis. Similarly, the current study confirmed the role of FYLM in overcoming EGFR-TKI

10.3389/fphar.2023.1093017

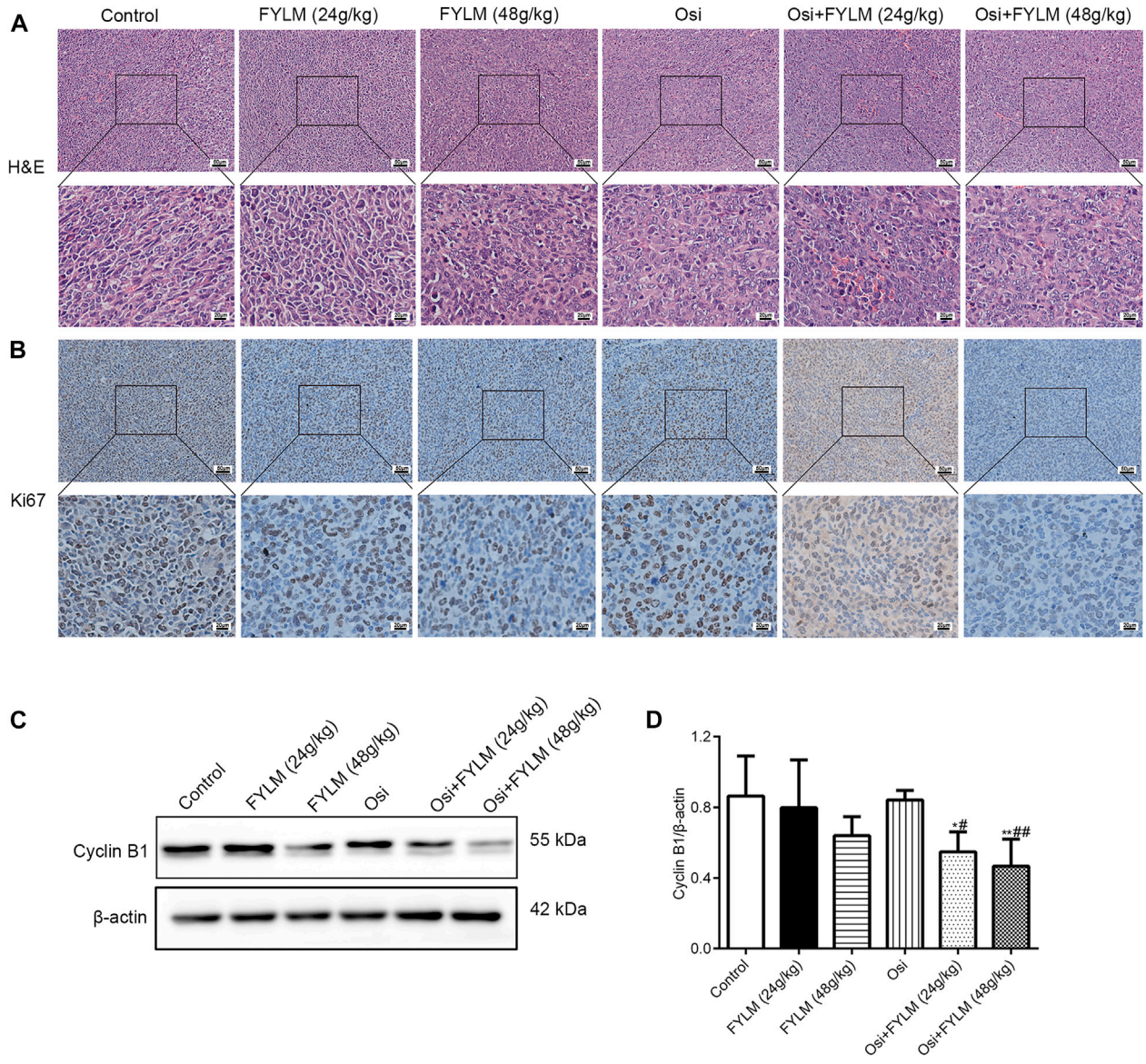

FIGURE 5
FYLM combined with osimertinib regulates cell proliferation and cell cycle in EGFR-Del19/T790M/C797S LLC tumor-bearing mice. **(A)** HE staining of tumor tissues. **(B)** Detection of Ki67 expression in tumor tissues by immunohistochemistry. **(C)** Cyclin B1 proteins were detected by western blotting. **(D)** Quantitative analysis of Cyclin B1 protein levels. *$p < 0.05$ and **$p < 0.01$ vs. Control; $^{\#}p < 0.05$ and $^{\#\#}p < 0.01$ vs. Osi. Osi, osimertinib. All data are shown as mean ± SD.

resistance in EGFR-mutated NSCLC. Specifically, we discovered that serum-containing FYLM inhibited cell growth both in triple-mutant cells and T790M-mutant cells. Animal experiments showed that the combination of FYLM and osimertinib suppressed tumor growth in LLC triple-mutant EGFR xenograft mice. In addition, the pathological changes of the tumor were observed by HE staining, and it was found that FYLM improved the malignancy of the tumor tissue in the xenograft model, decreased the density of nuclear, and decreased the nuclear-cytoplasmic ratio. Moreover, immunohistochemical results showed that FYLM also reduced the level of Ki-67 protein, and the effect of FYLM combined with osimertinib was more obvious. Ki-67 is mainly used to mark tumor cells in the proliferative cycle, and elevated Ki67 has a poor prognosis (Uxa et al., 2021). This suggests that the combination of FYLM and osimertinib has a synergistic effect in inhibiting the proliferation of EGFR-mutant NSCLC *in vitro* and *in vivo*.

Interestingly, we investigated the cyclin B1 (a cell cycle regulator) expression in mouse tumor tissues and found that the combination of FYLM and osimertinib downregulated the protein expression level of cyclin B1. Decreased expression of cyclinB1 causes G2 arrest, which is implicated in the mechanism of action of certain anticancer drugs (Lv et al., 2020). A previous report showed that the proliferation inhibition of NSCLC cells by sulforaphane was associated with cell cycle arrest caused by decreased cyclin B1 expression (Żuryń et al., 2019). It is well known that the most common hallmarks of cancer cells include sustained proliferation and attenuated apoptosis (Hanahan and Weinberg, 2011). Lately, research has shown that

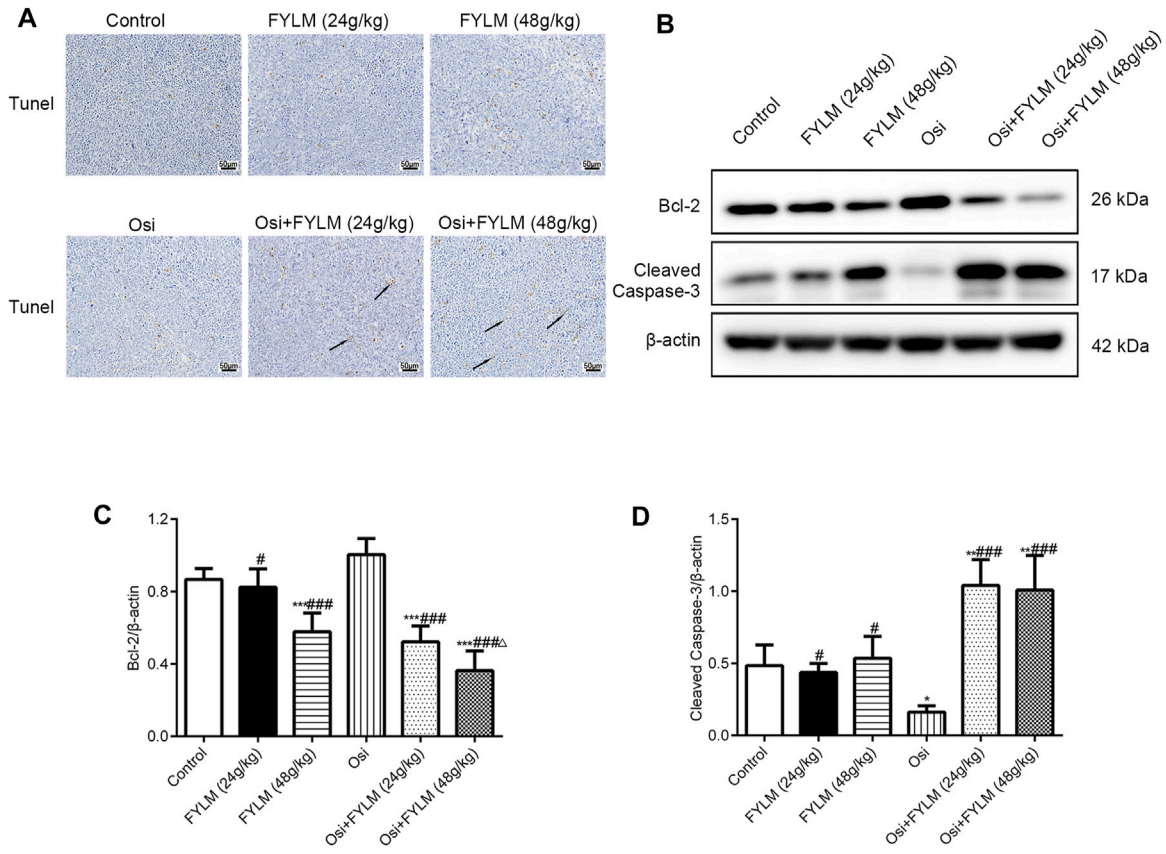

FIGURE 6
FYLM combined with osimertinib regulates apoptosis in EGFR-Del19/T790M/C797S LLC tumor-bearing mice. **(A)** Detection of apoptosis in tumor tissues by TUNEL staining. Arrows indicate brown-yellow apoptotic cells. **(B)** Bcl-2 and cleaved Caspase-3 proteins were detected by western blotting. **(C,D)** Quantitative analysis of Bcl-2 and cleaved Caspase-3 protein levels. $^{*}p < 0.05$, $^{**}p < 0.01$ and $^{***}p < 0.001$ vs. Control; $^{\#}p < 0.05$ and $^{\#\#\#}p < 0.001$ vs. Osi; $^{\triangle}p < 0.05$ vs. Osi + FYLM (24 g/kg). Osi, osimertinib. All data are shown as mean ± SD.

deoxypodophyllotoxin plays an important role in acquired resistance to gefitinib by inducing apoptosis in NSCLC cells (Kim et al., 2021). Consistent with the results, in our study, FYLM downregulated the expression of the apoptosis-related protein Bcl-2 while upregulating the cleaved caspase-3 in a mouse xenograft model. Furthermore, we investigated ALT, AST, ALP, CRE and BUN levels in the serum of xenograft-bearing mice and demonstrated that FYLM had no significant hepato-nephrotoxic side effects. In short, considering safety and efficacy, FYLM may be a natural, safe and promising adjunctive drug for the treatment of NSCLC harboring EGFR mutations. Overall, the above results suggest that FYLM reduces proliferation and arrests the cell cycle while increasing apoptosis to delay osimertinib resistance.

EGFR is a transmembrane receptor with tyrosine kinase activity that activates downstream signaling pathways *via* ligand-mediated autophosphorylation of intracellular tyrosine kinase domains (da Cunha Santos et al., 2011). Typically, EGFR downstream pathways are implicated in cell proliferation signaling, apoptosis, invasion, metastasis and angiogenesis (Levantini et al., 2022). Somatic mutations in the EGFR gene lead to ligand-independent activation of EGFR growth factor signaling (Harrison et al., 2020). Osimertinib, a potent EGFR inhibitor, competitively binds to the ATP site of the tyrosine kinase domain of EGFR, inhibits EGFR autophosphorylation, blocks the cell cycle and promotes apoptosis of tumor cells (Leonetti et al., 2019). Unfortunately, resistance mutations reduce osimertinib binding to EGFR, i.e., the development of acquired resistance, marking the agent's less effective inhibition of this pathway (Du et al., 2021). To date, no drug has been used to treat the $EGFR^{Del19/T790M/C797S}$ mutation caused by osimertinib. In our research, we chose a mouse Lewis lung carcinoma cell line harboring the Del19/T790M/C797S mutation generated by lentiviral transfection as a model of osimertinib resistance. Moreover, the H1975 cell line carrying the L858R/T790M mutation as control cells was sensitive to osimertinib. The triple mutant LLC cells were then injected subcutaneously into C57BL/6 mice to create an animal xenograft model. In addition, mouse Lewis lung cancer has been widely used as an experimental model for tumor research, especially in anti-tumor drug screening (Xu et al., 2018; Wang et al., 2021a). In *in vitro* study, we demonstrated that serum-containing FYLM downregulated the expression of p-EGFR protein in a dose-dependent manner, and the effect of the combination with osimertinib and FYLM was more obvious in triple-mutant cells. Similarly, FYLM synergizes with osimertinib to reduce the protein levels of p-EGFR and p-Akt in LLC triple-mutant tumor-bearing mice. The data show that combined treatment with FYLM and osimertinib inhibits the phosphorylation of EGFR in drug-resistant cells and triple-mutant xenografts.

10.3389/fphar.2023.1093017

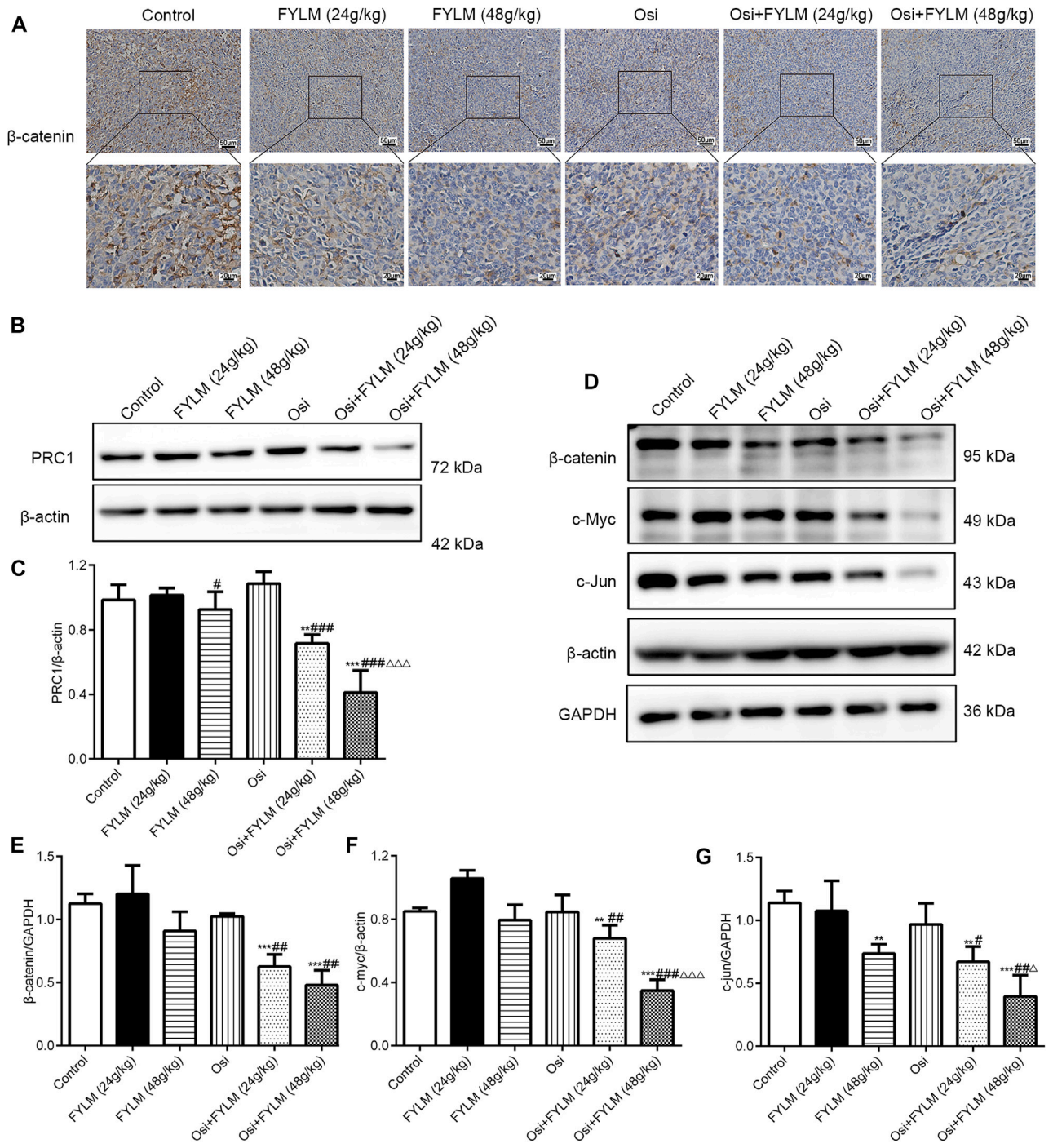

FIGURE 7
FYLM combined with osimertinib regulated PRC1/Wnt pathway in EGFR-Del19/T790M/C797S LLC tumor-bearing mice. **(A)** Detection of β-catenin expression in tumor tissues by immunohistochemistry. **(B,D)** PRC1, β-catenin, c-Myc and c-Jun proteins were detected by western blotting. **(C,E–G)** Quantitative analysis of PRC1, β-catenin, c-Myc and c-Jun protein levels. $^{**}p < 0.01$ and $^{***}p < 0.001$ vs. Control; $^{\#}p < 0.05$, $^{\#\#}p < 0.01$ and $^{\#\#\#}p < 0.001$ vs. Osi; $^{\triangle}p < 0.05$ and $^{\triangle\triangle\triangle}p < 0.001$ vs. Osi + FYLM (24 g/kg). Osi, osimertinib. All data are shown as mean ± SD.

Moreover, studies have shown that PRC1 is associated with poor prognosis in lung adenocarcinoma, and thus inhibition of PRC1 may be a promising therapeutic target for lung adenocarcinoma (Chen et al., 2016). More importantly, gene silencing of PRC1 could reduce the expression of β-catenin, cyclin D2, c-Myc and c-Jun in Wnt/β-catenin pathway in NSCLC cell lines (Zhan et al., 2017). In addition, the Wnt/β-catenin pathway mainly regulates important cellular functions such as cell proliferation, differentiation and apoptosis, and is involved in tumorigenesis and drug resistance of NSCLC (Stewart, 2014). In erlotinib-resistant HCC827/ER cells, suppressing the activation of the Wnt/β-catenin signaling can inhibit erlotinib resistance and cell migration (Wang et al., 2020). At the same time, EGFR mutations lead to nuclear accumulation of β-catenin,

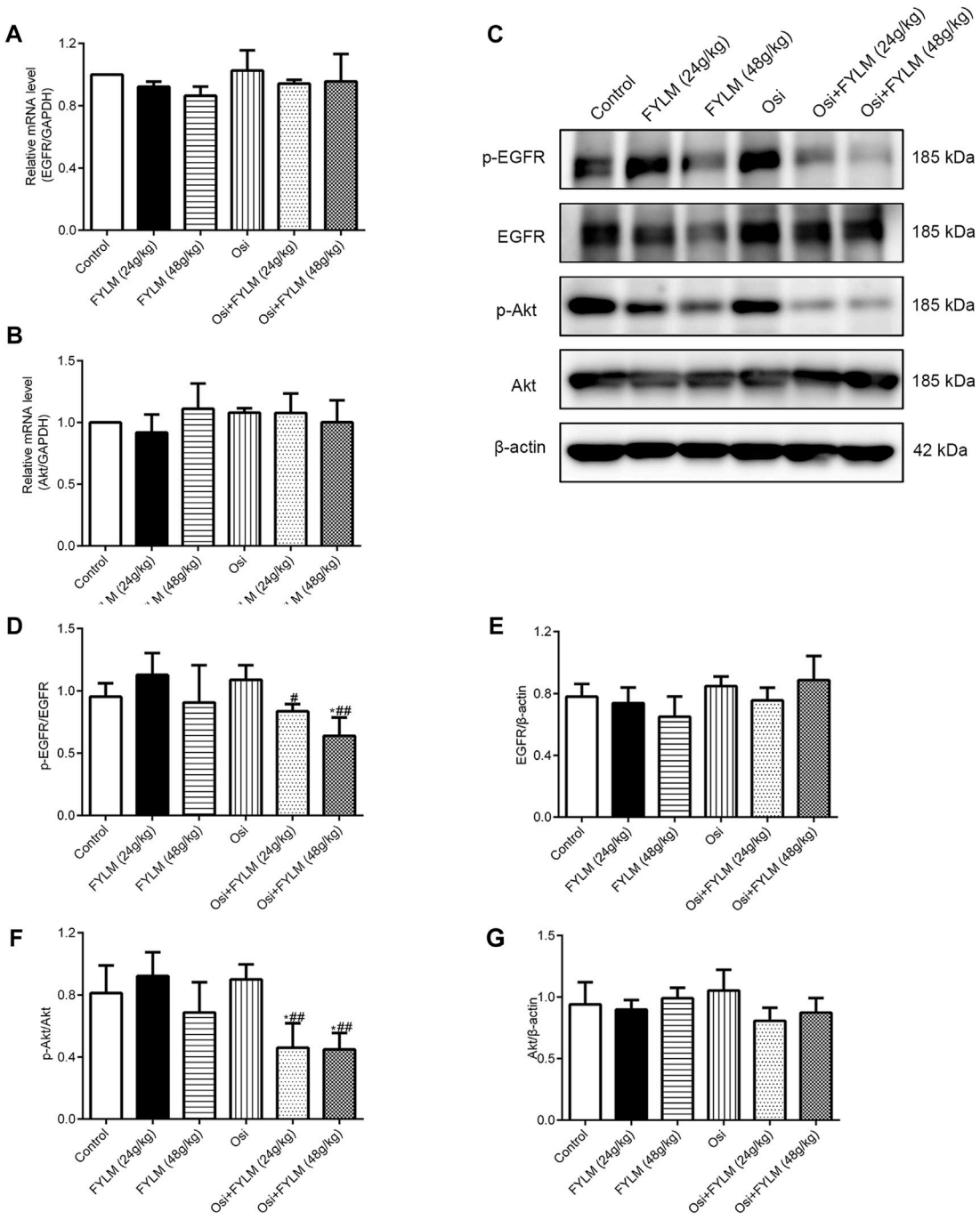

FIGURE 8
FYLM combined with osimertinib regulated EGFR pathway in EGFR-Del19/T790M/C797S LLC tumor-bearing mice. **(A,B)** mRNA levels of EGFR and Akt detected by real-time qPCR. **(C)** p-EGFR, EGFR, p-Akt and Akt proteins were detected by western blotting. **(D–G)** Quantitative analysis of p-EGFR/EGFR, EGFR, p-Akt/Akt and Akt protein levels. $^{*}p < 0.05$ vs. Control; $^{\#}p < 0.05$, $^{\#\#}p < 0.01$ vs. Osi. Osi, osimertinib. All data are shown as mean ± SD.

which activates the conduction of the Wnt pathway. The Wnt signaling pathway interacts with the EGFR signaling pathway to jointly regulate EGFR-TKI resistance. In our study, we discovered that FYLM not only decreased the PRC1 protein levels but also β-catenin, c-Myc and c-Jun protein levels in xenograft models. All of these results suggest that FYLM is associated with downregulation of PRC1 and Wnt/β-catenin pathway expression, reduced proliferation and increased apoptosis, thereby delaying resistance to osimertinib in drug-resistant cells and triple-mutant xenografts. Notably, FYLM can sensitize resistance-mutant NSCLC to osimertinib by affecting the PRC1/Wnt/EGFR pathway. However, this pathway may be regulated by multiple factors, and our current research did not carry out a retrospective experiment. In the next phase of research, pathway inhibitors should be applied for further validation. Another limitation of this study is that we only

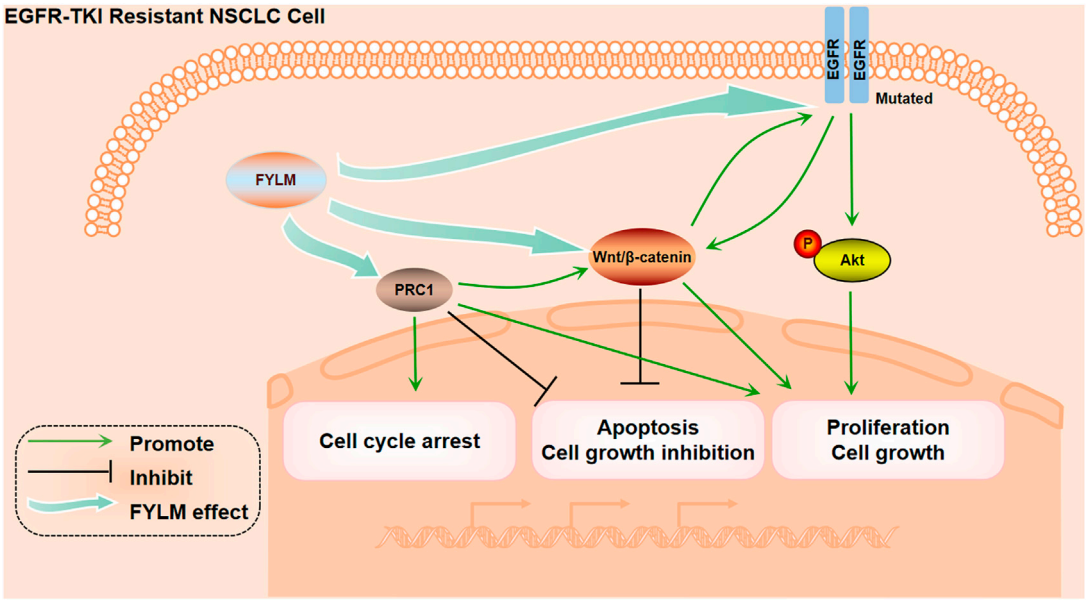

FIGURE 9
The Mechanism diagram of FYLM alleviating drug resistance.

evaluated the safety of liver function and kidney function in tumor-bearing mice, and further toxicity tests of FYLM still need to be conducted.

5 Conclusion

In summary, our study confirmed that FYLM synergistically reduces proliferation and increases apoptosis in EGFR mutant NSCLC cells. The mechanism of FYLM alleviating drug resistance may be related to reducing the expression of PRC1 and reducing the expression of Wnt pathway-related proteins. Furthermore, FYLM may be a promising adjunctive drug for patients with EGFR-mutant advanced NSCLC (Figure 9). The disadvantage of this study is that it only studied the research of FYLM in the treatment of lung cancer, and did not involve the research of FYLM in the treatment of other types of cancer. In order to better develop the medicinal value of FYLM, further research needs to be done.

Data availability statement

The original contributions presented in the study are included in the article/Supplementary Material, further inquiries can be directed to the corresponding author.

Ethics statement

The animal study was reviewed and approved by Ethics Review Committee of Shandong University of Traditional Chinese Medicine.

Author contributions

XZ and XL designed the experiments and provided technical guidance throughout the experiments. JS performed the experiments and wrote the manuscript. SH analyzed the data. YL performed part of the animal experiments. All authors approved the final version of the manuscript.

Funding

This research was supported by the Science and Technology Plan Project of Qingdao (No. 21-1-4-rkjk-17-nsh).

Acknowledgments

We thank the Science and Technology Plan Project of Qingdao (No. 21-1-4-rkjk-17-nsh) for financial support. We thank the Experimental Center, Shandong University of Traditional Chinese Medicine for providing the experimental platform. We thank the Chinese Medicine Antiviral Scientific Research Platform and Shandong Chinese Medicine Antiviral Engineering Research Center for providing technical support.

Conflict of interest

The authors declare that the research was conducted in the absence of any commercial or financial relationships that could be construed as a potential conflict of interest.

Publisher's note

References

Arasada, R. R., Shilo, K., Yamada, T., Zhang, J., Yano, S., Ghanem, R., et al. (2018). Notch3-dependent β-catenin signaling mediates EGFR TKI drug persistence in EGFR mutant NSCLC. *Nat. Commun.* 9 (1), 3198. doi:10.1038/s41467-018-05626-2

Cao, Y., Song, H., Sun, Q., Wng, S., and Zheng, X. (2016). Experimental study on inhibition of feiyuliu mixture on the growth of A549 nude mice transplanted tumors. *Shandong J. Traditional Chin. Med.* 35 (10), 901–904. doi:10.16295/j.cnki.0257-358x.2016.10.020

Chen, J., Rajasekaran, M., Xia, H., Zhang, X., Kong, S. N., Sekar, K., et al. (2016). The microtubule-associated protein PRC1 promotes early recurrence of hepatocellular carcinoma in association with the Wnt/β-catenin signalling pathway. *Gut* 65 (9), 1522–1534. doi:10.1136/gutjnl-2015-310625

Chen, X., Gao, A., Zhang, F., Yang, Z., Wang, S., Fang, Y., et al. (2021). ILT4 inhibition prevents TAM- and dysfunctional T cell-mediated immunosuppression and enhances the efficacy of anti-PD-L1 therapy in NSCLC with EGFR activation. *Theranostics* 11 (7), 3392–3416. doi:10.7150/thno.52435

Chen, Z., Huang, K. Y., Ling, Y., Goto, M., Duan, H. Q., Tong, X. H., et al. (2019a). Discovery of an oleanolic acid/hederagenin-nitric oxide donor hybrid as an EGFR tyrosine kinase inhibitor for non-small-cell lung cancer. *J. Nat. Prod.* 82 (11), 3065–3073. doi:10.1021/acs.jnatprod.9b00659

Chen, Z., Tian, D., Liao, X., Zhang, Y., Xiao, J., Chen, W., et al. (2019b). Apigenin combined with gefitinib blocks autophagy flux and induces apoptotic cell death through inhibition of HIF-1α, c-myc, p-EGFR, and glucose metabolism in EGFR l858r+t790m-mutated H1975 cells. *Front. Pharmacol.* 10, 260. doi:10.3389/fphar.2019.00260

Cooper, A. J., Sequist, L. V., and Lin, J. J. (2022). Third-generation EGFR and ALK inhibitors: Mechanisms of resistance and management. *Nat. Rev. Clin. Oncol.* 19 (8), 499–514. doi:10.1038/s41571-022-00639-9

da Cunha Santos, G., Shepherd, F. A., and Tsao, M. S. (2011). EGFR mutations and lung cancer. *Annu. Rev. Pathol.* 6, 49–69. doi:10.1146/annurev-pathol-011110-130206

Du, X., Yang, B., An, Q., Assaraf, Y. G., Cao, X., and Xia, J. (2021). Acquired resistance to third-generation EGFR-TKIs and emerging next-generation EGFR inhibitors. *Innov. (Camb)* 2 (2), 100103. doi:10.1016/j.xinn.2021.100103

Ettinger, D. S., Wood, D. E., Aisner, D. L., Akerley, W., Bauman, J. R., Bharat, A., et al. (2022). Non-small cell lung cancer, version 3.2022, NCCN clinical practice guidelines in oncology. *J. Natl. Compr. Canc Netw.* 20 (5), 497–530. doi:10.6004/jnccn.2022.0025

Geng, X., Wu, H., Li, Z., Li, C., Chen, D., Zong, J., et al. (2021). Jie-Yu-He-Huan capsule ameliorates anxiety-like behaviours in rats exposed to chronic restraint stress via the cAMP/PKA/CREB/BDNF signalling pathway. *Oxid. Med. Cell Longev.* 2021, 1703981. doi:10.1155/2021/1703981

Gesthalter, Y., Smyth, R., and Sullivan, D. (2022). Treatment of advanced-stage non-small cell lung cancer. *Am. J. Respir. Crit. Care Med.* 205 (5), P9–p10. doi:10.1164/rccm.2055P9

Hanahan, D., and Weinberg, R. A. (2011). Hallmarks of cancer: The next generation. *Cell* 144 (5), 646–674. doi:10.1016/j.cell.2011.02.013

Harrison, P. T., Vyse, S., and Huang, P. H. (2020). Rare epidermal growth factor receptor (EGFR) mutations in non-small cell lung cancer. *Semin. Cancer Biol.* 61, 167–179. doi:10.1016/j.semcancer.2019.09.015

Higgins, K. A., Puri, S., and Gray, J. E. (2022). Systemic and radiation therapy approaches for locally advanced non-small-cell lung cancer. *J. Clin. Oncol.* 40 (6), 576–585. doi:10.1200/jco.21.01707

Hsu, W. H., Yang, J. C., Mok, T. S., and Loong, H. H. (2018). Overview of current systemic management of EGFR-mutant NSCLC. *Ann. Oncol.* 29, i3–i9. doi:10.1093/annonc/mdx702

Huang, K. Y., Wang, T. H., Chen, C. C., Leu, Y. L., Li, H. J., Jhong, C. L., et al. (2021). Growth suppression in lung cancer cells harboring EGFR-C797S mutation by quercetin. *Biomolecules* 11 (9), 1271. doi:10.3390/biom11091271

Jiang, X. M., Xu, Y. L., Yuan, L. W., Zhang, L. L., Huang, M. Y., Ye, Z. H., et al. (2021). TGFβ2-mediated epithelial-mesenchymal transition and NF-κB pathway activation contribute to osimertinib resistance. *Acta Pharmacol. Sin.* 42 (3), 451–459. doi:10.1038/s41401-020-0457-8

Kim, H. S., Oh, H. N., Kwak, A. W., Kim, E., Lee, M. H., Seo, J. H., et al. (2021). Deoxypodophyllotoxin inhibits cell growth and induces apoptosis by blocking EGFR and MET in gefitinib-resistant non-small cell lung cancer. *J. Microbiol. Biotechnol.* 31 (4), 559–569. doi:10.4014/jmb.2101.01029

Krzyzanowska, M. K., Julian, J. A., Gu, C. S., Powis, M., Li, Q., Enright, K., et al. (2021). Remote, proactive, telephone based management of toxicity in outpatients during adjuvant or neoadjuvant chemotherapy for early stage breast cancer: Pragmatic, cluster randomised trial. *Bmj* 375, e066588. doi:10.1136/bmj-2021-066588

Leonetti, A., Sharma, S., Minari, R., Perego, P., Giovannetti, E., and Tiseo, M. (2019). Resistance mechanisms to osimertinib in EGFR-mutated non-small cell lung cancer. *Br. J. Cancer* 121 (9), 725–737. doi:10.1038/s41416-019-0573-8

Levantini, E., Maroni, G., Del Re, M., and Tenen, D. G. (2022). EGFR signaling pathway as therapeutic target in human cancers. *Semin. Cancer Biol.* 85, 253–275. doi:10.1016/j.semcancer.2022.04.002

Li, C., Niu, M., Wang, R., Zhou, X. W., Dong, B., Qi, S., et al. (2019). The modulatory properties of Si Jun Zi Tang enhancing anticancer of gefitinib by an integrating approach. *Biomed. Pharmacother.* 111, 1132–1140. doi:10.1016/j.biopha.2018.12.026

Li, J. (2010). *Clinical and experimental study on treating lung cancer with erlotinib and fei yiliu heji*. dissertation/master's thesis. Jinan (Shandong) University of Traditional Chinese Medicine.

Li, J., Dallmayer, M., Kirchner, T., Musa, J., and Grünewald, T. G. P. (2018). PRC1: Linking cytokinesis, chromosomal instability, and cancer evolution. *Trends Cancer* 4 (1), 59–73. doi:10.1016/j.trecan.2017.11.002

Li, L., Wang, S., Zheng, F., Wu, W., and Hann, S. S. (2016). Chinese herbal medicine Fuzheng Kang-Ai decoction sensitized the effect of gefitinib on inhibition of human lung cancer cells through inactivating PI3-K/Akt -mediated suppressing MUC1 expression. *J. Ethnopharmacol.* 194, 918–929. doi:10.1016/j.jep.2016.10.077

Lin, C., Huang, F., Shen, G., and Yiming, A. (2015). MicroRNA-101 regulates the viability and invasion of cervical cancer cells. *Int. J. Clin. Exp. Pathol.* 8 (9), 10148–10155.

Lv, S., Ning, H., Li, Y., Wang, J., Jia, Q., and Wen, H. (2020). Inhibition of cyclinB1 suppressed the proliferation, invasion, and epithelial mesenchymal transition of hepatocellular carcinoma cells and enhanced the sensitivity to TRAIL-induced apoptosis. *Onco Targets Ther.* 13, 1119–1128. doi:10.2147/ott.S225202

Michaelidou, K., Tzovaras, A., Missitzis, I., Ardavanis, A., and Scorilas, A. (2013). The expression of the CEACAM19 gene, a novel member of the CEA family, is associated with breast cancer progression. *Int. J. Oncol.* 42 (5), 1770–1777. doi:10.3892/ijo.2013.1860

Miller, M., and Hanna, N. (2021). Advances in systemic therapy for non-small cell lung cancer. *Bmj* 375, n2363. doi:10.1136/bmj.n2363

Molina, J. R., Yang, P., Cassivi, S. D., Schild, S. E., and Adjei, A. A. (2008). Non-small cell lung cancer: Epidemiology, risk factors, treatment, and survivorship. *Mayo Clin. Proc.* 83 (5), 584–594. doi:10.4065/83.5.584

Mössner, R. (2022). Severe side effects of targeted therapies. *J. Dtsch. Dermatol Ges.* 20 (6), 747–748. doi:10.1111/ddg.14827

Park, K., Tan, E. H., O'Byrne, K., Zhang, L., Boyer, M., Mok, T., et al. (2016). Afatinib versus gefitinib as first-line treatment of patients with EGFR mutation-positive non-small-cell lung cancer (LUX-Lung 7): A phase 2B, open-label, randomised controlled trial. *Lancet Oncol.* 17 (5), 577–589. doi:10.1016/s1470-2045(16)30033-x

Peng, Z., Zheng, X., Li, L., and Li, S. (2019). Effect of Feiyuliu ointment on PI3K/AKT pathway of Lewis lung cancer implanted tumor. *Chin. J. Gerontology* 39 (13), 3262–3266.

Ramalingam, S. S., Vansteenkiste, J., Planchard, D., Cho, B. C., Gray, J. E., Ohe, Y., et al. (2020). Overall survival with osimertinib in untreated, EGFR-mutated advanced NSCLC. *N. Engl. J. Med.* 382 (1), 41–50. doi:10.1056/NEJMoa1913662

Remon, J., Steuer, C. E., Ramalingam, S. S., and Felip, E. (2018). Osimertinib and other third-generation EGFR TKI in EGFR-mutant NSCLC patients. *Ann. Oncol.* 29, i20–i27. doi:10.1093/annonc/mdx704

Russo, A., Lopes, A. R., McCusker, M. G., Garrigues, S. G., Ricciardi, G. R., Arensmeyer, K. E., et al. (2020). New targets in lung cancer (excluding EGFR, ALK, ROS1). *Curr. Oncol. Rep.* 22 (5), 48. doi:10.1007/s11912-020-00909-8

Shao, N., Xiao, Y., Zhang, J., Zhu, Y., Wang, S., and Bao, S. (2021). Modified sijunzi decoction inhibits epithelial-mesenchymal transition of non-small cell lung cancer by attenuating AKT/GSK3β pathway *in vitro* and *in vivo*. *Front. Pharmacol.* 12, 821567. doi:10.3389/fphar.2021.821567

Sharma, S. V., Bell, D. W., Settleman, J., and Haber, D. A. (2007). Epidermal growth factor receptor mutations in lung cancer. *Nat. Rev. Cancer* 7 (3), 169–181. doi:10.1038/nrc2088

Siegel, R. L., Miller, K. D., Fuchs, H. E., and Jemal, A. (2022). Cancer statistics, 2016. *CA Cancer J. Clin.* 72 (1), 7–30. doi:10.3322/caac.21332

Stewart, D. J. (2014). Wnt signaling pathway in non-small cell lung cancer. *J. Natl. Cancer Inst.* 106 (1), djt356. doi:10.1093/jnci/djt356

Sun, S., Weil, M. H., Tang, W., Kamohara, T., and Klouche, K. (2004). Delta-opioid receptor agonist reduces severity of postresuscitation myocardial dysfunction. *Am. J. Physiol. Heart Circ. Physiol.* 287 (2), H969–H974. doi:10.1152/ajpheart.01171.2003

Sun, W., Ge, Y., Cui, J., Yu, Y., and Liu, B. (2021). Scutellarin resensitizes oxaliplatin-resistant colorectal cancer cells to oxaliplatin treatment through inhibition of PKM2. *Mol. Ther. Oncolytics* 21, 87–97. doi:10.1016/j.omto.2021.03.010

Sung, H., Ferlay, J., Siegel, R. L., Laversanne, M., Soerjomataram, I., Jemal, A., et al. (2021). Global cancer statistics 2020: GLOBOCAN estimates of incidence and mortality worldwide for 36 cancers in 185 countries. *CA Cancer J. Clin.* 71 (3), 209–249. doi:10.3322/caac.21660

Testa, U., Castelli, G., and Pelosi, E. (2018). Lung cancers: Molecular characterization, clonal heterogeneity and evolution, and cancer stem cells. *Cancers (Basel)* 10 (8), 248. doi:10.3390/cancers10080248

Thress, K. S., Paweletz, C. P., Felip, E., Cho, B. C., Stetson, D., Dougherty, B., et al. (2015). Acquired EGFR C797S mutation mediates resistance to AZD9291 in non-small cell lung cancer harboring EGFR T790M. *Nat. Med.* 21 (6), 560–562. doi:10.1038/nm.3854

Uchibori, K., Inase, N., Araki, M., Kamada, M., Sato, S., Okuno, Y., et al. (2017). Brigatinib combined with anti-EGFR antibody overcomes osimertinib resistance in EGFR-mutated non-small-cell lung cancer. *Nat. Commun.* 8, 14768. doi:10.1038/ncomms14768

Uxa, S., Castillo-Binder, P., Kohler, R., Stangner, K., Müller, G. A., and Engeland, K. (2021). Ki-67 gene expression. *Cell Death Differ.* 28 (12), 3357–3370. doi:10.1038/s41418-021-00823-x

Wang, Q., Liao, J., He, Z., Su, Y., Lin, D., Xu, L., et al. (2020). LHX6 affects erlotinib resistance and migration of EGFR-mutant non-small-cell lung cancer HCC827 cells through suppressing wnt/β-catenin signaling. *Onco Targets Ther.* 13, 10983–10994. doi:10.2147/ott.S258896

Wang, Y., An, E. K., Kim, S. J., You, S., and Jin, J. O. (2021a). Intranasal administration of codium fragile polysaccharide elicits anti-cancer immunity against Lewis lung carcinoma. *Int. J. Mol. Sci.* 22 (19), 10608. doi:10.3390/ijms221910608

Wang, Y., Wu, G., Li, R., Luo, Y., Huang, X., He, L., et al. (2021b). Chinese medicine combined with EGFR-TKIs prolongs progression-free survival and overall survival of non-small cell lung cancer (NSCLC) patients harboring EGFR mutations, compared with the use of TKIs alone. *Front. Public Health* 9, 677862. doi:10.3389/fpubh.2021.677862

Westover, D., Zugazagoitia, J., Cho, B. C., Lovly, C. M., and Paz-Ares, L. (2018). Mechanisms of acquired resistance to first- and second-generation EGFR tyrosine kinase inhibitors. *Ann. Oncol.* 29, i10–i19. doi:10.1093/annonc/mdx703

Wu, S. G., and Shih, J. Y. (2018). Management of acquired resistance to EGFR TKI-targeted therapy in advanced non-small cell lung cancer. *Mol. Cancer* 17 (1), 38. doi:10.1186/s12943-018-0777-1

Xu, F., Cui, W. Q., Wei, Y., Cui, J., Qiu, J., Hu, L. L., et al. (2018). Astragaloside IV inhibits lung cancer progression and metastasis by modulating macrophage polarization through AMPK signaling. *J. Exp. Clin. Cancer Res.* 37 (1), 207. doi:10.1186/s13046-018-0878-0

Yu, S., Sha, H., Qin, X., Chen, Y., Li, X., Shi, M., et al. (2020a). EGFR E746-A750 deletion in lung cancer represses antitumor immunity through the exosome-mediated inhibition of dendritic cells. *Oncogene* 39 (13), 2643–2657. doi:10.1038/s41388-020-1182-y

Yu, X., Gao, F., Li, W., Zhou, L., Liu, W., and Li, M. (2020b). Formononetin inhibits tumor growth by suppression of EGFR-Akt-Mcl-1 axis in non-small cell lung cancer. *J. Exp. Clin. Cancer Res.* 39 (1), 62. doi:10.1186/s13046-020-01566-2

Zhan, P., Zhang, B., Xi, G. M., Wu, Y., Liu, H. B., Liu, Y. F., et al. (2017). PRC1 contributes to tumorigenesis of lung adenocarcinoma in association with the Wnt/β-catenin signaling pathway. *Mol. Cancer* 16 (1), 108. doi:10.1186/s12943-017-0682-z

Żuryń, A., Krajewski, A., Klimaszewska-Wiśniewska, A., Grzanka, A., and Grzanka, D. (2019). Expression of cyclin B1, D1 and K in non-small cell lung cancer H1299 cells following treatment with sulforaphane. *Oncol. Rep.* 41 (2), 1313–1323. doi:10.3892/or.2018.6919

frontiers | Frontiers in Pharmacology

TYPE Original Research
PUBLISHED 24 February 2023
DOI 10.3389/fphar.2023.1150774

OPEN ACCESS

EDITED BY
Eswar Shankar,
The Ohio State University, United States

REVIEWED BY
Bhagavatula Moorthy,
Baylor College of Medicine, United States
Fei Chen,
Stony Brook University, United States
Yaguang Xi,
Louisiana State University, United States
Muthusamy Thangaraju,
Augusta University, United States

*CORRESPONDENCE
Chendil Damodaran,
chendamodar@tamu.edu

†These authors have contributed equally to this work

SPECIALTY SECTION
This article was submitted to Pharmacology of Anti-Cancer Drugs, a section of the journal Frontiers in Pharmacology

RECEIVED 24 January 2023
ACCEPTED 10 February 2023
PUBLISHED 24 February 2023

CITATION
Saran U, Chandrasekaran B, Tyagi A, Shukla V, Singh A, Sharma AK and Damodaran C (2023), A small molecule inhibitor of Notch1 modulates stemness and suppresses breast cancer cell growth.
Front. Pharmacol. 14:1150774.
doi: 10.3389/fphar.2023.1150774

A small molecule inhibitor of Notch1 modulates stemness and suppresses breast cancer cell growth

Uttara Saran[1†], Balaji Chandrasekaran[1†], Ashish Tyagi[1], Vaibhav Shukla[1], Amandeep Singh[2], Arun K. Sharma[2] and Chendil Damodaran[1*]

[1]Texas A&M University, College Station, TX, United States, [2]Penn State Cancer Institute, College of Medicine, The Pennsylvania State University, Hershey, PA, United States

Although breast cancer stem cells (BCSCs) are well characterized, molecularly targeting and eradicating this sub-population remains a challenge in the clinic. Recent studies have explored several signaling pathways that govern stem cell activation: We and others established that the Notch1 signaling plays a significant role in the proliferation, survival, and differentiation of BCSCs. Earlier, we reported that a newly developed small molecule, ASR490, binds to the negative regulatory region (NRR: The activation switch of the Notch receptor) of Notch1. *In vitro* results demonstrated that ASR490 significantly inhibited BCSCs ($ALDH^+$ and $CD44^+/CD24^-$) and breast cancer (BC) growth at nM concentrations, and subsequently inhibited the colony- and mammosphere-forming abilities of BCSCs and BCs. ASR490 downregulated the expressions of Notch1 intracellular domain (NICD: The active form of Notch1) and its downstream effectors Hey1 and HES1. Inhibition of Notch1-NICD facilitated autophagy-mediated growth inhibition by triggering the fusion of autophagosome and autolysosome in BCSCs. ASR490 was found to be non-toxic to healthy cells as compared to existing Notch1 inhibitors. Moreover, oral administration of ASR490 abrogated BCSC and BC tumor growth in the *in vivo* xenograft models. Together our results indicate that ASR490 is a potential therapeutic agent that inhibits BC tumor growth by targeting and abolishing Notch1 signaling in BCSCs and BC cells.

KEYWORDS

breast cancer, breast cancer stem cell (BCSC), ASR490, autophagy, NOTCH1

Introduction

Breast cancer stem cells (BCSCs) are a small population of cancer cells within breast tumors that are characterized by their self-renewal ability and relative resistance to current therapeutics (Al-Hajj et al., 2003). Furthermore, evidence suggests that BCSCs are not eliminated during cancer treatment (Shafee et al., 2008; Abravanel et al., 2015), consequently contributing to the development of therapeutic resistance and tumor recurrence in breast cancer (BC) patients (Dandawate et al., 2016; Bai et al., 2018). Hence, despite advances in early diagnosis and therapy (Harbeck et al., 2019), resistance and relapse of BC remain as significant challenges, resulting in this malignancy being the most prevalent cause of cancer-related deaths among women. Therefore, there is an urgent need to develop novel

therapeutic strategies to target the signaling pathways responsible for BCSCs and eradicate this subpopulation in BC patients.

The aberrant activation of Notch signaling has been shown to play a significant role in BC progression by maintaining cancer stem cells (Majumder et al., 2021; Ranganathan et al., 2011; D'Angelo et al., 2015). Notch1 is predominantly active in BCSCs, and its aberrant activation has been reported to enhance BCSCs metastatic phenotype by promoting invasiveness and chemoresistance (Reedijk et al., 2005; Phillips et al., 2006; Dickson et al., 2007; Sajithlal et al., 2010; Zang et al., 2010; Krop et al., 2012; Bolos et al., 2013; Suman et al., 2013; Kim et al., 2015; Li et al., 2015). Overexpression of Notch1 has been correlated with a poor prognosis (Yuan et al., 2015) and decreased overall recurrence-free survival (Abravanel et al., 2015) in BC patients. Hence, Notch1 is an attractive target for eradicating BCSCs, and several preclinical studies have confirmed its potential role as a therapeutic target in cancer treatment.

Several strategies can target Notch1, including Notch1 monoclonal antibodies, siRNA, natural products, γ-secretase inhibitors, pan-Notch inhibitors, etc. (Sorrentino et al., 2019). We and others have shown that inhibition of Notch1 *in vitro* using either genetic or pharmacological approaches enhanced the antitumor efficacy of chemotherapy agents by suppressing BCSCs (Qiu et al., 2013; Suman et al., 2013; Cao et al., 2015; Zhou et al., 2017). These studies suggest that targeting Notch1 signaling of BCSCs could be an effective therapeutic strategy for eradicating and preventing metastatic disease. However, to date, Notch1-targeted therapies for BC have not advanced to clinical trials due to their toxicity and anticancer efficiency. Therefore, it is imperative to develop effective and safer Notch1-targeted treatments for BC that selectively inhibit in a way distinct from currently known Notch inhibitors to circumvent toxicity issues. Earlier, we reported the potency of a non-toxic small molecule Notch1 inhibitor, ASR490, a pyridine-2-carboxylic acid prodrug analog of Withaferin-A developed in our laboratories based on structure-activity relationship (SAR) studies on compounds generated by the modifications of Withaferin A core structure, in downregulating Notch1 expression and abrogating the growth of colon cancer cells (Tyagi et al., 2020).

Here, we explored whether ASR490 inhibited BCSC growth in the *in vitro* and *in vivo* models and dissected its mechanism of action. Our results suggested that ASR490 eradicated BCSCs and inhibited BC growth in preclinical models. Furthermore, molecular studies revealed that ASR490's inhibition of Notch1 facilitated the induction of autophagy signaling resulting in the suppression of BCSCs.

Materials and methods

Cell culture and reagents

Human mammary immortalized cells (MCF10A), and the TNBC cell line MDA-MB-231 were purchased from American Type Culture Collection. MCF10A cells were grown in a 1: 1 mixture of Dulbecco's modified Eagle's medium (DMEM) and Ham's F12 medium with 20 ng mL^{-1} human epidermal growth factor, 100 ng mL^{-1} cholera toxin, 0.01 mg mL^{-1} bovine insulin, 500 ng mL^{-1} hydrocortisone, and 5% horse serum. MDA-MB-231 cells were grown in DMEM containing L-glutamine and sodium pyruvate, supplemented with 10% fetal bovine serum and 1% antibiotic and antimycotic solution in a humidified atmosphere of 5% CO2 at 37°C in an incubator. Human BCSC cells: $ALDH^+$ and $CD44^+/CD24^-$, and BC cells: ALDH- were purchased from Celprogen (San Pedro, CA, United States) and maintained in human BCSC expansion and undifferentiation media. DAPT (γ-secretase), cycloheximide (CHX), chloroquine (CQ), and MG132 were purchased from Sigma (St. Louis, MO).

Synthesis of ASR490

ASR490 was synthesized in our laboratory as reported previously (Tyagi et al., 2020).

Cell viability assays

$ALDH^-$, $ALDH^+$, and $CD44^+/CD24^-$ cells were first treated with vehicle control (DMSO) or treatment (ASR490, DAPT, MG132, or CQ) for prescribed doses and time points. Cell viability assays: Alamar blue (Life Technologies Corporation Eugene, OR) and EdU Cell Proliferation (using the EdU-Click 488 kit, cat# BCK-EdU488-1, Sigma), were then performed per the manufacturer's instructions.

Soft agar colony formation assay

Colony formation assays were performed to monitor anchorage-independent growth using the CytoSelect 96-well *in vitro* Tumor Sensitivity Assay kit (Cell Biolabs Inc., San Diego, CA, United States). The assay was performed as described previously (Suman et al., 2014).

Invasion assay

Invasion assays were performed and evaluated using Boyden chambers equipped with polyethylene terephthalate membranes with 8-mm pores (BD Biosciences, San Jose, CA, United States) as described previously (Das et al., 2014).

Wound healing migration assay

Control and ASR490-treated $ALDH^-$, $ALDH^+$, and $CD44^+/CD24^-$ cells were cultured in six-well plates and subjected to wound healing migration assays as described previously (Chandrasekaran et al., 2017).

Mammosphere formation assay

The mammosphere formation ability of $ALDH^-$, $ALDH^+$, and $CD44^+/CD24^-$ cells was determined by culturing the cells with MammoCult basal medium (StemCell Technologies) in ultra-low attachment plates (Corning, Acton, MA, United States). The cells were treated with either vehicle or ASR490 and allowed to form spheroids for 2–3 weeks. After the first-generation mammospheres were counted, the vehicle and ASR490 treated mammospheres were resuspended as single-cell suspensions, measured, and re-cultured without treatment to determine their second-generation mammosphere formation ability. The spheres formed after 3 weeks were counted, resuspended, and cultured for a third generation without treatment to determine their third generation mammosphere formation ability.

Immunofluorescence and microscopy

Immunofluorescence assays were performed to determine the Notch1 expression of the vehicle and ASR490-treated first, second,

and third-generation spheres as per the protocol described earlier (Suman et al., 2014). The spheres were imaged using a KEYENCE fluorescence microscope (BZ-X800/BZ-X810).

Apoptosis assay

Quantification of apoptosis was performed using the Annexin V-FITC apoptosis kit (BD Pharmingen, San Diego, CA, United States). After treatment with vehicle or ASR490 for 24 and 48 h, the ALDH$^-$, ALDH$^+$, and CD44$^+$/CD24$^-$ cells were suspended in 500 µL of binding buffer and stained with 5 mL of FITC-Annexin-V and 5 mL of propidium iodide for 15 min in the dark at room-temperature before being analyzed using a flow cytometer (Pal et al., 2018).

Transfection

ALDH$^+$ cells were transfected as per the protocol described elsewhere (Banks et al., 1985) with 20 nM of scrambled (SCR) or siRNA (siNOTCH1) obtained from OriGene Technologies Inc. (cat#: SR321124). Transfected cells were harvested after 48 h and used for cell proliferation, colony formation, and mammosphere assays following treatment with vehicle or ASR490. ALDH$^-$ cells were transfected with 500 ng plasmid concentration of pCMV6-NOTCH1 and vector pCMV6-Entry [NOTCH1 (NM_017617) Human ORF Clone] obtained from OriGene Technologies Inc. The cells were then harvested following treatment with vehicle or ASR490. Whole-cell lysates of transfected ALDH$^+$ and ALDH$^-$ were also prepared for Western blot analysis following treatment with vehicle or ASR490.

Proteasome activity

The proteasome activity of vehicle and ASR490-treated ALDH$^+$ cells was measured using a proteasome activity assay kit (BioVision) per the manufacturer's protocol. MG132 was used as the positive control.

RNA isolation, cDNA library construction, and RNA sequencing

Total RNA was isolated from ALDH$^+$ and ALDH$^-$ cells treated for 6 and 12 h with either vehicle or ASR490 using TRIzol (Thermo Fisher Scientific, Waltham, MA, United States). The quantity and quality of RNA were assessed using a NanoDrop™ spectrophotometer (Fisher Scientific). The cDNA library was prepared according to the manufacturer's instructions using Novogene Bioinformatics Technologies (Beijing, China) and a NEBNext Ultra TM RNA library kit for Illumina (New England Biolabs, Ipswich, MA, United States) by Novogene Bioinformatics Technologies Co. Ltd. The amplified cDNA library was then purified using the AMPure XP system (Beckman Coulter, Brea, CA, United States). The library quality was evaluated using the Agilent bioanalyzer 2,100 system. Finally, the enriched product was sequenced using the Illumina HiSeq 2,000/2,500 platform, and paired ends were generated. The raw data was analyzed and differential expression analysis was performed using the previously described method (Shukla et al., 2022).

Functional enrichment analysis

Gene set enrichment analysis (GSEA) was performed using GSEA software version 4.2.2 (16199517). Volcano plots were generated by SRplot (https://www.bioinformatics.com.cn/en), a free online platform for data analysis and visualization while ShinyGO was used to predict Kyoto Encyclopedia of Genes and Genomes (KEGG) pathways (Ge et al., 2020). Gene ontology (GO) analysis was performed by PANTHER (Mi et al., 2019).

Western blotting and immunoprecipitation (IP)

Cell lysates of ALDH$^-$, ALDH$^+$, and CD44$^+$/CD24$^-$ cells following treatment with vehicle and treatment (ASR490, DAPT, MG132, CHX, or CQ) for prescribed doses and time points, were prepared with RIPA buffer (Thermo Scientific, Rockford, IL, United States) per the manufacturer's protocol. Western blotting was performed using specific antibodies against Notch1 (CST, #3608), HES1 (Sigma, #SAB2108472), Hey1 (Proteintech, #19929-1-AP), NFκB p65 (CST, #8242), Bcl-2 (CST, #15071), Bcl-xL (CST, #2764), Vimentin (CST, #46173), Slug (CST, #9585), E-Cadherin (CST, #3195), β-catenin (CST, #8480), Ubiquitin (CST, #3933), Cleaved-PARP (CST, #5625), Cleaved-caspase-9 (CST, #20750), BAX (CST, #41162), Notch2 (CST, #D76A6), Lamp1 (CST, #9091), and LC3B (Proteintech, #14600-1-AP). β-Actin (CST, #4970) was used as the loading control. Protein bands were visualized using the Bio-Rad ChemiDocTM imaging system. For IP experiments, protein samples were immunoprecipitated with Notch1 antibody as per the protocol described elsewhere (Chandrasekaran et al., 2020), and Western blots were performed with ubiquitin antibody.

Xenograft studies

The *in vivo* efficiency of ASR490 in abrogating ALDH$^+$ and ALDH$^-$ tumorigenesis was evaluated by subcutaneously injecting each cell type (ALDH$^+$: 0.5×10^6 cells and ALDH$^-$: 0.8×10^6 cells) into female athymic mice (The Jackson Laboratory). ASR490 was dissolved in DMSO and then diluted in PBS by sonication to create a 0.1% solution. Once the tumors were approximately ~50 mm^3, the mice bearing ALDH$^+$ and ALDH$^-$ tumors were randomized into the vehicle (0.1% DMSO in PBS) and treatment (25 mg/kg, ASR490) groups (n = 6). ASR490 was administered orally for 7 days over 4 weeks. The mice were monitored daily, and tumor volumes and body weight were measured weekly. After 4 weeks of treatment, all mice were euthanized by CO_2 asphyxiation, and the xenograft tumors were collected for immunohistochemical analyses. All experimental animals were approved by the University of Louisville's ethical committee and maintained by the Institutional Animal Care and Use Committee-approved protocols.

Immunohistochemistry (IHC) analysis

Tumor specimens from the vehicle and ASR490-treated ALDH$^+$ and ALDH$^-$ xenografts were fixed in 10% formalin and processed for IHC analysis per the protocol previously described (Chandrasekaran et al., 2020). IHC analyses were performed for Notch1, HES1, and Ki67 expression, and images (40x) were captured using an Olympus BX43 microscope (Olympus America, Center Valley, PA).

Statistical analysis

Statistical analyses were performed using GraphPad Prism 8.0 software (GraphPad Software Inc., La Jolla, CA, United States). Values were presented as mean ± SD. One-way or two-way ANOVA and unpaired two-tailed Student's t-tests were performed to determine the significance between groups. A p-value of < 0.05 was considered statistically significant.

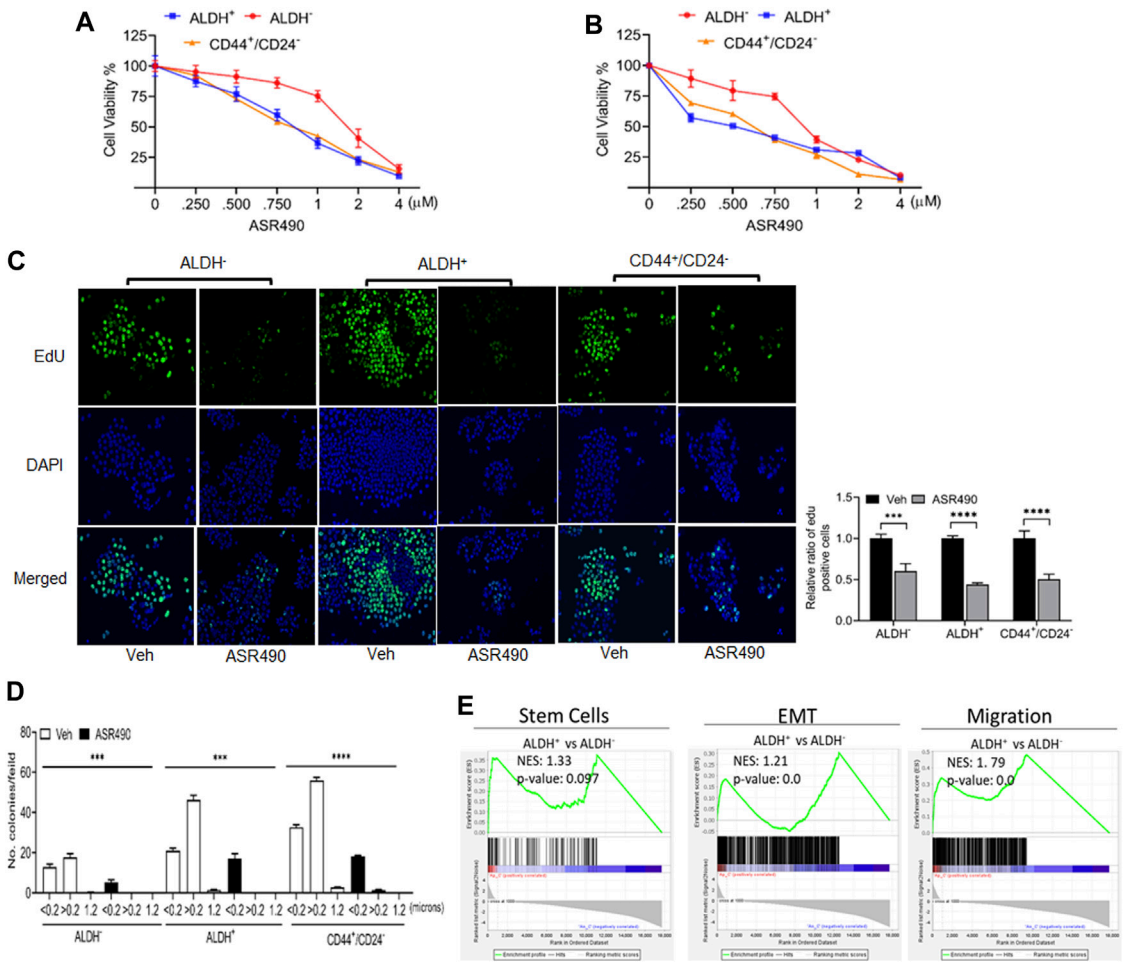

FIGURE 1
ASR490 suppresses the growth of ALDH$^-$, ALDH$^+$, and CD44$^+$/CD24$^-$ **(A, B)**. MTT cell viability assays performed on ALDH$^-$, ALDH$^+$, and CD44$^+$/CD24$^-$ cells following treatment with various concentrations of ASR490 (0, 0.250, 0.500, 0.750, 1, 2, and 4 μM) for 24 **(A)** and 48 h **(B)** (n = 6). **(C)** Representative images of EdU cell proliferation assay performed on vehicle and ASR490-treated ALDH$^-$, ALDH$^+$, and CD44$^+$/CD24$^-$ cells. Data were quantified by counting the cells demonstrating EdU (5-ethynyl-2′-deoxyuridine) expression per treatment group for each cell type using Image J software (n = 4, *** $p < 0.001$ and **** $p < 0.0001$). p values are based on two-way ANOVA with the *post hoc* Sidak test. **(D)** Colony-forming assay of the vehicle and ASR490-treated ALDH$^-$, ALDH$^+$, and CD44$^+$/CD24$^-$ cells (n = 6; *** $p < 0.006$ and **** $p < 0.0001$). p values are based on one-way ANOVA with a *post hoc* LSD test. **(E)** GSEA analyses of RNAseq data showing enrichment of genes in stem cell, EMT, metastasis signaling pathways in ALDH$^+$ vs. ALDH$^-$ cells (n = 4).

Results

ASR490 inhibits the growth of BCSCs and BC

ALDH$^+$ and CD44$^+$/CD24$^-$ are reported to be the top two markers enriched in BCSC populations (Douville et al., 2009; Charafe-Jauffret et al., 2010) which exhibit elevated Notch1 activity, and consequently, higher tumorigenic capability (D'Angelo et al., 2015; Ginestier et al., 2007). To determine ASR490's inhibitory function, we performed two cell proliferation assays on the ALDH$^-$, ALDH$^+$, and CD44$^+$/CD24$^-$ cells. Cell viability assays demonstrated that ASR490 effectively inhibited the viability of all three cell types, though its effects on Notch1-positive BCSCs (ALDH$^+$: IC50: 770 nM at 24 h, and 443 nM at 48 h; and CD44$^+$/CD24$^-$: IC50: 800 nM at 24 h, and 541 nM at 48 h) was more profound than its effect on ALDH$^-$ BC cells (IC50: 1.6 μM at 24 h and 836 nM at 48 h) (Figures 1A, B). Similar results were confirmed by EdU-proliferation analyses on all three cell types (Figure 1C). Next, we determined if ASR490 could inhibit the anchorage-independent growth of ALDH$^-$, ALDH$^+$, and CD44$^+$/CD24$^-$ cells. As seen in Figure 1D, vehicle-treated ALDH$^+$ and CD44$^+$/CD24$^-$ cells showed a higher number of <0.2, >0.2, and 1.2 micron-sized colonies compared to vehicle-treated ALDH$^-$ cells; however, treatment with ASR490 significantly suppressed the colony-formation ability of ALDH$^+$ and CD44$^+$/CD24$^-$ cells as compared to their respective vehicle-treated controls. Similar results were seen in ALDH$^-$ BC cells.

Next, we performed transcriptomic analysis to determine the possible mechanistic action of ASR490 on the stem cells. GSEA of vehicle control treated ALDH$^+$ and ALDH$^-$ cells revealed a significant enrichment of genes involved in the mammary stem

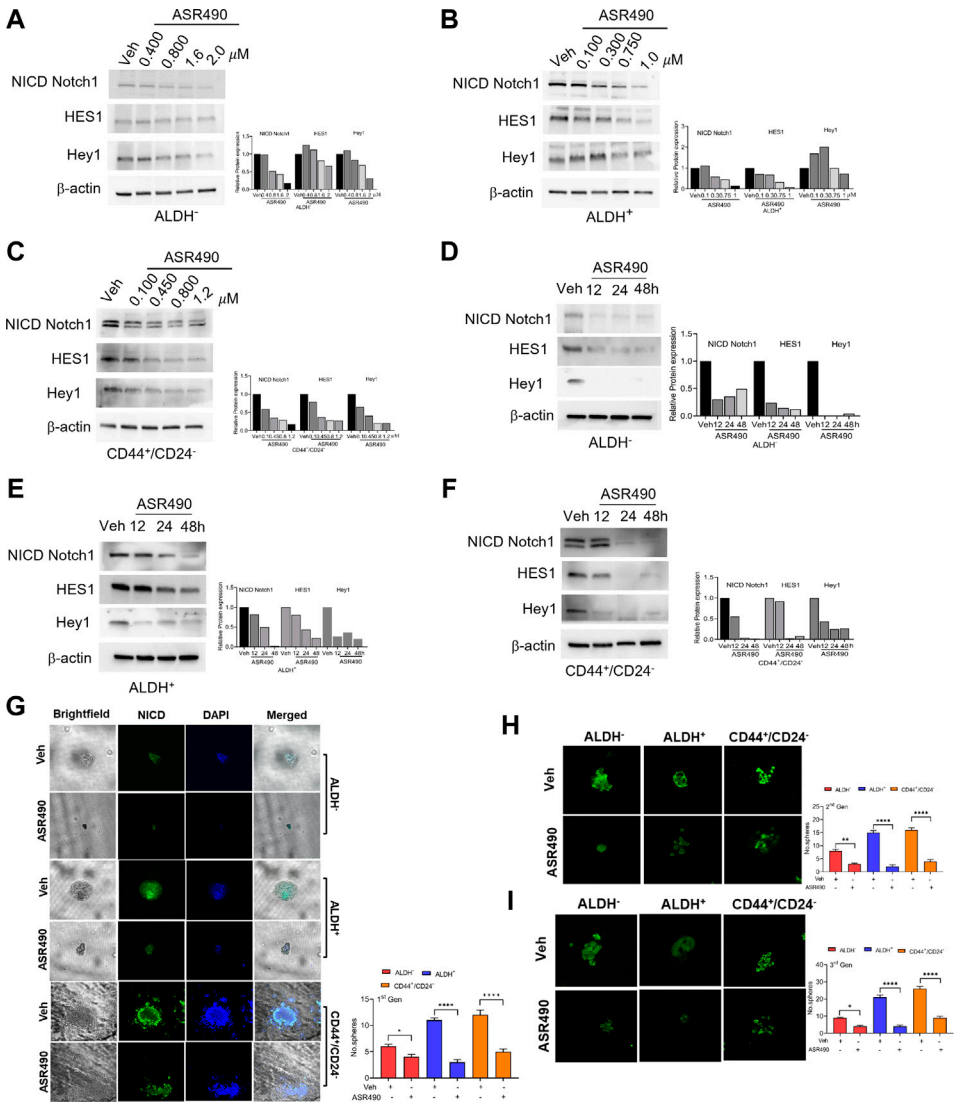

FIGURE 2
ASR490 mediates its effect by specifically inhibiting Notch1-NICD signaling and self-renewal capacity. **(A–F)** Western blots for Notch1-NICD (the active form of Notch1), HES1, and Hey1 expression to assess the dose- **(A–C)** and time-dependent **(D–F)** effects of ASR490 on ALDH$^-$, ALDH$^+$, and CD44$^+$/CD24$^-$ cells. **(G)** Representative brightfield and immunofluorescent images of Notch1-NICD (active form of Notch1) expression in vehicle and ASR490-treated first-generation mammospheres of ALDH$^-$, ALDH$^+$ and CD44$^+$/CD24$^-$ cells. The number of spheroids per group and cell type were quantified and presented graphically (n = 4, * p < 0.02 and **** p < 0.0001). **(H)** Immunofluorescent images of Notch1-NICD expression and number of spheroids quantified for second generation of serially passaged first-generation vehicle and ASR490-treated ALDH$^-$, ALDH$^+$, and CD44$^+$/CD24$^-$ mammospheres (n = 4, ** p < 0.007 and **** p < 0.0001), **(I)** Third generation of serially passaged second-generation spheroids. (n = 4, *, p < 0.02 and ****, p < 0.0001). Second and third-generation cells were not subjected to ASR490 treatment. p values are based on one-way ANOVA with *post hoc* Dunnett's test.

cells and their related signaling pathways (epithelial-mesenchymal transition (EMT) and migration) in the ALDH$^+$ cells compared to the ALDH$^-$ cells. (Figure 1E). In contrast, ASR490-treated ALDH$^+$ cells showed significant downregulation of stem cell signaling compared to their ALDH$^-$ counterparts (Figure 1E). We also performed a volcano plot-based filtering analysis to identify genes with significantly differential expression among these groups (Supplementary Figure S1). Further, KEGG analysis revealed that ASR490 inhibited Notch-mediated proliferation and EMT signaling in ALDH$^+$ cells (Supplementary Figure S2).

ASR490 specifically inhibits Notch1-NICD signaling in ALDH$^+$ and CD44$^+$/CD24$^-$ cells

Based on the GSEA analyses, we first validated the Notch1 targets in ASR490-treated ALDH$^-$, ALDH$^+$, and CD44$^+$/CD24$^-$ cells. Figures 2A–F show a dose and time-dependent downregulation of Notch1-NICD (the active form of Notch1) and its downstream effectors HES1 and Hey1 in all three cell types. Interestingly, the basal expression of Notch-1 in ALDH$^+$ and CD44$^+$/CD24$^-$ BCSCs was significantly higher when compared to the ALDH$^-$ BC cells. As one of stem cell

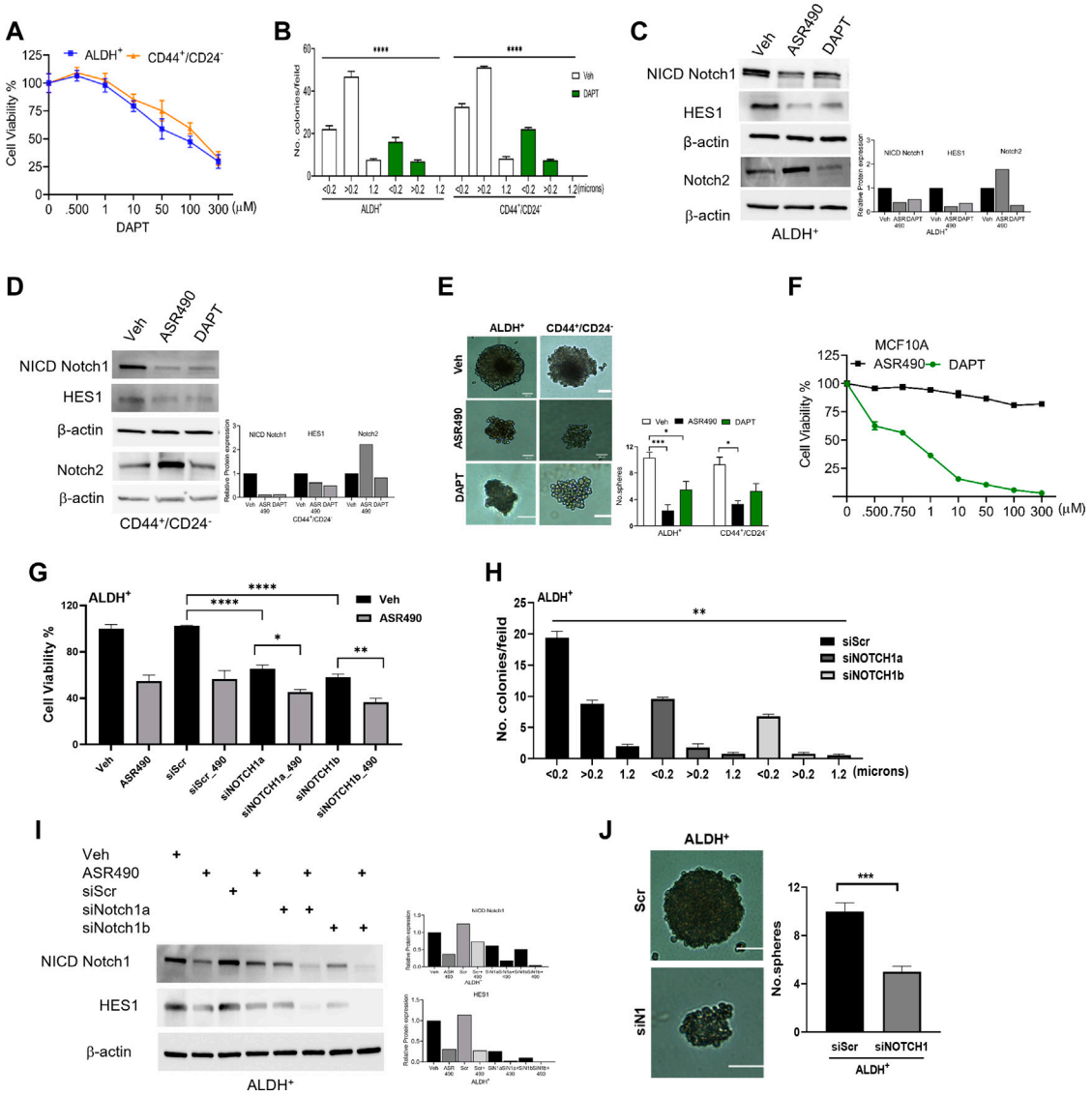

FIGURE 3
Pharmacological and genetic approaches to inhibit Notch1 signaling in BCSCs. **(A)** MTT cell viability assay performed on ALDH$^+$ and CD44$^+$/CD24$^-$ cells following treatment with various concentrations of DAPT (0, 0.500, 1, 10, 100, and 300 μM) for 24 h (n = 6). **(B)** Colony-forming assay of vehicle and DAPT-treated ALDH$^+$ and CD44$^+$/CD24$^-$ cells (n = 6; **** $p < 0.0001$). **(C, D)** Western blots for Notch1-NICD (the active form of Notch1), HES1 and Hey1 and Notch2 of vehicle, ASR490 and DAPT-treated ALDH$^+$ **(C)** and CD44$^+$/CD24$^-$ **(D)** cells. **(E)** Mammosphere assay performed for vehicle, ASR490, and DAPT-treated ALDH$^+$ and CD44$^+$/CD24$^-$ cells (n = 4, * $p < 0.02$ and *** $p < 0.007$). p values are based on one-way ANOVA with a *post hoc* LSD test. **(F)** MTT cell viability assay performed on MCF10A cells following treatment with various concentrations (0, 0.500, 0.750, 1, 10, 50, 100, and 300 μM) of ASR490 and DAPT for 24 h (n = 6). **(G)** Cell viability and **(H)** colony forming assays for vehicle and ASR490 treated non-transfected, SCR-siRNA, and Notch1-siRNA transfected ALDH$^+$ cells for 24 h (n = 6; * $p < 0.01$, ** $p < 0.008$, and **** $p < 0.0001$). p values are based on one-way ANOVA with a *post hoc* LSD test. **(I)** Western blots for Notch-NICD and HES-1 expression were performed on vehicle or ASR490 treated SCR-siRNA, and Notch1-siRNA transfected ALDH$^+$ cells. **(J)** Mammospheres assay performed for vehicle and ASR490 treated SCR-siRNA, and Notch1-siRNA transfected ALDH$^+$ cells (n = 6; *** $p < 0.001$). p values are based on one-way ANOVA with a *post hoc* LSD test.

characteristics is the formation of mammospheres, we next determined whether inhibition of Notch1 affected the self-renewal properties of the BCSCs. Both vehicle-treated ALDH$^+$ and CD44$^+$/CD24$^-$ cells significantly developed more prominent and numerous spheroids than their ALDH$^-$ counterparts (Figure 2G). As expected, ASR490 treatment resulted in a dramatic decrease in the number and size of spheroids in all three cell types, albeit its effect was significantly more profound in the ALDH$^+$ and CD44$^+$/CD24$^-$ cells. We then performed immunofluorescence for Notch1 expression in vehicle and ASR490-treated spheres to determine whether ASR490's inhibitory effects were mediated *via* its suppression of Notch1 expression in these cells. As expected, vehicle treated BCSCs (ALDH$^+$ and CD44$^+$/CD24$^-$) were found to express significantly higher Notch1 expression as compared to ALDH$^-$ BC cells, and the significantly decreased size and number of

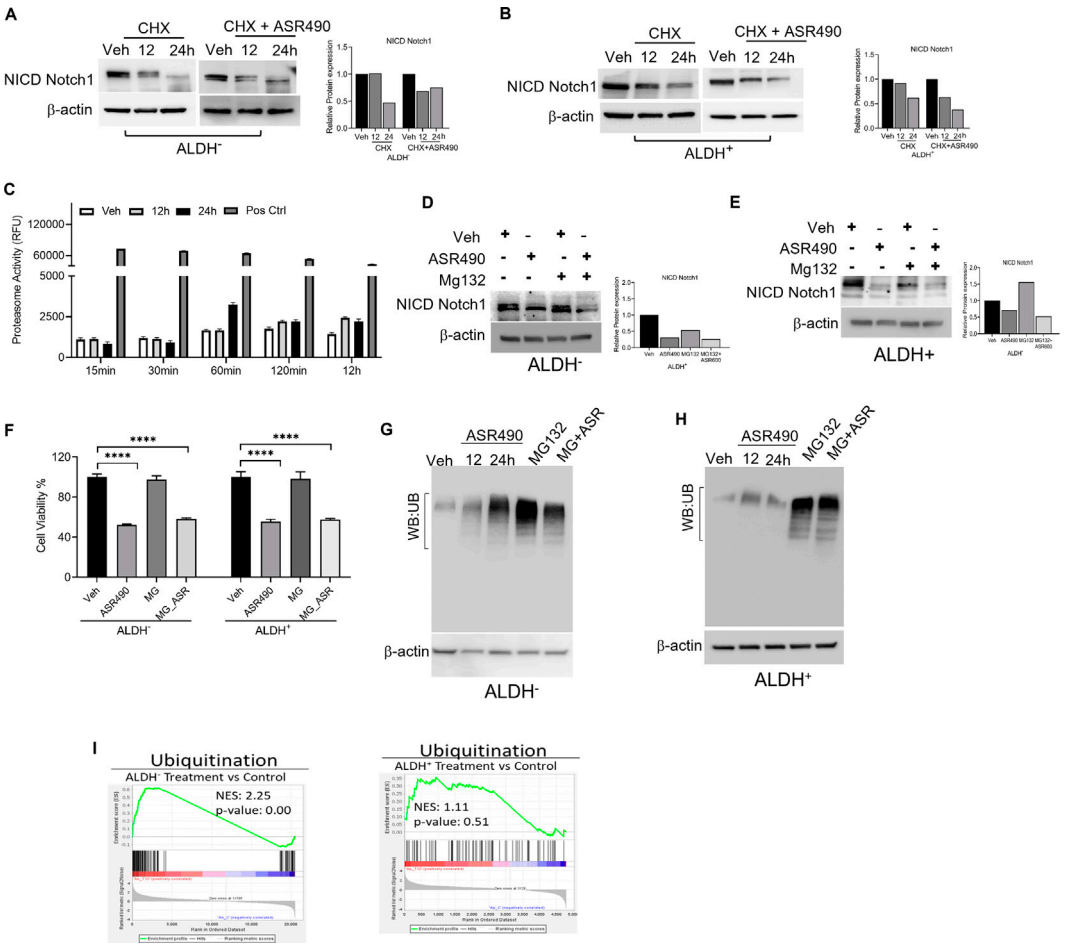

FIGURE 4
Molecular signaling responsible for NICD downregulation in ASR490 treated in ALDH$^-$ and ALDH$^+$ cells. **(A, B)** Western blots performed for Notch1-NICD expression in ALDH$^-$ and ALDH$^+$ cells treated with ASR490, CHX (50 μM), or combinations at the indicated time points. **(C)** Proteasome activity measured for ALDH$^+$ cells treated with ASR490 at the indicated time points. **(D, E)** Western blots showing Notch1-NICD expression in ALDH$^-$ and ALDH$^+$ cells treated with ASR490, MG132 (10 μM), or combinations at the indicated time points. **(F)** MTT cell viability assays performed on ALDH$^-$ and ALDH$^+$ following treatment with ASR490, MG132, or combinations (n = 6; **** $p < 0.0001$). p values are based on one-way ANOVA with a *post hoc* LSD test. **(G, H)** Western blots for ubiquitin protein expression performed for ASR490-treated ALDH$^-$ and ALDH$^+$ cells. MG132 was used as a positive control. **(I)** GSEA of RNA-seq data demonstrating alterations in ubiquitin signaling in ASR490-treated ALDH$^+$ and ALDH$^-$ cells.

spheroids in the treatment group was found to be directly correlated with ASR490's inhibition of Notch1 in all three cell types (Figure 2G).

To evaluate the potency of ASR490, these first-generation mammospheres were passaged for two more consecutive generations, though the second and third-generation spheroids were not exposed to ASR490 treatment. Analyses of the second and third-generation mammospheres revealed that ASR490 seemed to exert a prolonged effect on these cells, i.e., despite the two latter generations not being subjected to additional ASR490 treatment, the spheroids formed by the treatment groups continued to express significantly lower levels of Notch1, and consequently, formed smaller spheroids than their predecessors (Figures 2H, I; Supplementary Figure S3). This was in complete contrast to the vehicle-treated cells, which showed elevated Notch1 expression and larger spheroids.

To confirm ASR490's specificity in targeting Notch1, we compared its efficacy with a known pharmacological Notch inhibitor, DAPT (a γ-secretase), and by genetic inhibition (using siRNA for Notch1). Cell viability assays demonstrated that DAPT inhibited the growth of ALDH$^+$ and CD44$^+$/CD24$^-$ in the μM range (IC_{50}: ALDH$^+$: 81 μM and CD44$^+$/CD24$^-$:135 μM), underscoring the higher comparative potency of ASR490 in nM concentrations against Notch1-dependent cell growth (Figure 3A). DAPT was also found to inhibit the colony-forming abilities of ALDH$^+$ and CD44$^+$/CD24$^-$ cells (Figure 3B). Subsequent immunoblotting analyses revealed that in contrast to DAPT, ASR490 specifically only inhibited Notch1 and its downstream effector, HES-1, and did not affect the expression of Notch2 in ALDH$^+$ and CD44$^+$/CD24$^-$ (Figures 3C, D). Further, head-to-head comparison of ASR490 and DAPT in mammospheres assays demonstrated that ASR490 was more effective than DAPT at curtailing the self-renewal capacity of the BCSCs (Figure 3E).

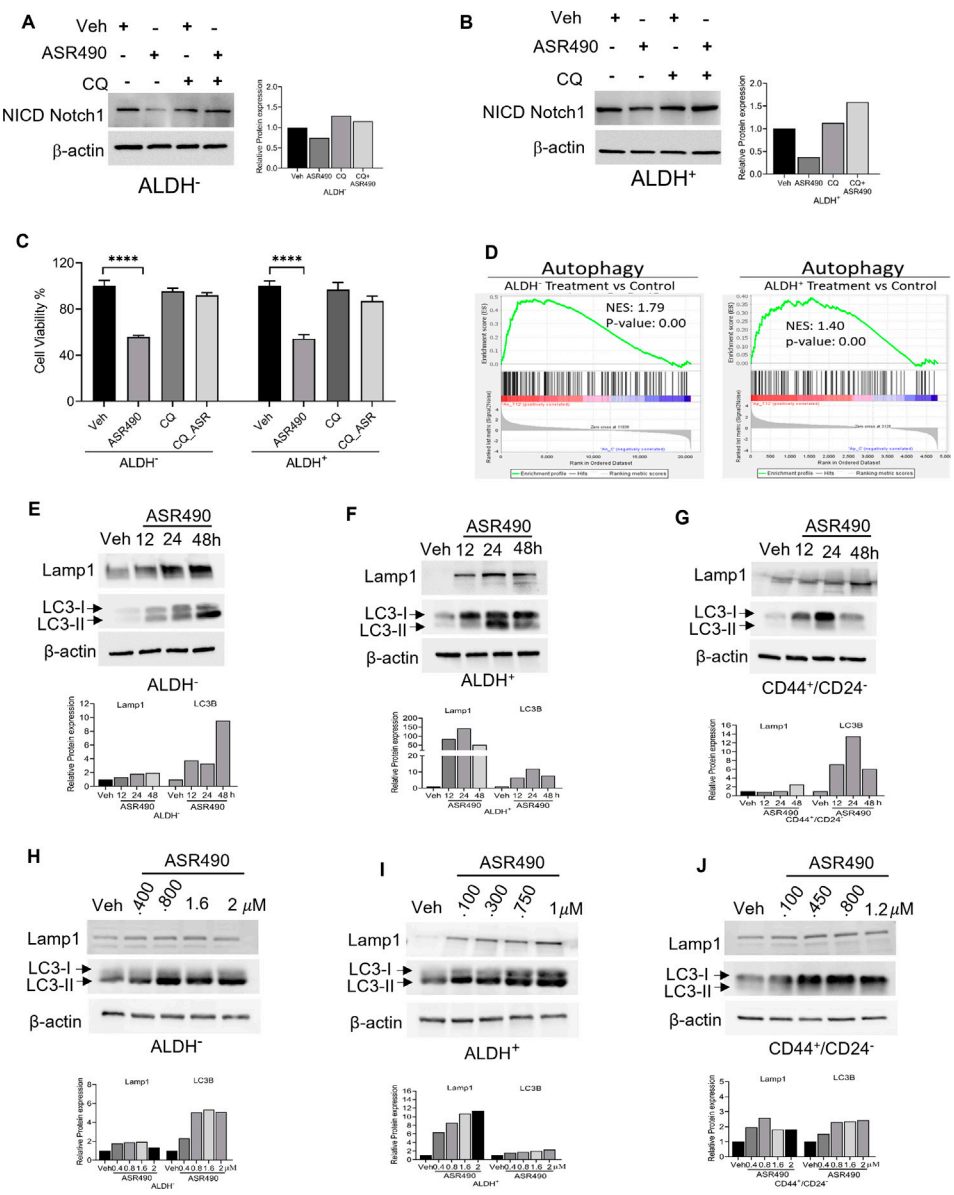

FIGURE 5
ASR490 abrogates both breast cancer and BCSC growth by activating autophagy pathways. **(A, B)** Western blots for Notch1-NICD expression in ALDH$^-$ and ALDH$^+$ cells treated with ASR490, CQ (50 μM), or combinations at the indicated time points. **(C)** MTT cell viability assays performed on ALDH$^-$ and ALDH$^+$ following treatment with ASR490, CQ, or combinations. (n = 6; **** $p < 0.0001$). p values are based on one-way ANOVA with the *post hoc* Tukey test. **(D)** GSEA of RNA-seq data demonstrating downregulation in autophagy-regulated genes in ASR490-treated ALDH$^+$ and ALDH$^-$ cells. **(E–J)**. Western blots showing time- **(E–G)** and dose-dependent **(H–J)** effects of ASR490 treatment on autophagy markers Lamp1 and LC3B in ALDH$^-$, ALDH$^+$, and CD44$^+$/CD24$^-$ cells.

Finally, the IC_{50} concentration at which DAPT mediated its inhibitory effect on BCSCs was found to be toxic to healthy breast epithelial cells (MCF10A) as compared with ASR490 (Figure 3F).

Similar approaches were executed using SCR and Notch1 siRNA transfected ALDH$^+$ to examine their cell viability, Notch1(NICD) and HES1 protein expressions, as well as colony- and mammosphere formation abilities following treatment with vehicle or ASR490. Results demonstrated that siNOTCH1-transfected cells showed significantly reduced cell viability and colony-forming abilities as compared to SCR-siRNA transfected ALDH$^+$ cells. Interestingly, treatment with ASR490 further inhibited the growth of the siNOTCH1-transfected ALDH$^+$ cells (Figures 3G, H). Similarly, while siNOTCH1-transfected ALDH$^+$ cells demonstrated decreased Notch1-NICD and HES1 expression levels compared to SCR-siRNA-transfected cells (Figure 3I), ASR490 treatment further inhibited Notch1 signaling in these cells. Finally, mammosphere assays demonstrated that the spheroids formed by siNOTCH1-transfected cells were smaller than those of scrambled transfected cells (Figure 3J),

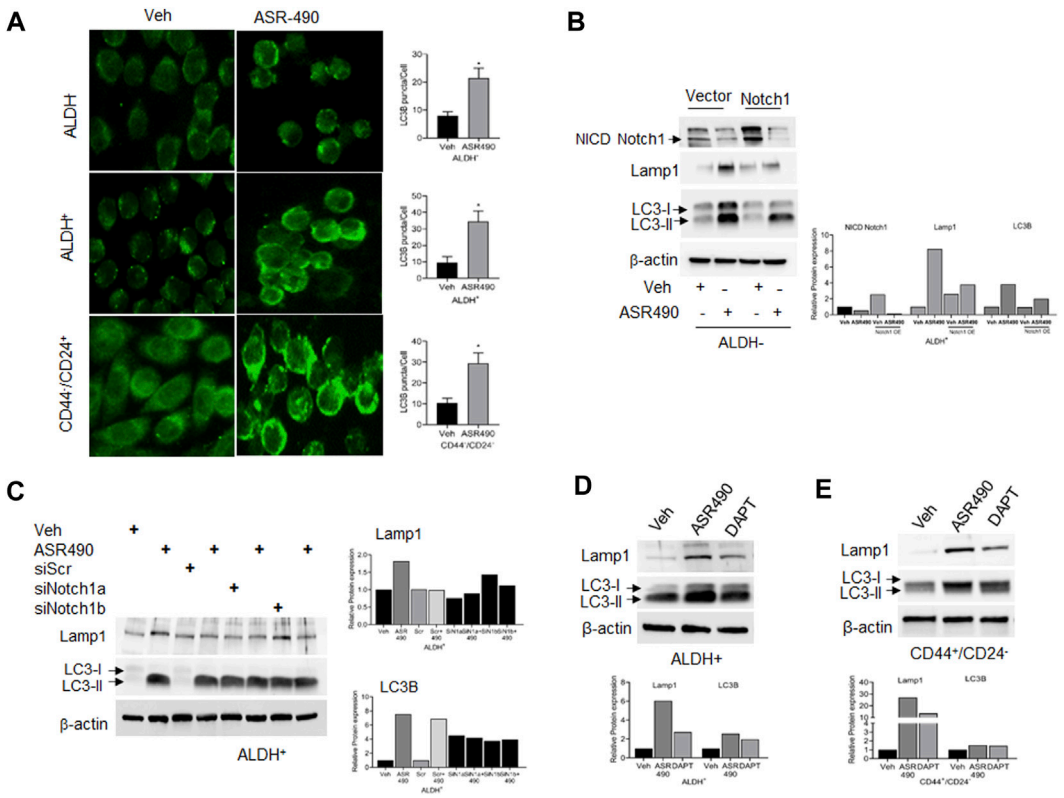

FIGURE 6
Notch-1 regulates autophagy in BCSC and BC cells. **(A)** Representative images of immunofluorescence analyses for LC3B punctae in vehicle and ASR490 treated ALDH$^-$, ALDH$^+$, and CD44$^+$/CD24$^-$ cells. **(B, C)** Western blots for Lamp1 and LC3B expression in vehicle and ASR490-treated pCMV- and Notch1-transfected ALDH$^-$ cells **(B)** and SCR-siRNA, and Notch1-siRNA transfected ALDH$^+$ cells **(C)**. **(D,E)** Western blots analysis of Notch1-NICD, Lamp-1, and LC3B for vehicle, ASR490, and DAPT-treated ALDH$^+$ and CD44$^+$/CD24$^-$ cells.

suggesting that Notch1 is an essential target for inhibiting BCSC growth.

Inhibition of Notch1 facilitates autophagy-mediated cell death in ASR490-treated BCSCs

Interestingly, in this study, no significant changes in Notch1 expression was observed from our transcriptomic analysis of ASR490-treated BCSCs (data not shown). So, we postulated that ASR490 might post-translationally regulate Notch1 in BCSCs. To corroborate this, ALDH$^+$ and ALDH$^-$ cells were treated with protein synthesis inhibitor CHX in the presence and absence of ASR490. While reduced Notch-NICD expression was observed in both ALDH$^+$ and ALDH$^-$ cells at 24 h in the CHX-alone treated group, the combination of ASR490 + CHX resulted in significantly greater suppression of Notch-NICD levels in both cell types (Figures 4A, B), suggesting that ASR490 may mediate its inhibitory effects through Notch1-NICD degradation.

As several studies have reported that Notch1 degradation can occur either *via* the ubiquitin-proteasome or lysosome pathways (Jehn et al., 2002; McGill and McGlade, 2003; Ahn et al., 2016; Wu et al., 2016). We first analyzed the possibility of ASR490 being another proteasome inhibitor like MG132 by measuring proteasome activity using a chymotrypsin-like compound with a 7-amido-4-methyl coumarin (AMC)-tagged peptide substrate induction of proteasome activity in ALDH$^+$ cells. Commercially available positive and negative controls were used for these experiments. Induction of proteasome activity was measured at different time points, and no significant changes were noted until 12 h in ASR490-treated ALDH$^+$ cells (Figure 4C). This suggests that ASR490 was not a proteasomal inhibitor. To further verify whether ASR490 mediates its effects *via* the proteasomal pathway, we performed cell viability and immunoblot analyses of vehicle and ASR490 treated ALDH$^+$ and ALDH$^-$ in the presence and absence of MG132 (10 μM). Results demonstrated that MG132 could not rescue ASR490-mediated inhibition of Notch1-NICD expression in both cell types (Figures 4D–F). Further, we analyzed the ubiquitin expression in ASR490-treated cells and found no significant induction of ubiquitin in either cell type following 12 and 24 h of treatment with ASR490 (Figures 4G, H). GSEA analysis of ASR490-treated cells demonstrated that ASR490 downregulated ubiquitin signaling in ALDH$^-$ cells but not in ALDH$^+$ cells (Figure 4I; Supplementary Figure S4).

In contrast, Western blots for Notch1-NICD and viability assays demonstrated that treatment with lysosome inhibitor (CQ) rescued NICD expression in ASR490 treated ALDH$^+$ and ALDH$^-$

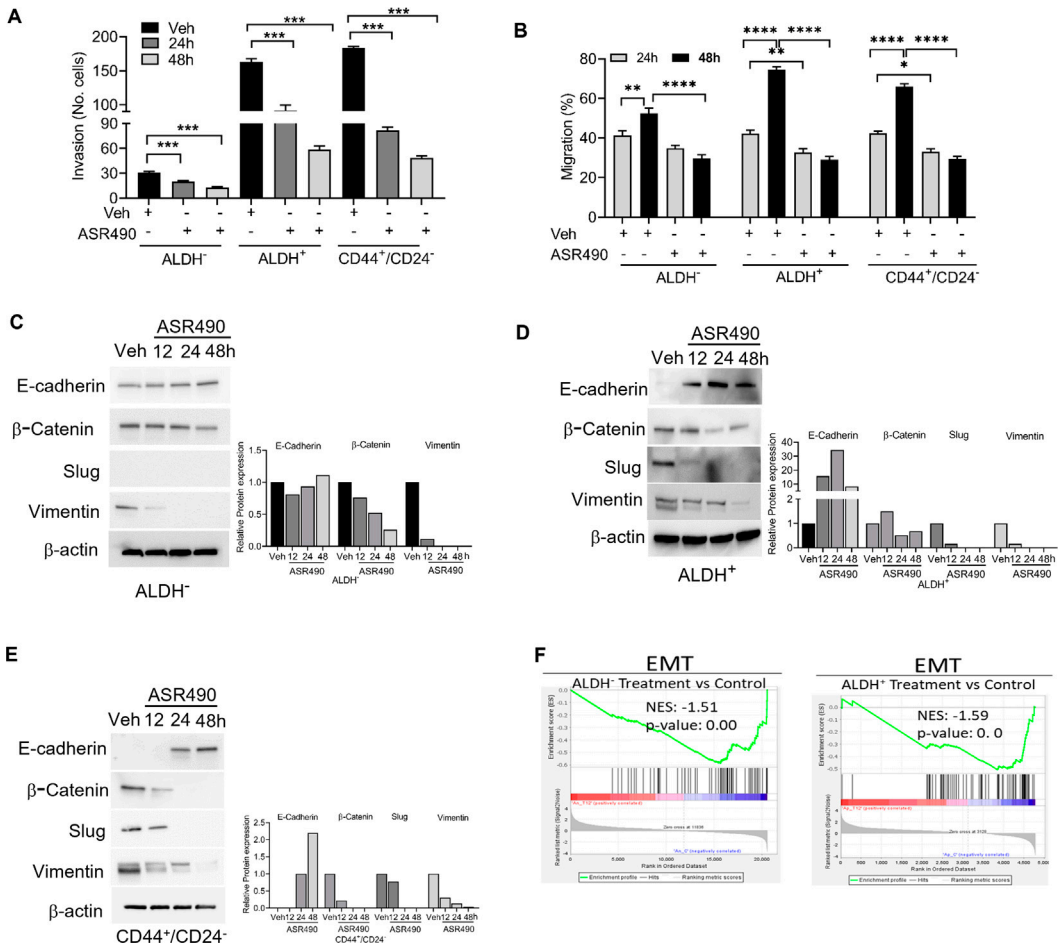

FIGURE 7
ASR490 inhibits the invasive and migratory abilities of BC and BCSCs. **(A)** Boyden chamber invasion assay was used to assess the time-dependent effects of ASR490 on the invasive ability of ALDH$^-$, ALDH$^+$, and CD44$^+$/CD24$^-$ cells (n = 3, **** $p < 0.0001$). **(B)** Time-dependent effects of ASR490 on the migratory abilities of ALDH$^-$, ALDH$^+$ and CD44$^+$/CD24$^-$ cells were assessed using a scratch wound assay (n = 3, * $p < 0.03$, ** $p < 0.007$ and **** $p < 0.0001$). p values are based on one-way ANOVA with *post hoc* Tukey's test. **(C–E)** Western blots showing time-dependent effects of ASR490 treatment on EMT markers (E-Cadherin, β-Catenin, Slug, and Vimentin) in ALDH$^-$, ALDH$^+$, and CD44$^+$/CD24$^-$ cells. **(F)** GSEA of RNA-seq data demonstrating downregulation of EMT-regulated genes in ASR490-treated ALDH$^-$ and ALDH$^+$ cells.

cells, signifying the possible involvement of lysosome signaling in ASR490-mediated NICD degradation (Figures 5A–C). GSEA analysis suggested significant enrichment of autophagy regulatory genes in ASR490-treated ALDH$^+$ and ALDH$^-$ cells (Figure 5D). This was further corroborated by Western blots that demonstrated a significant time- and dose-dependent upregulation of autophagy markers Lamp1 and LC3B in ASR490-treated BCSCs and BC cells (Figures 5E–J). Immunofluorescence analysis showed a significant accumulation of LC3B puncta, indicative of autophagy involvement, in ASR490 treated BCSCs and BC cells (Figure 6A). To demonstrate that Notch1 mediates autophagy signaling, we first overexpressed Notch1 in ALDH$^-$ cells, inhibiting endogenous and ASR490-induced LAMP1 and LC3B expressions (Figure 6B), suggesting that Notch1 activation impairs autophagy signaling in BC cells. Next, to confirm that Notch1 regulates autophagy signaling, we silenced Notch1 expression using siRNA Notch1 in ALDH$^+$ cells and showed that inhibition of Notch1 reverts both LAMP1 and LC3B expression (Figure 6C). Inhibition of Notch1 using pharmacological Notch1 inhibitors also facilitated the induction of autophagy markers in BCSCs (Figures 6D, E), confirming the molecular interaction between Notch1 and autophagy signaling in BCSCs.

ASR490 inhibits the proliferation, invasive and migratory abilities of BCSCs and BC

Invasion and wound healing migration assays demonstrated that treatment with ASR490 significantly inhibited the invasive and migratory potential of both BCSCs and BC cells (Figures 7A, B), albeit ASR490's effect was more profound on the BCSCs (ALDH$^+$ and CD44$^+$/CD22$^-$ than the BC (ALDH$^-$) cells. In addition, assessment of the expressions of essential EMT genes demonstrated a time-dependent increase of epithelial marker

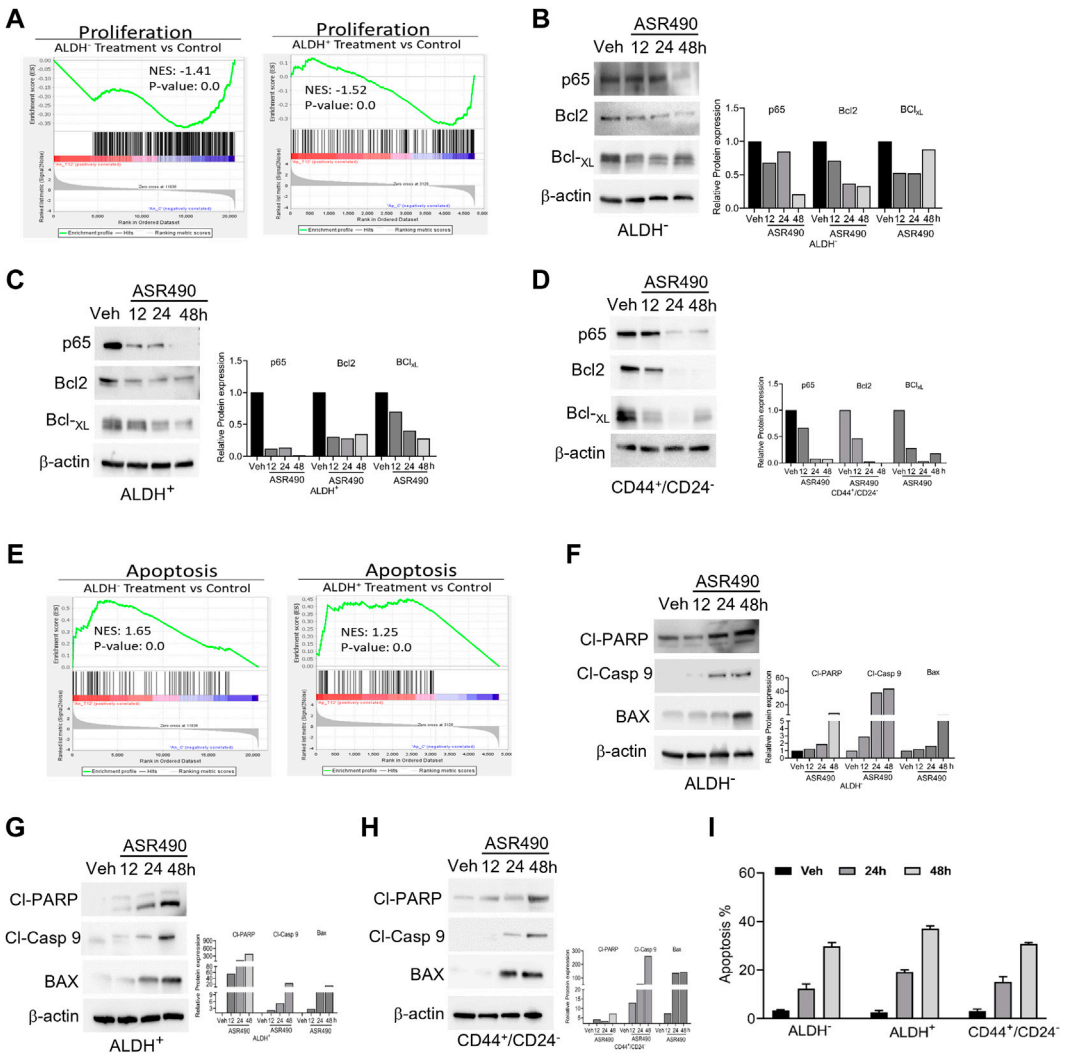

FIGURE 8
ASR490 inhibits the pro-survival signaling of BCSCs. **(A)** GSEA of RNA-seq data demonstrating alterations in proliferation signaling pathways in ASR490-treated ALDH⁻ and ALDH⁺ cells. **(B–D)** Western blots showing time-dependent effects of ASR490 treatment on pro-survival markers NFkB p65, Bcl2, and Bcl-$_{XL}$ expression in ALDH⁻, ALDH⁺, and CD44⁺/CD24⁻ cells. **(E)** GSEA of RNA-seq data demonstrating alterations in proapoptotic signaling in ASR490-treated ALDH⁻ and ALDH⁺. **(F–H)**. Western blots showing time-dependent effects of ASR490 treatment on the proapoptotic markers Cleaved-PARP, Cleaved-Caspase 9, and BAX in ALDH⁻, ALDH⁺, and CD44⁺/CD24⁻ cells. **(I)** FACS analyses (Annexin V–FITC and PI staining) performed for vehicle and ASR490-treated ALDH⁻, ALDH⁺, and CD44⁺/CD24⁻ cells.

E-cadherin and decrease of mesenchymal markers β-catenin, Slug, and Vimentin in ASR490 treated BCSCs and BC cells (Figures 7C–E). This was further corroborated by GSEA results which demonstrated a significant decline in EMT-enriched genes in ASR490-treated cells compared to the enrichment of EMT and metastasis genes in control cells (Figure 7F).

GSEA analyses also revealed that treatment with ASR490 also curbed the proliferative ability of both BCSCs and BC cells as evident by the decreased enrichment of proliferation genes in treated cells vs. control cells (Figure 8A). This was also confirmed by Western blots demonstrating a time-dependent downregulation of pro-survival genes (NFκB [p65], Bcl2, and BCL-xL) in ASR490-treated BCSCs and BC cells (Figures 8B–D). While both GSEA analysis (Figure 8E) and Western blots (Figures 8F–H) for apoptotic markers (Cleaved Caspase-9, cleaved-PARP, and BAX) demonstrated a time-dependent upregulation of apoptosis in ASR490 treated cells. Subsequent FACS analysis revealed that this induction was not significant (Figure 8I).

ASR490 abrogates *in vivo* growth of both ALDH⁺ and ALDH⁻ tumors

Next, the anticancer effect of ASR490 was evaluated *in vivo* using ALDH⁺ and ALDH⁻ xenografted mice. Oral administration of ASR490 significantly reduced the tumor burden of both ALDH⁺ and ALDH⁻ xenografted mice (Figure 9), although its effect was more profound in the ALDH⁺ group (Figure 9A). The weight of ASR490-treated tumors was also lower than that of the vehicle-treated tumors

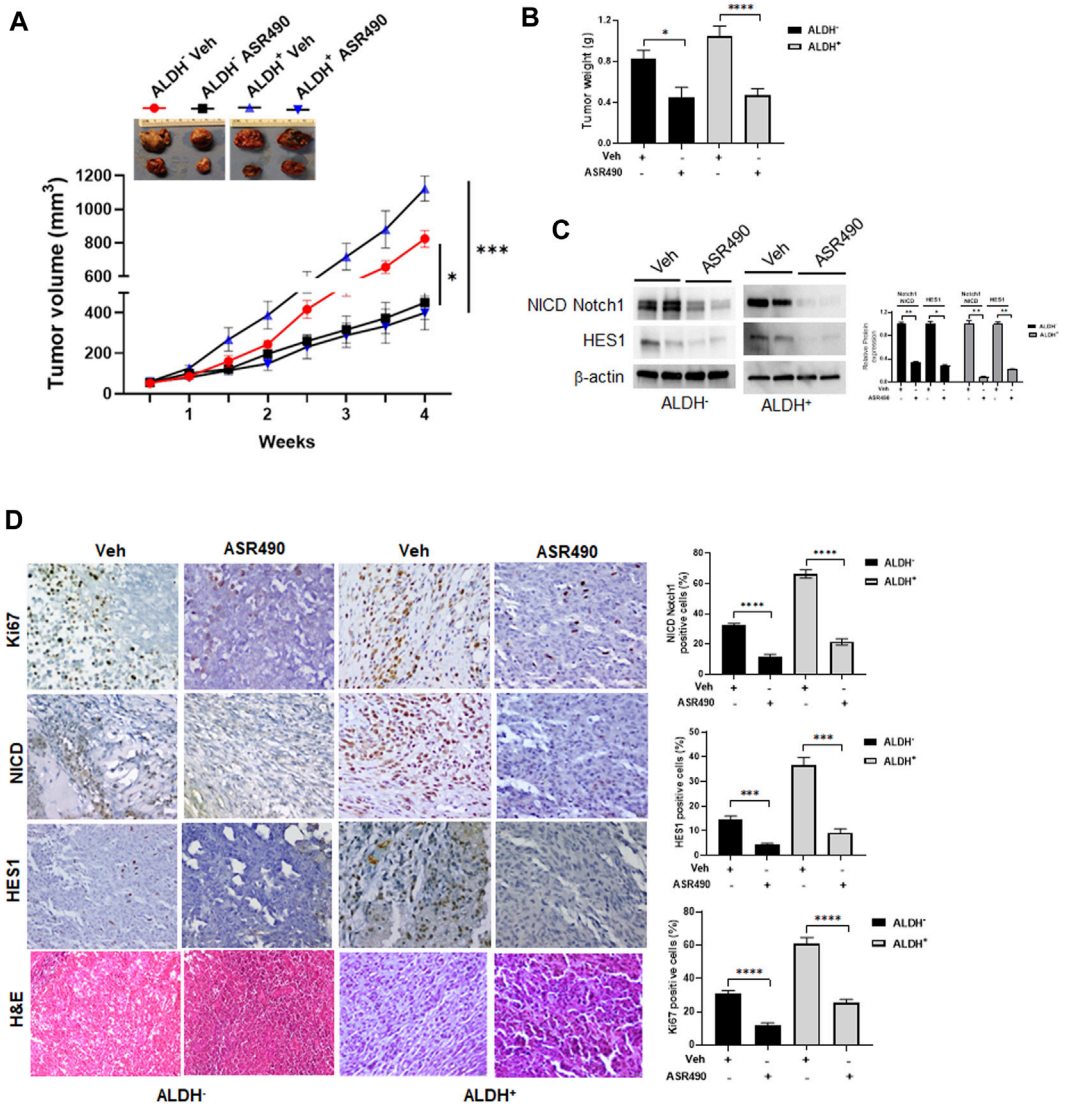

FIGURE 9
ASR490 reduces the tumor burden of xenotransplanted breast tumors. **(A)** Oral administration of ASR490 (25 mg/kg) significantly inhibited the growth of ALDH⁻ and ALDH⁺ xenotransplanted tumors ($n = 6$, $^{*}p < 0.01$, $^{***}p < 0.001$). **(B)** Tumor weight of vehicle and ASR490 treated ALDH⁻ and ALDH⁺ tumors. **(C)** Western blots performed for Notch1-NICD and HES1 on vehicle and ASR490-treated ALDH⁻ and ALDH⁺ tumors. **(D)** IHC analyses was performed on vehicle and ASR490-treated ALDH⁻ and ALDH⁺ tumors to evaluate the expressions of Notch1-NICD, HES1, and Ki67 (proliferation marker). *p* values were calculated using a two-sided Student's t-test.

(Figure 9B). Assessment of ASR490 treatment on Notch1 signaling in tumor tissue lysates showed significantly decreased Notch1-NICD and HES1 protein expression in the ASR490-treated groups compared to the vehicle-treated groups (Figure 9C). This finding was corroborated by IHC analyses, which showed significant downregulation of NICD, Hes1, and Ki67 (proliferation marker) expressions in the ASR490-treated tumors (Figure 9D).

Discussion

This study provides evidence that the newly developed potent small molecule, ASR490, explicitly suppresses Notch1 expression in BCSCs and BC by inhibiting cell proliferation and tumor growth in both *in vitro* and *in vivo* models. For more than twodecades, there has been a growing interest in targeting Notch1 signaling, resulting in the development of several approaches to inhibit Notch1 signaling in preclinical models. In fact, to date, almost all Notch1 inhibitors have largely failed in their clinical management due to gastrointestinal toxicities, non-selective Notch inhibition, and effective therapeutic doses to curb tumor growth (Imbimbo, 2008; Wu et al., 2010).

Our newly developed molecule, ASR490, is a selective Notch1 inhibitor that attenuates tumor growth in BCSC and BC models. ASR490 differs from existing Notch1 inhibitors due to its specificity towards NRR, oral bioavailability, and non-toxicity to

normal breast cells. Our dose and time-dependent analyses demonstrated that ASR490 inhibited Notch1 activity in both BCSCs ($ALDH^+$ and $CD44^+/CD24^-$) and BC ($ALDH^-$) cells. In addition, we observed that ASR490's effects were more prominent in cells expressing higher levels of Notch1 (i.e., $ALDH^+$ and $CD44^+CD24^-$) than in lower-Notch1-expressing $ALDH^-$ cells. We also demonstrated that this inhibitor specifically inhibited Notch1 expression without affecting the expression of Notch2, in contrast to the pan-Notch inhibitor DAPT and minimal or no toxicity was observed following treatment with ASR490 in both *in vitro* and *in vivo* models. Remarkably, serial passaging of ASR490-treated BCSCs and BC cells demonstrated that ASR490 has long-term effects on these cells, as evidenced by the diminished spheroid forming ability that was carried over for at least two successive generations.

The presence of both $ALDH^+$ and $CD44^+CD24^-$ populations have been previously correlated with a poor prognosis of BC patients (Ginestier et al., 2007; Ohi et al., 2011) and were showed to be able to induce lung metastasis (Sheridan et al., 2006). Moreover, others have shown that chemotherapy can enrich ALDH + populations within tumors, making them more resistant (Tanei et al., 2009). Interestingly, recent studies have suggested a role for Notch1 in drug-resistant BCSCs where exposure to chemo- and anti-hormonal therapies result in the enrichment of drug-resistant $ALDH^+$ BCSCs (Osipo et al., 2008; Suman et al., 2013; Baker et al., 2018). These results along with the well-established oncogenic role of Notch1 in BC (Reedijk et al., 2005; Hu et al., 2006; Mohammadi-Yeganeh et al., 2015), where its increased expression has been shown to enhance metastatic phenotype (Zang et al., 2010; Li et al., 2015), suggests that inhibition of Notch1 could eliminate BCSCs and increase drug sensitivity. Our results indicate that ASR490 is a potent compound that can overcome Notch1 mediated BCSCs accumulation and resistance in BC.

In our studies, ASR490's inhibition of Notch1 facilitated autophagy-mediated cell death in both BCSC and BC cells. The autophagy function is highly context-dependent (Chavez-Dominguez et al., 2020). For example, inhibition of Notch1 in glioblastoma cell lines induced the oncogenic function of autophagy; however, in combination with γ-secretase inhibitor RO4929097 (GSI) and a natural compound, Resveratrol, resulted in the accumulation of autophagosomes and subsequent growth inhibition by inducing apoptosis (Giordano et al., 2021). Whereas in lung cancer models, the induction of autophagy resulted in the downregulation of NICD expression and the eventual inhibition of EMT signaling (Zada et al., 2022). Our results suggest that Notch1 regulates the pro-apoptotic function of autophagy. Silencing of Notch1 in $ALDH^+$ cells induced autophagy signaling, while in contrast overexpression of Notch1 blocked ASR490-mediated autophagy, suggesting that Notch1 regulates autophagy function in BCSC cells.

Moreover, autophagy has been implicated to play a critical role specifically in BCSCs populations. For example, the impairment of autophagy has been shown to affect the maintenance of BCSCs by limiting EMT and the $CD44^+/CD24^-$ phenotype (Cufi et al., 2011). Analysis of the mechanism of action revealed that ASR490 mediated its effects by suppressing Notch1-induced EMT signaling in BCSCs and BC cells. The loss of E-cadherin and the upregulation of β-catenin expression is a classical molecular switch for EMT that initiates the loss of apical polarity by altering cytoskeleton organization and leads to spindle-shaped morphologic features (Leong et al., 2007; Gangopadhyay et al., 2013). We found that induction of E-cadherin and inhibition of β-catenin expression in ASR490-treated BCSCs and BC cells suggest the abrogation of this EMT phenomenon by ASR490. Activation of the pro-survival transcription factor NFκB (p65) is involved in EMT induction (Thiery et al., 2009) and is a crucial activator of BCSCs (Liu et al., 2010). Our results showed that ASR490 inhibited p65 expression as well as the expression its downstream targets Bcl-2 and BCL-xL in both BCSCs and BC cells.

ASR490 is an orally available potent inhibitor of Notch1-mediated activation that significantly abrogates the growth of BCSC and BC tumors. Moreover, the maximum tolerated dose of ASR490 was found to be 500 mg/kg (data not shown), which is approximately 20 times more than the dose used in our current study, indicative of ASR490's high therapeutic index. Therefore, with its potent activity and lack of apparent toxicity, ASR490 provides the necessary selectivity and therapeutic window for cancer therapeutics targeting the Notch1 pathway and selectively inhibiting BCSC populations within tumors.

In conclusion, our results demonstrate a novel therapeutic strategy for BCSCs specifically for TNBC, by inhibiting Notch1 signaling, which curtails self-renewal and tumorigenicity. Also, the inhibition of Notch1 facilitates autophagy signaling, which resulted in the inhibition of EMT, and survival signaling to eradicate tumor growth. Hence, our small molecule ASR490 is a promising therapeutic agent, and the inhibition of Notch1 is an ideal strategy for BCSC and BC.

Data availability statement

The original contributions presented in the study are included in the article/Supplementary Material, further inquiries can be directed to the corresponding author.

Ethics statement

The animal study was reviewed and approved by the University of Louisville's Ethical Committee and maintained by the Institutional Animal Care and Use Committee-approved protocols.

Author contributions

Conceptualization, CD and AKS; methodology, CD, AKS, US, BC, VS, and AT; formal analysis, US, BC, VS, and AT; investigation, US, BC, AT, and AS; resources, CD and AKS, and writing—original draft, US, BC, AT, and CD; supervision, CD and AKS.

Conflict of interest

The authors declare that the research was conducted in the absence of any commercial or financial relationships that could be construed as a potential conflict of interest.

Publisher's note

Supplementary material

The Supplementary Material for this article can be found online at: https://www.frontiersin.org/articles/10.3389/fphar.2023.1150774/full#supplementary-material

SUPPLEMENTARY FIGURE S1
Volcano plot analyses of differentially expressed genes between ALDH$^-$ treatment vs control, ALDH$^+$ treatment vs. control, and ALDH$^+$ vs. ALDH$^-$ is plotted on the X axis, and the False Discovery Rate (FDR) significance is plotted on the Y axis (–log10 scale). The grey dots represent no significant change, red dots represent logFC of >1.5 and FDR < 0.05 and blue represent logFC < –1.5 and FDR <0.05.

SUPPLEMENTARY FIGURE S2
KEGG pathway for differential expressed genes based on RNA-seq data for ALDH$^-$ treatment vs. control, ALDH$^+$ treatment vs. control and ALDH$^+$ against ALDH$^-$. Each bubble's color and size correspond to the amount of differentially expressed mRNAs that are enriched in a certain GO keyword or KEGG pathway, respectively. The cutoff utilized to choose KEGG keywords was p<0.05.

SUPPLEMENTARY FIGURE S3
Representative brightfield and immunofluorescent images of Notch1-NICD (active form of Notch1) expression in vehicle and ASR490-treated second and third generation mammospheres of ALDH$^-$, ALDH$^+$ and CD44$^+$/CD24$^-$ cells.

SUPPLEMENTARY FIGURE S4
Gene Ontology analysis for differential expressed genes based on RNA-seq data for ALDH$^-$ treatment vs. control, and ALDH$^+$ treatment vs. control.

References

Abravanel, D. L., Belka, G. K., Pan, T. C., Pant, D. K., Collins, M. A., Sterner, C. J., et al. (2015). Notch promotes recurrence of dormant tumor cells following HER2/neu-targeted therapy. *J. Clin. Invest.* 125 (6), 2484–2496. doi:10.1172/JCI74883

Ahn, J. S., Ann, E. J., Kim, M. Y., Yoon, J. H., Lee, H. J., Jo, E. H., et al. (2016). Autophagy negatively regulates tumor cell proliferation through phosphorylation dependent degradation of the Notch1 intracellular domain. *Oncotarget* 7 (48), 79047–79063. doi:10.18632/oncotarget.12986

Al-Hajj, M., Wicha, M. S., Benito-Hernandez, A., Morrison, S. J., and Clarke, M. F. (2003). Prospective identification of tumorigenic breast cancer cells. *Proc. Natl. Acad. Sci. U. S. A.* 100 (7), 3983–3988. doi:10.1073/pnas.0530291100

Bai, X., Ni, J., Beretov, J., Graham, P., and Li, Y. (2018). Cancer stem cell in breast cancer therapeutic resistance. *Cancer Treat. Rev.* 69, 152–163. doi:10.1016/j.ctrv.2018.07.004

Baker, A., Wyatt, D., Bocchetta, M., Li, J., Filipovic, A., Green, A., et al. (2018). Notch-1-PTEN-ERK1/2 signaling axis promotes HER2+ breast cancer cell proliferation and stem cell survival. *Oncogene* 37 (33), 4489–4504. doi:10.1038/s41388-018-0251-y

Banks, J., Kingsbury, J., Raboy, V., Schiefelbein, J. W., Nelson, O., and Fedoroff, N. (1985). The Ac and Spm controlling element families in maize. *Cold Spring Harb. Symp. Quant. Biol.* 50, 307–311. doi:10.1101/sqb.1985.050.01.039

Bolos, V., Mira, E., Martinez-Poveda, B., Luxan, G., Canamero, M., Martinez, A. C., et al. (2013). Notch activation stimulates migration of breast cancer cells and promotes tumor growth. *Breast Cancer Res.* 15 (4), R54. doi:10.1186/bcr3447

Cao, Y. W., Wan, G. X., Sun, J. P., Cui, X. B., Hu, J. M., Liang, W. H., et al. (2015). Implications of the Notch1-Snail/Slug-epithelial to mesenchymal transition axis for lymph node metastasis in infiltrating ductal carcinoma. *Kaohsiung J. Med. Sci.* 31 (2), 70–76. doi:10.1016/j.kjms.2014.11.008

Chandrasekaran, B., Dahiya, N. R., Tyagi, A., Kolluru, V., Saran, U., Baby, B. V., et al. (2020). Chronic exposure to cadmium induces a malignant transformation of benign prostate epithelial cells. *Oncogenesis* 9 (2), 23. doi:10.1038/s41389-020-0202-7

Chandrasekaran, B., Tyagi, A., Sharma, A. K., Cai, L., Ankem, M., and Damodaran, C. (2017). Molecular insights: Suppression of EGFR and AKT activation by a small molecule in non-small cell lung cancer. *Genes Cancer* 8 (9-10), 713–724. doi:10.18632/genesandcancer.154

Charafe-Jauffret, E., Ginestier, C., Iovino, F., Tarpin, C., Diebel, M., Esterni, B., et al. (2010). Aldehyde dehydrogenase 1-positive cancer stem cells mediate metastasis and poor clinical outcome in inflammatory breast cancer. *Clin. Cancer Res.* 16 (1), 45–55. doi:10.1158/1078-0432.CCR-09-1630

Chavez-Dominguez, R., Perez-Medina, M., Lopez-Gonzalez, J. S., Galicia-Velasco, M., and Aguilar-Cazares, D. (2020). The double-edge sword of autophagy in cancer: From tumor suppression to pro-tumor activity. *Front. Oncol.* 10, 578418. doi:10.3389/fonc.2020.578418

Cufi, S., Vazquez-Martin, A., Oliveras-Ferraros, C., Martin-Castillo, B., Vellon, L., and Menendez, J. A. (2011). Autophagy positively regulates the CD44(+) CD24(-/low) breast cancer stem-like phenotype. *Cell Cycle* 10 (22), 3871–3885. doi:10.4161/cc.10.22.17976

D'Angelo, R. C., Ouzounova, M., Davis, A., Choi, D., Tchuenkam, S. M., Kim, G., et al. (2015). Notch reporter activity in breast cancer cell lines identifies a subset of cells with stem cell activity. *Mol. Cancer Ther.* 14 (3), 779–787. doi:10.1158/1535-7163.MCT-14-0228

Dandawate, P. R., Subramaniam, D., Jensen, R. A., and Anant, S. (2016). Targeting cancer stem cells and signaling pathways by phytochemicals: Novel approach for breast cancer therapy. *Semin. Cancer Biol.* 40-41, 192–208. doi:10.1016/j.semcancer.2016.09.001

Das, T. P., Suman, S., and Damodaran, C. (2014). Induction of reactive oxygen species generation inhibits epithelial-mesenchymal transition and promotes growth arrest in prostate cancer cells. *Mol. Carcinog.* 53 (7), 537–547. doi:10.1002/mc.22014

Dickson, B. C., Mulligan, A. M., Zhang, H., Lockwood, G., O'Malley, F. P., Egan, S. E., et al. (2007). High-level JAG1 mRNA and protein predict poor outcome in breast cancer. *Mod. Pathol.* 20 (6), 685–693. doi:10.1038/modpathol.3800785

Douville, J., Beaulieu, R., and Balicki, D. (2009). ALDH1 as a functional marker of cancer stem and progenitor cells. *Stem Cells Dev.* 18 (1), 17–25. doi:10.1089/scd.2008.0055

Gangopadhyay, S., Nandy, A., Hor, P., and Mukhopadhyay, A. (2013). Breast cancer stem cells: A novel therapeutic target. *Clin. Breast Cancer* 13 (1), 7–15. doi:10.1016/j.clbc.2012.09.017

Ge, S. X., Jung, D., and Yao, R. (2020). ShinyGO: A graphical gene-set enrichment tool for animals and plants. *Bioinformatics* 36 (8), 2628–2629. doi:10.1093/bioinformatics/btz931

Ginestier, C., Hur, M. H., Charafe-Jauffret, E., Monville, F., Dutcher, J., Brown, M., et al. (2007). ALDH1 is a marker of normal and malignant human mammary stem cells and a predictor of poor clinical outcome. *Cell Stem Cell* 1 (5), 555–567. doi:10.1016/j.stem.2007.08.014

Giordano, F., Montalto, F. I., Panno, M. L., Ando, S., and De Amicis, F. (2021). A Notch inhibitor plus Resveratrol induced blockade of autophagy drives glioblastoma cell death by promoting a switch to apoptosis. *Am. J. Cancer Res.* 11 (12), 5933–5950.

Harbeck, N., Penault-Llorca, F., Cortes, J., Gnant, M., Houssami, N., Poortmans, P., et al. (2019). Breast cancer. *Nat. Rev. Dis. Prim.* 5 (1), 66. doi:10.1038/s41572-019-0111-2

Hu, C., Dievart, A., Lupien, M., Calvo, E., Tremblay, G., and Jolicoeur, P. (2006). Overexpression of activated murine Notch1 and Notch3 in transgenic mice blocks mammary gland development and induces mammary tumors. *Am. J. Pathol.* 168 (3), 973–990. doi:10.2353/ajpath.2006.050416

Imbimbo, B. P. (2008). Therapeutic potential of gamma-secretase inhibitors and modulators. *Curr. Top. Med. Chem.* 8 (1), 54–61. doi:10.2174/156802608783334015

Jehn, B. M., Dittert, I., Beyer, S., von der Mark, K., and Bielke, W. (2002). c-Cbl binding and ubiquitin-dependent lysosomal degradation of membrane-associated Notch1. *J. Biol. Chem.* 277 (10), 8033–8040. doi:10.1074/jbc.M108552200

Kim, B., Stephen, S. L., Hanby, A. M., Horgan, K., Perry, S. L., Richardson, J., et al. (2015). Chemotherapy induces Notch1-dependent MRP1 up-regulation, inhibition of which sensitizes breast cancer cells to chemotherapy. *BMC Cancer* 15, 634. doi:10.1186/s12885-015-1625-y

Krop, I., Demuth, T., Guthrie, T., Wen, P. Y., Mason, W. P., Chinnaiyan, P., et al. (2012). Phase I pharmacologic and pharmacodynamic study of the gamma secretase (Notch) inhibitor MK-0752 in adult patients with advanced solid tumors. *J. Clin. Oncol.* 30 (19), 2307–2313. doi:10.1200/JCO.2011.39.1540

Leong, K. G., Niessen, K., Kulic, I., Raouf, A., Eaves, C., Pollet, I., et al. (2007). Jagged1-mediated Notch activation induces epithelial-to-mesenchymal transition through Slug-

induced repression of E-cadherin. *J. Exp. Med.* 204 (12), 2935–2948. doi:10.1084/jem.20071082

Li, Z. L., Chen, C., Yang, Y., Wang, C., Yang, T., Yang, X., et al. (2015). Gamma secretase inhibitor enhances sensitivity to doxorubicin in MDA-MB-231 cells. *Int. J. Clin. Exp. Pathol.* 8 (5), 4378–4387.

Liu, M., Sakamaki, T., Casimiro, M. C., Willmarth, N. E., Quong, A. A., Ju, X., et al. (2010). The canonical NF-kappaB pathway governs mammary tumorigenesis in transgenic mice and tumor stem cell expansion. *Cancer Res.* 70 (24), 10464–10473. doi:10.1158/0008-5472.CAN-10-0732

Majumder, S., Crabtree, J. S., Golde, T. E., Minter, L. M., Osborne, B. A., and Miele, L. (2021). Targeting Notch in oncology: The path forward. *Nat. Rev. Drug Discov.* 20 (2), 125–144. doi:10.1038/s41573-020-00091-3

McGill, M. A., and McGlade, C. J. (2003). Mammalian numb proteins promote Notch1 receptor ubiquitination and degradation of the Notch1 intracellular domain. *J. Biol. Chem.* 278 (25), 23196–23203. doi:10.1074/jbc.M302827200

Mi, H., Muruganujan, A., Ebert, D., Huang, X., and Thomas, P. D. (2019). PANTHER version 14: More genomes, a new PANTHER GO-slim and improvements in enrichment analysis tools. *Nucleic Acids Res.* 47 (D1), D419–D426. doi:10.1093/nar/gky1038

Mohammadi-Yeganeh, S., Mansouri, A., and Paryan, M. (2015). Targeting of miR9/NOTCH1 interaction reduces metastatic behavior in triple-negative breast cancer. *Chem. Biol. Drug Des.* 86 (5), 1185–1191. doi:10.1111/cbdd.12584

Ohi, Y., Umekita, Y., Yoshioka, T., Souda, M., Rai, Y., Sagara, Y., et al. (2011). Aldehyde dehydrogenase 1 expression predicts poor prognosis in triple-negative breast cancer. *Histopathology* 59 (4), 776–780. doi:10.1111/j.1365-2559.2011.03884.x

Osipo, C., Patel, P., Rizzo, P., Clementz, A. G., Hao, L., Golde, T. E., et al. (2008). ErbB-2 inhibition activates Notch-1 and sensitizes breast cancer cells to a gamma-secretase inhibitor. *Oncogene* 27 (37), 5019–5032. doi:10.1038/onc.2008.149

Pal, D., Tyagi, A., Chandrasekaran, B., Alattasi, H., Ankem, M. K., Sharma, A. K., et al. (2018). Suppression of Notch1 and AKT mediated epithelial to mesenchymal transition by Verrucarin J in metastatic colon cancer. *Cell Death Dis.* 9 (8), 798. doi:10.1038/s41419-018-0810-8

Phillips, T. M., McBride, W. H., and Pajonk, F. (2006). The response of CD24(-/low)/CD44+ breast cancer-initiating cells to radiation. *J. Natl. Cancer Inst.* 98 (24), 1777–1785. doi:10.1093/jnci/djj495

Qiu, M., Peng, Q., Jiang, I., Carroll, C., Han, G., Rymer, I., et al. (2013). Specific inhibition of Notch1 signaling enhances the antitumor efficacy of chemotherapy in triple negative breast cancer through reduction of cancer stem cells. *Cancer Lett.* 328 (2), 261–270. doi:10.1016/j.canlet.2012.09.023

Ranganathan, P., Weaver, K. L., and Capobianco, A. J. (2011). Notch signalling in solid tumours: A little bit of everything but not all the time. *Nat. Rev. Cancer* 11 (5), 338–351. doi:10.1038/nrc3035

Reedijk, M., Odorcic, S., Chang, L., Zhang, H., Miller, N., McCready, D. R., et al. (2005). High-level coexpression of JAG1 and NOTCH1 is observed in human breast cancer and is associated with poor overall survival. *Cancer Res.* 65 (18), 8530–8537. doi:10.1158/0008-5472.CAN-05-1069

Sajithlal, G. B., Rothermund, K., Zhang, F., Dabbs, D. J., Latimer, J. J., Grant, S. G., et al. (2010). Permanently blocked stem cells derived from breast cancer cell lines. *Stem Cells* 28 (6), 1008–1018. doi:10.1002/stem.424

Shafee, N., Smith, C. R., Wei, S., Kim, Y., Mills, G. B., Hortobagyi, G. N., et al. (2008). Cancer stem cells contribute to cisplatin resistance in Brca1/p53-mediated mouse mammary tumors. *Cancer Res.* 68 (9), 3243–3250. doi:10.1158/0008-5472.CAN-07-5480

Sheridan, C., Kishimoto, H., Fuchs, R. K., Mehrotra, S., Bhat-Nakshatri, P., Turner, C. H., et al. (2006). CD44+/CD24-breast cancer cells exhibit enhanced invasive properties: An early step necessary for metastasis. *Breast Cancer Res.* 8 (5), R59. doi:10.1186/bcr1610

Shukla, V., Chandrasekaran, B., Tyagi, A., Navin, A. K., Saran, U., Adam, R. M., et al. (2022). A comprehensive transcriptomic analysis of arsenic-induced bladder carcinogenesis. *Carcinog. Cells.* 11 (15), 2435. doi:10.3390/cells11152435

Sorrentino, C., Cuneo, A., and Roti, G. (2019). Therapeutic targeting of Notch signaling pathway in hematological malignancies. *Mediterr. J. Hematol. Infect. Dis.* 11 (1), e2019037. doi:10.4084/MJHID.2019.037

Suman, S., Das, T. P., and Damodaran, C. (2013). Silencing NOTCH signaling causes growth arrest in both breast cancer stem cells and breast cancer cells. *Br. J. Cancer* 109 (10), 2587–2596. doi:10.1038/bjc.2013.642

Suman, S., Kurisetty, V., Das, T. P., Vadodkar, A., Ramos, G., Lakshmanaswamy, R., et al. (2014). Activation of AKT signaling promotes epithelial-mesenchymal transition and tumor growth in colorectal cancer cells. *Mol. Carcinog.* 53, E151–E160. doi:10.1002/mc.22076

Tanei, T., Morimoto, K., Shimazu, K., Kim, S. J., Tanji, Y., Taguchi, T., et al. (2009). Association of breast cancer stem cells identified by aldehyde dehydrogenase 1 expression with resistance to sequential Paclitaxel and epirubicin-based chemotherapy for breast cancers. *Clin. Cancer Res.* 15 (12), 4234–4241. doi:10.1158/1078-0432.CCR-08-1479

Thiery, J. P., Acloque, H., Huang, R. Y., and Nieto, M. A. (2009). Epithelial-mesenchymal transitions in development and disease. *Cell* 139 (5), 871–890. doi:10.1016/j.cell.2009.11.007

Tyagi, A., Chandrasekaran, B., Kolluru, V., Baby, B. V., Sripathi, C. A., Ankem, M. K., et al. (2020). ASR490, a small molecule, overrides aberrant expression of Notch1 in colorectal cancer. *Mol. Cancer Ther.* 19 (12), 2422–2431. doi:10.1158/1535-7163.MCT-19-0949

Wu, X., Fleming, A., Ricketts, T., Pavel, M., Virgin, H., Menzies, F. M., et al. (2016). Autophagy regulates Notch degradation and modulates stem cell development and neurogenesis. *Nat. Commun.* 7, 10533. doi:10.1038/ncomms10533

Wu, Y., Cain-Hom, C., Choy, L., Hagenbeek, T. J., de Leon, G. P., Chen, Y., et al. (2010). Therapeutic antibody targeting of individual Notch receptors. *Nature* 464 (7291), 1052–1057. doi:10.1038/nature08878

Yuan, X., Zhang, M., Wu, H., Xu, H., Han, N., Chu, Q., et al. (2015). Expression of Notch1 correlates with breast cancer progression and prognosis. *PLoS One* 10 (6), e0131689. doi:10.1371/journal.pone.0131689

Zada, S., Hwang, J. S., Lai, T. H., Pham, T. M., Ahmed, M., Elashkar, O., et al. (2022). Autophagy-mediated degradation of NOTCH1 intracellular domain controls the epithelial to mesenchymal transition and cancer metastasis. *Cell Biosci.* 12 (1), 17. doi:10.1186/s13578-022-00752-3

Zang, S., Chen, F., Dai, J., Guo, D., Tse, W., Qu, X., et al. (2010). RNAi-mediated knockdown of Notch-1 leads to cell growth inhibition and enhanced chemosensitivity in human breast cancer. *Oncol. Rep.* 23 (4), 893–899. doi:10.3892/or_00000712

Zhou, Y. F., Sun, Q., Zhang, Y. J., Wang, G. M., He, B., Qi, T., et al. (2017). Targeted inhibition of Notch1 gene enhances the killing effects of paclitaxel on triple negative breast cancer cells. *Asian Pac J. Trop. Med.* 10 (2), 179–183. doi:10.1016/j.apjtm.2017.01.005

frontiers | Frontiers in Pharmacology

TYPE Original Research
PUBLISHED 03 March 2023
DOI 10.3389/fphar.2023.1137783

OPEN ACCESS

EDITED BY
Eswar Shankar,
The Ohio State University, United States

REVIEWED BY
Prem P. Kushwaha,
Case Western Reserve University, United States
Yong Li,
Baylor College of Medicine, United States
Jayadev Joshi,
Cleveland Clinic, United States
Vinata Lokeshwar,
Augusta University, United States

*CORRESPONDENCE
Chendil Damodaran,
chendamodar@tamu.edu

†These authors have contributed equally to this work and share first authorship

SPECIALTY SECTION
This article was submitted to Pharmacology of Anti-Cancer Drugs, a section of the journal Frontiers in Pharmacology

RECEIVED 04 January 2023
ACCEPTED 08 February 2023
PUBLISHED 03 March 2023

CITATION
Chandrasekaran B, Tyagi A, Saran U, Kolluru V, Baby BV, Chirasani VR, Dokholyan NV, Lin JM, Singh A, Sharma AK, Ankem MK and Damodaran C (2023), Urolithin A analog inhibits castration-resistant prostate cancer by targeting the androgen receptor and its variant, androgen receptor-variant 7. *Front. Pharmacol.* 14:1137783. doi: 10.3389/fphar.2023.1137783

Urolithin A analog inhibits castration-resistant prostate cancer by targeting the androgen receptor and its variant, androgen receptor-variant 7

Balaji Chandrasekaran[1†], Ashish Tyagi[1†], Uttara Saran[1], Venkatesh Kolluru[2], Becca V. Baby[2], Venkat R. Chirasani[3], Nikolay V. Dokholyan[3,4], Jyh M. Lin[4], Amandeep Singh[3], Arun K. Sharma[3], Murali K. Ankem[2] and Chendil Damodaran[1,2*]

[1]Department of Pharmaceutical Science, College of Pharmacy, Texas A&M University, College Station, TX, United States, [2]Department of Urology, University of Louisville, Louisville, KY, United States, [3]Department of Pharmacology, Penn State Cancer Institute, Penn State College of Medicine, Hershey, PA, United States, [4]Department of Biochemistry and Molecular Biology, Penn State College of Medicine, Hershey, PA, United States

We investigated the efficacy of a small molecule ASR-600, an analog of Urolithin A (Uro A), on blocking androgen receptor (AR) and its splice variant AR-variant 7 (AR-V7) signaling in castration-resistant prostate cancer (CRPC). ASR-600 effectively suppressed the growth of AR^+ CRPC cells by inhibiting AR and AR-V7 expressions; no effect was seen in AR^- CRPC and normal prostate epithelial cells. Biomolecular interaction assays revealed ASR-600 binds to the N-terminal domain of AR, which was further confirmed by immunoblot and subcellular localization studies. Molecular studies suggested that ASR-600 promotes the ubiquitination of AR and AR-V7 resulting in the inhibition of AR signaling. Microsomal and plasma stability studies suggest that ASR-600 is stable, and its oral administration inhibits tumor growth in CRPC xenografted castrated and non-castrated mice. In conclusion, our data suggest that ASR-600 enhances AR ubiquitination in both AR^+ and AR-V7 CRPC cells and inhibits their growth *in vitro* and *in vivo* models.

KEYWORDS

CRPC, Androgen Receptor, AR-Splice Variants, N-terminal domain, small molecule, growth inhibition

Introduction

Androgen receptor (AR) signaling plays a key role in prostate cancer (CaP) pathogenesis (Schmidt and Tindall, 2013; Tan et al., 2015). Androgen deprivation therapy (ADT) that either represses androgen synthesis (van Poppel and Nilsson, 2008) or inhibits AR function (Tran et al., 2009) is the initial treatment for both localized and advanced CaP (Loblaw et al., 2007). Structurally, full-length AR (AR-FL) comprises three domains: The N-terminal activation domain (NTD), DNA-binding domain (DBD), and ligand binding domain (LBD) (Shafi et al., 2013). Current ADTs block the AR LBD directly with anti-androgens or indirectly with androgen biosynthesis inhibitors (Lu et al., 2015; Imamura and Sadar, 2016). Second-generation ADT agents such as abiraterone and enzalutamide are often recommended as first-line therapeutics for castration-resistant prostate cancer (CRPC)

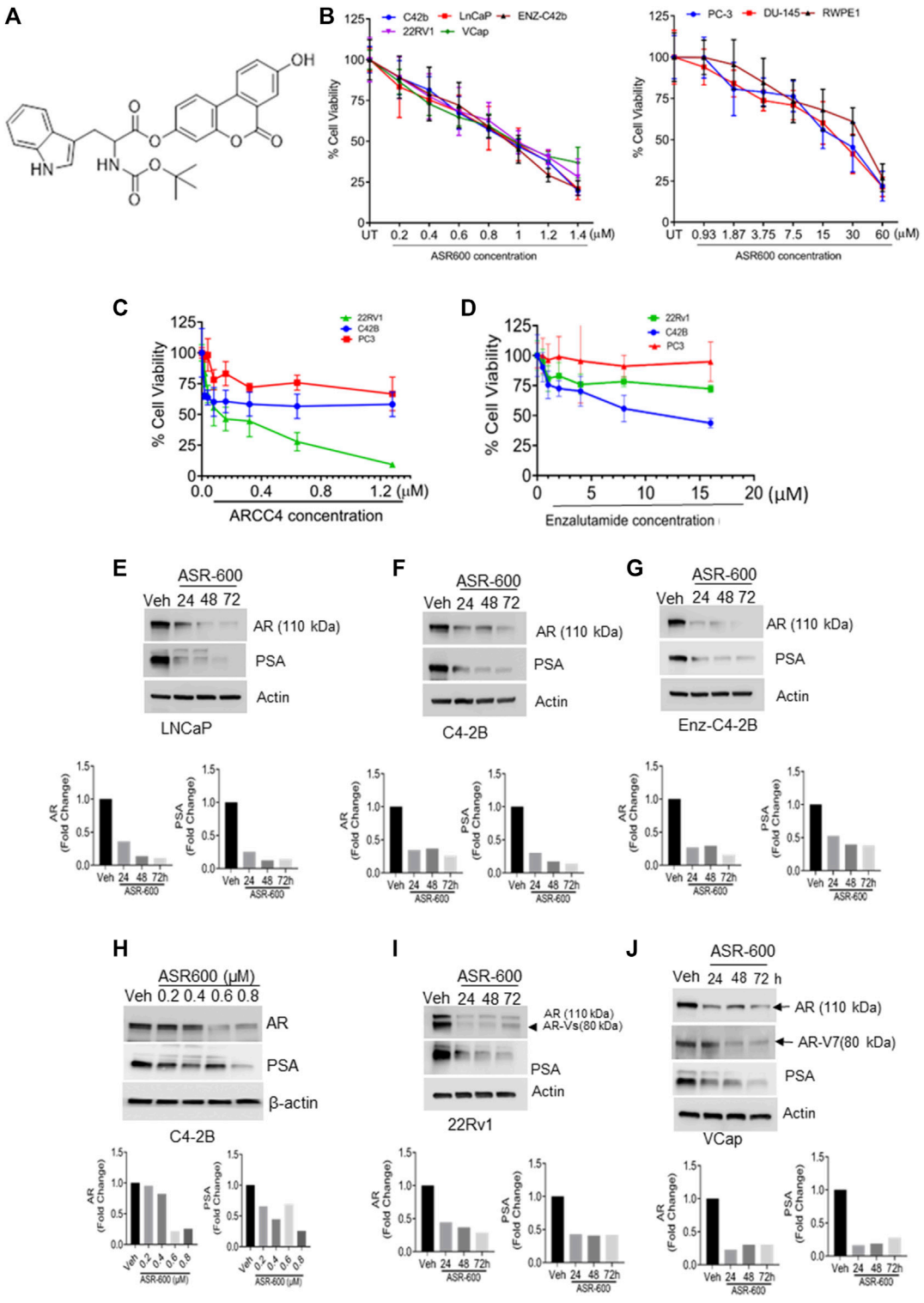

FIGURE 1
ASR-600 inhibits the AR and AR-V7 expression and abolishes the growth of AR$^+$ CaP cells. **(A)**. The molecular structure of ASR-600. **(B)**. MTT cell viability assays performed on AR$^+$ (C4-2B, LNCaP, EnZ-C4-2B, VCaP, and 22Rv1), AR- (PC-3 and DU-145) CaP, and normal prostate epithelial cell line (RWPE-1) with vehicle (DMSO) or different concentrations of ASR600. **(C, D)**. MTT cell viability assays were performed on AR$^+$ C4-2B and 22Rv1, as well as AR- (PC-3) cells treated with vehicle (DMSO) or different concentrations of ARCC4 and Enzalutamide. **(E–G, I, J)** immunoblots for AR, AR-V7and PSA expressions following treated with vehicle (DMSO) or ASR-600 for 24, 48, and 72 h **(H)**. Immunoblots for AR and PSA expressions following treatment with vehicle (DMSO), ASR-600 (at indicated concentrations).

(Beer et al., 2014). While patients are initially responsive toward ADT, tumor relapse often occurs, leading to the development of CRPC (de Bono et al., 2011). A characteristic feature of CRPC is its continued reliance on AR signaling; however, the mechanisms underlying AR reactivation remain unclear.

The truncated AR protein encoded by AR splice variants (AR-Vs) lacks the LBD domain while retaining the transactivating NTD domain. This results in ligand-independent activation and resistance to ADTs (Moon et al., 2018). The AR variant 7 (AR-V7) is the most commonly expressed variant identified to date and contains an intact AR NTD and DBD, as well as a unique C-terminal of 16-amino acids in place of the LBD (Antonarakis et al., 2016). This variant, unlike the AR-FL, is continuously localized to the nucleus (Hu et al., 2009) and has been reported to play a key role in promoting CRPC progression and metastasis, as well as developing resistance to ADT and anti-androgens (Guo et al., 2009; Li et al., 2013; Antonarakis et al., 2014). Moreover, heterogeneity among AR-driven CRPC is extensive, and AR-Vs is known to heterodimerize with the AR-FL (Brady et al., 1999; O'Neill et al., 2015). Thus, combining existing therapeutics with an AR-Vs-targeting agent may be a viable approach to overcome the acquired resistance of CRPC.

Recently, more attention was paid to post-translational regulation of AR activation, either by ubiquitination or lysosome degradation. Currently, three ubiquitination sites have been identified: K845 and K847 at the ligand-binding C-terminal (Xu et al., 2009; Linn et al., 2012) and another site K311 in the NTD (McClurg et al., 2017). Similarly, several preclinical studies suggest that induction of the lysosome pathway (autophagy) promotes CaP progression, and inhibition of lysosomal signaling abrogates the CaP growth (Finkbeiner, 2020; Machado et al., 2021). It has been reported that the AR activation is modulated by post-translational modifications, including ubiquitination (van der Steen et al., 2013).

Urolithin (UroA), a dietary gut microbiota-derived metabolite of ellagic acid, has been shown to exert anti-cancer effects on many cancer types (Sanchez-Gonzalez et al., 2016; Gonzalez-Sarrias et al., 2017; Dahiya et al., 2018; Komatsu et al., 2018; Zhao et al., 2018; Totiger et al., 2019). Interestingly, UroA has been shown to inhibit the proliferation of both androgen-dependent (LNCaP) and -independent (DU-145) CaP cells (Komatsu et al., 2018). In our prior study, our group demonstrated that UroA effectively inhibits AR^+ CRPC growth in both *in vitro and in vivo* models compared to AR^- CRPC growth (Dahiya et al., 2018). UroA was also found to inhibit AR signaling in the AR^+ CRPC cells, Moreover, the reintroduction of AR expression in AR-null PC-3 cells sensitized them to subsequent UroA treatment. Based on these results, we hypothesized that UroA might be a promising lead compound for developing potent and target-specific small UroA analogs to treat CRPC by directly targeting AR and AR-Vs.

We synthesized several O-methylated amino acids (tryptophan) and sulfonamide-/sulfoxide-conjugated analogs of UroA and tested their therapeutic effect on CRPC cell lines. Through structure-activity relationship (SAR) studies, we identified ASR-600 (an N-Boc-protected tryptophan analog, Figure 1A) as the most potent analog that effectively targeted both AR-FL and AR-V7 and suppressed the growth of AR^+ CaP and enzalutamide resistant cells in both *in vitro* and *in vivo* models.

Methods

Cell lines and reagents

Human CaP (LNCaP, PC-3, DU-145, VCaP, and 22Rv1), normal prostate epithelial (RWPE-1), and HEK-293T cell lines were purchased from the American Type Culture Collection (Manassas, VA, USA). C4-2B cells were obtained from ViroMed Laboratories (Minneapolis, MN, USA). The cells were grown on a specified medium, as described previously (Dahiya et al., 2018; Chandrasekaran et al., 2020). Dihydrotestosterone (DHT), cycloheximide (CHX), chloroquine (CQ), and MG132 were purchased from Sigma (St. Louis, MO). MG132 (10 μM) was used as the working concentration for experiments.

Synthesis of ASR-600 (8-Hydroxy-6-oxo-6H-benzo [c]chromen-3-yl (tert butoxycarbonyl)tryptophanate)

ASR-600 was synthesized from Urolithin A according to a synthetic strategy recently developed in our laboratory. Briefly, Urolithin A (1.0 g, 4.38 mmol) was reacted with Nα-Boc-tryptophan (1.38 g, 4.38 mmol) in the presence of coupling agents 1-ethyl-3-(3-dimethyl aminopropyl) carbodiimide hydrochloride (0.67 g, 4.38 mmol), hydroxy benzotriazole (0.59 g, 4.48 mmol), and triethylamine (0.88 g, 8.76 mmol) in acetonitrile at room temperature to afford ASR-600 as the major product. The compound was purified by silica gel column chromatography to yield ASR-600 as an off-white solid and characterized by proton nuclear magnetic resonance (^{1}H NMR, Bruker Avance 500 MHz)) and mass spectrometry (MS, Expression-S Compact Mass Spectrometer) and its purity (≥98%) was determined by high-performance liquid chromatography (HPLC). ^{1}H NMR (500 MHz, DMSO-d_6), 1.40 (s, 9H, 3 x CH_3), 3.17–3.29 (m, 2H, CH_2), 4.45–4.49 (m, 1H, CH), 6.77–6.85 (m, 1H, Ar-H), 6.85–6.87 (m, 1H, Ar-H), 7.01 (t, J = 10 Hz, 1H, Ar-H), 7.10 (t, J = 7.5 Hz, 1H, Ar-H), 7.37–7.41 (m, 1H, Ar-H), 7.57–7.61 (m, 2H, Ar-H), 7.75–7.76 (m, 1H, Ar-H), 8.15 (d, J = 9.0 Hz, 1H, Ar-H), 8.26 (d, J = 9.0 Hz, 1H, Ar-H), 8.30 (d, J = 8.5 Hz, 1H, Ar-H), 10.38 (s, 1H, OH), 10.93 (s, 1H, NH). MS m/z 457.92 [M^+ (514.17) - t-butyl]. Melting point, 200°C–202°C.

Cell viability assays

RWPE-1 and CaP cell lines were treated with vehicle control (DMSO) or different ASR-600 concentrations (200 nM–30 μM) for 24 h and then subjected to cell viability (MTT) assays as described before (Dahiya et al., 2018).

Immunoblot and immunoprecipitation

Cell lysates (vehicle, ASR-600, DHT, DHT + ASR-600, AR transfected cells + ASR-600, empty vector-transfected cells + ASR-600) of CaP cells were prepared following treatment for

24 h in a 6-well plate. Immunoblots were performed as described previously (Dahiya et al., 2018) for the following antibodies: AR-V7 (abcam #ab198394), PSA (abcam#53774), PTEN (abcam# 31392), AR-FL (CST #5153), AKT (CST#4691), pAKT^{ser473} (CST #4060), pmTOR^{Ser2481}(CST #5536), mTOR (CST #2972), ERα (CST#8644), PR (CST#3176), Ubiquitin (CST#3933), and Lamin A. β-Actin was used as the loading control (more details are given in Supplementary File S1). For immunoprecipitation (IP) experiments, protein samples were immunoprecipitated with the AR antibody per the protocol described before (Chandrasekaran et al., 2020). Briefly, in immunoprecipitation experiments, protein samples (40 μg) were extracted from cells using radioimmunoprecipitation assay (RIPA) buffer, then immunoprecipitated with AR antibody at 4°C under agitation overnight. The immunoprecipitated protein was pulled down using protein A-agarose beads (Thermo Fisher Scientific, Rockford, IL) at 4°C under rotary agitation for 3 h. Subsequently, centrifugation was followed by resuspension of the pellets in sample buffer, which was then heated for 5 min at 95°C for sodium dodecyl sulfate-polyacrylamide gel electrophoresis and immunoblot analysis for ubiquitin expression. All uncropped immunoblot images are presented as Supplementary File S3.

Transfection

PC-3 and HEK-29 cells were seeded on 6-well plates in a respective medium supplemented with 10%FBS and were allowed to attach overnight. They were then transfected with either a control vector or AF-FL plasmid, using Lipofectamine-2000 reagent in Opti-MEM medium. After 24 h, these cells were treated with ASR-600 at different time points. Finally, the cells were lysed, protein was extracted, and AR expression was assessed using immunoblot and IP. Briefly, the transfected cells were treated with IC_{50} concentrations of ASR-600 and AR expression was assessed using immunoblots and IP.

Real-time quantitative PCR

RNA was extracted from control and ASR600-treated cells using the RNAeasy Mini Kit (Qiagen, Hilden, Germany). This was followed by reverse transcription using the iScript DNA Synthesis Kit (Bio-Rad, Hercules, CA). RT-PCR using SYBR Green PCR Master Mix (Applied Biosystems, Foster City, CA) with specific AR and PSA primers as per the protocol described previously (Dahiya et al., 2018). β-actin was used as the internal control.

Immunofluorescence and immunohistochemistry analysis

Immunofluorescence analysis for AR and AR-V7 was performed on control, ASR-600, DHT or ASR-600 + DHT, MG132 or MG132+ASR-600 treated cells as described previously (Dahiya et al., 2018). Immunohistochemical analyses were performed for Ki-67, AR and PSA expression on vehicle control and ASR-600 treated xenograft tumors (22RV1 and C2-4B).

Proteasome activity

Proteasomal activity of control and ASR-600 treated C4-2B cells was measured using a Proteasome activity assay kit (BioVision) per the manufacturer's protocol. MG132 was used as the positive control.

Molecular docking

Molecular docking of ASR-600 to AR-NTD was conducted using MedusaDock 30, 32, 37, a docking program that incorporates structural flexibility during simultaneous sampling of conformational states of protein and ligand (Wang and Dokholyan, 2019). Due to the presence of low-complexity regions, the structural conformation of NTD is unknown. Therefore, we performed *ab initio* modeling to decipher its 3D structure. We submitted the FASTA sequence of NTD to the I-TASSER (Iterative Threading ASSEmbly Refinement) server (Yang et al., 2015), which utilizes a hierarchical approach to predict the structure of the query protein. Steric clashes were most prevalent in modeled and redesigned structures. Subsequently, we performed discrete molecular dynamics (DMD) simulations (Dokholyan et al., 1998; Lazaridis and Karplus, 2000; Shirvanyants et al., 2012; Ding and Dokholyan, 2013) for 6×10^6-time steps to remove steric clashes and to optimize the energy of the modeled structure. The structures were clustered using Gromacs tools (Cherinka et al., 2018), and the optimal representative structure of NTD was extracted for subsequent docking studies with ASR-600. The optimized structure of ASR-600 was built using a Marvin sketch workspace (Cherinka et al., 2018).

Nuclear magnetic resonance (NMR)

The proton NMR experiment was carried out with Bruker Avance 600 MHz NEO NMR equipped with the TCI cyroprobe. The purified NTD protein (5 μM/L) was mixed with ASR-600 (500 μM/L; dissolved in DMSO-d_6) in 500 μL of 20 mM phosphate buffer made up of 100% deuterium oxide. The NMR saturation transfer difference (STD) experiment was carried out with a standard pulse program from the Bruker pulse library. Two parallel experiments: the reference (A, without saturation, blue spectra; with decoupler set at δ= −30 ppm) and one with selective saturation on the AR protein (B, red spectra; decoupler set at δ= 0.8 ppm) were executed. The peak intensity differences are shown by spectra C (green spectrum). The binding affinity was measured based on the peak intensity by the different spectra.

Xenograft studies

The *in vivo* effect of ASR-600 was evaluated by subcutaneously injecting castrated and non-castrated 6–8 weeks old BALB/c male athymic nude mice (nu/nu), purchased from the Jackson Laboratory (Bar Harbor, ME, USA), with either 22Rv1 or C4-2B cells. ASR-600 first dissolved in DMSO was diluted in PBS to make a 0.1% solution. Mice bearing 22Rv1 and C4-2B xenografts were then randomized

into control (placebo) and treatment (20 mg/kg, ASR-600) groups. All mice were euthanized *via* CO_2 asphyxiation after 4 weeks of treatment, and the xenograft tumors were removed and fixed in 10% formalin for histopathological studies. All experimental animals were approved by the University of Louisville's ethical committee and maintained following Institutional Animal Care and Use Committee approved-protocols.

Microsomal incubation and sample preparation for liquid chromatography–mass spectrometry (LC-MS)

Pooled mouse liver microsomes were procured from BioIVT (USA). The ASR-600 metabolic stability was analyzed using previously established protocol (Attwa et al., 2020). A detailed procedure is given in the Supplementary Material. Briefly, 7.5 µL compound working solution was incubated with 592.5 µL microsomal/S9 mixture/vial and the metabolic reactions were initiated using NADPH (1 mM) for a specific time. Reactions were stopped at 14, 28, and 42 min by adding acetonitrile (ACN) containing 100 ng/mL tolbutamide. From the generated data after sample analysis, ASR-600 metabolic stability curve was established, and the *in vitro* intrinsic clearance was calculated (detailed procedure was given in Supplementary File S2).

Statistical analysis

All statistical analyses were performed using GraphPad Prism 8.0a software (GraphPad Software, Inc., La Jolla, CA). Unpaired two-tailed Student's *t*-tests and one-way ANOVA analysis were performed for two-group and multiple group comparisons, respectively. p-values <0.05 were considered statistically significant and values were presented as either mean ± SD.

Results

ASR-600 inhibits the growth of CaP cells

To develop more potent and target-specific compounds based on the lead UroA structure, a series of UroA analogs such as *O*-methylated and amino acid- and sulfonamide-/sulfoxide-conjugated analogs were synthesized. SAR studies based on cytotoxicity towards CaP cells led to the identification of ASR-600 (Figure 1A), an N-Boc-protected tryptophan analog, as the most potent compound. The inhibitory effect of ASR-600 on CaP cell growth in well-characterized human CaP cell lines (AR^+: LNCaP, C4-2B; AR-Variant: 22Rv1, VCaP; AR-null: PC-3 and DU-145) and normal prostate epithelial cells (RWPE1) was assessed by MTT assay. ASR-600 treatment inhibited the viability of C4-2B (IC_{50}: 824 nM), LnCaP (811 nM), 22Rv1 (IC_{50}: 919 nM) and VCaP (IC_{50}: 923 nM) cells in a concentration-dependent manner at 24 h. Similarly, treatment with ASR-600 for 24 h also significantly inhibited the viability of enzalutamide resistant C4-2B cells (IC_{50}: 815 nM). However, IC_{50} of AR-null CaP cell lines PC-3 (18 µM) and DU-145 (19.5 µM) are higher than AR-null CRPC cells. Interestingly, the RWPE1 cells remained unaffected (IC_{50}: 37 µM) with ASR-600 treatment (Figure 1B). We used AR inhibitors/degraders, such as enzalutamide and ARCC4, as controls for our experiments. The inhibitory effect of ASR-600 was significantly higher as compared to enzalutamide. ARCC4 was effective in 22RV1 (AR-FL/AR-V7) cells compared to ASR-600 (Figures 1C, D). These results suggested that AR^+ CaP cell lines are sensitive to ASR-600 compared to AR-null CaP or the RWPE1 cells.

ASR-600 targets AR and AR-V7 expression in CaP cell lines

Because the AR^+ CaP cell lines were found to be sensitive to ASR-600 treatment, we next sought to determine whether ASR-600 mediated its effects *via* targeting AR signaling. A time-dependent downregulation of AR expression as well as a concomitant decrease of AR downstream target prostate-specific antigen (PSA), was seen in a panel of CaP (C4-2B, LNCaP, EnZ-C4-2B, VCaP and 22Rv1) cell lines after treatment with their respective IC_{50} concentrations of ASR-600 (Figures 1E-G, I, J). A dose-dependent decline in AR expression was also observed in C4-2B cells (Figure 1H). We also noted that ASR-600 decreased the expression of AR-V7 in 22Rv1 and VCaP cells, suggesting that ASR-600 targets not only the AR-FL but also AR-Vs, which is associated with aggressive CaP phenotypes. We next explored the effects of ASR-600 on DHT-induced AR signaling in C4-2B and 22Rv1 cells. Results indicated that ASR-600 treatment abolished DHT-induced AR signaling in both cell lines, as confirmed by the decreased expressions of AR and PSA (Figures 2A, B). Next, to understand whether the inhibitory activity of ASR-600 is specifically through AR signaling, we overexpressed AR in 293T and prostate-specific AR-null PC-3 cells. ASR-600 suppressed the expression of AR-FL in both cell lines (Figures 2C, D). Together these data confirm AR could be a target for ASR-600. Subsequent immunofluorescence analysis reconfirmed that ASR-600 treatment resulted in the overall loss of AR in DHT-treated 22Rv1 and VCaP cells (Figures 3A, B) and inhibiting proteasomal activity by MG132 (10 µM) inhibited loss of AR in ASR-600 treated 22Rv1 cells (Figure 3C).

ASR-600 inhibits AR-V7 expression in CaP cells

We examined the cytosolic and nuclear expression of AR-V7 in ASR-600 treated 22Rv1 cells. Results demonstrate that ASR-600 decreases both cytoplasmic and nuclear AR-V7 in a time-dependent manner (Figure 4A). Subsequent, immunofluorescence analysis revealed a significant reduction in nuclear expression of AR-V7 in ASR-600 treated 22Rv1 and VCaP cells when compared to vehicle-treated cells (Figures 4B, C). As a proof of principle, we overexpressed AR-V7 in PC-3 and 293T cells and observed that ASR-600 completely abolished AR-V7 expression in both cell lines (Figures 4D, E). These results confirm that ASR-600 inhibits AR-V7 expression in CaP cell lines. Next, we analyzed the effect of ASR-600 on the transcriptional levels of AR and PSA in CaP cells.

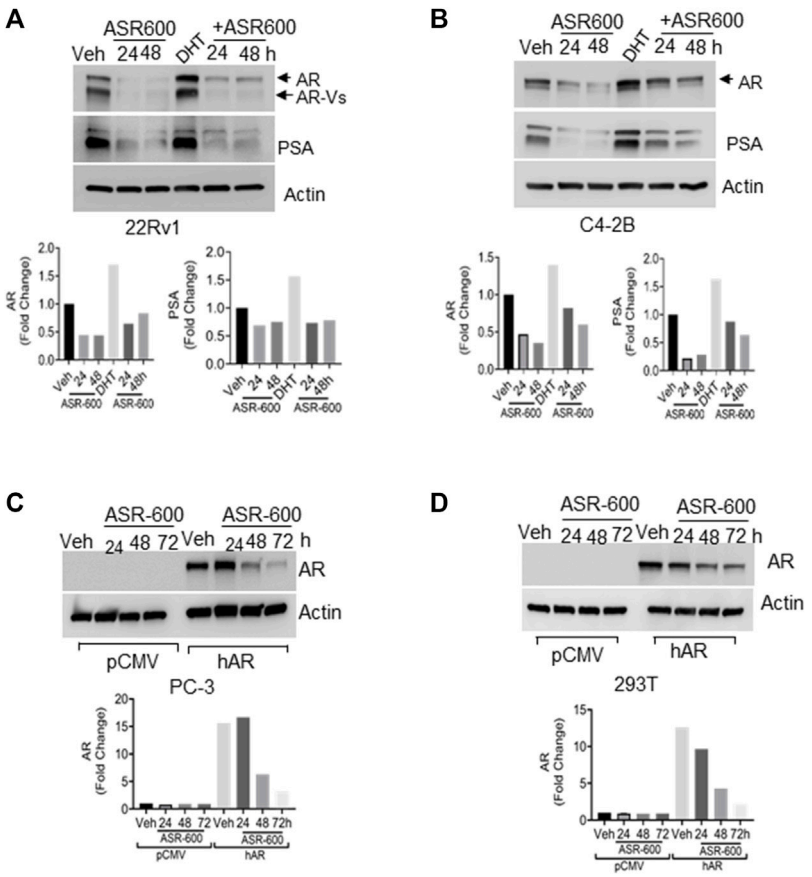

FIGURE 2
ASR-600 inhibits DHT-induced AR/AR-V7 expression. **(A, B)**. Immunoblots for AR, AR-V7and PSA expressions following treated with vehicle (DMSO) or ASR-600, DHT or DHT+ASR600 for 24 and 48 h in 22Rv1 and C4-2B cells. **(C, D)** Immunoblots for AR-expression in empty vector or AR transfected PC-3 or 293T cells following ASR-600 treatment for 24, 48, and 72 h.

Surprisingly, no significant reduction of AR mRNA levels was observed. However, a significant reduction of PSA levels was seen in the CaP cells suggesting that AR inhibition by ASR-600 may be post-transcriptionally regulated (Figures 4F, G).

Downregulation of AR by ASR-600 may involve ubiquitin signaling

As ASR-600 seems to have an inconsistent inhibitory effect on AR mRNA, as compared to AR protein levels, we investigated ASR-600 post-translational regulation of AR. We found that treatment with protein synthesis inhibitor CHX alone and in combination with ASR-600 resulted in a time-dependent decrease of AR expression in C4-2B cells (Figures 5A–C), suggesting the possible involvement of AR degradation signaling in ASR-600 mediated effects. To further explore these results, we examined degradation pathways that may be involved in the ASR-600-regulated decrease of AR. As the ubiquitin-proteasome or lysosome pathways are the predominant mechanisms for AR degradation, C4-2B cells were treated with ASR-600 in the presence or absence of a proteasome (MG132) and lysosome (CQ) inhibitor for 9 h. While the decrease in AR levels upon ASR-600 treatment was significantly rescued when MG132 was used to inhibit proteasomes, the same was not observed when cells were treated with the lysosomal inhibitor (Figures 5D-E). These results suggest that AR degradation is caused by proteasome activation.

Next, we examined ubiquitination-associated AR degradation in ASR-600 treated CaP cells. Increased ubiquitin expressions were seen in ASR-600 treated C4-2B and 22Rv1 cells (Figures 5F, G). MG132 treatment which inhibits proteasome mediated degradation of proteins causes polyubiquitination. Hence, we have used MG-132 as a positive control in these experiments. To confirm that ASR-600 specifically ubiquitinates AR, we analyzed ubiquitin expression in ASR-600 treated AR-null PC-3 and 293T cells. No change in ubiquitin expression was observed (Figures 5J, K). These results further confirm that ASR-600 treatment specifically ubiquitinates AR. However, when we overexpressed AR in AR-null PC-3 cells and treated them with ASR-600, we observed an increased expression of ubiquitin compared to the vehicle which suggests that ASR-600 specifically targets AR in CRPC cells (Figure 5L). We also examined ubiquitination-associated AR degradation by immunoprecipitation (IP) with AR and immunoblot for ubiquitin antibody on CaP cell lysates treated with MG-132, ASR-600 and combinations. ASR-600 induced AR ubiquitination in both C4-2B and 22Rv1 cells.

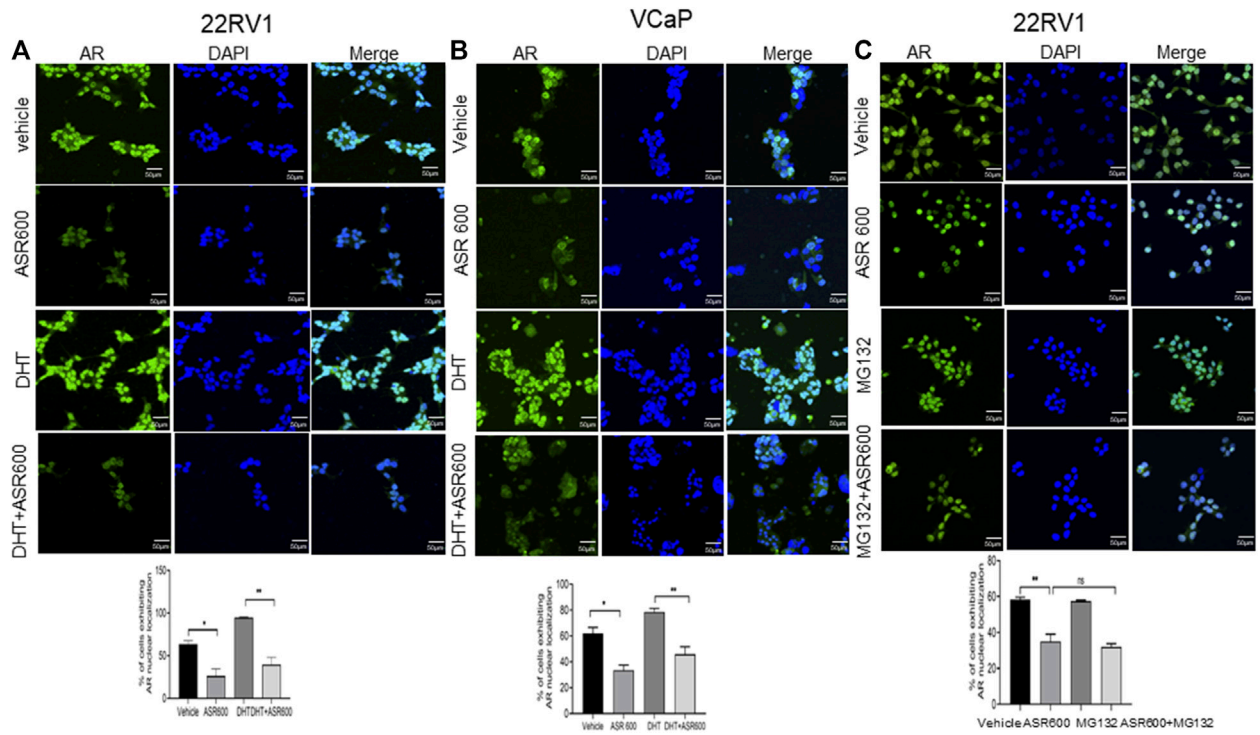

FIGURE 3
Nuclear accumulation of AR abolished by ASR-600. **(A, B)**. Immunofluorescence analysis of cyto-nuclear localization of AR expression in ASR-600, DHT, or ASR 600 + DHT treated 22RV1 and VCaP cells. **(C)**. Immunofluorescence analysis of cyto-nuclear localization of AR expression in ASR-600, MG132 (10 μM), or ASR 600 + MG132 treated 22RV1 cells.

Moreover, MG-132 increased AR ubiquitination which was further increased in both cell lines on treatment with a combination of MG-132 and ASR-600 (Figures 5H, I). To determine whether ASR-600 could be a proteasome inhibitor, we measured proteasomal activity using a chymotrypsin-like compound with a 7-amido-4-methylcoumarin (AMC)-tagged peptide substrate. An induction of proteasome activity was measured at 15 and 30 min and no significant changes were noted until 12 h in ASR-600-treated CaP cells (Figure 5M). We used commercially available positive and negative controls for these experiments. These results suggest that ASR-600 is not a proteasome inhibitor. Together, these results indicate that ASR-600 is a potent ubiquitination agent for AR in CaP cells.

ASR-600 specifically targets AR signaling

To confirm whether ASR-600 affects other pro-survival signaling pathways apart from AR in CRPC, we examined AKT, mTOR, Estrogen receptor (ER), and Progesterone receptor (PR) expressions in prostate and breast cancer cell lines. No significant changes in the expressions pAKTser243 were observed in the ASR-600 treated PC-3 cells (Figure 6A). Similarly, we confirmed that ASR-600 did not alter the expression of $pmTOR^{Ser2481}$, and $pAKT^{ser243}$ in DU-145 cells (Figure 6B). Moreover, assessment of ASR-600 effect on other closely related receptors in T47D cells, revealed that ASR-600 did not affect ER and PR levels. Moreover, no changes in the PTEN levels were seen in the ASR-600 treated cells (Figure 6C). As expected, ASR-600 failed to inhibit the growth of breast cancer cells (Figure 6D), which supports the notion that ASR-600 specifically targets AR in CaP cells.

ASR-600 binds to NTD of AR

We performed *ab initio* modeling to decipher the 3D structure of AR-NTD and used molecular docking studies to assess the binding affinity of ASR-600 to the NTD domain of AR. Visual inspection of the NTD-ASR-600 docked structures revealed compact binding between the ligand and NTD (Figure 7A). The interaction energy of ASR-600 with NTD displayed a moderate (−29.71 kcal/mol) binding energy. Next, we confirmed that ASR-600 binds to NTD by using a commercially available kit which works on a different principle (differential scanning fluorimetry). The first derivate of the fluorescence curve (-dF/dT) was plotted against temperature to calculate Tm (the temperature at which 50% of the double-stranded DNA dissociates into single strands) (lowest−dF/dT value). The purified NTD protein alone had a melt temperature of approx. 35.0°C and ASR-600 treatment shifted the melt temperature (ΔTm) by 12°C–15°C (median of 13.5°C) in a distribution that appeared normal (Figure 7B).

Finally, we utilized NMR spectroscopic studies to confirm the binding of ASR-600 to AR-NTD. The principle of this experiment is that in the bound state, the most abundant molecule governs the

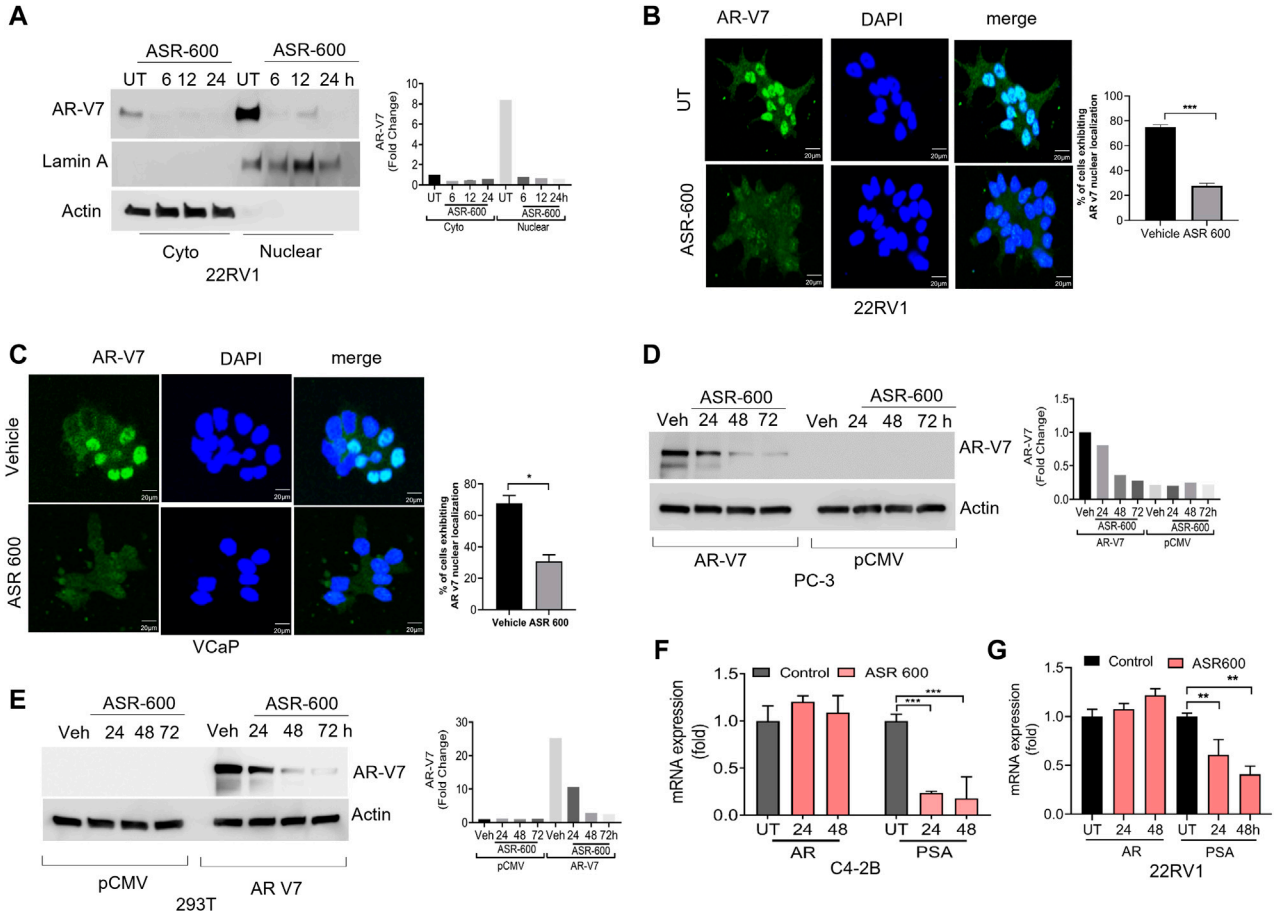

FIGURE 4
ASR-600 inhibited AR-V7 expression in CaP cells. **(A)** Immunoblots demonstrating subcellular fractionation in 22RV1 cells treated with ASR-600 for 6, 12, and 24 h. Lamin A and ß-actin were used as the internal controls. **(B, C)** Immunofluorescence analysis of cyto-nuclear localization of AR-V7 expression in ASR-600 treated 22Rv1 and VCaP cells. **(D, E)** Immunoblots for AR-V7 expression in PC-3 or 293T cells transfected with AR V7 or empty vector and treated with ASR-600 for 24, 48 and 72 h. **(F, G)** AR and PSA mRNA expression of ASR-600 treated C4-2B and 22Rv1 cells.

hydrodynamic properties of both ligand and receptor. Thus, the magnetization transfer in the on-resonance experiment leads to a significant reduction in signal intensities for the ligand, which is recorded in the spectra. The off-resonance irradiation experiment will not affect the spectra intensities of the ligand because there is no transfer of magnetization from protein to ligand, which serves as the reference spectra. Subtraction of the on-resonance spectra from off-resonance spectra indicates the binding interaction between ligand and protein (Figure 7C). In contrast, subtraction of the no-binding ligands will result in a flat line spectrum because no magnetization transfer takes place during both on- and off-resonance irradiation (This distinction provides the basis for NMR screening experiments. The STD effects observed were 30–18%, indicating a significant binding to NTD (Figure 7C).

In vitro metabolic stability

In vitro systems, such as human liver microsomes (HLM) and human hepatocytes, are the best models to predict a drug's hepatic clearance (Gajula et al., 2021). At a concentration of 0.5 μM, the elimination rate constant k) of ASR-600 in mice liver microsome metabolism was >0.48 min^{-1} (control: Midazolam, k = 0.250 min^{-1}) with a half-life (t½) of <1.4 min (Midazolam, t½ = 2.773 min) (Figures 8A, B, Table 1).

ASR-600 intrinsic clearance (CLint) was also calculated based on the *in vitro* t½ (Baranczewski et al., 2006) so the CLint of ASR-600 was 47.9 mL/min/g (Midazolam, 24.0 mL/min/g). ASR-600 was highly stable in the mouse plasma *in vitro*, 93.7% remaining after 2 h incubation time as compared to 25% in control i.e., Eucatropine (Figure 8D, E, Table 2). The high stability of ASR-600 in the mouse plasma suggests that ASR-600 is not subject to cleavage of any significant levels by the enzymes resided in the systemic circulation after it is intravenously administered to the animals.

ASR-600 inhibits the growth of CRPC tumors in castrated and non-castrated xenograft mouse models

The anti-cancer effect of ASR-600 was also evaluated *in vivo* using castrated and non-castrated CRPC xenograft mouse

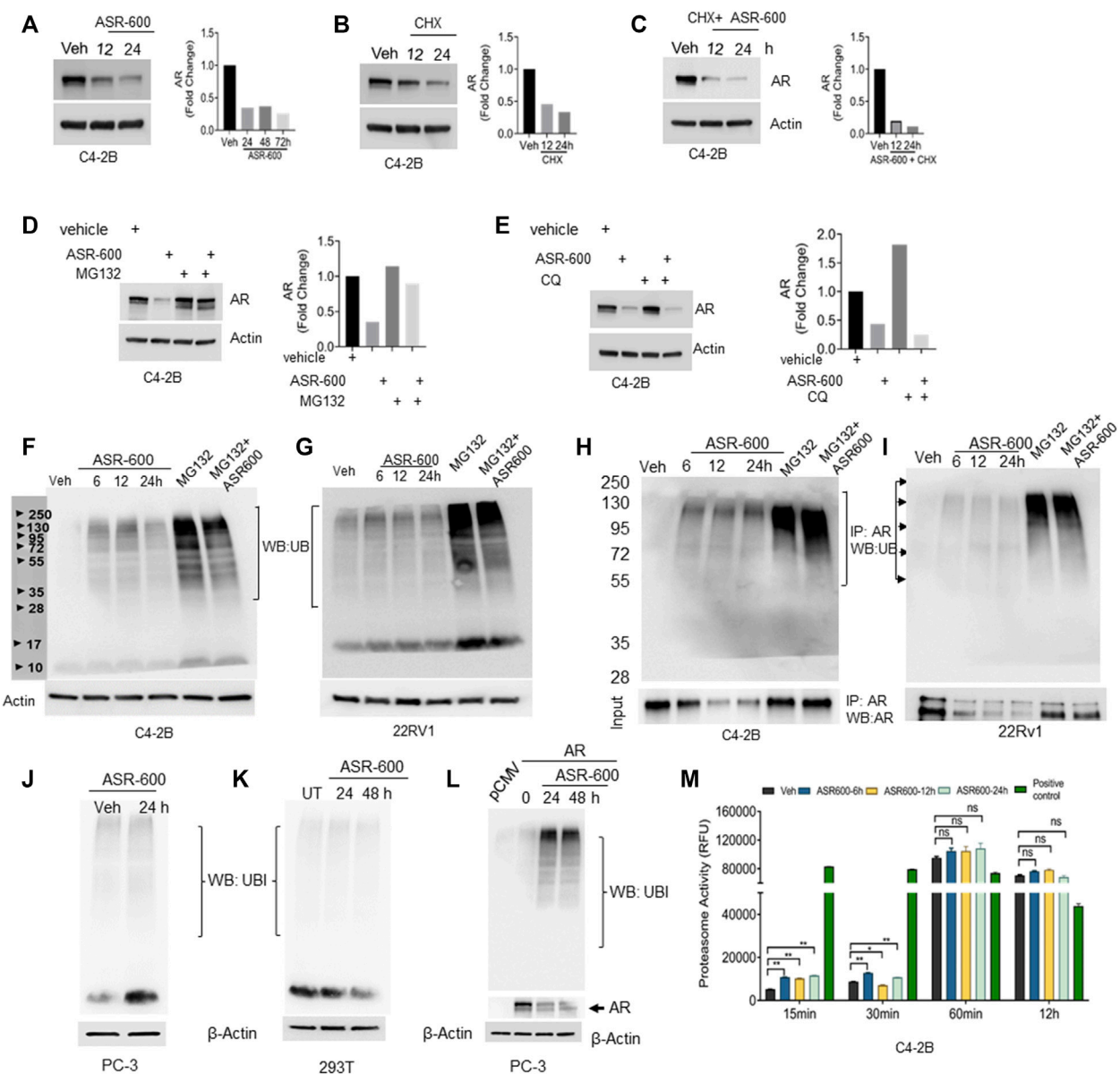

FIGURE 5
Ubiquitination of AR in ASR-600 treated CaP cells. **(A–C)** Immunoblots of AR expression in C4-2B cells treated with ASR-600, CHX (50 μM) or combinations at the indicated time points. **(D,E)** Immunoblots of AR expression in C4-2B cells treated with ASR-600, MG-132(10 μM) or CQ (50 μM), or combinations. **(F,G)** Immunoblots for ubiquitin protein expression in C4-2B and 22Rv1 cells were treated with MG-132, ASR-600, veh, or combinations for 6, 12, and 24 h **(H,I)**. Cell lysates were IP with AR antibody and subjected to WB with ubiquitin antibody. The input cell lysates were WB with AR. **(J,K)** Immunoblots of ubiquitin expression in PC-3 and 293T cells were treated with ASR-600 at the indicated time points. **(L)** PC-3 cells transfected with AR and treated with Veh or ASR600 for 0, 24, and 48 h. **(M)** The proteasomal activity was measured in C4-2B cells treated with ASR-600 at the indicated time points.

models. ASR-600 treatment was highly effective in reducing tumor volumes of both 22Rv1 and C4-2B xenograft models (Figures 9A, C). The weights of tumors from ASR-600 treated mice were also lower than that of the vehicle-treated group (Figures 9B, D). IHC analysis revealed that ASR-600 decreased AR and PSA expression in treated tissues. This confirms that ASR-600 effectively decreases AR levels and downregulates AR signaling. ASR-600 treated tumors also showed low Ki67 + nuclei, which confirms the growth inhibitor effect of ASR-600 in CRPC xenograft models (Figures 9E, F). Examination of the body weight of the treated mice revealed that ASR-600 had no toxic pathological effect on their growth during the treatment period (data not shown). These results suggest that the 20 mg/kg dose of ASR-600 used did not induce any significant toxicity in the mice.

Next, we evaluated the ability of ASR-600 to inhibit the growth of 22RV1 tumors in castrated mice. 22RV1 cells were injected into the right dorsal flank of castrated male nude mice. ASR-600 (20 mg/kg) was administered by oral gavage throughout the experiment period. ASR-600 significantly

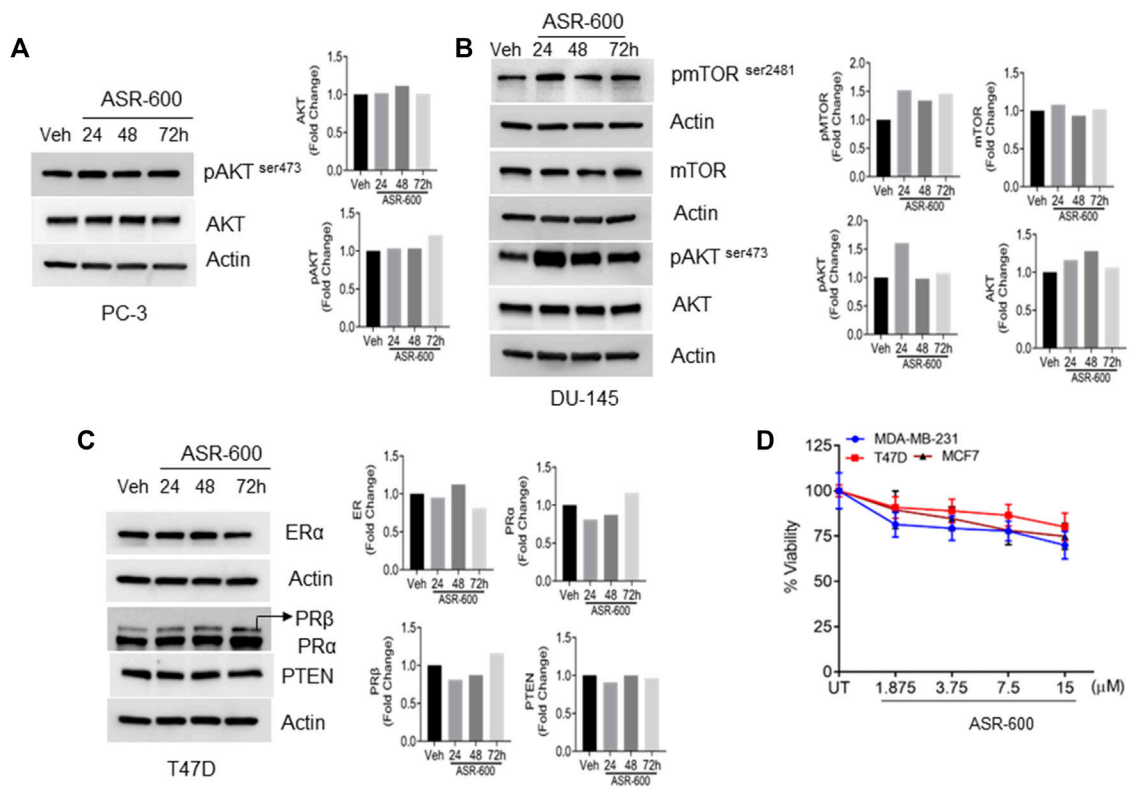

FIGURE 6
ASR-600 specifically targets AR in CaP cells: **(A–C)**. Immunoblots of indicated antibodies in vehicle or ASR-600 treated PC-3, DU-145, and T47D cell lines. **(D)**. Cell viability assay results of vehicle or ASR-600 treated ER-positive and ER-negative breast cancer (MCF-7, T47D, and MDA-231) cell lines.

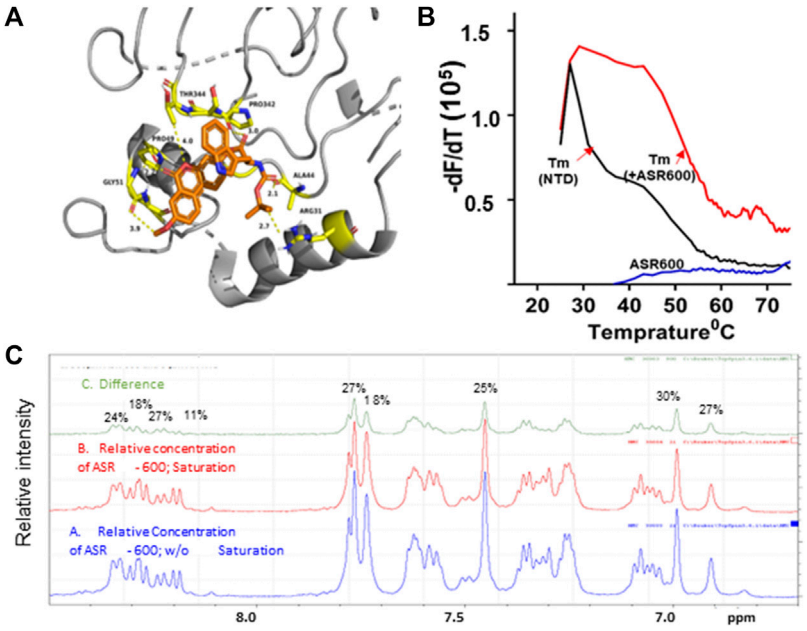

FIGURE 7
Physical interaction between ASR 600 and AR- NTD: **(A)**. AR-NTD residues participating in potential electrostatic and steric interactions with ASR-600 are depicted in yellow stick representation. The AR-NTD backbone is shown as a cartoon in gray, and ASR-600 is represented as an orange stick representation. **(B)**. GloMelt™ thermal shift assay was performed on NTD (5 μg) in the presence of ASR-600. The binding stabilized the protein, as indicated by the shift in the melting curves. **(C)**. NMR STD experiment results of ASR-600 with AR-NTD; the STD effect varied from 18 to 30%. The figure shows the aromatic region as proton peaks of ASR-600: the blue spectrum-without saturation; the red - with saturation; and the green depicts the difference in the spectrum observed.

Microsomal Stability: **Control** **ASR-600**

A

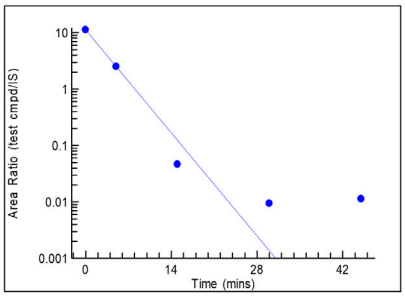

Parameter	Value	Std Error
Initial Value	11.22309891	0.045819195
Rate constant	0.300525385	0.003718136

B

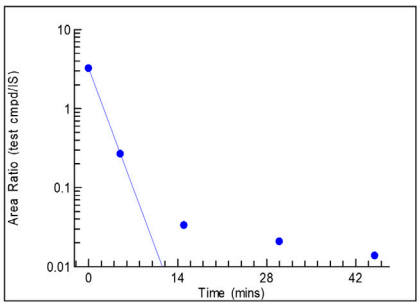

Parameter	Value	Std Error
Initial Value	3.225064461	0.023149003
Rate constant	0.498707978	0.017431737

Table:1 Microsomal stability

Microsomal Stability (Mouse, Compound Conc=0.5μM, n=1)			
Control	Midazolam		
Test compound	Elimination rate constant (k) (min-1) *	Half-life (t1/2) (min) **	Intrinsic Clearance (CLint) (mL/min/g liver)***
ASR600	>0.48	<1.4	47.9
Midazolam	0.250	2.773	24.0

Plasma Stability: **Control** **ASR-600**

C

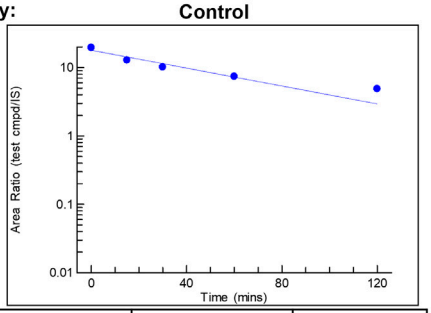

Parameter	Value	Std Error
Initial Value	17.96741793	1.552650707
Rate constant	0.015063865	0.003349679

D

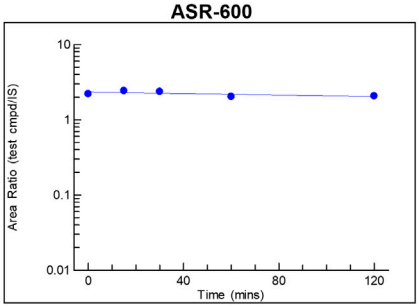

Parameter	Value	Std Error
Initial Value	2.33199864	0.100611778
Rate constant	0.001121809	0.000745459

Table:2 Plasma Stability

Area Ratio (test cmpd/IS) / Time (mins), Control = Eucatropine							
Compound	0	15	30	60	120	Stability (% Remaining)	Rate Constant
ASR600	2.2067	2.4259	2.3653	2.0324	2.0681	93.7	0.00112
Control	19.5832	12.8423	10.1686	7.4245	4.8971	25.0	0.0151

y=(A*exp(((-1)*B)*x))
A= initial value
B= elimination rate constant (k)

FIGURE 8
Microsomal and plasma stability ASR-600. Mouse microsomes were thawed and mixed with ASR-600 or control (Midazolam) **(A)**. ASR-600 and microsomes were incubated with or without cofactor (+NADPH) for indicated time points and plotted against area ratio. **(B)**. The area ratio was plotted against indicated time points for Midazolam **(Table:1)** Mouse microsomal stability. The elimination rate constant, half-life and intrinsic clearance of ASR-600 and control: Midazolam. Mouse plasma was mixed with ASR-600 or control (Eucatropine) **(C)**. ASR-600 and mouse plasma were incubated for indicated time points and analyzed with LC-MS/MS. **(D)**. The area ratio was plotted against indicated time points for Midazolam **(Table:2)** Plasma stability. Stability and rate constant of ASR-600 and control: Eucatropine.

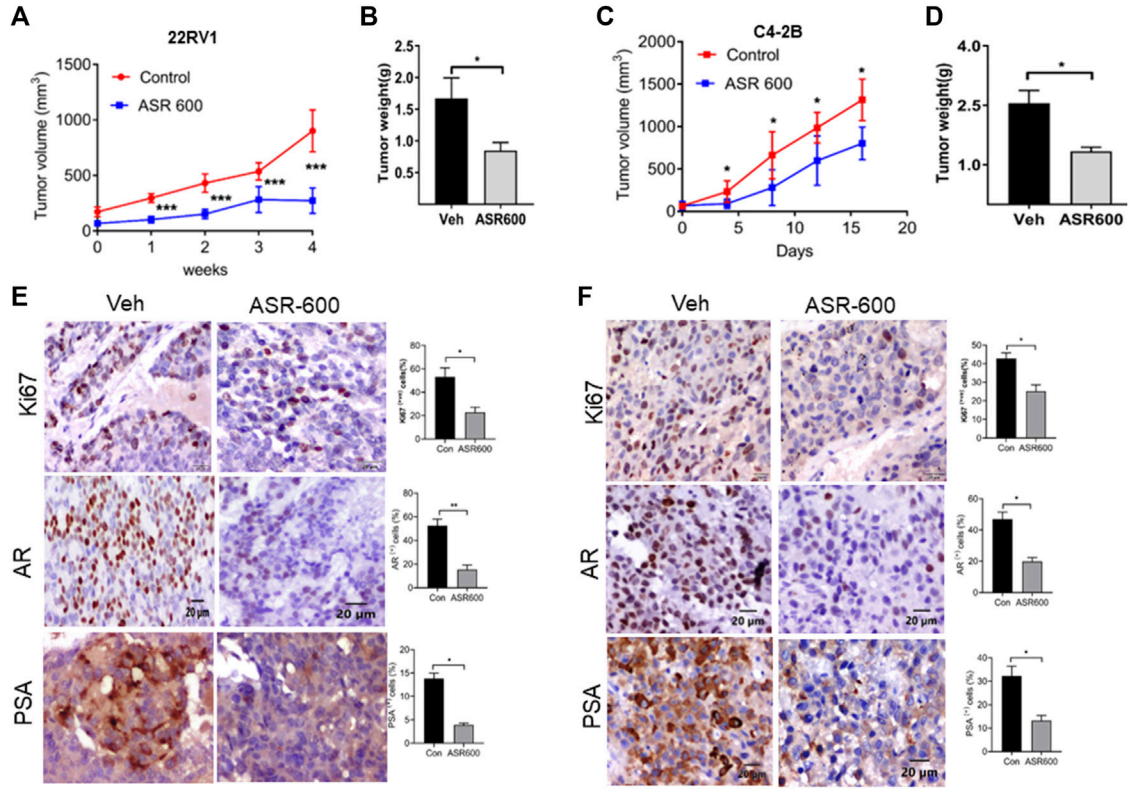

FIGURE 9
The therapeutic effect of ASR-600 on Xenotransplanted prostate tumors. **(A, C)** Oral administration of ASR-600 (20 mg/kg) inhibited the xenotransplanted tumors from 22Rv1 & C4-2B tumors. Tumor volumes were measured once per week for 4 weeks, and a line graph was plotted to compare tumor growth volume (mm^3). **(B, D)** Tumor weight for vehicle and ASR 600-treated 22Rv1 and C4-2B tumors. **(E, F)** Immunohistochemistry analyses of tumor samples were performed to evaluate the expression of Ki67, AR and PSA in 22Rv1 and C4-2B xenografted tumors.

inhibited the growth of 22RV1 tumors and decreased the tumor weights of treated mice (Figures 10A, B). IHC analysis of the xenograft tumors revealed that ASR-600 decreased AR and PSA expression in treated tissues (Figure 10C). This confirms that ASR-600 effectively decreases AR levels and downregulates AR signaling. ASR-600 treated tumors also showed low Ki67 + nuclei, which confirms the growth inhibitory effect of ASR-600 in CRPC castrated xenograft models. Our results indicate that ASR-600 may be a useful treatment for CRPC.

Discussion

We show here that ASR-600, an analog of UroA, is more potent than its parent compound and that it specifically targets and causes AR-FL and AR-V7 degradation in CRPC and enzalutamide resistant CaP cells *via* ubiquitin-mediated pathway. NMR and ITC studies revealed that ASR-600 binds to the AR-NTD domain and enhances ubiquitin-mediated degradation of both AR-FL and AR-V7 without inhibiting proteasome activity.

Upregulation or reactivation of AR signaling is a hallmark of CaP progression to CRPC (Chen et al., 2004; Schmidt and Tindall, 2013; Tan et al., 2015; Cato et al., 2019), which resulted in the development of anti-AR drugs (abiraterone and enzalutamide) targeting the AR axis (de Bono et al., 2011; Beer et al., 2014). Abiraterone reduces androgen production by blocking cytochrome P450 17 alpha-hydroxylase (CYP17) (Attard et al., 2009); enzalutamide has a three-fold effect it competitively inhibits androgen binding to AR, prevents AR translocation to the nucleus, and inhibits AR binding to androgen response elements in the nucleus (Tran et al., 2009; Watson et al., 2010). Although these modalities block AR signaling, they do not target AR (e.g., degradation of AR), which may continue to function through other stimuli (e.g., growth factors), resulting in disease relapse and progression. Moreover, the emergence of constitutively active AR-Vs that lack the LBD has contributed to the development of resistance in CRPC patients (Guo et al., 2009; Hu et al., 2009; Li et al., 2013; Scher et al., 2016; Welti et al., 2016). Hence, targeting both AR-FL and AR-Vs may not only disrupt these interactions but also curb the growth of CRPC.

Recently, a phase-1 clinical trial on the AR-NTD inhibitor (EP1-506) was terminated because it achieved a minor decline in serum PSA levels (a surrogate marker of disease progression) (4–29%), and only 3 out of 21 patients with metastatic CRPC (Ronan Le Moigne et al., 2019). Another agent (ARV-110), a PROTAC® drug that uses an E3 ligase to tag and degrades "clinically relevant mutated AR proteins", has been introduced in a limited Phase-I dose escalation for patients with metastatic CRPC. Hence, as of now, enzalutamide, abiraterone, and

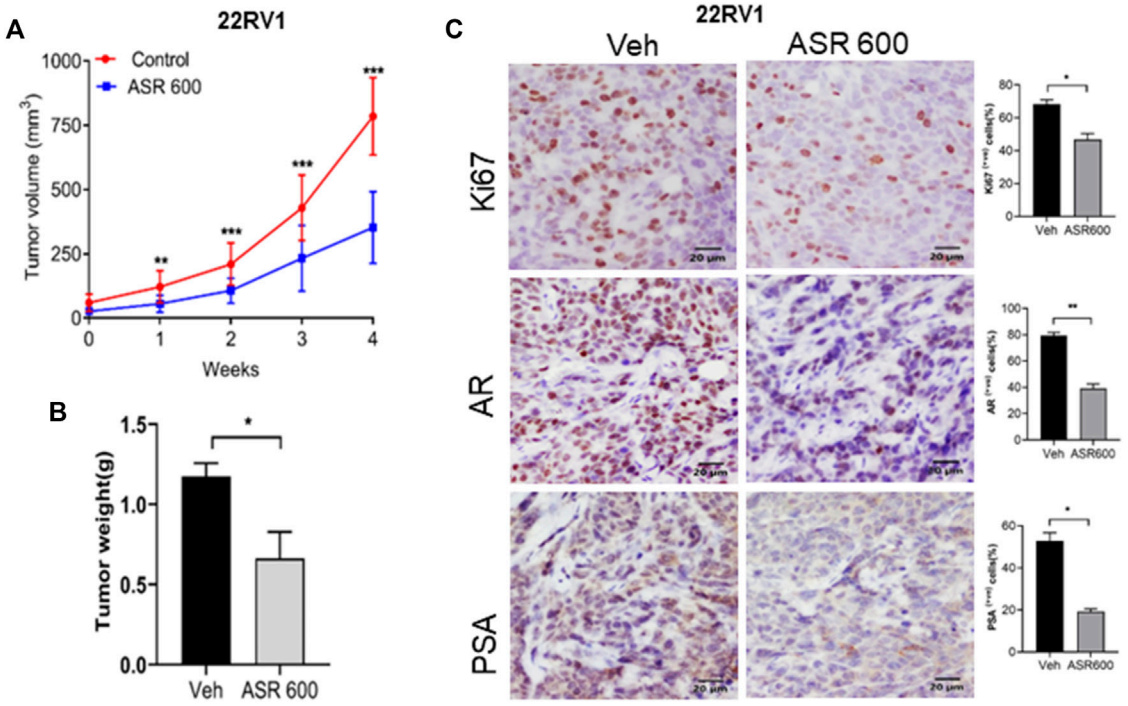

FIGURE 10
Oral administration of ASR-600 inhibits the growth of 22Rv1 xenograft tumors in castrated mice. 22Rv1 cells were inoculated into castrated nude mice. When the tumors reached ~50 mm^3, the mice were treated with 20 mg/kg ASR-600 through oral gavage. **(A)**. Mean tumor volumes. **(B)**, Individual tumor weight was measured. **(C)**. Immunohistochemistry analyses of tumor samples were performed to evaluate the expression of Ki67, AR and PSA in 22Rv1 xenografted tumors.

apalutamide are the US FDA-approved agents for treating CRPC. Considering that CRPC is the leading cause of 30,000 CaP-related mortalities every year in the US (American Cancer Society, 2019), there is an unmet clinical need for developing orally bioavailable and minimally toxic drug-like small molecules to effectively treat CRPC.

Previously, we reported that the anti-cancer properties of UroA occurred when the compound was administered in micromolar (IC_{50}: 35 μM) concentrations (Dahiya et al., 2018). However, in the present study, we found that novel UroA analog ASR-600 inhibited the growth of AR^+ CRPC, including enzalutamide resistant cells, at nanomolar concentrations, a dose that is 40-times lower than that of UroA (Boakye et al., 2018). Moreover, ASR-600 was found to be non-toxic to normal prostate epithelial cells. Our results also revealed that ASR-600 specifically targets AR. It is well known that UroA inhibits AKT and mTOR while upregulating PTEN in many cancer types (Zhou et al., 2016; Liberal et al., 2017; Boakye et al., 2018). These target genes are also expressed by AR null PC-3 and DU-145 CaP cells, and ASR-600 failed to inhibit pAKT and mTOR in AR-null CaP cells. This compound did not affect on PTEN levels as well as the ER and PR receptors in T47D cells. Similarly, although both DU-145 and PC-3 cells express the glucocorticoid receptor (Guo et al., 2018), ASR-600 still failed to inhibit the growth of both cell lines. Recently, Sharp et al. (2019) reported that while AR-V7 is rarely expressed in primary CaP, it is predominantly expressed in CRPC and frequently detected in CaP cases following ADT treatment and further increased following treatment with abiraterone or enzalutamide. We observed that ASR-600 decreased the expression of AR-V7 in 22Rv1 and VCaP cells and ectopically overexpressed AR-V7 293T cells. These results suggest that ASR-600 can target both AR-FL and AR-V7.

The ubiquitin-proteasome pathway is the predominant mechanism for AR degradation. Liu et al. (2018) discovered that the ubiquitin-mediated proteolysis pathway and proteasome activity are suppressed in enzalutamide and abiraterone-resistant CaP cells, which may trigger the over-expression of oncoproteins such as the AR-Vs. They noted that the half-life of AR-V7 is significantly extended in enzalutamide-resistant CaP cells suggesting that the treatment may alter the CaP ubiquitin-proteolysis system and stabilize the AR-V7 protein. Similarly, our results show that co-treatment of ASR-600 and CHX, a protein synthesis inhibitor, induced a ~90% decrease in AR protein levels, suggesting that ASR-600 mediated AR degradation may occur either by ubiquitin or lysosome pathways (Dikic, 2017). It is interesting to consider that AR downregulation in C4-2B cells was reversed by treatment with MG-132, a proteasome inhibitor (Steinhilb et al., 2001), but not with CQ, a lysosomal inhibitor. Thus, our mechanistic studies revealed that ASR-600 causes AR and AR-Vs degradation in CRPC and enzalutamide-resistant CRPC cells through a ubiquitin-mediated pathway. Biophysical analysis based on NMR and ITC studies indicated that ASR-600 binds to NTD and enhances ubiquitin-mediated degradation of both AR and

AR-Vs without inhibiting proteasome activity. Our ongoing experiments may suggest the possible ASR-490 ubiquitin binding sites at NTD of AR. We believe that if we ubiquitinate AR, regardless of whether or how much androgen or other stimuli of AR signaling are present in CRPC, it would be a novel approach to eradicate the deadly disease.

Results assessing ASR-600 *in vivo* efficacy using castrated and non-castrated xenograft mice models showed that ASR-600 exhibited a high therapeutic index in that it was able to significantly inhibit tumor growth at just 20 mg/kg [<4% of the maximum tolerated dose (MTD)]. Considering that the MTD of the oral dose of ASR-600 in mice was >500 mg/kg of body weight, it is safe to assume that oral dose can be increased without any concerns of ASR-600 being systemically toxic.

In conclusion, despite progress in this field, many second-generation anti-androgens have limited clinical success owing to their inability to block AR-V7 signaling in CRPC. Thus, to develop more efficient and target-specific treatments, a greater understanding of the regulatory mechanisms of AR-V7, its upstream and downstream effectors, and target genes is essential. Our findings highlight the importance of targeting AR-Vs, particularly AR-V7 in CRPC, and provides mechanistic insight into how UroA analog ASR-600 can target both AR-FL and AR-V7 in CRPC.

Data availability statement

The original contributions presented in the study are included in the article/Supplementary Materials, further inquiries can be directed to the corresponding author.

Ethics statement

The animal study was reviewed and approved by the ethical committee of the University of Louisville, KY and maintained in accordance with the Institutional Animal Care and Use Committee approved protocols.

Author contributions

Conceptualization, CD, MA, and AS; methodology, CD, AKS, ND, BC, and AT; formal analysis, BC, AT, US, VK, VC, and JL; investigation, BC, AT, US, VK, VC, AS, JL, and AKS; resources, CD, AKS, and MA; writing—original draft, BC, AT, US, and CD; supervision, CD, AKS, ND, and JL; funding acquisition, CD, AKS, and ND.

Funding

We acknowledge support from the National Institutes for Health, RO1 CA 257370 to CD, AKS, 1R35 GM134864 to ND and the Passan Foundation. The project described was also supported by the National Center for Advancing Translational Sciences, National Institutes of Health, through Grant UL1 TR002014.

Conflict of interest

The authors declare that the research was conducted in the absence of any commercial or financial relationships that could be construed as a potential conflict of interest.

Publisher's note

All claims expressed in this article are solely those of the authors and do not necessarily represent those of their affiliated organizations, or those of the publisher, the editors and the reviewers. Any product that may be evaluated in this article, or claim that may be made by its manufacturer, is not guaranteed or endorsed by the publisher.

Supplementary material

The Supplementary Material for this article can be found online at: https://www.frontiersin.org/articles/10.3389/fphar.2023.1137783/full#supplementary-material

References

American Cancer Society (2019). Key statistics for prostate cancer. https://www.cancer.org/cancer/prostate-cancer/about/key-statistics.html.

Antonarakis, E. S., Armstrong, A. J., Dehm, S. M., and Luo, J. (2016). Androgen receptor variant-driven prostate cancer: Clinical implications and therapeutic targeting. *Prostate Cancer Prostatic Dis.* 19 (3), 231–241. doi:10.1038/pcan.2016.17

Antonarakis, E. S., Lu, C., Wang, H., Luber, B., Nakazawa, M., Roeser, J. C., et al. (2014). AR-V7 and resistance to enzalutamide and abiraterone in prostate cancer. *N. Engl. J. Med.* 371 (11), 1028–1038. doi:10.1056/NEJMoa1315815

Attard, G., Reid, A. H. M., A'Hern, R., Parker, C., Oommen, N. B., Folkerd, E., et al. (2009). Selective inhibition of CYP17 with abiraterone acetate is highly active in the treatment of castration-resistant prostate cancer. *J. Clin. Oncol.* 27 (23), 3742–3748. doi:10.1200/JCO.2008.20.0642

Attwa, M. W., Kadi, A. A., and Darwish, H. W. (2020). Metabolic stability assessment of larotrectinib using liquid chromatography tandem mass spectrometry. *Drug Des. Devel Ther.* 14, 111–119. doi:10.2147/DDDT.S235934

Baranczewski, P., Stańczak, A., Sundberg, K., Svensson, R., Wallin, A., Jansson, J., et al. (2006). Introduction to *in vitro* estimation of metabolic stability and drug interactions of new chemical entities in drug discovery and development. *Pharmacol. Rep.* 58 (4), 453–472.

Beer, T. M., Armstrong, A. J., Rathkopf, D. E., Loriot, Y., Sternberg, C. N., Higano, C. S., et al. (2014). Enzalutamide in metastatic prostate cancer before chemotherapy. *N. Engl. J. Med.* 371 (5), 424–433. doi:10.1056/NEJMoa1405095

Boakye, Y. D., Groyer, L., and Heiss, E. H. (2018). An increased autophagic flux contributes to the anti-inflammatory potential of urolithin A in macrophages. *Biochim. Biophys. Acta Gen. Subj.* 1862 (1), 61–70. doi:10.1016/j.bbagen.2017.10.006

Brady, M. E., Ozanne, D. M., Gaughan, L., Waite, I., Cook, S., Neal, D. E., et al. (1999). Tip60 is a nuclear hormone receptor coactivator. *J. Biol. Chem.* 274 (25), 17599–17604. doi:10.1074/jbc.274.25.17599

Cato, L., de Tribolet-Hardy, J., Lee, I., Rottenberg, J. T., Coleman, I., Melchers, D., et al. (2019). ARv7 represses tumor-suppressor genes in castration-resistant prostate cancer. *Cancer Cell* 35 (3), 401–413 e6. doi:10.1016/j.ccell.2019.01.008

Chandrasekaran, B., Dahiya, N. R., Tyagi, A., Kolluru, V., Saran, U., Baby, B. V., et al. (2020). Chronic exposure to cadmium induces a malignant transformation of benign prostate epithelial cells. *Oncogenesis* 9 (2), 23. doi:10.1038/s41389-020-0202-7

Chen, C. D., Welsbie, D. S., Tran, C., Baek, S. H., Chen, R., Vessella, R., et al. (2004). Molecular determinants of resistance to antiandrogen therapy. *Nat. Med.* 10 (1), 33–39. doi:10.1038/nm972

Cherinka, B., Andrews, B. ~H., Sánchez-Gallego, J., Brownstein, J., Argudo-Fernández, M., Blanton, M., et al. (2018), Marvin: A toolkit for streamlined access and visualization of the SDSS-IV MaNGA data set. arXiv e-prints

Dahiya, N. R., Chandrasekaran, B., Kolluru, V., Ankem, M., Damodaran, C., and Vadhanam, M. V. (2018). A natural molecule, urolithin A, downregulates androgen receptor activation and suppresses growth of prostate cancer. *Mol. Carcinog.* 57 (10), 1332–1341. doi:10.1002/mc.22848

De Bono, J. S., Logothetis, C. J., Molina, A., Fizazi, K., North, S., Chu, L., et al. (2011). Abiraterone and increased survival in metastatic prostate cancer. *N. Engl. J. Med.* 364 (21), 1995–2005. doi:10.1056/NEJMoa1014618

Dikic, I. (2017). Proteasomal and autophagic degradation systems. *Annu. Rev. Biochem.* 86, 193–224. doi:10.1146/annurev-biochem-061516-044908

Ding, F., and Dokholyan, N. V. (2013). Incorporating backbone flexibility in MedusaDock improves ligand-binding pose prediction in the CSAR2011 docking benchmark. *J. Chem. Inf. Model* 53 (8), 1871–1879. doi:10.1021/ci300478y

Dokholyan, N. V., Buldyrev, S. V., Stanley, H. E., and Shakhnovich, E. I. (1998). Discrete molecular dynamics studies of the folding of a protein-like model. *Fold. Des.* 3 (6), 577–587. doi:10.1016/S1359-0278(98)00072-8

Finkbeiner, S. (2020). The autophagy lysosomal pathway and neurodegeneration. *Cold Spring Harb. Perspect. Biol.* 12 (3), a033993. doi:10.1101/cshperspect.a033993

Gajula, S. N. R., Nadimpalli, N., and Sonti, R. (2021). Drug metabolic stability in early drug discovery to develop potential lead compounds. *Drug Metab. Rev.* 53 (3), 459–477. doi:10.1080/03602532.2021.1970178

Gonzalez-Sarrias, A., Nunez-Sanchez, M. A., Garcia-Villalba, R., Tomas-Barberan, F. A., and Espin, J. C. (2017). Antiproliferative activity of the ellagic acid-derived gut microbiota isourolithin A and comparison with its urolithin A isomer: The role of cell metabolism. *Eur. J. Nutr.* 56 (2), 831–841. doi:10.1007/s00394-015-1131-7

Guo, J., Ma, K., Xia, H. M., Chen, Q. K., Li, L., Deng, J., et al. (2018). Androgen receptor reverts dexamethasoneinduced inhibition of prostate cancer cell proliferation and migration. *Mol. Med. Rep.* 17 (4), 5887–5893. doi:10.3892/mmr.2018.8566

Guo, Z., Yang, X., Sun, F., Jiang, R., Linn, D. E., Chen, H., et al. (2009). A novel androgen receptor splice variant is up-regulated during prostate cancer progression and promotes androgen depletion-resistant growth. *Cancer Res.* 69 (6), 2305–2313. doi:10.1158/0008-5472.CAN-08-3795

Hu, R., Dunn, T. A., Wei, S., Isharwal, S., Veltri, R. W., Humphreys, E., et al. (2009). Ligand-independent androgen receptor variants derived from splicing of cryptic exons signify hormone-refractory prostate cancer. *Cancer Res.* 69 (1), 16–22. doi:10.1158/0008-5472.CAN-08-2764

Imamura, Y., and Sadar, M. D. (2016). Androgen receptor targeted therapies in castration-resistant prostate cancer: Bench to clinic. *Int. J. Urol.* 23 (8), 654–665. doi:10.1111/iju.13137

Komatsu, W., Kishi, H., Yagasaki, K., and Ohhira, S. (2018). Urolithin A attenuates pro-inflammatory mediator production by suppressing PI3-K/Akt/NF-κB and JNK/AP-1 signaling pathways in lipopolysaccharide-stimulated RAW264 macrophages: Possible involvement of NADPH oxidase-derived reactive oxygen species. *Eur. J. Pharmacol.* 833, 411–424. doi:10.1016/j.ejphar.2018.06.023

Lazaridis, T., and Karplus, M. (2000). Effective energy functions for protein structure prediction. *Curr. Opin. Struct. Biol.* 10 (2), 139–145. doi:10.1016/s0959-440x(00)00063-4

Li, Y., Chan, S. C., Brand, L. J., Hwang, T. H., Silverstein, K. A. T., and Dehm, S. M. (2013). Androgen receptor splice variants mediate enzalutamide resistance in castration-resistant prostate cancer cell lines. *Cancer Res.* 73 (2), 483–489. doi:10.1158/0008-5472.CAN-12-3630

Liberal, J., Carmo, A., Gomes, C., Cruz, M. T., and Batista, M. T. (2017). Urolithins impair cell proliferation, arrest the cell cycle and induce apoptosis in UMUC3 bladder cancer cells. *Invest. New Drugs* 35 (6), 671–681. doi:10.1007/s10637-017-0483-7

Linn, D. E., Yang, X., Xie, Y., Alfano, A., Deshmukh, D., Wang, X., et al. (2012). Differential regulation of androgen receptor by PIM-1 kinases via phosphorylation-dependent recruitment of distinct ubiquitin E3 ligases. *J. Biol. Chem.* 287 (27), 22959–22968. doi:10.1074/jbc.M111.338350

Liu, C., Lou, W., Yang, J. C., Liu, L., Armstrong, C. M., Lombard, A. P., et al. (2018). Proteostasis by STUB1/HSP70 complex controls sensitivity to androgen receptor targeted therapy in advanced prostate cancer. *Nat. Commun.* 9 (1), 4700. doi:10.1038/s41467-018-07178-x

Loblaw, D. A., Virgo, K. S., Nam, R., Somerfield, M. R., Ben-Josef, E., Mendelson, D. S., et al. (2007). Initial hormonal management of androgen-sensitive metastatic, recurrent, or progressive prostate cancer: 2006 update of an American society of clinical oncology practice guideline. *J. Clin. Oncol.* 25 (12), 1596–1605. doi:10.1200/JCO.2006.10.1949

Lu, J., Van der Steen, T., and Tindall, D. J. (2015). Are androgen receptor variants a substitute for the full-length receptor? *Nat. Rev. Urol.* 12 (3), 137–144. doi:10.1038/nrurol.2015.13

Machado, E. R., Annunziata, I., van de Vlekkert, D., Grosveld, G. C., and d'Azzo, A. (2021). Lysosomes and cancer progression: A malignant liaison. *Front. Cell Dev. Biol.* 9, 642494. doi:10.3389/fcell.2021.642494

McClurg, U. L., Cork, D. M. W., Darby, S., Ryan-Munden, C. A., Nakjang, S., Mendes Cortes, L., et al. (2017). Identification of a novel K311 ubiquitination site critical for androgen receptor transcriptional activity. *Nucleic Acids Res.* 45 (4), 1793–1804. doi:10.1093/nar/gkw1162

Moon, S. J., Jeong, B. C., Kim, H. J., Lim, J. E., Kwon, G. Y., and Kim, J. H. (2018). DBC1 promotes castration-resistant prostate cancer by positively regulating DNA binding and stability of AR-V7. *Oncogene* 37 (10), 1326–1339. doi:10.1038/s41388-017-0047-5

O'Neill, D., Jones, D., Wade, M., Grey, J., Nakjang, S., Guo, W., et al. (2015). Development and exploitation of a novel mutant androgen receptor modelling strategy to identify new targets for advanced prostate cancer therapy. *Oncotarget* 6 (28), 26029–26040. doi:10.18632/oncotarget.4347

Ronan Le Moigne, H.-J. Z., Obst, J. K., Adriana Banuelos, C., Jian, K., Williams, D., Peter, V., et al. (2019). Lessons learned from the metastatic castration-resistant prostate cancer phase I trial of EPI-506, a first-generation androgen receptor N-terminal domain inhibitor. *JCO* 37, 257. doi:10.1200/jco.2019.37.7_suppl.257

Sanchez-Gonzalez, C., Ciudad, C. J., Izquierdo-Pulido, M., and Noe, V. (2016). Urolithin A causes p21 up-regulation in prostate cancer cells. *Eur. J. Nutr.* 55 (3), 1099–1112. doi:10.1007/s00394-015-0924-z

Scher, H. I., Lu, D., Schreiber, N. A., Louw, J., Graf, R. P., Vargas, H. A., et al. (2016). Association of AR-V7 on circulating tumor cells as a treatment-specific biomarker with outcomes and survival in castration-resistant prostate cancer. *JAMA Oncol.* 2 (11), 1441–1449. doi:10.1001/jamaoncol.2016.1828

Schmidt, L. J., and Tindall, D. J. (2013). Androgen receptor: Past, present and future. *Curr. Drug Targets* 14 (4), 401–407. doi:10.2174/1389450111314040002

Shafi, A. A., Yen, A. E., and Weigel, N. L. (2013). Androgen receptors in hormone-dependent and castration-resistant prostate cancer. *Pharmacol. Ther.* 140 (3), 223–238. doi:10.1016/j.pharmthera.2013.07.003

Sharp, A., Coleman, I., Yuan, W., Sprenger, C., Dolling, D., Rodrigues, D. N., et al. (2019). Androgen receptor splice variant-7 expression emerges with castration resistance in prostate cancer. *J. Clin. Invest.* 129 (1), 192–208. doi:10.1172/JCI122819

Shirvanyants, D., Ding, F., Tsao, D., Ramachandran, S., and Dokholyan, N. V. (2012). Discrete molecular dynamics: An efficient and versatile simulation method for fine protein characterization. *J. Phys. Chem. B* 116 (29), 8375–8382. doi:10.1021/jp2114576

Steinhilb, M. L., Turner, R. S., and Gaut, J. R. (2001). The protease inhibitor, MG132, blocks maturation of the amyloid precursor protein Swedish mutant preventing cleavage by beta-Secretase. *J. Biol. Chem.* 276 (6), 4476–4484. doi:10.1074/jbc.M008793200

Tan, M. H., Li, J., Xu, H. E., Melcher, K., and Yong, E. l. (2015). Androgen receptor: Structure, role in prostate cancer and drug discovery. *Acta Pharmacol. Sin.* 36 (1), 3–23. doi:10.1038/aps.2014.18

Totiger, T. M., Srinivasan, S., Jala, V. R., Lamichhane, P., Dosch, A. R., Gaidarski, A. A., 3rd, et al. (2019). Urolithin A, a novel natural compound to target PI3K/AKT/mTOR pathway in pancreatic cancer. *Mol. Cancer Ther.* 18 (2), 301–311. doi:10.1158/1535-7163.MCT-18-0464

Tran, C., Ouk, S., Clegg, N. J., Chen, Y., Watson, P. A., Arora, V., et al. (2009). Development of a second-generation antiandrogen for treatment of advanced prostate cancer. *Science* 324 (5928), 787–790. doi:10.1126/science.1168175

van der Steen, T., Tindall, D. J., and Huang, H. (2013). Posttranslational modification of the androgen receptor in prostate cancer. *Int. J. Mol. Sci.* 14 (7), 14833–14859. doi:10.3390/ijms140714833

van Poppel, H., and Nilsson, S. (2008). Testosterone surge: Rationale for gonadotropin-releasing hormone blockers? *Urology* 71 (6), 1001–1006. doi:10.1016/j.urology.2007.12.070

Wang, J., and Dokholyan, N. V. (2019). MedusaDock 2.0: Efficient and accurate protein-ligand docking with constraints. *J. Chem. Inf. Model* 59 (6), 2509–2515. doi:10.1021/acs.jcim.8b00905

Watson, P. A., Chen, Y. F., Balbas, M. D., Wongvipat, J., Socci, N. D., Viale, A., et al. (2010). Constitutively active androgen receptor splice variants expressed in castration-resistant prostate cancer require full-length androgen receptor. *Proc. Natl. Acad. Sci. U. S. A.* 107 (39), 16759–16765. doi:10.1073/pnas.1012443107

Welti, J., Rodrigues, D. N., Sharp, A., Sun, S., Lorente, D., Riisnaes, R., et al. (2016). Analytical validation and clinical qualification of a new immunohistochemical assay for androgen receptor splice variant-7 protein expression in metastatic castration-resistant prostate cancer. *Eur. Urol.* 70 (4), 599–608. doi:10.1016/j.eururo.2016.03.049

Xu, K., Shimelis, H., Linn, D. E., Jiang, R., Yang, X., Sun, F., et al. (2009). Regulation of androgen receptor transcriptional activity and specificity by RNF6-induced ubiquitination. *Cancer Cell* 15 (4), 270–282. doi:10.1016/j.ccr.2009.02.021

Yang, J., Yan, R., Roy, A., Xu, D., Poisson, J., and Zhang, Y. (2015). The I-tasser suite: Protein structure and function prediction. *Nat. Methods* 12 (1), 7–8. doi:10.1038/nmeth.3213

Zhao, W., Shi, F., Guo, Z., Zhao, J., Song, X., and Yang, H. (2018). Metabolite of ellagitannins, urolithin A induces autophagy and inhibits metastasis in human sw620 colorectal cancer cells. *Mol. Carcinog.* 57 (2), 193–200. doi:10.1002/mc.22746

Zhou, B., Wang, J., Zheng, G., and Qiu, Z. (2016). Methylated urolithin A, the modified ellagitannin-derived metabolite, suppresses cell viability of DU145 human prostate cancer cells via targeting miR-21. *Food Chem. Toxicol.* 97, 375–384. doi:10.1016/j.fct.2016.10.005

Frontiers in Pharmacology

Explores the interactions between chemicals and living beings

The most cited journal in its field, which advances access to pharmacological discoveries to prevent and treat human disease.

Discover the latest Research Topics

See more →

Frontiers

Avenue du Tribunal-Fédéral 34
1005 Lausanne, Switzerland
frontiersin.org

Contact us

+41 (0)21 510 17 00
frontiersin.org/about/contact